RACE for 2030

RELIABLE
AFFORDABLE
CLEAN
ENERGY

FINAL REPORT

Digital Twin Enabled Sustainable Sunshine Precinct

April 2026

Final report

Research Theme CT9: Digital Twin Enabled Sustainable Sunshine Precinct
Incorporating end users in whole of system design

ISBN: 978-1-922746-81-8

April 2026

Citations

Yang, R., Liu, C., Abuseif, M., Carre, A., Jayasuriya, S., Zhao, H., Zhao, Y., Zhang, J., Gunarathna, C., Little, L., McRae, B., Wagner, M., Seymour, J., Liu, C., Amani, A.M., Wakefield, R., Sun, C., Rajagopalan, P., Duckham, M., Shiwakoti, N., Stasinopoulos, P., Bao, N., Hurley, J., Francis, M. . (2026). Digital Twin enabled Sustainable Sunshine Precinct Development. Prepared for RACE for 2030.

Project team (include cash & in-kind contributors)

RMIT University

Rebecca Yang, Chengyang Liu, Majed Abuseif, Andrew Carre, Sajani Jayasuriya, Hongying Zhao, Yusen Zhao, Jiatong Zhang, Chathuri Gunarathna, Chen Liu, Ali Moradi Amani, Ron Wakefield, Chayn Sun, Priya Rajagopalan, Matt Duckham, Nirajan Shiwakoti, Peter Stasinopoulos, Nic Bao, Joe Hurley, Matthew Francis.

Department of Transport and Planning

- Laura Little
- Brendan McRae

Monash University

- Markus Wagner

Centre for New Energy Technologies (C4NET)

- James Seymour

Project partners

RMIT University, Department of Transport and Planning (DTP), Centre for New Energy Technologies (C4NET), Monash University.

Acknowledgements

Details are provided at the end of the report.

Acknowledgement of Country

The authors of this report would like to respectfully acknowledge the Traditional Owners of the ancestral lands throughout Australia and their connection to land, sea and community. We recognise their continuing connection to the land, waters, and culture and pay our respects to them, their cultures and to their Elders past, present, and emerging.

What is RACE for 2030?

Reliable, Affordable Clean Energy for 2030 (RACE for 2030) is an innovative cooperative research centre for energy and carbon transition. We were funded with $68.5 million of Commonwealth funds and commitments of $280 million of cash and in-kind contributions from our partners. Our aim is to deliver $3.8 billion of cumulative energy productivity benefits and 20 megatons of cumulative carbon emission savings by 2030. racefor2030.com.au

Disclaimer

Project Context

The value of integrated urban planning

The Sunshine Precinct is a key urban area situated at a vital junction between Melbourne's city centre and the western growth areas, offering strong connections to regional hubs, major transport routes, and economic infrastructure (State of Victoria Department of Transport, 2021). Planned infrastructure upgrades through major government projects will further boost accessibility and development opportunities in the precinct.

As the precinct is expected to experience a significant increase in both population and employment density, it faces the risk of growing environmental pressures. Without a sustainable design framework, issues such as urban heat, water scarcity, high energy costs and inefficient land use could compromise the precinct's liveability. To ensure that growth is managed responsibly and the area remains resilient to future challenges, it is essential to embed environmental sustainability into the core of precinct planning.

Figure 1 presents the key areas for growth and change identified for the Sunshine Precinct. The Victorian Department of Planning and Transport (DTP) provided RMIT with existing plans (referred to in this report as a base case) based on the Sunshine Precinct Opportunity statement[1] that foresees significant growth potential in the areas of Sunshine Station, Albion Precinct and Sunshine CBD (Town Centre). Within this analysis there was a strong focus on analysis of the Albion Precinct, which was undergoing a process of structure planning by the department.

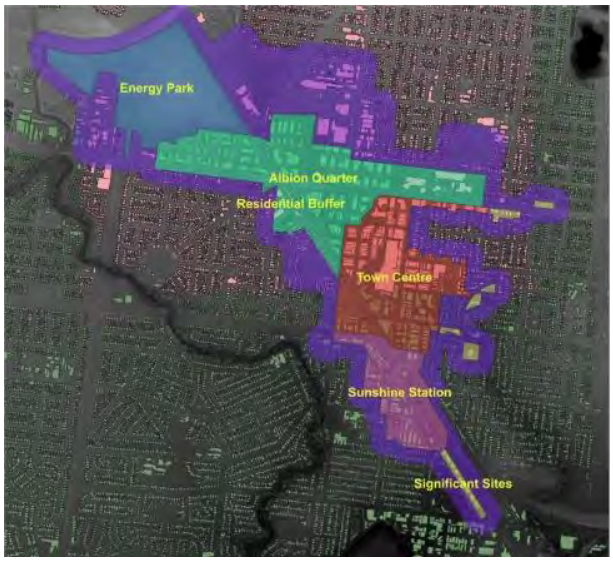

This project explores opportunities to enhance precinct renewal, through the application of digital twin technology. Digital Twins enable integrated, data-driven modelling of critical urban infrastructure such as power and water, as well as outcomes like urban heat, wind patterns and embodied carbon. This

[1] https://www.vic.gov.au/sites/default/files/2023-11/Sunshine_Precinct_Opportunity_Statement_Document_FINAL-%281%29.pdf

informs strategic planning decisions and ultimately opportunities to enhance urban resilience to climate change and other environmental challenges.

Leveraging digital twin modelling

Between the launch of the Sunshine Precinct Opportunity statement in 2021 to this report's publication in 2026, there have been significant advancements in our ability to capture data and to use it within digital twin modelling frameworks, helping us to explore alternative urban futures that can lead to better outcomes for the public.

In 2022, DTP launched the Digital Twin Victoria (DTV) platform[2] built in partnership with CSIRO. A defined aim of DTV was to "allow the planning and building industries to virtually manage a development precinct or project area. Using the platform tools, it was envisioned they can virtually model things like overshadowing and underground utilities, before shovel hits the ground[3]".

Realising the aspirational goal for the DTV requires significant contributions from industry and research, to develop and seamlessly link appropriate computational tools. This project developed and explored some of the tools needed to meet the DTV goal and applied these to the Sunshine Precinct as an exemplar of a more digitally enhanced future in planning.

Digital twins can enable more effective, integrated systems modelling, leading to more informed investment decisions in urban infrastructure and planning, while highlighting the potential for future, compounding costs and benefits.

Digital twins have great potential to transform the future planning and investment of sustainable cities. When used operationally, digital twins include representation of a physical entity (e.g. a building or precinct) and develop a virtual model that represents the performance of the real-world analogue (e.g. through machine learning, predictive models etc.). They capture live data flows from a range of tools (sensors, IoT devices, weather data, operational data that keep the virtual model synchronised) to update these predictive models in real-time to assist operators safely and efficiently deliver services.

For planning activities (as used in this study), the models typically concentrate on linking data with predictive models that include higher degrees of specificity and granularity (e.g. utilising non-linear physics-based models such as PowerFactory[4] for power simulation or ENVI-met[5] for environmental conditions) rather than learning based models that react to current data settings (e.g. temperature, solar radiation etc).

Depending on the nature of the problem being explored, these models can be soft-linked, helping to explore interactions between urban design decisions. For example, to explore how precinct specific temperature predictions from a model such as ENVI-met, affects electricity demand as an input into power flow models.

[2] https://www.land.vic.gov.au/maps-and-spatial/digital-twin-victoria

[3] https://www.land.vic.gov.au/maps-and-spatial/maps-and-spatial-news/2022/digital-twin-victoria-platform-now-live

[4] https://www.digsilent.de/en/powerfactory.html

[5] https://envi-met.com/

Digital Twin insights from the Sunshine Precinct

This study developed the processes and tools to examine sustainable urban design strategies across scales, from precinct-level outcomes to microclimates within the precinct, including the impact of street layouts and building forms.

The research was structured around four key focus areas being: (1) urban heat, (2) water and vegetation, (3) embodied carbon, and (4) energy. Two primary scenarios were analysed: a base scenario and an updated scenario, each including multiple alternatives to assess the impacts of varying urban design interventions.

The base scenario comprised a precinct model developed by the DTP for 2050, reflecting proposed developments within the Albion Quarter, Sunshine Station, and Town Centre. The updated scenario introduced modifications to the base model, including variations in built form, street design, and open space configuration.

Figure 2 illustrates, at a high level of abstraction, the interconnectivity of factors influencing outcomes such as urban heat, energy use and embodied carbon.

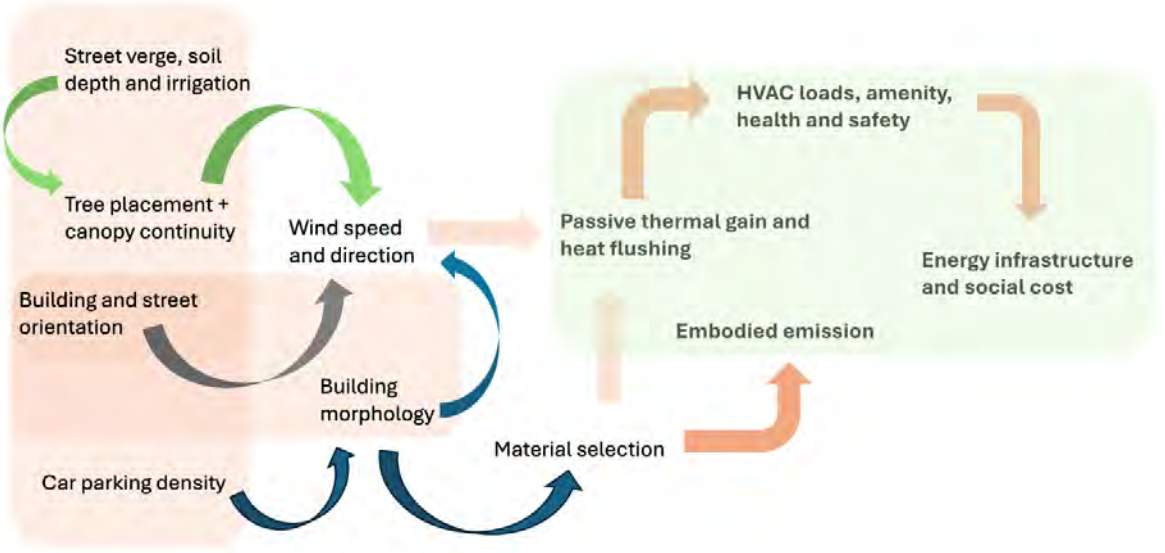

Figure 2. System connectivity considered in the Sunshine Precinct

For example, we can see the compounding impact that design elements such as street verge width and soil depth, irrigation and tree canopy, as well as building heights and orientation, have on wind speed and direction. Car parking density compounds the impact on wind speed, by its influence on building heights in particular, and material selection.

All of these design elements combine, with consequences for cooling energy demand (HVAC loads), amenity and health at street level, due to heat stress exposure.

The nature of a highly connected system (as shown in Figure 2) will often result in positive and negative changes as different input criteria are varied when examining alternative scenarios and comparing to the counterfactual of a base case. Graphical methods are particularly useful for providing clarity on

those impacts. Outcomes from the modelling employed in this study have been made available in a format compatible with the DTV platform for this purpose and for broader knowledge sharing.

Exploring system connectivity: Energy Park

Illustrating urban system connectivity is best done using a modelling case study. Here we consider changes to wind flow and urban heat outcomes across Energy Park (a Council owners former landfill proposed to transition to public use), through re-imagining the way in which green space is designed.

Figure 3(a) represents the base case green space allocation, with trees spread across the Energy Park to meet a 30% coverage target. In **Error! Reference source not found.**(b), an alternative case is a djusted to include provision of a sports stadium, a few service buildings, and activities including four playing fields with irrigated grass. This alternative case also meets the 30% canopy target.

Finally, Figure 3(c) illustrates a reimaging of the green structure to maximise airflow and reduce hotspots by rearranging trees including strategic grouping to serve as wind channels, while providing targeted, overlapped canopies to cool the park. This arrangement also exposed the four irrigated surfaces to increased airflow, enhancing evaporative cooling and distributing the cooled air within the park, while allowing it to move out of the park and cool the surrounding area.

(a)

(b

(c)

Figure 3. (a) Energy Park design based on the base case scenario; (b) Energy Park design based adjusting the base case scenario for addition of a stadium and playing fields; (c) Energy Park design to maximise airflow and reduce hotspots

Impact of design choice on urban heat

Strategic positioning and grouping of trees in the Energy Park (Figure 3(c) above) was clearly shown to reduce temperatures across the region.

Figure 4 illustrates the temperature profile in the Energy Park in the base case scenario for the hottest hour modelled. The Energy Park showed the highest temperatures across the precinct in the base case. Temperatures are relatively uniform across the Energy Park and in this case lead to an exceedance of state thermal comfort thresholds.

In contrast, Figure 5 clearly shows that strategic planning of vegetation and active irrigation (providing evaporative cooling) can substantially reduce ambient temperatures. The new design reduces predicted median air temperature across the Energy Park by 3.3 °C, with a maximum reduction of 10.9 °C. These impacts were shown to extend up to 550 m downwind.

The new design eliminates the extreme heat stress in the park and places a significant portion of the park within the moderate heat stress zone.

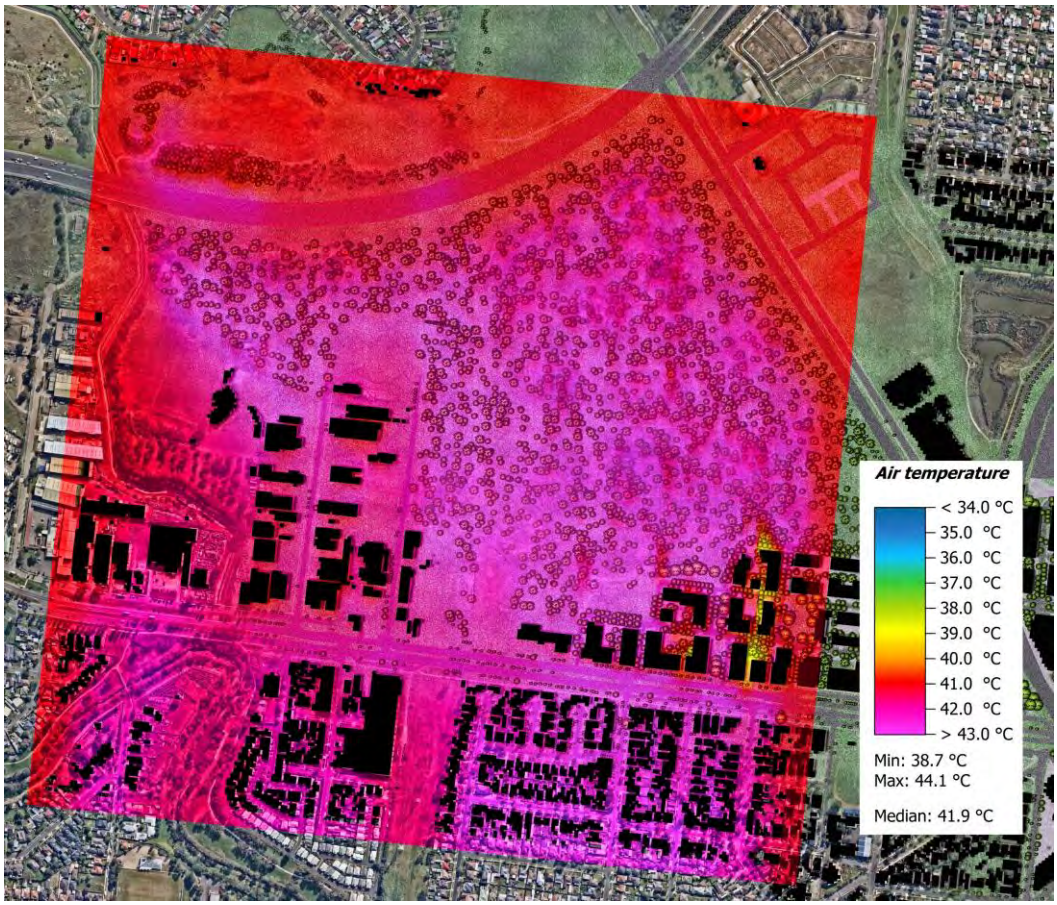

Figure 4. Energy Park temperatures for the base case

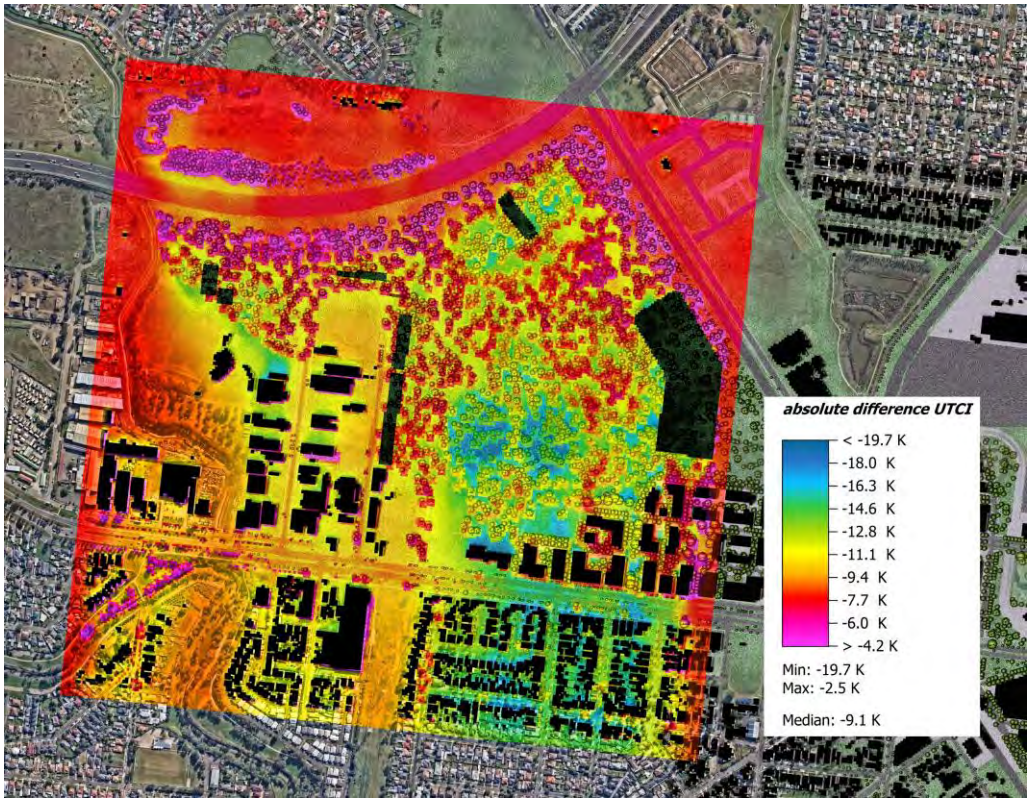

Figure 5. Differential temperatures across the Energy Park when design to maximise airflow and reduce hotspots

Impact on water needs

While the impact of tree placement and irrigation strategies provide a substantial reduction in ambient temperatures on extreme heat days, they require adequate water to allow for the evapotranspiration potential to be realised.

Figure 6 demonstrates that water requirements far exceed the effective rainfall (assumed to be 50% of annual rainfall) in the Energy Park. Up to 21.2 ML/yr of supplementary water is required for cooling in addition to the 36.6 ML/yr required for typical irrigation practices to maintain sports fields.

Effective rainfall is adjusted in 2050 to account for reductions likely from climate change however this change is relatively immaterial when compared with irrigation needs for the fields and for the additional water needed to cater for enhanced cooling on days exceeding 35°C (predicted to occur approximately 20 days each summer under CSIRO's RCP 4.5 scenario).

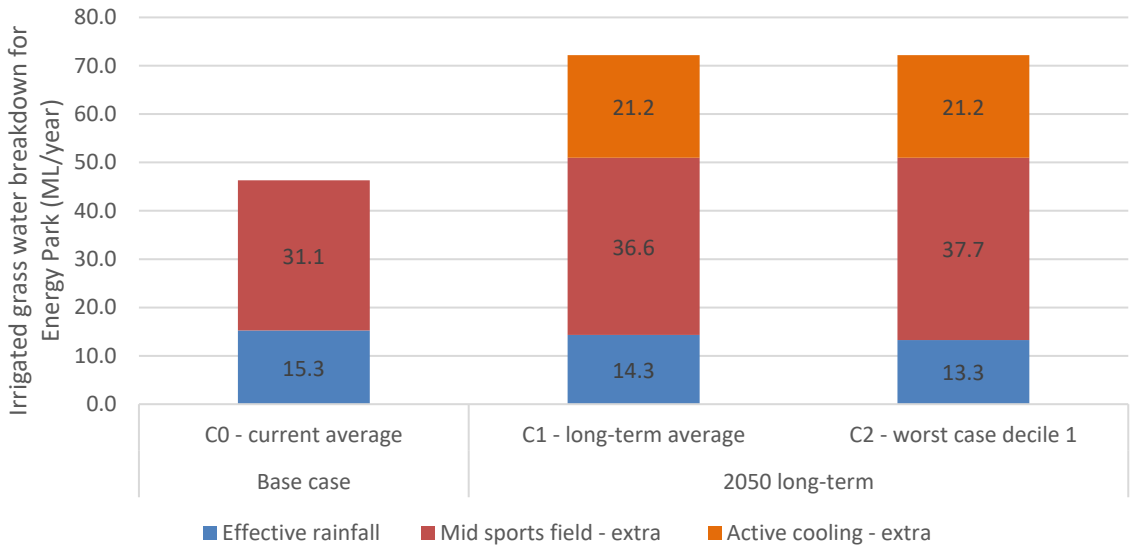

Figure 6. Grass water breakdown for the proposed irrigation area in Energy Park (ML/year)

Impact on energy demand

The ENVI-Met model used for urban heat impacts above was also used to estimate cooling loads on buildings adjacent to Energy Park. This was done for the base case and the updated case. Impacts in a specific section of the region was also explored (buildings 18-21). These buildings were chosen because they are located next to the energy park.

Figure 7 demonstrates the effects of greening strategies on cooling requirements for buildings adjacent to the Energy Park. Results show that on the hottest day, greening in the Energy Park significantly reduces overall cooling needs. Compared with the base case, the largest reduction occurs under the specific-zone (buildings 18-21), while adopting the Energy Park's average meteorological conditions also produces a noticeable decrease.

Greening strategies significantly reduce peak loads during the high-temperature period from 14:00 to 17:00, with reductions of 10–15% under specific-zone meteorological conditions shown in Figure 8. This suggests that local microclimate improvements brought by greening (cooling, increased humidity, and optimized wind speed) can have a strong effect in alleviating cooling demand during extreme periods. This can enhance energy system security and reduce costly infrastructure built to meet peak demand conditions.

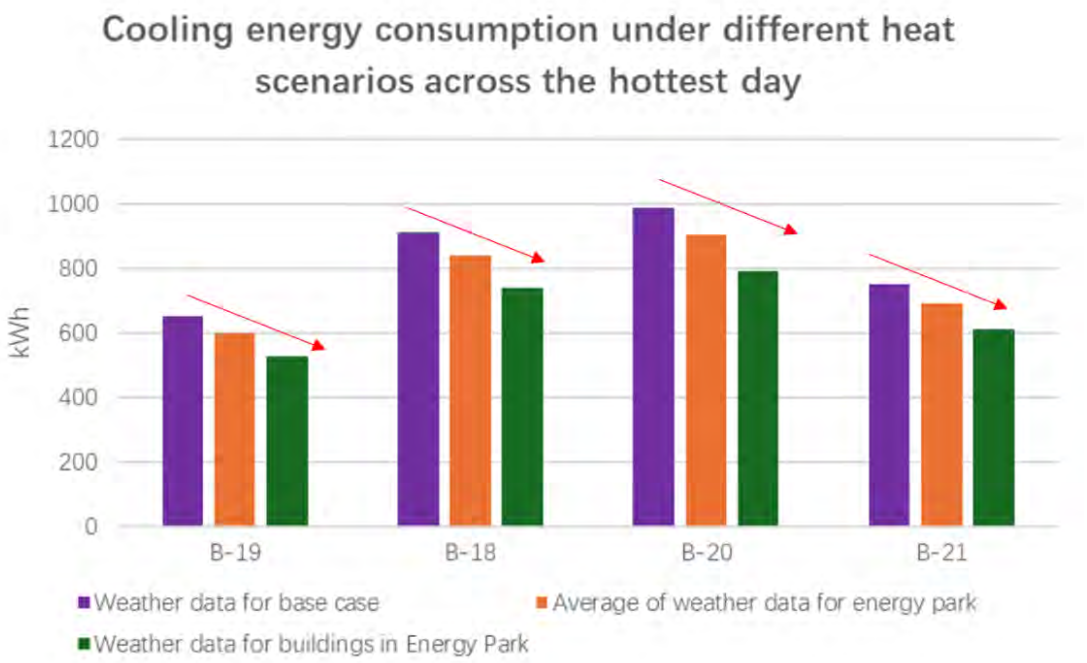

Figure 7. Cooling energy consumption under different heat scenarios across the hottest day.

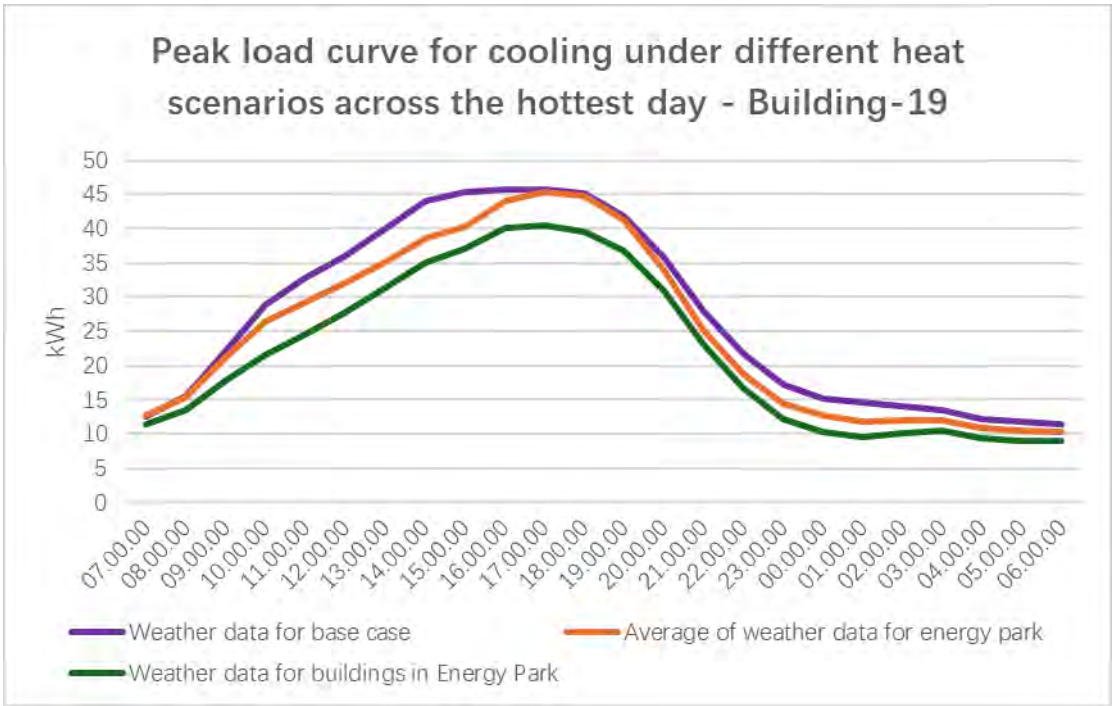

Figure 8. Peak cooling load curve under different heat scenarios across the hottest day – Building 19

Analysis of cooling loads at different floor levels of the buildings reveals the vertical variability of the greening effect. In a 30-meter-high building, the largest reductions (15–20%) are observed on the lower floors (0–2 floors). As building height increases, the reductions gradually diminish, with upper floors (7–8 floors) experiencing less than a 10% decrease. This indicates that greening in the Energy Park has a more pronounced effect on near-ground meteorological conditions, while the cooling and wind-

speed improvements weaken with height, thereby limiting the effect on upper-floor cooling energy consumption.

Overall, greening strategies in the Energy Park can effectively reduce both total cooling energy consumption and peak cooling loads by improving near-ground meteorological conditions. Areas with higher local greening coverage and more significant microclimate improvements achieve greater energy savings than the district-wide average.

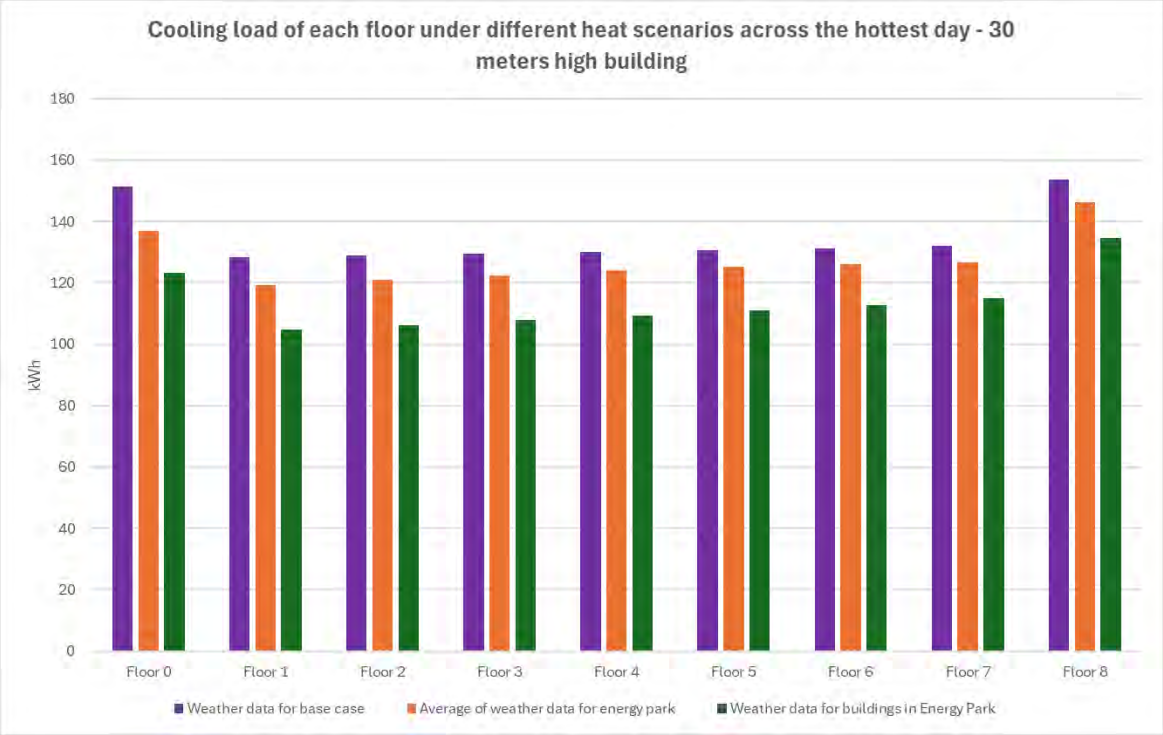

Figure 9. Cooling load of each floor under different heat scenarios across the hottest day – 30m high building

Overall impact

One of the difficulties in urban planning is the trade-off that inevitably arises as multiple actions are considered and multiple objectives targeted. The Energy Park case study demonstrates this challenge by highlighting significant reduction in urban heat and energy use in extreme conditions that is contingent on exploiting the benefits of evapotranspiration that requires sufficient water to be available.

This water can be provided in several ways, or through a combination of methods, such as piped supply, local storage facilities or through enhanced water capture in structured soils. While costs of these options have not been explored in this study, it is recognised that reductions in energy infrastructure from reduced loading and lower health costs through reductions in heat stress would provide significant economic value likely to outweigh the cost of water supply. Future analysis should estimate these impacts.

Executive Summary: Key research findings

A summary of key findings and where possible, recommendations from the detailed study are provided in this section.

Two major scenarios, both high-density, were tested:

- A Base Scenario –buildings from 2 to 15 storeys with a median height of 8 storeys, limited use of podiums and relatively more public realm.
- An Updated Scenario –buildings from 4 to 30 storeys with a median height of 14 storeys, widespread use of podiums, significantly more carparking, and relatively less public realm.

These scenarios are described in more detail in the Research Framework section of the report. Within each main scenario there were various sub-scenarios undertaken for different subject areas, to address specific research questions.

When examining the impacts of specific urban design choices for the Sunshine Precinct, it should be recognised that factors such as aligning streets or buildings to a North-South or East-West direction reflect outcomes based on specific meteorological conditions more prevalent at this site (see section 10) and do not necessarily generalise to other locations in Victoria or beyond.

Detailed findings are provided for urban heat, water, embodied carbon and energy in section 2 to 5 respectively.

Urban heat

In a future, warmer climate, the management of urban heat emerges as a fundamental and overarching design objective. Urban heat directly influences energy demand, outdoor amenity and public health outcomes, and therefore has a critical bearing on the long-term liveability, resilience and viability of urban precincts.

This study demonstrates that effective heat mitigation cannot be achieved through single-variable interventions, but instead depends on the interaction between built form, vegetation, irrigation, surface materials and airflow. Key findings from the modelling indicate that the following principles should inform effective urban heat mitigation:

- **Strategic irrigation of open spaces is the most effective driver of cooling at the precinct scale**

  Dispersed and linear irrigated open spaces function as primary cooling anchors, delivering substantial reductions in air temperature and thermal stress at the pedestrian level. Cooling effects were shown to propagate downwind for several hundred metres, provided that airflow pathways are maintained. This indicates that the spatial placement of irrigated landscapes relative to prevailing wind directions is more influential than uniform distribution. Targeted irrigated corridors and open spaces can therefore provide precinct-wide benefits without the need for irrigation everywhere.

The effectiveness of this approach was demonstrated most clearly in the Sunshine Energy Park ('Energy Park') and Albion Quarter scenarios. In the revised Energy Park design, median air temperature was reduced by 3.3°C, with maximum reductions of up to 10.9°C during extreme heat conditions. Thermal comfort improved substantially, eliminating extreme heat stress across much of the park. These benefits were strongly localised near irrigated surfaces but were amplified and extended through improved airflow, particularly closer to ground level where evapotranspiration is most effective.

- Airflow is as critical as shading in determining heat outcomes

Across all scenarios, areas with restricted ventilation consistently exhibited higher air temperatures, even where shading was present. Dense or poorly arranged tree canopy and compact built forms were shown to obstruct airflow, creating hot pockets and limiting the spread of cooling benefits from irrigated areas. Conversely, maintaining ventilation corridors allowed cooled air to disperse more effectively, enhancing the impact of irrigation and shading, as well as enhancing passive cooling.

This finding was reinforced in the Updated Scenario (tree optimisation sub-scenario) for Albion Quarter, where active tree placement and selective canopy adjustment improved airflow. Although precinct-wide average temperature reductions were modest, localised cooling reached up to 8.4°C, with significant reductions in thermal stress in high-risk locations. These results confirm that airflow management is a prerequisite for translating local cooling interventions into broader precinct benefits.

- Tree canopy should be optimised for spatial performance rather than uniform planting

The analysis shows increasing canopy coverage alone does not guarantee cooling. Trees are excellent at providing shade however their cooling performance varies depending on canopy density, shading context, local wind speeds and irrigation.

In areas with high solar exposure, it is critical that tree canopy is overlapping, to protect pedestrians and surfaces from direct and reflected solar radiation. In ventilation corridors,particularly close to irrigated areas, balance is needed between shading and allowing airflow. Street-scale analysis demonstrated that large trees could reduce air temperature when aligned with airflow, but may increase temperatures where they block ventilation, particularly in North-South ('N-S') streets. Small trees improve airflow but provide limited shading.

These trade-offs indicate tree canopy should be planned as a spatial system integrated with street geometry and wind behaviour, rather than delivered through uniform planting.
For the specific conditions of the Sunshine Precinct this means providing overlapping tree canopy on the southern side of East-West ('E-W') streets. Less dense planting may be feasible in N-S streets *if* these are well shaded by buildings and where there is limited airflow due to building configurations. Overlapping canopy is also required in streets otherwise unshaded by

buildings due to adjacent open space or infrastructure, although breaks may be required at strategic points to enable airflow.

- Water availability and evapotranspiration underpin vegetation cooling performance

  Cooling from vegetation was strongly dependent on soil moisture and sustained evapotranspiration. Drought-resistant trees with limited soil moisture showed reduced cooling capacity and, in some cases, contributed to higher daytime temperatures during peak heat due to suppressed transpiration. Diurnal analysis confirmed that cooling benefits diminish during the hottest hours when trees close their stomata under water stress.

  These findings highlight the importance of aligning vegetation selection, irrigation provision and realistic water management strategies. While irrigation imposes additional demand on water systems, its targeted application yields disproportionate cooling benefits, particularly when combined with airflow-aware design.

  It is important to note this finding is focused particularly on very hot days. For most hot days (excluding more extreme conditions), drought-resistant trees play an important role in pedestrian shading and protecting surfaces from solar radiation, and these benefits potentially outweigh the risk of slightly higher temperature on extreme heat days.

- Built form configuration significantly influences heat accumulation and dispersion

  In the Updated Scenario, increased building heights and more uninterrupted built form on the north side of Ballarat Road resulted in higher air temperatures due to trapped airflow and reduced ventilation in E-W streets. Taller buildings also altered wind patterns, intensifying wind speeds in N-S corridors while limiting heat dissipation in E-W corridors. In contrast, areas with greater spacing between buildings and access to irrigated landscapes performed better thermally.

  The analysis also indicates that low embodied carbon (i.e., mass timber) buildings have a limited influence on outdoor air temperature at the precinct scale, with variations of ±0.2°C. However, they do affect the timing of heat release, with lower embodied carbon materials reducing daytime temperatures at the expense of slightly higher night-time temperatures. The implications of this dynamic in a multi-day heatwave are unknown as this was not modelled in the study. The complexity suggests that material selection should consider both carbon and thermal performance.

- Heat risk is highly localised and should be addressed accordingly

  Across all scenarios, the most meaningful improvements were observed in high-risk locations such as Energy Park, compact street canyons and exposed paved spaces. Precinct-wide averages masked these outcomes and should not be relied upon as the primary indicator of

success. Instead, heat mitigation strategies should focus on identifying, prioritising and treating hotspots through coordinated landscape, irrigation and built-form interventions.

Water

Rainfall in the Sunshine region, even if fully captured, remains at levels below expected demand for irrigation. However, water is critical to the survival of vegetation and can act to reduce temperatures through the latent heat of evaporation (directly from wet sources or transpired through plant stomata). Understanding the supply anddemand balance and maximising co-benefits from its use is critical for efficient precinct development.

Given the overlap with urban heat and its mitigation through evapotranspiration, some outcomes for water are captured in the Urban Heat key findings. Additional research findings include:

- **The climate projections of lower rainfall, increased temperatures and drought, will create challenges to achieving greening outcomes**
  Average climate projections for 2050 point to an up to 13% decrease in annual rainfall *and* a 10% increase in evapotranspiration, creating a widening gap between available rainfall and tree water demand. In addition, lower rainfall and more frequent drought means that standard soil volumes for street trees are at risk of not providing sufficient water storage capacity to cover long dry periods over the summer. These dynamics create challenges for achieving greening objectives in the precinct, particularly on streets, and make provision of sufficient soil and water infrastructure critical.

- **Achieving overlapping tree canopy on streets requires investment in soil and water infrastructure beyond typical practices**

  To protect pedestrians and surfaces from solar radiation it is important that tree canopy is overlapping. Research in this study shows that investment in soil and water, frequently beyond typical practices, is needed to create this overlapping canopy.

  In relation to streets, analysis found that 3 metre verges with structural soil, or 5m verges (no structural soil), created the potential for overlapping canopy. A 2 metre verge was insufficient - even when supplementary water was provided. Active and passive irrigation of street trees is also critical. Efficient passive irrigation is required as a baseline measure to create overlapping canopy. Even increasing soil volume from 3 metres to 5metres, water remains a limiting factor, with overlapping canopy not achievable without passive irrigation for either verge width.

  Supplementary active irrigation – potentially through low-cost drip irrigation systems – enhances this overlapping effect, enabling mature tree growth to be realised more quickly and providing security against drought conditions.

  Where space is constrained, there is opportunity to focus the investment in overlapping canopy in areas with particularly high solar exposure in summer. These areas can be identified through shading analysis of a 3D built form model.

- **A 30% tree canopy target is unlikely to be met in the Sunshine Precinct without increasing the amount of public realm and/or increasing canopy provision on private land beyond current policy**

  Tree canopy was below 30% for both the Base and Updated Scenarios. In both scenarios increasing canopy cover on private land to 20% improved canopy percentages but did not reach the 30% target (25% for the Base Scenario and 22% for the Updated Scenario). This suggests that reaching this target would require more allocation of space to the public realm for greening, and/or additional private land canopy, such as above ground canopy on podiums (in addition to ground-level canopy).

- **Irrigation for cooling of open spaces requires investment in alternative water supplies**

  Irrigation of open space for cooling requires short bursts of intensive irrigation on days above 35 degrees. This equates to an annual water use of approximately 3.75ML per hectare in Sunshine, based on long term climate projections of 20 such days per annum.

  The analysis showed that significant water could be captured from road runoff and building rooftops across the precinct, however there are competing uses for this water. Road runoff is required for passive irrigation of street trees. Regarding rooftop water, a significant volume can be captured, however, for high density residential buildings that water is likely to be fully utilised for the building and private gardens. Given that, water capture from low rise commercial and industrial buildings or other infrastructure, or other alternative sources may be required to avoid reliance on mains water for irrigation.

Embodied carbon

As precincts electrify and their supply becomes dominated by renewable energy, the embodied carbon in construction materials becomes a more significant contributor to precinct-level emissions. This is because the electricity grid is decarbonising more quickly than manufacturing processes for steel or concrete, which depend on direct burning of coal or gas. Concrete and steel account for the largest portions of the carbon footprint, highlighting the crucial role of material selection.

Key findings from the research were:

- **Material selection was able to reduce embodied carbon from between 14% to 46%**

  Material selection was seen to reduce embodied carbon by 14% when equivalent lower carbon materials (e.g., low carbon cement) were selected, highlighting the benefits achievable when carbon is prioritised during procurement.

  More ambitious low-carbon material palettes such as light-weight and mass timber approaches, in combination reduced the embodied carbon of the precinct by 46%.

Concrete and steel were found to be the largest contributors to embodied carbon across most scenarios. Mostly for this reason, the upper floor elements of buildings were found to be the largest contributors to embodied carbon across most scenarios. Consistent with the literature, as buildings get taller, embodied carbon intensity typically increases. Furthermore, some forms of low-carbon construction approaches become difficult in taller buildings – such as light weight timber construction - which is uncommon in buildings above six (6) storeys.

- **Carparking within buildings was found to contribute significantly to embodied carbon**
  The removal of carparking (within the building) from the Base Scenario was seen to reduce embodied carbon by 15%.

  At the same time a tripling of carparking (between the Base Scenario and Updated Scenario) led to a 30% increase in embodied carbon.

- **The impact of basements on embodied carbon was relatively modest where carparking was retained elsewhere**
  Moving carparking from basements to the upper floors of buildings reduced embodied carbon by only 4%, where carparking was retained.

- **A study of the precinct carbon life cycle showed that reducing grid supplied electricity emissions currently has more impact potential than reducing embodied carbon, although this is projected to change over time as the grid decarbonises**

  At current grid emissions intensity, embodied carbon comprises between 7% and 12% of lifecycle emissions, depending on the extent of on-site renewable energy being used. Long term projections of electricity grid emissions intensity suggest the share of embodied carbon will increase to 53% of emissions over a 60-year lifecycle, if projections are realised. That is, we can expect the relative importance of reducing embodied carbon will increase over time.

Energy

Urban precinct design and energy infrastructure requirements are becoming more deeply connected as household electrification, PV, small scale/community battery storage and electric vehicles become more pervasive. Demand for electricity is a function of the type of services being sort, primarily hot water and space heating or cooling but increasingly electric transport (EVs). Heating and cooling loads are directly influenced by the built environment with material choices being particularly critical as well as meteorological processes that affect factors such as heat gain and local energy production.

Unique constraints on energy economic modelling resulted in the research focus being on exploring the relationship between built form and renewable energy outcomes, as well as high level, in-principle insight to inform planning processes and decisions. For example, we cannot reliably say what energy market wholesale conditions might look like in 2050, or customer uptake of variable pricing, therefore solar, battery and EV charge management modelling focused on identifying issues to be managed within current local grid constraints, as opposed to the financial value of localised solutions to precinct stakeholders.

The DER units and energy management system were controlled by a fuzzy-inference-system (FIS), which is a policy-based control system that coordinates battery charge and discharge according to generation, load, and predicted load profile.

A follow up study could build on the modelling approach developed in this report and focus on better quantifying the value gap between a standard roll out of distributed energy resources (DER) at the precinct level, and a co-ordinated rollout that balances the objectives of stakeholders. This value gap is a function of both the deployment and management of DER assets, as well as the cost of delivering a comparable solution via grid supplied energy. For example, if the policy goal was for a precinct to be 100% supplied with renewable energy, on a 24x7 basis, the cost of delivering that outcome via centralised grid assets would need non-trivial work to quantify.

Key findings from this current research are:

Climate change and energy

- **Climate change is expected to both increase cooling loads and reduce heat loads, resulting in a net increase in energy demand**
  Increased temperatures in 2050 were projected to increase cooling loads in the Base Scenario by 50%, while reducing heating loads by 20%, with a net 2.58% increase in total thermal load.

Urban form

- **In a medium to high-density urban form, building thermal performance improvements depend more on urban morphology than the thermal design of individual buildings**
  The Updated Scenario (with 14-20 storey buildings and widespread use of podiums) had a thermal load 15.8% higher than a somewhat less intensive Base Scenario (with an urban form of 8-10 storey buildings and limited use of podiums).

  Modelling indicated that this change was not due to deficiencies in individual building envelope performance but rather the result of increased mutual shading of buildings combined with the heat retention effects of more condensed urban form. The results suggest that in dense urban environments, the dominant mechanism of building energy consumption shifts from building envelope control to urban morphology control. Urban morphology control in this instance refers to shading levels at the precinct scale and the extent of narrow deep urban canyons that exacerbate heat retention.

- **More intensive urban form concentrates energy demand spatially and increases reliance on energy from the grid. Within a high-density typology, there was a significant different between an urban form of predominantly 8 to10 storeys buildings with few podiums, which can achieve self-sufficiency of up to 45%, compared to 14 to 20 storeys with widespread use of podiums which has a maximum self-sufficiency of up to 30%.**
  The Base Scenario was able to achieve higher levels of energy autonomy under a wider range of operational strategies compared to the Updated Scenario.

  While taller urban forms improve renewable generation intensity per unit land area through increased façade exposure, they also concentrate energy demand and operational loads. Where

functional floor area increases faster than renewable collection surfaces, renewable generation is diluted when assessed per unit of usable space.

Overall, the more intensive urban form creates a bigger gap between energy generation potential and energy demand. This results in lower self-sufficiency, reduced utilisation of on-site generation, and lower local energy autonomy compared with less compact urban forms. It also translates into higher relative costs of renewable energy deployment as the marginal benefit of investment is lower when the investment covers a smaller proportion of overall demand.

- **Changes in built form create materially different electricity network impacts, even with identical energy configurations**

  Network constraints emerged more readily in the Updated scenario than the Base scenario, under identical energy deployment assumptions. This was due to the greater transformer loading associated with serving larger buildings where both midday reverse power flows from building integrated photovoltaics and evening electric vehicle charging loads are concentrated. While there were options to meet demand within existing network constraints under both scenarios, there were fewer options under the Updated Scenario. This highlights the sensitivity of the network to spatial concentration effects at the building level.

Electric Vehicles

- **EVs have the potential to be a major driver of infrastructure upgrades requirements**
  Across the urban forms of the Base and Updated Scenarios, EV uptake emerges as the dominant driver of infrastructure upgrades. In the Base Scenario, a sharp threshold is observed between 20% and 50% EV penetration, beyond which infrastructure upgrades become more necessary. At penetration levels above 50% (1 per 50% of dwellings) the probability of upgrade rapidly approaches 100%, indicating that existing network capacity can no longer accommodate the coincident charging demand. In the Updated Scenario, this threshold behaviour is preserved, but the baseline probability of upgrades is systematically higher at lower EV penetration levels, reflecting the higher demand intensity associated with the vertically intensified built form.

- **Managing evening demand, in particular EV charging, is critical to longer term network performance. Smart charging combined with solar generation and battery storage can improve energy utilisation by 13-15%**

  Given the potential stress of EV charging on network infrastructure, coordinating charging strategies (i.e. smart charges) are critical. This is likely to be most effective when combined with façade PV and medium-to-high battery storage capacity, which helps smooth the mismatch between supply and demand. Modelling indicated that the combination of smart charging, additional generation and storage could improve consumption profile stability (load factor) by approximately 13–15%.

Solar PV

- **There is complementarity between rooftop and façade PV, which can support local renewable generation usage**

Evaluation of PV production across the precinct demonstrates a clear complementarity between rooftop and façade-integrated PV. Rooftop systems deliver strong summer peaks but significantly lower winter output. Façade-integrated PV produces less energy in absolute terms, but its relative contribution is higher during winter and shoulder seasons due to the advantages of vertical and east–west orientations under low solar elevation conditions. As such there are opportunities to exploit complementarities in renewable generation through combined rooftop and façade-integrated PV deployment, particularly if building integrated solar comes down the cost curve over time.

- Increasing northern façade PV is highly effective for improving energy autonomy but rapidly breaches infrastructure constraints

  Increasing the proportion of north-facing façade PV leads to a strong increase in energy self-sufficiency. However, beyond approximately 20% of the available north-facing façade PV coverage, infrastructure upgrades become both inevitable and economically significant.

- East–west façade PV expands the feasible envelope with comparatively low network risk
  Higher east–west façade coverage increases energy self-sufficiency proportionally with urban size, without systematically increasing network stress. This makes it an infrastructure-resilient pathway for increasing renewable penetration in dense urban contexts.

- Spatial concentration of PV deployment across feeders can have significant network impacts

  Scenarios with higher concentrations of building integrated photovoltaics on specific feeders exhibit increased exposure to reverse power flows and voltage constraints. This suggests that feeder aware deployment strategies, rather than uniform capacity expansion, may be important as photovoltaic penetration increases.

Batteries

- Medium-high battery use increases the potential to use local distributed energy resources (DER) and helps manage peak loads but does not eliminate network constraints

  Scenarios with low battery capacity are more likely to approach transformer loading limits during evening peaks, whereas medium and high battery configurations consistently reduce peak loading through targeted discharge. This confirms that investment in batteries is important if the intent is to maximise local PV generation and use localised DER to meet evening demand. However, it does not eliminate network constraints if overall load volumes remain significantly higher. As such battery deployment must be carefully coordinated with generation scale and network capacity rather than pursued as a stand-alone optimization lever, reinforcing the value of planning frameworks and processes that enable coordinated investment and management of battery assets

Grid performance

The scope of the research focused on avoiding infrastructure upgrades and the research findings reflect this constraint. There may be broader benefits in upgrading infrastructure to encourage higher uptake of EVs and DER, which could be explored in future research.

The research found that achieving zero upgrades is not about aggressive electrification but rather maintaining loads below critical network thresholds. Financially viable outcomes depend less on maximizing individual technologies than on maintaining balance across façade orientation, storage scale, EV penetration, and infrastructure impacts.

- Electricity demand could be met within the existing network constraints under both the Base and Updated Scenarios, under defined energy management scenarios. The range of scenarios was more restricted under the typology of the Updated Scenario

  Under both scenarios, transformer constraints are localised rather than systemic, with overall network performance shaped by a small number of spatially clustered bottlenecks in higher density mixed residential and commercial areas. This pattern indicates that targeted, asset specific interventions would be sufficient to unlock additional hosting capacity, rather than requiring widespread network augmentation.

- EV uptake and north-facing BIPV define the most restrictive feasibility boundaries

  Across unfeasible scenarios, binding constraints were primarily associated with transformer thermal limits driven by evening EV charging demand, and local voltage rise occurring during midday periods of concentrated PV generation.

  Beyond approximately 50% EV penetration and 20% north-facing façade PV coverage, infrastructure upgrades become both inevitable and economically significant.

- Built form impacts network constraints

  Under the Updated Scenario, the power system was able to operate safely but the feasibility envelope was notably narrower than in the Base Scenario. Compared with the Base Scenario, the Updated Scenario includes fewer but higher buildings, resulting in higher absolute levels of façade PV and battery capacity per building for the same percentage-based deployment assumptions. Consequently, binding constraints emerge more readily at specific assets, particularly at transformers serving larger buildings where both midday reverse power flows from building integrated photovoltaics and evening EV charging loads are concentrated.

  For infrastructure planning, this implies the Updated Scenario would require stronger reliance on external energy supply or more off-site renewable sources to meet demand, while the Base Scenario offers a broader range of pathways toward improved generation-to-load balance and meeting more energy demand locally.

- Network constraints are location- and asset-specific rather than universal

  Under both scenarios transformer constraints are localised rather than systemic, with overall network performance shaped by a small number of spatially clustered bottlenecks in higher density mixed residential and commercial areas. This pattern indicates that targeted, asset specific interventions would be sufficient to unlock additional hosting capacity, rather than requiring widespread network augmentation.

- Infrastructure impacts are threshold-driven rather than incremental

Rapid EV uptake and uncoordinated or unoptimized PV deployment can trigger sharp feasibility transitions, beyond which infrastructure upgrades become unavoidable and escalate rapidly in cost.

Economic analysis

The below findings focus on analysis which seeks to minimise network upgrade costs. A broader analysis that compares the impacts of significant network upgrade costs has not been undertaken. The findings below should be considered with that caveat in mind.

- Urban renewable systems are governed by trade-offs rather than a single optimum

  The challenge of integrating planning decisions with energy asset deployment, is that energy autonomy (i.e., used of localised DER), private investor returns and infrastructure constraints are often in competitive tension. Further work is needed to better quantify the value gap between 'business as usual' energy asset deployment, and precinct optimisation. Increasing urban density will translate into higher electricity demand. This can be met through renewable energy from either the grid, or local DER, or a combination of both. Built form design imposes constraints on how much renewable energy can be generated locally compared to demand. Further analysis is needed to determine whether there is value to be generated from meeting this energy demand through local generation, or whether, from an overall perspective of land economics, this demand is better met through grid scale renewables.

  This gap will then inform how much investment could or should be committed by policy makers, in pursuing innovations in the planning process (to adapt built form to facilitate precinct scale energy management), or in precinct scale energy supply models.

- Urban form influences the economic viability of different energy deployment strategies

  Vertically intensified urban form compresses the options available and lowers the ceiling of what can be simultaneously achieved across the objectives of energy autonomy, private sector returns and network capacity While outcomes are feasible that balance these objectives, under both Scenarios, there are fewer balanced outcomes under the Updated Scenario, and those that are have weaker performance in terms of energy autonomy and private sector returns than the Base Scenario.

  Intensified urform form also amplifies the economic penalties associated with renewable energy maximizing strategies and increases reliance on policy or financial support mechanisms to these. Renewable energy deployment was relatively more expensive and produced less energy autonomy under the Updated Scenario as compared to the Base Scenario.

  There are also comparatively fewer attractive private market investments under the Updated Scenario as compared to the Base Scenario.

  These findings reinforce that urban form fundamentally conditions the effectiveness, cost, and scalability of renewable energy transitions locally, even when identical technologies and optimization frameworks are applied. The Updated Scenario is a systematically more constrained

urban configuration where there are fewer feasible options, and with a compressed upper envelope for both economic and energy performance

- **Precinct scale battery storage expands the economic envelope and simplifies the control optimisation problem, but not the infrastructure envelope**
  Precinct scale battery energy storage systems (BESS) - for example a single large battery servicing an apartment block, as opposed to individual batteries for each apartment - tends to enhance economic performance in dense urban systems due to its lower capital cost per kWh, resulting in higher Internal Rate of Return and Net Present Value outcomes than household batteries. This advantage provides increasing flexibility to absorb additional capital costs as storage size increases. While utility BESS shifts many scenarios from financially unviable to investable, it does not remove the underlying infrastructure thresholds associated with high EV uptake or excessive north-facing BIPV deployment. In other words, utility BESS can make more scenarios economically viable, but it may not fundamentally relax network-driven limits on renewable and electrification intensity especially at the higher end of renewable penetration and/or electrification.

- **Investment coordination is critical to value creation**

  With network constraints potentially being a key limit on EV uptake, and the combination of solar PV, battery, EV and smart energy management an important source of value to precinct stakeholders, planning frameworks and processes that enable investment co-ordination are critical. For example, co-ordinated investment can help bring down the cost of battery deployment and EV charging infrastructure, while also simplifying the task of implementing control strategies that make best use of local energy assets within network constraints.

Recommendations

The key recommendations from the four workstreams are based on case studies, and include a degree of specificity to the Sunshine Precinct, particularly in terms of geometrical arrangement and use of local features.

While recommendations are presented by workstream, the greatest benefits are achieved when combining insights from across workstreams, as demonstrated in the connectivity analysis for Energy Park.

An overarching recommendation therefore is to employ integrated digital planning tools to explore the potential for perverse outcomes or hidden benefits, arising from the interaction of urban design elements. This includes minimising unnecessary heat stress caused by hot air pockets, minimising embodied carbon in buildings, providing adequate water critical for the survival of local vegetation and the cooling effects on extreme heat days, and ensuring the value of local distributed energy resources is maximised with co-ordinated management.

Urban heat

Impacts of urban heat were examined through complex non-linear modelling of built form that considers factors such as reflectivity, heat gain, shading and air flow. Preferential outcomes are obtained when

controls are put in place that maximise ventilation through the precinct and allow water to provide cooling through the latent heat of evaporation. Changes to building morphology can also reduce the impact of reflected and radiated heat from man-made structures. Specific recommendations from the research suggest to:

- Create a network of irrigated open spaces spread throughout the precinct that are placed strategically to take advantage of prevailing winds.
  Open space which has airflow to the south will spread more cool air (specifically in the weather conditions in the Sunshine Precinct). It is also important to maintain some gaps in the vegetation in open spaces to enable airflow, provide irrigation to maintain soil moisture, and target daytime actions such as active watering in high temperatures, to provide cooling. Active irrigation for cooling specifically is required only in very hot conditions (e.g. 35°C plus, expected to occur approximately 20 days per year in 2050).

- Plan for sufficient airflow in the precinct in summer, and moderation of wind speeds in winter
  Building height, spacing and podium continuity should be considered as part of heat mitigation. In the Sunshine Precinct context:
  - control wind through use of vegetation on NW/NE streets to prevent wind channelling.
  - avoid long, continuous podium structures, to prevent wind channelling and improve airflow.
  - increase setbacks between towers and buildings, and limit building heights to allow more airflow in summer and prevent hot pockets.
  - avoid trees in the middle of streets where airflow is important.
  - provide for airflow southwards in dead-ends and cul-de-sacs.

- Plan tree canopy as a spatial system that considers locations where shading and ventilation is required.
  For the specific context of the Sunshine Precinct, that means prioritising the southern sides of E-W streets for shading with overlapping canopy, planting dense irrigated vegetation on the south side and low-density vegetation on the north-side (which is shaded by buildings). For N-S corridors that means balancing shading and ventilation. Shading from buildings can be utilised in summer, allowing somewhat less dense vegetation to enhance airflow. Soil and water infrastructure is required to support vegetation, as outline in the Water section below.

- Irrigate vegetation and maintain soil moisture to support cooling. This will also support tree growth, as described in the Water section below.

- Use climate-responsive material selection at the pedestrian scale. In highly sun-exposed locations, prioritise high-thermal-mass and low-reflectivity finishes where reflected radiation is likely to affect pedestrians or nearby surfaces. High-reflectivity materials remain appropriate where solar radiation can be reflected primarily toward the sky. These strategies should be applied selectively and, where needed, balanced with measures that support effective nighttime heat release and cooling.

- **Identify, prioritise and treat targeted hotspots through coordinated landscaping, irrigation and built form interventions, rather than focusing on precinct-scale averages**. Micro-climate modelling, such as the Envi-met modelling used in the research, can be used to identify hotspots and test the impact of different interventions.

Water

Specific recommendations for the use of water are highly correlated with urban heat (above) which relies on adequate moisture for evapotranspiration. Specific additional recommendations suggest to:

- **Ensure adequate soil volume, and active and passive irrigation to support overlapping tree canopy growth, particularly in priority areas for shading.**
  Create 3m verges with structural soil or 5m verges with passive and active irrigation. Passive irrigation is critical to achieving overlapping canopy, while supplementary active irrigation is important to enable trees to meet maturity more quickly and to protect against drought conditions.

- **Provide *efficient* passive irrigation systems for street trees.**
  Supply of additional water beyond rainfall is critical to achieving tree canopy in the precinct. There is a significant difference in outcome between efficient and inefficient systems, so investment in a well-designed, efficient system is important.

- **Provide an alternative water capture systems to provide water for active cooling of public open space.**
  Aim for 11-12ML per annum *above* the amount already allocated to maintain a mid-range sports level. Water capture from low rise commercial and industrial buildings, or other infrastructure, could be good alternatives – if other sources of water (e.g., residential building rooftops and road runoff) are already fully utilised.

- **Encourage capture of alternative water on private land.**
  Water capture can support increased soil moisture in summer (for urban cooling purposes) and to support achievement of canopy targets on private land.

- **If a 30% canopy target is a priority, consider options to increase canopy cover across the precinct.**
  Options include increasing canopy cover on private land and allocation of additional public open space for greening.

Embodied carbon

The amount of embodied carbon was highly influenced by building morphology, carparking and precinct design approach. Specific recommendations suggest to:

- **Facilitate low-carbon building designs.**

Results show that substituting typical construction materials with low carbon equivalents can reduce embodied carbon by 14%. This could be improved to a 46% if low carbon (lightweight and mass timber) approach was adopted.

As embodied carbon becomes an increasing share of lifecycle emissions, encouraging material changes over the long term will be important to reducing built form emissions. This may entail some changes to built form, as research (Pomponi et al. 2021) suggests that low embodied carbon buildings are easier to achieve when they are shorter.

- **Reduce private car parking.**
  Carparking within buildings was found to contribute significantly to embodied carbon of the precinct designs assessed. By removing carparking (within the building) from the Base Scenario embodied carbon was reduced by 15%. Moving carparking from basements to the upper floors of buildings had lesser impact, reducing embodied carbon by 4%. Public transport systems will be expected to reduce the embodied carbon of buildings by removing the need for personal carparking space or by shifting such space to lower embodied carbon alternatives (such as remote carparking).

- **Use the Digital Twin to maximise the embodied carbon value of precinct designs while at the same time aiming for a net-zero carbon outcome.**
  Embodied carbon can be viewed as a cost to development that needs to be managed like any other cost. It was clear from that significant improvements in embodied carbon 'value' were achievable through various initiatives outlined above None of the precinct designs achieved a 'net zero' carbon outcome over the life cycle, even when the carbon sequestration potential of mass-timber was included. The ability of mass-timber and other biogenic materials to store carbon presents a theoretical opportunity for a precinct to achieve a net-zero carbon outcome if this goal is prioritised.

Energy

Energy provision within an urban precinct requires a complex trade-off between the capacity required to meet current and future demand and the potential for over-building capacity leading to pressures from economic regulations and the public. This has become more challenging as the world shifts toward full electrification of end-use devices including EVs. Analysis in this report considered the demand for energy services and local renewable supply and storage options within the constraints of the existing network. Urban heat recommendations highlight demand management opportunities through advanced microclimate management. Additional recommendations from the study suggest to:

For Distribution Network Service Providers (DNSPs)

- Implement spatially differentiated connection standards and incentives to encourage DER deployment on underutilised feeders.
- Require explicit evening discharge targets and standardised inverter volt–var and volt–watt settings for batteries and PV.

- Prioritise shared or utility-scale BESS where it delivers peak substitution, voltage control, and ramp-rate reduction.
- Use constraint classification frameworks to distinguish between scenarios requiring infrastructure augmentation and those addressable through operational or spatial measures.
- Coordinate EV smart charging programs to target load-factor improvement, not just peak avoidance.

For Planning Authorities

- Develop a strategic direction for energy management at the precinct scale that outlines the extent to which renewable energy and EV deployment is a priority, and how this can be addressed.
- Incentivise east–west façade-integrated PV through planning controls, design guidelines, or floor-space bonuses.
- Require shading, orientation, and energy performance analysis at early design stages for high-density developments to maximise passive heating and cooling and onsite renewable energy usage at a precinct neighbourhood scale.
- Support shared-service PV and battery business models (e.g. precinct energy services, community batteries).
- Understand potential EV loads based on proposed charging infrastructure and carparking capacity in new developments, and engage with DNSPs about the implications
- Encourage smart charging infrastructure.
- Incorporate consideration of urban form in any localised renewable energy deployment strategy.

For Developers and Precinct Proponents

- Design buildings to maximise usable PV surfaces, particularly east–west façades in high-rise contexts.
- Treat rooftop and façade PV as integrated energy assets, not optional add-ons.
- Invest in smart EV charging infrastructure rather than reducing parking capacity – although noting that reduced carparking capacity has positive benefits for embodied carbon.
- Consider shared or utility-scale battery solutions to improve project economics and manage peak demand.
- Evaluate projects using integrated metrics (IRR/NPV, self-consumption, network impacts) from early feasibility stages.

Research impact and future work

The learnings and methodologies developed through this project have the potential to be applied to other precincts across Melbourne and Victoria as well as interstate, advancing the integration of environmental, social and economic objectives in major urban planning projects.

There are several benefits or co-benefits that have not been quantified as part of this study given its relatively limited scope. Additional quantification and inclusion of costs in the digital twin or alongside the digital twin as part of future work could help inform decision making especially as they relate to making well informed trade-offs and prioritising effort.

Benefits of an improved precinct to be explored in more depth include:

- **Economic benefits (retail owners and landlords):** more people out walking or attracted to a commercial area encourages foot traffic, which in turn may benefit retail business owners and in turn potentially higher rental for landlords.
- **Economic benefits (health):** a reduced burden on the medical system through lower heat stress for pedestrians and a higher likelihood of a more active community. Better performing buildings will also assist with better sleep and all-round health of the community.
- **Social benefits (amenity):** a green and well-designed precinct to live, meet, work and gather in offers intangible social benefits, and likely improves mental health through increasing activity and reducing isolation. A biophilic, connected environment and walking community improves social cohesion, improved mental and physical health and well-being for communities.
- **Economic benefits (asset values, rental premium):** desirability likely increases in more liveable (cool and green) precincts, which in turn may lead to projects having a greater economic viability and increasing demand for housing supply.
- **Economic benefits (avoided costs):** smart precinct design combined with renewables and smart scheduling of CER can maximise the value of local energy resources, increase resilience and reduce costs of additional infrastructure. This could lead to lower energy bills for tenants and building users (lower peaks and associated demand charges), and lower overall energy use through onsite renewables and storage.

This digital twin project took a scenario approach that provides information about the positive or negatives effects of certain decisions like irrigation on various outcomes like urban heat for example. Future work could explore real-time data capture and integration inclusive of cost information to provide support for integrated decision-making involving trade-offs between various options. More work from industry and research is needed to provide a truly integrated precinct scale solution however this work demonstrates benefits from an integrated approach to design.

CONTENTS

TABLES

FIGURES

1. Background and Approach

This report is structured to provide an introduction to the Sunshine Precinct study and its purpose, followed by summaries of key research outcomes in section 2 to section 5 for Urban Heat, Water, Embodied Carbon and Energy. Underlying assumptions and detailed model settings are contained in the Appendices along with a review of the climatic conditions for the Sunshine area.

1.1 Project background

The Sunshine Precinct is a key urban area situated at a vital junction between Melbourne's city centre and the western growth areas, offering strong connections to regional hubs, major transport routes, and economic infrastructure (State of Victoria Department of Transport, 2021). Planned infrastructure upgrades through major government projects will further boost accessibility and development opportunities in the precinct. As the precinct is expected to experience a significant increase in both population and employment density, it faces the risk of growing environmental pressures. Without a sustainable design framework, issues such as urban heat, water scarcity, high carbon output, and inefficient land use could compromise the precinct's liveability and long-term performance. To ensure that growth is managed responsibly and the area remains resilient to future challenges, it is essential to embed environmental sustainability into the core of precinct planning. Figure 1.1 presents the key areas for growth and change.

The distinct zones in Figure 1.1 include:

1. Energy Park
2. Albion Quarter
3. Town Centre
4. Sunshine Station

Figure 1.1. Sunshine Precinct
Source: State of Victoria Department of Transport (2021)

This project explores the opportunities to transform the Sunshine Precinct into a leading example of sustainable urban development. By leveraging digital twin technology within urban planning processes, the initiative aims to provide robust, data-driven decision-making support that enhances urban resilience to climate change and other environmental challenges. The integration of critical urban elements such as energy, water, embodied carbon and urban heat within the digital twin framework facilitates more informed and strategic planning decisions.

This project is a collaboration between Department of Transport and Planning (DTP), RMIT University, RACE for 2030 and Centre for New Energy Technologies (C4NET). The focus is on the key environmental risks for the Sunshine Precinct, particularly related to urban heat, water supply, embodied carbon and the broader risks and opportunities associated with the energy transition. During the project process, the team has engaged communications and discussions with key stakeholders such as Development Victoria, Greater Western Water, Brimbank City Council, Powercor, Solar Victoria/Department of Energy, Environment and Climate Action. We also consulted industry and academic specialists in building design, embodied carbon, trees and water demand to refine the assumptions we have used (detailed names are shown in Acknowledgement). Stakeholder engagement is an integral component of the project, ensuring the relevance and credibility of the modelled outcomes while facilitating informed policy development and meaningful community dialogue.

The learnings and methodologies developed through this project have the potential to be applied to other precincts within Victoria and interstate, thereby contributing more broadly to advancing best practice precinct planning.

1.2 Scope and objectives

The scope of this project includes contributing to the Sunshine Precinct Opportunity Statement[6] through providing a comprehensive analysis of a wide spectrum of sustainable urban design strategies.

Key objectives include:

1. To design and implement a comprehensive digital twin that integrates key environmental and spatial data: temperature, energy, water, embodied carbon, and street design to support scenario analysis and strategic urban planning.
2. To enable evidence-based planning through modelling, supporting policies that address climate resilience, resource efficiency, and sustainable growth in the Sunshine Precinct.
3. To contribute to the Sunshine Precinct vision goals by evaluating and demonstrating sustainable urban design strategies focused on reducing urban heat, improving water efficiency, and transitioning to renewable energy.
4. To engage key stakeholders including government agencies, industry, and researchers, to ensure the modelled outcomes are relevant, credible, and useful in guiding community engagement, policy and investment decisions.

[6] https://www.vic.gov.au/sites/default/files/2023-11/Sunshine_Precinct_Opportunity_Statement_Document_FINAL-%281%29.pdf

5. To develop transferable tools, methods, and insights that can be applied to other precincts within Victoria and Australia, contributing to the advancement of best practice precinct planning and policy.

1.3 Research framework

The study examined the future development of the Sunshine Precinct through to 2050, concentrating on proposed building projects within the Albion Quarter, Sunshine Station, and Town Centre. A comprehensive analysis of sustainable urban design strategies was conducted across a range of scales. The research considered both the precinct as a whole, and specific elements within it, such as microclimates, built forms, and street designs to ensure the strategies were contextually relevant and effectively targeted. This multi-scale approach allowed for the identification of tailored interventions that address the unique environmental and infrastructural challenges faced by the Sunshine precinct.

This study was conducted under 4 main focus areas: (1) Urban heat, (2) Water, (3) Embodied carbon and (4) Energy. Each focus area considered 2 primary scenarios: (1) base case scenario and (2) updated scenario. Under each primary scenario, multiple alternative scenarios were explored to understand the impact of diverse environmental and infrastructural settings.

This report is structured with results from each section for the Base Case and Updated Scenarios including alternative scenarios where used. Details of the modelling setup and data sources are contained in the appendices to simplify navigation of the results. Key findings and recommendations for each of the four study areas are provided at the beginning of each results chapter.

1.4 Comparison between modelling scenarios

The study focuses on the modelling of two design scenarios provided by DTP: the S1 base case scenario and the S3 updated scenario. The base scenario comprised a precinct model developed by the DTP for 2050, reflecting proposed developments within the Albion Quarter, Sunshine Station, and Town Centre. The updated scenario introduced modifications to the Albion Quarter, as this is the area currently being considered for planning changes. These modifications include variations in built form, street design, and open space configuration. The updated scenario focuses solely on changes within the Albion Quarter and does not consider other areas included in the base case. Table 1.1 summarises the key details of modelling scenarios. Figure 1.4 presents the digital models of the base case and updated scenarios.

Table 1.1. Comparison between modelling scenarios

	Base (S1)	Base (S1) (Albion Quarter only))	Updated (S3) (Albion Quarter only)
Total building numbers (excluding existing buildings in the buffer zone)	322	207	230
Total dwelling number	10336	7768	8363
Average height of buildings (M)	16.78	13.50	38.58
Maximum height of buildings (M)	44.04	44.04	77.00
Number of Storeys	3–13	4–13	8–30
% of buildings with podium structure	18.32%	6.28%	96%
Average Podium Height (M)	11.08	9.00	18.63
Total project zone land size	2,257,992	803,901	803,901

Gross floor area (GFA - m²)	2,501,108	1,223,781	2,002,459
Functional floor area (FFA – m²)	2,252,395	1,080,672	1,380,761
Residential floor area (m²)	1,126,333	678,718	803,884
Commercial floor area (m²)	1,014,386	258,124	576,875
FFA to GFA Ratio	90.06%	88.31%	68.95%
Carparking area as % of GFA	10%	12%	41%
FFA to project land size Ratio	99.75%	134.43%	171.76%
Total area of public open space (excluding Energy Park)			
Without Stony Creek corridor	-	43,850	41,510
With Stony Creek Corridor	-	68,658	67,470
Total street area (excluding Ballarat Road)	332,046	132,348	92,413
Total private land open space area	-	85,822	61,010
Canopy area (m²)	-	108,179	60,908 (BAU) 72,610 (BAU double) 113,452 (Better/Best)

- Base scenario (S1) vs (S3)– Buildings, public realm and open space

The diagrams in

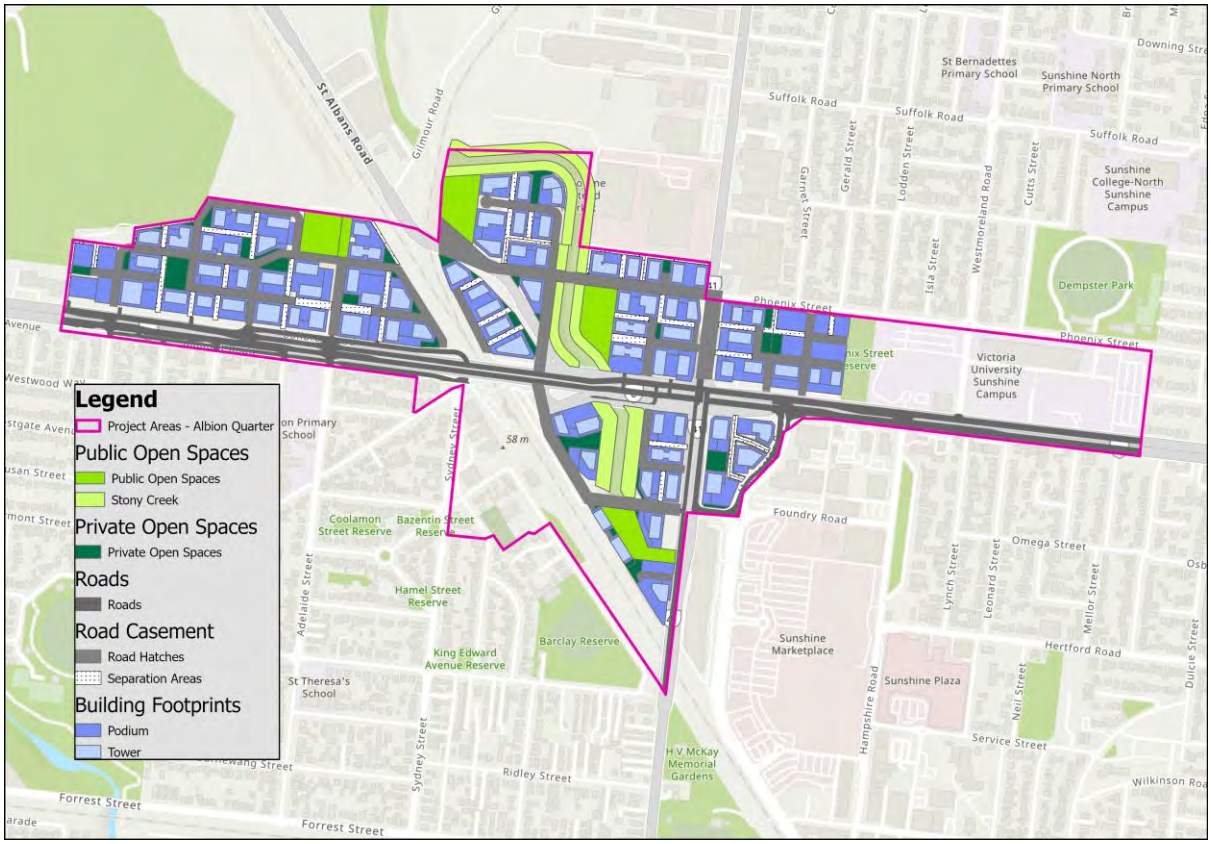

Figure 1.2 show the more distributed form of public open space across the Albion Quarter in S1, and the greater road area, compared to S3. S3 also has a much larger proportion of podium and tower structures in the Albion Quarter compared to the Base Scenario.

S1

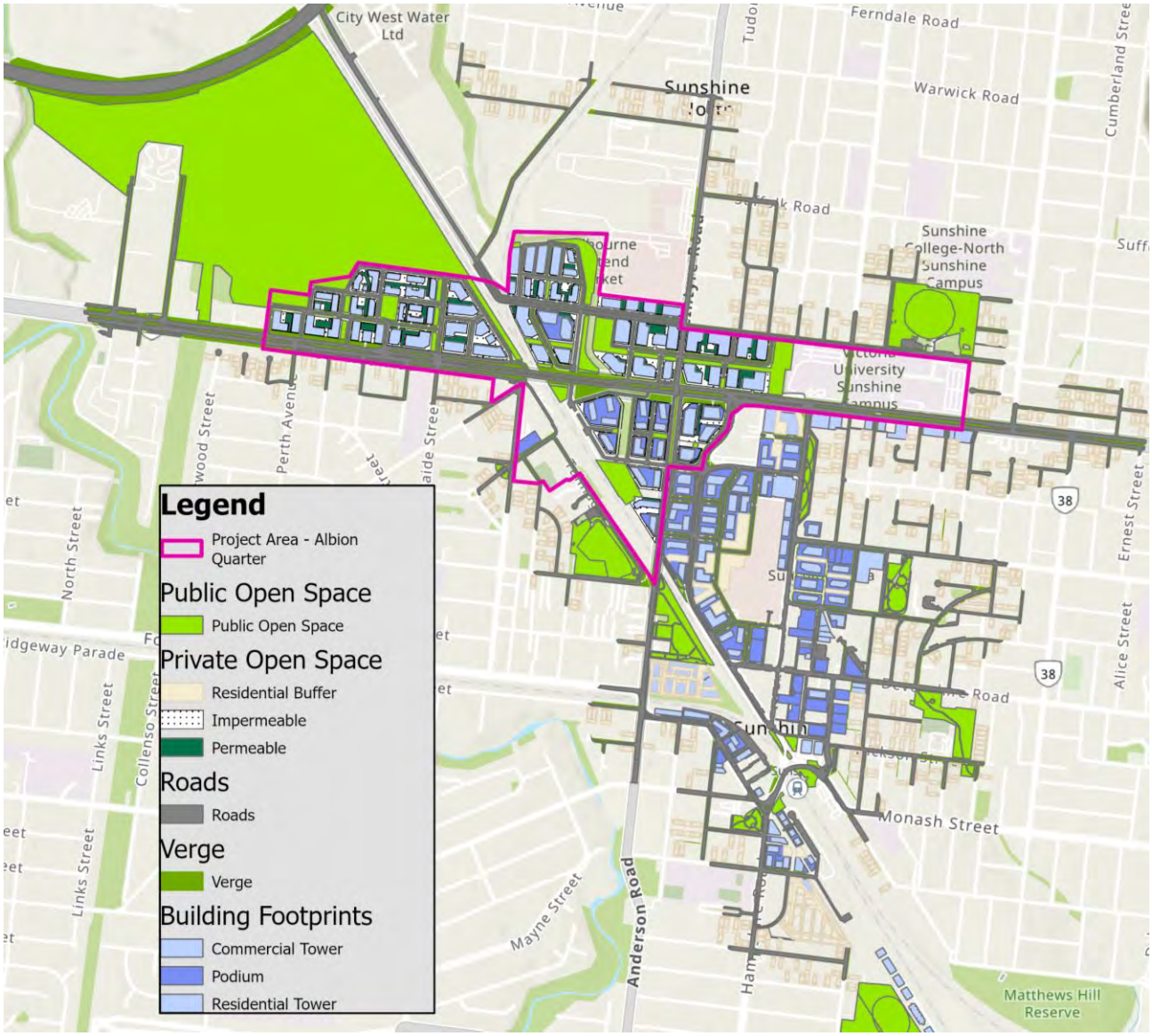
City West Water Ltd
Ferndale Road
Warwick Road
Sunshine
Sunshine College-North Sunshine Campus
University Sunshine
Legend
Project Area - Albion Quarter
Public Open Space
Public Open Space
Private Open Space
Residential Buffer
Impermeable
Permeable
Roads
Roads
Verge
Verge
Building Footprints
Commercial Tower
Podium
Residential Tower
North Street
Links Street
Collenso Street
Perth Avenue
Mayne Street
Anderson Road
Monash Street
Alice Street
Ernest Street
Matthews Hill Reserve
38

S3

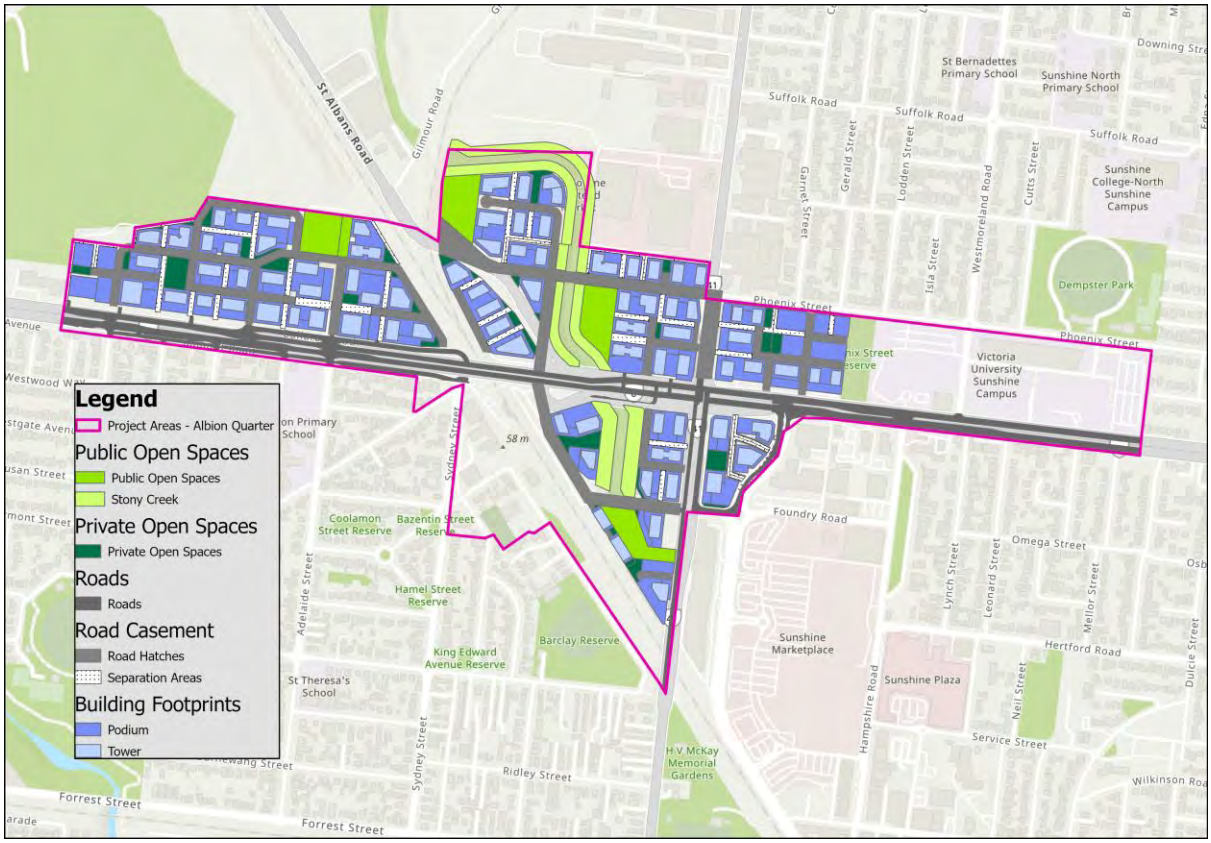

Figure 1.2. Base scenario (S1) vs (S3)– Buildings, public realm and open space

- Base scenario (S1) vs (S3)– Building heights and form

Building heights are typically higher in S3 with widespread use of podiums compared to S1 which has fewer podiums, lower heights and smaller podium structures.

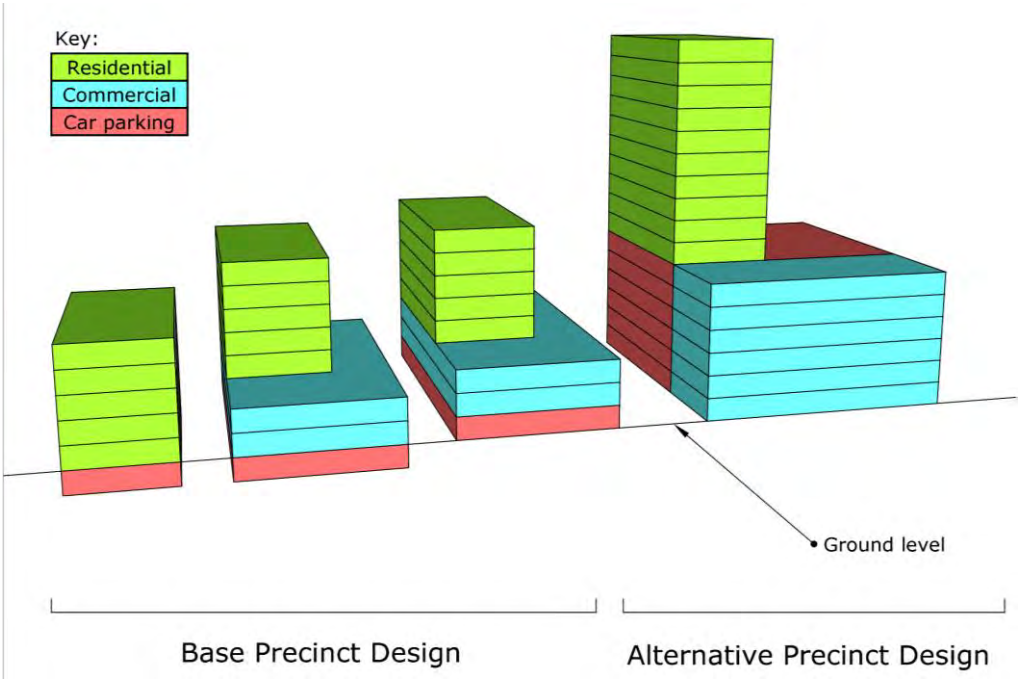

Figure 1.3. Base scenario (S1) vs (S3)– Building heights and form

The cumulative impact at the precinct scale is evident in the 3D visuals below with the first diagram, S1 showing predominantly lower heights and smaller structures compared to S3.

S1

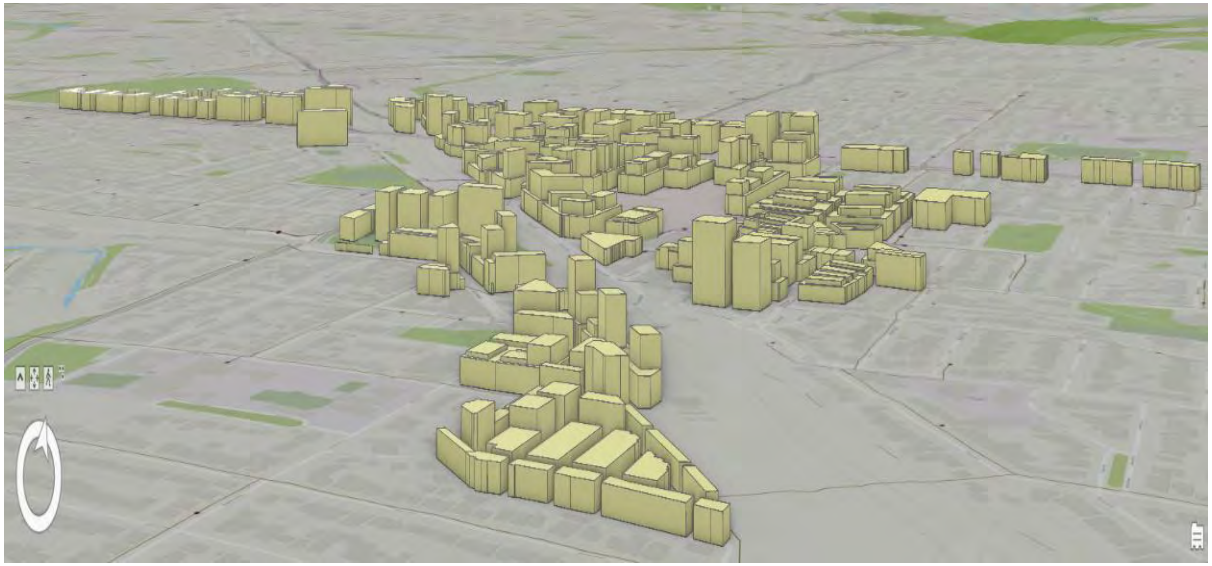

S3

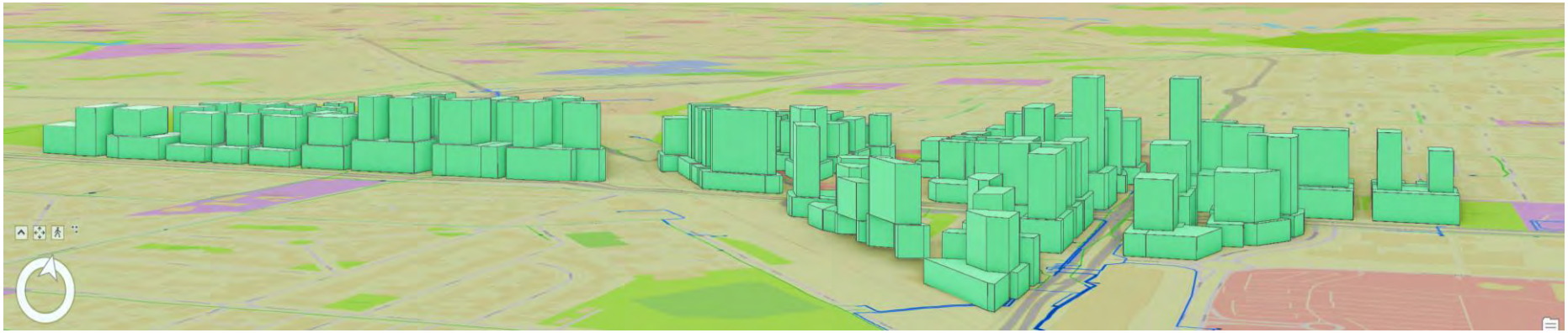

Figure 1.4. Digital models of the base case and updated scenarios

1.5 Key assumptions

The study was based on a set of primary assumptions, along with several subgroup-specific assumptions, to guide the development of both the base case and alternative scenarios. These assumptions were necessary to address data gaps, align the modelling with broader planning objectives, and ensure that the scenarios tested were both contextually relevant and analytically robust. These assumptions were validated by key stakeholders and experts (Detailed in Section 1.1). The key primary assumptions are outlined below. Detailed assumptions are provided in the appendices.

1. Future built forms and urban greening, from DTP, based on the Sunshine Precinct Opportunity Statement growth target.
2. Future electricity consumption and generation – buildings, PV, batteries, EV based on AEMO 2024 Integrated System Plan (ISP) and National Construction Code (NCC) Section J.
3. Building materials and energy performance based on NCC standards.
4. Roof water capture and building water consumption based on DEECA guidance.
5. Sparse canopy trees were used and classified based on 5m intervals (5m, 10m, 15m, and 20m) to simplify the modelling process. The model is based on a 5m×5m grid; hence, the trees were selected at this scale to align with the modelling cells.
6. Natural material colours (material's original state) were used in urban heat modelling.
7. Urban heat assessment resolution is based on a 5mx5m grid and focuses on the hottest day and a typical hot day from CSIRO climate projections in 2050 for an RCP4.5 scenario.
8. All residential building windows are double glazed for future buildings.
9. Window to wall ratio is 40%[7] (Foo & Shen, 2018).

The overall research design is presented in Figure 1.5.

[7] https://www.researchgate.net/profile/Grace-Foo/publication/350190665_Australian_Commercial_Buildings_Window_to_Wall_Ratios/links/6055640ca6fdccbfeafocd55/Australian-Commercial-Buildings-Window-to-Wall-Ratios.pdf

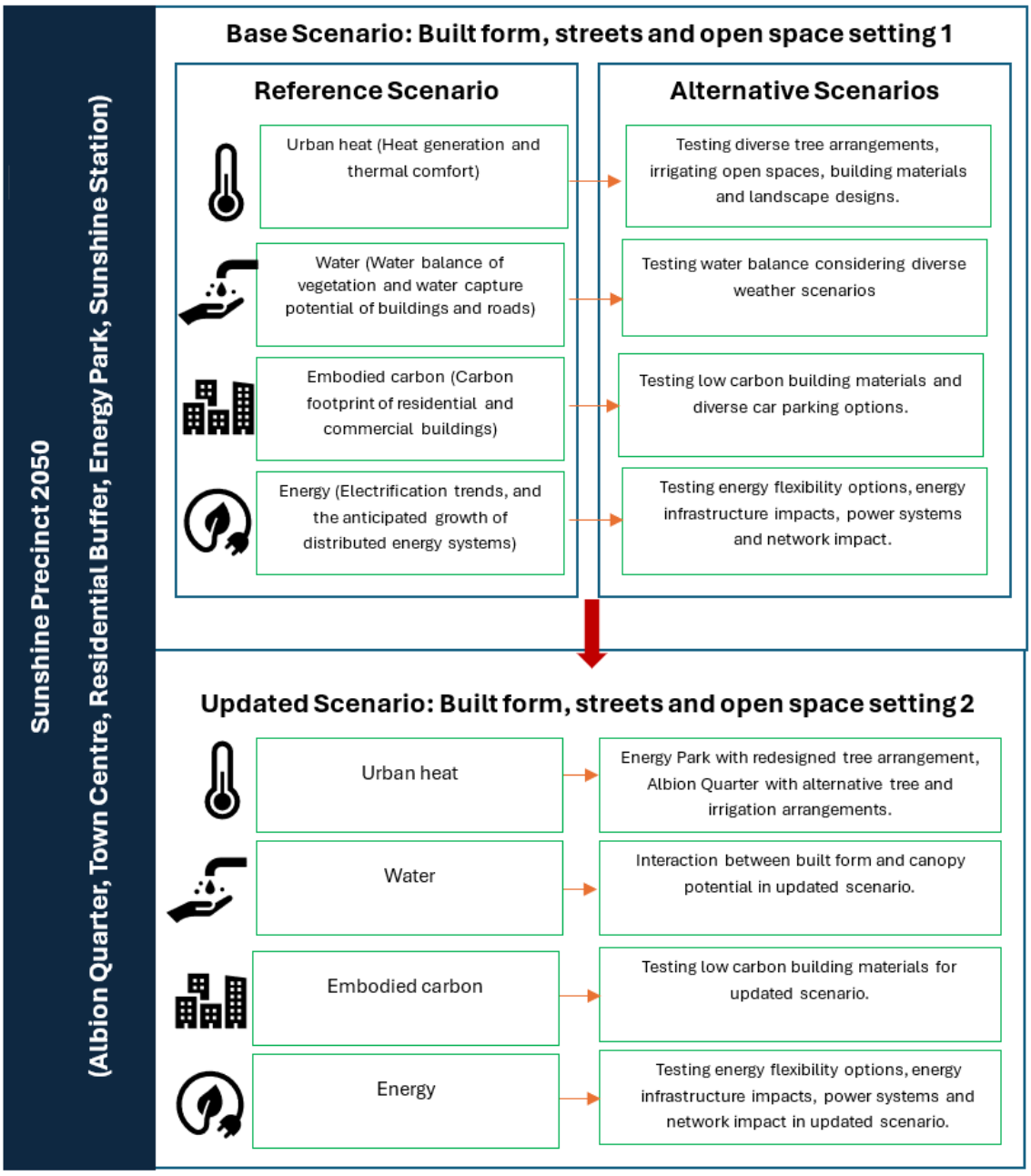

Figure 1.5. Overall research design

2. Urban Heat Results

Urban heat analysis was conducted in three stages. The first stage focused on the base case design, followed by testing various design strategies across alternative scenarios, and finally, evaluating the updated scenario against alternative scenarios to identify further improvements. Details for the scenarios and assumptions are provided in section 10.

The precinct was divided into overlapped tiles (Tiles 1 to 5 in Figure 2.1) to capture the whole non-linear project area, including key elements such as the Albion Quarter core and the proposed Energy Park, which is part of the updated scenarios. Although ENVI-met operates on an orthogonal grid and a single large domain could theoretically be used, practical limitations related to computational load and the need to minimise empty-edge artefacts meant that multiple smaller overlapping tiles were required. Each tile was therefore modelled at 5 m by 5 m resolution with deliberate overlap to maintain boundary stability and simulation quality. Base case analysis was conducted for all five tiles. Updated scenarios were applied to Tiles 1 and 2 because Tile 1 contains the core Albion Quarter area, where most design changes occur, while Tile 2 contains the future Energy Park, which undergoes substantial redesign in the alternative scenarios.

Input meteorological conditions for the model were taken from CSIRO's climate projections in 2050 for an RCP4.5 scenario. These projections were derived from an ensemble of up to 40 global climate models and are provided at an approximate 5 kms spatial resolution through CSIRO's application-ready climate datasets (DCCEEW, 2025). By their nature, these models provide a relatively coarse assessment of meteorology across a wide region. The ENVI-met model used here (detailed in section 10) calculates a set of outcomes with a much higher degree of specificity for the local area, considering the coarser input meteorological conditions as initial settings (detailed in section 10).

Comparisons provided consider the change in meteorological conditions (temperature, humidity etc.) between the base input data (from the high-level modelling) and the more granular outcomes from capturing details of the urban form with the ENVI-met model.

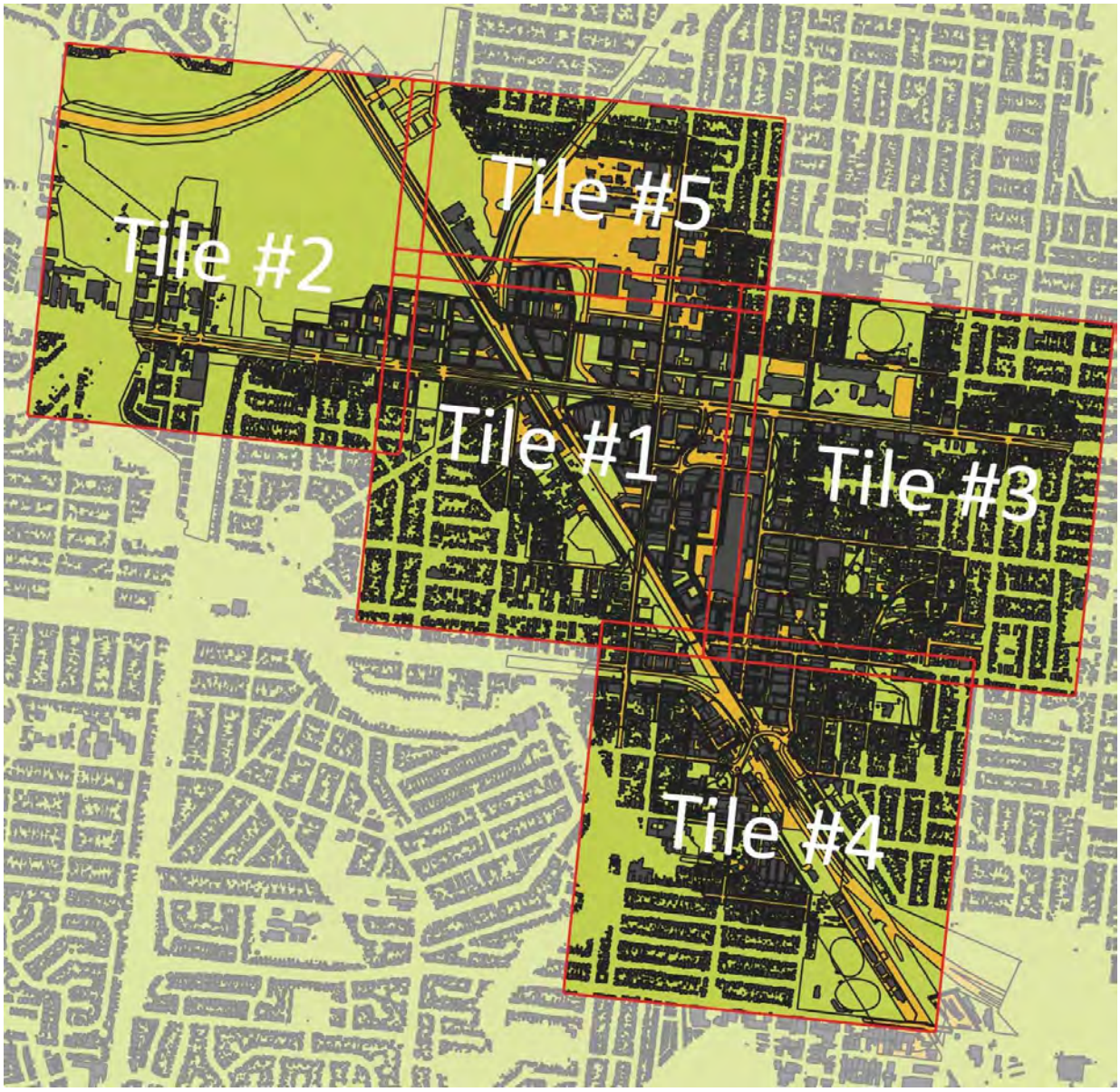

Figure 2.1. The identified tiles for urban heat simulations

2.1 Key findings and recommendations

2.1.1 Key findings

This study demonstrates that urban heat outcomes in the Sunshine development are driven not by single variables, but by the interaction between built form, surface materials, vegetation configuration, irrigation, and airflow. Across the base case and alternative scenarios, the modelling consistently shows that local microclimate conditions can vary substantially within the same precinct, particularly during extreme heat events. The findings below synthesise the most material outcomes that explain where, why, and how heat accumulates or is mitigated.

- Under extreme heat conditions, the Sunshine development increases median air temperature by 1.4 °C relative to the boundary input, with internal variations of up to 12.5 °C across the

precinct. These variations are spatially patterned rather than isolated, aligning with land cover, shading, ventilation and moisture availability.

- Irrigated landscapes and water bodies consistently perform as the most effective cooling elements. In the base case, irrigated open spaces and Stony Creek produced the lowest air temperatures and thermal stress, even as ambient temperatures increased. In alternative scenarios, irrigated open spaces reduced air temperature by up to 7.5 °C and UTCI by up to 10.2 °C, with cooling effects propagating downwind for up to 550 m.
- Tree canopy alone does not guarantee cooling. In both the base case and street-tree scenarios, dense or poorly arranged canopy obstructed airflow and created hot pockets, particularly in confined street canyons and open spaces with limited ventilation. Large trees provided effective shading but could increase temperatures in some situations when they suppressed wind-driven heat removal.
- Canopy continuity is critical for reducing direct and reflected solar exposure. Overlapping tree canopies consistently lowered both direct and reflected solar radiation, whereas non-overlapping trees allowed high radiation levels to reach pedestrian zones, explaining counterintuitive hotspots beneath vegetation.
- Reflected solar radiation is a significant but often overlooked contributor to pedestrian heat exposure. Medium- and light-reflective surfaces can contribute up to 450 W/m² of reflected radiation when reflections are directed toward pedestrians or adjacent built surfaces, particularly near north-facing facades and unshaded paved areas. In these locations, dry grass and light-coloured pavements tend to amplify heat exposure. Reflective materials remain appropriate in other locations, provided reflected radiation is directed away from pedestrian spaces and does not concentrate on nearby surfaces. In contrast, irrigated and darker surfaces absorb more radiation and can support evaporative cooling, helping to moderate pedestrian-level thermal stress.
- Mean radiant temperature represents a major health risk driver. Median MRT during the hottest hour reached 58.2 °C, exceeding the 5% mortality-risk threshold. Locations combining direct exposure, reflective surfaces and limited shading recorded the highest MRT and health risk, while shaded and irrigated areas remained below critical thresholds.
- Wind plays a dual role in heat mitigation and comfort. Reduced wind speeds contributed to heat accumulation in poorly ventilated areas such as the base design of Energy Park and compact street canyons, while excessive wind speeds occurred in exposed corridors such as Albion Station. Cooling benefits from irrigation and vegetation were strongly dependent on the ability of airflow to transport cooled air beyond its source.
- Night-time cooling was sufficient in the simulated conditions, as indicated by a Heat Index of -1.6 °C. However, this finding is constrained by the modelling of a single night and does not capture the cumulative effects of multiple warm nights during prolonged heatwaves.
- Street tree size and irrigation interact strongly with airflow. Large trees improved shading and evapotranspiration but could raise temperatures where they blocked ventilation. Small trees improved airflow but reduced shading. Neither approach alone consistently improved conditions, underscoring the importance of location-specific design.
- Drought-resistant trees with limited soil moisture increased median air temperature by 0.2 °C and up to 1.3 °C during peak hours due to suppressed evapotranspiration. Diurnal analysis

showed that cooling performance depends on sustained soil moisture, not tree presence alone.

- Changes to building materials to reduce embodied carbon had a limited effect on outdoor air temperature, with differences between -0.2 °C and +0.2 °C. Low-embodied-carbon materials (specifically mass timber) reduced daytime temperatures but slightly increased night-time temperatures, indicating that material selection should consider both carbon and thermal performance.
- Among the updated scenarios, the Best Investment Case (BIC) achieved the strongest local cooling outcomes. Targeted irrigation, active tree placement and improved airflow reduced air temperature by up to 8.4 °C and UTCI by up to 11.6 °C in high-risk locations, although precinct-wide average reductions remained modest due to spatial averaging.

2.1.2 Recommendations

The modelling results point to a clear shift away from uniform, single-metric heat mitigation strategies toward spatially targeted, airflow-aware design. The recommendations below translate the findings into actionable guidance for precinct-scale planning, urban design and staging decisions.

- Irrigated open spaces should be treated as primary cooling anchors. The largest and most reliable reductions in air temperature and thermal stress were delivered by irrigated parks, ovals and linear landscapes, with benefits extending hundreds of metres downwind. These spaces should be located strategically to align with prevailing wind directions rather than being distributed uniformly.
- Airflow should be accommodated first, and shading should be configured second. Ventilation corridors should be protected and reinforced through building spacing, podium articulation and selective canopy placement. Shading strategies should be implemented in ways that complement, rather than obstruct, airflow, particularly in N-S streets that function as primary ventilation corridors.
- Tree canopy should be planned as a spatial system. Canopy continuity, height relative to buildings and placement within wind corridors should be considered. Overlapping canopy should be applied where shading is required and airflow is not critical, while gaps should be maintained in key ventilation corridors. For Sunshine Precinct this means providing overlapping tree canopy on the southern side of E-W streets. This is less critical in N-S streets *if* these are well shaded by buildings and where there is limited airflow due to building configuration. Overlapping canopy is also required in streets otherwise unshaded by building due to adjacent open space or infrastructure, although breaks may be required at strategic points to enable airflow.
- Irrigation should be integrated with vegetation selection and placement. Cooling performance is dependent on sustained evapotranspiration, so tree species and landscape typologies should be matched to realistic soil moisture regimes, recognising that drought-stressed vegetation provides limited cooling during extreme heat, although play an important role on typical hot days.
- Reliance on dry, reflective ground surfaces should be reduced. Dry grass and light pavements were associated with increased reflected radiation and pedestrian heat exposure. Where

irrigation is not feasible, darker or moisture-retaining surfaces at the pedestrian level should be considered to limit reflected solar load. While government policy has previously recommended use of light, solar reflective surfaces to reduce urban heat, current literature suggests that this approach is problematic when applied to the pedestrian level. Above the pedestrian level (i.e., rooftops and upper floors of buildings) radiation can be reflected to the sky, whereas at the pedestrian level light and reflective surfaces reflect heat and radiation directly to the pedestrian, affecting pedestrian health. Darker surfaces will, however, retain heat and potentially radiate this at night, meaning they should be used only in sun-exposed areas and accompanied by other nighttime cooling strategies.

- Water-sensitive landscapes should be used to moderate humidity and heat. Moderate humidity levels supporting thermal comfort were maintained near water bodies and irrigated vegetation without suppressing evaporative cooling. These elements should be integrated into public realms and connected to airflow paths.
- Heat risk should be addressed through targeted intervention rather than precinct-wide averages. The most meaningful improvements occurred in high-risk locations such as the old design of Energy Park, compact street canyons and exposed open spaces. Future design iterations should be directed toward identifying and treating hotspots rather than pursuing marginal average reductions.
- Summer cooling should be balanced with winter comfort. Increased airflow supports summer heat dissipation but may require mitigation in winter through selective sheltering, seasonal planting strategies or adaptive design elements.
- Landscape interventions should be combined with built-form optimisation. Trees and irrigation alone cannot compensate for poorly ventilated urban form. Building height, spacing, orientation and podium continuity should be considered alongside green infrastructure to achieve durable heat mitigation.
- Future refinement should be supported through staged implementation and monitoring. Given sensitivities to canopy density, soil moisture and airflow, a staged approach that enables monitoring and adjustment over time should provide greater resilience than fixed, prescriptive solutions.

2.2 Base case scenario

This subsection presents the urban heat results for the base case during extreme heat conditions, focusing on the pedestrian level at 1.5 m above ground. The section begins with outcomes of an initial screening. It is then followed by an overall summary of the base case results, focusing on the simulated 24 hours from 6 am on the 25th of February to 6 am on the 26th of February. This is followed by a detailed analysis of the various meteorological findings across the development, focusing on the hottest hour of the simulated day, 3 pm.

2.2.1 Initial screening for base case

At the early stage of the project, a comparison focused on air temperature at pedestrian level because the research aims to evaluate thermal exposure and comfort conditions experienced directly by users of the precinct. In addition to air temperature, several parameters were examined to provide a more complete understanding of the processes that drive heat accumulation and pedestrian thermal stress

in the precinct. Air temperature alone cannot represent the full dynamics of urban heating, which are influenced by the absorption and re-radiation of shortwave and longwave energy from materials, the intensity of direct solar exposure, the availability of humidity to moderate heat transfer and the ability of airflow to dissipate warmed air. For this reason, the analysis considers direct shortwave reflection, mean radiant temperature, relative humidity and UTCI. Together, these indicators provide a clearer picture of why air temperature increases in certain locations and how pedestrians may experience these conditions. For both days, model outputs were assessed at 3 pm, which represents the period of highest simulated thermal stress; the model input conditions used to drive these simulations are documented in Appendix 4. On the hottest day (25 February 2050), the model predicts an ambient boundary temperature of 40.3°C, while air temperatures within the Sunshine development range from 32.5°C to 45.0°C, producing an internal variation of approximately 12.5°C across the precinct. The median air temperature was 41.7 °C, indicating that the development increases the heat by 1.4 °C, Figure 2.2.

During a typical hot day, the input air temperature was 36.2°C, resulting in an air temperature in the Sunshine development that ranged between 31.6°C and 40.4°C, with a nearly 9°C difference between the hottest and coolest air temperatures. The median air temperature was 37.6°C, with an identical air temperature increase to the hottest day of 1.4 °C. It should be noted that temperatures are reported in Celsius, while absolute temperature differences are reported in Kelvin.

(a)

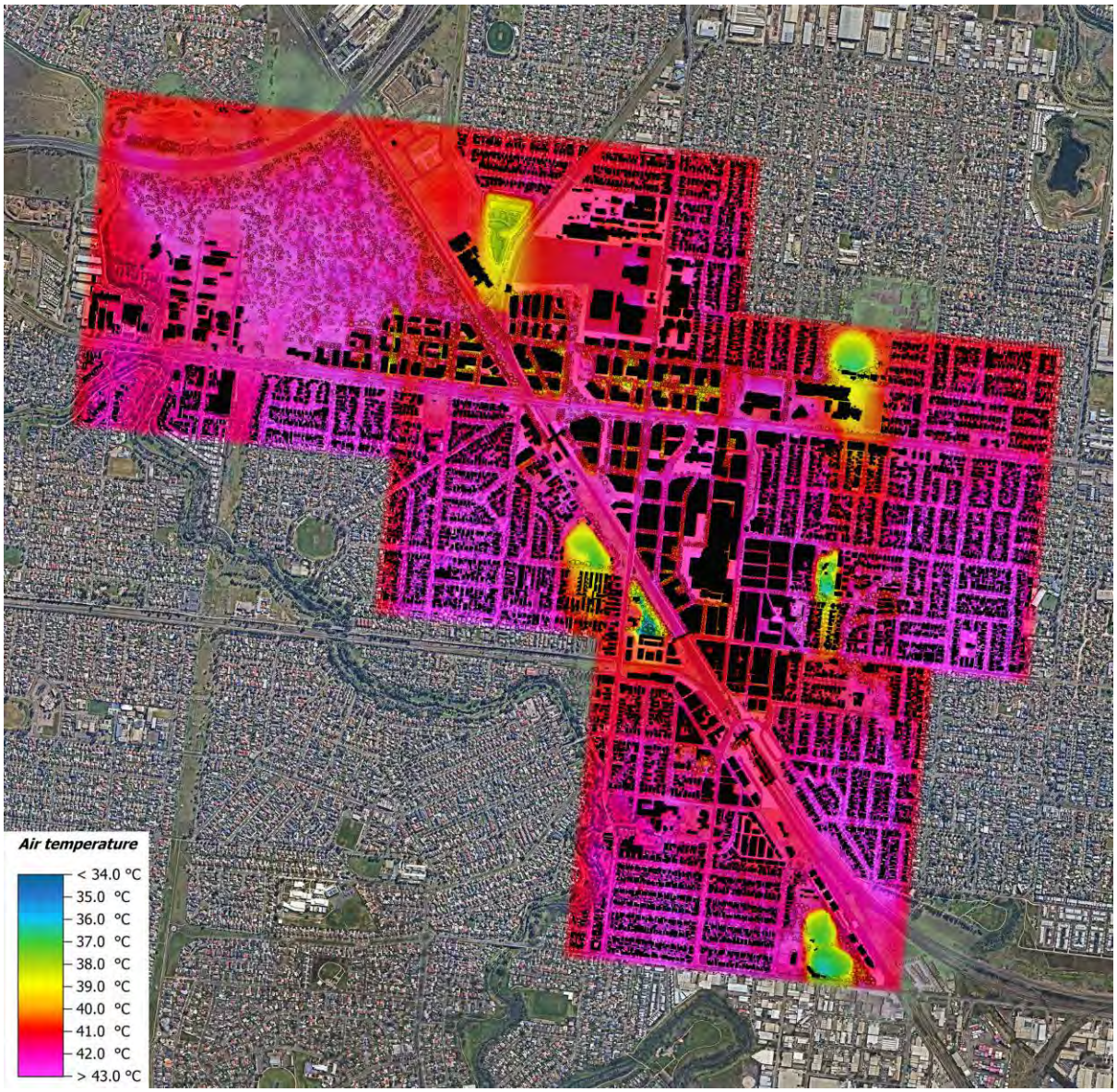
Air temperature
< 34.0 °C
35.0 °C
36.0 °C
37.0 °C
38.0 °C
39.0 °C
40.0 °C
41.0 °C
42.0 °C
> 43.0 °C

(b)

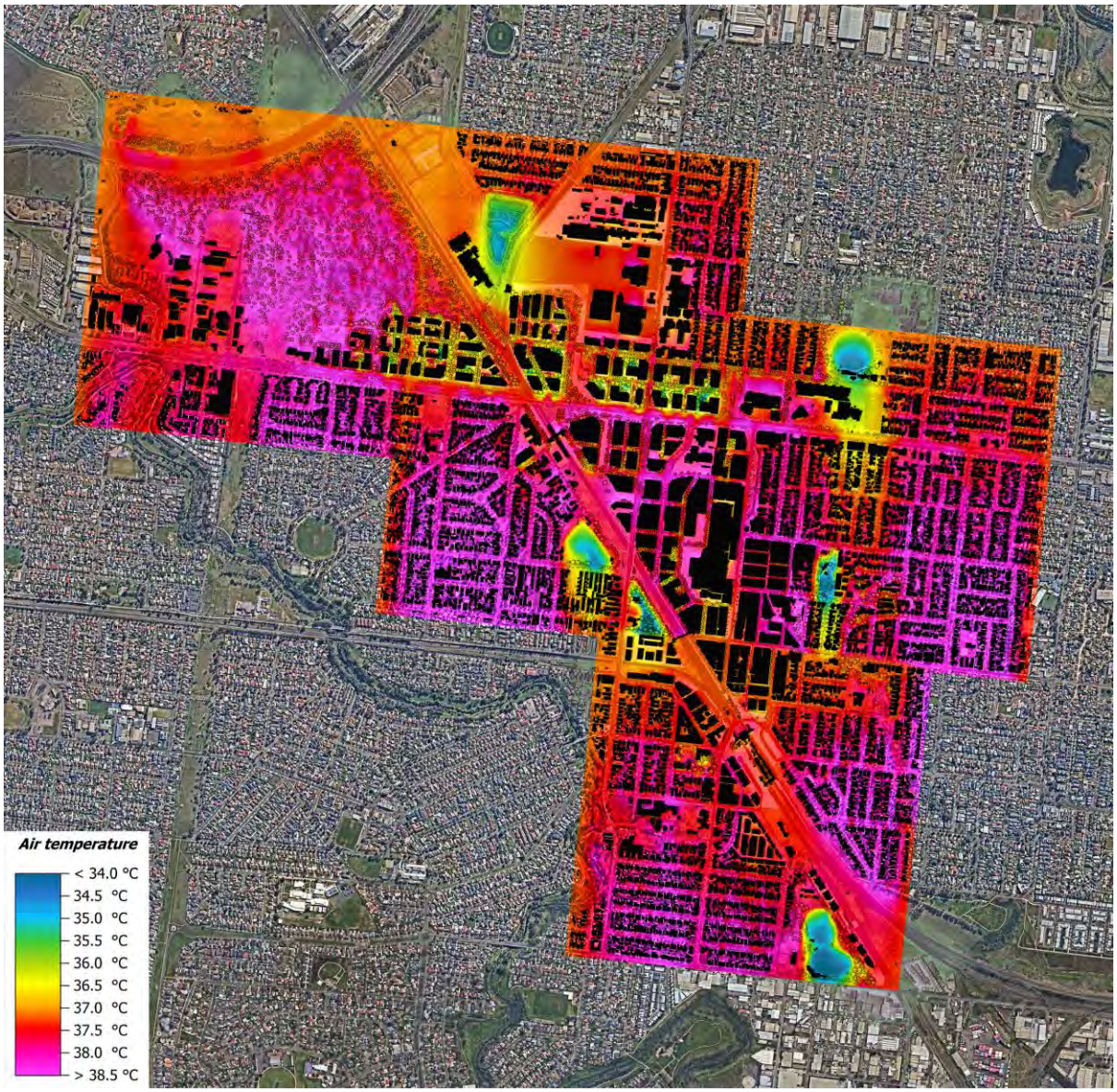

Figure 2.2. Air temperature at 3 pm at 1.5 m above the ground level, (a) during the hottest day, (b) during the typical hot day

Although the increase in median air temperature relative to the input air temperature was identical on both days, performance differed across urban settings due to the heat-retention capacity of the materials used. While the air temperature difference in the input data was 4.1°C between the two days, the air temperature difference in the Sunshine development ranged from 0.6 K to 5.6 K, Figure 2.3, and the urban settings with exposed surfaces and restricted airflow became hotter as temperatures rose.

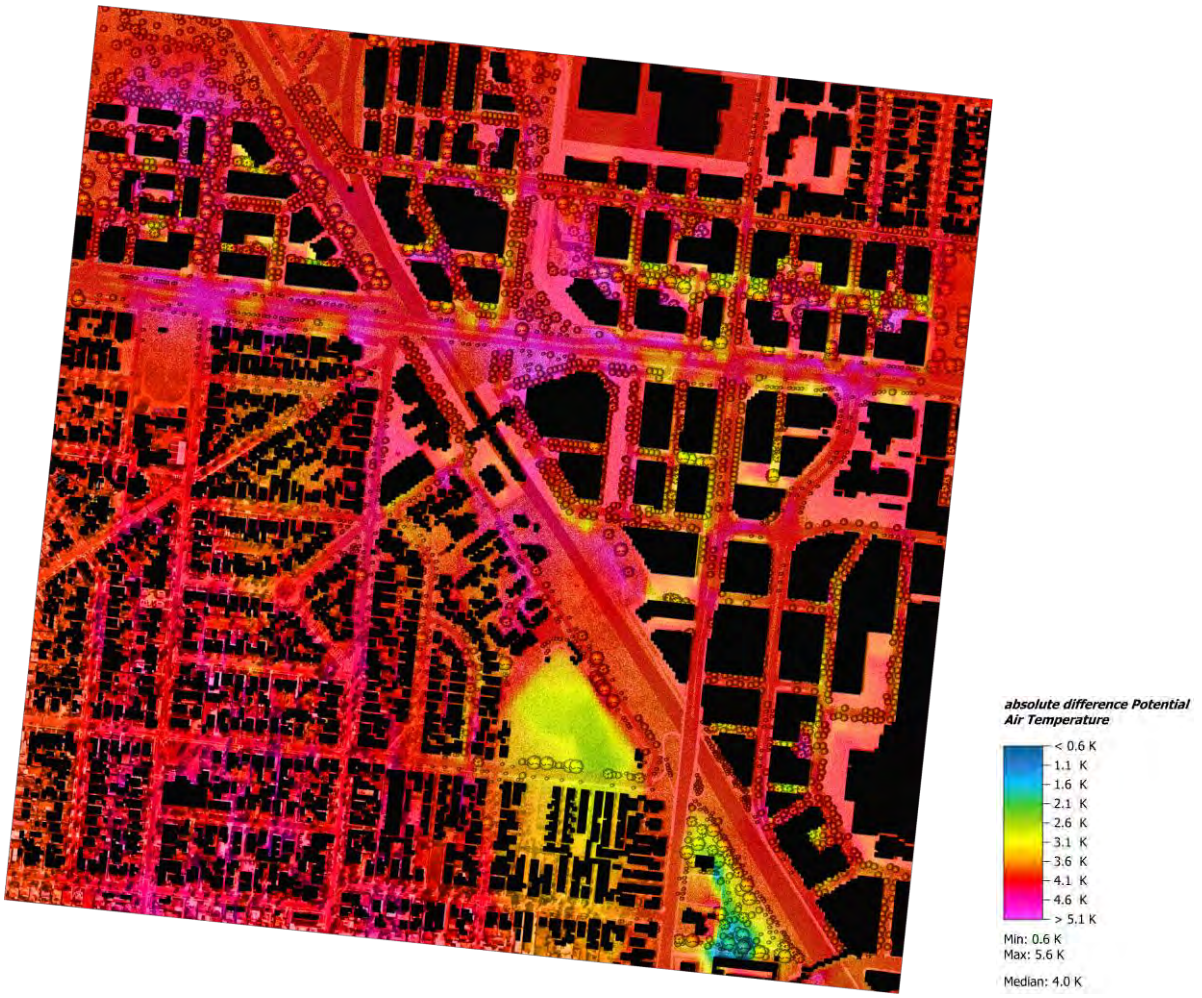

Figure 2.3. Absolute air temperature comparing the Sunshine development performance based on the conditions of the typical day to the hottest day

These results help identify the performance of the various urban settings in the development. Irrigated open spaces, for example, successfully mitigated heat and maintained conditions within the thermal comfort zone, even as ambient air temperatures increased. In contrast, areas exposed to solar radiation with limited airflow intensified heat by up to 4.7 °C. These patterns indicate that the integrated passive cooling strategies perform well under hotter conditions, while other settings amplify heat as temperatures rise. Because this divergence becomes more pronounced during extreme events, the following analysis focuses on the hottest conditions to better understand where interventions are most needed and to develop targeted heat-mitigation strategies.

2.2.2 Summary of base case

The median air temperature in the development was higher than the input data between 11 am and 4 pm, shifting the highest temperature to 3 pm rather than 5 pm due to impacts from the built form.

The highest modelled air temperature was 45.0°C at 3 pm, driven primarily by limited ventilation and high solar reflectance from adjacent hard surfaces. In contrast, the lowest temperature during the hottest hour was 32.5°C, occurring in irrigated vegetated areas and near water bodies. The cooling or warming influence of vegetation depended strongly on its location and arrangement, particularly in

relation to airflow pathways and reflective surfaces. Irrigated vegetation positioned within well-ventilated corridors produced measurable cooling, whereas dense or poorly arranged vegetation in confined spaces restricted airflow and contributed to local heat accumulation. These findings highlight the importance of strategic tree placement, irrigation provision, and maintaining open ventilation corridors as key planning and design considerations to manage precinct-scale heat.

The modelled median mean radiant temperature (MRT) during the hottest hour was 58.2°C, which is classified as level 2, with a 7.5% increased mortality risk (Thorsson et al., 2014), primarily due to a lack of shading and solar reflection. Some locations are exposed to high wind risk, while others have poor ventilation, which can reduce air quality and passive cooling.

From a thermal comfort perspective, very high heat stress (46-38 (Zare et al., 2018)) is recorded in some locations between 11 am and 5 pm. These conditions are most commonly associated with areas that combine poor ventilation, lack of irrigation and high surface exposure, rather than a single identifiable point. The specific hotspots vary across tiles, but the pattern consistently aligns with compact built forms and exposed hard surfaces. The median relative humidity during the hottest hour reached 14%, which could increase the risk of dehydration, irritated skin, and respiratory issues, but also provides a significant opportunity to integrate evaporative cooling strategies to control the heat. The analysis revealed that the site Heat Index has a value of -1.6 °C, which indicates that the Sunshine development under these conditions has sufficient night cooling. Therefore, while the modelled night-time conditions indicate reduced concern about accumulated heat, this conclusion is limited by the fact that only one night was simulated, and Melbourne can experience multiple successive warm nights during heatwaves. With this caveat, the mitigation strategy is directed primarily toward managing the daytime increase in heat. Finally, Figure 2.4 presents the air temperature distribution in the development throughout the simulated day and illustrates how pedestrians might perceive these conditions in terms of thermal comfort.

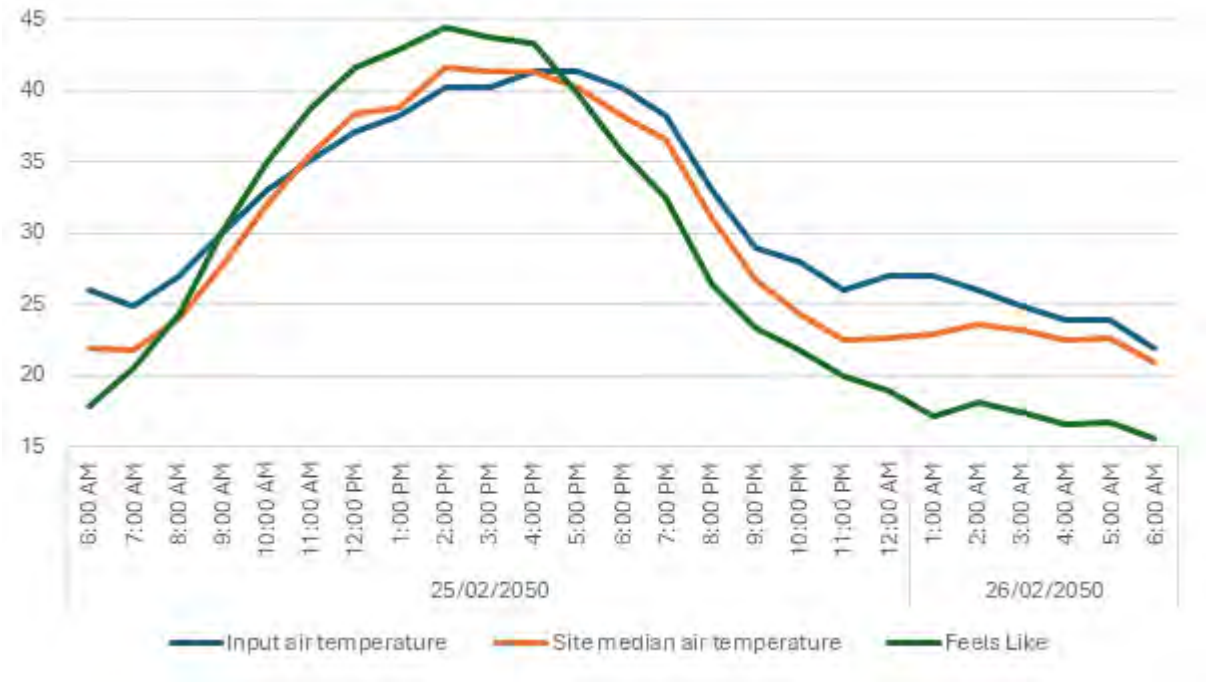

Figure 2.4. Air temperature and thermal comfort anticipation in the development during the hottest day in 2050

2.2.3 Direct solar exposure

The exposed surfaces in the development have received approximately 880 W/m² of direct solar radiation, Figure 2.5. This radiation level reflects the RCP4.5 input used in the model, which assumes moderate climate response actions. Direct solar radiation represents the amount of energy falling onto surfaces without shading, meaning that areas lacking canopy cover or structural shade experience substantially higher surface heating.

Two main factors determine how this energy affects temperatures at ground level: 1) whether surfaces or pedestrians are directly shaded, for example, by overlapping tree canopy; and 2) the thermal characteristics of the materials receiving the radiation. Based on the thermal properties of the main surfaces in the precinct, an increase in direct solar energy leads to surface temperature rises of approximately 0.7°C for soil, 0.2°C for water, 1°C for concrete and 1.2°C for glass. Although materials with higher thermal mass, such as concrete and brick, do not reduce heat gain outright, they slow the rate at which surfaces heat up, acting as a buffer or shock absorber. Over long periods or consecutive warm nights, however, these materials may also release stored heat back into the environment.

The spatial pattern of heating in the Base Case reflects these processes. Areas with continuous or overlapping tree canopy experience reduced exposure to direct radiation, while locations with gaps between trees, where the canopy does not overlap, still receive intense radiation even though vegetation is present. This explains several counterintuitive hotspots under or near trees that do not provide complete shading. Similarly, differences in surface material (for example, concrete compared with soil or water) lead to higher or lower temperature responses under identical solar exposure. Finally, exposure to direct solar radiation at this level can be detrimental to human health. For instance, a person may experience an increase in core body temperature of up to 0.5°C in light clothing and up to 1°C in dark clothing after 10 minutes of exposure. This matter is further explored in the following subsections.

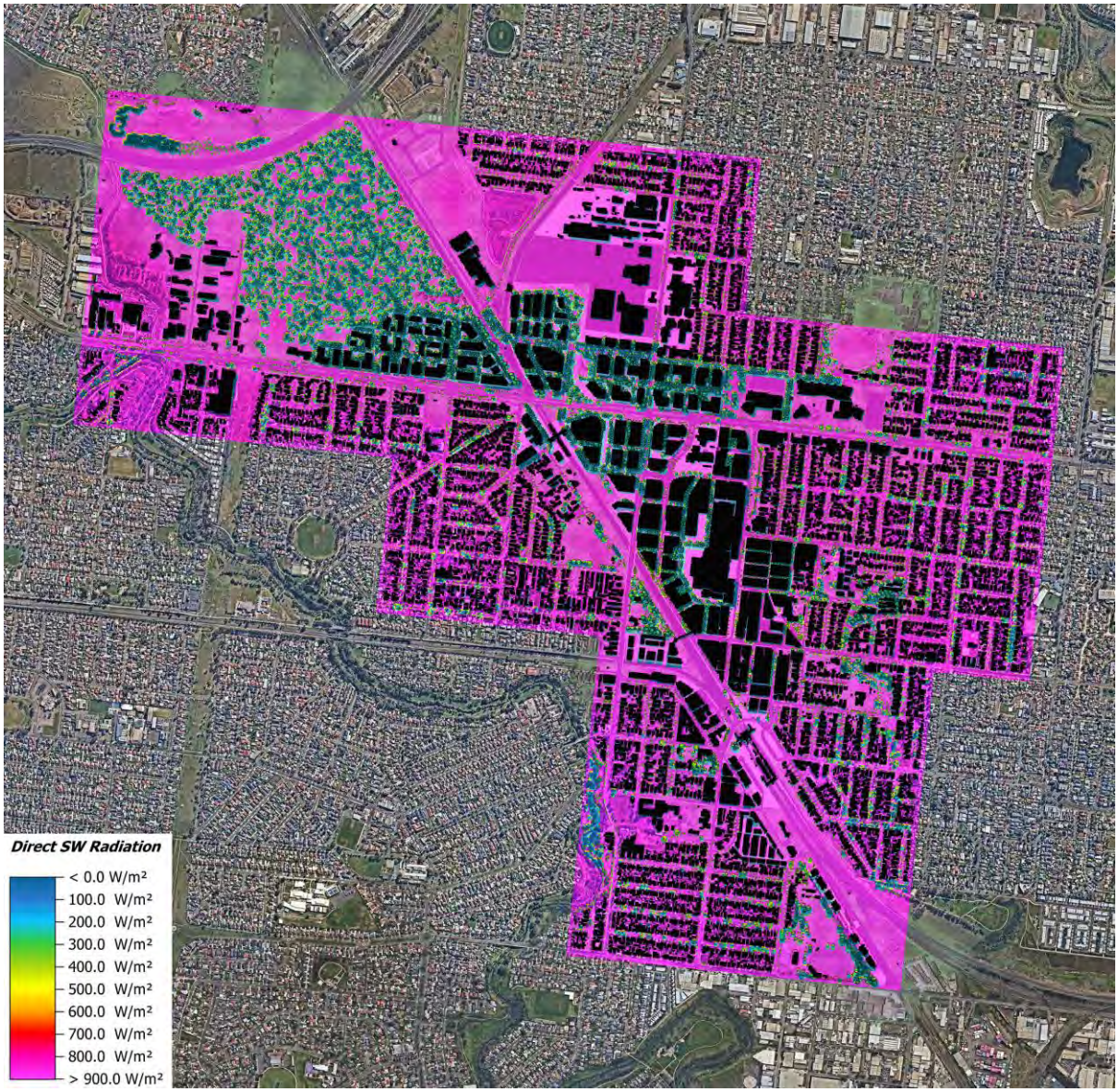

Figure 2.5. Direct solar radiation map at 3 pm during the hottest day in 2050

2.2.4 Reflected solar exposure

Reflective solar radiation[8] is not well studied in the literature due to its complexity, and most studies have focused on the direct impact of solar radiation. However, understanding the level of reflected solar radiation and identifying the areas of its concentration within the Sunshine development, as well as the causes, can significantly help in pinpointing the suitability of mitigation strategies. It can be seen that buildings with a medium level of reflective materials contribute up to 450 W/m² on their north side, which is exposed to direct solar radiation, Figure 2.6. In the context of this precinct, medium-reflective materials generally refer to surfaces such as standard concrete or mid-tone facade finishes,

[8] reflective radiation is the portion of sunlight that bounces back into the surrounding environment, rather than being absorbed

consistent with the National Construction Code classification of light, medium and dark colours. Dark surfaces (for example, asphalt) absorb more radiation, whereas lighter facade materials produce higher reflectance. It has been found that water bodies and irrigated grass sufficiently absorb direct solar radiation, and the energy gained contributes to evaporation, thus reducing air temperature, while dry surfaces and specifically dry grass, contribute up to 250 w/m² of reflected solar radiation, which can target the pedestrian and nearby surfaces and increase their temperatures. These effects are visible in several open spaces in the base case where unirrigated grass or light-coloured pavements reflect radiation toward adjacent footpaths and facades, increasing their surface temperature. For instance, trees next to light surfaces contribute up to 150 w/m² due to reflectance between the surface and the tree canopy. In contrast, trees next to irrigated grass and dark surfaces do not contribute reflected radiation. This distinction occurs because the darker and irrigated surfaces absorb a large proportion of incoming shortwave energy rather than scattering it upward toward the canopy or pedestrians. Lastly, overlapping tree canopies reduce not only direct solar radiation but also reflected solar radiation, because their continuous cover intercepts reflections before they reach pedestrian level. This effect is observable along sections of the precinct where mature, overlapping canopy creates shaded corridors, compared with nearby areas containing spaced or non-overlapping trees that allow direct and reflected radiation to reach the ground and surrounding surfaces. Although the temperature impact cannot be precisely quantified for each point without extensive cell-by-cell extraction, the pattern is consistent: overlapping canopy conditions correspond to lower reflected radiation values and therefore contribute to cooler pedestrian zones. These findings reinforce that canopy continuity, rather than simply the presence of individual trees, is a key determinant of reflected-radiation exposure and therefore an important design consideration explored further in the alternative scenarios.

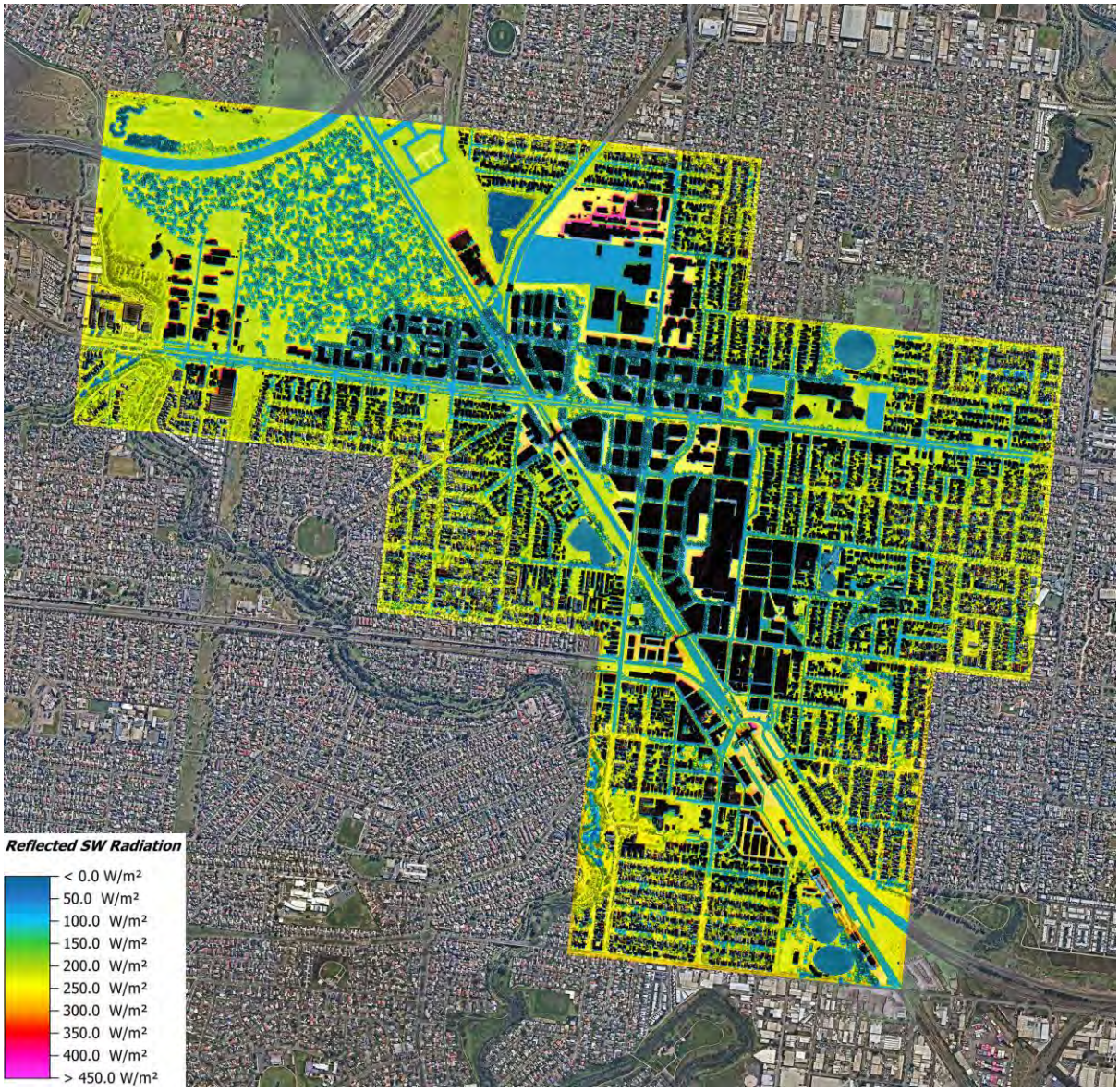

Figure 2.6. Reflected solar radiation map at 3 pm during the hottest day in 2050

2.2.5 Mean radiant temperature (MRT)

MRT represents the average temperature of all surrounding surfaces that exchange thermal radiation with a person, weighted by their view factors (the proportion of radiation received from each surface), which is a direct influence on their thermal comfort. It is also used to identify the risk levels to which humans can be exposed, and that might impact their health. For instance, exceeding the threshold of 57.1 °C could increase the risk of mortality by 5% for all age groups (Thorsson et al., 2014); therefore, this threshold was used in analysing the results. Overall, the Sunshine development has a high level of MRT with a median of 58.2°C. The minimum observed MRT was 25.0°C, and the maximum was 75.0°C, Figure 2.7. It can be noticed that all exposed spaces to solar radiation exceeded the safe threshold and have a mortality risk above 5%, particularly in open paved areas and locations immediately adjacent to medium- and high-reflective facades where surfaces are oriented to receive both direct and reflected solar radiation. These zones typically occur along north-facing building edges and unshaded paved forecourts where view factors to heated and reflective surfaces are high. Exposed spaces near

reflective surfaces show even higher MRT, often exceeding the 10% mortality-risk equivalent. These areas share common features, including limited shading, light to medium-toned materials and close proximity to facades that receive strong afternoon sun. There are also small, localised pockets with limited access for pedestrians, carrying mortality risk levels above 15%. These are very restricted areas that result from extreme combinations of direct exposure, adjacent reflective surfaces and confined geometry, rather than primary pedestrian routes. In contrast, shaded areas from buildings and vegetation have MRT values under the threshold, which emphasise the importance of shading. In addition, irrigated spaces recorded lower levels of MRT due to the sufficient absorbance of the direct solar radiation.

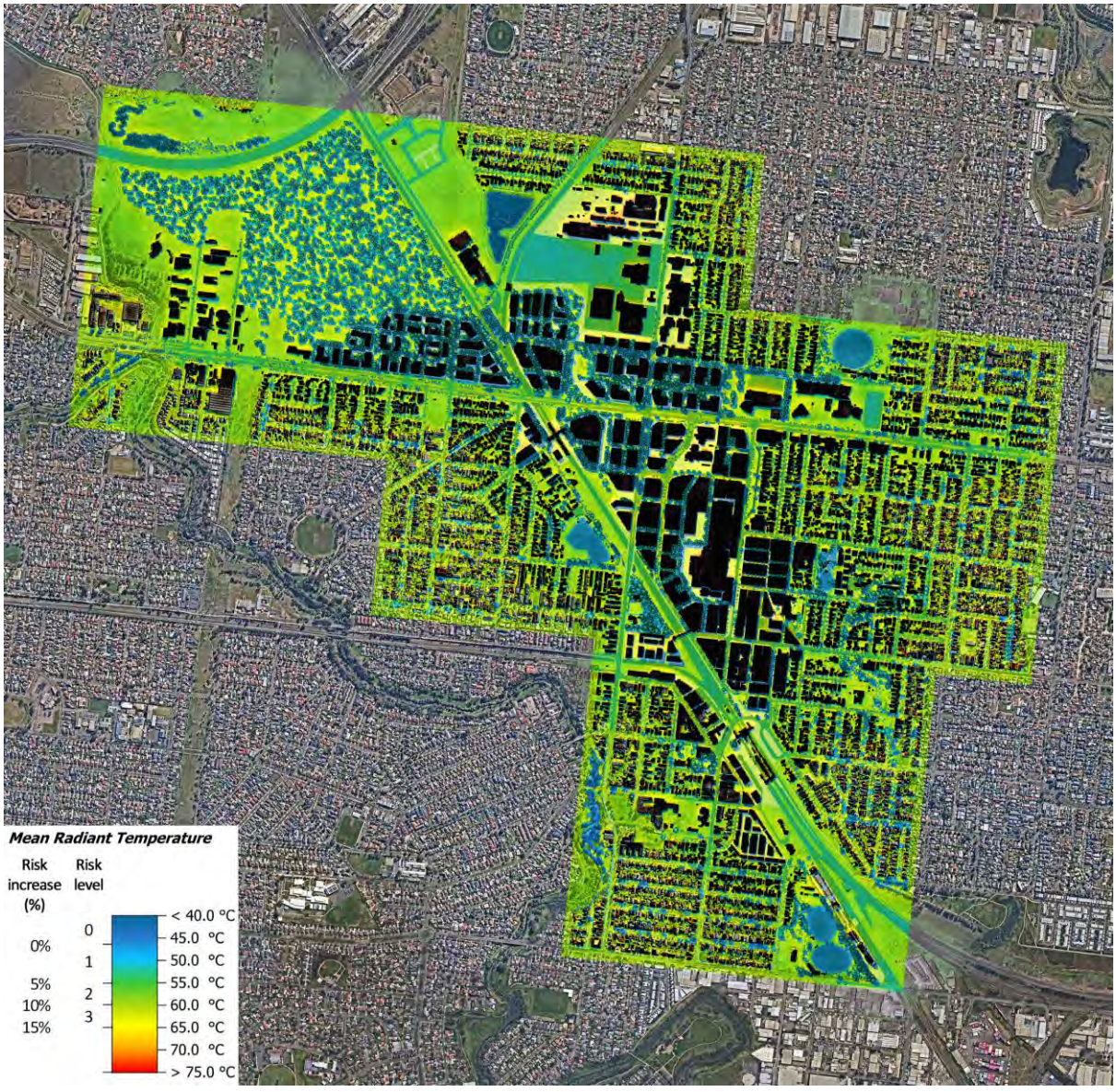

Figure 2.7. Mean radiant temperature and mortality risk levels at 3 pm during the hottest day in 2050

2.2.6 Wind characteristics

Wind plays a critical role in determining air temperature in urban environments because airflow disperses accumulated heat, removes warm air from exposed surfaces and supports evaporative cooling. Wind is also important from an amenity and safety perspective, as both excessively low and

excessively high wind speeds can negatively affect pedestrian comfort and public space usability. Although the wind input parameters were constant, they were significantly altered due to the built environment settings. For instance, at 3 pm, the input wind speed was 5 m/s, with a direction of 0 degrees, approaching from the north. The built form alters these settings, resulting in a median wind speed of 2.6 m/s at the pedestrian level. The minimum wind speed was 0 m/s, where the built form blocked the wind flow, and the maximum reached 4.86 m/s in open spaces that lacked vegetation and buildings, allowing an unobstructed airflow from the north, Figure 2.8.

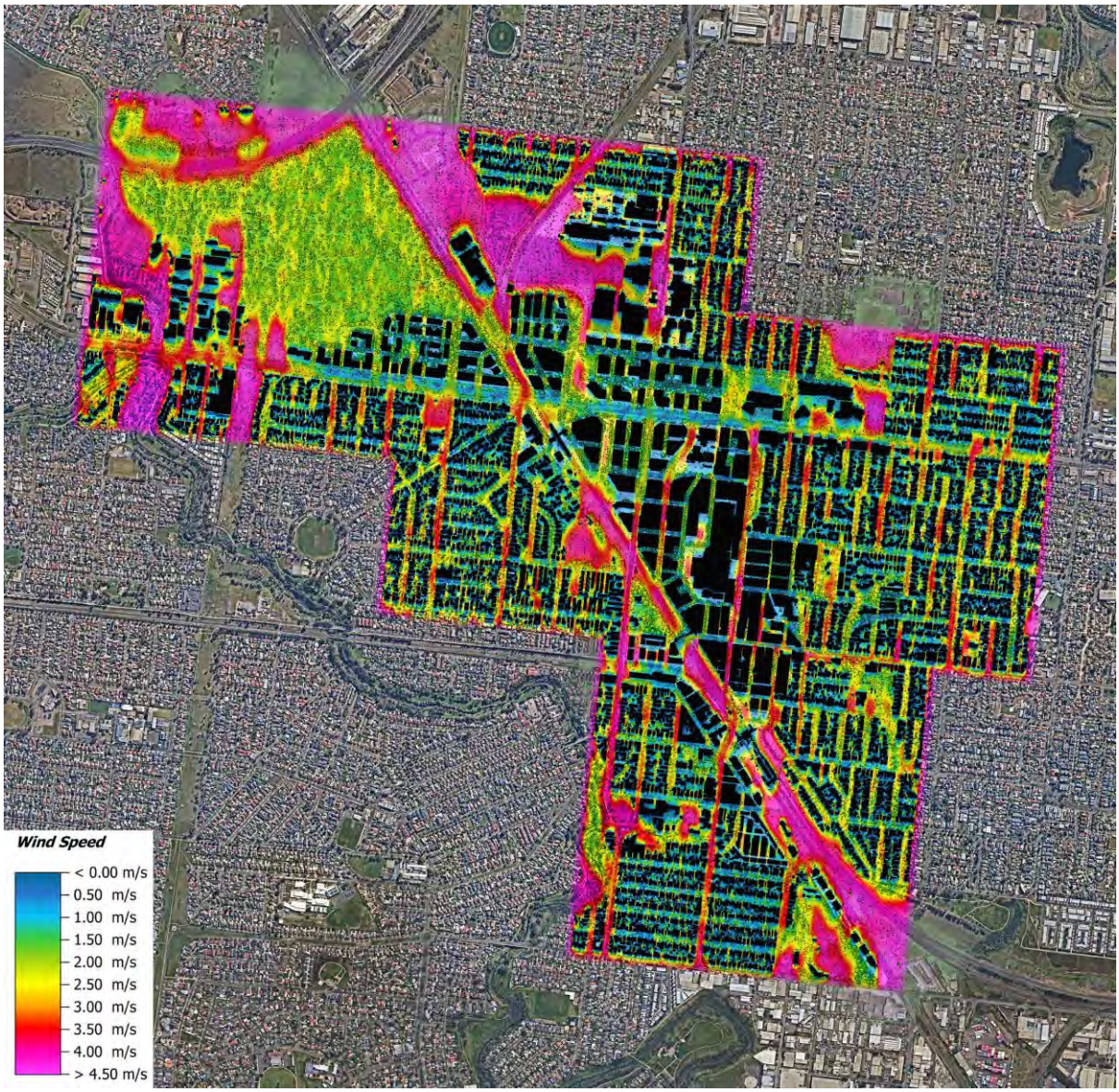

Figure 2.8. Wind Characteristics at 3 pm during the hottest day in 2050

The main key factors that controlled the wind speed were street orientation, location of open space, building heights, orientation, vegetation location, canopy density, and proximity. The results helped identify areas that lack ventilation, which impact passive cooling, such as Energy Park, and some street canyons and public areas exposed to high wind speed risks, including the Albion train station. These findings inform recommendations such as increasing shading and vegetation in highly exposed areas, enhancing ventilation corridors in poorly ventilated spaces and reviewing built form placement where

wind speeds exceed comfort or safety thresholds. In addition, by analysing the impact of the built form on wind speed recovery, the results revealed that the wind speeds need up to three times the height of the built form to recover, in this modelling setup. This recovery distance is influenced by the constant boundary wind-speed assumptions and should be interpreted as indicative rather than absolute. Understanding this distance is important because design decisions seek a balance between excessive sheltering, which suppresses ventilation and contributes to heat build-up, and excessive exposure, which can create pedestrian discomfort. Built form height, canyon geometry and vegetation placement all contribute to whether wind is slowed too much or channelled too strongly, Figure 2.9. The impact of vegetation on wind characteristics in street canyons varied due to inconsistencies in canopy size within the street canyons; therefore, it was further analysed by uniforming the canopy size and reported in the alternative scenarios. It should be noted that from an urban design perspective, very low wind speeds are desirable for comfort and safety, whereas from an urban heat perspective, a moderate wind speed is preferable to zero wind speed because it supports heat removal.

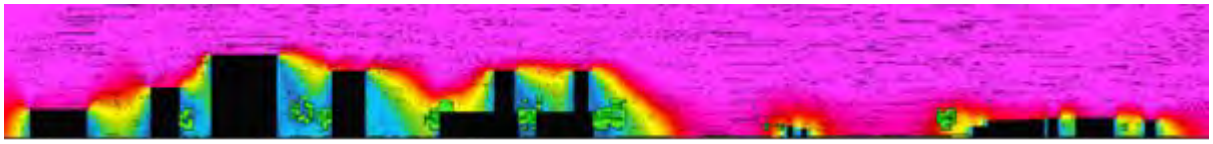

Figure 2.9. A section illustrating the wind characteristics at 3 pm during the hottest day in 2050. The section scale ratio in the height-to-width is 3:1

2.2.7 Relative humidity

The input climate conditions used in the model indicate naturally low summer humidity, and the ENVI-met outputs reflect how the built environment further modifies these conditions. For instance, in the hottest hour, the mean relative humidity in open areas was 13%. The Sunshine development has not significantly altered the median value, which was 14% (see Figure 2.10). However, the various settings in the development had both positive and negative impacts on the relative humidity in different locations. The lowest relative humidity was 11%, observed near the built forms where vegetation and air ventilation were limited. In comparison, the maximum relative humidity was 33%, observed near water bodies and irrigated vegetation in open spaces. Higher values in these locations result from evaporation from the water bodies and transpiration from actively irrigated vegetation. Relative humidity influences thermal comfort in a non-linear way: very low humidity can increase the risk of dehydration, while very high humidity can reduce the body's ability to cool itself. The desirable range is generally moderate humidity, which supports thermal comfort without inhibiting evaporative cooling. In this context, water bodies and irrigated vegetation maintained moderate humidity levels, supporting improved outdoor comfort compared with the driest parts of the precinct. These findings emphasise the value of irrigation and moisture-retaining landscapes as part of an urban cooling strategy. Further discussion of humidity in relation to air temperature and UTCI is provided in the following subsections.

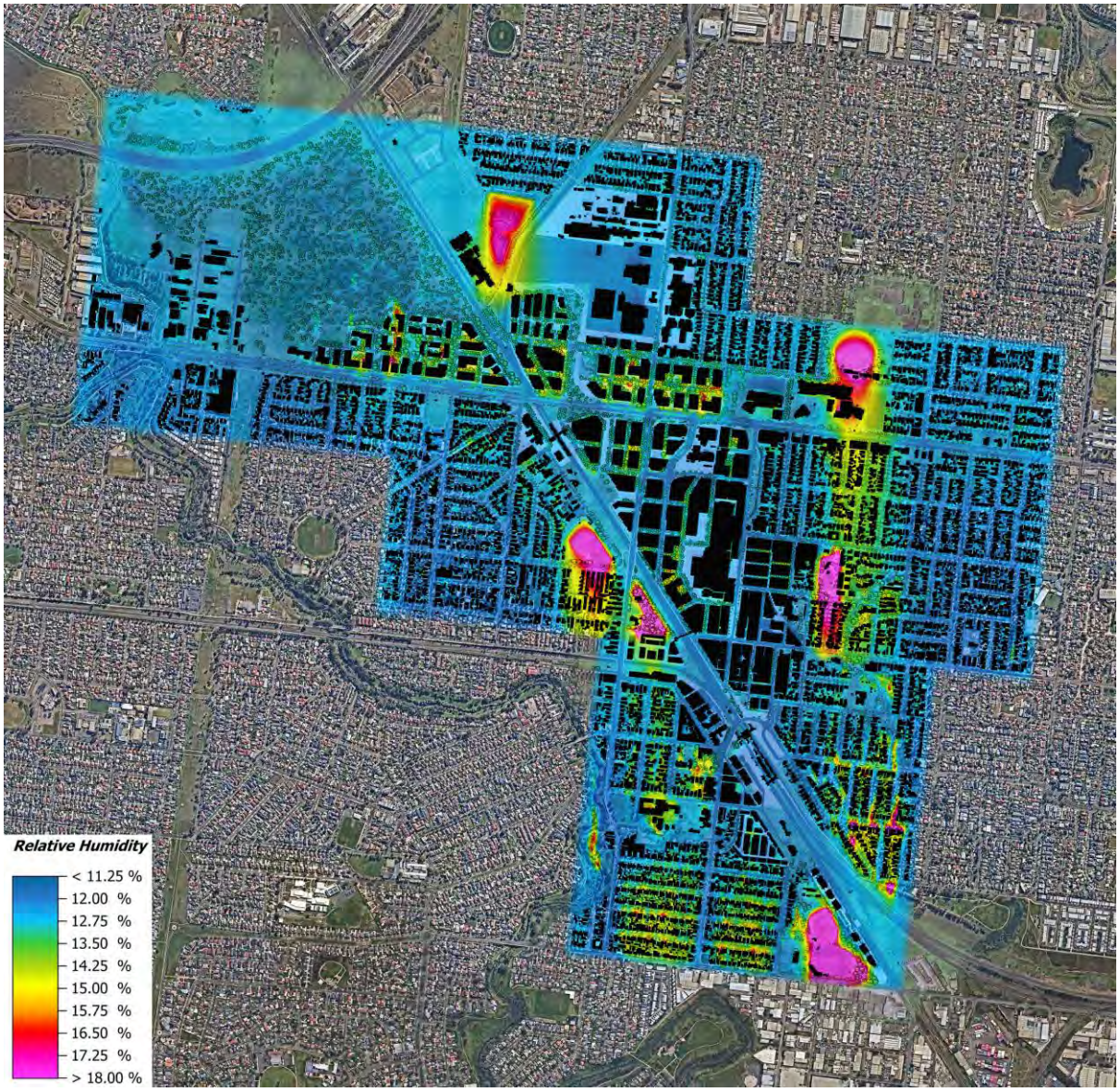

Figure 2.10. Relative humidity levels at 3 pm during the hottest day in 2050

2.2.8 Air temperature

The air temperature results from the interaction of nearby surfaces and objects, which influence its value through heat exchange. For the cross-sections assessed at 3 pm, the boundary input temperature was 40.3°C, while the air temperature in the development ranged between 32.5°C and 45.0°C, (see Figure 2.11). The median temperature was 41.7°C, indicating that the development resulted in a 1.4°C increase in air temperature. The spatial variation is associated with typical land-cover patterns rather than isolated points. The coolest values occurred around irrigated landscapes and water bodies, while the highest were concentrated in unshaded hard surfaces and restricted street canyons. There was an almost 12.5°C difference between the hottest and coolest ground surfaces at the pedestrian level. The lowest air temperatures were observed above and near surfaces with sufficient moisture, such as Stony Creek and irrigated open spaces, due to the evaporation and evapotranspiration effect. This provides a strong link between the relationship between relative humidity and air temperature and the power of evaporative cooling in this climate due to the initial low humidity.

In contrast, the highest air temperatures were recorded mainly in two locations. These included the central portion of the Energy Park and several compact street canyons that lacked shading or ventilation. The former was due to reduced relative humidity, as the park is not irrigated, combined with low ventilation and elevated reflected solar radiation from dry grass. Street canyons with limited ventilation displayed elevated temperatures when aligned perpendicular to the prevailing wind (for example, E-W orientations), while canyons parallel to the wind showed lower temperatures but increased exposure to direct solar radiation. These dynamics are examined further in the alternative scenarios section, which consolidates the contributing factors into design recommendations.

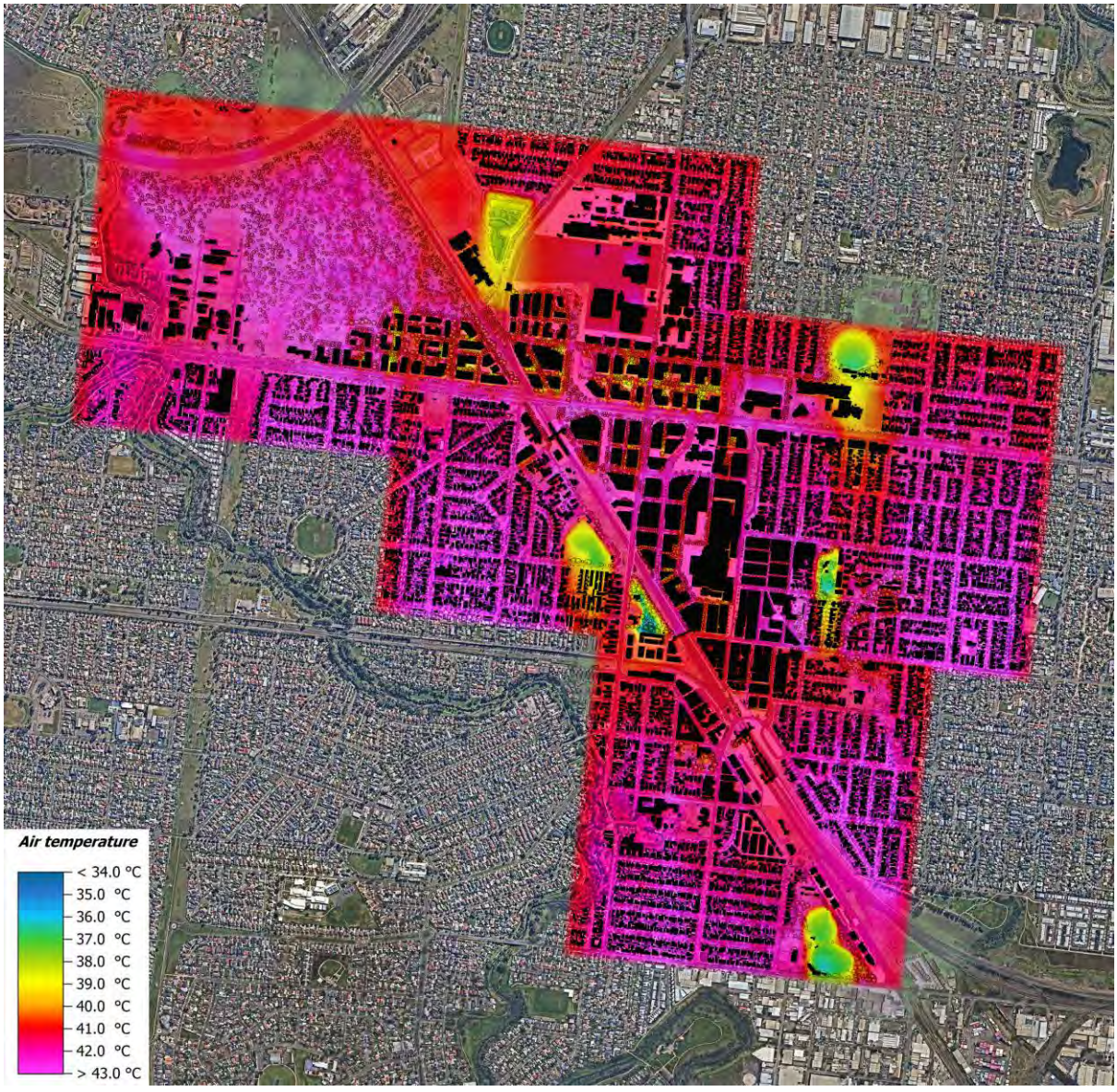

Figure 2.11. Air temperature at the pedestrian level at 3 pm during the hottest day in 2050

The surface materials and their characteristics, as well as the characteristics of air and wind, have a significant impact on the distribution of heat in the built environment, as illustrated in Figure 2.12. Lower wind speeds, higher surface absorption and increased reflectance all contributed to higher air temperatures in areas with limited shading or ventilation. These themes have been integrated to avoid duplication across sections.

Additionally, water availability in the soil reduces surface temperature and increases evapotranspiration, thereby lowering air temperature. Due to the different pressures and wind patterns, the positive impact of irrigated grass on air temperature reduction reached up to 30m in height and 550m in wind direction.

The analysis also revealed that trees are excellent at providing shade; however, their cooling performance varies depending on irrigation, canopy density, shading context and local wind speeds. Trees surrounded by hot, reflective surfaces or limited airflow exhibit reduced cooling potential, whereas trees in irrigated and shaded environments demonstrate stronger cooling effects. These results highlight the importance of matching canopy conditions and irrigation levels to local microclimate objectives rather than relying solely on tree presence.

Figure 2.12. A section illustrating the air temperature at 3 pm during the hottest day in 2050. The section scale ratio in the height-to-width is 3:1

2.2.9 Thermal comfort (UTCI)

Thermal comfort is a measure of human satisfaction with the thermal environment in the built environment, reflecting the combined influence of the analysed parameters above and their clothing insulation, activity level and metabolic rate. The median UTCI temperature observed in the development was 44.6°C, with a minimum of 31.1°C and a maximum of 50.9°C, following a pattern similar to air temperature and MRT, with a difference between the minimum and maximum temperatures of 19.8 °C, Figure 2.13. According to UTCI classification, the median value of 44.6°C falls within the very strong to extreme heat stress categories, indicating that under the Base Case conditions, the precinct experiences thermal environments that substantially exceed recommended outdoor comfort thresholds.

The lower UTCI temperature was within the moderate heat stress range for pedestrians, which was observed under shading and in areas above and nearby irrigated open spaces and Stony Creek. The highest observed UTCI, representing extreme heat stress and elevated health risk, was in various locations, including the central and eastern portions of the Energy Park, unshaded open spaces with dry grass, and compact street canyons with direct or reflected solar exposure. These zones share consistent causal factors: absence of shading, dry surfaces with limited evaporative cooling and reduced ventilation pathways.

Due to the observed relevant patterns between air temperature, MRT, and thermal comfort, the analysis of alternative scenarios focused on air temperature as an indicator of alternative heat control strategy effectiveness, as well as an easier parameter to understand by non-expert stakeholders.

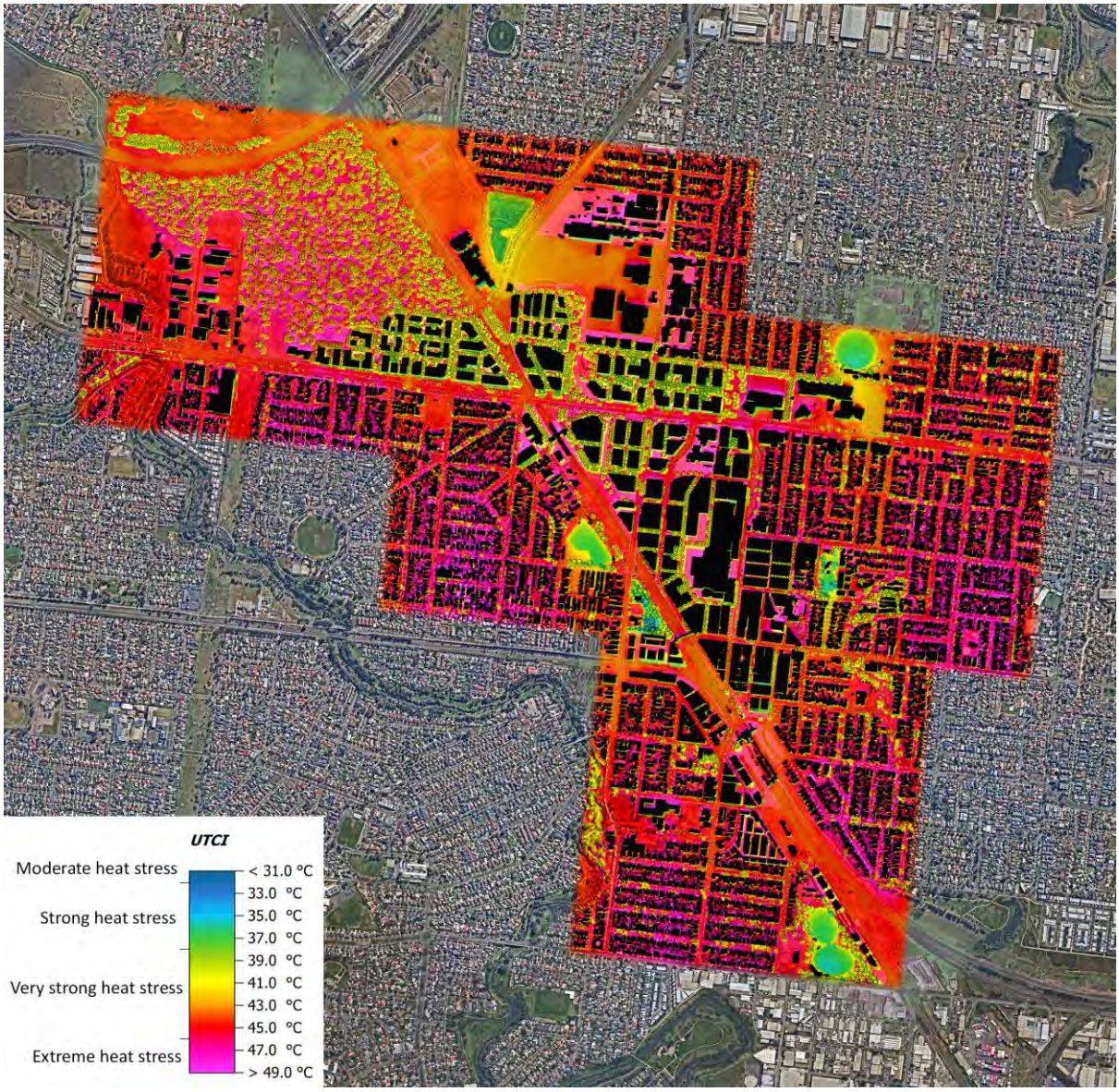

Figure 2.13. Thermal comfort and heat stress levels at 3 pm during the hottest day in 2050

2.3 Alternative scenarios - Street trees

The street trees were thoroughly investigated regarding their size and location within the various street canyons in the development. The following subsection reports the investigation steps and results. It should be noted that the tree arrangements in this section follow the water analysis described in section 3.4.2, which also explains the various settings of the implemented tree configuration for urban heat analysis.

2.3.1 Impact of large and small trees

The built environment at street levels in the base case features various settings, including different tree sizes in street canyons (small, medium, large), varying verge widths (or no verge), and isolated and overlapping trees (see section 10.1.6). In some streets, the tree canopy is high, while in other streets near the residential area, it is low. However, all the settings had one thing in common: the absence of irrigation.

In general, the overlapped canopy provided excellent shading on the east-west axis but significantly impacted airflow on the north-south axis (see Figure 2.14). Additionally, the limited number of trees in the housing area in the S-W area contributed to increased temperature. The small trees had a limited cooling effect, while the large canopy blocked airflow and, in some locations, created hot pockets. Due to the various settings in the base case, it was challenging to generate recommendations for trees in street canyons.

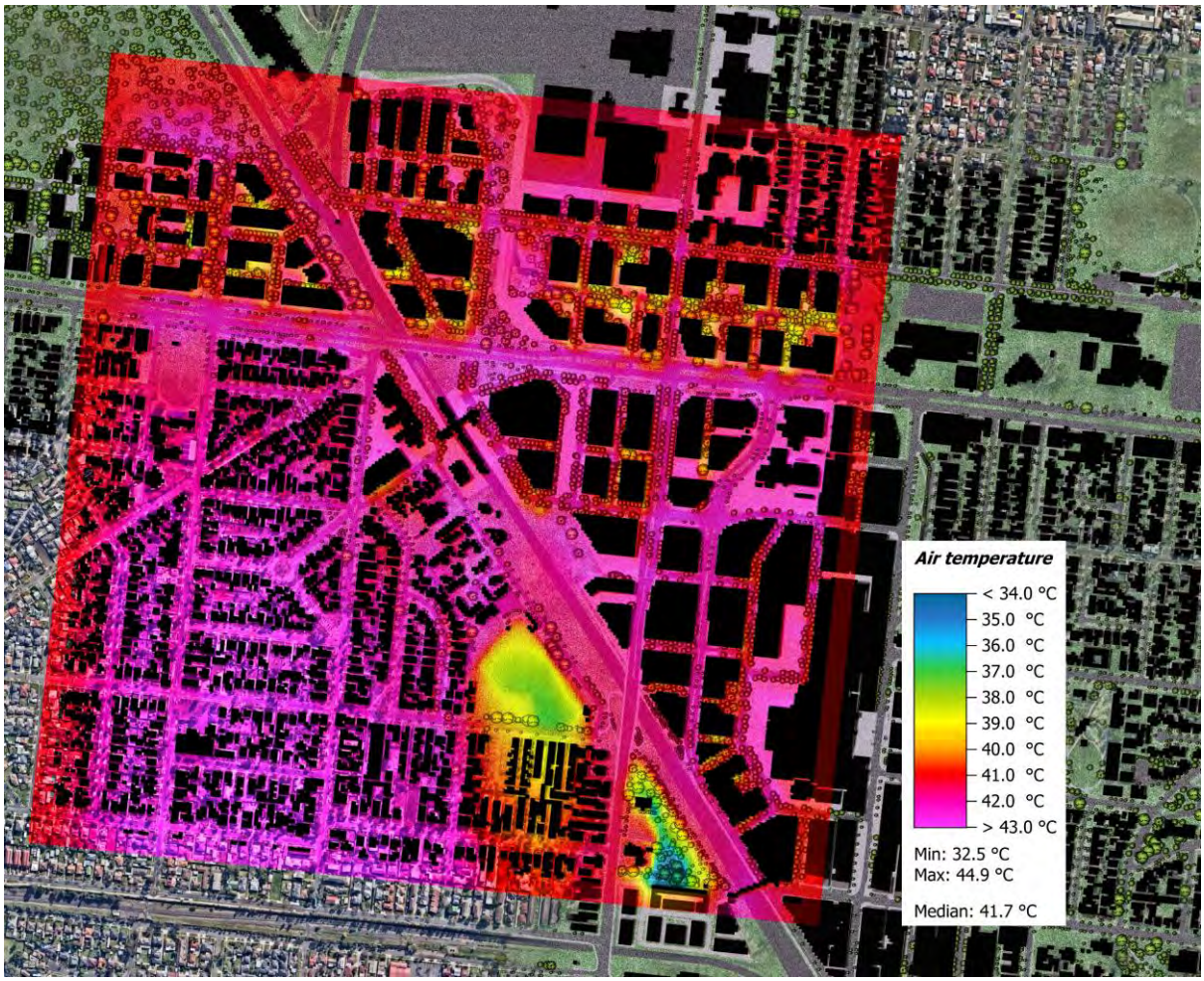

Figure 2.14. Median air temperature at 3 pm at the pedestrian level during the hottest day in 2050

Therefore, all the trees in street canyons have been replaced with large trees (defined as 15m wide canopy), without altering the number or location of these trees, to test the effect of incorporating large trees in the precinct. Overall, the median temperature of the new setting remained unchanged, with increases of up to 1.2 °C and reductions of up to -3.1 °C at the street canyon levels (see Figure 2.15). Generally, the enhanced cooling was attributed to increased shading and evapotranspiration resulting from the increased canopy percentage. However, in some locations, this increase created hot pockets by obstructing airflow and reducing it, which in turn raised the temperature.

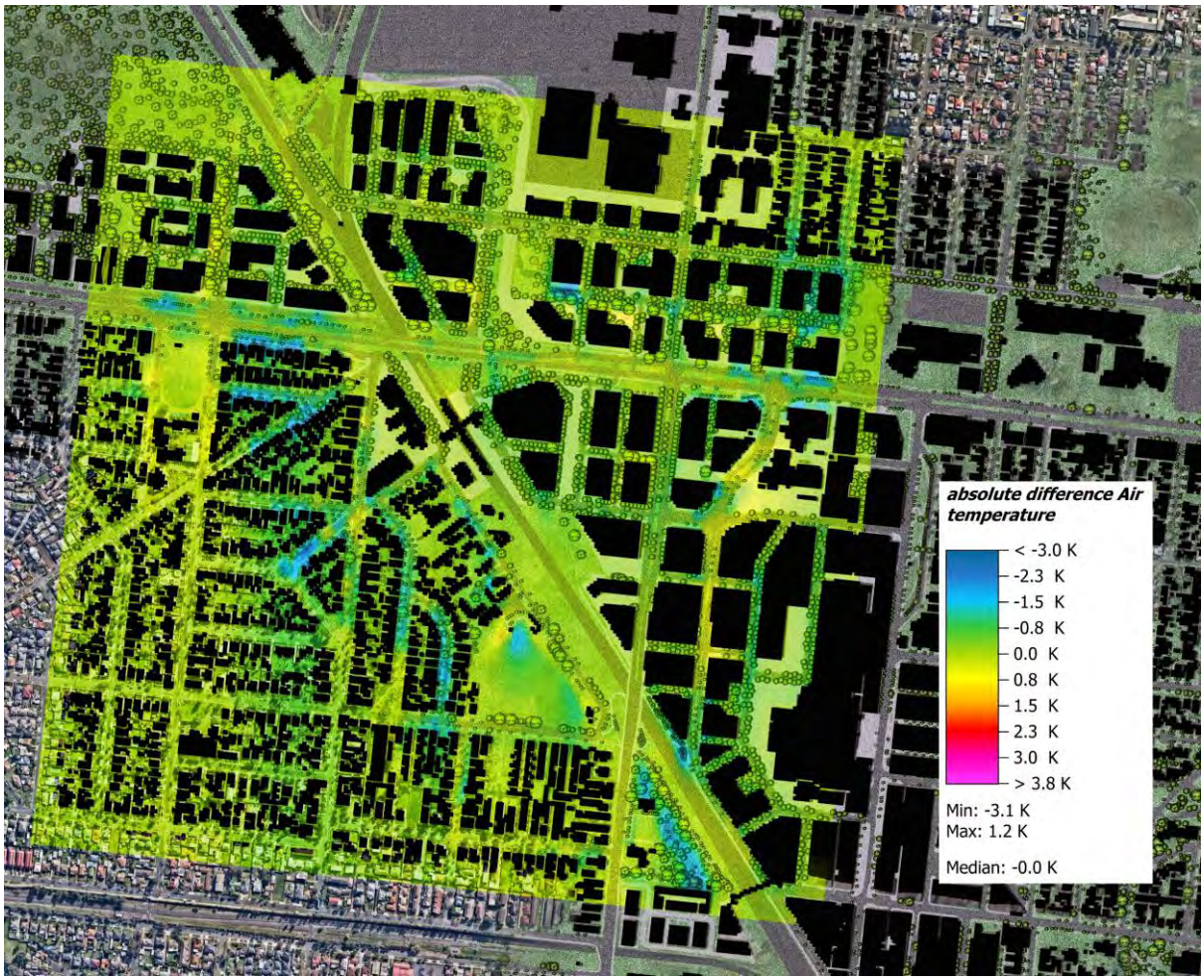

Figure 2.15. Median air temperature at 3 pm at the pedestrian level during the hottest day in 2050

The second trial was to change all the trees to small (defined as 5m wide canopy), similarly to the large trees' scenario. Overall, the median air temperature has increased by 0.1 °C, with the highest increases of up to 3.9 °C and reductions of up to -1.5 °C at the street canyon levels (see Figure 2.16). Generally, the increase in air temperature was due to reduced shading and evapotranspiration resulting from lowering the canopy coverage. In contrast, the enhanced cooling was due to improved airflow. These results suggest that the size of the trees may have a positive or negative impact, depending on their location.

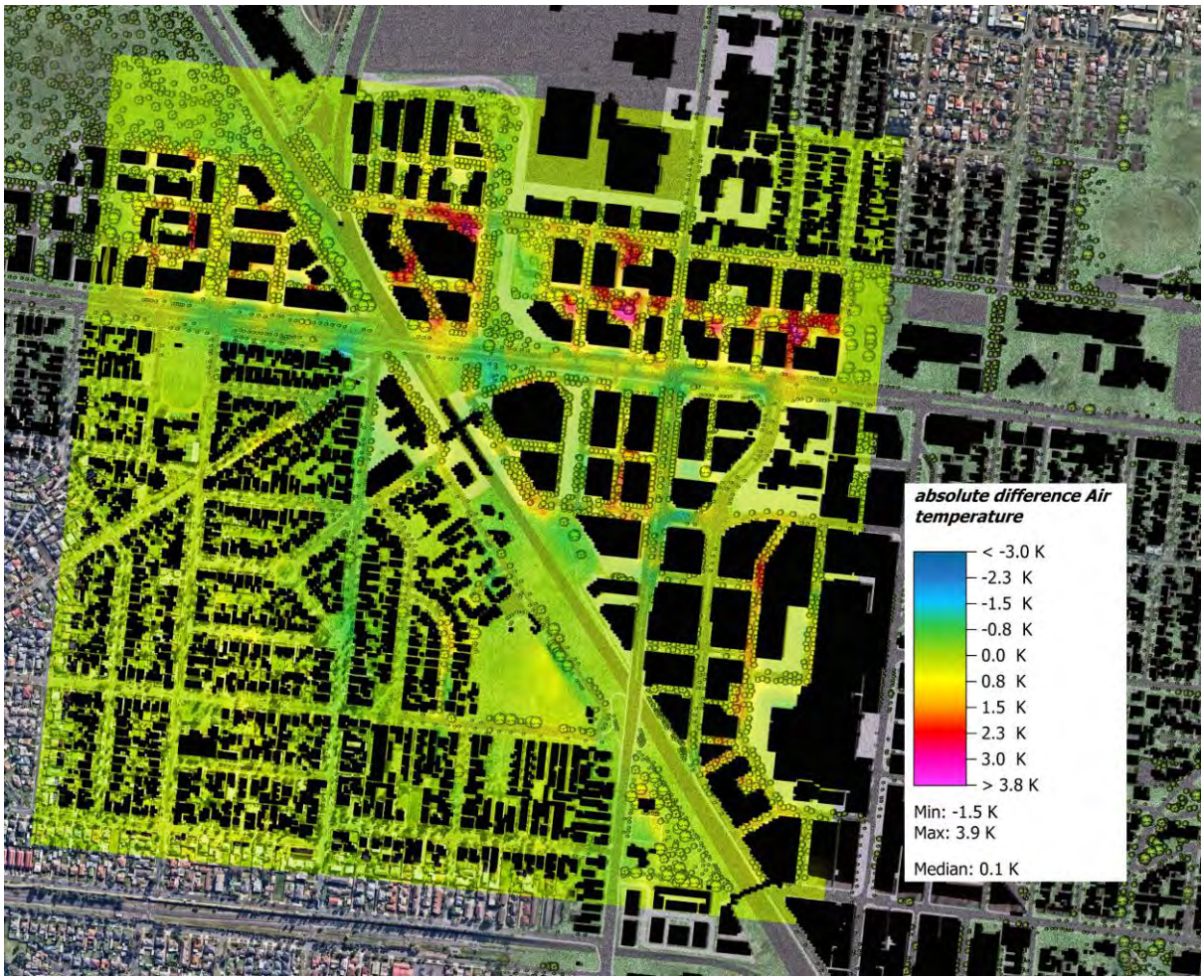

Figure 2.16. Median air temperature at 3 pm at the pedestrian level during the hottest day in 2050

To better understand the impact of large and small trees in street canyons, the absolute difference between the two proposed alternatives was analysed (see Figure 2.17). When replacing small trees with large trees and comparing the results in the same scenario, some or part of the street canyons may experience a reduction in air temperature, while others may experience an increase. These changes have been noticed regardless of the street width and orientation. Therefore, additional parameters were investigated to understand better the impact of changes in the tree canopy on air temperature.

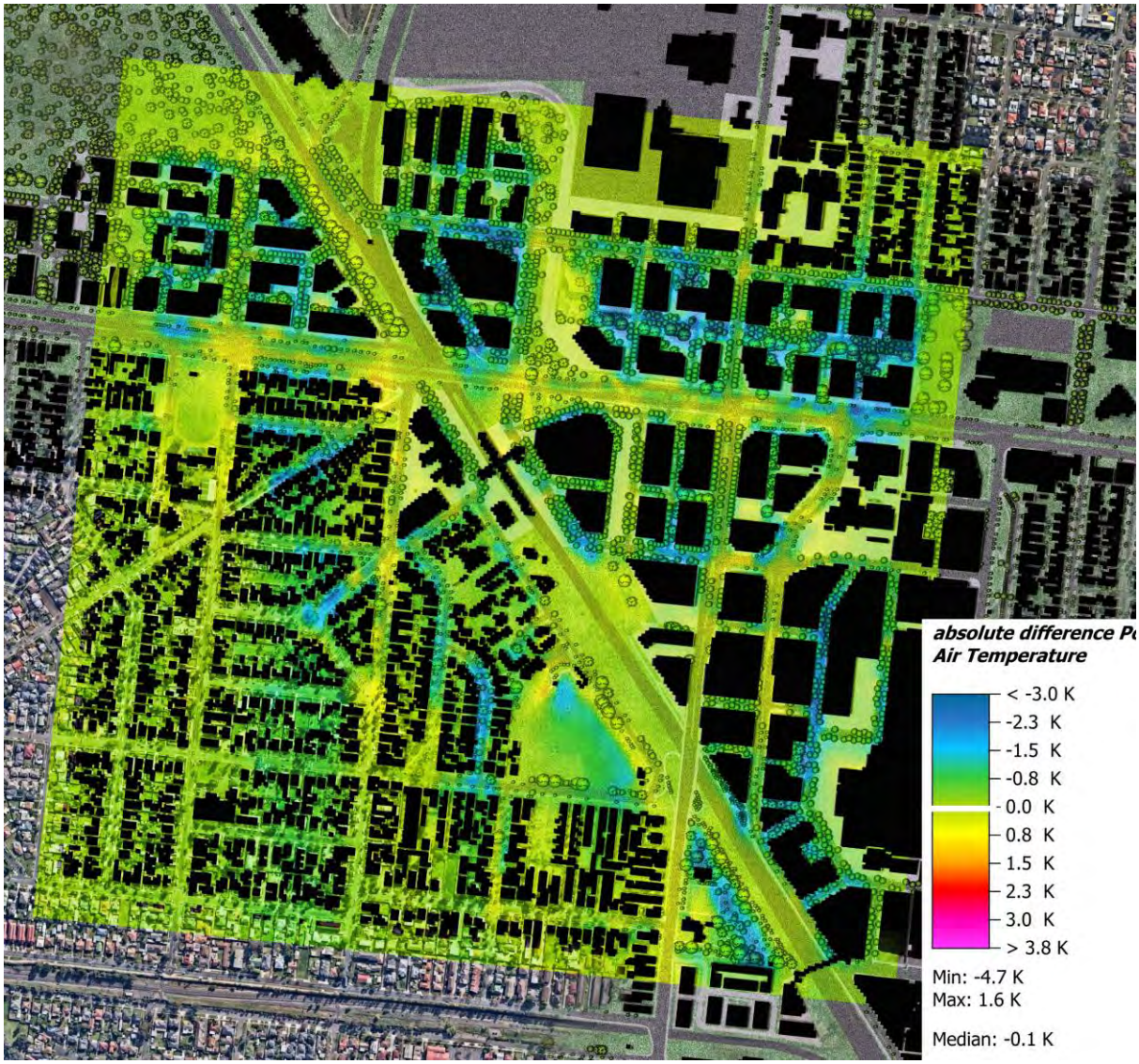

Figure 2.17. Air temperature at 3 pm at the pedestrian level during the hottest day in 2050

From the shading aspect, the direct solar radiation was analysed at the pedestrian level (see Figure 2.18). The maximum observed solar radiation was in open spaces, reaching up to 880 W/m². The increased canopy coverage, provided by large trees, successfully mitigates solar radiation in some locations, offering more shading for pedestrians under the canopy. At the same time, it has no impact or a negative impact in other places due to an increase in reflected solar radiation, which results in no changes to the median radiation within the small and large tree scenarios. The trees near the south building facades had no impact on shading unless the tree was taller than the building (mainly in residential areas with low-rise housing). In contrast, shading increases significantly under trees near the north building facades. There was a medium to high shading increase on N-S streets, and the median and south side of E-W streets. Lastly, medium shading increases on the N-E side of NW-SE oriented streets, while high shading increases on the S-W side. These shading patterns directly influence local microclimate conditions: locations receiving effective canopy shading generally correspond to lower air temperature, lower MRT and improved thermal comfort, whereas areas with limited or fragmented shading show higher heat stress due to exposure to both direct and reflected

radiation. The results, therefore, highlight that shading effectiveness is highly dependent on canopy continuity, building orientation and surface reflectance rather than simply tree presence.

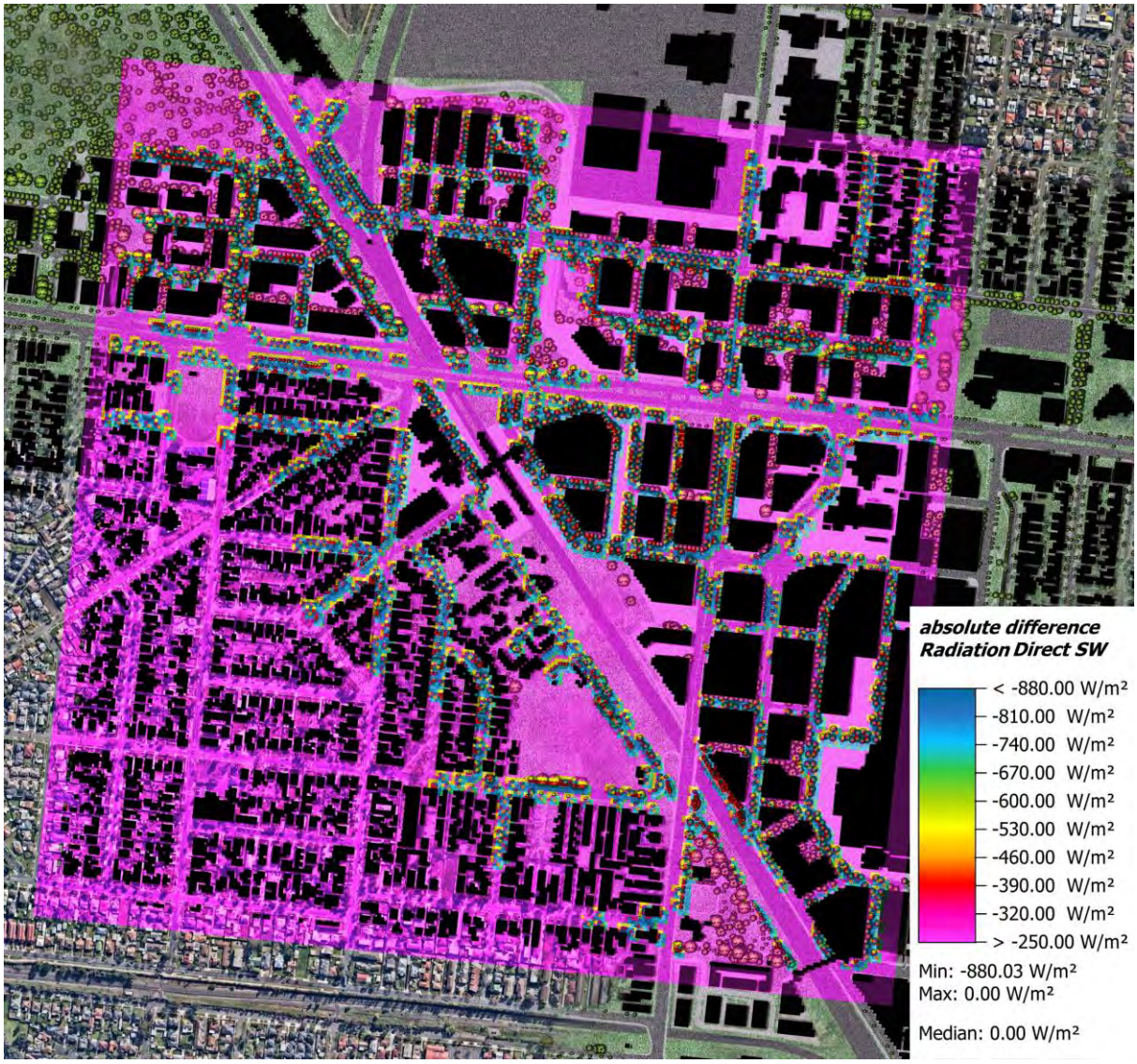

Figure 2.18. Direct solar radiation at 3 pm at the pedestrian level during the hottest day in 2050

The wind analysis provided significant insights, facilitating an understanding of the air temperature differences within the scenario. Figure 2.19 illustrates the impact of the increased tree canopy on wind speed. The figure shows that reduced wind speed significantly influences the increase in air temperature (see Figure 2.17). Large trees (15m wide) significantly reduced ventilation, passive cooling, and wind speed on N-S streets. However, N-S streets with obstructed airflow and limited trees have not been impacted by tree size, which also does not contribute to an increase in air temperature. For E-W streets, tree size has a limited impact on wind speed, except near the intersection, that are influenced by the wind speed reduction from the obstructed wind from N-S streets.

The integrated analysis of air temperature, shading, and wind speed reveals that large trees can reduce air temperature if they do not significantly affect wind speed. However, if they reduce wind speed, their cooling effect is diminished or absent, and significant reductions in wind speed may contribute to an

increase in air temperature. These findings highlight the importance of strategic tree placement that aligns with precinct-scale airflow patterns. Trees should be located to maximise shading while preserving key ventilation corridors. During heatwaves, canopy shading can reduce the accumulation of radiant heat in surfaces and provide net thermal benefits. However, canopy density and placement should be carefully managed to avoid impeding passive cooling or redirecting airflow in ways that intensify heat, particularly in narrow or low-ventilation street canyons.

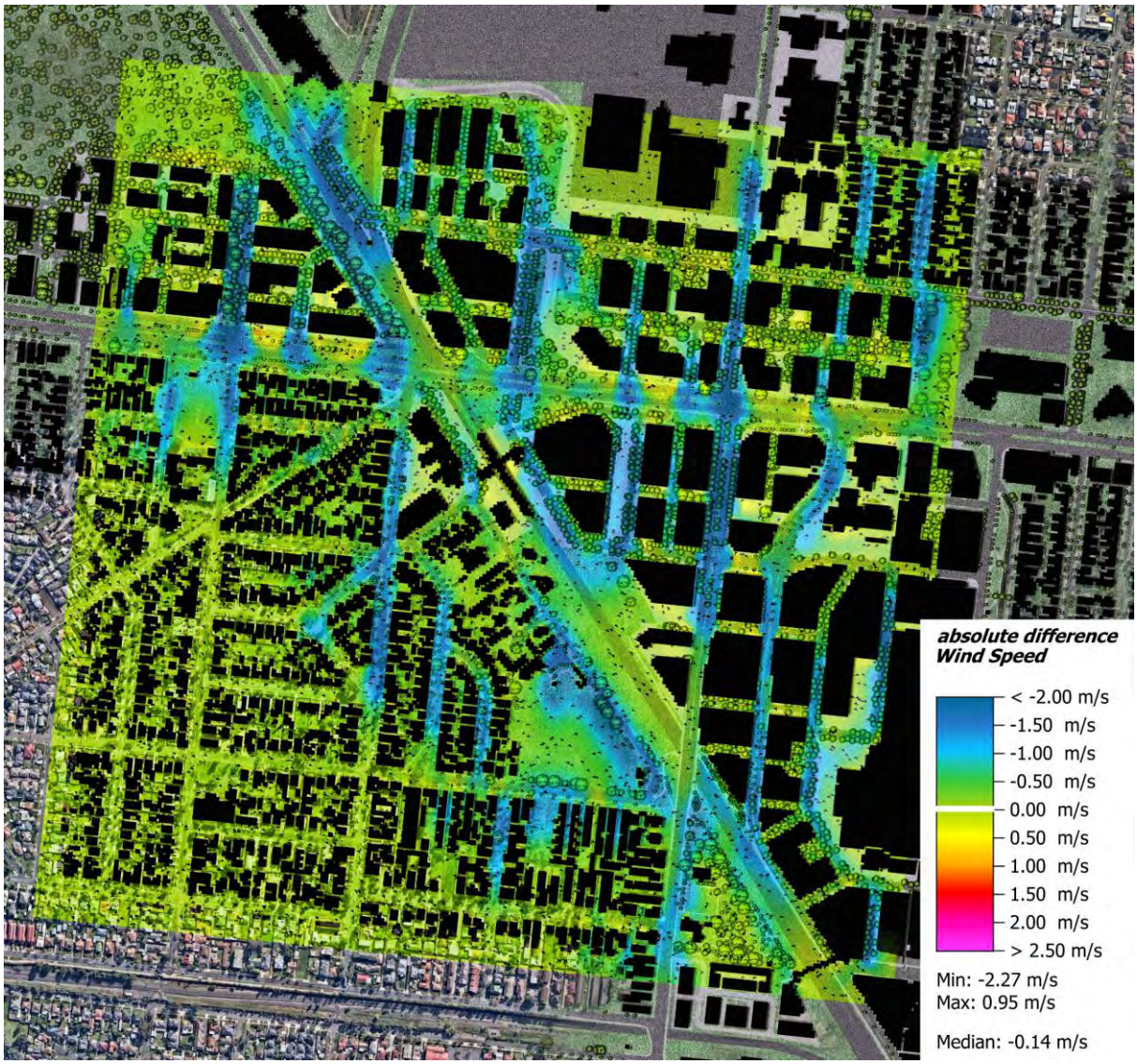

Figure 2.19. Median wind speed and direction at 3 pm at the pedestrian level during the hottest day in 2050

2.3.2 Impact of drought-resistant trees with limited soil moisture

Planting drought-resistant trees with limited soil moisture levels, which maintain physiological function under dry conditions, compared to medium-water-intake trees in the base case, which have modest soil moisture, resulted in a 0.2 °C increase in the median air temperature during the hottest hour. There are a few spots where the air temperature has increased by up to 2.3 °C near the trees and by up to 1.6 °C in wider areas around these trees (see Figure 2.20).

The increase in temperature was primarily observed in areas where airflow was limited due to obstructions from the tree canopy, overlapping canopies, or built forms. In contrast, in other regions with unrestricted airflow, no increase was noted. This increase resulted from reduced evapotranspiration and localised shading effects that alter the energy balance. In this scenario, drought-stressed canopies have limited cooling capacity, so their net effect depends on both canopy density and the reflectance of surrounding surfaces.

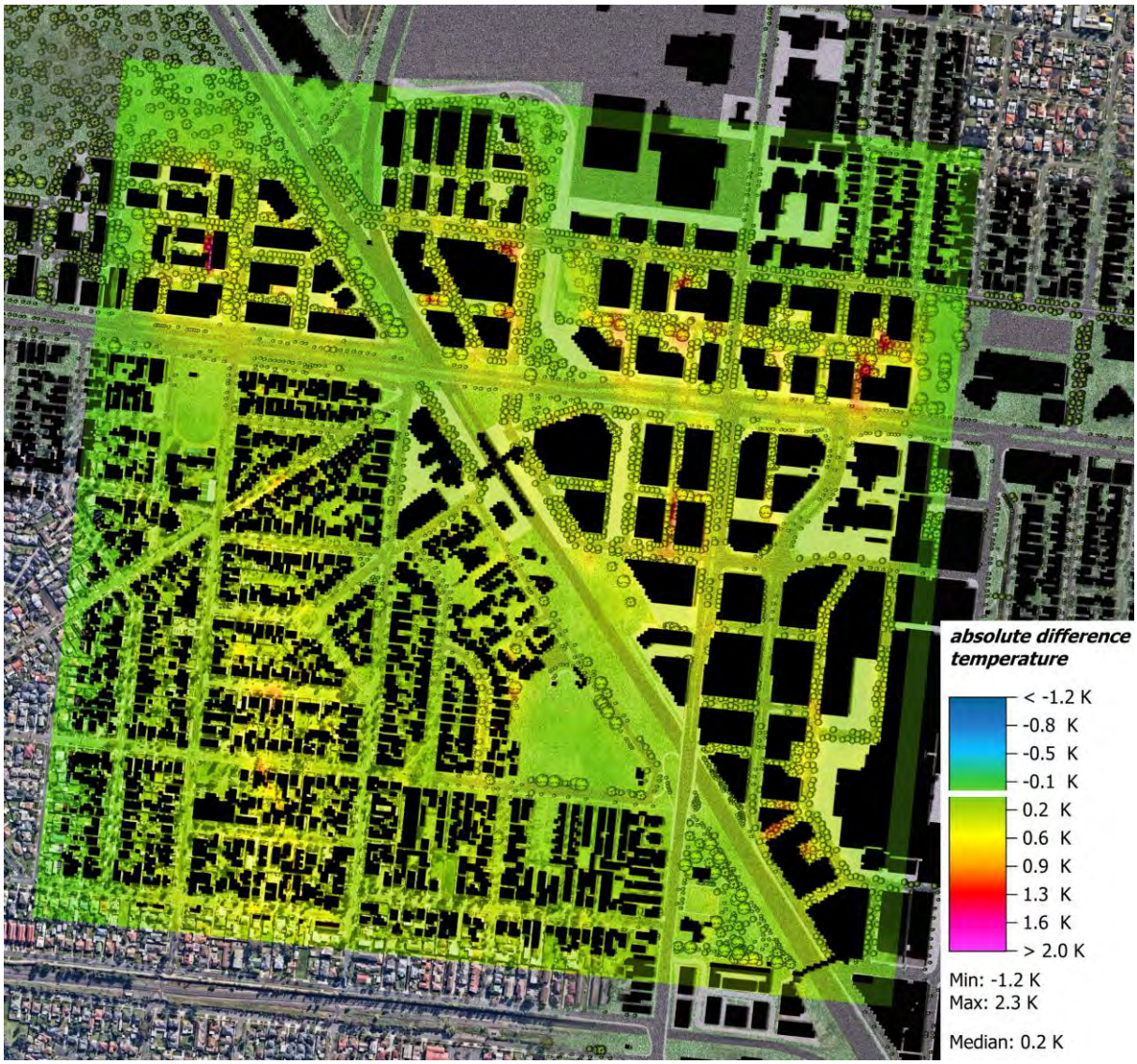

Figure 2.20. Median air temperature at 3 pm at the pedestrian level during the hottest day in 2050

These mechanisms become more pronounced during the hottest hours of the day, when trees close their stomata to conserve water and evapotranspiration is largely suppressed. As a result, drought-stressed canopies provide little active cooling, and the combined effects of canopy density, surface reflectance and restricted airflow described above lead to additional temperature increases. Assessing the diurnal pattern is therefore essential. The smallest increase occurred at 6 am (0.1°C), while the largest was at 1 pm (1.3°C), with an average daytime increase of 0.4°C. This pattern reinforces the critical role of soil moisture in enabling evaporative cooling. It demonstrates the importance of selecting tree species and irrigation strategies that can sustain transpiration under hot conditions to

support passive cooling and reduce urban heat. At the same time, however, even if not reducing temperatures through evapotranspiration, drought resistant trees can still play an important role in reducing direct and indirect solar radiation. This is important in protecting pedestrian health and reducing heat accumulation in ground surfaces - which is particularly important in a heatwave.

2.4 Alternative scenarios - Irrigating open spaces

As evidence of the impact of irrigation and increased soil moisture on reducing air temperature and enhancing the thermal comfort of the development (see section 2.2.8), further investigation has been conducted to assess the impact of increasing irrigated open spaces. The investigation began with water analysis, where locations were identified as possibly irrigated, and the water and soil requirements are reported in section 3. The urban heat simulation for this scenario followed the proposed setting in section 3.3. The results were compared to the base case, as can be seen in Figure 2.21. These proposed open spaces have significantly reduced air temperature and thermal comfort in the open spaces up to 7.5 °C and 10.2 °C, respectively. The positive impact travelled downwind, gradually fading for up to 550m. This provides evidence that irrigation is more influential in reducing air temperature than increasing the tree canopy coverage percentage. These findings highlight the strategic value of locating irrigated open spaces and parks in relation to precinct-scale wind flows. By positioning irrigated areas at appropriate intervals and aligning them with prevailing ventilation corridors, it is possible to achieve substantial cooling benefits across the precinct without the need for widespread irrigation. This offers a targeted, resource-efficient approach to improving outdoor thermal comfort.

(a)

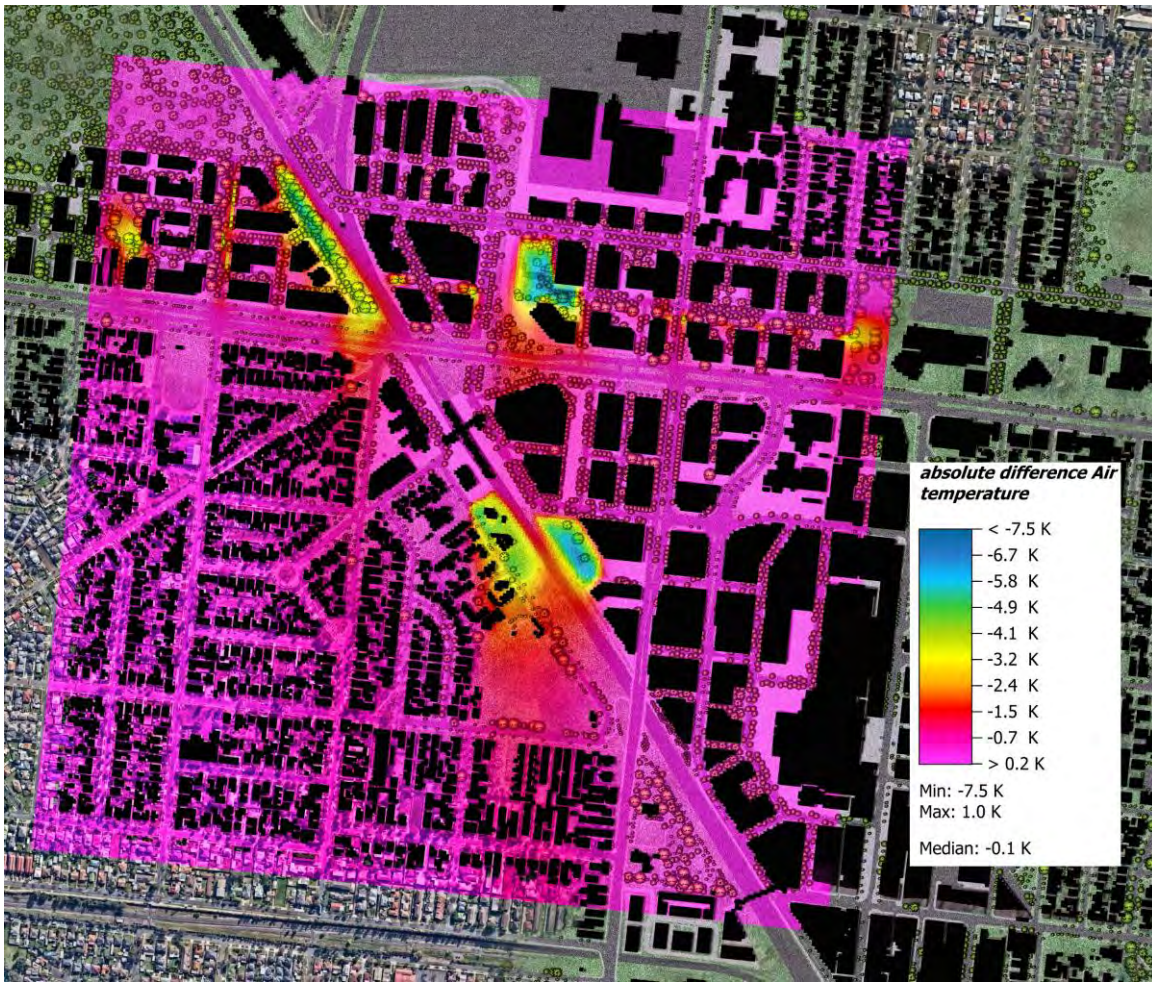
absolute difference Air temperature
< -7.5 K
-6.7 K
-5.8 K
-4.9 K
-4.1 K
-3.2 K
-2.4 K
-1.5 K
-0.7 K
> 0.2 K
Min: -7.5 K
Max: 1.0 K
Median: -0.1 K

(b)

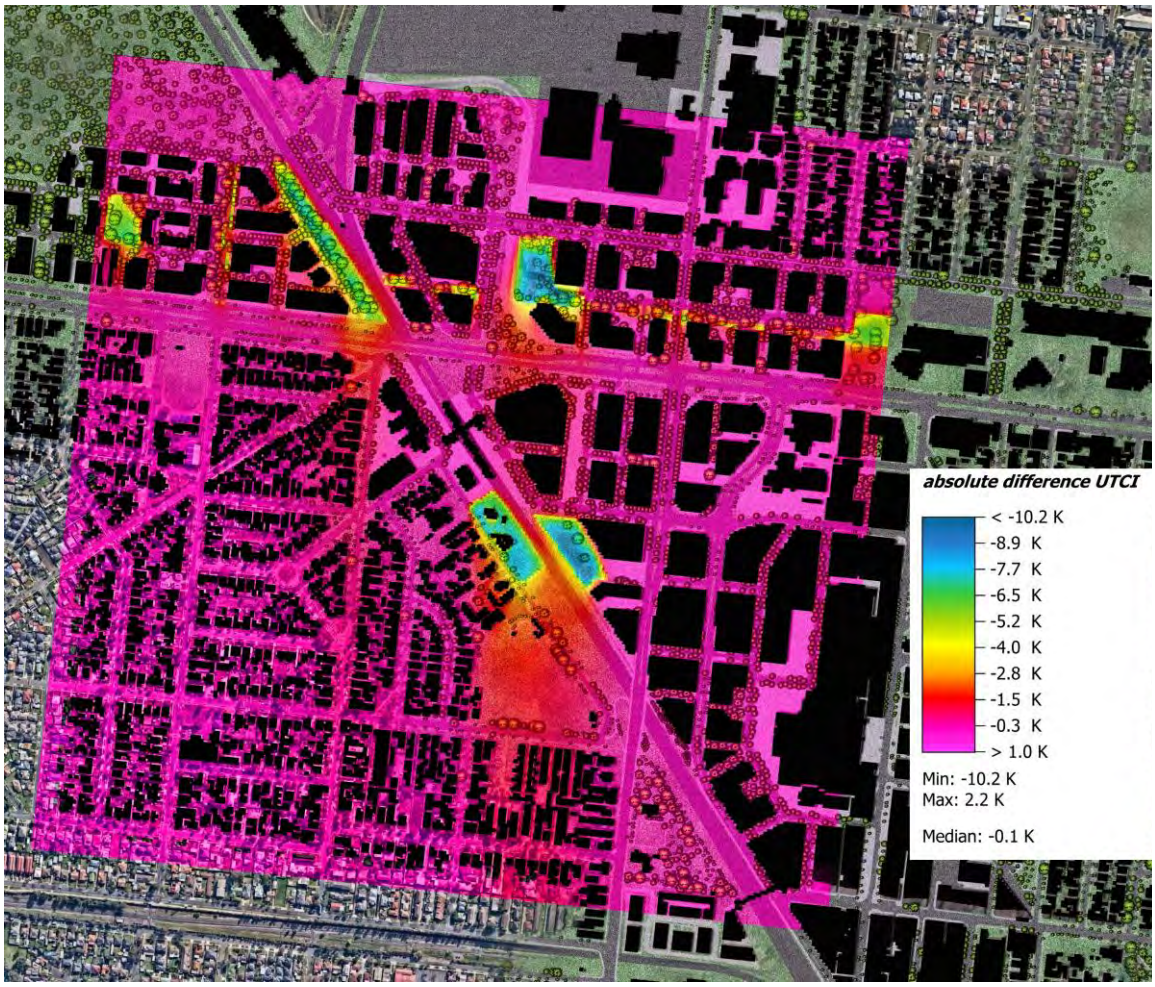

Figure 2.21. Median thermal performance at 3 pm at the pedestrian level during the hottest day in 2050. (a) median absolute air temperature, (b) median absolute thermal comfort.

2.5 Alternative scenarios - Buildings embodied carbon and urban heat

As one of the project's aims is to create net-zero carbon development, several options were investigated to reduce the embodied carbon (EC) of the development, with a focus on building materials. After careful consideration, a new scenario was developed, incorporating low embodied carbon materials for selected buildings where these alternative materials could be allocated - see Table 10.4 for materials selected and their thermal properties. A few key of the scenario was the use of mass timber in building construction.

The new scenario was modelled, simulated, and compared with the base case scenario. It was observed that between 6:00 AM and 8:00 AM, there is no significant difference in outdoor air temperature between the high-EC and low-EC building scenarios (see Figure 2.22). After 8:00 AM, the outdoor temperature in the high-EC scenario increases more rapidly than in the low-EC scenario, peaking at a 0.2 °C difference at 10:00 AM. This difference remains constant until 4:00 PM, with a slight reduction to 0.1 °C at 2:00 PM. After 4:00 PM, the temperature difference between the two scenarios gradually decreases, reaching 0 °C between 6:00 PM and 7:00 PM. After 7:00 PM, the outdoor air temperature in the low-EC scenario exceeds that of the high-EC scenario by up to 0.2 °C. Overall, the air

temperature difference between the two scenarios ranges from -0.2°C to 0.2°C, indicating relatively low variability. The high-EC scenario yields higher daytime air temperatures, whereas the low-EC scenario results in higher nighttime temperatures. A multi-day heatwave was not modelled, so the longer-term behaviour of materials, particularly the accumulation of heat in the built environment, cannot be directly assessed. This is important, as cumulative heat storage rather than short-term air temperature is a key driver of thermal risk during heatwaves. The slightly higher nighttime temperatures observed in the low-EC scenario are likely related to differences in thermal mass and heat release timing, rather than greater overall heat accumulation. Based on established thermal behaviour, higher-mass materials such as concrete are more likely to store and re-radiate heat over successive hot days than lower-mass timber systems, suggesting that cumulative heat accumulation would be greater under the high-EC scenario. Given that, , low embodied carbon building materials are likely to be preferable, as they help reduce air temperatures when most needed and offer greater potential for lowering the project's overall embodied carbon.

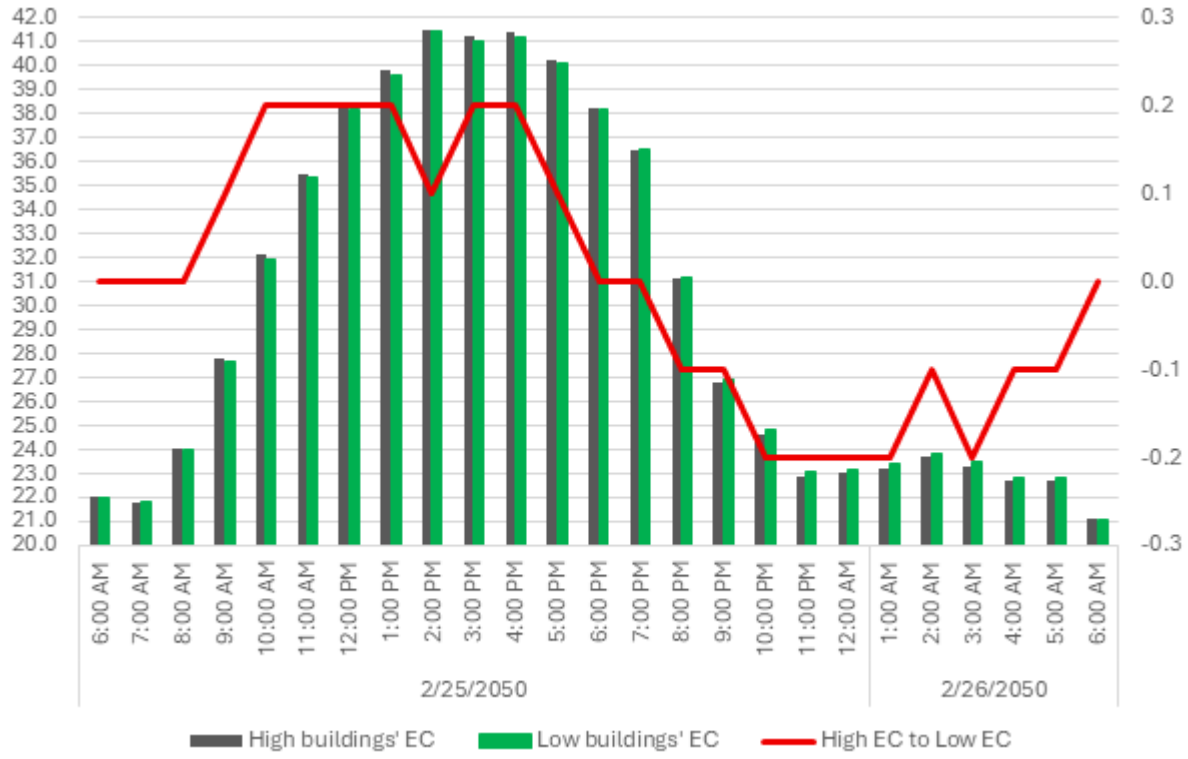

Figure 2.22. Median air temperature during the simulated 24 hours on the hottest day at the pedestrian level in 2025

2.6 Updated scenario

The updated scenario options were developed and provided by DTP. The analysis was performed on Tiles 1 and 2, as these two tiles host the majority of the changes across the five tiles. Details of the setup and structure are provided in the Appendix (see section 10). Simulation of this stage was based on five models. The first model focused on an Energy Park following the same design layout of the base case, except for the tree arrangement, which was redesigned and idealised based on the analysis in the base case to free the airflow and enhance the passive cooling, as the park was one of the hottest spots in the base case and mainly due to the tree arrangement. Three scenarios focused on Albion Quarter

with alternative tree and irrigation arrangements as outlined in Figure 2.23. The three Albion Quarter scenarios are Best Investment Case (BIC), Reasonable Investment Case (RIC), and Business As Usual (BAU). The settings of these scenarios are listed in Figure 2.23. The last scenario was developed to ensure a valid comparison across all simulations. The updated scenarios include taller buildings, which required a larger ENVI-met modelling domain. Therefore, the base case was re-simulated within the expanded geometry so that all scenarios could be compared under consistent model dimensions and boundary conditions.

Scenario	Streets					Public open space			Private realm			
	Active irrigation priority	Active irrigation all	Tree overlap priority	Tree overlap all	Structural soil	Active irrigation	30% canopy	% hardstand	Active irrigation	10% ground canopy	Podium canopy	Internal streets with trees
Best Investment case	O	O	O	X	O	O 30%	O	X	O 20%	O	X	O
Reasonable investment case	O	X	O	X	O	O 20%	O	X	X	O	X	O
BAU	X	X	X	X	X	X	O	X	X	O	X	O

Assumptions	Definition
Priority Street	Street sides that will be unshaded in summer
All Streets	All street sides, regardless of orientation and shading
Tree Overlap	Trees that are close enough together or large enough that canopy overlaps
Structural Soil	Extra soil put under footpath and on-street carparking to support tree growth and facilitate tree canopy overlap
Active Irrigation	Drip irrigation to enable street tree growth (street trees). For open space, the equivalent of active irrigation for cooling purposes
% hardstand	The amount of open space not covered by grass
30% canopy	Coverage of 30% of open space with tree canopy
Podium canopy	Trees planted on top of carparking podiums

Figure 2.23. Assumptions and definitions of Albion Quarter scenarios for the updated scenario simulations

2.6.1 Impact of the new design of the Energy Park compared to the base case scenario

The design of the Energy Park in the base case included 30% tree canopy coverage and was mainly covered by grass. The trees overlapped in some locations, while they did not in others, and all the vegetation was unirrigated (see Figure 2.24a). The air temperature in the park was one of the highest in the whole development, as reported earlier in section 2.2.8. It was noticed that the park's air temperature significantly impacts the microclimate and the surrounding area, specifically on the south side of the park, Figure 2.24b. One of the main factors contributing to the increase in air temperature was the tree arrangement, which significantly reduced wind flow, creating hot pockets in the park. Although the trees provided good shading in the park, the heat accumulation outweighed the benefits of shading.

(a) (b)

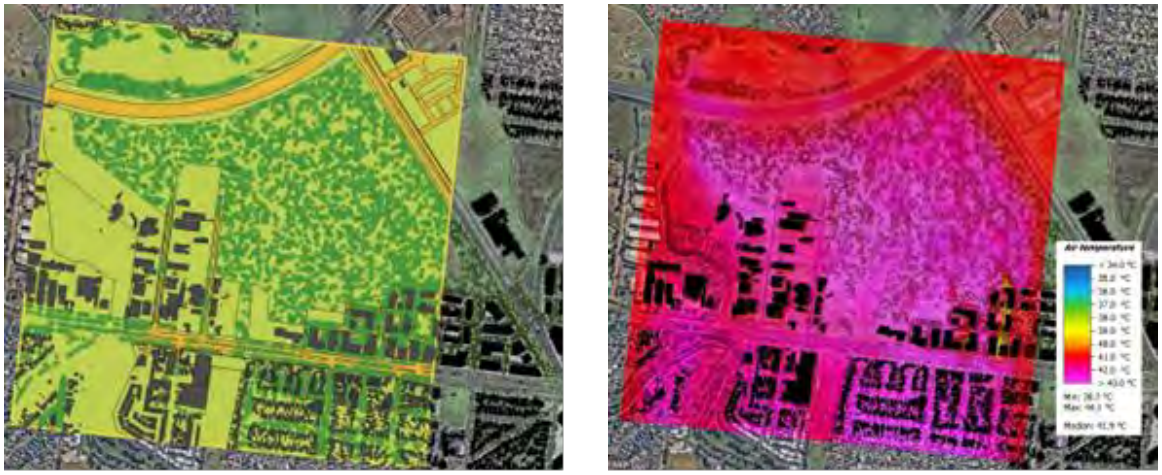

Figure 2.24. Energy Park design and thermal performance. (a) the design based on the base case scenario, (b) the air temperature during the hottest hour at the pedestrian level in 2025

The proposed design of the Energy Park includes adding a stadium, a few service buildings, and activities (see Figure 2.25 a). The tree canopy coverage in the park remains 30% and includes four play fields with irrigated grass. However, based on the lessons learned from the base case, it was concluded that even though the added field will contribute to air temperature reduction, its impact will be localised around the grass due to the arrangement of trees, which will reduce wind speed and block natural ventilation. Therefore, a decision was made to keep the design while rearranging the trees, which was influenced by the wind flow and characteristics in the base case. Trees were reduced in the north to allow the wind to penetrate through the park. Additionally, the trees within the park were strategically grouped to serve as wind channels, while providing targeted, overlapped canopies to cool the park, Figure 2.25 b. This arrangement also exposed the four irrigated surfaces to increased airflow, enhancing evaporative cooling and distributing the cooled air within the park, while allowing it to move out of the park and cool the surrounding area.

(a) (b)

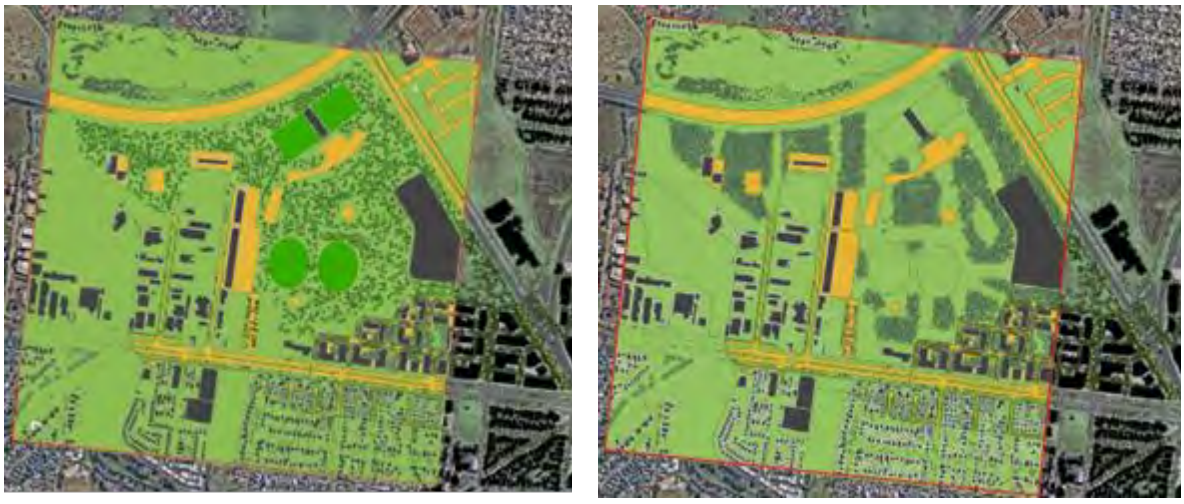

Figure 2.25. Energy Park proposal. (a) the proposal based on the structural plan, (b) the modified proposal for better ventilation and passive cooling

The new design successfully reduced the median air temperature by 3.3 °C, with a minimum reduction of -1.5 °C (see Figure 2.26a) The highest reduction was significant, reaching up to 10.9 °C, which was observed in the oval irrigated grass area due to the enhanced cooled airflow from the north and the irrigated grass. In addition, the enhanced arrangement of the trees significantly improved the wind flow, which carried this positive impact up to 550 m downwind. Additionally, the evaporative cooling resulting from the irrigated grass was the primary factor in enhancing air temperature. Furthermore, the targeted airflow and tree grouping play a crucial role in improving the microclimate and distributing benefits throughout the park. The design also enhances relative humidity and reduces reflected solar radiation, both of which contribute to improved thermal comfort. The median UTCI has been reduced by 9.1 °C (see Figure 2.26 b), with a minimum reduction of 2.5 °C and a maximum of 19.7 °C. The new design successfully eliminates the extreme heat stress in the park and places a significant portion of the park within the moderate heat stress zone. In contrast, in the base case, the majority of the park was located at the extreme heat stress level.

(a)

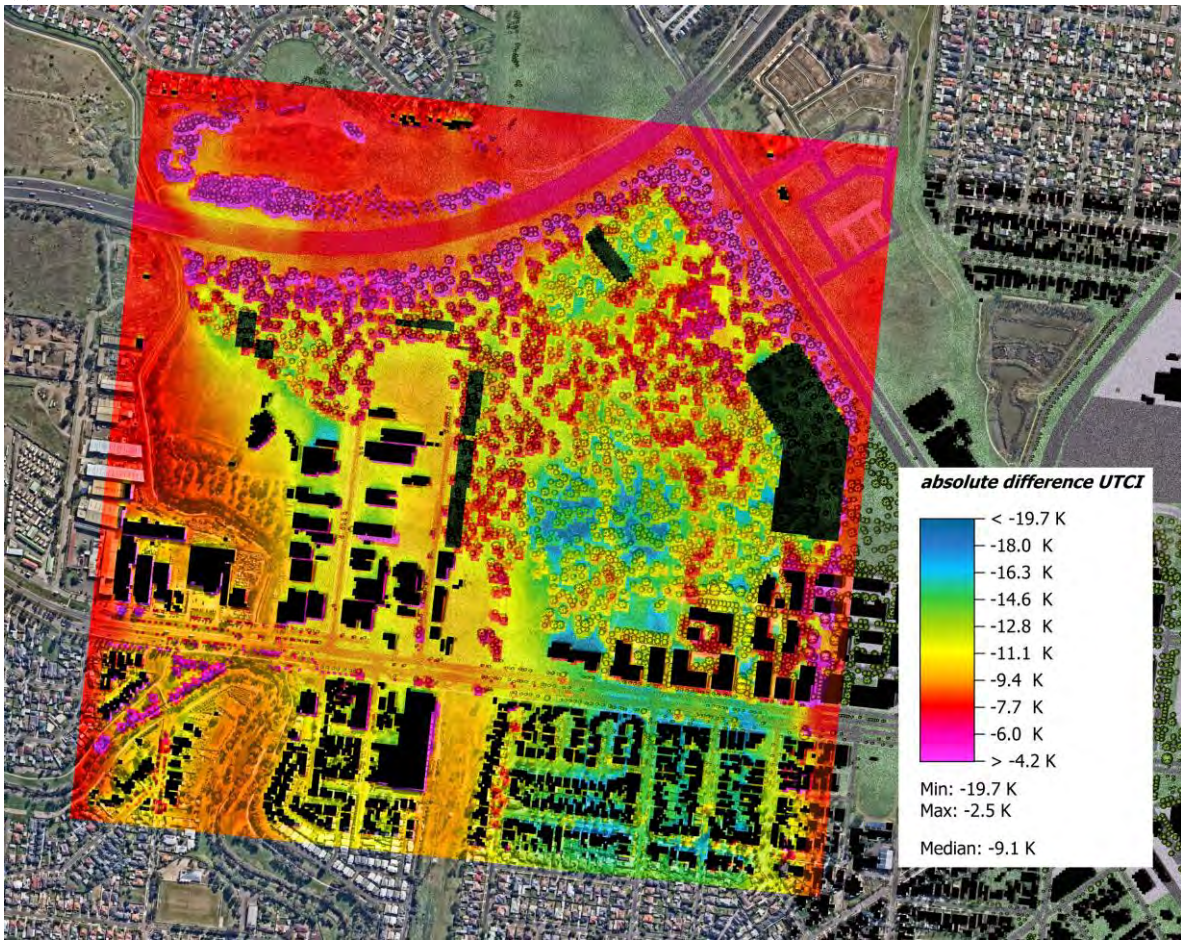

(b)

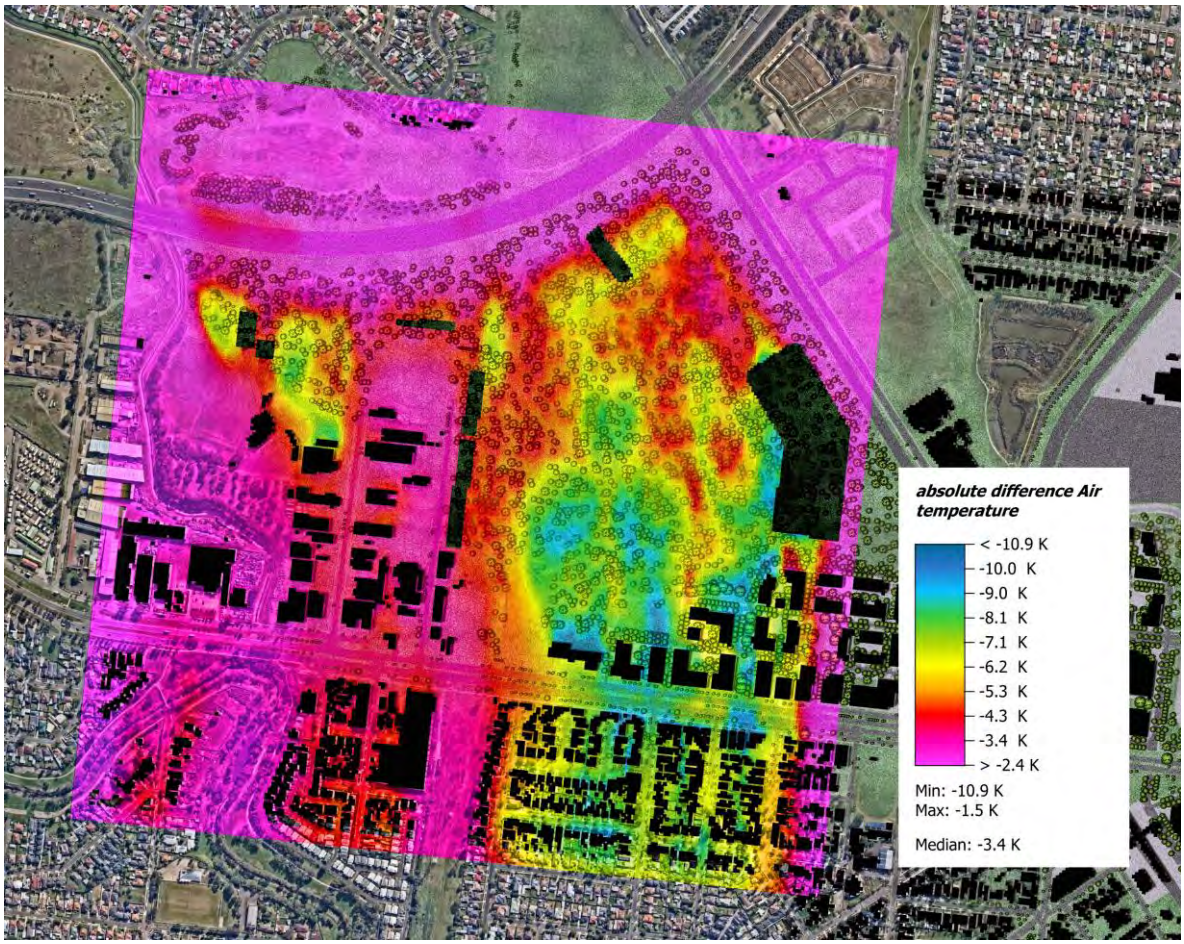

Figure 2.26. Thermal performance comparison between the base case and the developed design of the Energy Park during the hottest hour in 2050 at the pedestrian level. (a) thermal comfort, (b) air temperature

2.6.2 Comparison between Base Case and BAU

The updated Albion Quarter design increased the floor area and height of buildings, mainly on the north side of Ballarat Road. This change introduced taller, more continuous building forms and narrowed the spacing between buildings and streets, resulting in higher temperatures on that side of the area due to trapped airflow between the buildings, creating hot pockets (Figure 2.27). In addition, this change increased wind speed in the main N-S streets (see Figure 2.28) as airflow became more channelled between taller facades and the increased airflow resistance from the larger E-W facades. The housing area on the south side performed better than the north side, the opposite of the base case. This indicates that the new design at the north side of Ballarat Road negatively impacts the by increasing air temperature, restricting ventilation within E–W streets due to taller buildings and reduced street widths, and intensifying wind speeds along N–S corridors. These outcomes highlight the importance of urban layout decisions, particularly the provision of adequate spacing between buildings, discontinuous podium forms and the retention of open spaces that previously allowed lateral airflow and heat dissipation.

In addition, the increased heights of buildings further reduced airflow at higher levels and allowed for more radiation absorption by the building envelopes, contributing to higher local air temperatures and further modification of wind patterns within the precinct. Further, since the BAU scenario does not include irrigation, the cooling effect of vegetation was limited and only noticeable in exposed or heavily shaded areas. This pattern is evident in open spaces and street edges where tree shading reduced direct solar exposure, and in locations where wind exposure supported limited evapotranspiration. The first reason was the shading benefits of the trees. At the same time, the second result was influenced by evapotranspiration, which resulted from the regulated temperature caused by the building's shading and exposure to airflow with increased wind speed in N-S streets, facilitating the process. Lastly, there was a noticeable cooling effect in Stony Creek on the south side of Ballarat Road, with temperatures dropping by up to 5.2 °C around the entire Creek and its surrounding open spaces, due to the presence of a narrow waterline, wet gravels, and mud at this location. In contrast, the north side of Ballarat Road contains limited vegetation and little available surface moisture, which restricts evaporative cooling and contributes to higher temperatures. The cooling effect does not travel far from this area because the buildings on the south side obstruct the airflow. This reinforces that effective cooling at the precinct scale depends not only on irrigation and water-sensitive landscapes, but also on facilitating wind flow to allow cooled air to spread beyond its source. Seasonal performance should also be considered, as increased wind exposure may be beneficial for summer cooling but may require mitigation in winter to maintain pedestrian comfort.

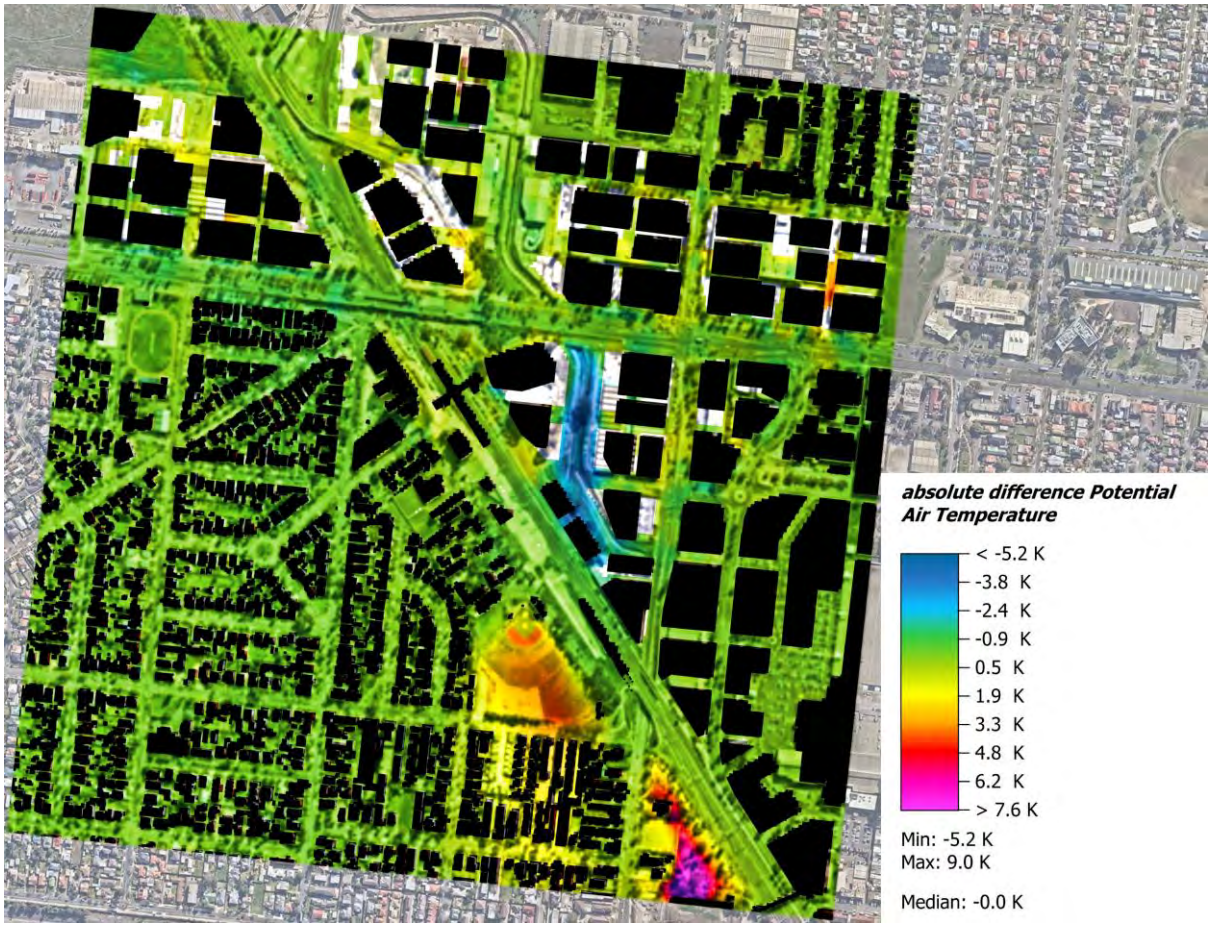

Figure 2.27. Comparison between Base Case and BAU, Air temperature during the hottest hour at 1.5m height

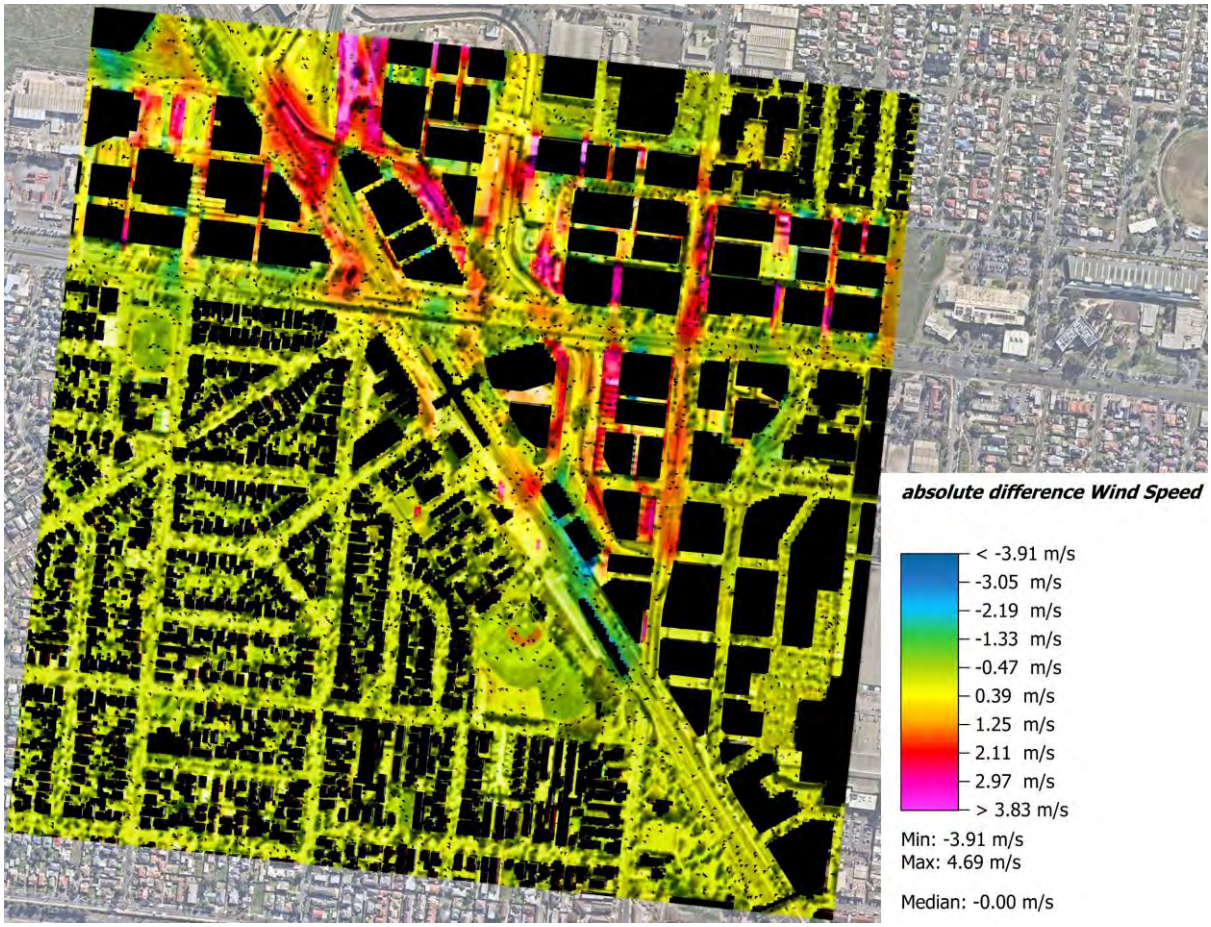

Figure 2.28. Comparison between Base Case and BAU, Wind speed and direction during the hottest hour at 1.5m height

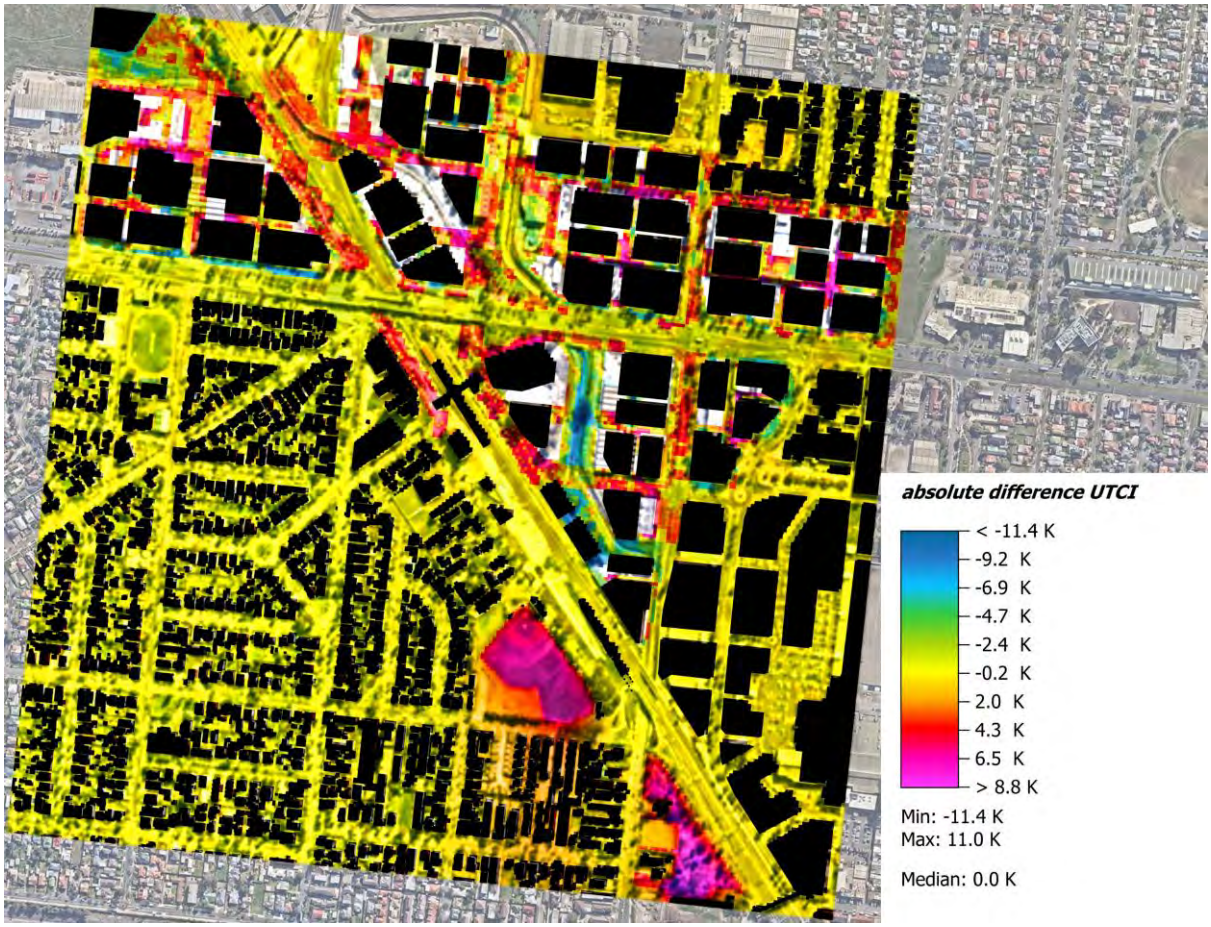

Figure 2.29. Comparison between Base Case and BAU, UTCI during the hottest hour at 1.5m height

2.6.3 Comparison between BAU and RIC

The RIC includes increased canopy coverage by prioritising overlapping tree canopy, with additional structural soil to support tree growth. These trees and the open public spaces are irrigated to reach up to a 20% soil moisture level, enhancing the cooling effect and facilitating their development. It can be noticed from the illustrated results in Figure 2.30 that the irrigated open spaces and street trees have positively enhanced the cooling effect by reducing the temperature up to 4.2 °C.

The results indicate that larger, continuous irrigated open spaces generate cooling effects that extend further into the surrounding precinct, whereas smaller irrigated areas produce more localised benefits. It was also observed that some locations experienced an increase in air temperature up to 1 °C. The increase was due to the creation of hot pockets and the reduction of passive cooling due to obstructed airflow from the overlapped canopy, (see Figure 2.31). This outcome highlights that increased canopy coverage alone does not always lead to lower air temperatures if it significantly restricts ventilation. While dense canopy may still deliver important shading and amenity benefits, particularly during extreme solar exposure or in winter wind mitigation, its effectiveness for heat reduction during heatwaves depends on its interaction with airflow. This observation is consistent with previous studies that emphasise the need to balance shading provision with the preservation of ventilation pathways in urban environments (Middel et al., 2015; Ng & Cheng, 2012).. In this scenario, the competing effects of irrigation-driven cooling and canopy-induced airflow obstruction resulted in a limited average air temperature reduction of 0.1 °C across the precinct. This outcome demonstrates the limits of relying

on trees and irrigation alone without concurrent consideration of their placement relative to airflow patterns and built form.

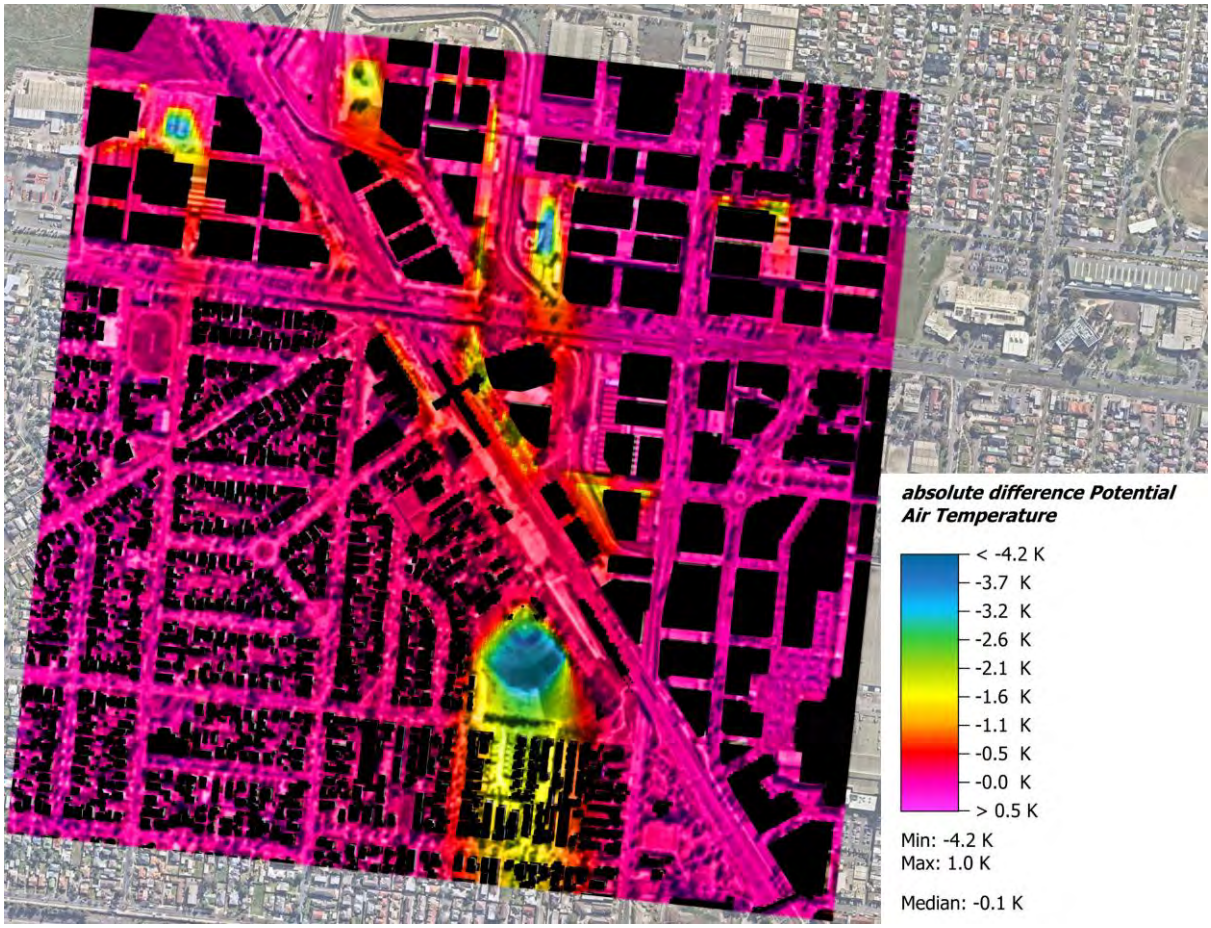

Figure 2.30. Comparison between BAU and RIC, Air temperature during the hottest hour at 1.5m height

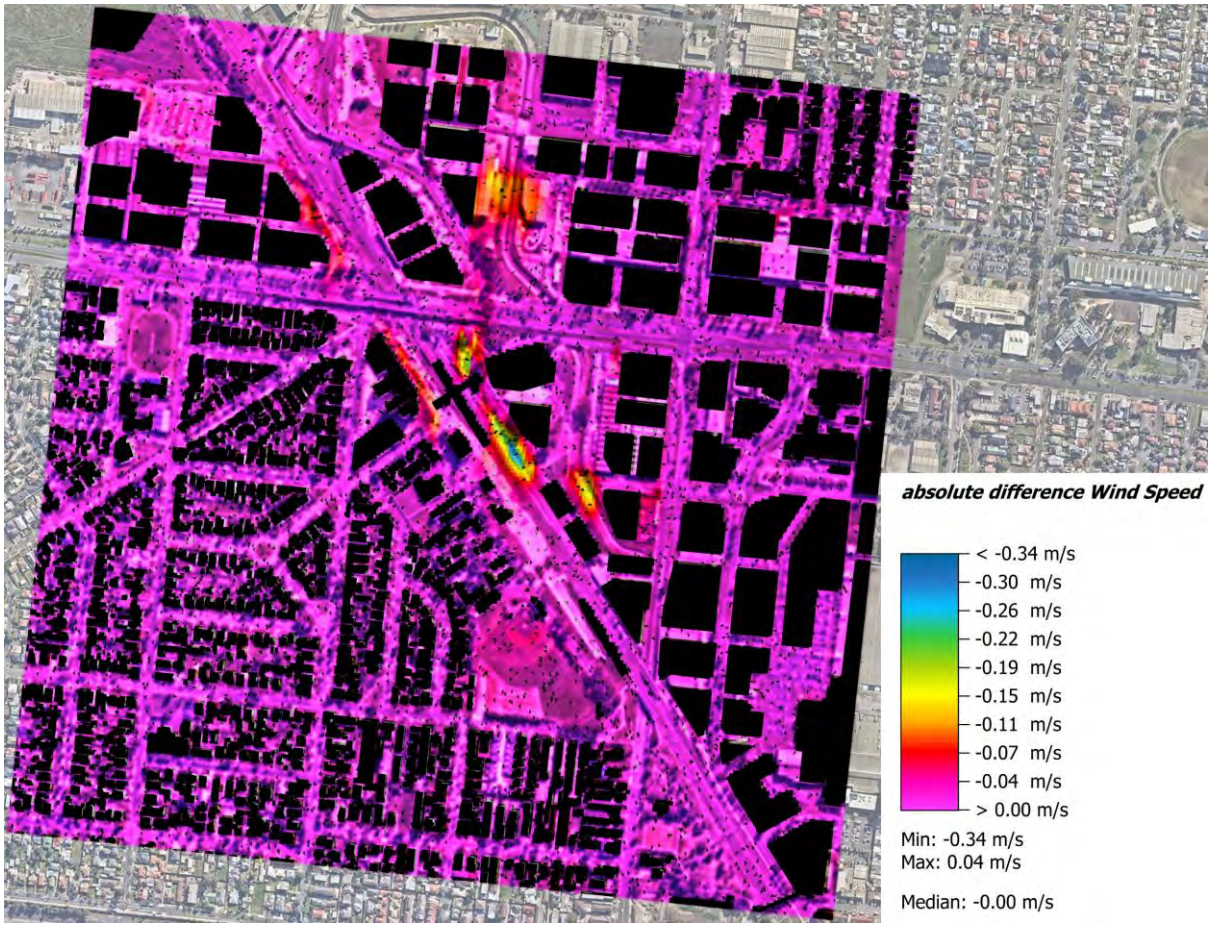

Figure 2.31. Absolute wind speed and direction showing the differences between the BAU and RIC at 1.5 m above the ground level

The thermal comfort followed a similar pattern to the air temperature changes (see Figure 2.32). The reduction was mainly above and around the irrigated open areas up to 8.1 °C. In the main streets where the irrigation and extra trees were added, there was also a reduction of up to 4.9 °C. However, increases were observed across several other locations, reaching up to 2.6 °C, due to obstructed airflow caused by the interaction between the built form and overlapping canopy, as shown in Figure 2.31. These areas largely correspond to locations where the urban form limits ventilation, and this pattern is consistent with the Base Case, although the magnitude of change is slightly altered by the additional trees and irrigation. When averaged across the entire modelled area, the localized increases and decreases offset one another, resulting in limited average thermal comfort reduction up to 0.1 °C at the precinct scale. This outcome reflects spatial redistribution of comfort conditions rather than uniform improvement or degradation, with substantial local benefits in irrigated areas counterbalanced by minor increases in other locations, as can be seen in Figure 2.32.

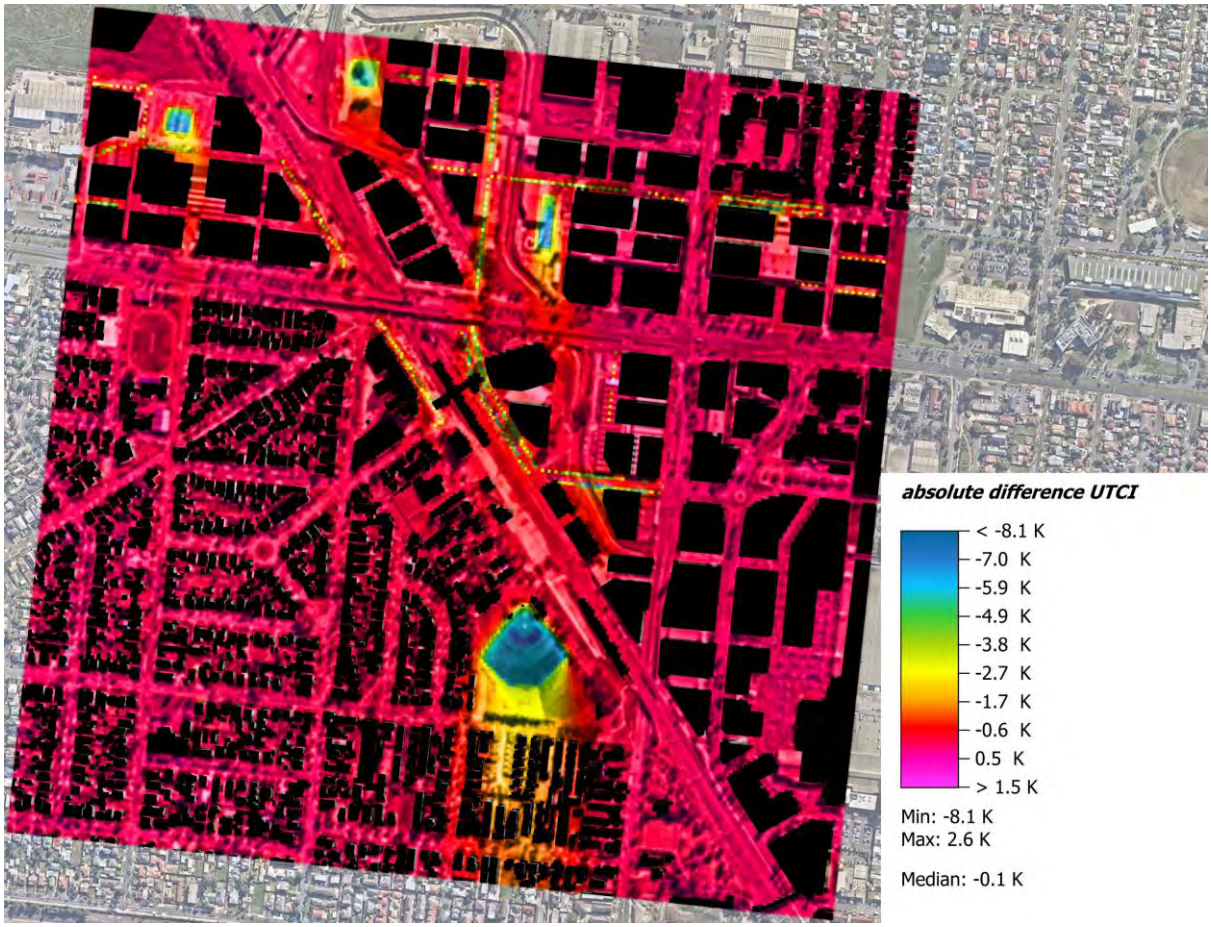

Figure 2.32. Absolute UTCI differences between BAU and RIC at 1.5 m above the ground level.

2.6.4 Comparison between BAU and BIC

The BIC includes similar enhancements to the RIC, while the irrigation increased to reach up to 30% for the street trees and open spaces. In addition, it provides irrigation up to 20% for private open spaces. After analysing RIC, it was observed that the increased canopy affected airflow. Consequently, active tree placement was introduced as part of the BIC, and some trees at critical locations that hindered airflow or created hot pockets were rearranged to improve ventilation and facilitate passive cooling. This targeted adjustment resulted in localised airflow enhancement in these specific locations (see Figure 2.34). The enhanced airflow and increased irrigated area both played a vital role in improving cooling, which reached up to 8.4 °C (see Figure 2.33), including an additional reduction of 4.2 °C compared to the RIC as explained earlier in the above section. This new arrangement also reduced the air temperature in the hot pockets by up to 2.9 °C. These cooling effects were strongest in and immediately downwind of the irrigated and ventilated areas, with influence diminishing with distance, consistent with the airflow patterns observed in the model. While the average air temperature across the entire precinct decreased by approximately 0.2 °C, this value reflects spatial averaging across heterogeneous conditions rather than the magnitude of localised benefits. The key performance improvement of the BIC lies in the substantial cooling achieved in targeted high-risk locations rather than a uniform precinct-wide reduction.

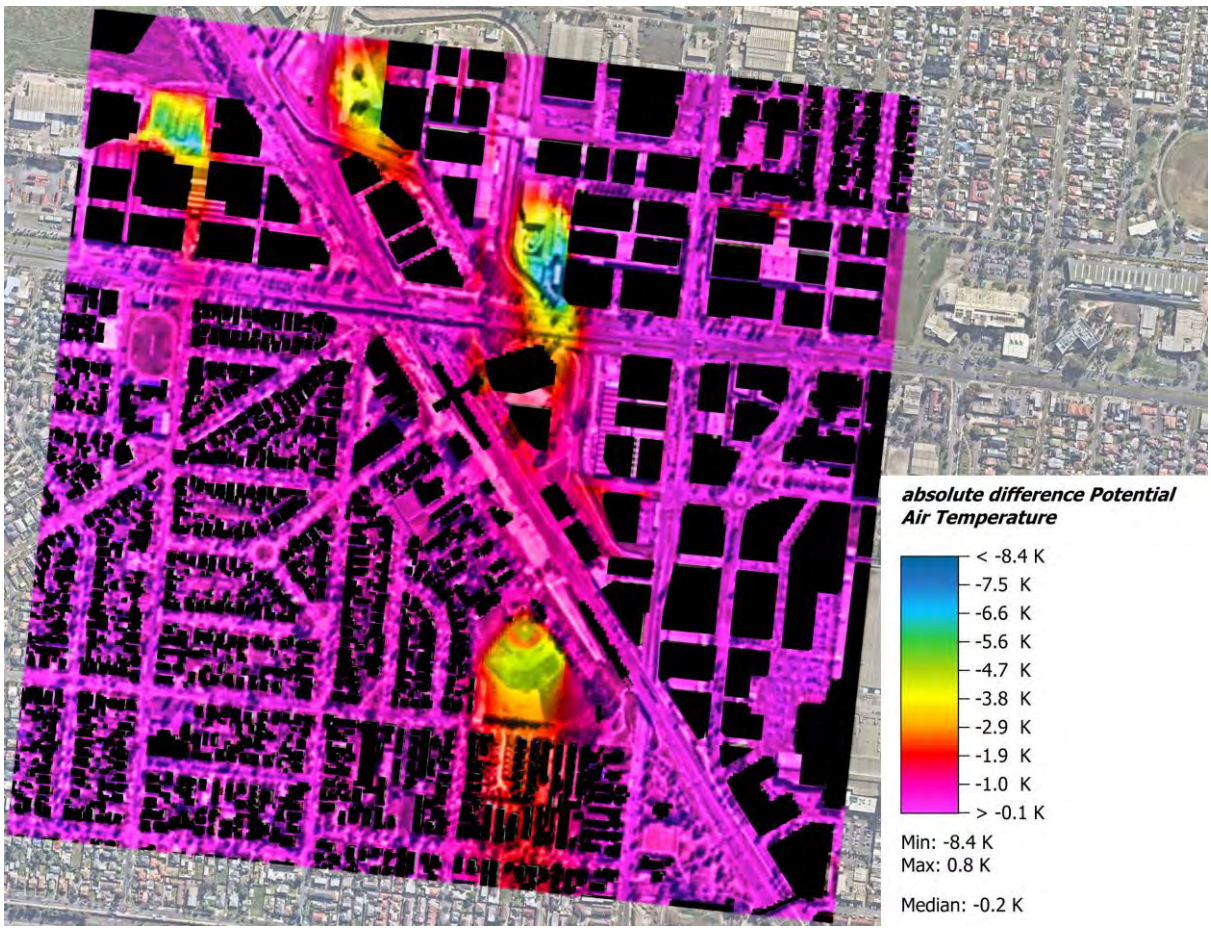

Figure 2.33. Comparison between BAU and BIC, Air temperature during the hottest hour at 1.5m height

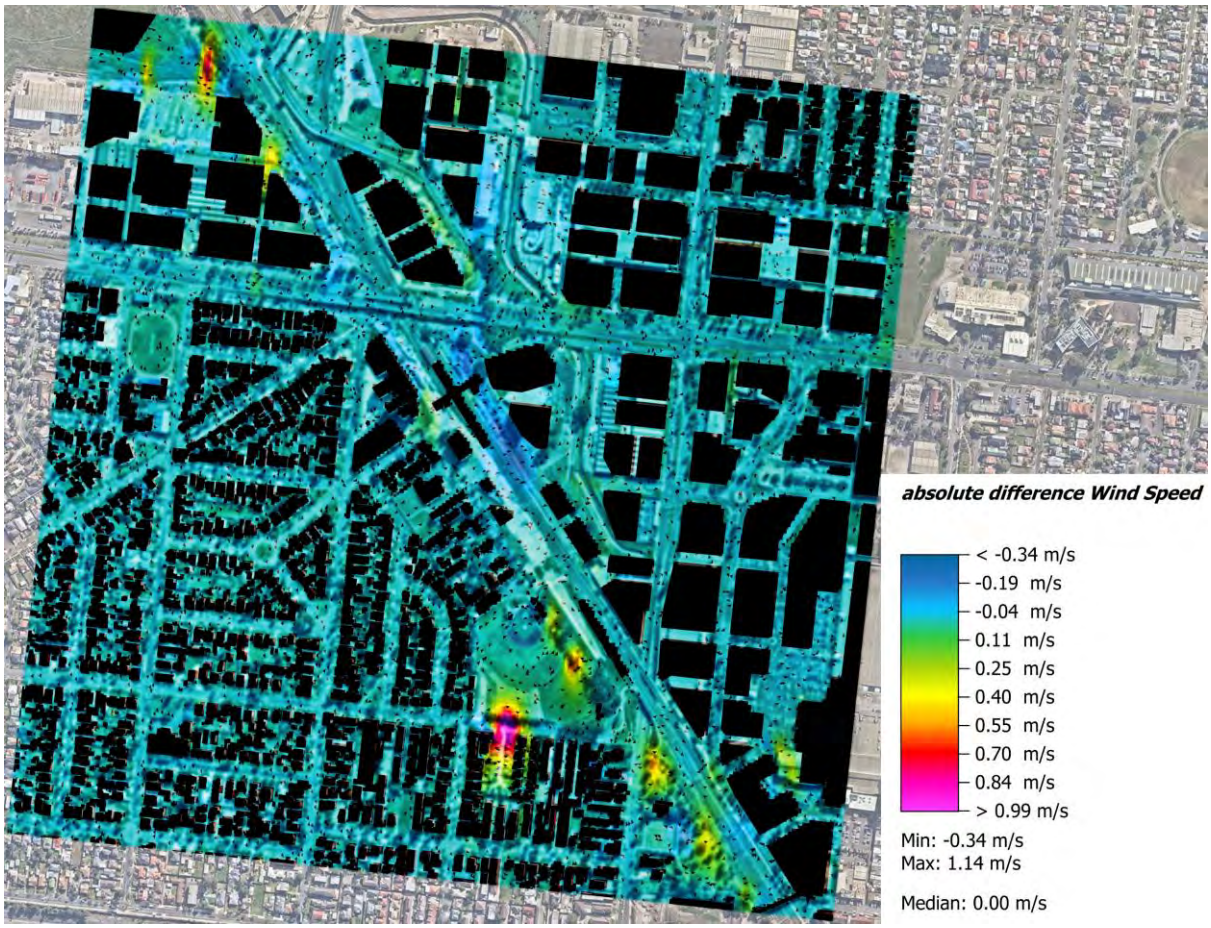

Figure 2.34. Absolute wind speed and direction showing the differences between the BAU and BIC at 1.5 m above the ground level

Similar to the RIC, the UTCI followed a similar pattern to the air temperature (see Figure 2.35). The reduction was greatest above and around the irrigated open spaces, reaching up to 11.6 °C. These reductions represent substantial, material improvements in thermal comfort within the irrigated zones and their immediate surroundings. It can also be noticed that the reduction spread more after the irrigated spaces up to 200 m and reduced by at least 1 °C following the airflow. Notably, the reduction on the streets was 3.5 °C, compared to 1.9 °C in RIC, due to changes in the canopy in the targeted locations. While the average reduction across the entire development was approximately 0.2 °C, this value reflects spatial averaging rather than the effectiveness of the intervention. The primary benefit of the BIC lies in the significant localised reductions achieved near irrigated open spaces and along ventilation corridors, rather than a uniform precinct-wide improvement. These results indicate that extending comfort benefits to areas further away would require either additional strategically located irrigated open spaces, changes to built form to facilitate airflow, or a combination of both.

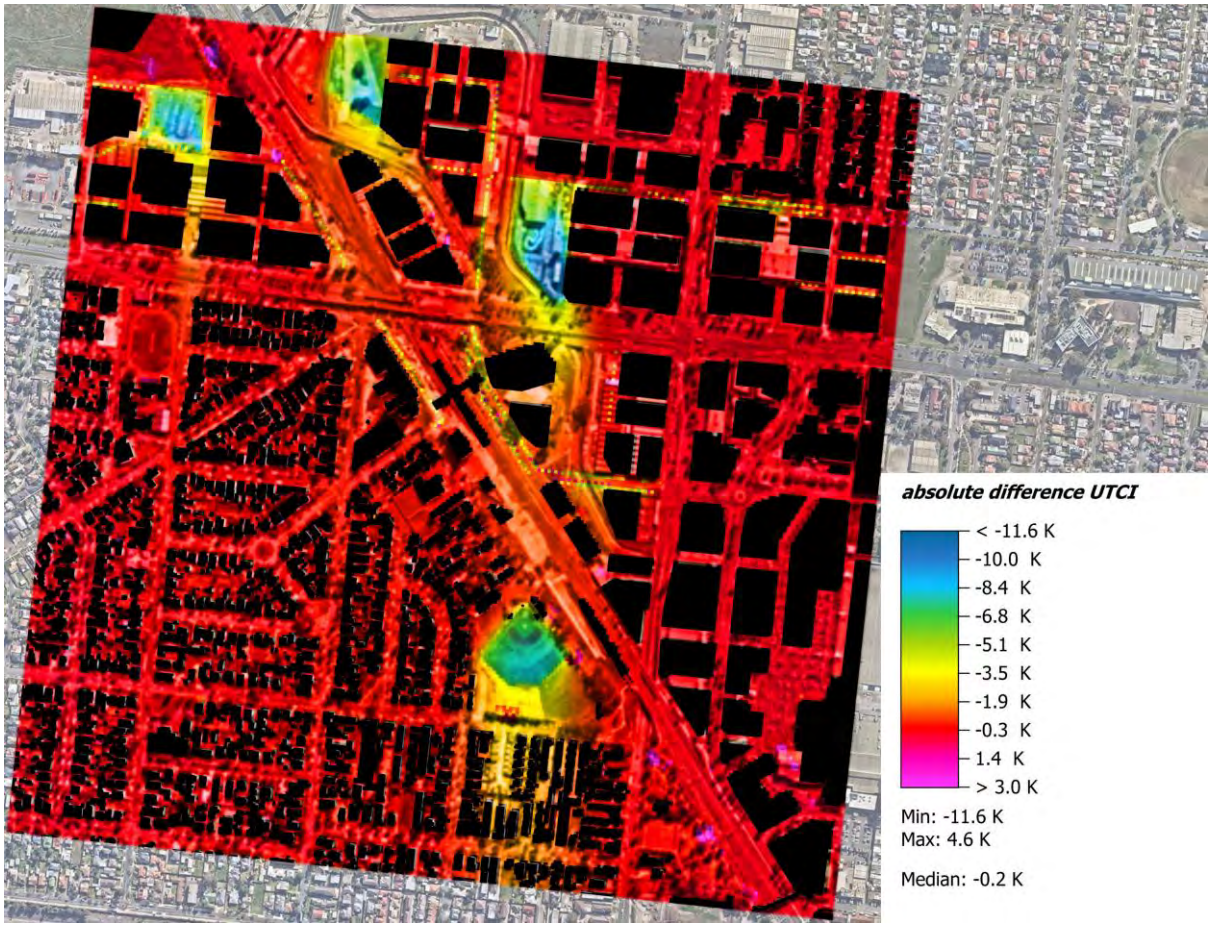

Figure 2.35. Absolute UTCI differences between BAU and BIC at 1.5 m above the ground level.

2.6.5 Comparison between RIC and BIC

The accumulated cooled air from the irrigated public spaces, along with the cooled air from the irrigated private open spaces, resulted in an overall reduction in three locations, where the irrigation is introduced, by up to 7.5 °C. While in the RIC, the enhancement in air temperature was localised (see Figure 2.36). The removal of some trees to improve airflow helped distribute the cooling effect further toward the south, although the resulting reduction in the precinct-wide average air temperature was modest (approximately 0.1°C). This value reflects spatial averaging across the entire modelled area rather than the magnitude of the localised cooling benefits. These findings reinforce that airflow plays a critical role in determining how far cooling benefits can propagate beyond irrigated areas. While targeted tree placement alone does not produce a large precinct-wide temperature reduction, it influences the spatial distribution of cooling. Decisions regarding tree placement should therefore consider canopy density, ventilation pathways and broader urban form, rather than pursue uniform planting.

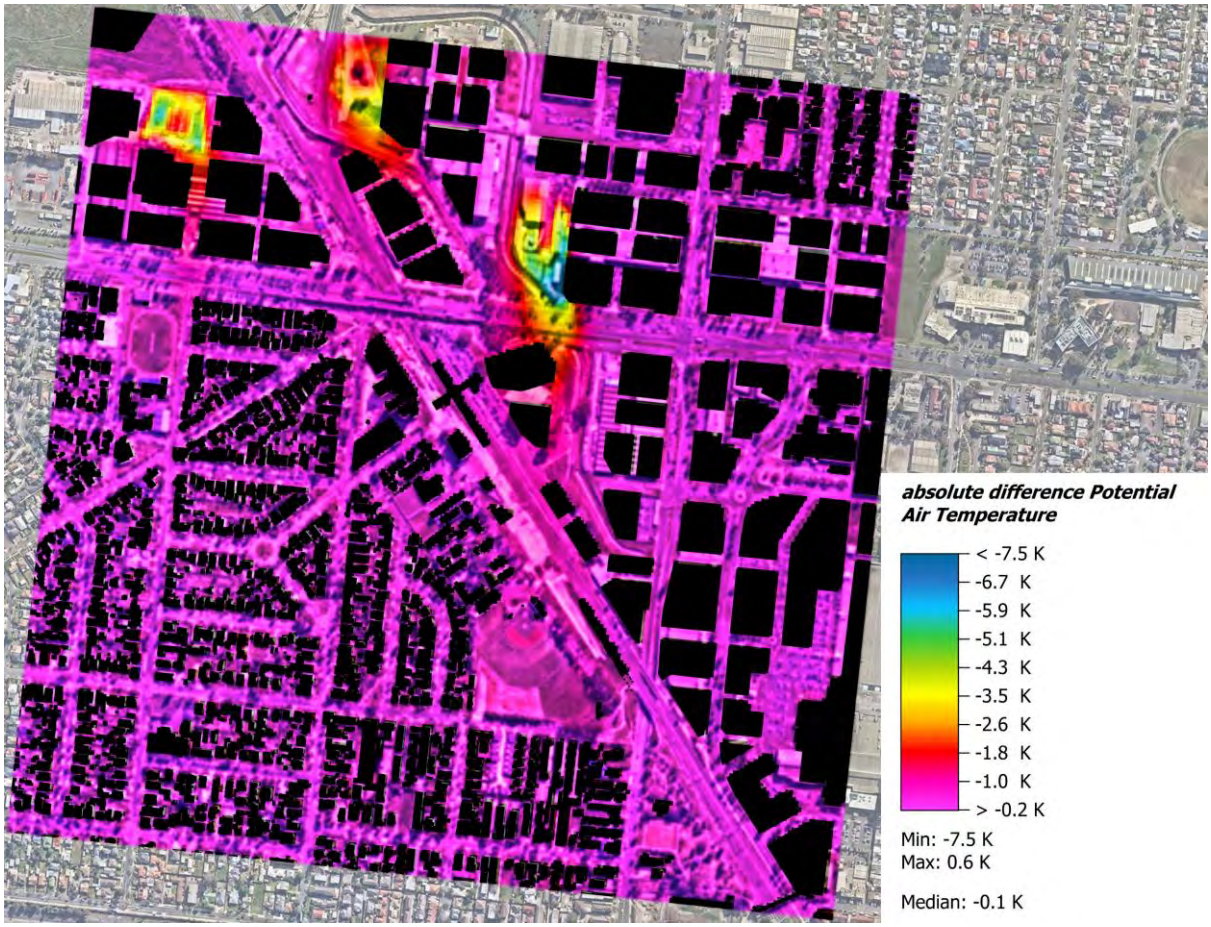

Figure 2.36. Comparison between RIC and BIC, Air temperature during the hottest hour at 1.5m height

It can be seen in Figure 2.37 that the removal of some of the trees, which obstructed the airflow in RIC helped in facilitating the cooling by increasing the wind speed by 1.14 m/s, which also facilitates moderating the high wind speed in N-S open corridors with the same values, this supports the previous results and recommendations of the importance of providing a balanced open corridor to mitigate the high wind speed and enhance the ventilation.

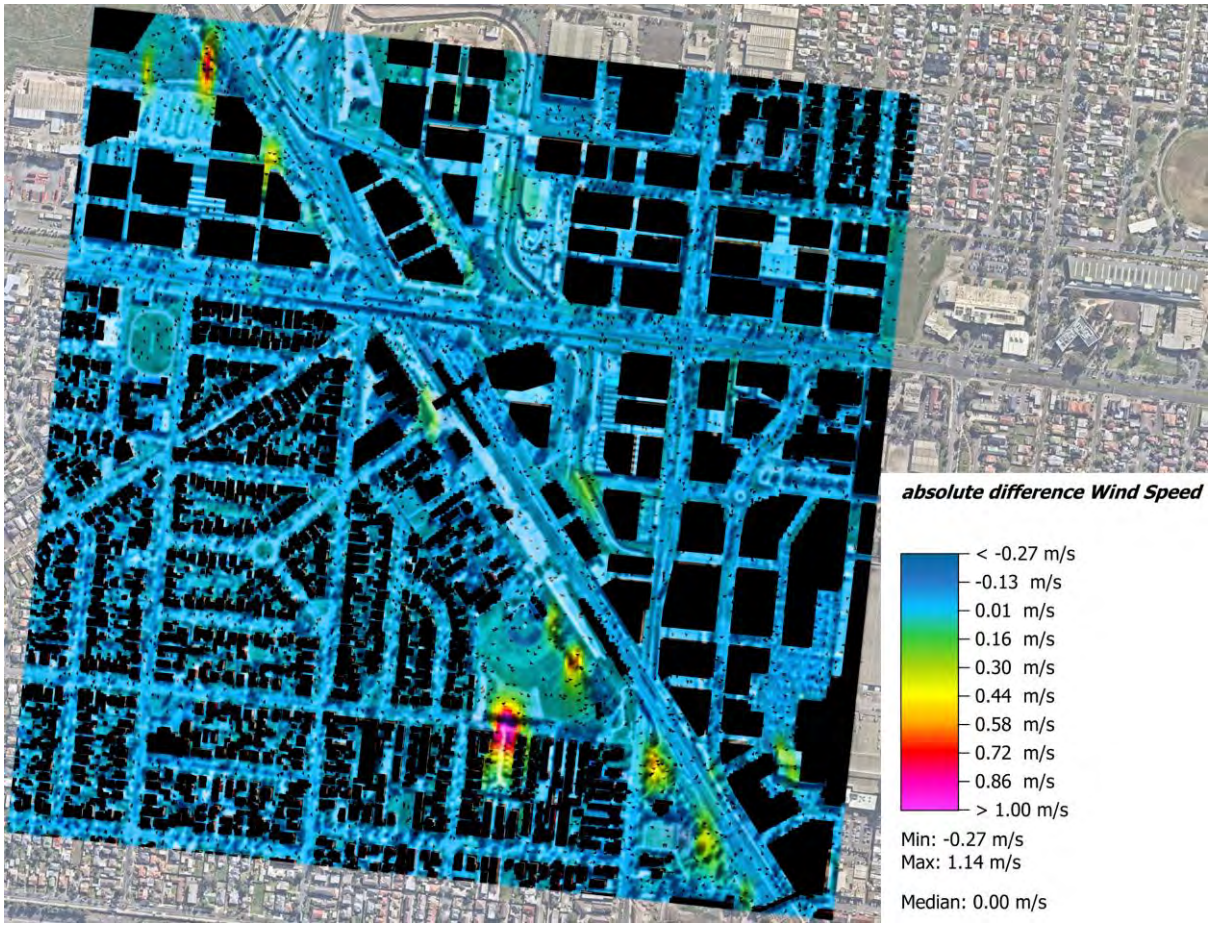

Figure 2.37. Absolute wind speed and direction showing the differences between the RIC and BIC at 1.5 m above the ground level

On the thermal comfort level, it can be seen in Figure 2.38 that the enhancements in BIC were totally positive and resulted in reductions up to 10.7 °C above and around the newly irrigated areas, and the reduction of the tree coverage did not contribute to temperature increase. This supports the previous results and recommendations that increasing the canopy cover does not always contribute to temperature reduction, while in some cases, reducing the canopy cover, specifically to facilitate the airflow, could result in temperature reduction. It is important to note that only very modest reduction in tree canopy at specific, strategic locations – particularly around irrigated spaces – is required to achieve this effect. For example, this might involve removing a few trees in a long row of tree canopy to allow airflow. Whether this is appropriate in specific locations needs to be weighed against the imperatives for shading and the amenity benefit of trees in these locations.

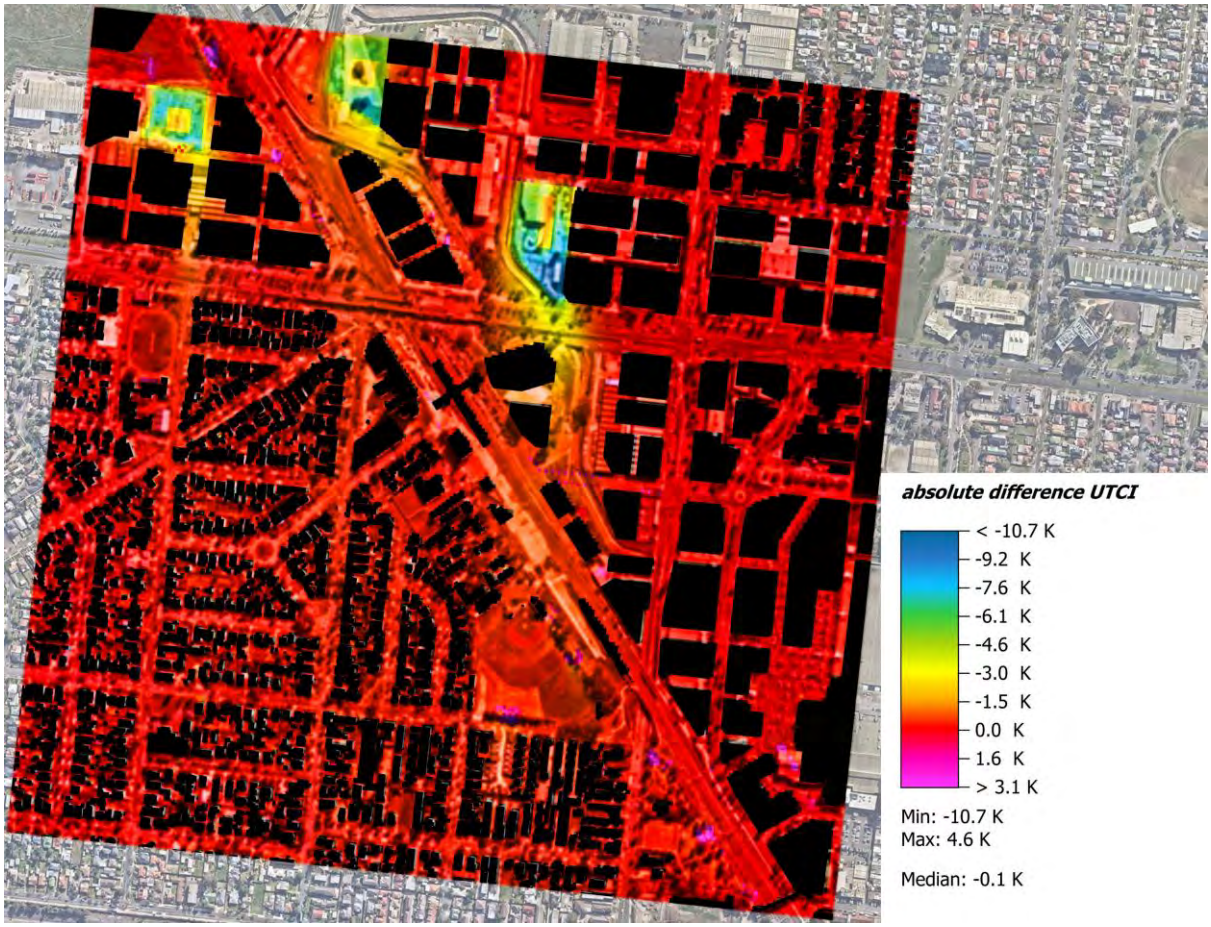

Figure 2.38. Absolute UTCI differences between RIC and BIC at 1.5 m above the ground level.

3. Water Results

Expanding urban canopy cover can help address the impacts of climate change and urbanisation. A dense and healthy tree canopy provides amenity while offering shade for pedestrians and contributing to local cooling through shade and evapotranspiration. Under heatwave conditions, human thermal stress reflects the combined influence of air temperature, radiation, humidity and wind, with the relative importance of each factor varying across locations. Tree canopy shade contributes to reducing radiant heat load, while water-based interventions support additional cooling through evaporative processes.

The CSIRO predict Melbourne's west will have more frequent high temperature extremes and less rainfall in 2050. Achieving a future resilient and broad canopy cover in a priority precinct like Sunshine, that has a low tree canopy cover today, is challenging.

The drive for significant housing and employment growth creates competition for space, directly constraining greening efforts by limiting the areas available for permeable soil and water infiltration. Increased temperatures and reduced rainfall pose a direct threat to maintaining, let alone increasing, urban tree canopy. In Sunshine, a projected 13% decrease in annual rainfall and a 10% increase in evapotranspiration due to rising temperatures creates a growing gap between rainfall water supply and plant water demand.

A key challenge in planning for the Sunshine Precinct is how to create a climate-resilient and comfortable living environment under these pressures and competing priorities. This section considers the practical challenge of achieving a 30% tree canopy target outlined in the Victorian Government's *Plan for Victoria* policy, through an assessment of the precinct's tree canopy potential under different soil volumes, water availability, solar access and space competition constraints. In addition, this section assesses the potential water supply implications of irrigating urban green spaces in the Sunshine precinct for cooling objectives.

The policy focus in this area is:

- Amenity - achieving sufficient tree canopy coverage to provide liveability
- Heat mitigation – providing sufficient shading of pedestrians and reducing air temperatures (either through cooling from tree canopy shade and transpiration or evapotranspiration from water used in irrigation of urban green spaces).

The research intent was to understand future urban and climate conditions, to test what strategies were most effective to achieve a high tree canopy and adequate water supply for tree health and active cooling.

Results presented in this section are based on an initial assessment (base case), a set of alternative scenarios and the updated scenario.

The base case involved a Macro-Scale Assessment that considered the base case urban form provided by DTP. A set of alternative scenario cases was then considered for streets, public open spaces and park tree planting strategies to evaluate the practical feasibility of achieving the target canopy

outcomes. Streets were considered in the most detail as they offer the greatest opportunity for direct government intervention through detailed planning policies, such as mandating wider verges, specifying soil volumes, and integrating irrigation systems.

The updated scenario considers three distinct zones based on their unique characteristics, management structures, and development constraints: streets, public open spaces, and private lands. This zoned approach allows for the development of tailored strategies that address the specific challenges and opportunities within each landscape type. Details of the methodological approach and underlying data can be found in section 11.

3.1 Key findings and recommendations

3.1.1 Key findings

- Established areas like Sunshine Station and Sunshine Town Centre provide the least opportunity for increased greening and cooling. Providing additional space for trees requires expensive or technically challenging solutions like tree pits to support growing conditions. While these can likely be incorporated at strategic locations, it is less practical to do at a scale that could achieve a 30% canopy cover. Reprioritising road space provides the best opportunities for greater canopy cover here.
- Large sites and "brownfield" areas like Albion Quarter provide the greatest opportunity for increased tree canopy, however a typical planning approach of 10% of private land having deep soil planting, 6% of all land being open space and typical cross sections with 2m wide verges are unlikely to achieve a 30% canopy target. Requiring greater deep soil areas on private land and/or delivering a much higher percentage of open space provides the best opportunities for greater canopy cover here (Refer to Section 3.4.1 and summarized in Table 3.1)
- Investment in a 3-metre verge, structural soil, active and passive irrigation is important to create overlapping canopy. These investments are important to safeguard tree canopy in a future climate (Refer to Section 3.4.2.1)
- Active and passive irrigation of all street trees is important to address the growing rainfall deficit under climate change and the greater drought risks (Refer to Section 3.2.1)
- Building rooftops are unlikely to provide a significant source of alternative water supply for irrigation of public spaces as water captured is likely to be fully consumed by building operations and/or private gardens on site (Refer to Section 3.2.2)
- Not all areas in a high-density precinct are exposed to direct sunlight in summer so investment in overlapping canopy could be prioritised based around shading/street orientation (Refer to Section 3.4.2.2)
- Irrigation of open space for cooling requires supplementary water beyond rainfall and routine irrigation used for sports field maintenance; however, this additional water use can deliver co-benefits through reduced urban heat exposure and improved thermal comfort during extreme heat events (Refer to Section 3.3).
- Current soil provision (0.6 m^3 loam per m^2 canopy) is broadly adequate for low water use species but insufficient for medium water use trees, with summer water storage remaining well below the 50-day resilience benchmark and declining further under future climate scenarios; improving soil

quality and/or increasing soil volume can enhance summer water storage and partially improve resilience (Refer to Section 3.2.1).

3.1.2 Recommendations

- Invest in structural soil, active and passive irrigation and soil volume, particularly in priority areas for shading
- Invest in active and passive irrigation on all new streets to support tree growth
- Provide alternative water supply to support open space irrigation for cooling and active irrigation of street trees
- Consider options to provide more tree canopy on private land
- Increase soil volume and/or use higher quality soil to improve summer water storage

3.2 Base case scenario

3.2.1 Tree Water Demand

Figure 3.1 compares the annual water consumption per m² of canopy area (L/m² canopy/year) for medium and low water use street trees with the corresponding rainfall supply per m² of soil surface (L/m² soil/year) under three climate scenarios: current long-term average (C0), 2050 long-term average (C1), and a 2050 low decile year (C2).

For medium-water-use trees, the annual water demand consistently exceeds both total and effective rainfall across all climate scenarios. In contrast, while low-water-use trees consume less than the total annual rainfall, the effective rainfall is still insufficient, though the gap is smaller.

As outlined in Table 11.2, street trees and trees in public open space are generally assumed to be low water use species, while trees on private land could be either medium or low water use species. The figure shows that water availability is marginal even for low water use street trees when considered on a per-m² basis. In other words, the same square metre of soil surface is unlikely to fully support an equivalent square metre of tree canopy without supplementary water. Under current conditions (C0), effective rainfall is just sufficient to meet the annual demand of low water use species but falls short for medium water use species in all scenarios (C0, C1, C2).

The gap between total and effective rainfall highlights that not all rainfall contributes to plant water use. Losses result from interception of rainfall, seasonal mismatches between rainfall and demand, high-intensity events exceeding infiltration rates, and soils already at capacity. In sites with limited or no supplementary irrigation, low water use trees remain the most viable option; however, their reduced canopy density and transpiration rates also mean a lower cooling effect compared to higher water use species.

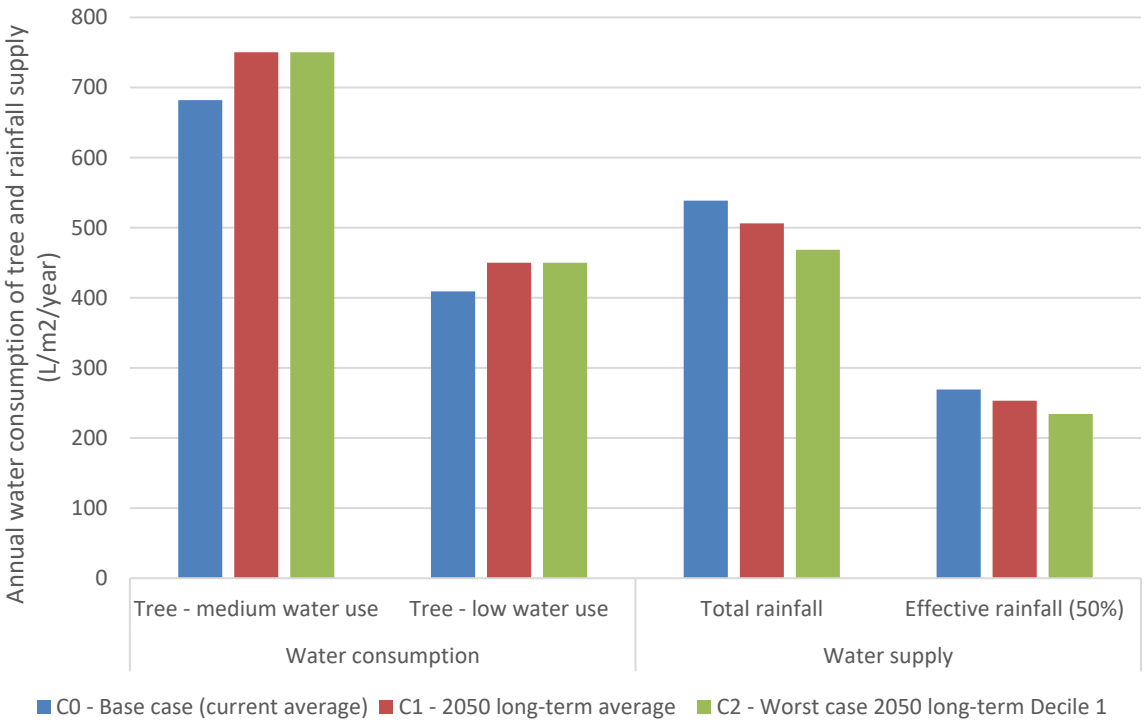

Figure 3.1. Annual water consumption of tree and rainfall supply (L/m²/year)

Given Melbourne's characteristic summer climate, which features long dry periods and only four to six days of effective rainfall per month, the capacity of soil to store water is a critical factor for urban tree survival. While abundant rainfall before summer can improve soil moisture, this reserve is often insufficient to sustain trees, particularly medium water use species, through the extended dry spells. Therefore, this section focuses specifically on analysing the number of summer water storage days provided by typical soil conditions.

The analysis reveals a critical relationship between tree selection, soil volume, and climate resilience. When compared against a performance target of 50 days of water storage, the standard soil provision of 0.6 m³ of loam per m² of canopy yields vastly different outcomes. As detailed in Figure 3.2, low water use trees are at or near the target, with 54 days of storage under current conditions and 49 days in future scenarios (+10% ETo). This indicates the current soil provision is generally adequate for these species although will become more marginal in a changing climate. In contrast, medium-water-use trees fall significantly short, with the same soil volume providing only 32 days of water storage currently, a figure that drops to 29 days under future climate projections.

This shortfall demonstrates that the standard soil provision is inadequate for medium water use trees. To meet the 50-day resilience target for these species, improvements to the soil environment are essential. As suggested in Figure 11.3, to achieve a higher summer storage target, it is necessary to provide a higher quality soil. For example, by using loam with higher organic content, an additional four days of storage for medium water use trees and an extra seven days for low water use trees can be provided. Increasing the soil volume available to each tree can also increase the resilience and help achieve the 50-day target.

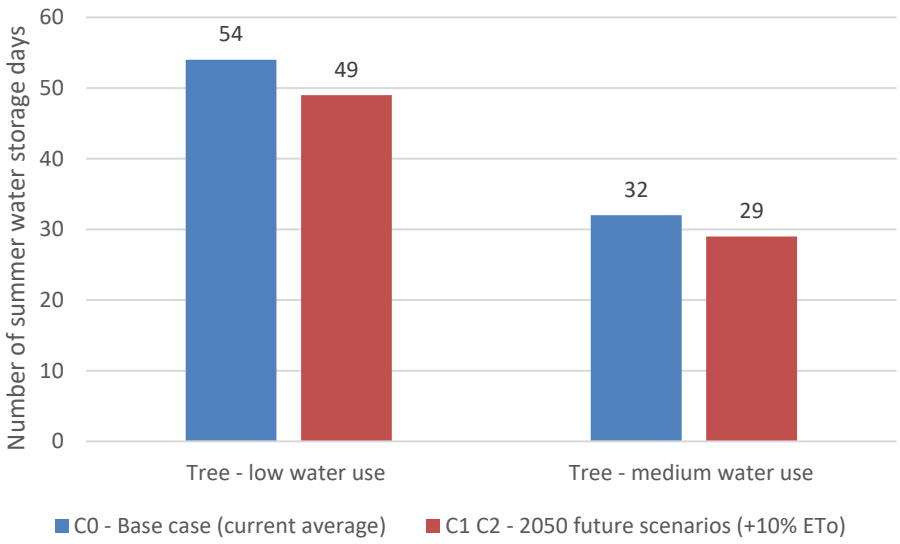

Figure 3.2. Number of summer water storage days under standard soil provision (0.6 m³/m² canopy)

3.2.2 Water capture results and implications

Based on the established tree design for the base case, an analysis of supplementary water availability was conducted. This analysis quantifies the potential annual rainwater capture from the two primary hard surfaces within the precinct: building roofs and roads. The calculation of the two rainwater capture methods is explained in Section 11.4.5 The results establish theoretical water resource available for irrigation under different climate scenarios.

In the base case, the spatial distribution of potential roof and road catchments is illustrated in Figure 3.3 which maps the road areas and roof areas of proposed residential and commercial towers within the Sunshine CBD, Albion Quarter, and Sunshine Station precincts. The total road surface area is 332,046 m², while the total roof area for all proposed buildings is 375,217m².

Figure 3.3. Maps of building roof (left) and road (right) capture for the base case

Figure 3.4 presents the resulting capture volumes. Under current conditions (Co), building roofs could capture approximately 76 ML/year and roads an additional 36 ML/year, giving a combined total of 112

ML/year. In the 2050 long-term average scenario (C1), capture potential decreases slightly to 72 ML/year from roofs and 34 ML/year from roads. In the 2050 worst-case low decile scenario (C2), capture potential reduces further to 66 ML/year from roofs and 31 ML/year from roads.

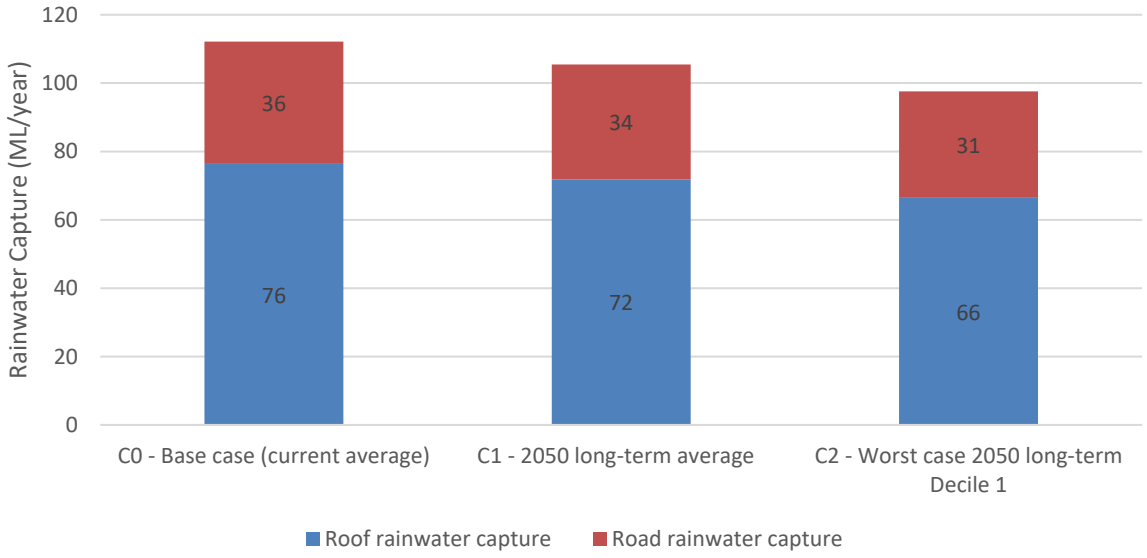

Figure 3.4. Roof and road rainwater capture (ML/year) in the base case

Figure 3.5 shows the total annual water consumption of residential and commercial buildings within the study area. For residential buildings, consumption is calculated using a rate of 0.12 ML per dwelling. Across 142 proposed residential buildings, accommodating 6,049 dwellings, this equates to an estimated total demand of 726 ML/year. Commercial building consumption is based on a total gross floor area (GFA) of 231,621 m² across 67 buildings. Historical data indicate that prior to 2021, commercial water use averaged 363 L/m²/year (equivalent to 83 ML/year). More recent consumption data from 2023–2024 show a reduced rate of 191 L/m²/year (equivalent to 44 ML/year).

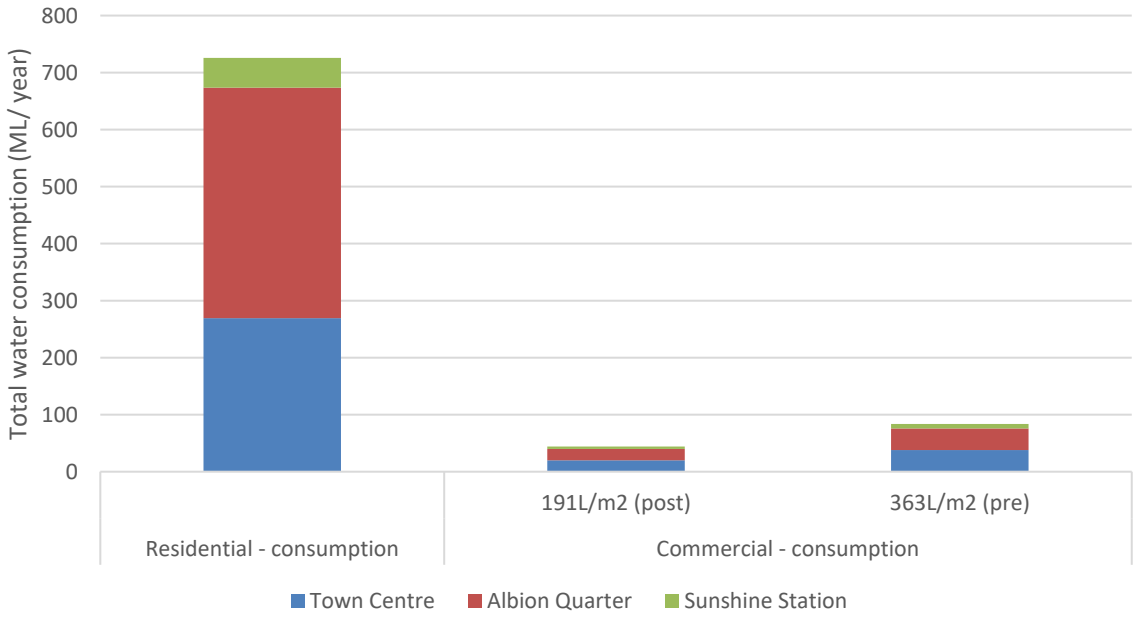

Figure 3.5. Total water consumption of residential and commercial towers (ML/year) in the base case

As shown in the results, there is a substantial imbalance between the buildings' internal water demand and roof capture. Therefore, it is highly probable that harvested rainwater will be prioritized for internal building operations, such as greywater systems. Given these constraints, it is unrealistic, in this specific precinct, to consider building roof runoff as a reliable, large-scale supplementary water source for public assets like street trees and parks.

In the S3 model, taller buildings drive higher on-site demand, widening the gap further between roof capture and building consumption. In this situation rooftop harvesting from private residential buildings that are retained on parcel is unlikely to provide a meaningful surplus for public-realm irrigation. Depending on development patterns there may still be some low rise commercial and industrial buildings or other infrastructure, from which roof water could be captured, however this is less certain.

Given the above, subsequent scenario testing in this report moves to focus specifically on the potential of road capture. This focused approach allows for a detailed and practical analysis of how this viable water source can be harnessed to address the growing rainfall deficit and support the health of the precinct's public green infrastructure.

3.3 Alternative scenarios – Irrigation for active cooling

While a dense tree canopy is foundational for providing shade and baseline cooling, its effectiveness can be limited during prolonged heatwave conditions when trees are under stress. In contrast, the targeted irrigation of green open spaces can significantly reduce ambient air temperatures through evaporation, offering a critical heat mitigation strategy when it is needed most.

Figure 3.6 demonstrates the comparison between annual water consumption of different grass and effective rainfall supply under three climate scenarios. The highest quality of grass is the most water-intensive, which requires around 11 ML/ha/year under current conditions, increasing to 12 ML/ha/year in future scenarios. Mid-range irrigation for sports turf requires roughly 8–9 ML/ha/year, while unirrigated grasses, typically warm-season species such as kikuyu and couch, consume about 4 ML/ha/year, drawing primarily on rainfall. This intensive water use is directly tied to a key trade-off: irrigated grass uses more water but provides cooling, whereas dry, unirrigated grass uses less water but has a hotter surface and contributes to higher air temperatures.

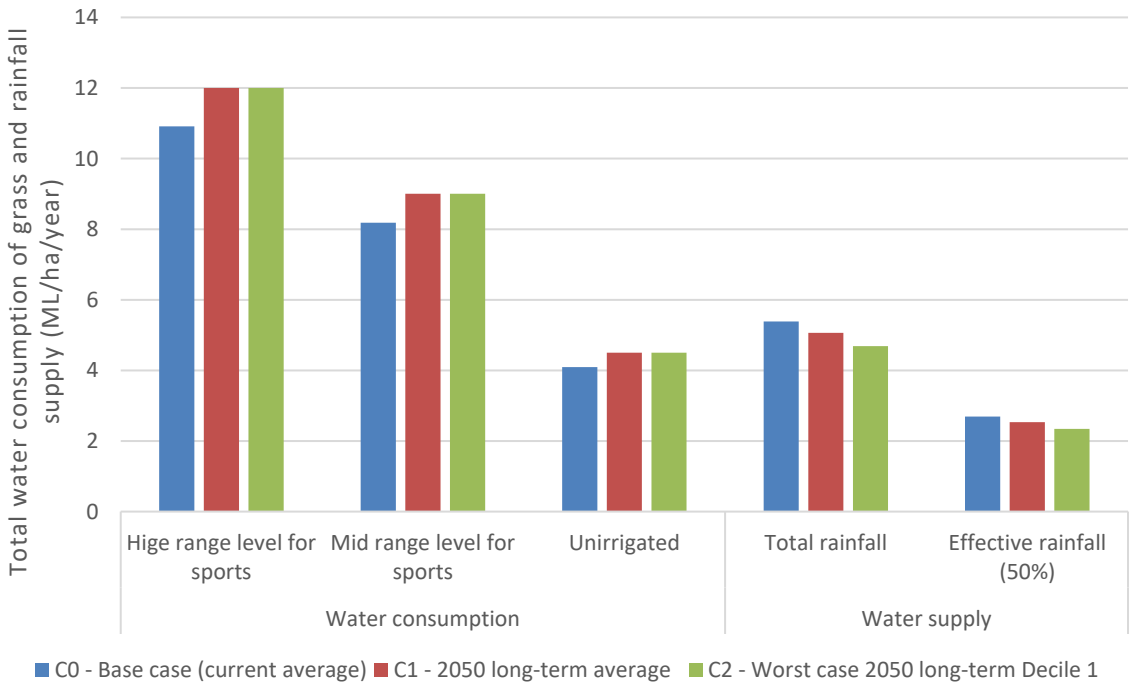

Figure 3.6. Total water consumption of grass and rainfall (ML/ha/year)

To calculate the water demand for this strategy, a targeted approach was modelled. Supplementary irrigation is applied only on days of extreme heat, defined as when the temperature reaches or exceeds 35°C. Under the future climate scenarios, this is predicted to occur approximately 20 days each summer. An annual water use rate of 3.75 ML per hectare has been assumed for cooling purposes.

3.3.1 Energy Park irrigation

The additional cooling method was applied to scenario testing for Energy Park. The base case scenario was replaced with an alternative scenario with sports ovals and fields shown in bright green on the figure to the right, with heat modelling results shown in Figure 2.25 38. Irrigation was assumed for the sporting fields; however, this is contingent upon a specific caveat regarding Energy Park's landfill legacy. Site-specific irrigation management is required to regulate where water is held within the soil profile, thereby mitigating risks of instability or environmental contamination associated with the legacy site conditions.

Figure 3.7 provides a detailed breakdown of the resulting annual water budget for the proposed areas. It distinguishes between the base water supply from effective rainfall, the extra water needed for mid-level sports fields, and the total volume required for the active cooling strategy for C1 and C2 scenario. For the existing 5.66 hectares of irrigated land in Energy Park, this targeted approach requires an additional 21.2 ML of water per year dedicated solely to active cooling.

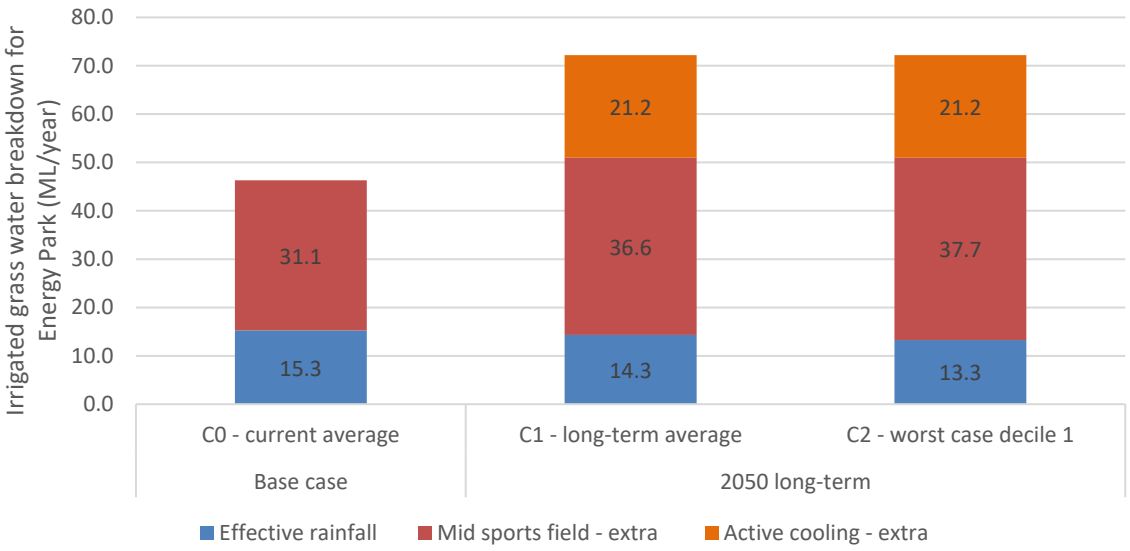

Figure 3.7. Grass water breakdown for the proposed irrigation area in Energy Park (ML/year)

3.3.2 Open space irrigation

The analysis focuses on the specific open space areas identified in Figure 3.8, which include a potential 3.07 hectares for future irrigation. The resulting annual water budget, detailed in Figure 3.9, shows that this targeted cooling strategy requires a substantial volume of water beyond effective rainfall and base irrigation for sports fields. For the proposed 3.07-hectare area for public open space, the strategy would demand an additional 11.5 ML of water per year.

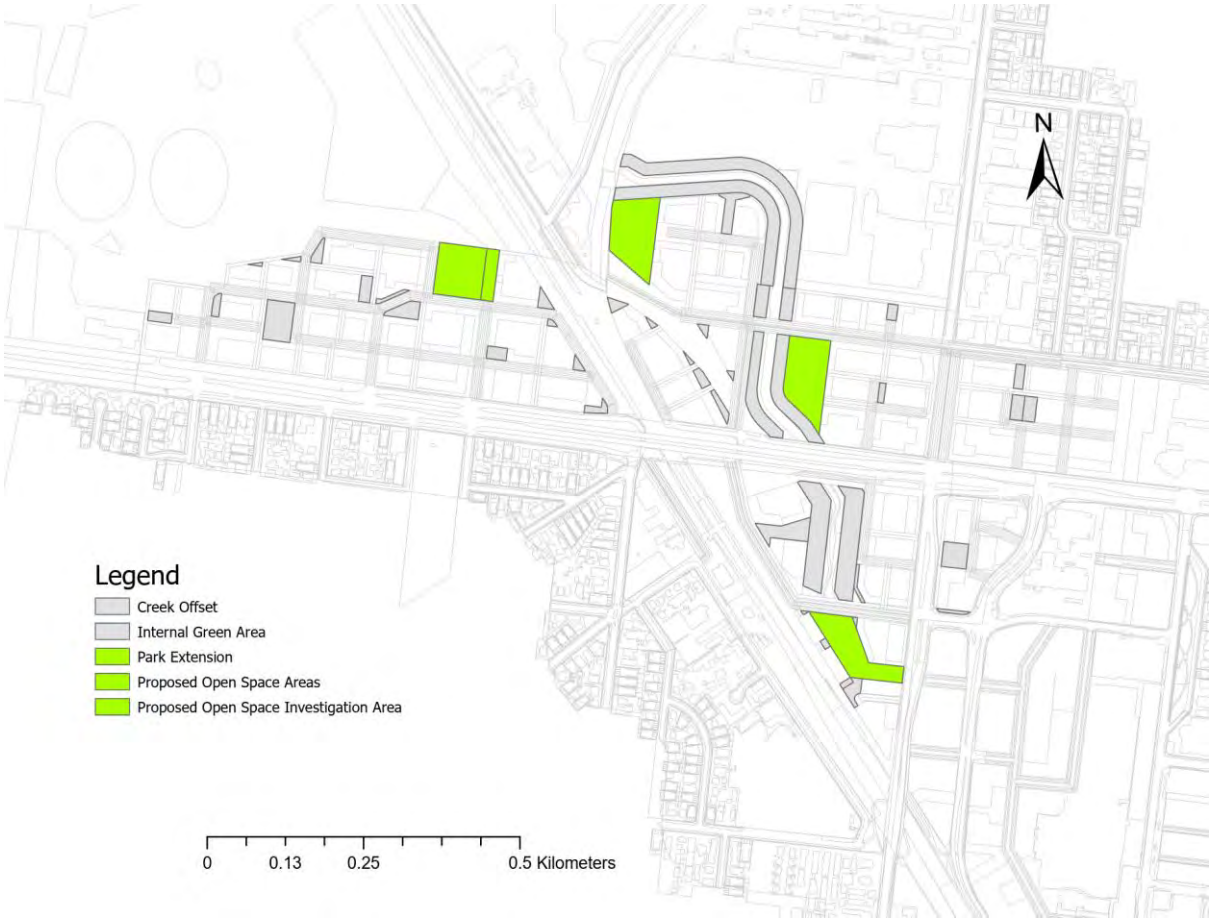

Figure 3.8. Map of Irrigated Areas for public open space using S3 model

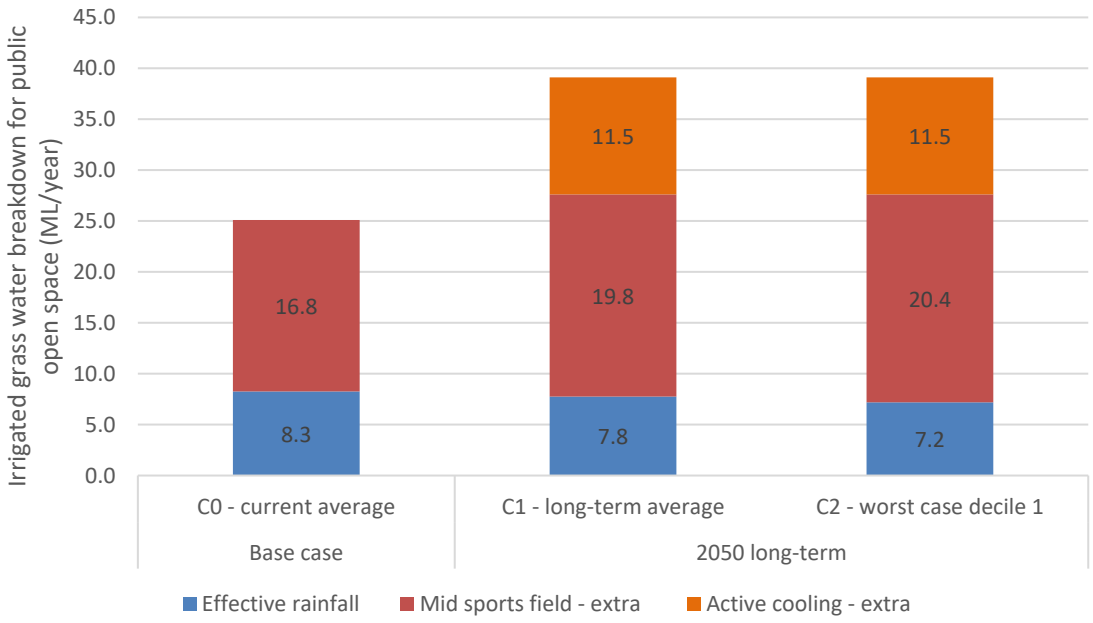

Figure 3.9. Grass water breakdown for public open space using S3 model (ML/year)

3.4 Updated scenario

For scenario testing, the precinct was disaggregated into three distinct types based on their characteristics, management structures, and development constraints: streets, public open spaces, and private lands. This approach allows for the development of tailored strategies that address the specific challenges and opportunities within each landscape type.

The most detailed analysis within this report is focused on the streetscape. This emphasis is intentional for two key reasons. First, unlike private land, there is currently a lack of specific, robust guidelines governing the design and implementation of street trees. Second, as public infrastructure, streets offer the greatest opportunity for direct intervention through detailed planning policies, such as mandating wider verges, specifying soil volumes, and integrating irrigation systems.

In contrast, private land is already governed by an existing 10% canopy coverage requirement for residential development. While this limits the scope for entirely new policy, this study investigates the potential impact of exceeding this baseline and the levers required to encourage a greater contribution.

Public open spaces, such as parks, offer significant potential for large-canopy trees due to greater soil availability. However, this potential is tempered by site-specific constraints. For example, areas along Stony Creek may have limitations due to potential land contamination, which restricts planting opportunities. Trees also competing with other requirements for open space, such as open sports fields.

A critical finding emerging from this analysis is the concept of a ‘canopy ceiling’. The analysis reveals that even if canopy coverage is maximized across all public lands (e.g. Street and public open space), their relatively small proportion of the total precinct area means that alone is unlikely to achieve a high

overall target like 30%, which is the current canopy target under the Victorian Government's Plan for Victoria policy.

This reality underscores that achieving a transformative precinct-wide target is fundamentally dependent on securing a substantial contribution from private land or reducing the amount of private land space. This finding does not diminish the importance of the public realm, but rather sharpens the focus on where the most direct and impactful interventions can be made.

Streetscapes represent a powerful lever for change. They are the spaces where direct investment in soil, water, and tree selection can create a resilient, high-quality canopy that directly enhances the public experience through shade and cooling. Therefore, while acknowledging the role of private land and open space in achieving overall scale, this report prioritizes actionable strategies for the public realm, as this is where targeted investment can build a genuinely climate-resilient and comfortable environment for the community. Based on the analysis in Section **Error! Reference source not found.**, t wo different street tree strategies are discussed in terms of their implications for precinct canopy outcomes:

Basic Approach: This method represents typical practice. It assumes trees are planted in a 3m verge and rely solely on this soil, with:

- No structural soil.
- Road rainwater capture: 20% of annual rainfall from the road surface is used for passive irrigation.
- Trees: All trees are of a uniform size.

Sophisticated Approach: This method incorporates advanced techniques to improve growing conditions. It includes:

- Structural soil: 0.9 m depth installed under footpaths and on street carparking spaces, with an effective soil ratio of 20%.
- Road rainwater capture: 20% of annual rainfall from the road surface is used for passive irrigation.
- Varied Planting: A staggered arrangement of alternating large and small canopy trees in areas of high solar exposure.
- Supplementary water to meet remaining tree water demand: through improving road rainwater capture potential to 90% of total rainfall, and/or active drip irrigation.

The following sections detail the analysis of streets, public open space and private land, quantifying their individual potential and highlighting the specific strategies required to maximize their contribution to the precinct's overall canopy goal.

3.4.1 Comparison of precinct canopy coverage outcomes under different street tree and private land design scenarios

This analysis reveals that the high-density built form, limited permeable surfaces, and scarce public open space fundamentally constrain canopy expansion within the public realm. Table 3.1 summarizes

the comparison of potential canopy coverage across private land, public areas, and streets under several scenarios, focused specifically on Albion Quarter

The scenarios modeled are:

- **Base Scenario:** the initial scenario modelled focused on the Albion Quarter. This has relatively more public realm – open space and street area – compared S3, with street tree assumptions delivering a mix of overlapped and dispersed canopy, akin to the Better/Best Practice approach described below.
- **S3 Business as Usual (BAU):** This relates to Scenario 3, which has relatively less public open space and street area compared to the Base scenario. 'BAU' represents theBasic Approach to street tree planting(outlined above).
    - BAU means using the Basic approach to street tree planting everywhere, assuming 50% rainfall efficiency.
    - BAU with water doubled through active drip irrigation means using the Basic approach to street tree planting everywhere, but assuming active drip irrigation to double the water.
- **S 3 Better/Best Practice:** This relates to Scenario 3 and reflects the application of the Sophisticated approach to street tree planting *where overlapping tree canopy is required to provide shading* (refer to section 3.4.2.3 for discussion of the shading analysis component).The Basic Approach is applied for the remaining streets where significant shading is already provided by buildings during summer. For this scenario, it is assumed that active drip irrigation is used to double the water. The difference between the two practices of Better and Best is the soil moisture assumptions shown Figure 10.3. This was taken into account in urban heat modelling but is not relevant for tree canopy percentage calculations.
- **S 3 Private Land Scenarios:** These tests were designed to quantify the precinct-wide impact of increasing canopy on private land in Scenario 3. The distinct scenarios were modeled:
    - BAU with No Enforcement: A conservative variation assuming only 5% canopy cover is achieved on private land.
    - Private land 20% assumes that private, ground-level land achieves a 20% canopy coverage.
    - Private land (10%) with 50% podium models a baseline 10% canopy on private, ground-level land, plus an additional 50% canopy coverage on all private podium areas.
    - Private land (20%) with 50% podium assumes a 20% canopy on private, ground-level land plus 50% canopy coverage on all private podium areas.

Details about the street tree differences in the BAU and Better/Best Practice scenarios can be found in Section 11.

The results indicate that under current land use and street typologies – both the Base Case and S3 options - achieving a high overall target like 30% is challenging without either a significant increase in canopy on private land and/or a major investment in creating additional public realm.

The Base Scenario – with relatively more public realm compared to S3 – was able to achieve 19.9% canopy cover, 10% below the 30% policy target. The comparable scenario under S3 (Best Practice),

reached 6% below this amount, demonstrating that allocating more space for open space and streets can be an important enabler of tree canopy at the precinct scale. To achieve similar coverage under the more intensive S3 development required doubling the private land canopy. The impact of increasing private land greening is also significant. Under the more intensive S3 development scenario, increasing tree canopy on private parcels from 10% to 20% raises total precinct-wide canopy coverage from 11.7% to 22%, representing an 11-percent-point gain. Under the less intensive base case, a 6% improvement in canopy cover was achieved through doubling private land greening. This highlights the importance of private land as a key opportunity for canopy delivery, particularly where the public realm is under pressure.

Table 3.1. Comparison of canopy coverage outcomes under different scenarios

Scenario	Private land		Public area (including stony creek)		Street		Overall	
	Canopy area (m^2)	% of All Areas	Canopy area (m^2)	% of All Areas	Canopy area (m^2)	% of All Areas	Canopy area (m^2)	% of All Areas
Base Case (Albion Quarter)								
Base - Tree akin to Better Practice	23677	4.6%	33287	6.4%	51215	9.9%	103194	19.9%
Base – Private land 20%	47354	9.1%	33287	6.4%	51215	9.9%	103194	25.4%
Scenario 3								
BAU With No Enforcement	18045	3.5%	16808	3.2%	12763	2.5%	47615	9.2%
BAU	31337	6.0%	16808	3.2%	12763	2.5%	60908	11.7%
BAU With Water Doubled	31337	6.0%	16808	3.2%	21422	4.1%	69567	13.3%
Better Practice	31337	6.0%	16808	3.2%	24465	4.7%	72610	13.9%
Best Practice	31337	6.0%	16808	3.2%	24465	4.7%	72610	13.9%[1]
Private Land 20%	72179	13.9%	16808	3.2%	24465	4.7%	113452	21.9%

Private Land (10%) With 50% Podium	100614	19.4%	16808	3.2%	24465	4.7%	141886	27.4%
Private land (20%) with 50% podium	136703	26.4%	16808	3.2%	24465	4.7%	177976	34%

[1] *The Better Practice and Best Practice scenarios share the same canopy rate; the difference between them lies in the Urban Heat Model assumptions, specifically regarding soil moisture conditions.*

Note: The potential canopy impact of podium greening was not tested for the Base Scenario, as there was only a small number of podiums due to the different building typology. Rooftop gardens could be an option in this space but this was not tested in terms of canopy impact.

3.4.2 Street design and canopy cover

The research analysed the implications of specific street design strategies for the achievement of canopy cover over streets. The analysis of street trees began at the unit scale (a 100-meter street segment, see Section 11.4.6) and was then scaled up to represent the overall precinct.

3.4.2.1 100-meter street tree design

To conduct a detailed and controlled assessment of street tree potential, a representative 100-metre road cross-section was modelled as the primary unit of analysis. The specific parameters and design of this section are provided in Section 11.4.6. Figure 3.10illustrates the cross-section of a typical 100-meter street segment utilized in the analysis.

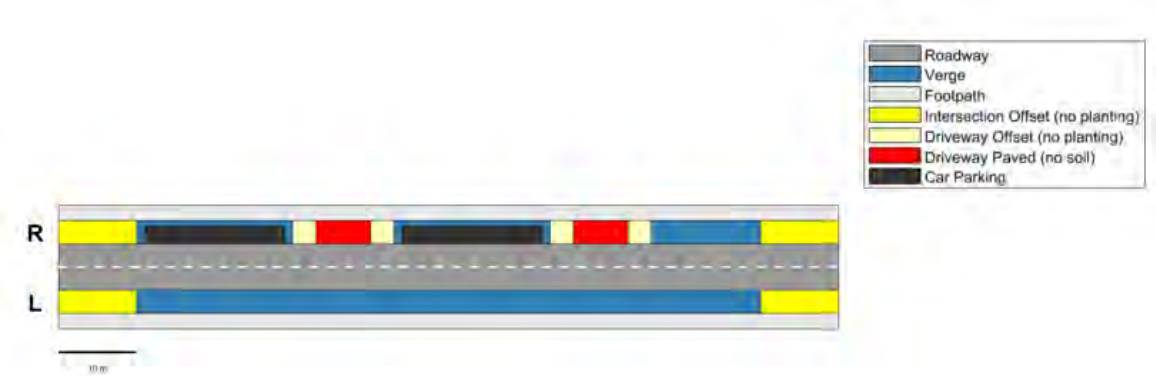

Figure 3.10. A typical living street configuration of 100m

A sensitivity analysis was then undertaken to quantify how design and environmental factors influence achievable canopy coverage, moving beyond a single static outcome to test a range of realistic conditions. The analysis focused on three key variables:

- Verge Width: Evaluated at 2 m and 3 m to measure the effect of increased soil volume.
- Water availability: Compared a baseline condition assuming 50% effective rainfall with a supplementary irrigation scenario, in which effective water availability is doubled relative to the baseline through additional irrigation (e.g. active drip irrigation applied to the roadside verge).

- Design Interventions: Tested the benefits of introducing structural soil and passive irrigation relative to the baseline condition.

Together, these variables define the soil volume and water availability that determine canopy performance. By quantifying their effects, the analysis identifies which interventions deliver the greatest improvement per unit of investment under future climate conditions (see Section **Error! R eference source not found.** for detailed parameters and calculation methods).

Nine street tree segments are compared in Table 3.2 and **Error! Reference source not found.**, including visualizations of their canopy cover. The analysis begins with a minimum baseline scenario representing the most restrictive conditions for street tree growth. This scenario (Segment 1) assumes a 2 m verge width, no structural soil, no road runoff capture, and rainfed conditions with 50% effective rainfall. Under these constraints, canopy establishment is highly limited, achieving only 10% canopy cover over the street area. It should be noted that underground service conflicts were not explicitly modelled; therefore, actual worst-case conditions may be even more restrictive.

- The Impact of Verge Width: A narrow 2 m verge without investment in water infrastructure is insufficient to support an overlapping tree canopy. Comparison of Segments 1 and 2 shows that increasing verge width from 2 m to 3 m under baseline rainfed conditions results in an increase in street canopy cover from 10% to 16%. Further increasing verge width to 5m results in an increase to 22%.

- The Impact of providing passive irrigation: Introducing passive irrigation results in measurable gains relative to baseline conditions without passive systems. Comparing Segment 4 and Segment 6 and 11, a designed passive system with 20% capture increases canopy cover by approximately 8% for a 3m verge and 5% for a 5m verge. At higher capture efficiency, the benefits increase further. A high-efficiency passive system capturing 90% of road runoff (Segment 8 and 12) achieves 53% canopy cover for a 3m, exceeding the performance of standard active drip irrigation (Segment 4, 31%), and a 51% canopy for a 5m verge

- The Impact of Enhanced Water Availability: Water availability is a significant lever for canopy expansion and impacts how quickly trees reach maturity. Comparing the baseline rain-fed scenario (Segment 2, 16%) with the active irrigation scenario (Segment 4, 31%) confirms that doubling effective water input roughly doubles canopy coverage.

- The Impact of Structural Soil: The comparison between Segments 6 and 7 highlights that in a hybrid scenario (where water is present but not unlimited), adding structural soil under the footpath in a 3m verge significantly boosts canopy cover from 39% to 47%. However, when water availability is already maximised through high-efficiency passive irrigation (Segments 8 vs 9), the additional benefit of structural soil becomes marginal (53% to 55%). This suggests that structural soil is most valuable as a strategy to extend the root zone in constrained or moderately watered environments, but water remains the primary limiting factor.

Table 3.2. Summary of the twelve 100 m street tree segments

Segment	Verge width	Structural soil	Road runoff capture	Tree size	Water source / availability	Canopy cover	Overlapping (Y/N)
1	2 m	No	None	All same (4m)	50% effective rainfall (Baseline)	10%	N
2	3 m	No	None	All same (4m)	50% effective rainfall (Baseline)	16%	N
3	2 m	No	None	Big (7m) & small (4m)	Active drip irrigation (Doubled water)	21%	N
4	3 m	No	None	Big (7m) & small (4m)	Active drip irrigation (Doubled water)	31%	N
5	3 m	No	20%	Big (7m) & small (4m)	50% effective rainfall	22%	N
6	3 m	No	20%	Big (7m) & small (4m)	Active drip irrigation (Doubled water)	39%	N
7	3 m	Yes	20%	Big (7m) & small (4m)	Active drip irrigation (Doubled water)	47%	Y
8	3 m	No	90%	Big (7m) & small (4m)	50% effective rainfall (Baseline)	53%	Y
9	3 m	Yes	90%	Big (7m) & small (4m)	50% effective rainfall	55%	Y
10	5m	No	None	Big (7m) & small (4m)	50% effective rainfall	22%	N
11	5m	No	20%	Big (7m) & small (4m)	50% effective rainfall	29%	N
12	5m	No	90%	Big (7m) & small (4m)	50% effective rainfall	51%	Y

Table 3.3. Visualization of canopy percentage for the twelve 100 m street tree segments

Segment	Canopy cover	Visual Segment
1	10%	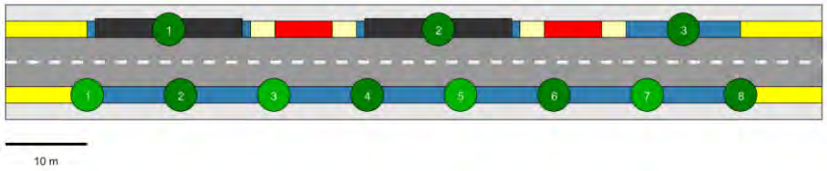
2	16%	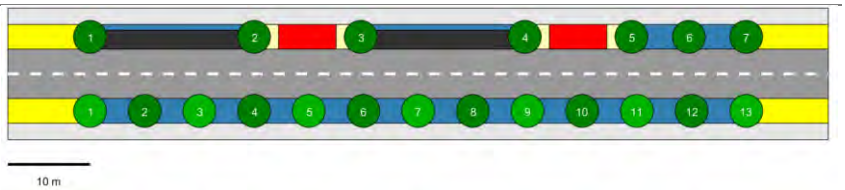
3	21%	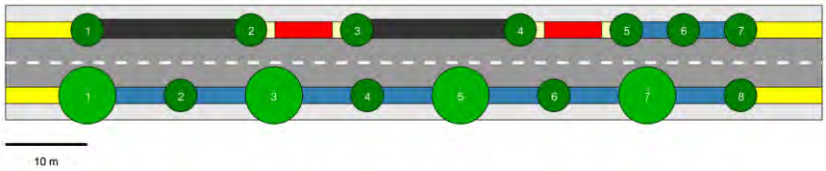
4	31%	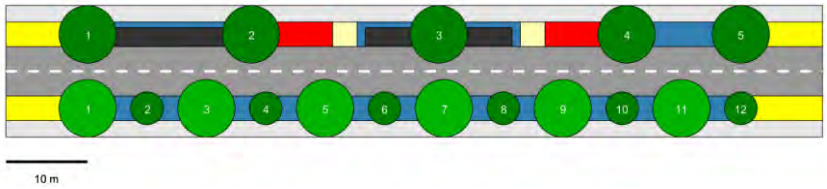
5	22%	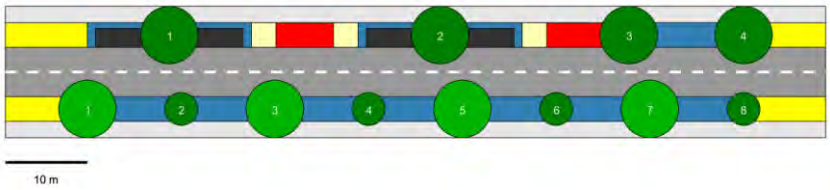
6	39%	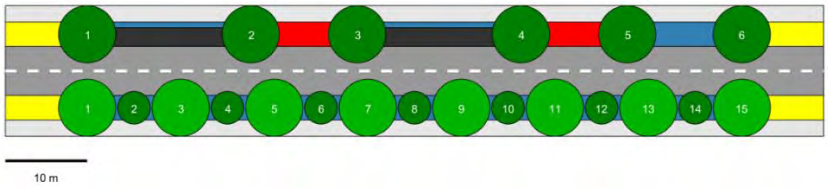
7	47%	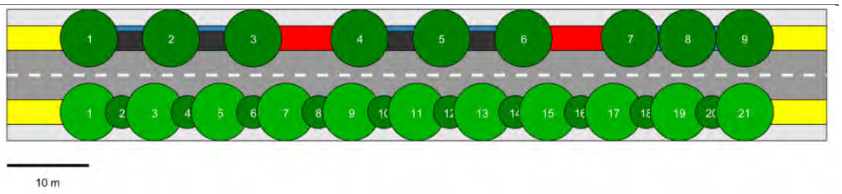
8	53%	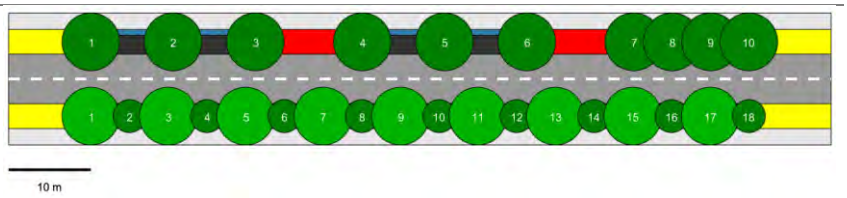

9	55%	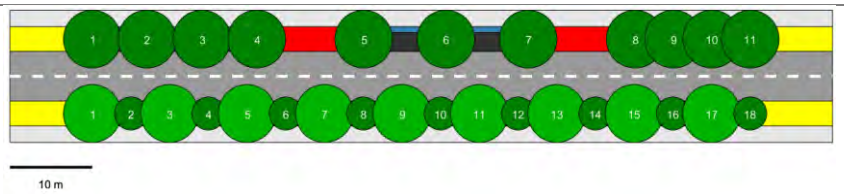
10	22%	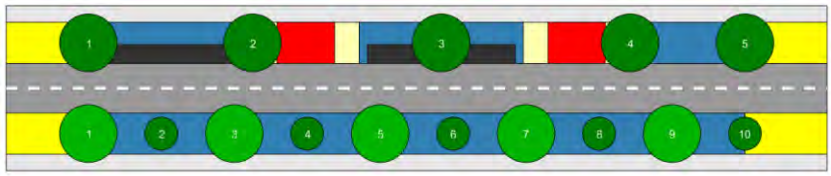
11	29%	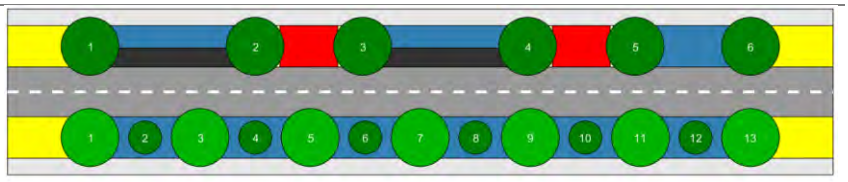
12	51%	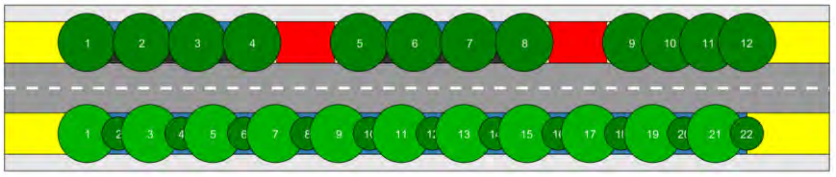

Therefore, the final optimal design could incorporate the recommended measures derived from the scenario testing, including:

- A wide 3-metre verge with structural soil, OR a 5m verge
- The implementation of passive irrigation from road capture.
- A doubling of effective water availability relative to the baseline, achieved through more efficient roadwater capture (90% efficiency) and/or active supplementary irrigation .
- A staggered planting arrangement of alternating large and small tree species on the sun-exposed side to create a more diverse and effective canopy structure.

It should be noted that these results assume no spatial constraints from underground utilities, which in practice could further limit tree planting opportunities. Conversely, it assumed that additional soil and water was not available beyond the street area (i.e. from neighbouring private land).

Investment in soil volume (3m verge and structural soil or a 5m verge), active and passive irrigation is important in areas where the intent is to create overlapping canopy. While it's possible that canopy could be achieved with a lesser amount in practice, via, for example, trees sourcing water from broken pipes or roots extending under footpaths to adjoining private land, these outcomes can't be guaranteed. Investments in soil and irrigation are important to safeguard tree canopy, particularly in a future, more unpredictable climate.

3.4.2.2 Precinct street tree planting strategy

While the analysis in Section 3.4.2.1 is founded on the primary constraints of soil and water, the project's evolution toward a high-density built form made it essential to incorporate shading. As the design progressed from the lower-height base case to the taller S3 model, the impact of building shadows on street trees became an equally critical consideration.

In this high-density environment, sun exposure directly influences tree health and growth potential. The shading analysis was used to create a more realistic and targeted street tree design. Instead of a uniform planting plan, the design strategy was prioritized based on the sun exposure available in different street corridors.

3.4.2.3 Priority based on shading conditions and precinct scale impacts of planting strategies

Figure 5.14 illustrates the significant difference in shading impact, comparing the lower building heights of the base case to the taller buildings modelled in the Stage 3 built form. The modelling demonstrated that as building heights increase, the resulting shadows significantly reduce the amount of direct sunlight reaching the street level.

To create a responsive and effective planting plan, the tree placement strategy was therefore adapted to these varied light conditions by selectively applying the two design methods defined in Section 11.2:

- For streets that are highly affected by shading, the more conservative Basic Approach was adopted, acknowledging the less favourable growing conditions.
- Conversely, for streets with moderate shading and greater sun exposure, the Sophisticated Approach was applied to maximize canopy coverage and capitalize on the more suitable environment.

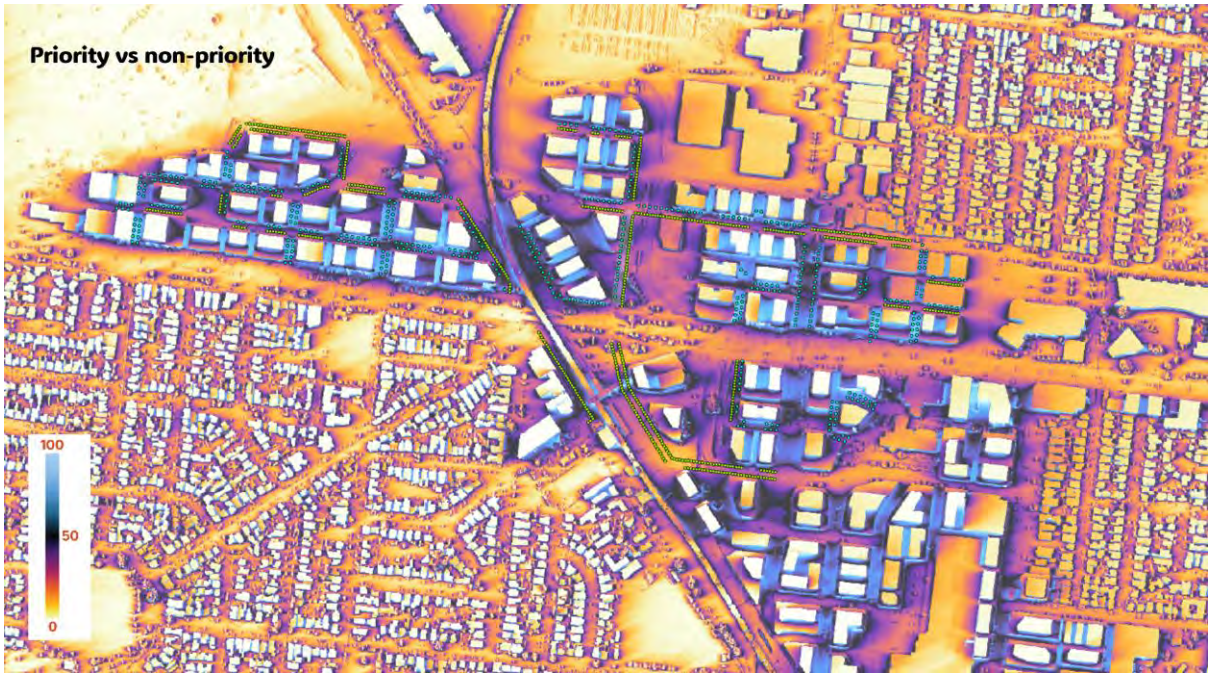

Figure 3.11. Priority and non-priority street design based on the shading condition of S3

By considering shading, the analysis ensures the tree design is not a uniform plan but rather a responsive strategy. This approach prioritizes investment and dense planting in locations with the most suitable growing conditions, as shown in Figure 5.14. Table 3.4. Details of the difference scenarios. presents the difference of the different scenarios in terms of the street tree placement. Figure 3.12 presents the street tree canopy maps for different scenarios.

Table 3.4. Details of the difference scenarios.

Scenario	Street tree placement strategy	Water availability
BAU	Basic approach	50% effective rainfall
BAU With Water Doubled	Basic approach	Equivalent to 100% effective rainfall (achieved via active drip irrigation)
Batter/Best Practice	Non- prioritized area - basic approach Prioritized area - sophisticated approach	Equivalent to 100% effective rainfall (achieved via active drip irrigation)

Figure 3.12. Street tree canopy maps for different scenarios

As summarized in Table 3.5, implementing Best Practice interventions for street trees increases their specific canopy coverage from 10% under the BAU and 17% under the BAU with water doubled through active drip irrigation to 20%. This targeted investment has a notable impact on the entire precinct, lifting the overall study area canopy coverage from 12% to 14%.

Table 3.5. Street tree canopy percentage changes

Scenario	Street		Overall	
	Canopy Area (m^2)	% of Street Areas	Canopy Area (m^2)	% of All Areas
BAU	12763	**10%**	60908	**12%**
BAU With Water Doubled	21422	**17%**	69567	**13%**
Best Practice	24465	**20%**	72610	**14%**

3.4.2.4 Cooling Benefits from of street tree strategy - BAU to Best Practice

While increasing the canopy rate is a primary goal, the analysis was also linked to the urban heat modelling to understand the quality of the thermal benefit provided by the BAU, Better Practice, and Best Practice scenarios.

According to Section 2.6.3, 2.6.4 and 2.6.5, analysis found that optimizing both shading (canopy) and ventilation (airflow) yields stronger and more widespread cooling effects. The Best Practice scenario, when modelled with 30% soil moisture and strategic gaps for ventilation, provided the most significant urban heat mitigation and the best thermal comfort.

Airflow is a critical factor, as increased canopy coverage can sometimes reduce cooling efficiency if it obstructs natural ventilation pathways. The urban heat modelling showed that strategically placing or removing trees at critical points enhanced airflow by 0.04 m/s, which helped alleviate hot pockets and reduce high wind speeds in N-S open corridors.

Therefore, from a purely thermal performance perspective, canopy alone is not enough. Without adequate irrigation (for active cooling) or sufficient airflow, additional canopy can have neutral or even adverse thermal effects. However, it must be noted that the value of an urban canopy extends beyond temperature reduction. Trees provide essential amenity value, such as direct shading for pedestrian comfort and benefits for mental health, which are also critical goals.

3.4.3 Precinct scale impacts of public open space greening

The analysis of public open spaces within the S3 model, which includes four parks and the Stony Creek corridor, indicates they contribute to a 20% canopy coverage for that specific land use zone and 14% of the entire areas. The tree canopy map is presented in Figure 3.13, where all trees are modelled with a 10-meter diameter.

Figure 3.13. Tree canopy map for public open space

This figure falls short of a more ambitious 50% canopy cover on open space due to the constraints of planting in the Stony Creek corridor – which is heavily contaminated – and the competing uses of open spaces for sporting activities. Table 3.6 demonstrates the contributions from the four open space areas and Stony Creek.

Table 3.6. Breakdown of canopy area within public open spaces

Public Open Space	Canopy Area (m^2)	% of Each Area	% of All Public Open Space Areas
Four Public Open Spaces	9582	31%	11%
Stony Creek	7226	13%	9%

If the constraints were overcome and a 50% canopy were achieved in four public open spaces, as summarized in Table 3.7, it would increase the precinct overall canopy coverage by an additional 1%. This limited effect reflects the fact that there is a relatively small amount of open space in the precinct.

Table 3.7. Public Open space tree canopy percentage changes

Scenario	Public Area		Overall	
	Canopy Area (m^2)	% of All Public Open Areas	Canopy Area (m^2)	% of All Areas

30% Public Open Space Canopy (all scenarios)[1]	16808	20%	72610	14%
50% Public Open Space Canopy[2]	22566	27%	78368	15%

[1] *The 30% scenario corresponds to the conditions presented above, where the four public open spaces achieve a 31% canopy rate, contributing 11% of the total public open space canopy.*

[2] *The 50% scenario increases the canopy rate of the four public open spaces while keeping the Stony Creek canopy constant.*

Beyond their role in providing canopy coverage, public open spaces are critical assets for active heat mitigation. As detailed in Section 3.3.2, these areas can be used for targeted irrigation, a strategy that provides significant cooling benefits to the surrounding environment during extreme heat events.

3.4.4 Precinct scale impacts of private land greening

Private land holds a critical role in achieving a high overall canopy target for the precinct due to its significant land share. However, realizing this potential is not straightforward, as it depends on the effective implementation of policy, clear design standards, and consistent compliance. Figure 3.14 demonstrates the tree canopy map for private land, accounting for 9% of the private land. (Note: coverage of 10% was not possible due to inconsistency between tree sizing in the model and the spatial configuration of private open space areas).

Figure 3.14. Tree canopy map for private land

The strategic leverage of private land is significant. As shown in Table 3.8 increasing the canopy coverage on private parcels from 9% to 20% results in an 8-percentage-point gain in the precinct's overall canopy (from 14% to 22%).

In addition to ground-level greening, podium landscapes present another valuable opportunity for expanding canopy cover. A separate scenario demonstrates that achieving 50% canopy coverage on podium areas could add approximately 19% canopy coverage within the private land portion, further underscoring the multiple pathways through which the private realm can substantially enhance overall precinct canopy outcomes.

However, it is important to note that rainfall remains a limiting factor, and achieving sustainable canopy growth will likely require the use of drought-resistant species and/or irrigation for medium water-use trees. Also as demonstrated in Section **Error! Reference source not found.**, if rainwater collected f rom roofs is used inside the building (e.g., for toilet flushing or non-potable uses), the captured water may not be sufficient for tree irrigation.

Table 3.8. Private land tree canopy percentage changes

Scenario	Private land		Overall	
	Canopy Area (m^2)	% of Private Lands	Canopy Area (m^2)	% of All Areas
10% Private Land[1]	31337	9%	72610	14%
20% Private Land	72179	20%	113452	22%
Private Land (10% ground cover) with 50% Podium	100614	28%	141886	27%
Private Land (20% ground cover) with 50% Podium	136703	38%	177976	34%

[1]*The 10% not able to be achieved in the 3D model due to tree size limitations*

4. Embodied Carbon Results

The goals of the embodied carbon assessment were to provide planners with an estimate of climate change impacts of the materials employed within the proposed precinct, in a manner that was sufficiently transparent to enable causes of impacts to be understood. Transparency of calculation was considered a priority as it was unclear as to exactly how planners might use climate impact information in decision making. The project therefore emphasised the building of a climate impact dataset that could be queried from multiple perspectives and that could be easily reconciled to precinct scale metrics.

The term 'embodied carbon' was used in this study to refer to the climate change impacts associated with materials and construction of the proposed Sunshine Precinct. This scope of consideration was referred to as the Embodied Carbon to Practical Completion (ECPC) and included the climate impact of materials when disposed of at the end of the precinct's life. A more precise definition of what was included in this definition is presented in Appendix 6 – Embodied carbon.

In addition to providing climate impact information for planners, the embodied carbon assessment also sought to identify a methodology whereby such information could be provided quickly and consistently with other allied analyses such as precinct energy demand/supply, urban heat island and water use. The ambition of responding in a consistent fashion to a given precinct design was considered a critical enabler of 'clash detection', thereby the avoiding the problem where competing goals of the design tend to contradict one another, leading to unintended burden shifting between design objectives.

The research goals can be summarised as follows:

1. Quantify the embodied carbon of the built environment of the precinct. Such quantification must be transparently calculated and readily connectable to precinct features such as its form and material.
2. Identify possible approaches that could be employed to reduce the embodied carbon of the Sunshine Precinct.
3. Identify a process that leverages the Digital Twin concept to calculate impacts quickly, consistently and transparently, in order to support informed decision making.

The embodied carbon assessment employed a parametric model above to consider 12 different ways of providing the functionality of the precinct that were distinguished by changes to precinct design, changes to built form, changes to carparking and changes to materials used to construct the buildings of the precinct. Two (2) precinct design scenarios, the Base Scenario and the Updated Scenario (explained in Section 1.4) were considered. In addition, two (2) built form alternatives were considered a) using buildings with basement carparking, and b) using buildings with upper floor carparking. The form alternatives were intended to consider the implications of basement excavation and construction versus upper level carparking provision. Three (3) carparking alternatives were also considered: a) Carparking levels of 0.6 per dwelling in the Base Scenario; b) Triple the level of carparking of the Base Scenario in the Updated Scenario; c) no carparking.

A summary of the alternatives considered is presented in Table 4.1, illustrating the focus on analysis of the Base Scenario under various form, carparking and materials assumptions. The Updated Scenario analysis was limited to changes in materials options. This approach was adopted as it was felt the main benefit of the Updated Scenario analysis was to assess how a planning approach that encouraged larger, taller buildings, with more carparking, would impact upon embodied carbon outcomes. Details regarding the scenarios considered and the methodology employed for analysis can be found in Appendix 6 – Embodied carbon.

Table 4.1. Scenarios considered. Scenario names used throughout the report are noted in bold.

Precinct Design	Precinct considered	Building Form	Car parking*	Materials		
				Typical	Best efforts	Low carbon
Base	Albion Quarter, Town Centre & Sunshine Station	Basement	100%	**B-T (Base case)**	**B-BE**	**B-LC**
		No Basement	100%	**NoB-T**	**NoB-BE**	**NoB-LC**
		No Basement	0%	**NoB-T-CP0**	**NoB-BE-CP0**	**NoB-LC-CP0**
Updated	Albion Quarter	No Basement	100%	**Upd-NoB-T**	**Upd-NoB-BE**	**Upd-NoB-LC**

* Carparking measured as proportion of functional capacity

Functionality of the precinct was defined in terms of the functional unit below:

- Functional unit: Provision of one (1) square meter of functional floor area (commercial and residential) and associated personal transport. Referred to as the Functional Floor Area (FFA).

Embodied carbon results were calculated for the provision of the functional unit for each of the scenarios described in **Error! Reference source not found.**. The intent of this approach was to c ompare the embodied carbon of various approaches to achieving the same functional outcome. To facilitate comparison to other studies, the commonly used reference unit of one (1) square meter of Gross Floor Area (GFA) was also used for embodied carbon assessment (but should not be considered the decision-making parameter). Further details and the implications of functional unit definition are presented in Appendix 6 – Embodied carbon.

The estimates of embodied carbon for the precincts considered are highly uncertain. There were many assumptions required to develop the estimates presented herein including building form, construction approach, supply chain production processes, end of life material fates and other assumptions. Efforts to manage uncertainty involved comparing construction material quantities to estimates developed by a quantity surveyor and by comparing results to other, similar studies. A discussion of processes employed to manage uncertainty can be found on Section 12.4.3.

4.1 Key findings and recommendations

4.1.1 Key findings

- The embodied carbon across all scenarios was found to vary significantly - between 144 and 457 kg CO2e/m2 of functional floor area (FFA) - highlighting the potential for design changes to lower embodied carbon.
- Carparking within buildings was found to contribute significantly to embodied carbon

a) Tripling the amount of carparking led to a 30% increase in embodied carbon (between the Base Scenario and Updated Scenario).

b) The removal of carparking entirely (within the building) from the Base precinct scenario was seen to reduce embodied carbon by 15%. This was based on a rate of 0.6 carparks per dwelling in this scenario.

- **The impact of basements on embodied carbon was relatively modest where carparking was retained elsewhere**
  Moving carparking from basements to the upper floors of buildings reduced embodied carbon by only 4%, where carparking was retained.

- **Material selection was able to reduce embodied carbon from between 14% - 46%**

  Concrete and steel were found to be the largest contributors to embodied carbon across most scenarios. This was driven by the upper floor elements of buildings, which were the largest contributors to embodied carbon across most scenarios.

  Material selection was seen to reduce embodied carbon by 14% when equivalent lower carbon concrete and steel were selected, highlighting the benefits achievable when carbon is prioritised during procurement.

  More ambitious low-carbon material palettes such as light-weight and mass timber approaches, in combination reduced the embodied carbon of the precinct by 46%

- **While the electricity grid remains carbon-intensive, reducing electricity supply from the grid has a much greater impact on lifecycle carbon over 60 years than embodied carbon. However, as the grid de-carbonises, embodied carbon will become increasingly important, potentially making up the majority 60-year lifecycle emissions, based on long term emission projections.**

  Without on-site generation and under existing grid supply conditions, electricity use and maintenance contributes 93% of total life cycle carbon impacts, compared with 7% from embodied carbon. Utilising rooftop and façade PV and batteries reduces lifecycle carbon emissions by 27% overall (based on current carbon intensity of the grid), but embodied carbon still only makes up 12% of emissions. However, if grid emissions intensity lowers with the transition to renewable energy embodied carbon will grow to 53% of carbon impacts over the 60-year life cycle.

- **The Digital Twin enabled the assessment of embodied carbon and the life cycle climate change impacts of the precinct thereby providing better information to planning decision makers.**

4.1.2 Recommendations

- **Plan to facilitate low-carbon building designs**

Lower carbon construction approaches were found to significantly reduce embodied carbon outcomes. Results show that substituting typical construction materials with low carbon equivalents can reduce embodied carbon by 14%. This could be improved to 46% if low carbon (lightweight and mass timber) approach is adopted.

As embodied carbon becomes an increasing share of lifecycle emissions, encouraging material changes over the long term will be important to reducing built form emissions. This may entail some changes to built form, as research (Pomponi et al. 2021) suggest that low embodied carbon buildings are easier to achieve when they are shorter. For example, it is unusual to see light-weight construction approaches in multi-residential buildings above six (6) storeys in Australia. Mass carbon approaches such as CLT currently achieve building heights of up to 10 storeys in Australia.

- **View carparking as a burden of transport, to be reduced as appropriate**

Carparking within buildings was found to contribute significantly to embodied carbon of the precinct designs assessed. By removing carparking (within the building) from the Base precinct scenario embodied carbon was reduced by 15%. Moving carparking from basements to the upper floors of buildings was seen to have a lesser impact, reducing embodied carbon by 4%.

By viewing carparking as a burden of the precinct transportation system, planners can consider alternatives to personal transport such as public transport systems. Public transport systems will be expected to reduce the embodied carbon of buildings by removing the need for personal carparking space or by shifting such space to lower embodied carbon alternatives (such as remote carparking).

- **Planners could use the Digital Twin to maximise the embodied carbon value of precinct designs while at the same time aiming for a net-zero carbon outcome**

Embodied carbon can be viewed as a cost to development that needs to be managed like any other cost. Indeed, it is possible to translate embodied carbon to a dollar cost using approaches such as the Social Cost of Carbon (Rennert et al. 2022) and other approaches. While an absolute cost may help educate certain stakeholders, the challenge for planners is likely to remain one informed by value rather than cost, where value is understood as the ratio between precinct utility and the climate price paid for it. It was clear from the precinct designs assessed in the study that significant improvements in embodied carbon 'value' were achievable through various initiatives outlined above. It was also clear that none of the precinct designs achieved a 'net zero' carbon outcome over the life cycle, even when the carbon sequestration potential of mass-timber was included. The ability of mass-timber and other biogenic materials to store carbon presents a theoretical opportunity for a precinct to achieve a net-zero carbon outcome if this goal is prioritised.

4.2 Base case and updated scenario

4.2.1 Embodied carbon assessment

The scenario analysis was based upon the variation of parameters that were believed to impact embodied carbon – the interventions. The interventions tested included:

- Precinct design – the form of the precinct
- Building form – the inclusion or exclusion of basements
- Carparking – the amount of building floor area devoted to carparking
- Materials – Typical, best efforts or low carbon building materials

To assess the impacts of these changes, that were assessed in isolation and in combination, the embodied carbon results presented in were sorted from the most adverse impact to the most beneficial impact

relative to the base scenario B-T. By arranging results in this way, it was possible to consider the impact of interventions upon the embodied carbon outcomes. The results of this analysis are shown in Figure 4.1.

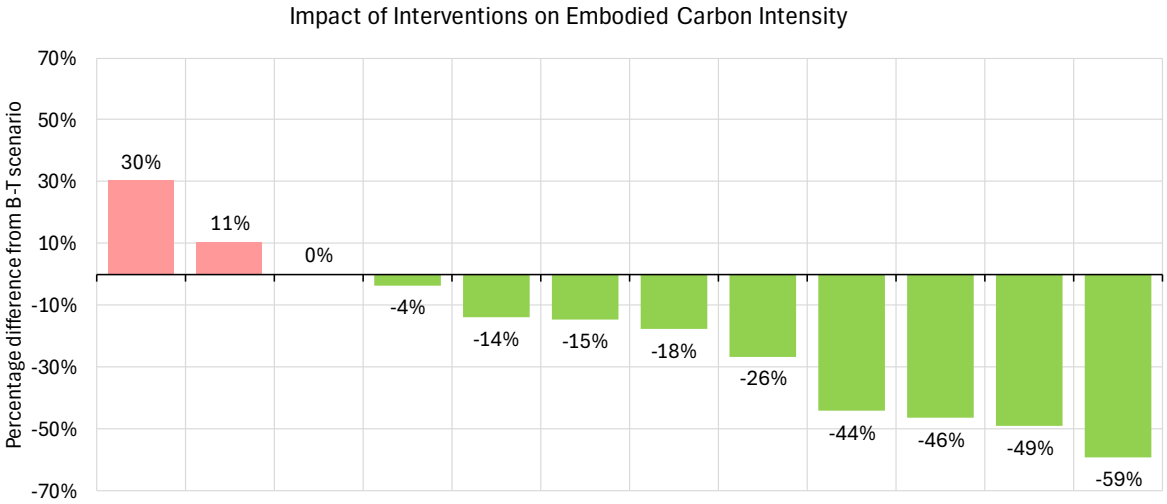

Scenario Name	Upd-NoB-T	Upd-NoB-BE	B-T	NoB-T	B-BE	NoB-T-CP0	NoB-BE	NoB-BE-CP0	Upd-NoB-LC	B-LC	NoB-LC	NoB-LC-CP0
Precinct design	Updated	Updated	Base	Base	Base	Base	Base	Base	Updated	Base	Base	Base
Precincts considered	Albion Qtr.	Albion Qtr.	Albion Qtr. Town Cen. Sun. Station	Albion Qtr. Town Cen. Sun. Station	Albion Qtr. Town Cen. Sun. Station	Albion Qtr. Town Cen. Sun. Station	Albion Qtr. Town Cen. Sun. Station	Albion Qtr. Town Cen. Sun. Station	Albion Qtr.	Albion Qtr. Town Cen. Sun. Station	Albion Qtr. Town Cen. Sun. Station	Albion Qtr. Town Cen. Sun. Station
Building form	No basemt.	No basemt.	Basement	No basemt.	Basement	No basemt.	No basemt.	No basemt.	No basemt.	Basement	No basemt.	No basemt.
Carpark area / FFA area	45%	45%	11%	11%	11%	0%	11%	0%	45%	11%	11%	0%
Materials	Typical	Best efforts	Typical	Typical	Best efforts	Typical	Best efforts	Best efforts	Low carbon	Low carbon	Low carbon	Low carbon
Total (t CO2e)	631,210	535,762	789,928	761,693	680,589	676,570	651,595	581,142	270,857	423,982	403,336	324,604
Impact per FFA (kg CO2e/m2)	**457**	**388**	**351**	**338**	**302**	**300**	**289**	**258**	**196**	**188**	**179**	**144**
% difference from Typical	**30%**	**11%**	**0%**	**-4%**	**-14%**	**-15%**	**-18%**	**-26%**	**-44%**	**-46%**	**-49%**	**-59%**

Figure 4.1. Impact of interventions on embodied carbon intensity. Adverse impacts shown in red; beneficial impacts shown in green. Baseline reference scenario (B-T) highlighted in orange.

The embodied carbon across all scenarios was found to vary between 144 and 457 kg CO_2e/m^2 (FFA), as shown in Figure 4.1. The differences seen in embodied carbon intensity can be attributed to the four (4) interventions considered, as follows:

Precinct design

The Updated Scenario (Upd-NoB-T) increased the carparking area in the Albion Quarter by 334% (refer Section **Error! Reference source not found.**) over the Base Scenario (B-T). Although the Updated S cenario did involve the elimination of basements and changes to the shapes of buildings, the bulk of the 30% increase in embodied carbon for the Upd-NoB-T scenario was due to the additional materials required to provide this extra carparking space (Figure 4.2). Importantly, the use of lower impact materials in the Upd-NoB-BE and Upd-NoB-LC scenarios were seen to partially and completely offset the impact of the increased carparking considered in the Updated Scenario. Indeed, the Upd-NoB-LC scenario achieved a 44% reduction versus the B-T scenario due to the large amounts of carbon stored in the mass-timber employed in the residential towers of this scenario.

Building form

The incorporation of basements was found to have less of an effect on embodied carbon than might be expected. Throughout the analysis it was assumed that basements would only be used for carparking, so the assessment of the basement was compared to the alternative of placing carparking in the building ground and upper floors. Embodied carbon intensity was seen to be slightly higher for carparking underground due to increased burdens associated with excavation and reinforcement versus creating the same parking area in an above ground structure. When B-T and NoB-T scenarios were compared the embodied intensity of the precinct only fell by 4% (Figure 4.2). The result suggests that for situations where one to two basement levels are being considered, the additional material and construction burden of this approach versus providing carparking above ground (in building structures) is not large.

Carparking

As mentioned in 'Precinct Design' above, carparking was seen to significantly impact embodied carbon because it was viewed as a precinct burden that did not contribute to FFA. To test the benefit of reducing carparking extreme scenarios were considered whereby carparking was eliminated from the precinct buildings. Comparing the B-T scenario to NoB-T-CP0 showed the impact of removing carparking and therefore basements to reduce the embodied carbon intensity of precinct by 15%. The reduction was not as large as the adverse increase seen in Upd-NoB-T because the Updated Scenario increased carparking by 334% versus the reduction considered NoB-T-CP0 which is effectively a 100% reduction.

It is unsurprising that carparking increases the carbon intensity of the precinct because it adds materials without adding FFA. When carparking is removed, it is assumed that the personal transport service considered within the system boundary (Figure 4.2) is provided elsewhere without incremental burden. This assumption may be justifiable if existing public transportation services are already being provided that have excess capacity, however this will often not be the case. Further detailed study of the incremental carbon burden associated with additional public transport capacity (and accessibility) would need to be conducted to properly assess the net carbon impact.

Materials

Material interventions were seen to reduce the embodied carbon impact of the precinct. Under the 'Best Efforts' scenario (B-BE), embodied carbon of the B-T scenario was reduced by 14%. This was a good result given that it only involved choosing lower impact materials and using the same fundamental precinct and building designs. When a more ambitious material palette was employed, which included lightweight and mass-timber construction approaches, the embodied carbon intensity was reduced by 46% (B-T vs B-LC). This benefit was seen to be achieved under the Updated Scenario as well (44% for Upd-NoB-LC). When combined with other interventions, such as removing basements and carparking, the low-carbon materials were seen to reduce the carbon intensity of the precinct by 59 % (B-T vs NoB-LC-CP0). Benefits from the use of low-carbon materials stem from the assumption that they are both low-impact to produce and that they store carbon in their structures in the long term, as discussed in Section 12.3.4.

4.2.2 Looking across the life cycle

A more holistic view of the climate change impact of the precinct was considered by including the operational phase of building life into the analysis (embodied carbon typically excludes this). To do this the embodied carbon of the precinct for Scenario B-T was added to estimated impacts associated with manufacturing photovoltaics (PV) and battery storage systems (BESS). This total embodied carbon was informed by the Energy Subgroup scenario P01F02N04S04B01E03 which assumed that buildings employed rooftop and façade solar as well as battery storage, where possible, to maximise grid stability. Building embodied carbon was assumed to support precinct function over a 60-year period, and PV and BESS 20 years (requiring two replacements over one building life).

The results of the life cycle assessment illustrated the relative contribution embodied carbon (ECPC scope) made to the overall life cycle climate impact of the precinct. The results (Figure 4.2) showed that without on-site generation and under existing grid supply intensities (Scenario 1), electricity use and maintenance contributes 93% of total life cycle carbon impacts (embodied carbon contributes 7%). When on-site generation from PV was included the contribution from electricity and maintenance falls to 88% of life cycle impact embodied carbon increases to 12% of climate impact (Scenario 2). When a longer view of grid emissions intensity was considered (lower grid emissions), combined with on-site generation, the contribution of grid supplied electricity and building maintenance fell to 47% of total life cycle emissions and the embodied emissions grew to 53% of life cycle climate impacts (Scenario 3).

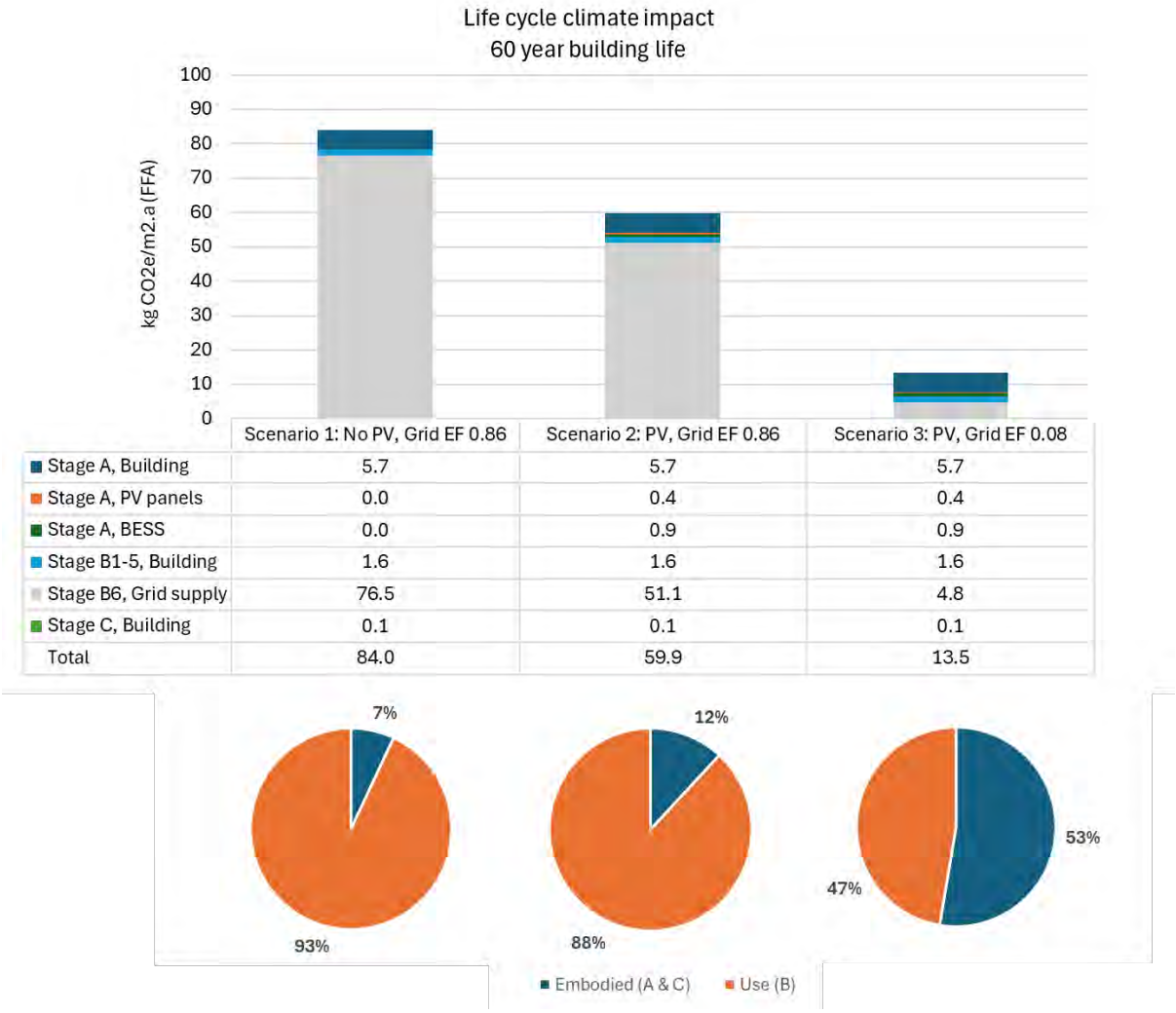

Figure 4.2. Life cycle climate impact breakdown by stage of precinct life.

When on-site electricity generation was considered, the life cycle carbon impact fell from 84 kg CO_2e/m2.a to 59.9 kg CO_2e/m2.a assuming the current carbon intensity of grid electricity supply (0.87 kg/kWh) as shown in Figure 4.2. This reduction represents a 27% reduction in life cycle carbon emissions. If the carbon intensity of grid electricity supply is assumed to achieve the forecasted average for the life period (0.08 kg/kWh), the life cycle emissions fall drastically to 13.5 kg CO_2e/m2.a, a reduction of 84%. While impressive, the assumption of a close to zero emissions intensity for grid supplied electricity is arguably very optimistic. Overall, these results demonstrated that initiatives, such as local electricity generation from solar PV, have the greatest impact upon life cycle climate change outcomes while emissions intensity of the electricity grid remains high.

While there is significant uncertainty associated with the analysis, the results illustrated the relative importance of embodied carbon is highly dependent on the expected future emissions intensity of grid electricity supply. In the existing emissions intensity environment (Scenario 1 and 2) embodied carbon plays a small part in the total life cycle impact of the precinct (7-12%). However, as the grid decarbonises over the life of the precinct the contribution of embodied carbon will be expected to increase – significantly (53% under Scenario 3). Given that the carbon emissions from the supply chains that provide

materials such as concrete and steel are not currently driven by electricity, it is likely that the embodied carbon of these materials will remain relatively constant, even as electricity supply emissions fall.

4.2.3 Conclusions

The embodied carbon analysis sought to assess the climate impacts of the materials employed within the proposed development (the 'embodied carbon') to identify interventions that might reduce those impacts and to pilot an assessment methodology that would exploit the rich data provided by a 'Digital Twin' and to compliment such data with embodied carbon information. To satisfy these goals, the research employed a linear analysis which quantified material quantities associated with a range of planning scenarios for the precinct from which climate impacts were estimated using climate impact factors drawn from EPDs. The analysis was conducted at a building-by-building level, where quantity survey techniques and assumptions where automated in an embodied carbon database to estimate total material quantities and supply chain climate impacts. Using the embodied carbon database, it was possible to assess the embodied carbon for a range of scenarios as well as considering the climate impacts over the life cycle of the precinct.

Conclusions were drawn vis a vis the research goals as follows:

Goal 1: Quantify the embodied carbon of the built environment of the precinct. Such quantification must be transparently calculated and readily connectable to precinct features such as its form and material.

> Embodied carbon was defined as the climate change impact associated Stage A (Production) and Stage C (End of Life) of the life cycle of the buildings within the precinct (shown in orange in Figure 4.2). The functional unit of the precinct was defined as the residential and commercial floor area provided by the buildings in the precinct (the FFA), excluding carparking area contained within buildings. Timber elements were assumed to store carbon indefinitely as they were assumed to be disposed of to landfill at the end of the precinct life (Section 12.3.4).
>
> The embodied carbon across all scenarios was found to vary between 144 and 457 kg CO_2e/m^2 (FFA). Embodied carbon was found to be highest in the Updated Scenario which included the most carparking (30% greater than the Base design). Importantly, when lower carbon materials were employed in the Updated Scenario, the impact of additional carparking was found to be partially and completely offset. When carparking was eliminated in the Base design scenario, embodied carbon was reduced by 15%.
>
> The study considered the contribution of materials and building elements to the total embodied carbon of the precinct. Concrete and steel were the materials contributing most to embodied carbon across most scenarios considered. This result was consistent with material quantity analysis which showed that concrete dominated building mass in all scenarios, accounting for 94% in the typical construction case (B-T) and 79% in the low-carbon case (B-LC), with total material mass ranging from 787 to 972 kg/m^2 GFA. Building upper floors were found to be the building elements which contributed the most to embodied carbon.
>
> When a 'best efforts' approach (selecting lower carbon but equivalent materials) to materials (by prioritising low carbon materials during procurement) was employed in the Base Scenario, embodied carbon was reduced by 14%. This improvement increased to 46% when more

ambitious low carbon materials and designs (i.e. light-weight and mass-timber constructions) were employed.

The incorporation of basements was found to have less of an effect on embodied carbon than might be expected. When the Base Scenario was considered using typical materials and equivalent carparking, the use of a basement was found to increase embodied carbon by 4%. The result demonstrated that for situations where one (1) to two (2) basement levels are being considered, the additional material and construction burden of this approach versus providing the same carparking area above ground (within the building) was not large.

Goal 2: Identify possible approaches that could be employed to reduce the embodied carbon of the Sunshine Precinct.

The analysis and conclusions which addressed Goal 1 (above) showed that reducing carparking, choosing lower carbon materials and removing basements all reduced embodied carbon. Further to these, it was also shown in the life cycle assessment that on-site electricity generation from renewable sources reduced climate change impacts over the life of the precinct by 27% if the carbon intensity of grid supplied electricity was assumed to remain as it is now over the life of the precinct. This reduction was greater than the entire contribution of embodied carbon (7%), demonstrating that while grid emissions remain as they are, electricity generation from renewables remains a more powerful strategy for reducing the precinct footprint.

As the carbon intensity of electricity supply improves into the future, it is expected that the role of embodied carbon in determining the life cycle climate impact will increase. The analysis showed that under the current grid intensity, the embodied carbon contributed 7% of life cycle emissions when no renewables were generated on site. The solar PV and BESS were included this grew to 12% of life cycle emissions. When a future grid carbon intensity, based on forecasts, was assumed, the contribution of embodied carbon to life cycle climate change impact increased to 53%. These results indicate that the role of embodied carbon in determining precinct impacts is likely to increase into the future, thereby requiring ongoing attention.

Goal 3: To identify a process that leverages the Digital Twin concept to calculate impacts quickly, consistently and transparently in order to support informed decision making.

The methodology employed in the study demonstrated a process for calculating embodied carbon at the precinct scale that was straight-forward and repeatable. The growth in credible carbon datasets such as the Australasian EPD Database, enabled an 'emission factor' method for assessing the carbon impacts of materials used in construction from estimated quantities. While quantity estimation from planning layouts involves significant uncertainty, the benefits of estimating quantities provide planners with immediate feedback as to the likely implications of their decisions, thereby enabling better decision making. Moving forward, it would be a straightforward improvement to the quantity model developed to incorporate missing data such as the impacts associated with shared infrastructure. Other improvements such as incorporation of maintenance and replacements (B1-5) would be challenging but also useful. Overall, the study showed the benefit of the Digital Twin approach when it comes to embodied carbon and climate change impact assessment to inform decisions.

5. Energy Results

This energy chapter considers an analysis of energy demand and supply across the Sunshine precinct considering detailed shading assessment, building material choice and end-use patterns for occupants including their transportation needs for electric vehicles (EV, see section 13.2.3). Demand-side supply options include traditional rooftop photovoltaics (PV), building façade PV and BESS. Building load as a function of material choice was linked to the ENVI-Met system employed in the urban heat analysis (see section 2).

A fuzzy inference-based energy management system (Section 13.2.4) was developed and used to treat the temporal optimisation of energy use and energy storage. This includes the ability to shift EV charging and to store and temporally shift production from local PV with onsite batteries (BESS).

Having established demand profiles, a power quality analysis was performed with PowerFactory to examine changes from various scenario settings on line-voltage and thermal limits and transformer ratings. A set of conditional constraints were used to establish options within each test case that ensured voltage and thermal limits of lines and transformers are able to operate within defined operational limits over a year of operation.

Table 5.1 illustrates the two scenarios examined and the various settings employed. The base case (S1) considers the full study area covering 322 buildings. For the base case there were a total 72 cases considered that included perturbations to PV, façade PV, BESS and EV. Additionally, a second set of 144 cases were analysed with higher degrees of specificity on façade PV (see section 13.2.2).

An alternative and updated case considers the Albion quarter in more detail. The alternative case (S3) covers both rooftop and façade PV modelling and power system simulation. The scenario testing focuses only on the iteration 2 (144 cases) which has more detailed system settings and rules out infeasible options.

Table 5.1. Scenario comparison

	S1	S3
Precinct Digital Model Version	S1 model covers full study area (322 buildings)	S3 model (Albion Quarter – 230 buildings)
Solar and shading mapping	Yes	Yes
Renewable generator	Rooftop and façade PV multiple scenarios	Rooftop and façade PV multiple scenarios
Load models	Baseline models + Load adjustment models	Load management models
Energy management system models	Baseline model + Adaptive EMS	Adaptive EMS

Adaptive EMS testing iterations	Two iterations including preliminary 72 scenario settings and expanded 144 scenario settings	One iteration with the expanded 144 scenario settings
Power system analysis	Yes	Yes

5.1 Base case scenario

5.1.1 Solar irradiance and shading exposure mapping

Figure 5.1 compares the shading impacts within the Sunshine precinct during two distinct seasonal periods: April to September (Autumn and Winter months) and October to March (Spring and Summer months). The maps use a colormap scheme to represent variations in sunlight exposure, clearly illustrating the extent of shading effects during daylight hours across these seasons.

Notably, shading impacts are considerably more pronounced from April to September, characterized by higher percentages of average daytime hours affected by shadows. Conversely, shading impacts from October to March are relatively less severe, reflecting the higher solar angles typical of the warmer months.

An important observation is that building rooftops within the precinct generally experience limited shading impacts, particularly during Spring and Summer. However, rooftops situated near taller or closely spaced buildings experience increased shading during Autumn and Winter, when lower solar elevation angles result in longer and more extensive shadows.

During the cooler months (April to September), significant shading (represented by darker blue shades) is observed along both East-to-West and North-to-South building corridors. This widespread shading is due to the lower solar altitude, which causes denser shadows. In contrast, during Spring and Summer (October to March), shading impacts predominantly affect North-to-South oriented corridors which is likely due to the closeness the buildings, while East-to-West corridors typically experience shading less than 50% of daylight hours. This seasonal shift occurs because the higher solar path in warmer months reduces shadow lengths along East-to-West alignments.

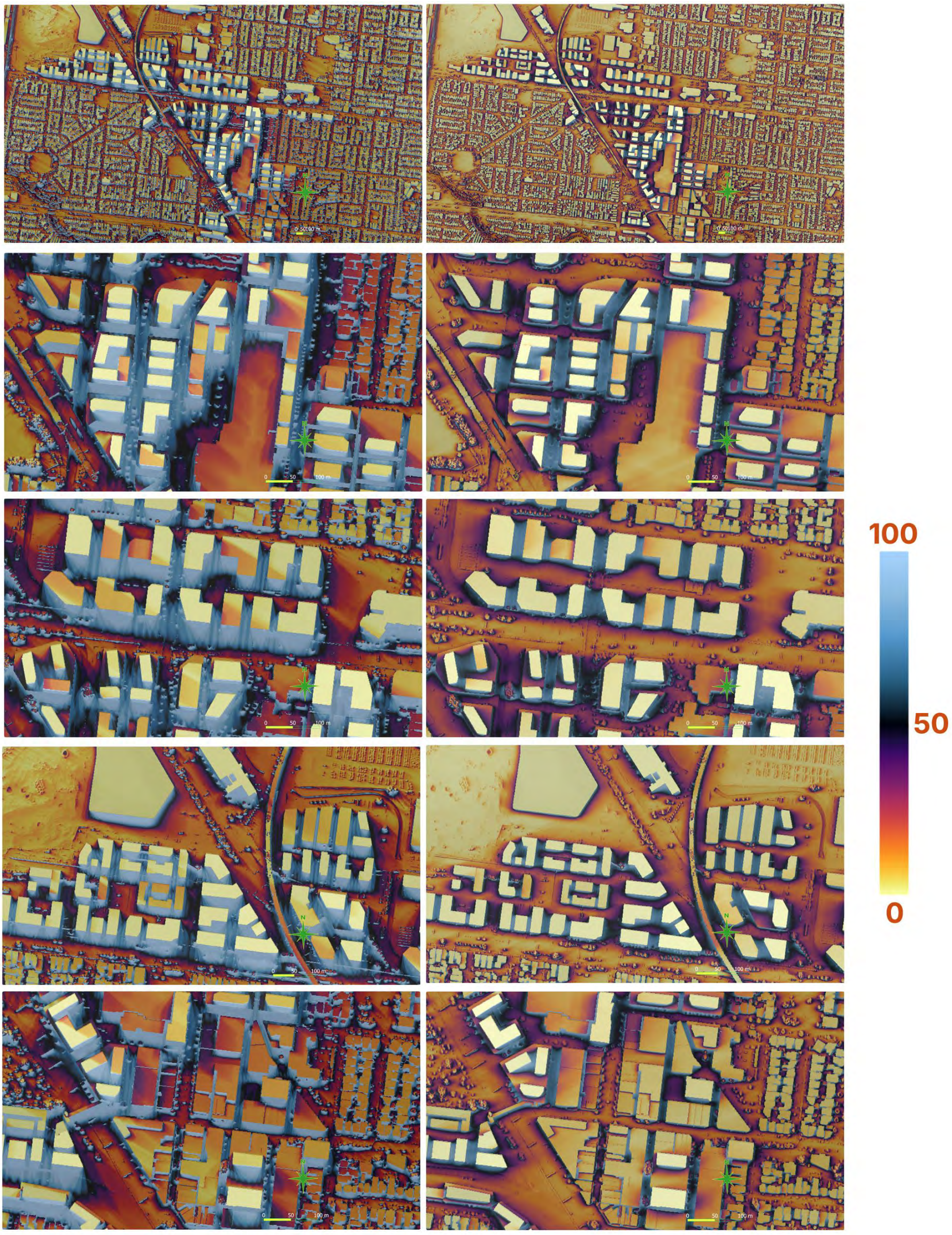

Figure 5.1. Shading impact analysis of S1

Figure 5.2. Average façade shading impact measured by average shading height (m) during daylight hours

Further, buildings oriented along the East-West axis generally exhibit more substantial shading impacts during Autumn and Winter, reinforcing the importance of orientation in urban design to optimize solar access.

The raster layer (Figure 5.2) maps the annual average shading height on building façades. Values are derived from hourly wall-shading simulations and averaged over the year. The colour scale indicates the percentage of each wall's height that is in shade on average. South- and east-facing façades generally show higher average shading, consistent with the solar path. Some north-facing walls also register high shading where adjacent buildings or structures are close enough to cast persistent shadows.

The Figure 5.3 maps the annual solar potential on building façades. Values are computed from hourly solar-irradiance simulations and aggregated over the year. Wall surfaces provide additional harvestable solar resource beyond rooftops. West-facing façades receive the greatest potential, while south- and east-facing façades have the lowest exposure.

Figure 5.3. Total solar potential on wall surfaces

5.1.2 Solar energy utilisation

The Figure 5.4 maps annual PV generation per square metre across the precinct for coverage setting of 50% of eligible rooftop area. The northern side of the precinct typically has good solar generation compared to the southern side, due to the shading path. Still, most of the new buildings within the redevelopment plan have reasonably good generation potential. It was also noted that different shapes and orientations of roof have effects to the predicted energy generation. Typically, north oriented roofs will have more hosting capacity than elsewhere oriented roofs.

Figure 5.4. Rooftop PV generation profile (kWh/m2/year) at 50% rooftop coverage ratio

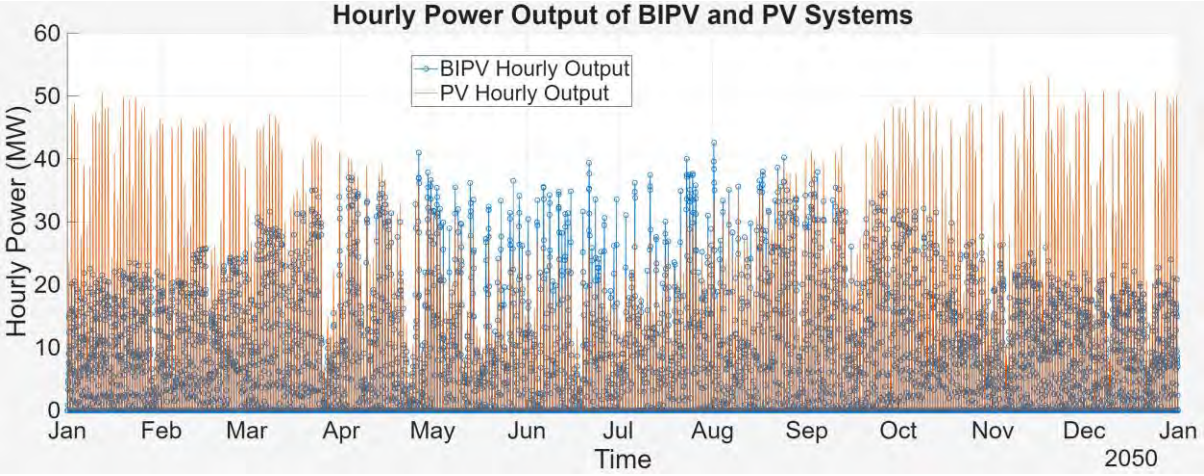

Figure 5.5. Seasonal matching effects of Façade PV systems and rooftop PV systems within the Sunshine Precinct

Figure 5.5 shows hourly, precinct-level generation from rooftop PV (orange) and façade BIPV (blue) across 2050. Rooftop PV exhibits the expected strong summer peaks (Nov–Feb) with frequent hours above 40–50 MW, and much lower winter output when the sun is lower and days are shorter. Façade PV contributes less absolute power overall, but its production is comparatively stronger through winter and the shoulder months (May–Sep), reflecting the advantage of vertical/east–west surfaces under low solar elevation and off-noon incidence.

Taken together, the two sources seasonally complement one another: rooftop PV supplies high summer energy, while BIPV lifts winter and shoulder-season generation and reduces the depth of the seasonal trough. This "matching" effect smooths the annual profile and improves the likelihood that local solar can meet demand outside peak-summer periods.

5.1.3 Energy load digitalization and simulation

This section presents the digitalised energy-load results for the precinct, including the annual end-use breakdown for HVAC, lighting, and appliances, the comparison of thermal loads under the current TMY and 2050 climate scenarios, and representative daily load profiles for different building types. The modelling was based on a consistent set of assumptions that are summarised in Section 13.1 (NCC 2022 J1V5, NCC 2022 J1V3, NABERS, and NaTHERS Handbook). All buildings are assumed to be fully electrified, including HVAC system, cooking and hot water.

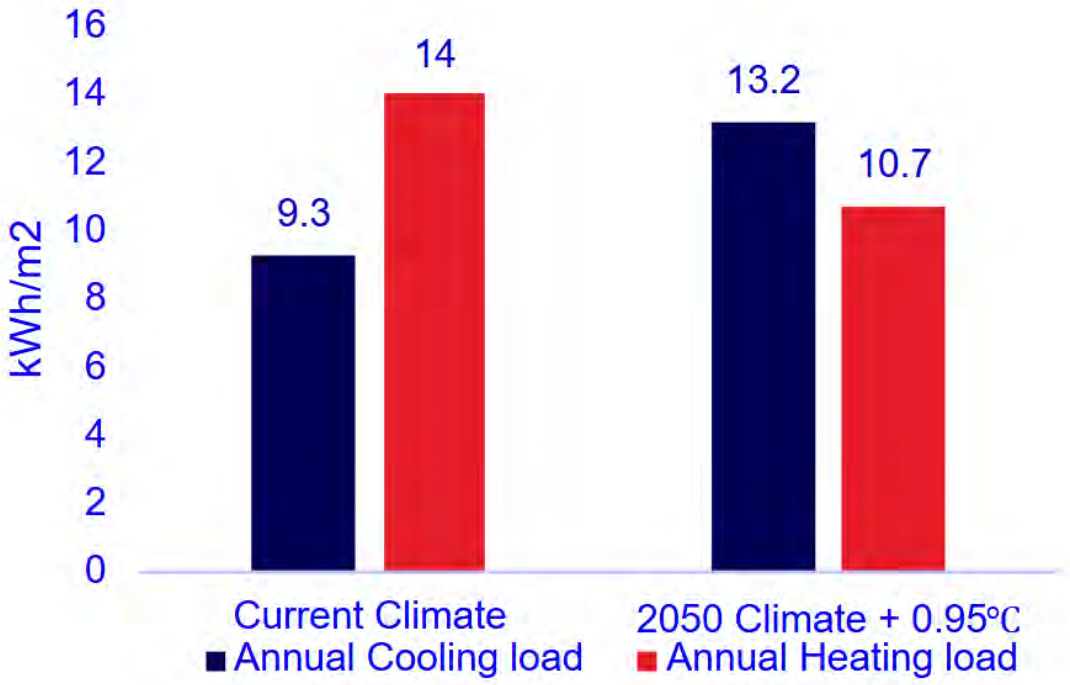

Figure 5.6. Heating and cooling load of current and 2050 climate

The results of the energy-load show several notable trends. Electric-vehicle charging increases annual electricity demand by 28% for residential buildings and 7% for commercial buildings. The electrification of hot water systems increases annual energy demand by 19% for residential users and 2% for commercial users. Residential buildings are considered to meet the NatHERS 7-star thermal performance standard. Future climate conditions are expected to reduce heating demand while increasing cooling demand (see Figure 5.6), resulting in a net 2.58% increase in total thermal load.

Based on the representative load profiles (Figure 5.7), commercial buildings exhibit higher demand during daytime hours, while residential buildings show two distinct peaks in the morning and evening, reflecting typical occupancy and activity patterns.

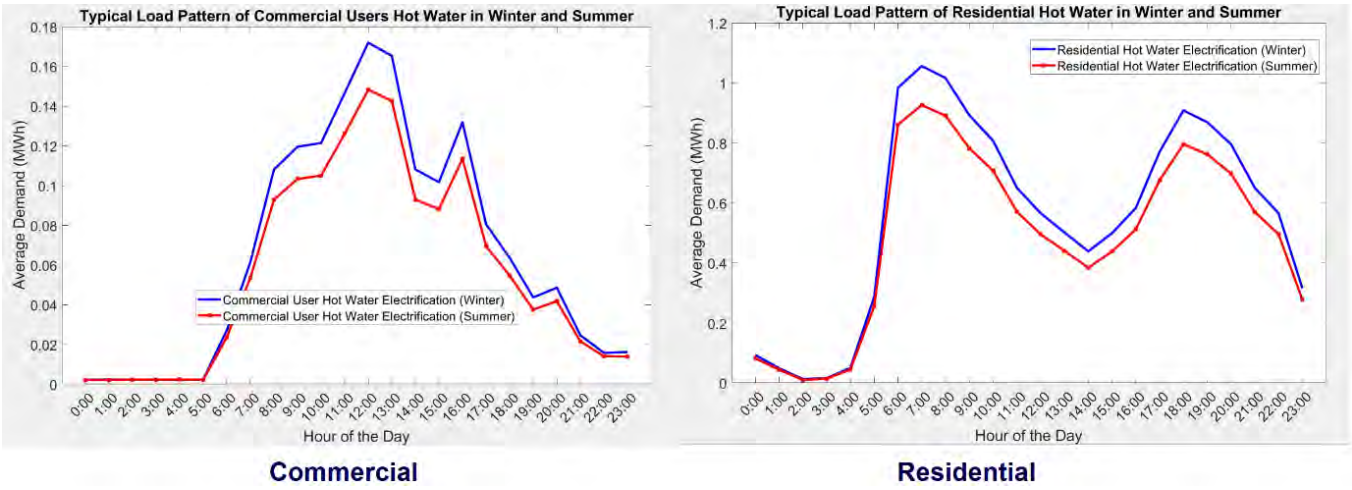

Figure 5.7. Energy consumption of two sectors under 2050

Figure 5.8 illustrates the projected 2050 energy-use breakdown for all residential units (excluding common areas) in Albion precinct, showing electrical appliances as the dominant end-use, followed by hot water and HVAC. Within the appliance category, kitchen cooking loads account for approximately 20% of the total appliance energy consumption.

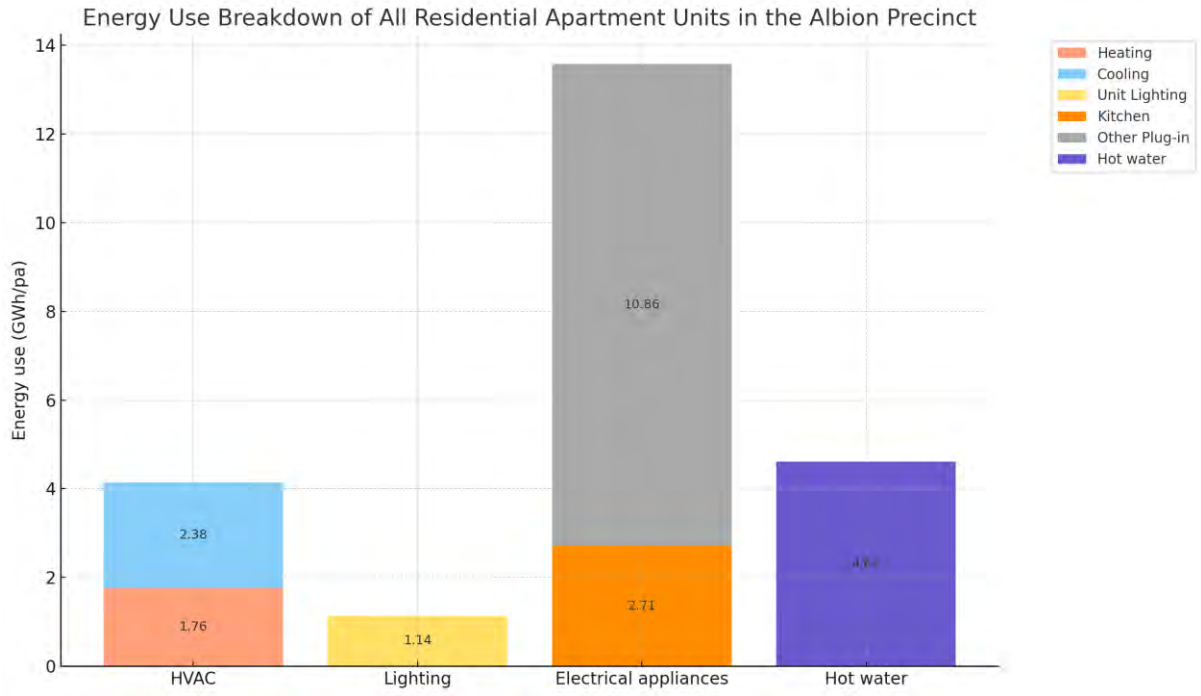

Figure 5.8. Energy consumption of all residential internal units' sector under 2050

As mentioned previously, this study, based on ENVI-met simulation outputs, quantitatively evaluates the effectiveness of greening strategies in reducing building cooling demand across the Energy Park, focusing on Buildings B-18 to B-20, as these buildings are located in close proximity to the Energy Park. The analysis compares overall building cooling energy consumption and peak load for cooling under three meteorological scenarios: (i) the Base Case without greening strategies, (ii) the Energy Park average weather conditions with greening strategies applied, and (iii) the localized weather conditions near the

B-18 to B-20 zone with greening strategies. It also examines the effects of greening strategies on cooling energy consumption for buildings across the area and at different heights.

As shown in Figure 5.9, under the hottest-day conditions, greening in the Energy Park significantly reduces overall cooling energy consumption during the day. Compared with the Base Case, the largest reduction occurs under the specific-zone meteorological conditions, while adopting the Energy Park's average meteorological conditions also produces a noticeable decrease, indicating a cooling effect across the entire Energy Park.

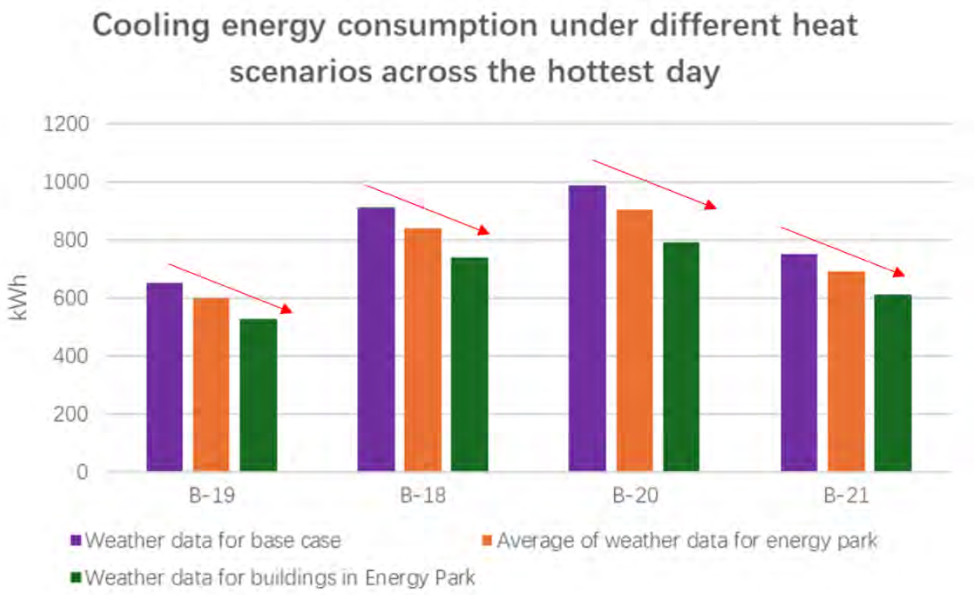

Figure 5.9. Cooling energy consumption under different heat scenarios across the hottest day

Figure 5.10 illustrates the reduction in peak cooling loads. Taking Building B-19 as an example, greening strategies significantly reduce peak loads during the high-temperature period from 14:00 to 17:00, with reductions of 10–15% under specific-zone meteorological conditions. This suggests that local microclimate improvements brought by greening (cooling, increased humidity, and optimized wind speed) have a strong effect in alleviating cooling demand during extreme periods.

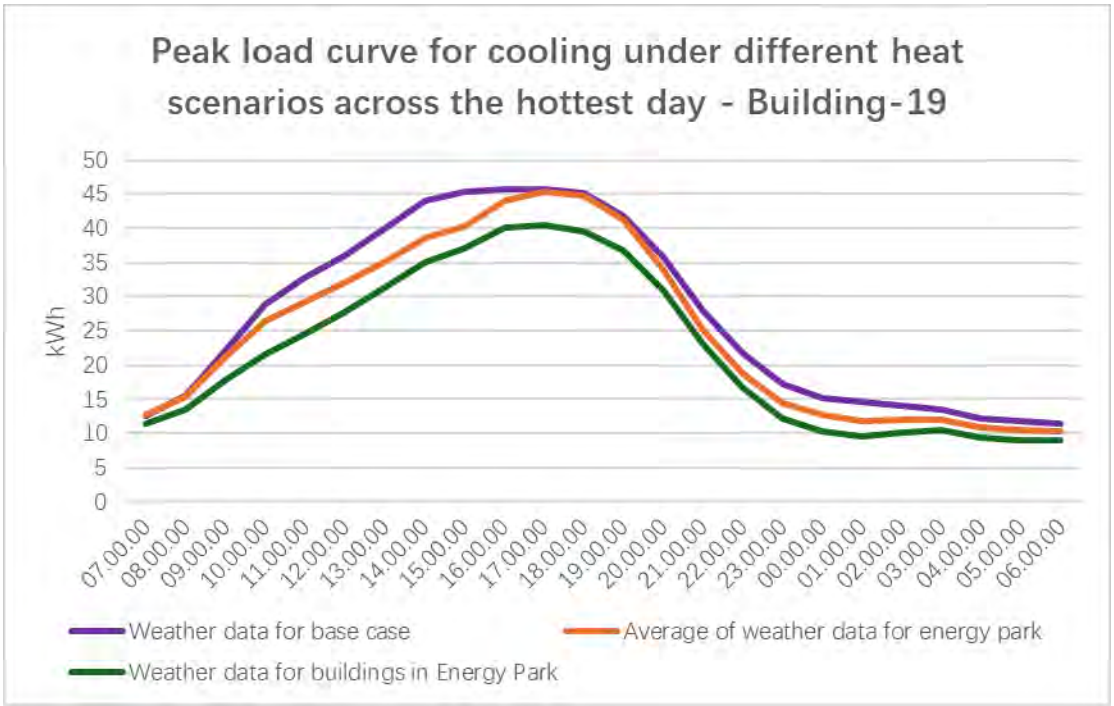

Figure 5.10. Peak cooling load curve under different heat scenarios across the hottest day – Building 19

Based on these meteorological files, an additional analysis was conducted for buildings with greater height. The analysis of cooling loads at different floor levels further reveals vertical variability in the greening effect, indicating that microclimate-induced cooling benefits are more pronounced at lower floors and diminish at higher floors. As shown in Figure 5.11, in a 30-meter-high building, the largest reductions 15–20%, are observed on the lower floors (0–2 floors). As building height increases, the reductions gradually diminish, with upper floors (7–8 floors) experiencing less than a 10% decrease. This indicates that greening in the Energy Park has a more pronounced effect on near-ground meteorological conditions, while the cooling and wind-speed improvements weaken with height, because these changes are primarily driven by latent heat fluxes associated with evapotranspiration and soil moisture at ground level, thereby limiting the effect on upper-floor cooling energy consumption.

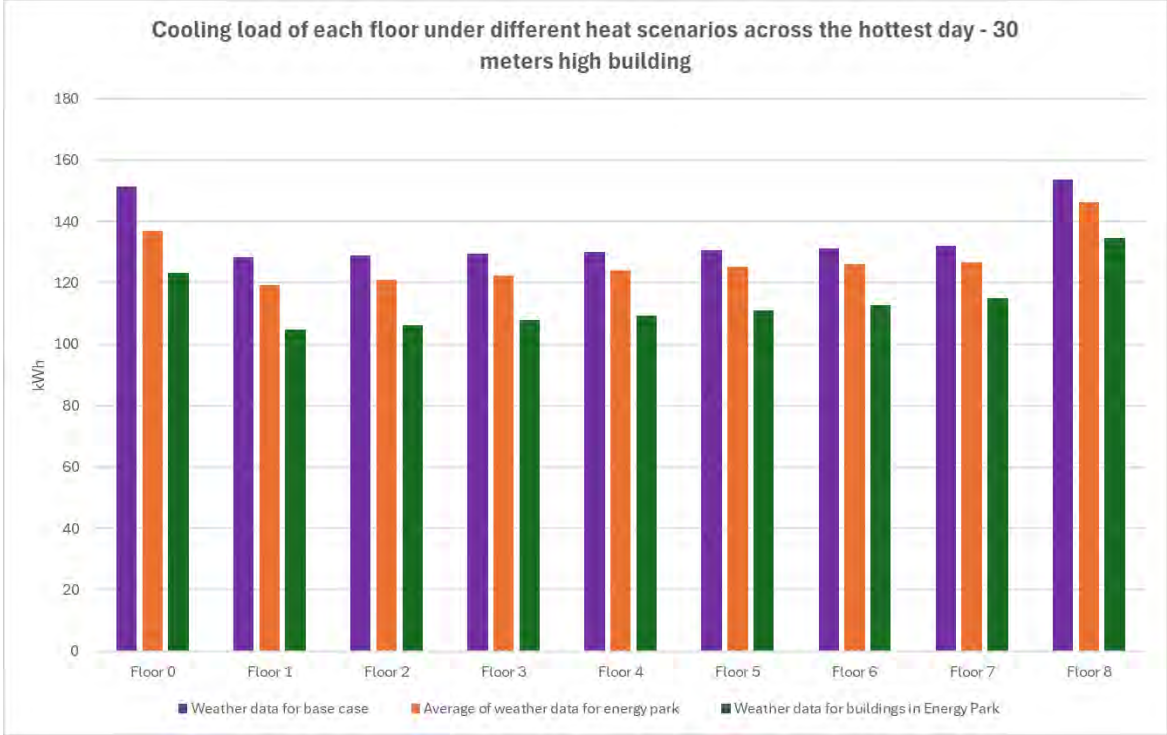

Figure 5.11. Cooling load of each floor under different heat scenarios across the hottest day – 30m high building

Overall, greening strategies in the Energy Park can effectively reduce both total cooling energy consumption and peak cooling loads by improving near-ground meteorological conditions. Areas with higher local greening coverage and more significant microclimate improvements achieve greater energy savings than the district-wide average. However, this cooling and energy-saving effect diminishes with building height. Therefore, in energy-efficient design for high-rise buildings, further solutions are required at upper floors, such green roofs.

5.1.4 Validation of the precinct-level energy management system

For both S1 and S3, multiple options were developed to test the different renewable energy, storage, and load options. For S1, two iterations of testing were carried out with option combinations shown in Table 13.2 and Table 13.3. Testing scenario iteration 2, with further detailed explanation presented in Section 13.2.1. The total number of option combinations is 72 for iteration 1 and 144 for iteration 2. For iteration 1, the purposes were to (1) Validate the effectiveness of FIS framework, (2) Examine the effectiveness of different energy options, and (3) Refine scope and modelling workflow. Following the analysis of the iteration 1, the option combinations were modified to refine the system options for façade PV and to exclude infeasible options in iteration 2. Therefore, with the project timeframe, for S3 specifically, only the iteration 2 was tested due to computational intensity and timeframe.

Two sets of indicators (load factor and variance coefficient) were used to examine the effectiveness of the FIS-based EMS in the iteration 1, further definition and calculation process of these variables can be found in Section 13.2.5.

The load factor results demonstrate that the FIS EMS consistently improves consumption efficiency across a broad range of configurations, with the improve rates in the top-performing scenarios ranging from +12.8% to +14.9%. These improvements are largely associated with the presence of façade PV and

medium-to-high battery capacities, indicating that additional generation sources and adequate storage play a critical role in smoothing the mismatch between supply and demand.

Rooftop PV capacity, however, does not exhibit a strong correlation with load factor improvements, suggesting that façade PV's orientation and generation profile may contribute more effectively to matching the local consumption profile. Carpark capacity appears to have minimal influence on consumption efficiency when EV smart charging is available, underscoring the dominant role of load scheduling over parking space availability. Conversely, the bottom-performing scenarios reveal that when both PV generation (rooftop and façade) and battery capacity are low, the addition of EV capacity can negatively impact load factor, even with smart charging, due to increased peak demands that cannot be offset by local generation or storage.

The variance coefficient (VC) results reveal a more nuanced picture of FIS EMS impacts on load stability. In the best-performing cases, the VC is reduced by up to 0.11, indicating a significant decrease in load variability. These scenarios typically combine low-to-medium rooftop PV, moderate storage capacities, and low carpark capacity, alongside EV smart charging. This configuration allows the EMS to exercise greater flexibility in load scheduling without introducing large fluctuations, as generation variability from high-capacity PV systems is minimised. Interestingly, the top VC improvements occur even in cases with relatively modest generation and storage, implying that stability benefits arise from the ability to shape demand rather than from the absolute size of supply assets.

While many configurations that improve LF also perform well in VC reduction, the relationship is not universal. Several high-LF scenarios, especially those with high rooftop PV and large batteries, appear among the worst VC outcomes. In these cases, the abundance of generation and storage may lead to more aggressive shifting of loads, creating sharper intra-day fluctuations and increasing variability (VC increases up to +0.11). This highlights a potential trade-off between maximising consumption efficiency and maintaining stability—overemphasis on one metric may degrade the other if control strategies are not carefully tuned.

The combined analysis of LF and VC suggests that the most effective EMS strategies require a balanced system design. Medium-scale PV and storage capacities, coupled with façade PV integration and coordinated EV smart charging, deliver simultaneous gains in both consumption efficiency and load stability. Over-sizing PV or battery systems without considering demand-side flexibility can undermine stability, even if efficiency improves. Therefore, scenario-specific optimisation is essential, and future work should explore multi-objective control approaches that explicitly account for both metrics to avoid unintended instability.

Table 5.2. Top 10 scenarios with improved consumption efficiency (Load Factor)

Scenarios	Rooftop PV (P)	Façade PV (F)	Battery capacity (B)	EV smart charging	Carpark capacity (E)	Load factor Original	Load factor with FIS EMS	Load Factor Difference
P03F02B03E02	High	Yes	High	Yes	Low	28.7%	43.6%	+14.9%
P02F02B03E02	Medium	Yes	High	Yes	Low	28.6%	43.2%	+14.7%
P03F02B03E03	High	Yes	High	Yes	Medium	26.1%	40.5%	+14.4%
P01F02B03E02	Low	Yes	High	Yes	Low	28.4%	42.5%	+14.1%
P03F02B03E04	High	Yes	High	Yes	High	24.9%	38.7%	+13.8%
P03F02B02E02	High	Yes	Medium	Yes	Low	28.7%	42.5%	+13.8%
P02F02B03E03	Medium	Yes	High	Yes	Medium	26.0%	39.7%	+13.7%
P02F02B02E02	Medium	Yes	Medium	Yes	Low	28.6%	41.8%	+13.3%
P02F02B03E04	Medium	Yes	High	Yes	High	24.7%	37.9%	+13.1%
P01F02B03E03	Low	Yes	High	Yes	Medium	25.8%	38.6%	+12.8%

Table 5.3. Bottom 10 scenarios with deteriorated consumption efficiency (Load Factor)

Scenarios	Rooftop PV (P)	Façade PV (F)	Battery capacity (B)	EV smart charging	Carpark capacity (E)	Load factor Original	Load factor with FIS EMS	Load Factor Difference
P01F01B01E01	Low	No	Low	No	Medium	26.0%	22.4%	-3.6%
P02F01B01E01	Medium	No	Low	No	Medium	26.5%	23.4%	-3.1%
P01F01B02E01	Low	No	Medium	No	Medium	26.0%	23.3%	-2.7%
P03F01B01E01	High	No	Low	No	Medium	26.9%	24.5%	-2.4%
P01F01B03E01	Low	No	High	No	Medium	26.0%	24.3%	-1.7%
P02F01B02E01	Medium	No	Medium	No	Medium	26.5%	25.2%	-1.3%
P03F01B02E01	High	No	Medium	No	Medium	26.9%	26.4%	-0.5%
P02F01B03E01	Medium	No	High	No	Medium	26.5%	26.3%	-0.2%
P03F01B03E01	High	No	High	No	Medium	26.9%	27.7%	+0.8%
P01F01B01E03	Low	No	Low	Yes	Medium	26.4%	27.5%	+1.1%

Table 5.4. Top 10 scenarios with improved load stability (variance coefficient)

Scenarios	Rooftop PV (P)	Façade PV (F)	Battery capacity (B)	EV smart charging	Carpark capacity (E)	VC Original	VC with FIS EMS	VC Difference
P01F01B03E02	Low	No	High	Yes	Low	0.49	0.38	-0.11
P01F02B01E02	Low	Yes	Low	Yes	Low	0.47	0.39	-0.08
P02F02B01E02	Medium	Yes	Low	Yes	Low	0.47	0.39	-0.08
P03F02B01E02	High	Yes	Low	Yes	Low	0.46	0.39	-0.07
P02F01B03E02	Medium	No	High	Yes	Low	0.49	0.39	-0.10
P02F01B02E02	Medium	No	Medium	Yes	Low	0.49	0.39	-0.10
P03F01B02E02	High	No	Medium	Yes	Low	0.48	0.40	-0.08
P03F01B01E02	High	No	Low	Yes	Low	0.48	0.40	-0.08
P01F01B02E02	Low	No	Medium	Yes	Low	0.49	0.41	-0.08
P01F01B03E02	Low	No	High	Yes	Low	0.49	0.38	-0.11

Table 5.5. Bottom 10 scenarios with deteriorated load instability (variance coefficient)

Scenarios	Rooftop PV (P)	Façade PV (F)	Battery capacity (B)	EV smart charging	Carpark capacity (E)	VC Original	VC with FIS EMS	VC Difference
P03F02B03E02	High	Yes	High	Yes	Low	0.46	0.57	+0.11
P02F02B03E02	Medium	Yes	High	Yes	Low	0.47	0.55	+0.08
P01F02B03E02	Low	Yes	High	Yes	Low	0.47	0.53	+0.05
P03F02B03E03	High	Yes	High	Yes	Medium	0.52	0.55	+0.03
P03F02B02E02	High	Yes	Medium	Yes	Low	0.46	0.49	+0.02
P02F02B03E03	Medium	Yes	High	Yes	Medium	0.53	0.54	+0.01
P02F02B02E02	Medium	Yes	Medium	Yes	Low	0.47	0.47	0.00
P01F02B03E03	Low	Yes	High	Yes	Medium	0.53	0.52	-0.01
P01F02B02E02	Low	Yes	Medium	Yes	Low	0.47	0.46	-0.02
P03F02B03E04	High	Yes	High	Yes	High	0.57	0.55	-0.02

To sum up the key observations of the scenario testing iteration 1, it is found that:

- Rooftop capacity above 20% does not contribute to consumption efficiency, and it is still unclear that what design factors among the façade PV contribute or worsen the load stability and consumption efficiency.
- EV smart charging is a fundamental requirement amid the expanding electrification.

Therefore, the iteration 2 of the scenario testing adopted further refinements of the scenario settings outlined in Section 13.2.1. With the validated FIS-EMS framework, following section conducts further analysis of power system dynamics and constraints using the iteration 2's refined scenario group of in total 144 scenarios.

5.1.5 S1 power system results

This section reports Base case (S1) network outcomes using the validated feeder and transformer model with hourly simulation for a full year in PowerFactory. Building side base load is aggregated by building group and then converted to a net load that combines base load, local generation, battery behaviour, and vehicle charging. Capacity assessment applies a planning envelope rather than a physical failure limit. For each distribution transformer the annual maximum utilisation is targeted to remain below ninety percent of the nameplate rating. This threshold is consistent with urban distribution planning practice, where the remaining margin caters for short duration peaks above the hourly average, diversity effects, and contingency operation. Within this envelope an annual mean loading close to sixty percent is treated as desirable rather than mandatory and is used as a heuristic indicator of available headroom or emerging bottlenecks.

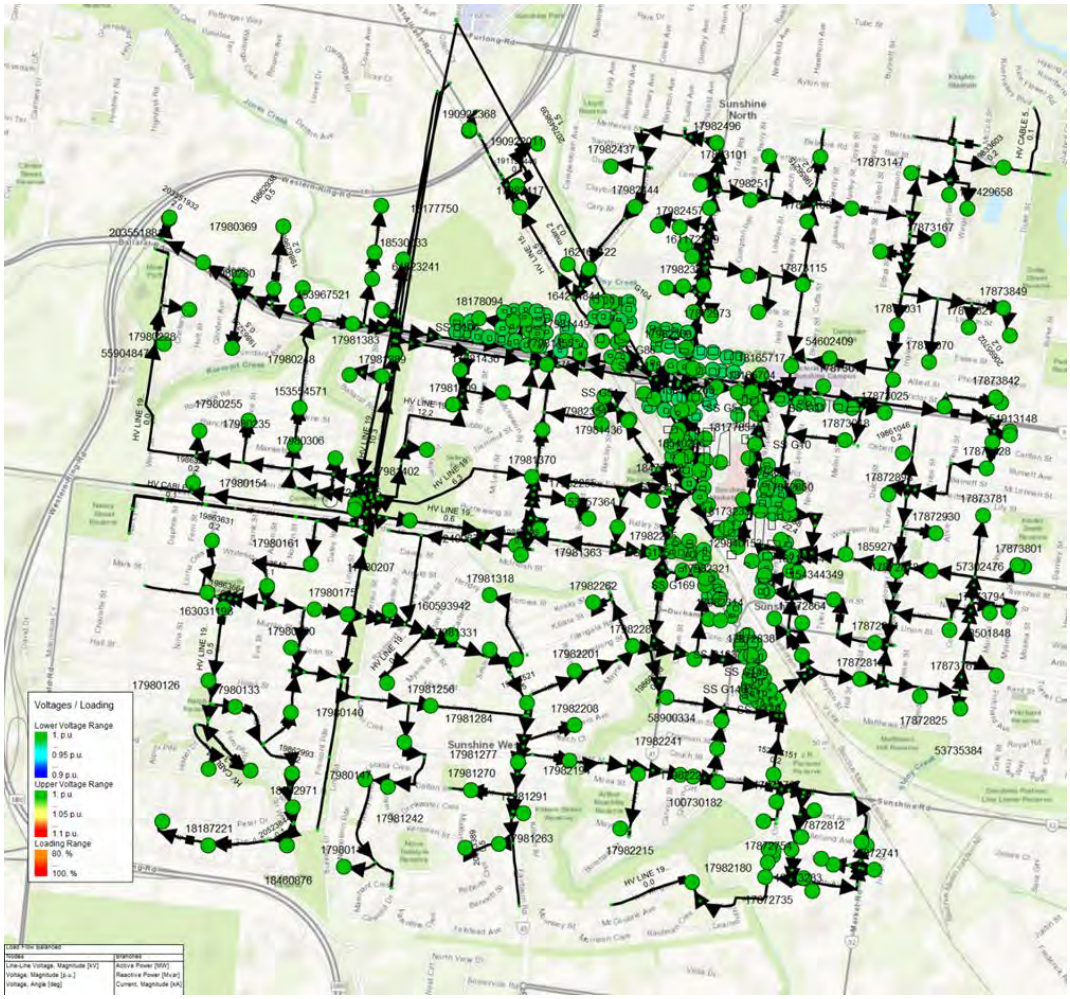

Figure 5.12. Overview of the distribution network supplying the precinct for Base Case

All power flow simulations run at hourly resolution for a full calendar year. For reporting and comparison, the hourly results are summarised into two planning windows that align with the dominant risk mechanisms in the precinct. The midday window covers the late morning to early afternoon period when photovoltaic output is strongest and reverse power flows are most likely. It is used to identify uplift risks such as elevated voltages and increased losses under high distributed generation. The evening window covers the late afternoon and early night period when residential and mixed-use demand peaks. It is used to test depression risks including voltage drop, transformer headroom, and thermal stress on heavily loaded feeders. These windows do not replace the underlying hourly simulation. They provide a consistent temporal filter so that indicators across scenarios are comparable and directly relevant to the specific planning questions.

Figure 5.12 and Figure 5.13 are used together to support interpretation of the power system results. Figure 5.12 presents the full distribution network supplying the precinct and is provided to show the overall feeder topology, upstream connectivity, and dominant power flow directions under the selected planning window. The network topology shown in figures is modelled on a one-to-one basis using the currently configured distribution network architecture. This overview establishes the broader network context within which the study area operates. Figure 5.13 provides a zoomed view focusing on the subset of feeders and distribution transformers that directly supply the aggregated building groups included in the

quantitative analysis. All feasibility screening, transformer loading, and capacity headroom results reported in the subsequent tables correspond to the assets shown in this zoomed view. Substations and feeders outside this focus area are retained in the overview figure for spatial and topological context only and are not included in the quantitative assessment.

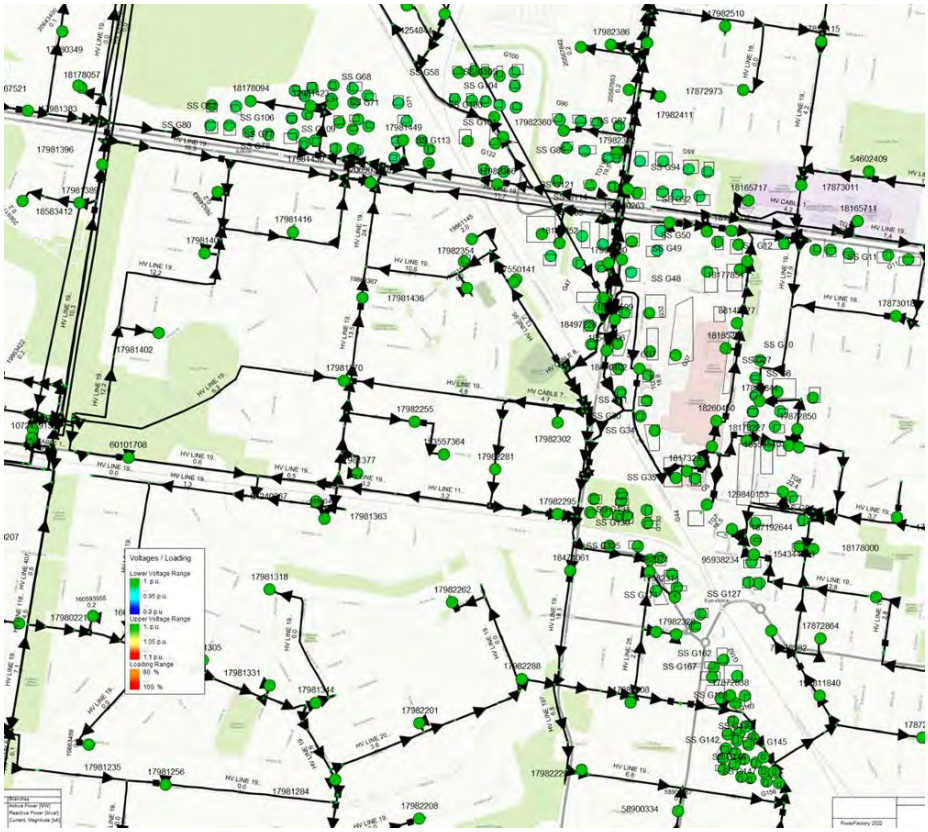

Figure 5.13. Zoomed view of the distribution network supplying the planning buildings analysed in Base Case

Feasible scenario set

This subsection defines the feasibility screen used for all power system results. All plots and tables that follow use only the scenarios that pass the hard constraints below. The full feasible scenarios appear in the Table 5.6.

Table 5.6. Base Case feasible scenarios used in results

scenario	rooftop PV coverage	BIPV coverage	BESS	EV
s1	20%	N:0%, S: 0%	Low	20%
s4	20%	N:0%, S: 0%	medium	20%
s7	20%	N:0%, S: 0%	high	20%
s10	20%	N:0%, S: 20%	low	20%
s13	20%	N:0%, S: 20%	medium	20%
s16	20%	N:0%, S: 20%	high	20%
s19	20%	N:0%, S: 50%	low	20%
s22	20%	N:0%, S: 50%	medium	20%
s25	20%	N:0%, S: 50%	high	20%

s28	20%	N:0%, S: 80%	low	20%
s31	20%	N:0%, S: 80%	medium	20%
s34	20%	N:0%, S: 80%	high	20%
s37	20%	N:20%, S: 0%	low	20%
s40	20%	N:20%, S: 0%	medium	20%
s43	20%	N:20%, S: 0%	high	20%
s46	20%	N:20%, S: 20%	low	20%
s49	20%	N:20%, S: 20%	medium	20%
s52	20%	N:20%, S: 20%	high	20%

Screening rules

A scenario is feasible if and only if all the following are satisfied for the full year and for both analysis windows.

a) Transformer loading. The annual maximum loading of one transformer over one hundred percent.
b) Voltage compliance. For every low voltage node, voltage not in operation band, 0.95p.u. – 1.05 p.u.
c) Thermal limits. No feeder or branch exceeds its continuous thermal rating in any hour.

NOTE. For clarity, voltage and thermal constraints reflect different physical mechanisms within the distribution network. Voltage at a given node is influenced by conditions both upstream and downstream along the feeder, including aggregated load and distributed generation. In contrast, thermal limits on feeders and branches are determined by the power flows to downstream nodes only, reflecting conductor current carrying capacity.

Feasible means all hard constraints pass. Infeasible means at least one hard constraint fails. While feasibility is defined strictly by compliance with all hard constraints, the type of binding constraint carries different planning implications. Scenarios that fail due to transformer loading limits typically indicate localised asset capacity issues, which in principle could be alleviated through targeted transformer upgrades. In contrast, infeasibility driven by voltage deviations or feeder thermal limits reflects broader network constraints that would require more extensive intervention, such as feeder reinforcement or coordinated voltage control strategies across the area.

Accordingly, the feasibility screening is not only used to exclude non-compliant scenarios, but also to identify the dominant constraint mechanisms shaping network performance. This distinction provides a basis for interpreting which scenarios are excluded due to fundamental network limitations, and which may remain technically viable subject to focused infrastructure upgrades, a question explored further in subsequent analysis.

Summary statement

The feasible set provides the evidence base for the subsequent power system analysis. Under the Base case configuration, which assumes the existing network architecture and no additional operational control or infrastructure augmentation, only eighteen scenarios satisfy all hard feasibility constraints.

These eighteen feasible scenarios form the basis for all subsequent power system results reported in this chapter.

Across the full set of one hundred and forty-four scenarios, all remaining scenarios fail at least one hard feasibility constraint. The dominant causes of infeasibility differ by time of day. During the midday period, high levels of coincident photovoltaic generation lead to excessive reverse power flows that exceed local network limits; during the evening period, concentrated electric vehicle charging demand places stress on transformers that were not originally designed to accommodate such coincident peaks, resulting in overload conditions or unacceptable voltage depression along weaker low voltage circuits and transmission line overloading.

Importantly, these infeasible scenarios are not interpreted as evidence of fundamental system failure. Rather, they identify specific locations where targeted interventions would be required to alleviate the observed constraints. In most cases the limiting factors are local and asset specific, indicating that measures such as spatial dispersion of photovoltaic capacity, managed evening discharge from distributed storage, or modest transformer upgrades could restore compliance. While the present study does not quantify the costs associated with these interventions, the results clearly distinguish between scenarios excluded due to hard feasibility constraints under the Base case assumptions and scenarios that remain technically viable subject to focused mitigation.

Transformer loading and capacity headroom

This subsection assesses transformer loading and capacity headroom under the Base case using hourly simulation results for the feasible scenario set. Transformer availability is evaluated relative to the planning criterion that annual maximum loading should remain below ninety percent of nameplate rating. The analysis adopts both an asset level perspective, to identify the most heavily loaded transformers, and a network wide perspective, to characterise the overall distribution of loading and remaining headroom across the study area.

Under the Base case, most distribution transformers operate comfortably within planning limits for annual maximum loading. Average utilisation remains moderate across large portions of the network, indicating that meaningful headroom is available in many locations where additional distributed generation or managed demand could be accommodated without immediate augmentation. However, a small subset of transformers operates close to the planning threshold during the evening window and therefore defines the binding constraints on network availability.

Table 13.8 summarises worst case transformer loading for each feasible scenario by reporting the maximum annual loading observed on the most heavily loaded device, together with the number of hours for which that device operates above eighty percent of its nameplate rating. These results highlight the specific assets that approach the planning limit under otherwise feasible operating conditions. Although all scenarios listed in Table 13.8 satisfy the hard feasibility constraints, several cases exhibit peak loadings close to ninety percent, typically concentrated over relatively short durations during the evening peak. This behaviour indicates proximity to localised capacity limits rather than sustained or system wide overload. The recurrence of the same transformers as worst performing devices across multiple scenarios further suggests that network availability is governed by a limited number of asset specific bottlenecks.

Table 13.9 provides a complementary network wide view of transformer availability by summarising the number of transformers operating above sixty percent, seventy percent, and eighty percent utilisation thresholds for each feasible scenario. This representation captures the dispersion of loading across the transformer population and provides an aggregate indication of remaining headroom. Across all feasible scenarios, a substantial number of transformers operate above sixty percent utilisation, reflecting active use of available capacity. In contrast, only a small subset exceeds seventy percent, and very few approach or exceed eighty percent of nameplate rating. This distribution confirms that, despite the presence of isolated high loading assets identified in Table 13.8, most of the scenarios retains meaningful capacity headroom under the Base case.

Taken together, Table 13.8 and Table 13.9 provide a planning level assessment of network availability and capacity headroom. The results demonstrate that transformer constraints under the Base case are localised rather than systemic, with overall network performance shaped by a small number of spatially clustered bottlenecks in higher density mixed residential and commercial areas. This pattern indicates that targeted, asset specific interventions would be sufficient to unlock additional hosting capacity, rather than requiring widespread network augmentation.

Voltage compliance

Since all feasible sets do not have voltage violation, all node voltage within 0.95 -1.05 p.u.

Network losses

Table 13.10 summarises annual and peak network losses across the feasible scenarios relative to the reference case. Overall, total annual losses remain within a narrow range across most scenarios, indicating that the distribution network operates under a broadly stable loss regime for the tested configurations.

For most scenarios, yearly total losses are marginally lower than the reference case, with reductions typically in the order of 1–3%. Mean and maximum instantaneous losses vary only slightly between scenarios, with mean losses clustered around 0.30–0.31 MW and maximum losses generally below 0.55 MW. Peak loss shares remain close to 0.17 across almost all cases, suggesting that differences in distributed energy resource configurations do not materially alter the timing or concentration of peak losses.

While small variations in annual losses are observed between scenarios, these differences are modest compared to the overall magnitude of system losses. This indicates that, within the feasible scenario set, changes in photovoltaic, battery, and electric vehicle configurations primarily affect the spatial and temporal distribution of power flows rather than driving substantial changes in aggregate network losses.

Renewable Utilisation Rate

Renewable Utilisation Rate (RUR) is defined as the ratio between the locally consumed renewable energy and the total renewable energy generated within the precinct over a year (Equation below). RUR captures how effectively the precinct absorbs its own PV/BIPV output after EV/BESS scheduling, excluding energy that is curtailed or exported.

$$RUR = E_{gen}/E_{cons}\ ,\ 0 \leq RUR \leq 1$$

Table 5.7. Summary of RUR by scenario for Base Scenario

Scenario	RUR	Energy generation / MWh	Energy consumption / MWh
s7	84.19%	9036.67	7608.37
s4	82.90%	9036.67	7491.58
s16	81.85%	11502.16	9414.88
s1	81.01%	9036.67	7320.36
s13	80.57%	11502.16	9267.47
s10	78.81%	11502.16	9064.86
s25	77.80%	15200.39	11825.25
s22	76.81%	15200.39	11675.09
s19	75.25%	15200.39	11438.23
s34	72.49%	18898.62	13699.76
s31	71.85%	18898.62	13579.39
s28	70.57%	18898.62	13336.60
s43	69.76%	22701.44	15836.78
s40	69.34%	22701.44	15741.40
s37	68.23%	22701.44	15489.92
s52	68.19%	25166.92	17160.75
s49	67.89%	25166.92	17086.50
s46	66.87%	25166.92	16830.05

EV (Smart Charging Compliance)

Smart Charging Compliance (SCC) is treated as an operational constraint rather than a performance outcome, reflecting the extent to which scheduled EV charging can be shifted away from the evening peak while remaining compatible with local network limits. All feasible scenarios share the same EV demand curve; what differs is the network and DER mix that EV charging must "fit into". Because SCC alone would look almost identical across scenarios, we added transformer loading compliance jointly evaluate:

(ii) how well the scheduler shifts EV power out of the evening peak (SCC logic);
(ii) whether the shift remains within safe transformer loading. This produces a fair, system-aware view of "how chargeable" each scenario is.

Metrics explanation:

Let:

- T be hours (here T=8736, due to the day one data).
- G be transformers (or LV feeders mapped to transformers).
- $L_{t,g}$ the loading (%) of device g at hour t under scheduled EV.
- $L^{base}_{t,g}$, the loading under baseline (unscheduled) EV.
- H_{peak} and H_{target} sets of peak and valley hours (our runs used 17:00–21:00 and off-peak windows).
- Loading limit Λ=80% (soft operational limit, configurable).

Note: Minor deviations are observed during the first simulation day due to initialisation effects associated with the commissioning of battery storage and electric vehicle charging. At this stage, devices may exhibit elevated charging activity to establish stable operating states from initial conditions. These effects are transient and limited to the first day of simulation and therefore do not affect the interpretation of annual results.

Loading Compliance Rate (LCR): fraction of system-hours that respect the limit, Values ~1 mean almost every hour/device is under 80%.

$$LCR = 1 - 1/TG \sum_{(t,g)} II\big(L_{(t,g)} > \Lambda\big)$$

Any Over Hours: Count of hours where any device exceeds Λ.

Over Mag Total: Cumulative over-limit magnitude, %-hours, this captures both how often and how far this index exceed the limit.

$$OverMagTotal = \sum_{t,g} \max\big(0, L_{t,g} - \Lambda\big)$$

P95 Loading (%): 95th percentile of $L_{t,g}$ within H_{target}, lower is more comfortable valley loading.

Target Headroom Avg (%): Average headroom to the limit in valley hours, values around 65% mean ample spare capacity while charging off-peak.

$$TargetHeadroomAvg = 1/\big(\big|H_{target}\big|G\big) \sum_{t \in H_{(target,g)}} \big(\Lambda - L_{(t,g)}\big)$$

Composite Score (0-1): this index aggregate after min-max normalisation (x) so that higher is better and "bad" metrics are inverted.

$$Score = w_1 LCR + w_2(1 - AnyOverHours) + w_3(1 - OverMagTotal) + w_4(1 - MaxLoading) + w_5(1 - P95Loading) + w_6 T\,\mathrm{arg}\,e\,tHeadroomAvg$$

$$\sum w_i = 1$$

$$w_1 \ldots w_6 = (0.25, 0.10, 0.15, 0.15, 0.10, 0.25),\ (configurable)$$

Table 5.8. Scenario ranking based on transformer loading performance relative to the 80% operational threshold for Base Case

Scenario	LCR	Any Over Hours	Over Mag Total	Max Loading	P95 Loading	Loading Avg	Score
s19	1.00000	0	0.00	77.74	29.66	65.37	0.9688
s22	1.00000	0	0.00	79.10	28.96	65.29	0.9604
s10	0.99989	1	2.69	82.69	30.09	65.20	0.9494
s25	1.00000	0	0.00	79.14	28.60	65.18	0.9486
s13	0.99966	3	6.16	83.91	29.42	65.10	0.9360
s16	0.99954	4	6.53	83.95	29.08	64.99	0.9239
s1	0.99931	6	15.11	86.13	30.45	64.96	0.9165
s4	0.99920	7	24.04	86.97	29.82	64.83	0.8996
s7	0.99920	7	23.82	87.02	29.53	64.71	0.8878
s37	0.99519	42	232.65	95.50	29.17	65.55	0.8872
s40	0.99451	48	277.14	95.50	28.30	65.54	0.8684
s43	0.99439	49	278.59	95.50	28.05	65.48	0.8609
s46	0.99245	66	384.59	98.67	28.88	65.64	0.8346
s49	0.99187	71	439.38	98.67	27.98	65.67	0.8169
s52	0.99176	72	443.99	98.67	27.79	65.60	0.8074
s28	0.98386	141	657.26	97.15	29.46	65.42	0.6750
s31	0.98352	144	664.39	97.14	28.75	65.35	0.6629
s34	0.98340	145	667.20	97.14	28.43	65.22	0.6482

To support comparison across feasible scenarios, a composite ranking is constructed based on transformer loading performance relative to the operational threshold. The metrics reported in Table 16 capture complementary aspects of network stress, including the frequency and magnitude of threshold exceedance, peak loading conditions, and overall utilisation levels.

The ranking score is designed as a normalised composite indicator that favours scenarios with high loading compliance, low exceedance duration, and reduced exposure to high loading extremes. It does not represent a physical quantity, but rather a comparative measure intended to distinguish scenarios that are more compatible with existing network capacity under smart charging operation. Accordingly, higher scores indicate scenarios that place lower operational stress on distribution transformers and therefore offer greater flexibility for EV charging without immediate augmentation.

Summary

Under the 18 feasible scenarios of Base case, all feasible scenarios share a common baseline of twenty percent rooftop photovoltaic coverage and twenty percent electric vehicle adoption. Differences in system performance therefore arise primarily from variations in the spatial distribution of building integrated photovoltaic capacity and the scale of distributed battery storage. Within this envelope, the power system is able to operate safely under existing planning limits; however, the results indicate that rising distributed energy penetration increasingly requires deliberate spatial and temporal management rather than uniform capacity expansion.

Across the feasible scenario set, results indicate that voltage compliance and transformer loading are sensitive to how additional photovoltaic capacity is spatially allocated across the network. Scenarios with higher concentrations of building integrated photovoltaics on specific feeders exhibit increased exposure to reverse power flows and voltage constraints, suggesting that feeder aware deployment strategies may be important as photovoltaic penetration increases.

The comparative analysis further shows that transformer loading, and voltage performance are most sensitive to evening demand conditions, which remain consistent across scenarios due to the EV demand profile. Scenarios with low battery capacity are more likely to approach transformer loading limits during the evening window, whereas medium and high battery configurations consistently mitigate peak loading through targeted discharge. This confirms that distributed storage plays a critical role in decoupling photovoltaic generation from evening demand, particularly as building integrated photovoltaic penetration increases.

Taken together, the feasible scenario results provide clear guidance on the types of grid infrastructure interventions that would be required to accommodate higher levels of photovoltaic and battery penetration. Among the full set of one hundred and forty-four scenarios, those that fail the hard feasibility constraints do so primarily due to either excessive reverse power flows during midday photovoltaic peaks or transformer loading exceedances during evening electric vehicle charging periods. Importantly, these infeasible scenarios are not excluded from further consideration on the basis of fundamental incompatibility with the network. Instead, they identify asset specific and location dependent constraints, indicating where targeted grid upgrades such as transformer capacity augmentation, feeder reinforcement, or enhanced voltage control would be necessary to restore technical feasibility. The implications of these required infrastructure upgrades, including their impact on system energy performance and associated costs, are examined in the subsequent section on energy performance and economic analysis.

5.2 Updated scenario results

5.2.1 Shading comparison across scenarios

Figure 5.14 presents a comparison of the shading impacts across scenarios S1 and S3. The seasonal variations between winter and summer months are generally consistent with the patterns discussed in Section **Error! Reference source not found.**. During summer, shading tends to be concentrated along t he streets oriented in the south–north direction, while in winter it shifts toward the east–west-oriented streets.

Among the two scenarios, S1 (the base scenario) shows the greatest extent of shading during the winter months. Although S3 features a taller urban form compared with S1, the shading impact in S3 is less significant throughout the seasons. This improvement can be attributed to the more coordinated building orientations, as most buildings are arranged in parallel with one another, reducing the extent of inter-building shadowing.

Base Case Scenario

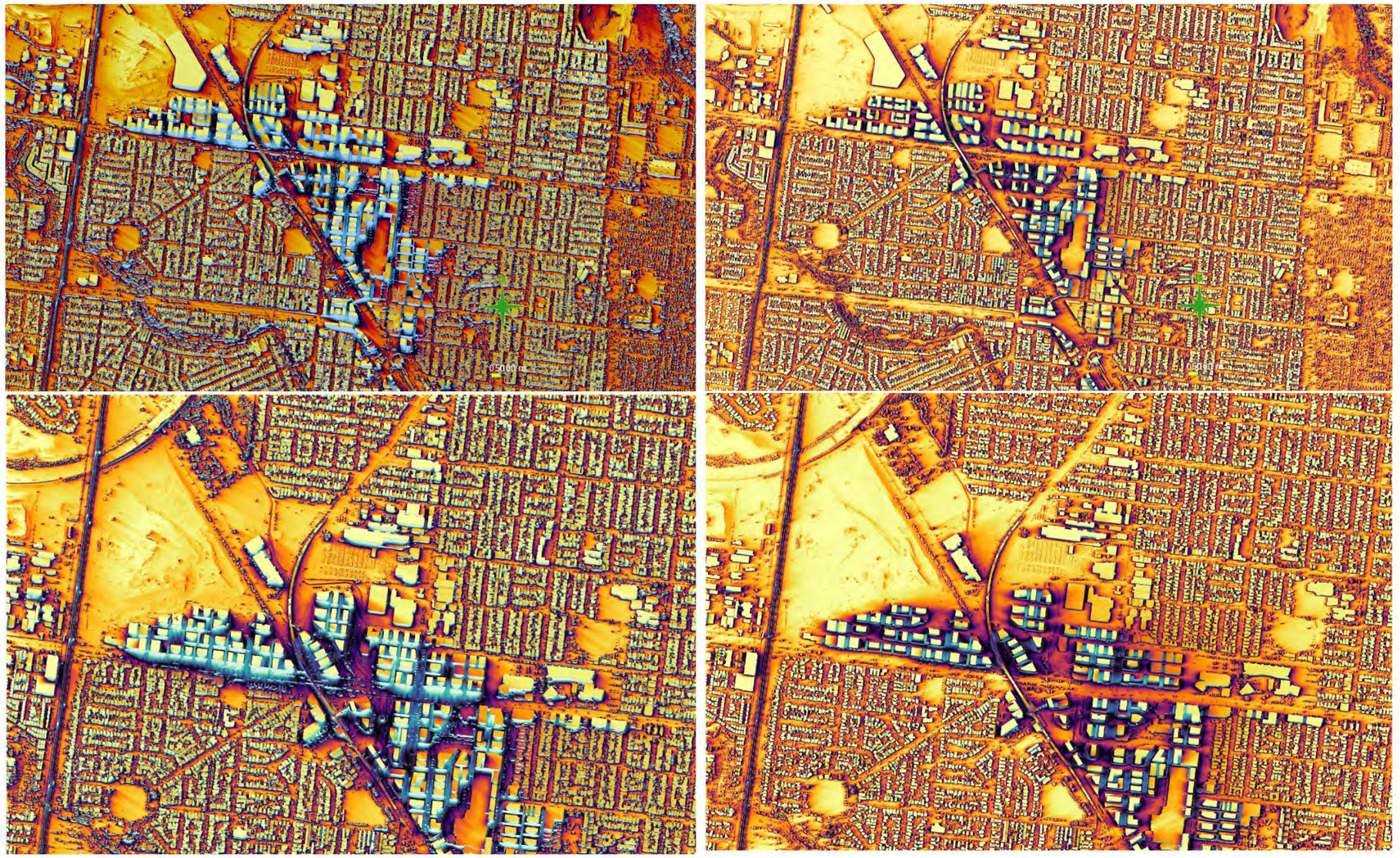

Figure 5.14. Shading comparison for winter/summer seasons across scenarios

5.2.2 Energy load digitalization and simulation

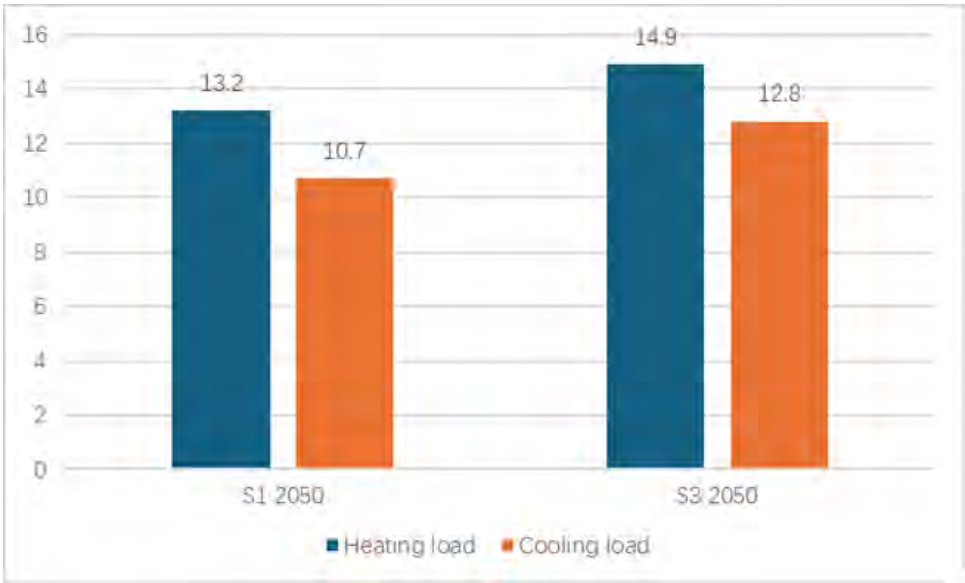

Figure 5.15. Heating and cooling load of S1 and S3

Simulation results of Scenario S3 indicate that when the urban form transitions from a layout dominated by detached buildings to a high-density configuration composed of tower–podium complexes, both heating and cooling loads increase even under identical meteorological boundary conditions. This is mainly because in the tower–podium configuration, 20% of residential units are located on the podium levels, and these podium façades experience much stronger shading from adjacent towers. A large proportion of the walls are facing the neighbouring parking podiums, resulting in weaker direct solar gains.

When the same window configuration as in S1 (U = 1.7 W/m²·K, SHGC = 0.25) is adopted and the window-to-wall ratio is kept at 40%, the heating demand in S3 rises significantly. After adjusting the window parameters to a higher solar heat gain coefficient and a slightly higher thermal transmittance (U = 1.9 W/m²·K, SHGC = 0.45), the heating load decreases markedly but remains higher than in S1; meanwhile, the cooling load also increases compared with S1. For the upper tower zones where mutual shading is less severe, the increased Solar Heat Gain Coefficient (SHGC), thereby contributing to the overall rise in cooling demand in S3.

In the high-density layout, the narrow spacing between podiums and enhanced mutual shading among buildings lead to a substantial reduction in the sky view factor and a decrease in direct solar gains on lower façades. At the same time, shortwave reflections between adjacent façades and ground surfaces intensify, while longwave radiation dissipation is constrained, resulting in elevated equivalent surface temperatures. Consequently, even with identical external weather conditions, building envelopes in dense areas receive a lower net radiative flux, leading to greater conductive heat transfer and increased heating demand. Compared with S1, even with a higher-performance window system, the heating load still increased by 13%.

Increasing the solar heat gain coefficient of windows (from 0.25 to 0.45) partly compensates for the loss of solar radiation on lower façades, thereby effectively reducing winter heating loads. However, this

adjustment simultaneously allows more direct solar radiation to penetrate the upper façades of towers during summer, raising cooling loads. The slightly higher thermal transmittance (U = 1.9) further amplifies the window's thermal exchange sensitivity, making the building's thermal response more dynamic.

Overall, the simultaneous increase in heating and cooling loads in Scenario S3 stems primarily from radiative coupling and heat retention effects inherent in the thinner/taller built forms in the S3, rather than deficiencies in individual envelope performance. The results suggest that in dense urban environments, the dominant mechanism of building energy consumption shifts from envelope control to morphology control. Within high-density urban morphologies, optimizing the building envelope can only partially mitigate the upward energy trend—building energy performance depends more on morphological-scale thermal environment regulation than on fine-tuning individual thermal parameters. Compared with S1, the total thermal load increased by 15.8%.

5.2.3 Power system analysis results

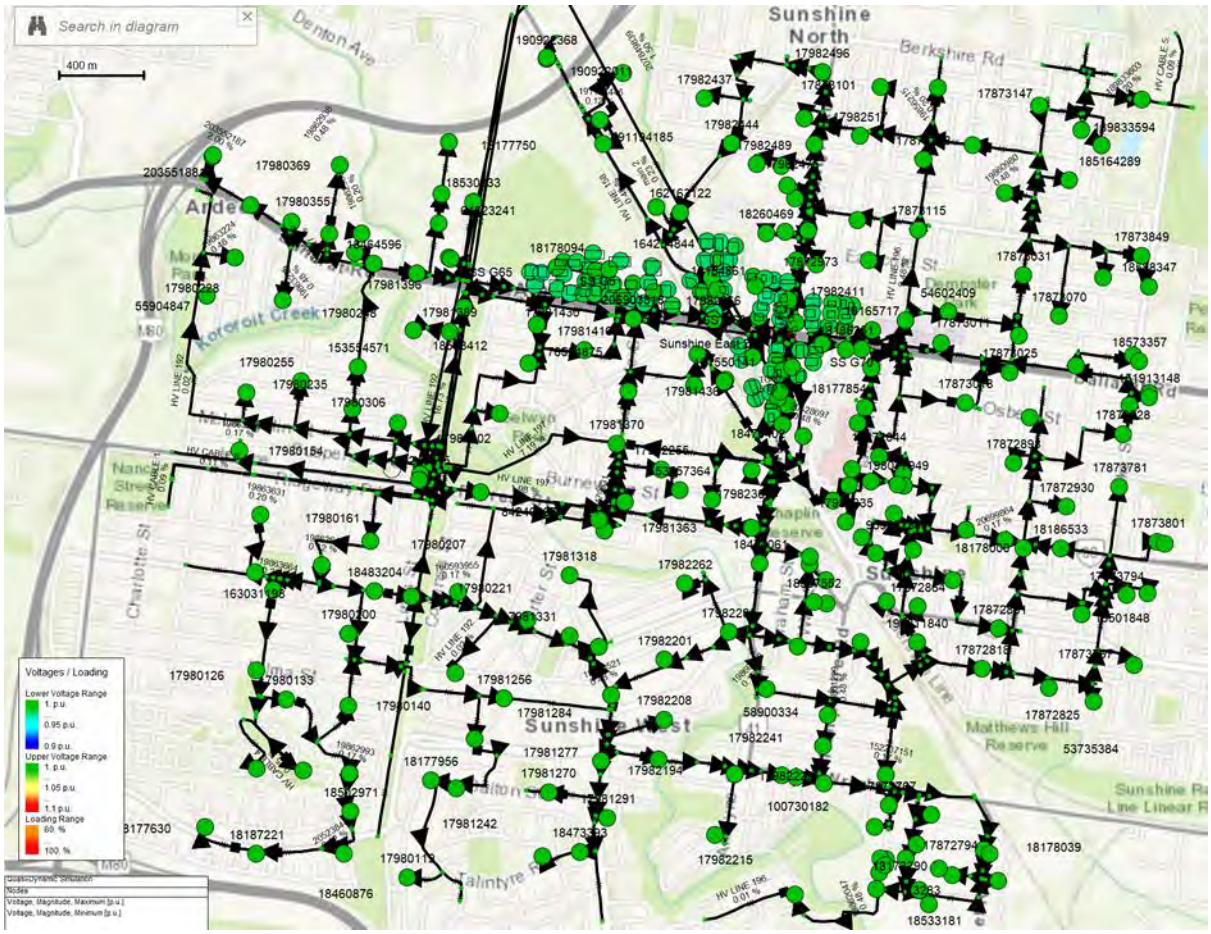

Figure 5.16. Study area network and analysis windows for scenario 3

This section reports S3 (Scenario 3) network outcomes using the validated feeder and transformer model with hourly simulation for a full year in PowerFactory. Building side base load is aggregated by building group and then converted to a net load that combines base load, local generation, battery behaviour, and vehicle charging. Capacity assessment follows the rule that the annual maximum loading must remain at or below ninety percent. The average loading should approach sixty percent subject to the maximum

constraint. Two analysis windows are used. The midday window identifies uplift risk from photovoltaic. The evening window identifies depression risk due to demand concentration.

Feasible scenario set

The feasible scenario set defines the subset of scenarios that satisfy all hard feasibility constraints and therefore form the basis for the subsequent power system analysis. These scenarios are not selected as alternative design options but rather emerge from the feasibility screening of the full set of 144 scenarios. While limited in number, the feasible scenarios span a representative range of photovoltaic integration patterns and battery storage levels that remain technically compatible with the existing network configuration.

Table 5.9. S3 feasible scenarios used in results

scenario	rooftop PV coverage	BIPV coverage	BESS	EV
1	0.2	N:0%, S: 0%	low	20%
4	0.2	N:0%, S: 0%	medium	20%
7	0.2	N:0%, S: 0%	high	20%
10	0.2	N:0%, S: 20%	low	20%
13	0.2	N:0%, S: 20%	medium	20%
16	0.2	N:0%, S: 20%	high	20%
19	0.2	N:0%, S: 50%	low	20%
22	0.2	N:0%, S: 50%	medium	20%
25	0.2	N:0%, S: 50%	high	20%
28	0.2	N:0%, S: 80%	low	20%
31	0.2	N:0%, S: 80%	medium	20%
34	0.2	N:0%, S: 80%	high	20%

Transformer loading and capacity headroom

Under Scenario 3, most transformers remain within planning limits for the annual maximum loading. A small subset operates close to the threshold in the evening window and should be watched in option testing. Average loading is moderate across many areas, which indicates usable headroom where additional distributed generation, or managed demand could be accommodated without immediate augmentation. Bottlenecks show spatial clustering in higher density mixed residential and commercial zones.

Table 5.10. Summary of transformer loading for Scenario 3

Scenarios	worst Device Max Loading/ %	Worst Device Over 80%_hours Count
s1	92.32	20
s7	92.32	19
s4	92.32	19
s10	92.31	18
s19	92.31	18
s13	92.31	18
s16	92.31	18

s28	92.31	18
s22	92.31	18
s25	91.31	12
s31	85.97	11
s34	85.97	10

Network losses

Under Scenario 3, total annual network losses range from approximately 2.19 to 2.26 GWh, representing a 1.6–2.9% reduction relative to the reference case for most feasible configurations. Mean losses remain stable at around 0.25–0.26 MW, while peak losses are reduced from 390 MW (reference) to approximately 369–385 MW, depending on the scenario. The peak loss share remains broadly consistent at ~0.17, indicating that loss reductions are driven primarily by overall load redistribution rather than changes in peak coincidence. Scenarios with higher distributed PV and storage penetration exhibit the largest reductions in both total and peak losses, whereas configurations closer to the reference show marginal increases (<0.5%). Overall, Scenario 3 delivers modest but consistent network loss improvements without introducing additional peak loss stress.

Table 5.11. Summary of network losses for Scenario 3

Row	Yearly Total Loss / MWh	Mean Loss / MW	Max Loss / MW	Peak Loss / MW	Peak Share	Mean Abs Delta / MW	Delta Total Vs Ref / MWh	Delta Total Vs Ref / %
s34	2189.16	0.25059	0.33981	369.17	0.16863	0.00325	-65.56	-2.91%
s31	2190.32	0.25072	0.33903	369.84	0.16885	0.00341	-64.4	-2.86%
s28	2193.01	0.25103	0.33749	370.47	0.16893	0.00368	-61.71	-2.74%
s25	2200.75	0.25192	0.35243	371.92	0.169	0.00351	-53.97	-2.39%
s22	2202.17	0.25208	0.35204	372.57	0.16919	0.00369	-52.55	-2.33%
s19	2204.43	0.25234	0.35141	373.14	0.16927	0.00393	-50.29	-2.23%
s16	2217.39	0.25382	0.36943	375.55	0.16937	0.00395	-37.33	-1.66%
s13	2218.43	0.25394	0.36895	376.08	0.16953	0.00411	-36.3	-1.61%

s10	2219.78	0.2541	0.3688	376.41	0.16957	0.00427	-34.94	-1.55%
refer	2254.72	0.2581	0.40109	390	0.17297	0.00483	0	0.00%
s7	2263.42	0.25909	0.39026	384.67	0.16995	0.00463	8.7	0.39%
s4	2263.95	0.25915	0.3904	384.99	0.17005	0.00473	9.23	0.41%
s1	2264.61	0.25923	0.38999	385.13	0.17006	0.00481	9.89	0.44%

Renewable Utilisation Rate

Renewable Utilisation Rate (RUR) is defined as the ratio between the locally consumed renewable energy and the total renewable energy generated within the precinct over a year (Equation below). RUR captures how effectively the precinct absorbs its own PV/BIPV output after EV/BESS scheduling, excluding energy that is curtailed or exported.

Table 5.12. Summary of RUR by scenario for Scenario 3

Scenario	RUR	Energy generation / MWh	Energy consumption / MWh
s7	0.993563	2328605	2313616
s4	0.9928	2328605	2311839
s1	0.991491	2328605	2308791
s16	0.913834	5291961	4835976
s13	0.907922	5291961	4804690
s10	0.900402	5291961	4764894
s25	0.78052	9736994	7599918
s22	0.773703	9736994	7533546
s19	0.762543	9736994	7424879
s34	0.656749	14182027	9314030
s31	0.652335	14182027	9251429
s28	0.642912	14182027	9117790

Summary

Under the S3 configuration, the power system can operate safely for a reduced subset of feasible scenarios; however, the feasibility envelope is notably narrower than in the Base case. This difference is primarily driven by structural characteristics of the S3 development, rather than changes in the underlying network topology or operating assumptions. Compared with the Base case, S3 includes fewer but higher buildings, resulting in higher absolute levels of BIPV and battery capacity per building for the same percentage-based deployment assumptions.

Consequently, binding constraints in S3 emerge more readily at specific assets, particularly at transformers serving larger buildings where both midday reverse power flows from building integrated photovoltaics and evening electric vehicle charging loads are concentrated. While transformer loading remains the dominant constraint across the feasible S3 scenarios, the reduced number of feasible configurations highlights the increased sensitivity of the network to spatial concentration effects at the building level.

These results indicate that the S3 outcomes are not a direct replication of the Base case findings but rather reflect a development structure in which identical percentage-based energy configurations translate into materially different network impacts. The S3 analysis therefore reinforces the importance of asset specific assessment when scaling distributed energy resources in precincts characterised by fewer, higher density buildings, even where overall penetration levels appear comparable.

5.3 Analysis and discussions

5.3.1 Introduction

This section presents an integrated assessment of energy performance, economic viability, and infrastructure feasibility for renewable energy deployment in dense urban environments. The analysis begins by examining how differences in urban form, spatial structure, and system configuration shape energy outcomes across alternative development scenarios (S1 and S3).

Energy viability is assessed using simplified energy supply costs and values for energy surplus (feed in) of 30c/kWh and 5c/kWh respectively. This may understate the value of energy technologies like battery storage in the short term, that can charge at lower prices and discharge at high prices when the energy customer at a premise is exposed to wholesale market contracts.

However, there is substantial uncertainty over future prices, price volatility and customer willingness to adopt wholesale price exposure. Further, the primary goal here is to inform planning decisions, as opposed to assess specific energy asset investments. For these reasons, the simplified energy cost structure has been chosen, as it helps us understand key technology constraints and planning opportunities that effect built form. Economic viability results should be read in that context - they are designed to inform planning choices, and do not necessarily reflect the economic viability of specific technologies today.

Differences in spatial efficiency and the concentration of functional floor area (FFA) play a critical role in mediating outcomes. Variations in building height and urban compactness influence renewable generation potential, energy demand intensity, and the interpretation of performance metrics under different normalisation approaches (e.g. project land area versus FFA). Explicitly accounting for these spatial effects enables a more transparent comparison between scenarios and avoids misattributing performance differences to technology choices alone.

Building on this scenario-level assessment, the section then considers economic and infrastructure implications from a multi-stakeholder perspective. Economic indicators, including net present value (NPV) and internal rate of return (IRR), are evaluated from the perspective of private investors and households, reflecting costs and benefits borne directly by renewable energy adopters. Infrastructure upgrade requirements included within the cost analysis are also assessed separately as an indicator of the potential impacts to the energy infrastructure. This structure enables trade-offs between private financial viability, infrastructure stability, and broader energy system objectives.

The analysis is based on a comprehensive exploration of a 145-scenario design space (144 scenarios in iteration 2 plus 1 BAU scenario) spanning variations in photovoltaic deployment, battery storage configurations (including both household and utility-scale systems), and electric vehicle (EV) uptake.

The key design variables examined include building-integrated photovoltaics (BIPV) differentiated by façade orientation (north-facing and east–west-facing), battery storage deployment, and EV uptake levels. Rooftop PV capacity is fixed at 20% of available roof area across all scenarios. This represents a relatively high but realistic penetration level given the spatial and geometric constraints typical of dense urban environments and is consistent with expectations under current National Construction Code (NCC)

requirements. Further subdivision of rooftop PV penetration within the 0–20% range was therefore not pursued, as the resulting marginal differences would be negligible relative to the broader system-scale effects investigated in this section.

Table 5.13 summarizes the key assumptions, parameter values, and literature sources underpinning the energy, economic, and infrastructure modelling in this analysis. This table provides the common reference point for the results presented throughout Section 5.3.

Table 5.13. Key assumptions for energy performance and economic analysis

Items	Assumptions	References/Notes
	Category 1: System cost settings	
PV cost	**Total system cost: 1200 AUD/kW** Equivalent to ~264 AUD/ m² for a 22% nameplate efficiency	The current rate as of 2025 sits at 1200 AUD per KW system as of the most recent APVI report: https://apvi.org.au/wp-content/uploads/2025/11/PViA-2024-v3.pdf
BIPV cost	**Total system cost: 481.70 AUD/m².** • Unit area cost for BIPV system: 503.30 AUD/m² (opaque) and 763.50 AUD/m² (semi-transparent). • Unit area cost offset through replacing original façade material: 251.8 AUD/m² (opaque) and 280.58 AUD/m2 (semi-transparent) • Estimated installation cost: 40% of the system cost. • Window-to-wall ratio: 4:6	Based on project team's BIPV database and research outputs: Economic viability of building integrated photovoltaics: A review of forty-five (45) non-domestic buildings in twelve (12) western countries - ScienceDirect
Battery system cost	**Home battery system: 1,200 AUD/kWh capacity** **Utility BESS: 575 AUD/kWh capacity excluding supporting transmission infrastructure** Note: *Network upgrade costs (distribution network upgrade for a battery within the precinct's distribution zone and transmission/distribution network upgrade for a battery outside the distribution zone) are not included into the calculation. **Land cost for utility BESS are not included in the calculation.	Ref: GEM 2024 Solar PV and Battery Projections Report Section 4.3 Page 42, Publisher: AEMO Ref: CSIRO Gen Cost 25-26 https://www.csiro.au/-/media/Energy/GenCost-2025-26-Draft/GenCost2025-26ConsultDraft_20251216-FINAL.pdf Section 4.3.13 Page 40.
Generation degradation rate	**0.05% per year**	This rate reflects the PV and BIPV systems' power degradation over time. It will affect future profitability through energy cost saving and energy export.
	Category 2: Electricity price	

Energy retail price	0.3 AUD/kWh (300 AUD/MWh) excluding supply charge	Estimated based on Victorian ESC default offer 2025 in Powercor distribution zone for domestic customers and small business customers. Victorian Default Offer | Essential Services Commission
Energy export price	0.0483 AUD/kWh (48.34 AUD/MWh)	Estimated based on the Victorian long-term average wholesale electricity prices (RRP) of NEM. AEMO | Aggregated price and demand data
Category 3: Financial benchmarking		
Deposit rate	3.60%/year The return rate threshold of low-risk return	Based on RBA Interest Rate Decision 2025 Australia Interest Rate
Weighted average cost of capital (WACC)	3.66% The discount rate for calculating net present value (NPV) of investment	• Deposit interest rate: 4.1%/year • Equity Rate: 4.8%/year (Estimated based on 10-year stock market return rate of ASX) • Debt ratio: 50% • Equity ratio: 50% • Corporate tax rate: 30%/year Australia Indicators Australia Stock Market Index - Quote - Chart - Historical Data - News | Trading Economics
Category 4: Infrastructure upgrade cost		
Infrastructure upgrade cost	62.57 AUD/KVA upgrade	Annual pricing proposal 2024-25

5.3.2 Analytic methods

Energy performance indicators

Following indicators were calculated for each scenario to analysis the energy performance:

- **Self-sufficiency rate (SSR):** The proportion of total energy demand that is met by on-site renewable energy generation (directly or via storage).

$$SSR = \frac{E_{Consumed\ Generation}}{E_{Total\ Load}}$$

- **Renewable energy utilisation rate (RUR):** The proportion of on-site renewable energy generation that is actually used locally rather than exported.

$$RUR = \frac{E_{Consumed\ Generation}}{E_{Total\ Generation}}$$

- **Generation-to-load ratio (GLR):** The ratio of total renewable energy generation to total energy demand over a given period.

$$GLR = \frac{E_{Total\ Generation}}{E_{Total\ Load}}$$

- **Net present value (NPV):** The present value of all future cash inflows minus outflows over the asset lifespan, discounted to year 0 using WACC. NPV is calculated with the following equations:

$$NPV = \sum_{t=0}^{T} \frac{B_t - C_t}{(1 + WACC)^t}$$

- Where T = 30 is the lifespan of the BESS and PV systems before a replacement is imminent.
- B_t is the benefit cashflow at year t, including annual incomes from energy cost saving, and energy export. The B_t gradually reduces over the lifespan which is a result of system degradation as outlined in Table 5.13.
- C_t is the cost cashflow at year t. For year 0, the cost includes:
  - Total system cost of utility or household BESS (See Table 5.13 for notes of utility BESS cost exclusion)
  - Rooftop PV system,
  - BIPV system,
  - Infrastructure upgrade cost.
- The capital cost assessment excludes EV-related costs and benefits. Electric vehicles are primarily purchased for mobility purposes, and the majority of their economic value is associated with transport utility rather than energy system participation. Incorporating EV costs into this analysis would therefore be inappropriate unless a dedicated assessment is undertaken to isolate and quantify the marginal costs and benefits attributable specifically to EV integration within the energy system, which is beyond the scope of this project.
- $WACC$ is the average rate of return a project or company is expected to pay to all its capital providers (bank and private equity). Where WACC = (% fraction of debt x debt rate x (1 – tax rate)) + (% fraction equity x equity rate). Key assumptions for the calculation are presented in Table 5.13

- **Internal rate of return (IRR):** The discount rate at which the net present value of a project equals zero, representing its expected annual return. IRR is calculated using the following criterion:

$$IRR = r, where\ NPV = \sum_{t=0}^{T} \frac{B_t - C_t}{(1 + r)^t} == 0$$

- **Infrastructure upgrade cost (Inf):** The cost for upgrading the transformer capacity to a level that can satisfy the import/export capacity within each scenario. Infrastructure upgrade cost is represented by the product of total required upgrade capacity (kVA) and the unit cost of upgrade (Table 5.13).

5.3.3 Comparison of key performance indicators between S1 and S3

This section presents a general comparison between S1 and S3, focusing on their energy profiles including total generation and load profiles and normalised profiles against the different urban built form.

5.3.3.1 Urban form comparison of S1 and S3

Table 5.14 highlights fundamental differences in spatial structure between the two urban models. While S1 covers a substantially larger project zone, the two scenarios exhibit relatively close total gross floor areas (GFA). This contrast indicates that S3 represents a much more compact urban form.

Table 5.14. Summary table of spatial comparison between S1 and S3 (Adapted from Embodied Carbon Section Error! Reference s ource not found.)

	S1	S3
Total project zone land size * Projected land area size of the entire project zone measured from geospatial model (Geo-reference: EPSG:7855 - GDA2020 / MGA zone 55)	2,257,992 (Albion Quarter, Town Centre, Energy Park, and Sunshine Station)	803,901 (Albion Quarter)
Gross floor area (GFA - m^2)	2,501,108	2,002,459
Functional floor area (FFA – m^2)	2,252,395	1,380,761
FFA to GFA Ratio	90.06%	68.95%
FFA to project land size Ratio	99.75%	171.76%

However, this compact urban form in S3 is accompanied by a substantially lower internal spatial efficiency, with an FFA-to-GFA ratio of 68.95% compared to 90.06% in S1. This indicates that a larger share of built volume in S3 is allocated to non-functional space (specifically, carparking). At the same time, the vertically intensified configuration of S3 results in a much higher concentration of functional floor area relative to land size, with an FFA-to-land ratio of 171.76% compared to 99.75% in S1. The coexistence of lower internal efficiency and higher functional density per unit land directly shapes the interpretation of energy demand and renewable generation intensities, depending on whether performance is normalised by gross floor area, functional floor area, or project land area.

The effects of these spatial differences are first reflected in the absolute energy metrics presented in Section 1 of Table 5.15. S1 achieves higher total renewable generation and higher total annual electricity demand across all EV penetration scenarios, driven by its broader precinct coverage. Increasing EV adoption leads to a consistent rise in annual demand in both S1 and S3, yet the proportional increase remains aligned with underlying floor area and land-use characteristics rather than the compactness of the urban form itself.

When energy metrics are normalised by total project land area (Section 2 of Table 5.15), S3 appears considerably more energy-intensive than S1. Renewable generation intensity in S3 is approximately 49.6% higher than in S1, reflecting the denser concentration of built form within the unit land size. This outcome is further influenced by the taller building typologies adopted in S3, which provide improved access to façade irradiance and enhance the deployment potential of building-integrated photovoltaics. Consequently, despite lower total generation in absolute terms, S3 demonstrates a higher renewable generation yield per unit of total precinct land area.

Table 5.15. Comparison of generation and load profiles of S1 and S3

	S1	S3
Section 1. Total Generation and Load Profiles		
Maximum renewable generation (GWh/year)	73.71	39.27
Annual Load without EV (GWh)	157.56	105.25
Annual Load with 20% EV (GWh)	169.32	114.20
Annual Load with 50% EV (GWh)	185.80	127.55
Annual Load with 80% EV (GWh)	202.56	140.88
Section 2. Generation and Load Intensity of Land Area		
Maximum generation intensity (kWh/sqm Precinct Land area)	32.64	48.85 (+49.64%)

Annual Load Intensity without EV (kWh/sqm Precinct Land area)	69.78	130.93 (+87.63%)
Annual Load Intensity 20% EV (kWh /sqm Precinct Land area)	74.99	142.06 (+89.44%)
Annual Load Intensity 50% EV (kWh /sqm Precinct Land area)	82.29	158.67 (+92.83%)
Annual Load Intensity 80% EV (kWh /sqm Precinct Land area)	89.71	175.25 (+95.35%)
Section 3. Generation and Load Intensity of FFA		
Maximum generation intensity (kWh/sqm FFA)	32.73	28.44 (-13.09%)
Annual Load Intensity without EV (kWh/sqm FFA)	69.95	76.23 (+8.97%)
Annual Load Intensity 20% EV (kWh/sqm FFA)	75.18	82.71 (+10.02%)
Annual Load Intensity 50% EV (kWh/sqm FFA)	82.49	92.38 (+11.99%)
Annual Load Intensity 80% EV (kWh/sqm FFA)	89.93	102.03 (+13.45%)

In contrast, land-area-normalised load intensity in S3 is markedly higher across all EV scenarios, exceeding S1 by approximately 88–95% (Section 2 of Table 5.15). This divergence increases with higher EV penetration, indicating that compact urban morphology amplifies energy demand pressure at the precinct scale. Under this metric, S3 presents a substantially more energy-intensive system per unit of land, with limited spatial flexibility to accommodate both rising demand and on-site renewable supply.

A different interpretation emerges when energy metrics are normalised by functional floor area (Section 3 of Table 5.15). Under this perspective, S3 consistently exhibits lower renewable generation intensity per unit of functional space, approximately 13% below that of S1. At the same time, load intensity per unit of functional floor area in S3 is systematically higher, by roughly 9–13% across increasing EV penetration levels.

To sum up the observations, the S3 overall has less shading intensity as summarised in Section 5.2.1, which result in a much higher solar generation per unit size of precinct's land. However, the S3 has an intensified energy usage per FFA due to the much higher FFA per unit land size, which also translates to lower generation per FFA, and potentially lower energy performance such as self-sufficiency. In the next section, the system-level energy performance across the two built forms will be discussed in further details.

5.3.3.2 Energy performance indicators

Figure 5.17, Figure 5.18, and Figure 5.19 present frequency histograms of three key energy performance indicators: self-sufficiency rate (SSR), generation-to-load ratio (GLR), and renewable energy utilisation rate (RUR) across 145 different energy management scenarios for each urban model (S1 - green boxes and S3 - red lines).

A histogram is an effective statistic tool that groups scenario outcomes into value ranges (bins) and shows how often results fall within each range. For example, in Figure 5.17, the green bar between 25% and 30% on the SSR axis with its top close to around 22 on number of scenarios axis means that there are around 22 scenarios in the S1 that achieved SSR within 25-30%.

Rather than presenting a single outcome, these histograms illustrate the spread, concentration, and limits of performance achievable under different operational assumptions. This approach allows the robustness and variability of each urban model to be assessed, rather than relying on a single representative case.

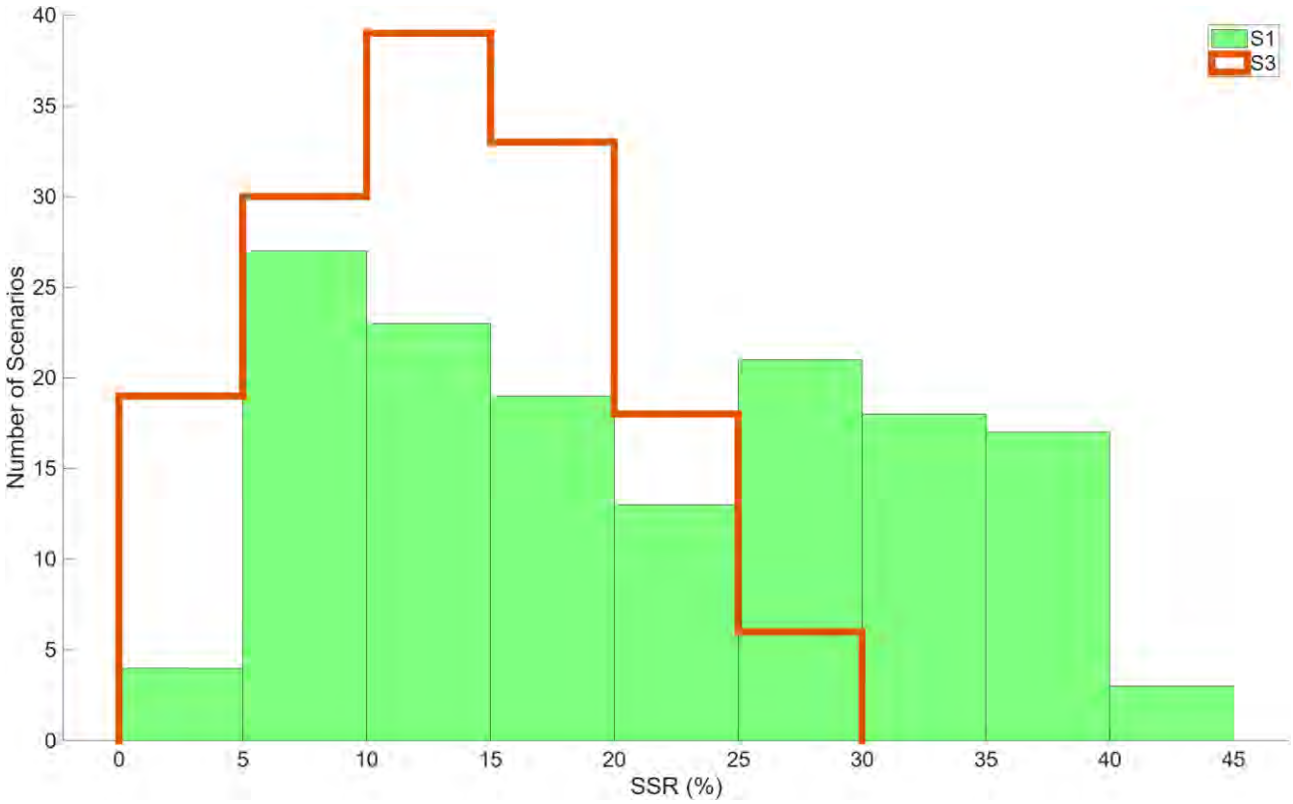

Figure 5.17. Histogram of self-sufficiency rate of S1 and S3

The SSR histogram (Figure 5.17) shows a clear structural separation between S1 and S3. Across the 145 scenarios, S1 tends to achieve higher self-sufficiency outcomes, with the majority of scenarios clustered at moderate to high SSR levels (10-25%) and a long upper tail extending beyond 30–40%. This indicates that S1 offers a broader operating envelope in which on-site renewable generation can offset a significant proportion of total demand.

In contrast, S3 exhibits a distribution concentrated at lower SSR values, with most scenarios falling below 20–25% and limited presence in higher self-sufficiency ranges. This reflects the combined effect of higher land-area load intensity and lower functional spatial efficiency in S3. Even though façade-based BIPV contributes to renewable generation, the compact and vertically intensified urban form constrains the overall ability to meet demand locally at the precinct scale. From a planning perspective, this suggests that S1 provides greater flexibility for achieving higher levels of energy autonomy under a wider range of operational strategies, whereas S3 is structurally constrained in this regard.

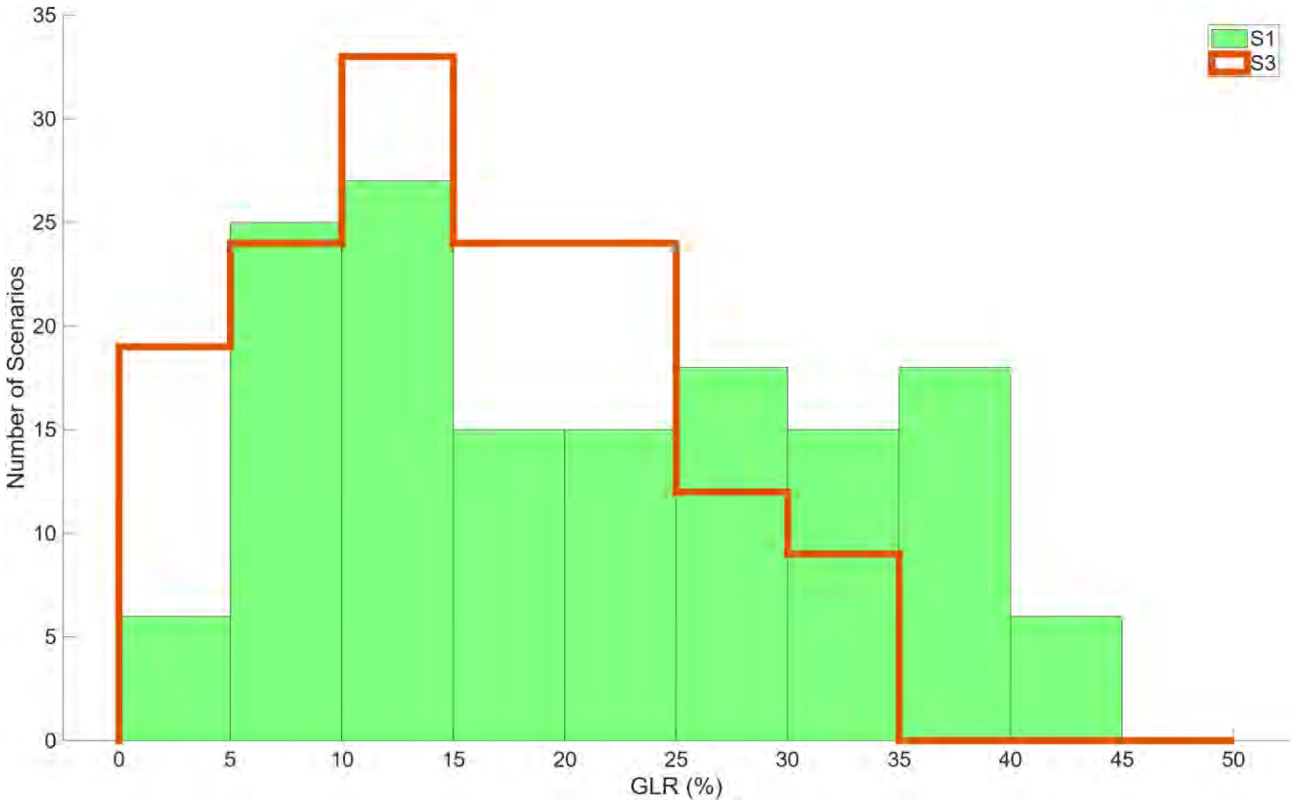

Figure 5.18. Histogram of generation-to-load ratio of S1 and S3

The GLR histograms (Figure 5.18) further reinforce the distinction between the two urban models. S1 displays a wider and right-shifted distribution, with many scenarios achieving relatively high ratios of renewable generation to total load. This indicates that, under favourable combinations of control strategies and demand assumptions, S1 can approach higher degrees of generation adequacy relative to its energy demand.

S3, by contrast, exhibits a distribution concentrated at lower GLR values, with a narrower spread and fewer scenarios achieving higher ratios. Although taller buildings and enhanced façade exposure increase renewable yield per unit land area, the higher load intensity of S3 limits the extent to which generation can keep pace with demand across scenarios.

For infrastructure planning, this implies that S3 would require stronger reliance on external energy supply or more off-site renewable sources to meet demand, while S1 offers a broader range of pathways toward improved generation-to-load balance.

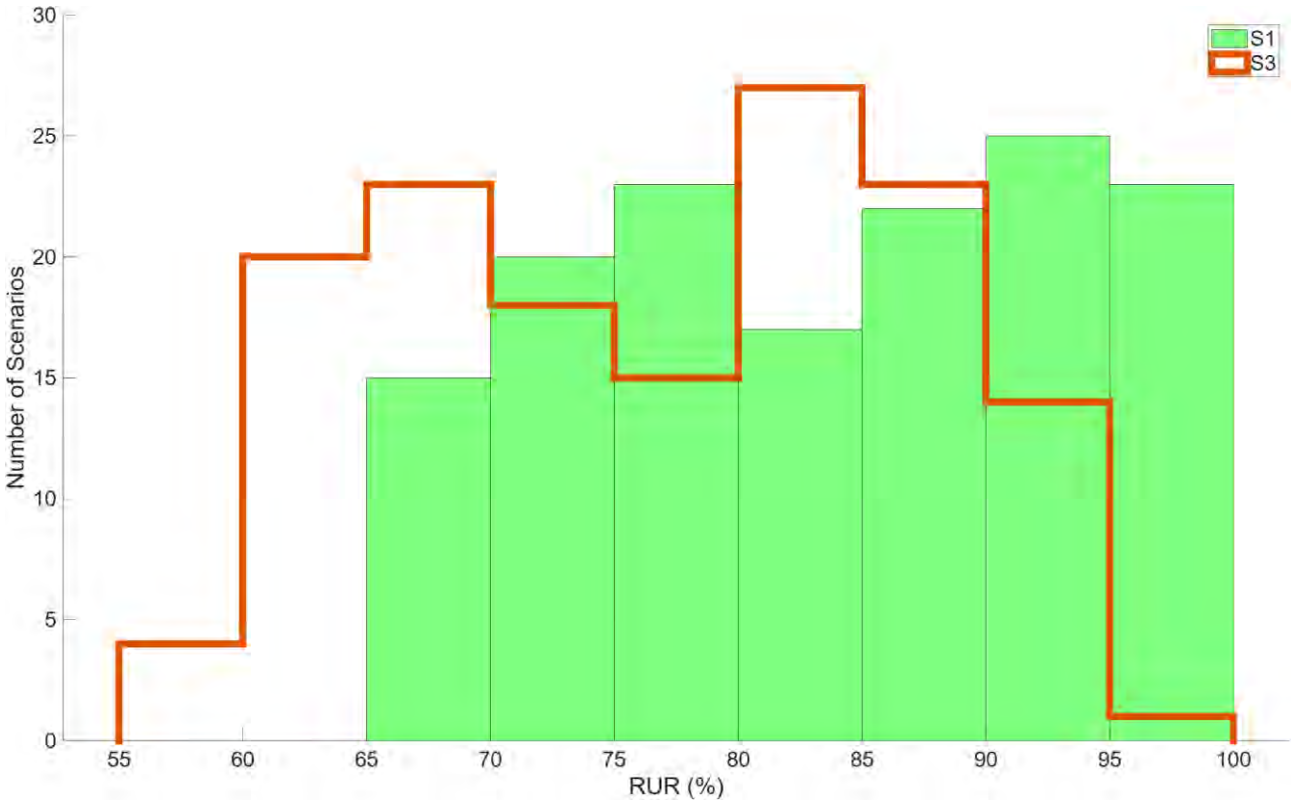

Figure 5.19. Histogram of renewable utilisation ratio of S1 and S3

Figure 5.19 presents the distribution of renewable energy utilization rate (RUR) for S1 and S3. RUR indicates the proportion of locally generated renewable energy that is consumed within the project area.

The observation is in general consistent with the previous ones. The histogram shows that S1 consistently achieves higher RUR outcomes across scenarios, with the majority of cases concentrated at higher utilization levels, frequently exceeding 80% and extending toward the upper end of the distribution. This indicates that, despite its larger land area and higher absolute generation capacity, S1 is generally able to align renewable generation with local demand through operational flexibility and load diversity across the precinct.

In contrast, S3 exhibits a distribution that is shifted toward lower RUR values, with a greater proportion of scenarios clustered in the mid-range of utilization (80-90%) and fewer cases achieving very high RUR. Although the compact and vertically intensified design of S3 supports effective façade-based renewable generation, the concentration of demand and limited operational diversity within a smaller land footprint reduce the ability to consistently absorb all locally generated energy under varying management strategies.

5.3.3.3 Summary

- **S3 achieves higher renewable generation intensity when normalised by total project land area**, primarily due to reduced inter-building shading across seasons and improved façade irradiance associated with its taller and more vertically articulated built form.

- **This generation advantage is substantially offset by significantly higher energy demand intensity**, with S3 exhibiting approximately **8–13% higher energy consumption per unit functional floor area (FFA)** compared to S1.
- **The elevated energy consumption per unit land area in S3 is a direct consequence of its vertically intensified urban form**, whereby a greater amount of conditioned floor space and activity is concentrated within a smaller land footprint.
- **The higher energy consumption per unit FFA indicates additional operational impacts beyond density alone**, consistent with the consumption modelling results presented in Section 5.2.2, which show that S3 experiences **up to 15% higher heating and cooling loads** relative to S1.
- **S3 simultaneously exhibits higher renewable generation per unit land area and lower generation per unit functional floor area**, reflecting its vertically intensified configuration. With an FFA-to-land ratio of approximately **170%**, compared to **~100% in S1**, functional floor area in S3 increases significantly faster with building height than renewable collection surfaces. As a result, renewable yield scales favourably with land use but is diluted when assessed per unit of functional space.
- **Statistical analysis presented in this section further confirms that the intensified concentration of functional floor area in S3 leads to systematically weaker energy performance**, with S3 exhibiting lower overall outcomes across all three indicators (SSR, GLR, and RUR) across the evaluated scenarios.
- Lower self-sufficiency rates (SSR) indicate reduced local energy autonomy in S3 compared to S1, while lower generation-to-load ratios (GLR) reflect a higher demand burden relative to on-site generation capacity. Together with lower renewable utilization rates (RUR), these results indicate that S3 faces structural constraints in both meeting and effectively absorbing its locally generated renewable energy.

5.3.4 Design variable impacts

From this section onwards, the report focuses on the Techno-economic-stakeholder assessment of the two scenarios (S1 and S3). The analysis covers the design space behaviours of the key design variables, economic viable design options, trade-offs and threshold analysis, and clustering analysis for different stakeholder groups.

This section examines how key system performance indicators vary across the renewable energy design space using exploratory data analysis (EDA). Rather than seeking a single optimal solution, the objective is to reveal structural trends, trade-offs, and non-linear behaviours that emerge as major design variables are adjusted. The analysis focuses on four primary decision dimensions: façade-integrated PV orientation, battery capacity, and EV uptake. Each was evaluated against energy performance, infrastructure impacts, and financial outcomes.

5.3.4.1 Impact of north-facing BIPV deployment

Figure 5.20, Figure 5.21, Figure 5.22, and Figure 5.23 present boxplots illustrating the distributions of self-sufficiency rate (SSR), infrastructure upgrade cost, and internal rate of return (IRR) under two financial representations of battery energy storage systems (BESS): household-level BESS and a utility-scale BESS proxy introduced as a comparative financial scenario. Results are shown for both the baseline urban

configuration (S1: Figure 5.20 (a), Figure 5.21 (a), Figure 5.22 (a), and Figure 5.23 (a)) and the alternative configuration (S3: Figure 5.20 (b), Figure 5.21 (b), Figure 5.22 (b), and Figure 5.23 (b)). Importantly, this comparison between household and utility BESS isolates financial effects only while operational behaviour, network constraints, and system control assumptions remain unchanged.

Across both S1 and S3, increasing the proportion of north-facing façade BIPV leads to a strong and monotonic increase in self-sufficiency. As shown in Figure 5.20 (a), median SSR in S1 rises substantially as north-facing coverage increases from 0% to 80%, reflecting the high annual solar yield achievable on north-oriented façades. The same structural relationship is observed in S3 (Figure 5.20 (b)), with SSR increasing consistently across the same façade coverage range. Absolute SSR values in S3 are lower than in S1, reflecting the smaller land area and reduced consumption performance as outlined in the previous section; however, the relative gains per increment of façade coverage remain comparable in the two scenarios. This indicates that the energy performance benefit of north-facing BIPV is robust to changes in urban scale and built-form density.

In both configurations, these energy gains are accompanied by a pronounced escalation in infrastructure upgrade costs, particularly beyond approximately 50% north-facing façade coverage. In S1, higher façade penetration results in rapidly increasing median upgrade costs and widening interquartile ranges, signaling growing variability and the rising likelihood of severe network upgrades. S3 exhibits similar threshold-driven behavior. The persistence of this pattern across both scenarios suggests that the underlying driver is not absolute system size, but the concentration of synchronous generation and export associated with extensive north-facing BIPV deployment.

From an investment perspective, IRR declines consistently with increasing north-facing BIPV under household-level BESS costs in both S1 and S3. At high penetration levels, median IRR becomes marginal or negative, reflecting capital concentration, declining self-consumption, and export-driven network stress. When evaluated under the utility-scale BESS cost assumption, IRR improves markedly across all façade ratios in both scenarios. Nevertheless, the downward trend with increasing north-facing coverage remains evident, indicating that while lower-cost storage can partially restore financial feasibility, generation-driven network constraints remain a dominant structural limiter.

Taken together, the S1 and S3 results demonstrate that north-facing BIPV is a highly effective lever for improving energy autonomy, but one that consistently defines a hard infrastructure and economic boundary when deployed at scale. The close alignment between the two scenarios confirms that this behavior is structural rather than site-specific, reinforcing the need to limit extensive north-facing façade deployment within a carefully managed design envelope.

a.

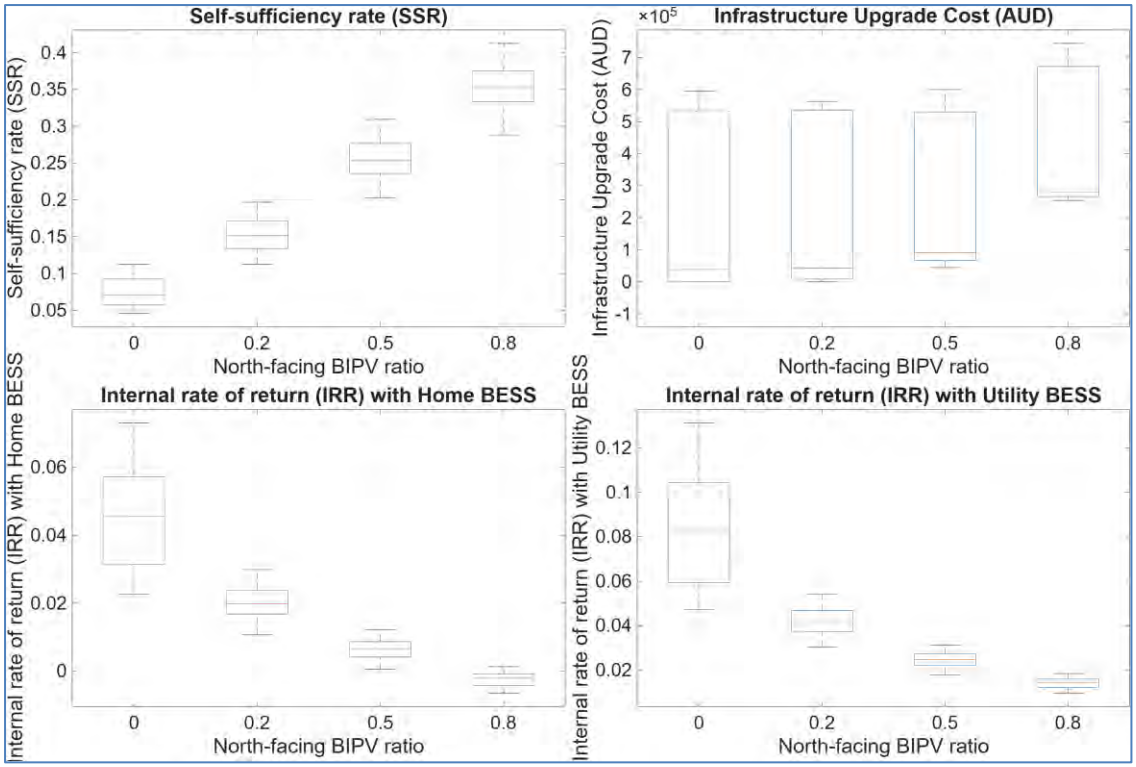

b.

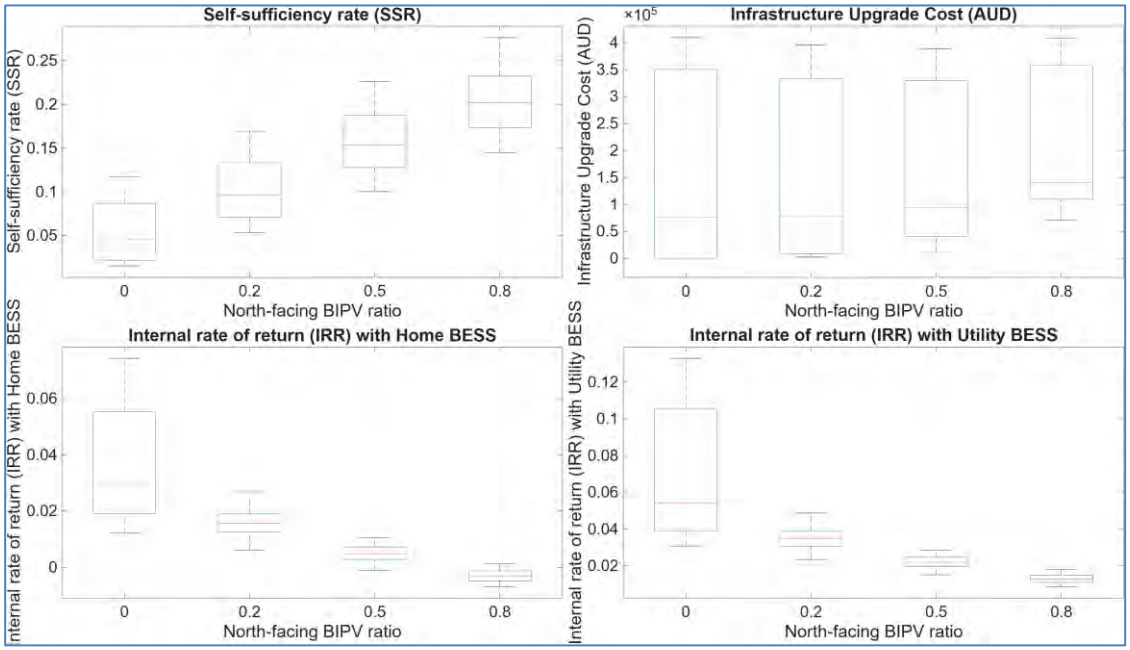

Figure 5.20. Boxplot of north-facing BIPV ratio against the key performance indicators (a – S1, b – S3)

5.3.4.2 Impact of east–west-facing BIPV deployment

In contrast to north-facing façades, Figure 5.21 shows that east–west (E/W) façade BIPV delivers a more moderate but structurally robust improvement in self-sufficiency across both urban configurations. In S1 (Figure 5.21 (a)), SSR increases steadily as E/W coverage rises from 0% to 80%, albeit at a slower rate than observed for north-facing deployment. The same monotonic but gradual improvement is evident in S3 (Figure 5.21 (b)), with lower absolute SSR values reflecting the considerably higher FFA built form of the precinct, but with a comparable relative response to increasing façade coverage. This consistency

indicates that the energy contribution of E/W BIPV scales proportionally with urban size while preserving its performance characteristics.

Crucially, infrastructure upgrade costs remain comparatively stable across the full range of E/W BIPV ratios in both scenarios. As shown in Figure 5.21 (a)–(b), upgrade cost distributions exhibit substantial overlap across façade coverage levels, with no sharp escalation or threshold behaviour even at high penetration. While median costs in S3 are lower in absolute terms due to reduced system scale, the absence of strong sensitivity to E/W coverage is common to both configurations. This contrasts sharply with the behaviour observed for north-facing BIPV and confirms that E/W deployment does not systematically exacerbate network stress.

From a financial perspective, IRR under household-level BESS declines gradually as E/W BIPV penetration increases in both S1 and S3, but remains positive across a substantially larger portion of the design space compared to north-facing façades (Figure 5.21 (a)–(b)). When evaluated under the utility-scale BESS cost assumption, IRR distributions shift upward in both scenarios while preserving their overall shape, reinforcing the interpretation that lower-cost storage improves financial viability without altering the underlying system response.

Notably, the minimum IRR associated with E/W BIPV remains within a narrow and stable range under both household and utility BESS assumptions and across both urban configurations. This indicates that increasing E/W façade coverage does not introduce additional downside financial risk, even at higher penetration levels. The persistence of this behaviour in both S1 and S3 confirms that E/W BIPV is not a primary cost driver and represents a structurally resilient pathway for expanding renewable generation in dense urban environments.

a.

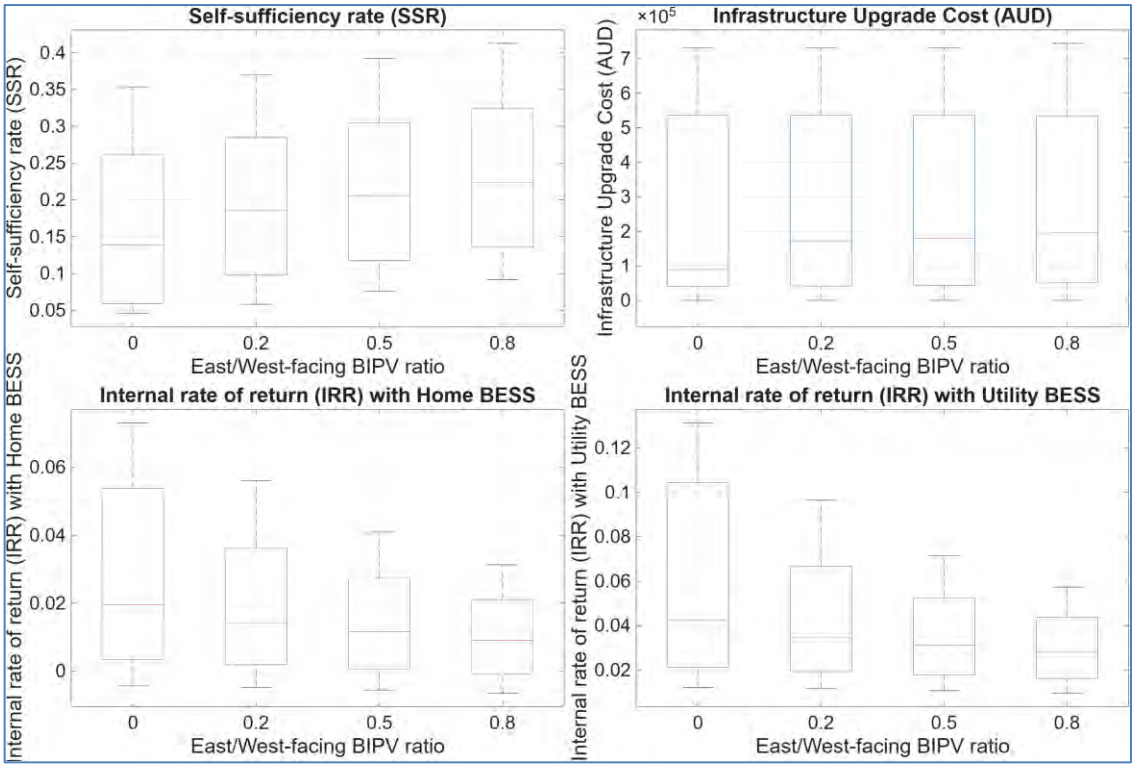

b.

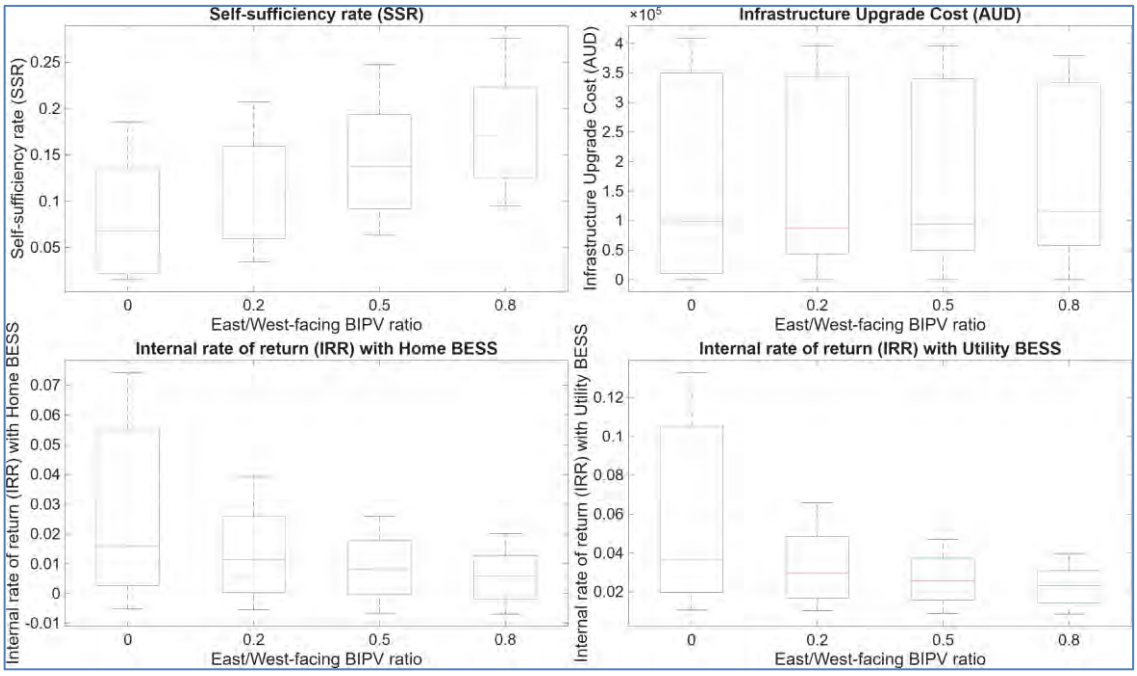

Figure 5.21. Boxplot of East/West- facing BIPV ratio against the key performance indicators (a – S1, b – S3)

5.3.4.3 Impact of battery capacity

Figure 5.22 illustrates the influence of increasing battery capacity on energy performance, infrastructure requirements, and financial viability under both household-level and utility-scale BESS cost assumptions. In S1 (Figure 5.22 (a)), higher battery capacity is associated with incremental improvements in self-sufficiency, reflecting enhanced temporal shifting of local generation and improved peak demand management. However, these gains exhibit clear diminishing returns beyond moderate deployment levels, with successive increases in capacity delivering progressively smaller improvements in SSR. The same

qualitative behaviour is observed in S3 (Figure 5.22 (b)). Importantly, the relative response to increasing storage capacity remains comparable between the two scenarios, indicating that the marginal contribution of additional storage scales proportionally with system size rather than being fundamentally altered by urban form differences.

Infrastructure upgrade costs exhibit a strongly non-linear response to battery capacity in both S1 and S3. At low to moderate capacities, upgrade costs display wide dispersion, indicating that local network conditions, load profiles, and charging patterns play a significant role in determining outcomes. As battery capacity increases, however, this dispersion collapses and high upgrade costs become increasingly unavoidable. This convergence at higher capacities is evident in both scenarios and is consistent with synchronized charging behavior and reverse power flow effects dominating network performance once storage penetration exceeds moderate levels.

From an investment perspective, IRR declines sharply with increasing battery capacity under household BESS cost assumptions in both S1 and S3. In S1, median IRR becomes marginal or negative beyond approximately 170–180 MWh, while in S3 this transition occurs at lower absolute capacities due to the reduced scale of S3 model, but again the patterns are generally comparable across the two scenarios. When evaluated under the utility-scale BESS cost assumption, IRR improves substantially across all capacity levels in both scenarios and remains positive even at very high storage capacities. Nevertheless, the downward trend with increasing capacity persists, indicating that while lower-cost storage can restore financial feasibility, it does not eliminate the structural penalties associated with over-deployment.

Overall, the results confirm that battery storage plays a supportive rather than dominant role in shaping feasible urban renewable systems. Moderate storage deployment can enhance self-consumption and mitigate variability, but large-scale battery capacity alone cannot overcome fundamental utilization limits and network constraints. This behavior is robust across both urban configurations within the precinct's distribution network constraints and reinforces the interpretation that battery deployment must be carefully coordinated with generation scale and network capacity rather than pursued as a stand-alone optimization lever.

a.

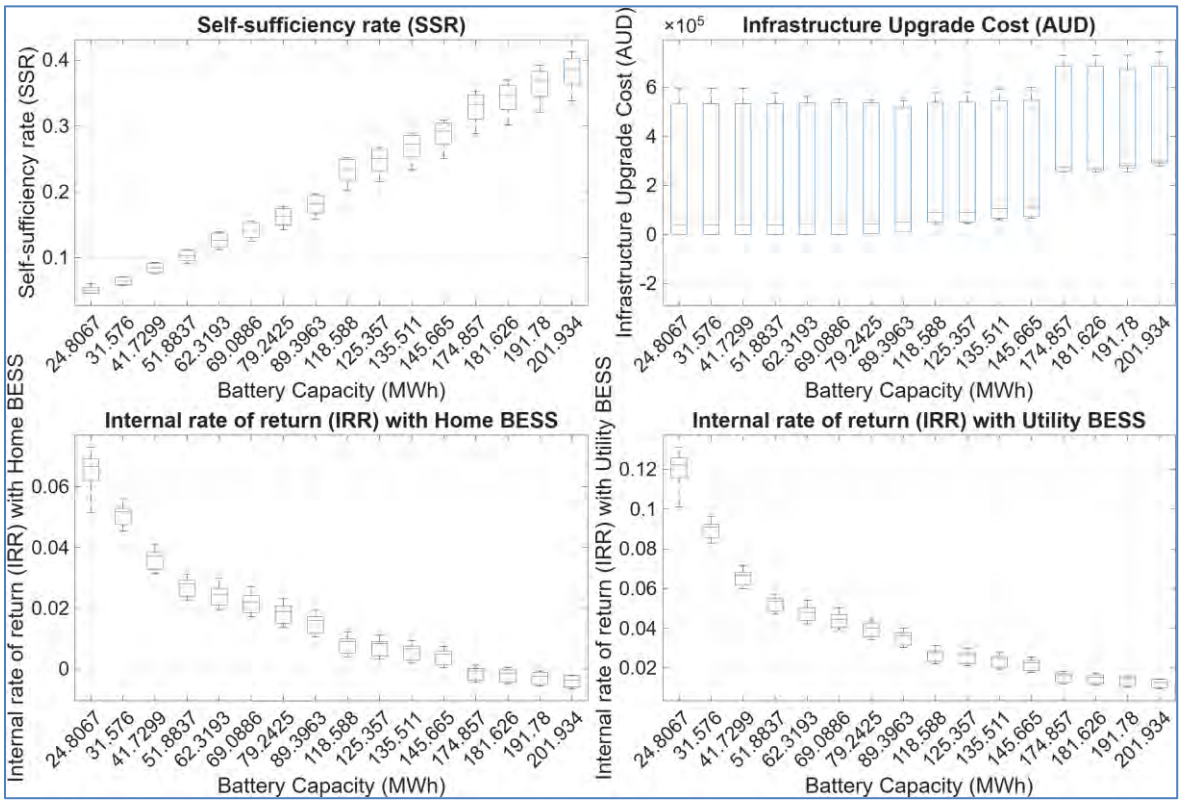

b.

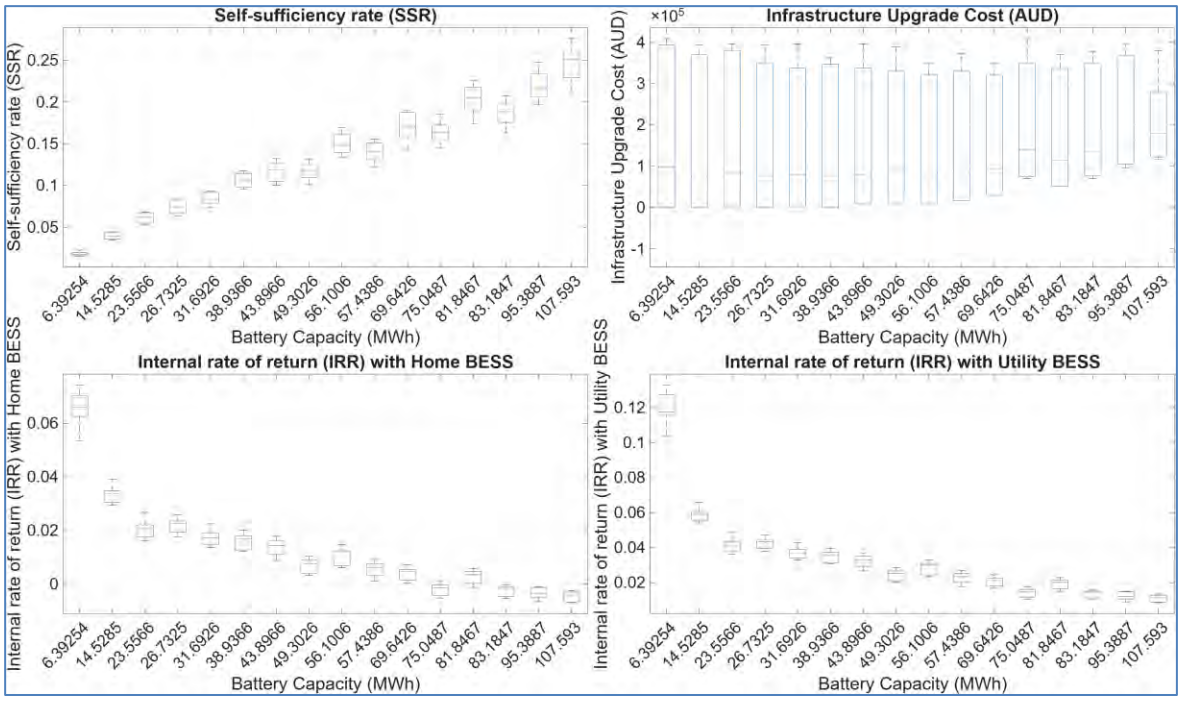

Figure 5.22. Boxplot of battery number against the key performance indicators (a – S1, b – S3)

5.3.4.4 Impact of EV uptake

Figure 5.23 illustrates the impact of EV uptake on energy performance, infrastructure requirements, and financial indicators for both urban configurations, with Figure 5.23 (a) corresponding to S1 and Figure 5.23

(b) to S3. Across both scenarios, EV uptake emerges as the most disruptive design variable from an infrastructure perspective, introducing sharp feasibility thresholds rather than gradual trade-offs.

In S1 (Figure 5.23 (a)), increasing EV penetration produces modest improvements in self-sufficiency, reflecting higher local utilisation of on-site renewable generation through electrified transport demand. However, these gains are relatively limited compared to those achieved through PV or BIPV deployment. In contrast, infrastructure upgrade costs increase sharply beyond approximately 50 percent EV uptake. The distributions transition from wide and context-dependent at low penetration levels to narrow and consistently high at 80 percent uptake, indicating that major network reinforcement becomes nearly unavoidable once EV penetration exceeds moderate levels.

The same qualitative pattern is observed in S3 (Figure 5.23 (b)), although absolute SSR values are lower due to the reduced scale of generation and demand within the smaller precinct footprint. Importantly, the infrastructure response to EV uptake remains similarly threshold-driven. In both scenarios, the concentration of high upgrade costs at elevated EV penetration levels confirms that demand-driven electrification places a fundamentally different type of stress on the network compared to generation- or storage-oriented interventions.

From a financial perspective, IRR distributions show limited sensitivity to EV uptake under both household and utility-scale BESS cost assumptions in S1 and S3. This relative stability reflects the modelling scope defined Section 5.3.1, where the capital costs and private benefits of EV adoption are excluded from the economic assessment. As a result, EV uptake primarily manifests as a system-level and infrastructure-level driver rather than a lever for improving private investment returns within the analysed scenarios.

Overall, the results confirm that EV uptake defines one of the hardest boundaries of the feasible design envelope. While moderate electrification can modestly enhance renewable utilisation, high EV penetration rapidly and predictably triggers substantial infrastructure upgrades in both urban configurations. This behaviour underscores the need for coordinated charging strategies, staged deployment, or complementary policy mechanisms if high EV adoption is to be pursued without imposing disproportionate network reinforcement costs.

a.

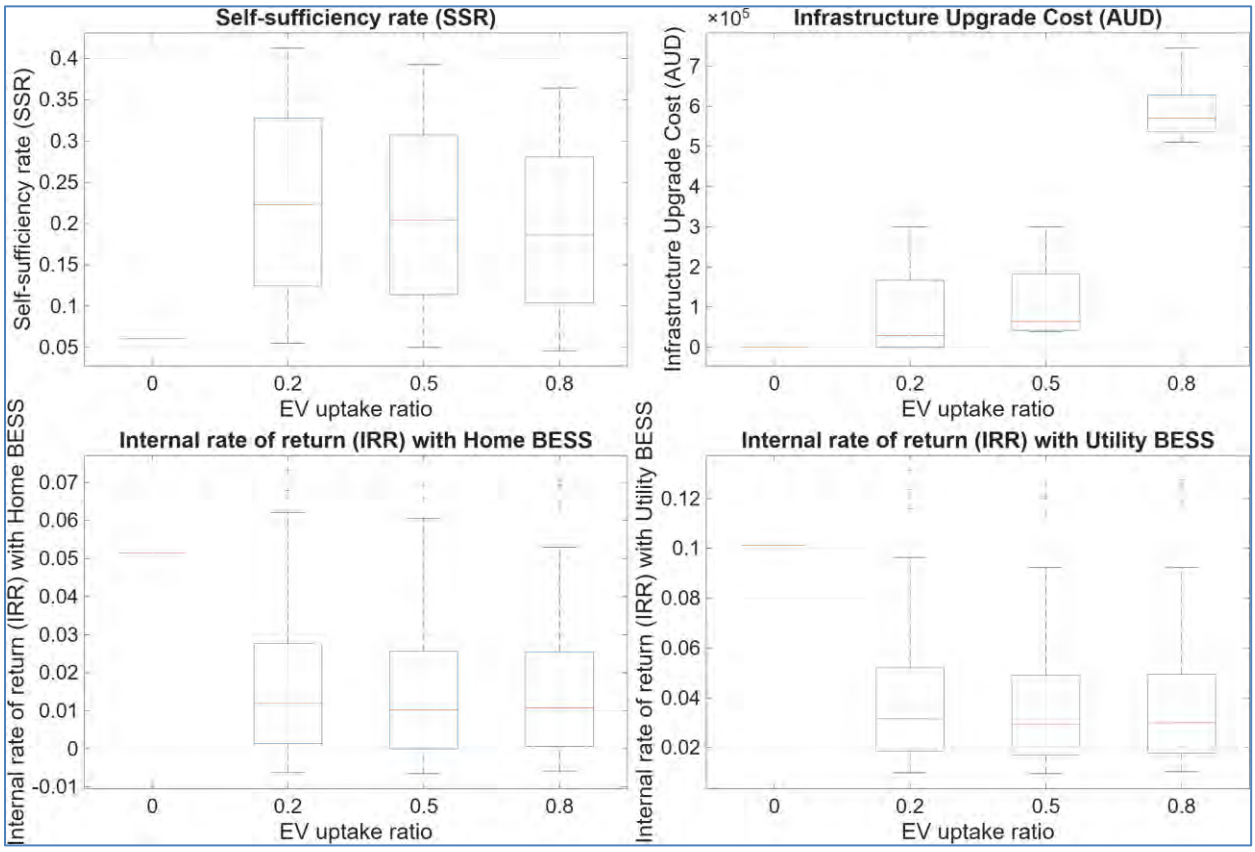

b.

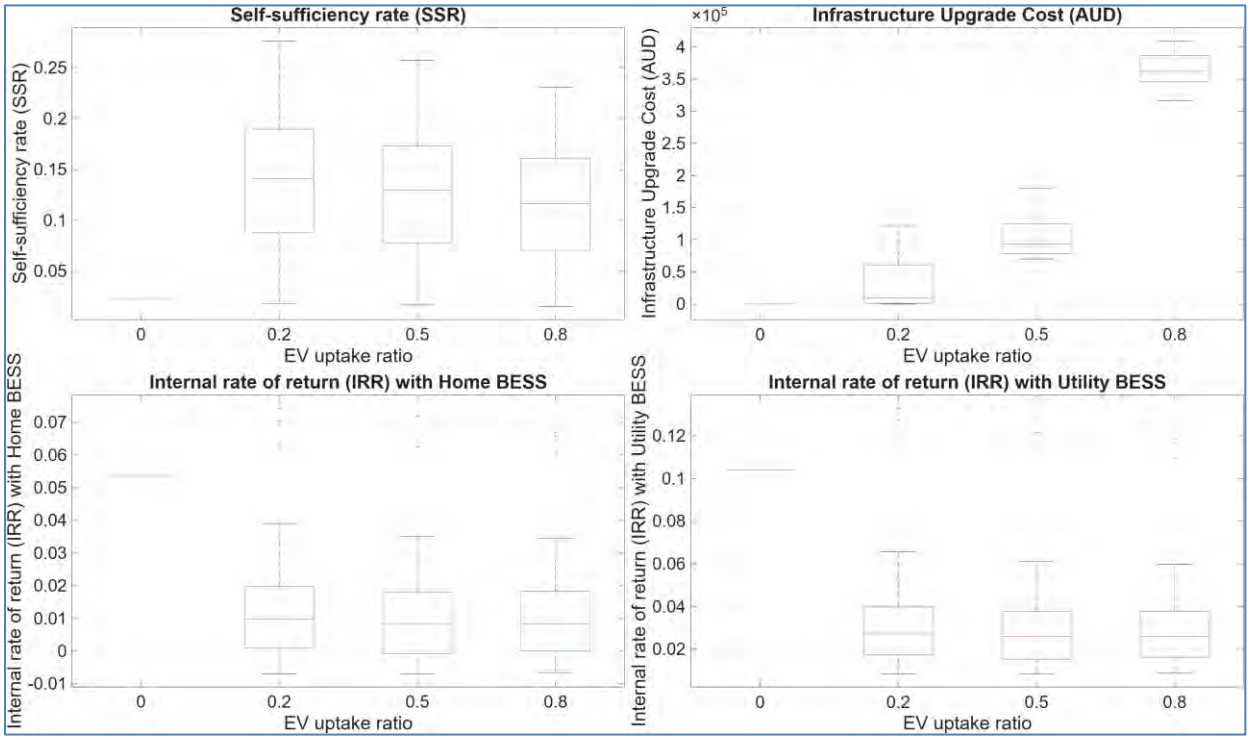

Figure 5.23. Boxplot of EV uptake ratio against the key performance indicators

5.3.5 Economic viable scenarios

Table 5.16 (S1) and Table 5.17 (S3) summarise all scenarios that achieve a positive net present value (NPV) under at least one battery cost assumption for S1 and S3, respectively, and therefore meet the minimum criterion for financial viability. Note that the scenarios that are viable only with utility BESS option are highlighted. In both urban configurations, economically viable scenarios constitute a relatively small and structured subset of the full design space, confirming that financial feasibility is highly selective rather than pervasive across system configurations. However, the number and composition of viable scenarios differ markedly between S1 and S3.

For S1, financially viable outcomes span a broader range of configurations, reflecting its lower demand intensity and more favourable balance between renewable generation and load. In contrast, S3 exhibits a noticeably smaller set of economically viable scenarios, consistent with its higher energy consumption per unit land area and per unit functional floor area. Despite S3 benefiting from improved façade irradiance and higher renewable generation intensity per unit land area, these advantages are systematically offset by the concentration of conditioned floor space and elevated operational demand, which dilute the financial effectiveness of on-site generation.

Across both S1 and S3, several consistent structural characteristics emerge among financially viable configurations. First, north-facing BIPV deployment is absent or strictly limited. In both tables, the highest-performing scenarios overwhelmingly operate with 0% north-facing BIPV, with only a small number incorporating modest coverage at 20%. This pattern reinforces earlier findings that north-facing façade deployment, while effective in increasing absolute generation, introduces capital costs and export-driven network pressures that are difficult to recover under current financial assumptions. The constraint is more pronounced in S3, where higher baseline demand further erodes the economic return of additional north-facing capacity.

Second, east–west (E/W) BIPV plays a central role in maintaining financial viability, particularly in S1 but also, to a rather limited extent, in S3. In S1, viable scenarios span the full range from 0% to 80% E/W façade coverage, with self-sufficiency rates (SSR) increasing steadily from approximately 5–6% in roof-only configurations to above 15–19% in high E/W BIPV cases, while remaining financially viable under selected battery and EV uptake levels. In S3, viable scenarios similarly favour E/W BIPV over north-facing deployment, but the achievable SSR range is systematically lower, reflecting the dilution effect of higher functional floor area relative to renewable collection surfaces. This confirms that E/W façade deployment remains a comparatively robust and economically resilient pathway in both urban forms, albeit with reduced absolute returns in more vertically intensified configurations.

Third, battery capacities in financially viable scenarios remain moderate in both S1 and S3. In S1, viable battery capacities predominantly fall between approximately 25 MWh and 90 MWh, while in S3 the viable range shifts downward, clustering at lower absolute capacities. Larger storage systems appear infrequently in both cases, consistent with the strong capital cost sensitivity and diminishing financial returns identified in the exploratory analysis. The narrower viable battery range in S3 further reflects its reduced tolerance for capital-intensive interventions due to higher underlying demand and lower per-unit functional energy yield.

Table 5.16. Summary of all financially viable scenarios within S1

Scenario Code	N- BIPV ratio	Side BIPV ratio (E–W)	Battery Capacity (MWh)	EV penetration (% of dwellings)	Infrastructure Cost (AUD)	Total IRR with Home BESS	Total IRR with Utility BESS	SSR
P01F02N01S01B03E02	0%	0%	24.8067	20%	$0	7.31%	13.12%	5.51%
P01F02N01S01B03E04	0%	0%	24.8067	80%	$533,910	7.05%	12.76%	4.60%
P01F02N01S01B02E04	0%	0%	24.8067	80%	$536,220	6.93%	12.58%	4.59%
P01F02N01S01B03E03	0%	0%	24.8067	50%	$38,793	6.92%	12.57%	5.02%
P01F02N01S01B02E02	0%	0%	24.8067	20%	$0	6.78%	12.37%	5.52%
P01F02N01S01B02E03	0%	0%	24.8067	50%	$38,793	6.57%	12.09%	5.02%
P01F02N01S01B01E04	0%	0%	24.8067	80%	$595,670	6.38%	11.82%	4.57%
P01F02N01S01B01E02	0%	0%	24.8067	20%	$0	6.21%	11.58%	5.49%
P01F02N01S01B01E03	0%	0%	24.8067	50%	$56,626	6.06%	11.37%	4.99%
P01F02N01S02B03E02	0%	20%	31.576	20%	$0	5.61%	9.64%	7.07%
P01F02N01S02B03E04	0%	20%	31.576	80%	$533,910	5.30%	9.24%	5.89%
P01F02N01S02B03E03	0%	20%	31.576	50%	$38,793	5.29%	9.23%	6.44%
P01F02N01S02B02E04	0%	20%	31.576	80%	$536,220	5.19%	9.10%	5.87%
P01F02N01S02B02E02	0%	20%	31.576	20%	$0	5.18%	9.09%	7.07%
BAU	0%	0%	24.8067	0%	$0	5.15%	10.12%	6.06%
P01F02N01S02B02E03	0%	20%	31.576	50%	$38,793	4.95%	8.80%	6.43%
P01F02N01S02B01E04	0%	20%	31.576	80%	$595,670	4.78%	8.58%	5.82%
P01F02N01S02B01E02	0%	20%	31.576	20%	$0	4.69%	8.47%	7.02%
P01F02N01S02B01E03	0%	20%	31.576	50%	$56,626	4.55%	8.29%	6.37%
P01F02N01S03B03E02	0%	50%	41.7299	20%	$0	4.09%	7.14%	9.23%
P01F02N01S03B03E04	0%	50%	41.7299	80%	$533,910	3.84%	6.83%	7.77%
P01F02N01S03B03E03	0%	50%	41.7299	50%	$38,793	3.83%	6.82%	8.49%
P01F02N01S03B02E02	0%	50%	41.7299	20%	$0	3.73%	6.71%	9.25%
P01F02N01S03B02E04	0%	50%	41.7299	80%	$536,220	3.72%	6.69%	7.72%
P01F02N01S03B02E03	0%	50%	41.7299	50%	$38,793	3.55%	6.48%	8.45%
P01F02N01S03B01E04	0%	50%	41.7299	80%	$595,670	3.30%	6.18%	7.57%
P01F02N01S03B01E02	0%	50%	41.7299	20%	$0	3.28%	6.16%	9.15%
P01F02N01S03B01E03	0%	50%	41.7299	50%	$50,369	3.14%	5.99%	8.30%
P01F02N01S04B03E02	0%	80%	51.8837	20%	$0	3.13%	5.73%	11.15%
P01F02N02S01B03E02	20%	0%	62.3193	20%	$0	2.99%	5.42%	13.89%
P01F02N01S04B03E04	0%	80%	51.8837	80%	$533,910	2.96%	5.53%	9.55%
P01F02N01S04B03E03	0%	80%	51.8837	50%	$38,793	2.92%	5.48%	10.38%
P01F02N01S04B02E04	0%	80%	51.8837	80%	$536,220	2.85%	5.40%	9.45%
P01F02N01S04B02E02	0%	80%	51.8837	20%	$0	2.81%	5.36%	11.22%
P01F02N02S02B03E02	20%	20%	69.0886	20%	$0	2.72%	5.04%	15.48%
P01F02N02S01B03E03	20%	0%	62.3193	50%	$41,171	2.70%	5.08%	12.81%
P01F02N01S04B02E03	0%	80%	51.8837	50%	$38,793	2.68%	5.20%	10.33%
P01F02N02S01B03E04	20%	0%	62.3193	80%	$536,290	2.65%	5.02%	11.70%
P01F02N02S01B02E02	20%	0%	62.3193	20%	$0	2.63%	5.00%	13.91%
P01F02N02S01B02E04	20%	0%	62.3193	80%	$536,290	2.45%	4.80%	11.54%
P01F02N02S02B03E03	20%	20%	69.0886	50%	$41,171	2.45%	4.73%	14.32%
P01F02N02S02B03E04	20%	20%	69.0886	80%	$536,290	2.41%	4.69%	13.08%
P01F02N01S04B01E04	0%	80%	51.8837	80%	$577,830	2.39%	4.87%	9.17%
P01F02N02S01B02E03	20%	0%	62.3193	50%	$41,171	2.38%	4.72%	12.67%
P01F02N01S04B01E02	0%	80%	51.8837	20%	$0	2.38%	4.85%	11.09%
P01F02N02S02B02E02	20%	20%	69.0886	20%	$0	2.38%	4.65%	15.53%
P01F02N02S03B03E02	20%	50%	79.2425	20%	$3,942	2.32%	4.51%	17.61%
P01F02N01S04B01E03	0%	80%	51.8837	50%	$50,369	2.27%	4.72%	10.07%
P01F02N02S02B02E04	20%	20%	69.0886	80%	$536,290	2.21%	4.46%	12.88%
P01F02N02S02B02E03	20%	20%	69.0886	50%	$41,171	2.15%	4.38%	14.16%
P01F02N02S01B01E02	20%	0%	62.3193	20%	$0	2.13%	4.42%	13.67%
P01F02N02S03B03E03	20%	50%	79.2425	50%	$42,735	2.08%	4.24%	16.45%
P01F02N02S03B03E04	20%	50%	79.2425	80%	$537,850	2.08%	4.24%	15.06%
P01F02N02S01B01E04	20%	0%	62.3193	80%	$563,510	2.03%	4.30%	11.23%

P01F02N02S03B02E02	20%	50%	79.2425	20%	$3,942	1.99%	4.14%	17.73%
P01F02N02S01B01E03	20%	0%	62.3193	50%	$52,747	1.96%	4.23%	12.36%
P01F02N02S04B03E02	20%	80%	89.3963	20%	$12,577	1.94%	4.03%	19.50%
P01F02N02S03B02E04	20%	50%	79.2425	80%	$537,850	1.89%	4.02%	14.80%
P01F02N02S02B01E02	20%	20%	69.0886	20%	$0	1.89%	4.08%	15.24%
P01F02N02S03B02E03	20%	50%	79.2425	50%	$42,735	1.81%	3.93%	16.27%
P01F02N02S02B01E04	20%	20%	69.0886	80%	$551,930	1.78%	3.96%	12.50%
P01F02N02S04B03E04	20%	80%	89.3963	80%	$546,490	1.76%	3.82%	16.91%
P01F02N02S02B01E03	20%	20%	69.0886	50%	$52,747	1.72%	3.90%	13.77%
P01F02N02S04B03E03	20%	80%	89.3963	50%	$51,370	1.72%	3.78%	18.38%
P01F02N02S04B02E02	20%	80%	89.3963	20%	$12,577	1.63%	3.68%	19.69%

Table 5.17. Summary of all financially viable scenarios within S3

Scenario Code	N- BIPV ratio	Side BIPV ratio (E–W)	Battery Capacity (MWh)	EV penetration (% of dwellings)	Infrastructure Cost (AUD)	Total IRR with Home BESS	Total IRR with Utility BESS	SSR
P01F02N01S01B03E02	0%	0%	6.3925	20%	$0	7.43%	13.29%	1.93%
P01F02N01S01B03E03	0%	0%	6.3925	50%	$98,235	7.18%	12.91%	1.72%
P01F02N01S01B02E02	0%	0%	6.3925	20%	$0	7.04%	12.75%	1.93%
P01F02N01S01B03E04	0%	0%	6.3925	80%	$393,570	6.68%	11.83%	1.56%
P01F02N01S01B02E03	0%	0%	6.3925	50%	$98,235	6.65%	12.16%	1.73%
P01F02N01S01B02E04	0%	0%	6.3925	80%	$393,570	6.57%	11.68%	1.53%
P01F02N01S01B01E02	0%	0%	6.3925	20%	$0	6.30%	11.71%	1.84%
P01F02N01S01B01E03	0%	0%	6.3925	50%	$98,235	6.26%	11.60%	1.67%
P01F02N01S01B01E04	0%	0%	6.3925	80%	$409,210	6.05%	10.94%	1.57%
BAU	0%	0%	6.3925	0%	$0	5.35%	10.39%	2.25%
P01F02N01S02B03E02	0%	20%	14.5285	20%	$0	3.91%	6.58%	4.51%
P01F02N01S02B03E03	0%	20%	14.5285	50%	$76,335	3.52%	6.11%	3.91%
P01F02N01S02B02E02	0%	20%	14.5285	20%	$0	3.46%	6.05%	4.35%
P01F02N01S02B02E04	0%	20%	14.5285	80%	$393,570	3.45%	5.98%	3.58%
P01F02N01S02B03E04	0%	20%	14.5285	80%	$362,280	3.38%	5.90%	3.49%
P01F02N01S02B02E03	0%	20%	14.5285	50%	$76,335	3.18%	5.71%	3.85%
P01F02N01S02B01E02	0%	20%	14.5285	20%	$0	3.09%	5.61%	4.36%
P01F02N01S02B01E03	0%	20%	14.5285	50%	$91,978	2.96%	5.45%	3.97%
P01F02N01S02B01E04	0%	20%	14.5285	80%	$393,570	2.96%	5.40%	3.51%
P01F02N02S01B03E02	20%	0%	23.5566	20%	$2,315	2.68%	4.86%	6.80%
P01F02N01S03B03E02	0%	50%	26.7325	20%	$0	2.59%	4.72%	8.38%
P01F02N01S03B03E03	0%	50%	26.7325	50%	$76,335	2.38%	4.48%	7.37%
P01F02N01S03B03E04	0%	50%	26.7325	80%	$362,280	2.35%	4.42%	6.39%
P01F02N01S03B02E02	0%	50%	26.7325	20%	$0	2.32%	4.41%	8.31%
P01F02N01S03B02E04	0%	50%	26.7325	80%	$346,640	2.28%	4.34%	6.72%
P01F02N02S01B03E03	20%	0%	23.5566	50%	$84,907	2.26%	4.38%	6.23%
P01F02N02S02B03E02	20%	20%	31.6926	20%	$2,315	2.25%	4.28%	9.32%
P01F02N02S01B02E02	20%	0%	23.5566	20%	$2,315	2.19%	4.31%	6.81%
P01F02N02S01B03E04	20%	0%	23.5566	80%	$380,240	2.14%	4.23%	5.46%
P01F02N01S03B02E03	0%	50%	26.7325	50%	$76,335	2.14%	4.20%	7.50%
P01F02N02S01B02E04	20%	0%	23.5566	80%	$380,240	2.07%	4.14%	5.32%
P01F02N01S04B03E02	0%	80%	38.9366	20%	$0	2.02%	3.98%	11.50%
P01F02N02S01B02E03	20%	0%	23.5566	50%	$84,907	1.95%	4.03%	6.33%
P01F02N01S03B01E02	0%	50%	26.7325	20%	$0	1.95%	3.98%	8.11%
P01F02N02S02B02E02	20%	20%	31.6926	20%	$2,315	1.94%	3.94%	9.18%
P01F02N01S03B01E04	0%	50%	26.7325	80%	$393,570	1.92%	3.94%	6.34%
P01F02N02S02B03E03	20%	20%	31.6926	50%	$78,650	1.91%	3.89%	8.46%
P01F02N02S02B03E04	20%	20%	31.6926	80%	$348,950	1.88%	3.85%	7.92%
P01F02N01S04B03E03	0%	80%	38.9366	50%	$76,335	1.86%	3.79%	10.93%
P01F02N02S03B03E02	20%	50%	43.8966	20%	$8,572	1.79%	3.70%	12.65%
P01F02N01S04B03E04	0%	80%	38.9366	80%	$346,640	1.79%	3.70%	9.84%
P01F02N02S01B01E02	20%	0%	23.5566	20%	$2,315	1.79%	3.85%	6.71%
P01F02N01S03B01E03	0%	50%	26.7325	50%	$70,078	1.76%	3.77%	7.09%
P01F02N02S02B02E04	20%	20%	31.6926	80%	$333,310	1.74%	3.69%	7.48%

P01F02N02S02B02E03	20%	20%	31.6926	50%	$78,650	1.73%	3.69%	8.23%
P01F02N02S01B01E04	20%	0%	23.5566	80%	$395,880	1.71%	3.74%	5.49%

Across financially viable scenarios in S1 (

Table **5.16**), EV penetration levels span a relatively wide range, from 20% up to 80%, demonstrating that EV adoption in of itself does not preclude economic feasibility. However, higher EV penetration is frequently associated with non-zero infrastructure upgrade requirements, typically in the range of approximately AUD 0.5–0.6 million. These upgrade costs exert downward pressure on investment returns and partially explain the progressive decline in IRR observed in high-EV configurations. This pattern is consistent with the threshold behaviour identified earlier; whereby EV-related demand amplification rather than generation capacity becomes the dominant driver of network stress.

Notably, a subset of financially viable S1 configurations achieves zero infrastructure upgrade cost, particularly at lower EV penetration levels (around 20%) combined with moderate PV and battery deployment. These cases consistently exhibit stronger economic performance and higher IRRs, underscoring the value of aligning distributed energy resource (DER) deployment with existing network capacity. The presence of these zero-upgrade scenarios highlights that financial viability is maximized not through aggressive electrification, but through configurations that remain below critical network thresholds.

In S3 (Table 5.17), a similar qualitative relationship between EV penetration, infrastructure cost, and financial performance is observed, but within a more constrained feasible space. While EV uptake levels among viable S3 scenarios also range between 20% and 80%, higher penetration levels more rapidly erode financial viability due to the combined effects of elevated demand intensity and infrastructure reinforcement. As a result, S3 exhibits fewer zero-upgrade viable scenarios, and those that do remain viable tend to cluster at lower battery capacities and lower EV uptake. This contrast reinforces the role of built-form-driven demand concentration in narrowing the economically feasible design envelope.

Another key feature observed in

Table 5.16 and Table 5.17 is the side-by-side comparison of financial performance under household BESS and utility-scale BESS cost assumptions. Across all S1 scenarios, the application of utility-scale BESS costs substantially improves financial performance. IRR values under the utility BESS assumption are typically 4–6 percentage points higher than their household BESS counterparts, and in several cases exceed conventional investment benchmarks. A similar uplift is observed in S3, although the absolute IRR levels remain lower due to higher underlying demand and reduced self-sufficiency.

Despite this improvement, the relative ordering of scenarios remains broadly consistent under both battery cost assumptions in both S1 and S3. Configurations that perform well under household BESS generally also perform well under utility BESS, indicating that the fundamental drivers of economic performance—such as BIPV orientation, battery sizing, EV penetration, and exposure to infrastructure

costs—remain structurally unchanged. The utility BESS assumption therefore expands the financially viable region but does not fundamentally alter the shape or boundaries of the feasible design space.

The business-as-usual (BAU) case remains economically viable in both S1 and S3 under both battery cost assumptions, with IRR values comparable to early-stage BIPV configurations. However, BAU scenarios consistently exhibit lower self-sufficiency rates relative to many alternative configurations. In both urban forms, several non-BAU scenarios achieve materially higher SSR while maintaining comparable or superior financial performance, particularly when moderate E/W BIPV deployment is combined with controlled battery sizing and limited infrastructure upgrade requirements.

Overall, the results demonstrate that economic viability is achievable but tightly constrained in both S1 and S3. Financially viable outcomes depend less on maximizing individual technologies than on maintaining balance across façade orientation, storage scale, EV penetration, and infrastructure impacts. While lower-cost utility-scale BESS assumptions materially improve absolute returns, they do not eliminate the underlying trade-offs that define viable urban energy system design, particularly in vertically intensified urban forms such as S3.

5.3.6 Trade-offs between utility and household batteries

a .

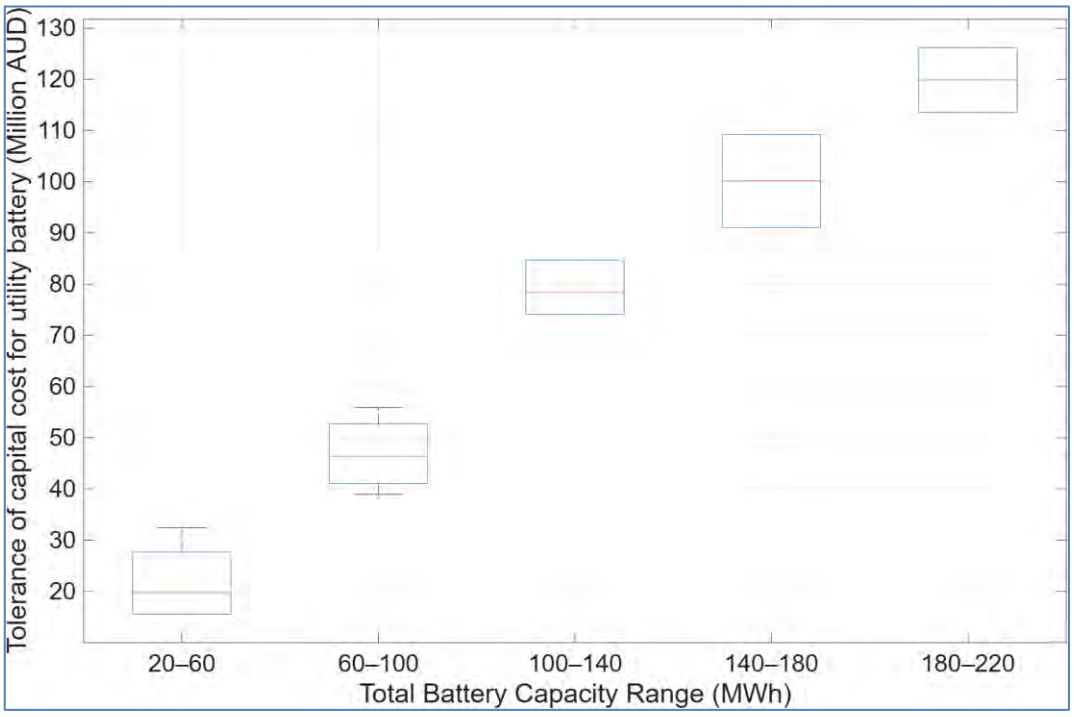

b.

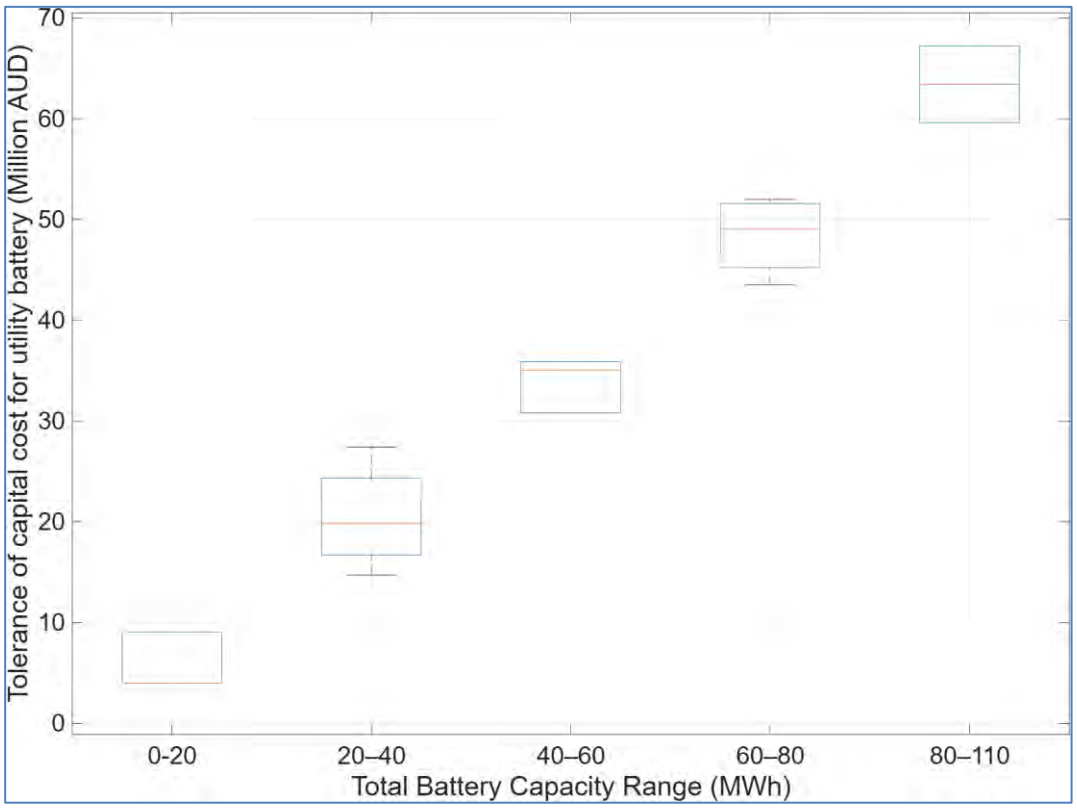

Figure 5.24. Capital cost tolerance of utility battery investment (a – S1, b – S3)

Figure 5.24 compares household battery systems and utility-scale battery systems by examining the tolerance of additional capital costs associated with utility-scale deployment. This tolerance represents the maximum level of excluded or unmodelled costs, such as land acquisition, local distribution network

reinforcement, or transmission upgrades, that utility-scale BESS could absorb before becoming economically less attractive than household batteries.

The tolerance is calculated as the difference in net present value (NPV) between the utility BESS and household BESS options for each scenario. Because utility BESS benefits from substantially lower assumed costs per kWh, it consistently achieves higher NPVs than household batteries under the base assumptions. The tolerance therefore defines a financial margin within which additional real-world costs could be accommodated without overturning the economic preference for utility-scale storage.

For example, in scenarios with a total battery capacity between 20–60 MWh, the upper whisker of the distribution in Figure 5.24 (a) indicates that utility BESS can tolerate up to approximately AUD 30–35 million in additional capital expenditure. Beyond this threshold, the economic advantage of utility BESS would be eroded, and household batteries would become the more competitive option. This provides a practical benchmark for assessing whether site-specific costs such as land values or grid connection upgrades are likely to invalidate the assumed cost advantage of centralised storage.

Across increasing capacity ranges, the tolerance of additional capital cost rises approximately linearly with total battery capacity. For mid-range deployments of 100–140 MWh, acceptable additional costs increase to around AUD 75–85 million, while at very high storage capacities of 180–220 MWh, the tolerance exceeds AUD 120 million. This scaling behaviour reflects the increasing system value of large-scale storage, which enables greater operational flexibility, improved peak management, and enhanced energy arbitrage potential, thereby generating larger economic returns that can absorb higher upfront investments.

In S3 (Figure 5.24 - b), the same qualitative relationship between battery capacity and cost tolerance is observed, but at systematically lower absolute levels. For comparable capacity ranges, the tolerable additional capital costs are reduced relative to S1, reflecting S3's higher demand intensity and lower overall self-sufficiency outcomes. For example, tolerance levels in the 20–40 MWh range are typically below AUD 25 million, and even at 80–110 MWh, the upper tolerance remains below AUD 70 million. This indicates that while utility-scale storage remains economically advantageous in S3, the margin within which unmodelled costs can be absorbed is narrower, making site-specific constraints more critical to feasibility.

Importantly, this analysis does not claim that such additional costs are negligible in practice. Rather, Figure 5.24 defines an upper-bound economic envelope within which utility-scale BESS remains preferable under the assumed operating and market conditions. The results highlight that the financial advantage of utility-scale storage is highly sensitive to site-specific capital costs, but also demonstrate that, particularly at larger capacities, this advantage can be sufficiently large to accommodate substantial non-trivial investments before household batteries become the economically dominant option.

5.3.7 Threshold behavior and upgrade drivers

Building on the exploratory analysis, this subsection explicitly isolates distribution network infrastructure as a critical but often under-examined constraint in urban renewable energy system design. While earlier sections revealed broad trade-offs between energy performance and economic outcomes across the

design space, they also exposed substantial non-linearities and abrupt shifts in feasibility that cannot be explained by energy or financial metrics alone.

In practice, network infrastructure frequently represents the binding constraint in high-density urban contexts, yet is commonly simplified, assumed away, or treated ex post in renewable energy studies. Here, infrastructure is treated as an explicit system dimension, recognizing that network capacity constraints can invalidate otherwise attractive energy and economic configurations. This subsection therefore focuses on identifying threshold behavior and upgrade drivers, distinguishing between gradual performance trade-offs and sharp transitions from feasible to infeasible regimes.

By separating the likelihood of infrastructure upgrades from their cost implications, the analysis establishes a clear basis for understanding which technology pathways induce manageable network stress and which push the system beyond practical limits. Figure 5.25 presents the probability of triggering infrastructure upgrades as a function of key design variables for both S1 (Figure 5.25 a) and S3 (Figure 5.25 b).

5.3.7.1 Threshold behavior and upgrade drivers

a.

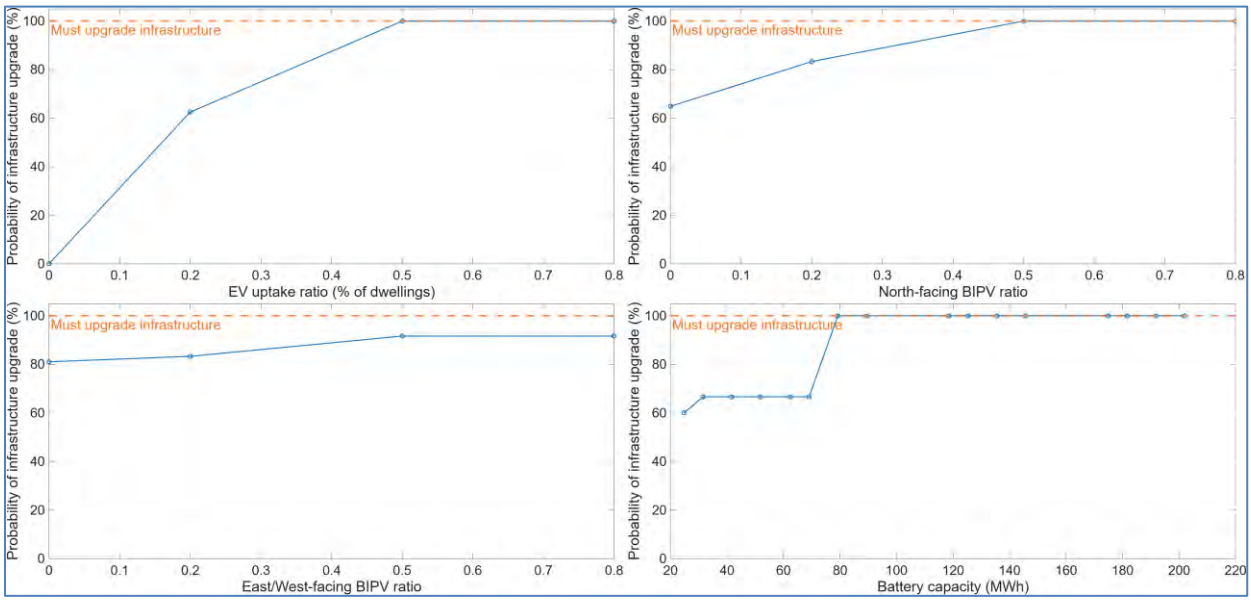

b.

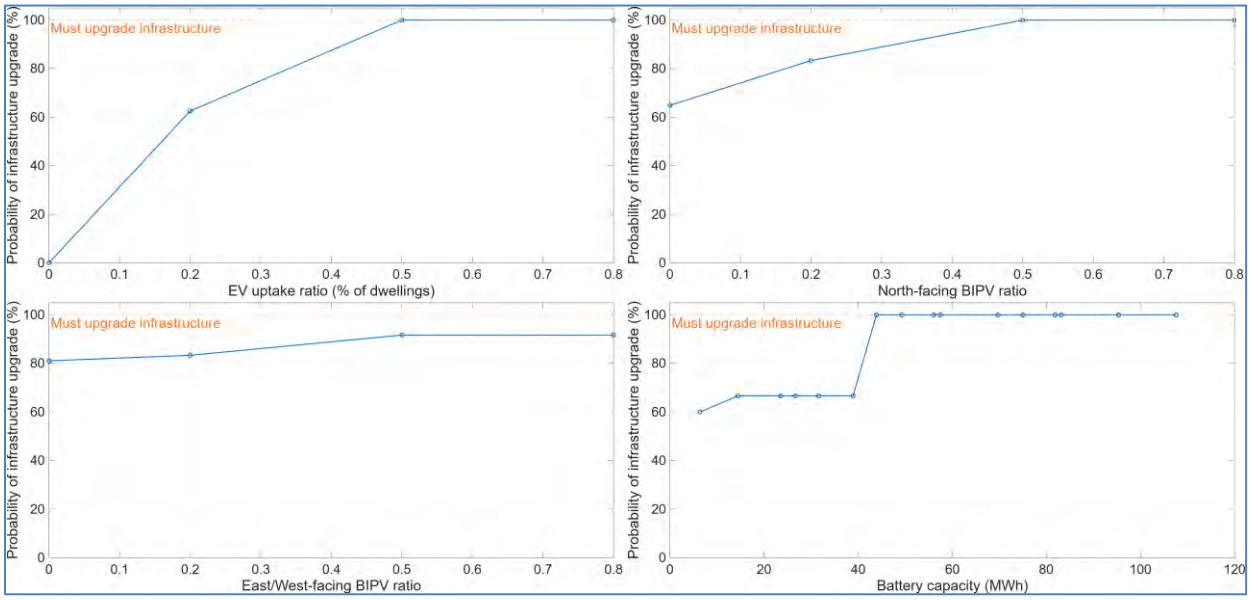

Figure 5.25. Upgrade likelihood vs key design variables (a – S1, b – S3)

Across both urban forms, EV uptake emerges as the dominant driver of infrastructure upgrades. In S1, a sharp threshold is observed between 20% and 50% EV penetration, beyond which infrastructure upgrades become effectively unavoidable. At penetration levels above 50%, the probability of upgrade rapidly approaches 100%, indicating that existing network capacity can no longer accommodate the coincident charging demand. In S3, this threshold behaviour is preserved, but the baseline probability of upgrades is systematically higher at lower EV penetration levels, reflecting the higher demand intensity associated with the vertically intensified built form.

High renewable generation penetration can also push the system into infeasibility, even in the absence of EV adoption. For both S1 and S3, a clear threshold is evident at approximately 50% north-facing façade BIPV coverage, beyond which infrastructure upgrades become inevitable. Unlike EV-driven constraints,

this behaviour reflects generation-driven limitations, such as export peaks and transformer loading, rather than increased demand. The transition is sharper in S3, indicating that the combination of higher load density and concentrated generation further reduces the system's tolerance to north-oriented façade deployment.

In contrast, east–west (E/W) BIPV exhibits a markedly different profile. In both S1 and S3, the probability of infrastructure upgrades is already relatively high at low E/W coverage, indicating that other system drivers dominate baseline network stress. Increasing E/W façade coverage does not substantially worsen feasibility beyond this baseline, and no distinct threshold behaviour is observed. This suggests that E/W-oriented BIPV distributes generation more evenly across the day, reducing the severity of export peaks and avoiding the sharp feasibility transitions associated with north-facing deployment.

Battery deployment exhibits a clear tipping-point behaviour when expressed in terms of total storage capacity. In S1, infrastructure upgrade probability remains relatively stable up to approximately 60–80 MWh of total battery capacity, beyond which upgrades rapidly become unavoidable. In S3, the corresponding threshold occurs at substantially lower capacities, around 40–60 MWh, reflecting the higher baseline loading and reduced headroom of the intensified urban form. In both cases, very large storage capacities are consistently associated with near-certain infrastructure upgrades, likely due to synchronised charging and reverse power flow exceeding network limits. These results indicate that while moderate battery deployment can smooth variability, storage alone cannot resolve network constraints beyond a critical scale.

Overall, infrastructure feasibility in urban renewable energy systems is governed by threshold behaviour rather than gradual trade-offs. EV uptake and north-facing BIPV deployment introduce sharp transitions from feasible to infeasible regimes, while east–west BIPV exhibits a more moderate and saturating impact. Battery storage moderates system variability but does not eliminate upgrade requirements once capacity thresholds are exceeded. Importantly, these threshold effects are consistently more restrictive in S3 than in S1, confirming that vertically intensified urban forms face tighter infrastructure constraints even when qualitative trade-off structures remain similar.

5.3.7.2 Trade-off between infrastructure upgrades and energy/economic benefits

a.

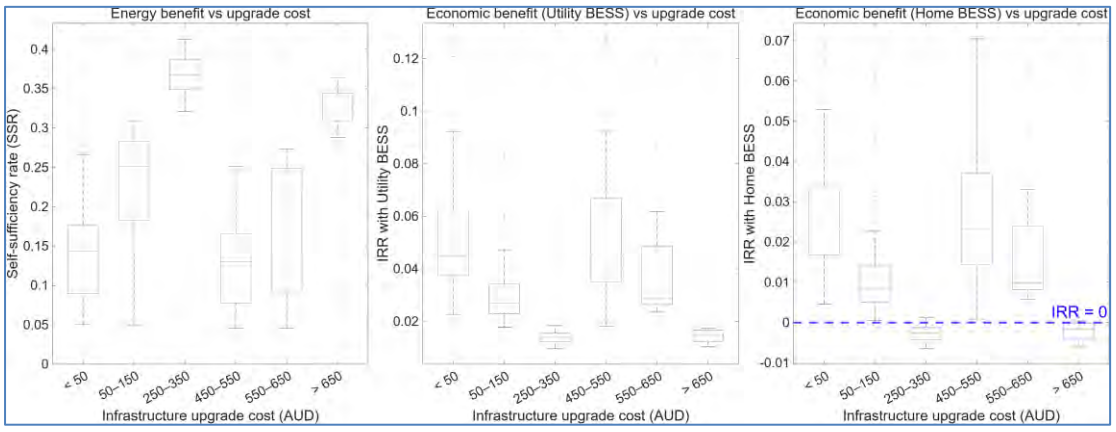

b.

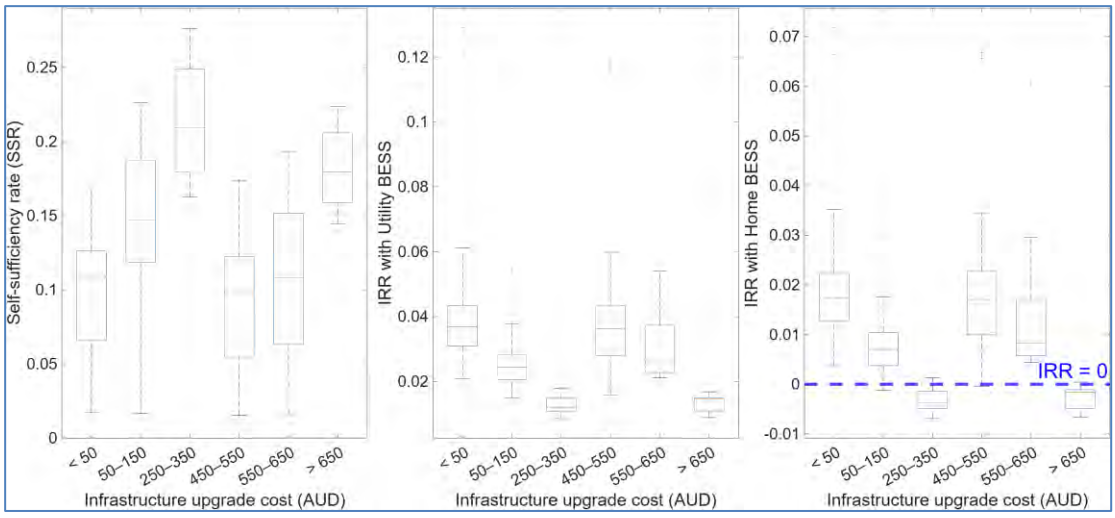

Figure 5.26. Trade-off between infrastructure upgrade cost and system benefits (a – S1, b – S3)

Figure 5.26 illustrates the trade-off between infrastructure upgrade costs and system-level energy and economic benefits by grouping scenarios into discrete upgrade cost bins and examining their associated self-sufficiency rates (SSR) and internal rates of return (IRR). The figure combines three complementary perspectives: energy performance (SSR), economic performance with utility-scale batteries, and economic performance with household batteries. Together, these panels demonstrate that infrastructure upgrade cost is not a monotonic indicator of system value but instead delineates distinct performance regimes with fundamentally different characteristics.

At low upgrade cost levels (< AUD 50 k), scenarios exhibit modest improvements in energy performance, with median SSR values typically in the range of approximately 0.12–0.18 in S1 and slightly lower values in S3. Importantly, both utility-scale and household battery configurations maintain predominantly positive IRR distributions in this regime. These outcomes correspond to low-stress system configurations, where limited infrastructure reinforcement enables incremental gains in self-sufficiency without undermining economic viability. This regime therefore represents a favourable balance between energy ambition, network impact, and financial performance.

As upgrade costs increase into the AUD 50–150 k range, SSR improves further, with median values rising towards 0.20–0.25, indicating enhanced local energy utilisation. However, this technical improvement is

accompanied by a clear deterioration in economic performance, particularly for household battery systems. While utility-scale batteries continue to exhibit positive IRR medians, household battery IRRs cluster closer to the zero line, signalling the onset of economic trade-offs. This divergence is more pronounced in S3, where higher baseline demand intensity and reduced network headroom amplify the sensitivity of decentralised storage economics to infrastructure stress.

The AUD 250–350 k upgrade cost range marks a critical transition regime. In this bin, SSR reaches its highest median values, approaching 0.35–0.38 in S1 and approximately 0.20–0.25 in S3, reflecting near-maximal energy autonomy within the explored design space. However, this energy peak coincides with systematically weak or negative economic outcomes for household batteries, with median IRRs falling below zero in both urban forms. Utility-scale batteries perform more robustly, but their IRR distributions also narrow and shift downward. This regime therefore represents an energy-maximising but economically constrained design space, where the pursuit of high self-sufficiency increasingly conflicts with financial feasibility.

At higher upgrade cost levels (> AUD 450 k), the relationship between infrastructure cost and system benefit becomes increasingly decoupled. SSR no longer increases systematically and instead stabilises or declines slightly, despite substantially higher upgrade expenditures. Economic performance deteriorates further: household battery IRRs remain consistently negative, while utility-scale battery IRRs fall to low but marginally positive levels. These scenarios are not driven by proportional gains in energy performance, but rather by reactive network reinforcements triggered by stress conditions such as high EV penetration, synchronised charging, reverse power flows, or transformer capacity limits. In this regime, infrastructure upgrades are corrective rather than value-generating.

Overall, Figure 5.26 demonstrates that infrastructure upgrades in urban renewable energy systems exhibit threshold-driven and regime-dependent behaviour. Moderate upgrades can deliver meaningful improvements in energy autonomy while preserving economic viability, particularly when combined with utility-scale storage. Beyond a bounded cost envelope, however, further infrastructure investment yields diminishing energy returns and rapidly erodes financial performance, most notably for household battery systems. The most expensive upgrades do not correspond to superior system outcomes, underscoring the importance of identifying feasible design envelopes that balance energy ambition with network and economic constraints, rather than pursuing maximal renewable penetration in isolation.

5.4 Stakeholder feasibility mapping and scenario clustering

The analysis in the previous sections demonstrated that infrastructure feasibility in urban renewable systems is governed by pronounced threshold behavior rather than gradual trade-offs. Key design variables such as EV uptake, battery penetration, and façade-oriented PV deployment were shown to trigger abrupt transitions from feasible to infeasible regimes, accompanied by sharp escalations in upgrade probability and cost. While these results identify critical stress drivers and system limits, they do not yet explain how such transitions are perceived, managed, or mitigated across different stakeholder perspectives. This motivates a further layer of analysis that explicitly accounts for the distribution of costs, benefits, and risks across actors involved in urban energy transitions.

The purpose of this section is therefore to move beyond aggregate system performance and examine stakeholder feasibility under infrastructure constraints. Rather than seeking a single optimal configuration, this section aims to map the design space according to how well different scenarios align with the objectives and constraints of key stakeholder groups. In doing so, it reframes feasibility not as a binary system property, but as a multi-dimensional concept shaped by competing priorities and unevenly allocated responsibilities.

Three broad stakeholder perspectives are considered in this analysis:

(1) Private investor

This represents residents, building owners, or energy adopters who directly invest in PV, BIPV, batteries, and EV charging infrastructure. From this perspective, feasibility is primarily evaluated through economic indicators such as internal rate of return (IRR) and net present value (NPV), which reflect private costs, savings, and revenues.

(2) Infrastructure-oriented stakeholder

This stakeholder category includes distribution network service providers (DNSPs) and public authorities responsible for maintaining system reliability and funding or approving network reinforcements. For this group, feasibility is governed by infrastructure upgrade requirements and associated costs.

(3) Energy or sustainability objective

This represents broader societal goals related to renewable energy utilization, self-sufficiency, and decarbonization, which are captured through system-level performance indicators such as the self-sufficiency rate (SSR).

These stakeholder perspectives are linked to distinct, but complementary, key performance indicators:

- **IRR** of the utility-scale battery is used to indicate investment attractiveness, while **negative NPV values** quantify the financial gap that would need to be addressed through external support for a scenario to become investable.
- **Infrastructure upgrade cost** is treated separately and interpreted as a system-level burden, reflecting investments typically undertaken by network operators or recovered through regulated mechanisms rather than borne directly by energy adopters.
- **SSR** is used as a proxy for energy autonomy and renewable effectiveness, capturing the extent to which local demand is met by on-site or precinct-level renewable generation. Importantly, infrastructure upgrade costs are not included in the IRR or NPV calculations, ensuring a clear separation between private financial viability and system-level feasibility.

Building on this stakeholder framing, the remainder of this Section develops a structured feasibility mapping of all scenarios using tiered classifications of economic performance, energy performance, and infrastructure impact. A heatmap-based representation is first used to visualise the distribution of scenarios across these dimensions and to reveal the absence of configurations that simultaneously maximise all objectives. This is followed by a stakeholder badge system and scenario clustering, which together identify balanced, renewable-forward, market-ready, and grid-stressed regimes. Through this

approach, the section aims to provide an interpretable decision framework that highlights unavoidable trade-offs, clarifies where policy support may be most effective, and delineates realistic envelopes for urban renewable deployment under network constraints.

5.4.1 Performance landscape of energy, economic viability, and infrastructure feasibility

To systematically examine how energy performance, economic viability, and infrastructure feasibility interact across the scenario set, a tier-based feasibility mapping approach is adopted in this section. The objective is to reveal how different combinations of stakeholder-relevant outcomes emerge across the design space, and to identify structural trade-offs that cannot be resolved through incremental optimisation.

Three key dimensions are considered: investment viability (Table 5.18), energy autonomy (Table 5.19), and infrastructure impact (Table 5.20). Each dimension is discretised into ordinal tiers using transparent and interpretable thresholds, as summarised in these tables. These tiers are designed to capture relative performance groupings within each scenario set rather than to impose externally defined notions of optimality, allowing the results to be interpreted in a planning and policy-relevant context.

Energy autonomy is represented by the self-sufficiency rate (SSR), which captures the proportion of local electricity demand met by on-site or precinct-level renewable generation. SSR tiers are defined using percentile-based thresholds derived from the full scenario set, ensuring that the classification reflects the achievable range of energy performance within the studied design space rather than externally imposed targets. Infrastructure feasibility is assessed using the required infrastructure upgrade cost, with scenarios grouped into no-upgrade, minor, moderate, and major upgrade tiers based on cost percentiles.

Table 5.18. Tier settings for IRR (Investment)

IRR Tier	Definition	IRR (S1)	IRR (S3)	Interpretation
IRR-1: Lowest	< 20th percentile	IRR < 1.60%	IRR < 1.50%	Not possible to achieve NPV > 0
IRR-2: Lower	20–40th	1.60% ≤ IRR < 2.56%	1.50% ≤ IRR < 2.26%	The scenarios that are unlikely to result in profits
IRR-3: Medium	40–60th	2.56% ≤ IRR < 4.03%	2.26% ≤ IRR < 3.27%	The scenarios that have return rate near deposit rate and WACC
IRR-4: Upper	60-80th percentile	4.03% ≤ IRR < 5.63%	3.27% ≤ IRR < 4.21%	Acceptable but not outstanding scenarios
IRR-5: Highest	>80th percentile	IRR ≥ 5.63%	IRR ≥ 4.21%	Scenarios with highest return rates

Table 5.19. Tier settings of SSR (Energy autonomy)

SSR Tier	Definition	SSR (S1)	SSR (S3)	Interpretation
SSR-1: Lowest	< 20th percentile	SSR < 9.35%	SSR < 6.76%	Lowest band of self-sufficiency
SSR-2: Lower	20–40th	9.35% ≤ SSR < 15.62%	6.76% ≤ SSR < 11.15%	Second lowest band of self-sufficiency
SSR-3: Middle	40–60th	15.62% ≤ SSR < 25.04%	11.15% ≤ SSR < 14.93%	Medium band of self-sufficiency
SSR-4: Upper	60-80th percentile	25.04% ≤ SSR < 32.41%	14.93% ≤ SSR < 19.09%	Second highest band of self-sufficiency
SSR-5: Highest	>80th percentile	SSR ≥ 32.41%	SSR ≥ 19.09%	Highest band of self-sufficiency

Table 5.20. Tier settings for infrastructure upgrade cost (Power system)

Infra Tier	Definition	Upgrade cost (S1)	Upgrade cost (S3)	Interpretation
INF-0: No upgrade	cost = 0	Upgrade Cost = 0	Upgrade Cost = 0	Fully network-compatible
INF-1: Minor	<25th percentile	0 < Upgrade Cost ≤ $51,683	0 < Upgrade Cost ≤ $76,335	Low level upgrade
INF-2: Moderate	P25 < cost ≤ P75	$51,683 < Upgrade Cost ≤ $536,287	$76,340< Upgrade Cost ≤ $346,637	Significant but manageable

INF-3: Major	cost > P75	Upgrade Cost > $536,287	Upgrade Cost > $346,637	System-level stress

Importantly, infrastructure upgrade costs are treated as a distinct system dimension, even though they are incorporated into the calculation of NPV and IRR. This separation preserves the analytical distinction between private financial viability and system-level feasibility and enables trade-offs between stakeholders to be examined explicitly rather than being obscured through aggregated metrics.

5.4.2 Performance differences between S1 and S3

Crucially, while the same tiering methodology is applied consistently to both S1 and S3 using Table 5.18, Table 5.19, and Table 5.20, the resulting tier boundaries reveal a systematic downward shift in the feasible performance envelope of S3. In particular, IRR tiers in S3 are compressed toward lower absolute values, with the lower bound of the upper investment tier (IRR-4) falling below the weighted average cost of capital (WACC = 3.66%) used in the NPV calculation. This indicates that even the relatively higher-performing configurations in S3 do not consistently satisfy conventional investment benchmarks in absolute terms, in contrast to S1 where upper-tier scenarios clearly exceed WACC and represent genuinely attractive investment opportunities.

A similar boundary shift is observed for energy autonomy. SSR tier thresholds in S3 are substantially lower than those in S1 across all percentile bands, indicating that the highest-achievable self-sufficiency levels in S3 correspond to only moderate performance in S1. This reflects the structurally intensified urban form of S3, where higher energy demand density and functional floor area concentration dilute renewable generation benefits when assessed relative to load. As a result, relative optimisation within S3 does not translate into equivalent absolute energy autonomy outcomes.

Taken together, these boundary shifts confirm that S3 represents a systematically more constrained urban configuration. While the same analytical workflow and tiering framework remain valid, the resulting feasibility landscape is fundamentally weaker, with a compressed upper envelope for both economic and energy performance. This distinction is critical for interpreting subsequent clustering and stakeholder alignment results, as it demonstrates that scenario optimisation is strongly conditioned by urban form and demand structure, not solely by technology selection or deployment intensity.

5.4.3 Heatmap of performance landscape

Using these tier definitions, all scenarios are mapped onto a two-dimensional heatmap for each infrastructure tier, with IRR tiers on the vertical axis and SSR tiers on the horizontal axis, as shown in Figure 5.27. Each cell in the heatmap represents a distinct combination of economic and energy performance under a given level of infrastructure impact and is annotated with both the number and proportion of scenarios falling within that category. Empty cells indicate combinations that are not achievable within the explored design space.

This heatmap-based feasibility landscape provides a compact visualisation of the multi-stakeholder trade-offs inherent in urban renewable system design. Rather than identifying a single optimal solution, it reveals the absence of scenarios that simultaneously achieve high energy autonomy, strong private economic performance, and minimal infrastructure intervention, and highlights the regimes in which compromises between these objectives become unavoidable. The resulting structure forms the basis for the

stakeholder badge system and scenario clustering discussed in the following subsections, enabling a transparent classification of scenarios according to balanced, renewable-forward, market-ready, and grid-stressed outcomes.

Figure 5.27 presents the distribution of all scenarios across three dimensions: energy performance (self-sufficiency rate, SSR tiers), private investment performance (IRR tiers), and infrastructure upgrade severity (INF tiers). The four panels jointly define a feasibility landscape that exposes both attainable configurations and structurally constrained combinations within the explored urban renewable design space, with Panels (a) and (b) corresponding to S1 and S3 respectively.

a.

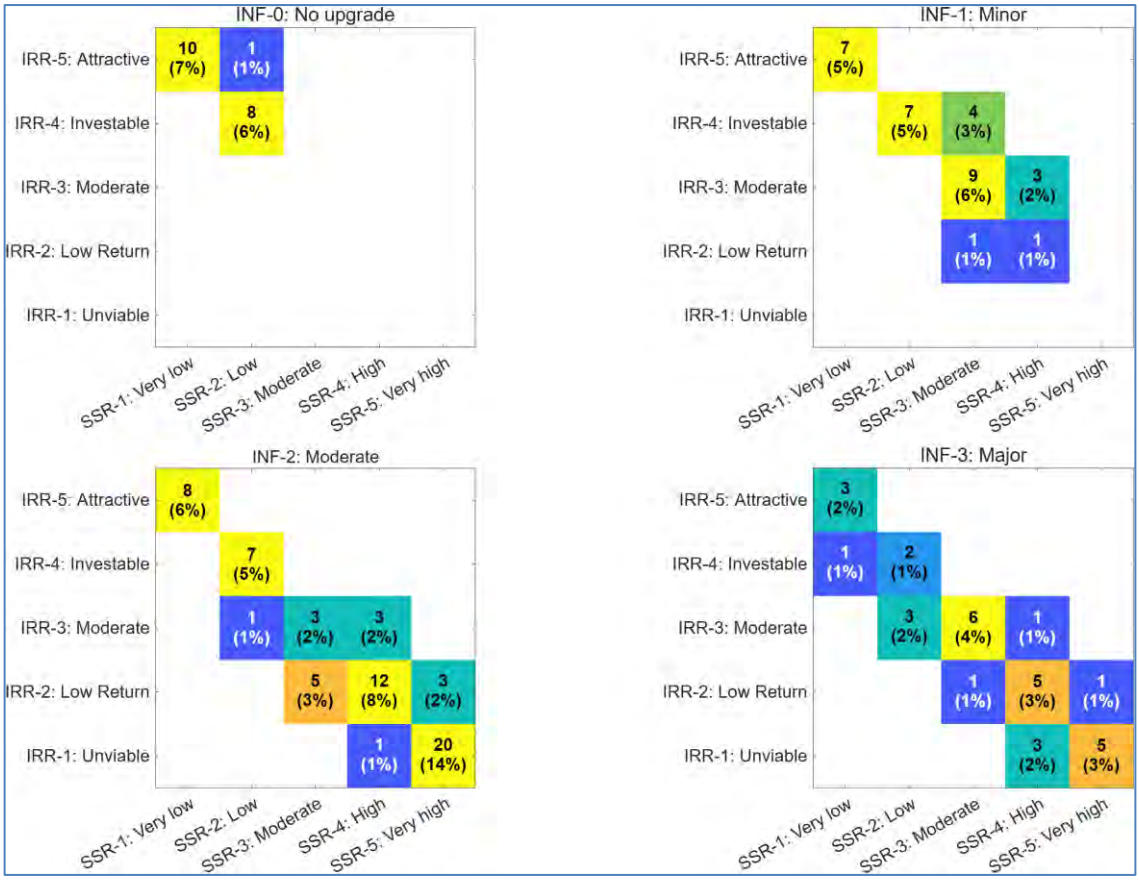

b.

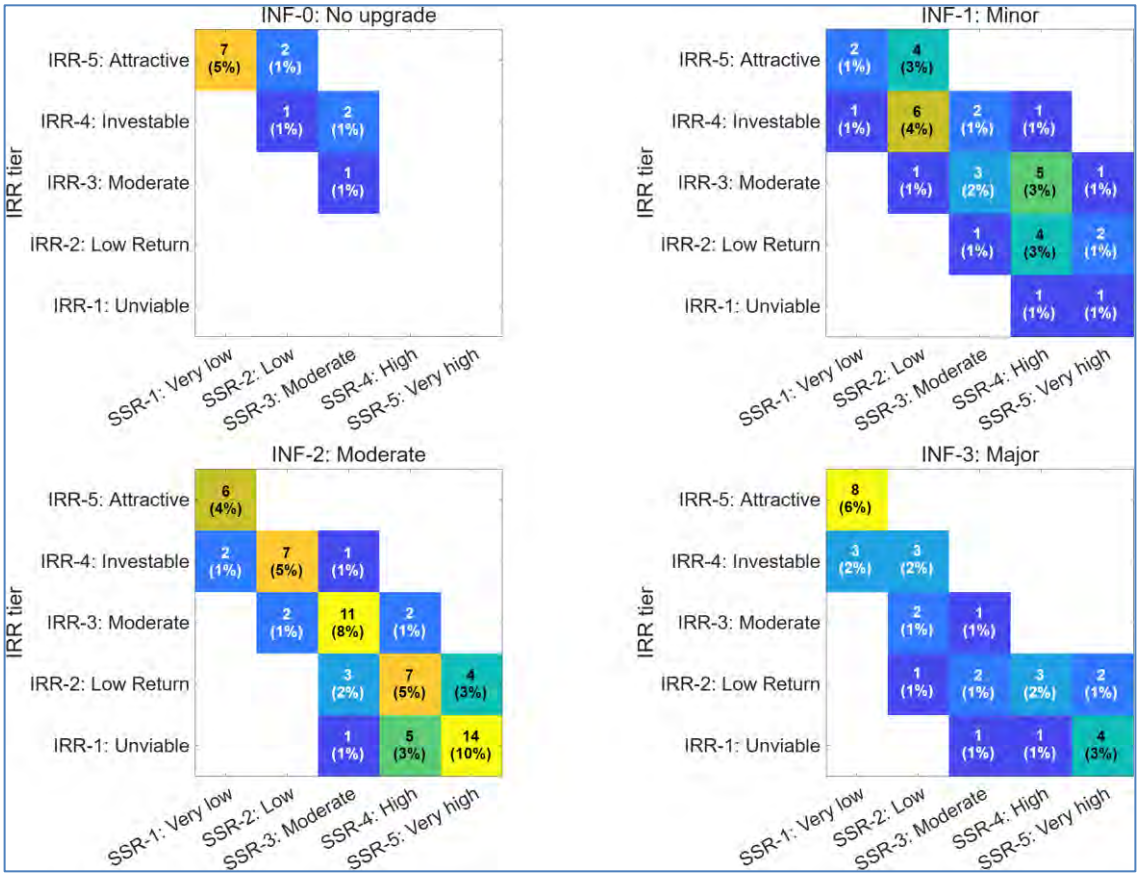

Figure 5.27. Scenario distribution heatmap across energy, economic, and infrastructure tiers (a – S1, b – S3)

A prominent feature common to both urban forms is the systematic absence of scenarios in the upper-right region of the heatmaps, corresponding to combinations of high or very high self-sufficiency (SSR-4/5), strong private investment performance (upper IRR tiers), and low or no infrastructure upgrades (INF-0/1). This empty region indicates that, under prevailing cost assumptions and network constraints, it is not possible to simultaneously maximise energy autonomy, private economic performance, and infrastructure compatibility. Importantly, this structural gap persists across both S1 and S3 and across infrastructure tiers, confirming that it reflects a fundamental trade-off rather than an artefact of scenario sampling or a peculiarity of urban form.

At the opposite extreme, the lower-left region of the heatmaps—representing scenarios with low self-sufficiency (SSR-1), weak economic performance (lowest IRR tier), and major infrastructure upgrades (INF-3)—is also sparsely populated in both cases. This suggests that configurations performing poorly across all three dimensions are relatively uncommon. In practice, even scenarios that impose substantial infrastructure stress tend to deliver either meaningful energy benefits or acceptable private returns, indicating that extreme "lose–lose–lose" outcomes are unlikely to arise unintentionally within realistic design envelopes.

Despite these shared structural features, clear and systematic differences emerge between S1 and S3 in both the density and organisation of feasible outcomes. In S1, scenario distributions form more compact and coherent clusters within specific regions of the feasibility space, indicating smoother transitions between energy, economic, and infrastructure regimes and the existence of comparatively robust design pathways. By contrast, S3 exhibits a noticeably sparser yet more widely dispersed distribution, with fewer scenarios per cell but spread across a larger number of distinct SSR–IRR–INF combinations. This fragmentation reflects the compounded constraints introduced by S3's vertically intensified built form, higher demand intensity, and reduced network headroom, which collectively compress the feasible performance envelope and increase sensitivity to design choices.

Scenarios achieving high or very high self-sufficiency are concentrated within the moderate and major infrastructure tiers (INF-2 and INF-3) in both urban forms and are frequently associated with weak or marginal economic performance. These configurations represent renewable-forward designs that prioritise energy autonomy at the expense of network stress and private financial viability. In S3, such outcomes occur less frequently but are more dispersed across infrastructure and economic tiers, reinforcing the finding that intensified urban form magnifies the penalties associated with energy-maximising strategies while offering fewer stable high-performance configurations.

Conversely, scenarios exhibiting stronger private investment performance and minimal infrastructure upgrades are clustered within the lower to moderate SSR tiers, representing market-aligned configurations that preserve network feasibility and economic viability but deliver limited gains in energy autonomy. In S3, these configurations are fewer in number and less densely clustered than in S1, indicating a reduced availability of scenarios that simultaneously satisfy economic and infrastructure constraints under higher baseline demand conditions.

Between these extremes, Figure 5.27 highlights intermediate regions where partial alignment between stakeholder objectives is achieved. These include scenarios combining moderate SSR with minor infrastructure upgrades and borderline economic performance, as well as economically viable and network-compatible configurations that fall short of higher energy autonomy targets. While such compromise solutions are present in both urban forms, they are notably more fragmented in S3,

suggesting that balanced outcomes become increasingly contingent on precise parameter combinations as urban intensity increases.

Overall, Figure 5.27 demonstrates that feasibility in urban renewable systems is governed not by a single optimal solution, but by a constrained and non-linear landscape shaped by interactions between energy performance, private economics, and infrastructure limits. The contrast between S1's denser and more coherent feasibility clusters and S3's sparser, more fragmented distribution underscores how intensified urban form systematically weakens absolute performance and compresses feasible solution spaces. The absence of "perfect" outcomes alongside the rarity of universally poor ones reinforces the need for explicit trade-off recognition and stakeholder-aware decision-making, rather than attempts to optimise all objectives concurrently. This insight directly motivates the subsequent clustering of scenarios into stakeholder-aligned outcome regimes and balanced feasibility envelopes.

5.4.4 Stakeholder trade-off and balanced outcomes

To translate the feasibility landscape into interpretable and decision-relevant insights, this section introduces a scenario clustering approach that identifies groups of configurations achieving partial but meaningful alignment between stakeholder objectives. Rather than attempting to define a single optimal solution or aggregate score, the objective is to distinguish outcome regimes that reflect different priorities, trade-offs, and constraint structures within the explored design space.

The clustering is based on a badge-style logic that evaluates each scenario against three stakeholder-aligned criteria: energy autonomy, private investment viability, and network feasibility. Each criterion is assessed using tier-based classifications introduced in Table 5.18, Table 5.19, and Table 5.20.

Three stakeholder-aligned criteria are defined:

- First, scenarios are considered energy-aligned if they achieve at least moderate self-sufficiency (SSR-2 or above), recognising that incremental improvements in energy autonomy are often policy-relevant even when the highest self-sufficiency levels are unattainable.
- Second, private investment alignment is evaluated using relative IRR tiers, with scenarios classified as economically favourable if they fall within the upper tiers of the distribution.
- Third, network alignment is assessed using infrastructure upgrade requirements, with scenarios considered network-compatible if they require no upgrade or only minor reinforcement.

Based on these criteria, four stakeholder-aligned outcome types are defined: (i) balanced outcomes satisfying all three objectives, (ii) renewable-forward configurations prioritising energy autonomy and network compatibility at the expense of private returns, (iii) market-aligned outcomes favouring economic performance and network feasibility but delivering limited energy autonomy, and (iv) technically and financially strong configurations constrained primarily by network capacity. Scenarios that fail to meet at least two stakeholder objectives are not clustered further, as they are unlikely to represent actionable deployment pathways under current planning and market conditions.

The clustering framework is applied separately to S1 and S3 in the following subsections. While the analytical criteria remain identical, the resulting clusters differ markedly in size, composition, and internal

coherence, revealing how urban form fundamentally shapes the availability of balanced and stakeholder-aligned renewable energy outcomes.

5.4.4.1 S1 Cluster analysis

Collectively, the S1 clustering results demonstrate that a compact but meaningfully populated feasibility space exists in which partial and, in some cases, full alignment between energy, investment, and network objectives can be achieved. Although fully balanced outcomes represent a relatively small proportion of the overall design space, their presence confirms that trade-offs between stakeholders are not irreconcilable under this urban form. Importantly, the distribution of clusters shows a graduated structure rather than a binary separation between viable and unviable outcomes: market-ready configurations, renewable-forward pathways, and balanced solutions coexist within adjacent regions of the feasibility landscape.

This structure indicates that, for S1, incremental design adjustments can shift scenarios between stakeholder-aligned regimes without triggering abrupt losses in feasibility. From a planning perspective, this suggests that S1 offers a degree of flexibility in negotiating energy ambition, private investment performance, and network constraints, making it a robust reference case for stakeholder-informed urban renewable energy design. The presence of all major outcome types within S1 provides a coherent basis for policy interpretation and comparison with more constrained urban forms in the subsequent analysis.

Table 5.21. Stakeholder-aligned outcome clusters across all scenarios in S1

Stakeholder feasibility alignment	Unique Scenario Count	% of total scenarios	Implications	Cluster ID
Energy ✓ Investor ✓ Network ✓	4	2.76	Balanced outcomes that simultaneously satisfy energy performance, private investment viability, and network feasibility objectives	Table 13.11. S1C1: Balanced outcomes
Energy ✓ Network ✓	14	9.66	Renewable-forward outcomes that achieve high energy autonomy with minimal infrastructure reinforcement, but require policy or financial support to achieve private investment viability	Table 13.12. S1C2: Renewable-forward (policy-supported)
Investor ✓ Network ✓	33	22.76	Market-ready and network-compatible outcomes that prioritise financial viability, but deliver limited energy autonomy	Table 13.13. S1C3: Market-ready (conservative)
Energy ✓ Investor ✓	0	0	Technically and financially attractive outcomes that are constrained by network capacity and therefore require significant infrastructure upgrades	-

The resulting clusters, summarised in Table 5.21 and detailed in Appendix Table 13.11, Table 13.12, and Table 13.13, provide a structured lens through which balanced outcomes, renewable-forward pathways, market-

ready configurations, and grid-limited opportunities can be examined. Together, they form the basis for the policy and planning insights discussed in the following subsections.

5.4.4.1.a Cluster S1C1 – Balanced outcomes

Cluster C1 represents the subset of scenarios that simultaneously satisfy energy performance, private investment viability, and network feasibility criteria. As such, this cluster defines the balanced outcome regime within the explored design space, where improvements in self-sufficiency, economic performance, and infrastructure compatibility are achieved without imposing disproportionate costs or constraints on any single stakeholder group. While Cluster C1 accounts for only 4 scenarios (2.76%) of the total design space, it plays a critical role as a feasibility benchmark against which other trade-off-driven clusters are evaluated.

Cluster C1 represents the subset of scenarios that simultaneously satisfy energy performance, private investment viability, and network feasibility criteria. As such, this cluster defines the balanced outcome regime within the explored design space, where improvements in self-sufficiency, economic performance, and infrastructure compatibility are achieved without imposing disproportionate costs or constraints on any single stakeholder group. While Cluster C1 accounts for only 4 scenarios (2.76%) of the total design space, it plays a critical role as a feasibility benchmark against which other trade-off-driven clusters are evaluated.

Table 5.22. Summary table of cluster S1C1

	Min	Max	Median	Mean
• *Design Variables*				
North BIPV	20%	20%	20%	20%
E/W BIPV	50.00%	80.00%	50.00%	57.50%
Battery Capacity (MWh)	79.24	89.40	79.24	81.78
EV uptake	20.00%	50.00%	20.00%	27.50%
• *Key Indicators*				
Infrastructure upgrade cost - AUD	3941.90	42735.00	8259.45	15798.95
SSR	16.45%	19.50%	17.67%	17.82%
IRR	4.03%	4.51%	4.19%	4.23%

Table 5.22 summarises the key design characteristics and performance indicators of Cluster C1, with individual scenarios detailed in Table 13.11. From a system design perspective, Cluster C1 is characterised by moderate and carefully distributed BIPV deployment rather than aggressive capacity maximisation. North-facing BIPV coverage is consistently limited to 20%, while east–west (E/W) BIPV exhibits higher penetration, ranging from 50% to 80%, with a median of 50%. This configuration reflects a deliberate emphasis on temporal generation smoothing and network-compatible energy delivery, consistent with earlier findings that E/W façade deployment mitigates peak export stress.

Battery deployment in Cluster C1 remains moderate and tightly bounded, with total battery capacity ranging from 79.24 to 89.40 MWh and a median of 79.24 MWh. This scale is sufficient to support self-consumption and peak load management while remaining well below the capacity levels associated with sharp increases in infrastructure upgrade probability and cost. EV uptake is similarly constrained, ranging from 20% to 50% of dwellings, with a median of 20%, reinforcing the role of controlled electrification in preserving network feasibility under existing infrastructure assumptions.

In terms of system performance, Cluster C1 achieves moderate but robust energy autonomy, with self-sufficiency rates (SSR) spanning 16.45% to 19.50% and a median of 17.67%. Although these values do not reach the highest SSR tiers observed elsewhere in the design space, they represent a meaningful improvement over low-autonomy configurations while avoiding the infrastructure stress associated with extreme renewable penetration. This confirms that balanced outcomes are associated with incremental, rather than maximal, gains in self-sufficiency.

From an economic perspective, Cluster C1 scenarios deliver stable and investable private returns. Internal rates of return (IRR) range from 4.03% to 4.51%, with a median of 4.19% and a mean of 4.23%, placing all scenarios comfortably within the investable range defined in this study. These returns are not driven by speculative upside but by consistent cost-performance alignment, reinforcing the notion that economic viability in urban renewable systems is achieved through disciplined system sizing rather than scale alone.

Crucially, infrastructure impacts in Cluster C1 are limited and manageable. Infrastructure upgrade costs remain low across all scenarios, ranging from AUD 3,942 to AUD 42,735, with a median requirement of AUD 8,259. Even at the upper bound, upgrade costs remain well below the major reinforcement thresholds identified elsewhere in the design space, confirming that Cluster C1 configurations are largely network-compatible and do not rely on extensive public infrastructure investment.

Overall, Cluster C1 defines a narrow but well-defined feasible envelope for urban renewable energy deployment. It demonstrates that balanced outcomes are achievable when system design prioritises moderation, diversification, and stakeholder alignment, rather than the optimisation of any single objective. While such configurations are relatively rare, they provide a critical reference point for understanding how departures toward greater renewable ambition, market-driven optimisation, or technical extremity introduce increasingly explicit and unavoidable trade-offs in subsequent clusters.

5.4.4.1.b Cluster S1C2 – Renewable growth and grid compatibility scenarios

Cluster C2 represents renewable-forward scenarios that prioritise higher levels of energy autonomy but require explicit policy or public support to remain economically viable. These scenarios sit between the balanced feasibility envelope of Cluster C1 and the high-stress regimes identified elsewhere, achieving materially higher self-sufficiency at the cost of reduced private investment attractiveness and increased infrastructure engagement. Cluster C2 accounts for 14 scenarios (9.66% of the design space) and plays a critical role in identifying where targeted intervention can unlock stronger energy outcomes without pushing the system into extreme network stress.

Table 5.23. Summary table of cluster S1C2

	Min	Max	Median	Mean
• *Design Variables*				
North BIPV	20%	50%	20%	33%
E/W BIPV	0.00%	80.00%	50.00%	43.57%
Battery Capacity (MWh)	79.24	125.36	89.40	101.18
EV uptake	20.00%	50.00%	20.00%	30.71%
• *Key Indicators*				
Infrastructure upgrade cost - AUD	3941.90	51683.00	48147.50	40272.71
SSR	15.72%	26.77%	19.56%	21.25%
IRR	2.26%	3.93%	3.16%	3.17%

As summarised in Table 5.23, Cluster C2 is characterised by a clear intensification of renewable and storage deployment relative to Cluster C1. North-facing BIPV penetration increases modestly, spanning 20–50% with a median of 20%, while east–west BIPV exhibits wide flexibility, ranging from 0–80% (median 50%). This reflects a deliberate expansion of façade-based generation to increase temporal coverage and total yield rather than simple capacity maximisation.

Battery deployment is notably higher than in C1, with capacities ranging from 79 to 125 MWh (median 89 MWh), indicating a shift toward storage-supported self-consumption and peak mitigation. EV uptake remains constrained to 20–50% (median 20%), suggesting that electrification growth is still moderated to avoid disproportionate network stress under existing infrastructure conditions.

From an energy perspective, Cluster C2 delivers a clear step-change in performance. Self-sufficiency rates range from 15.7% to 26.8%, with a median of 19.6% and a mean exceeding 21%, surpassing both BAU and Cluster C1 outcomes. These values place C2 firmly within the renewable-forward regime, where energy autonomy becomes a primary system objective.

However, this improvement comes with economic trade-offs. IRR values fall into a narrower and lower band (2.26–3.93%, median 3.16%), remaining above zero but below typical private investment thresholds. These scenarios are therefore marginally viable at best under market conditions, indicating that without intervention, private actors are unlikely to deliver these configurations at scale.

Infrastructure impacts remain moderate but non-negligible. Upgrade costs cluster between AUD 3,900 and AUD 51,700, with a median of approximately AUD 48,000, placing most scenarios in the INF-1 to INF-2 tiers. This confirms that Cluster C2 outcomes are not driven by severe network reinforcement, but rather by cumulative stress associated with higher distributed generation and storage penetration.

Policy Support Implications

To quantify the intervention needed to unlock these renewable-forward configurations, Table 5.24 estimates the policy support intensity required to make Cluster C2 scenarios economically viable, assuming that support is applied to one system component at a time within the scenarios captured by this cluster.

Importantly, the support values reported do not represent a combined subsidy package. Instead, each metric reflects the equivalent incentive level required if policy support were targeted solely at that specific system component, holding other components unchanged.

Table 5.24. Estimated policy support intensity required for Cluster S1C2 scenarios

	Median	Low - P25	High - P75	Units
Total Support Required	$12,051,000	$916,670	$25,844,000	AUD
Support per 1% SSR achieved	$1,036,300	$112,240	$1,645,600	AUD per +1% SSR
Support per kW PV/BIPV	$198	$19	$333	AUD per kW PV/BIPV
Support per kWh Battery Capacity	$127,150	$11,568	$217,930	AUD per battery unit
Support per 1% EV uptake	$398,040	$45,834	$1,292,200	AUD per 1% EV uptake

To translate these scenarios into actionable policy guidance, Table 5.24 quantifies the support intensity required to close the investment gap. By normalising negative NPVs against key deployment metrics, this table estimates the magnitude of financial support needed to render C2 scenarios economically viable.

Importantly, the support values reported do not represent a combined subsidy package. Instead, each metric reflects the equivalent incentive level required if policy support were targeted solely at that specific system component, holding other components unchanged.

Key observations include:

- The median total support required per scenario is approximately AUD 12.1 million, with a wide interquartile range (AUD 0.9–25.8 million), highlighting substantial heterogeneity within the cluster.
- When normalised by energy outcome, the median support required per additional 1% SSR is AUD 1.04 million, indicating that marginal gains in energy autonomy become increasingly costly beyond the balanced regime.
- In contrast, generation-focused support is relatively efficient: a median of AUD 198 per kW of PV/BIPV would be sufficient to render these scenarios viable. This implies that targeted incentives for façade and rooftop PV deployment can effectively unlock renewable-forward outcomes at moderate public cost.
- Battery-only support is significantly more expensive, with a median requirement of AUD 127,150 per kWh of battery capacity, reflecting the dominant role of storage capital costs in suppressing IRR in these scenarios.
- Support linked to electrification is similarly costly: achieving viability through EV-only incentives would require approximately AUD 398,000 per additional 1% EV uptake, reinforcing that EV penetration primarily acts as a stressor rather than a value driver under current tariff and infrastructure assumptions.

When interpreted jointly, these results indicate that direct support for PV and BIPV deployment constitutes the most cost-effective intervention pathway. Relatively modest incentives for generation capacity can unlock meaningful gains in energy autonomy at substantially lower public expenditure than interventions targeting battery storage or EV uptake alone. In contrast, battery-focused or EV-focused support mechanisms require significantly higher expenditure per unit of outcome, reflecting the high capital intensity of storage systems and the network-driven costs associated with electrified transport.

Consistent with the threshold behaviour identified in Section 5.3.7, façade-based BIPV particularly east–west oriented systems offer an additional strategic advantage by increasing renewable contribution without proportionally exacerbating infrastructure upgrade requirements. This makes BIPV a comparatively efficient policy lever for advancing self-sufficiency within constrained urban networks. By comparison, incentives directed toward large-scale battery deployment or accelerated EV uptake tend to deliver smaller marginal gains in SSR per dollar spent while simultaneously intensifying infrastructure stress, rendering these levers more system-sensitive and costly under the current network context.

Overall, Cluster C2 illustrates a policy-leveraged transition regime in which public intervention is required to align private investment behaviour with broader societal energy objectives. These scenarios are not market-ready in isolation, but they become feasible through targeted, technology-specific support mechanisms that prioritise high-impact renewable deployment while preserving network feasibility. This highlights the importance of selective, evidence-based policy design, rather than uniform incentives, in accelerating urban renewable energy transitions.

5.4.4.1.c Cluster S1C3 – Market ready outcomes

Cluster C3 represents scenarios that are financially attractive to investors and broadly compatible with existing network capacity, but deliver comparatively modest improvements in energy autonomy. As such, this cluster defines *the* market-ready and low-risk deployment regime, prioritising economic viability and infrastructure compatibility over ambitious renewable penetration.

As summarised in Table 5.25, Cluster C3 is characterised by restrained system sizing across all major design variables. North-facing BIPV deployment is minimal, with a median value of 0% and an upper bound of only 20%, while east–west BIPV penetration remains limited, with a median of 20%. This indicates a strong preference for conservative façade deployment strategies that avoid aggressive increases in installed capacity. Battery deployment is also moderate, with total capacity ranging from approximately 25 to 69 MWh and a median of 41.7 MWh, well below the levels observed in the renewable-forward Cluster C2. EV uptake spans a wider range but remains controlled overall, with a median value of 20%, suggesting that electrification proceeds incrementally rather than as a dominant driver of system design.

Table 5.25. Summary table of cluster S1C3

	Min	Max	Median	Mean
• *Design Variables*				
North BIPV	0%	20%	0%	6%
E/W BIPV	0.00%	80.00%	20.00%	29.70%
Battery Capacity (MWh)	24.81	69.09	41.73	46.23
EV uptake	0.00%	50.00%	20.00%	32.12%
• *Key Indicators*				
Infrastructure upgrade cost - AUD	0.00	50369.00	0.00	17447.45
SSR	5.02%	15.53%	9.25%	9.86%
IRR	4.08%	13.12%	5.99%	7.13%

From an infrastructure perspective, Cluster C3 scenarios are highly network compatible. The median infrastructure upgrade cost is zero, and even the upper bound remains below AUD 50,400, indicating that most configurations can be accommodated within existing distribution capacity or require only minor reinforcement. This confirms that the conservative sizing of renewable and storage assets effectively mitigates network stress, aligning with the low-upgrade regimes identified in Section 5.3.

In terms of performance outcomes, Cluster C3 delivers relatively low but stable energy autonomy. Self-sufficiency rates range from 5.0% to 15.5%, with a median of 9.3%, reflecting incremental gains over baseline conditions rather than transformative reductions in grid reliance. While these SSR levels fall well below those achieved in Cluster C2, they are achieved without triggering substantial infrastructure investment or operational constraints.

Economically, Cluster C3 represents the strongest private investment proposition across all clusters. IRRs span from 4.1% to 13.1%, with a median value of 6.0% and a mean of 7.1%, comfortably exceeding typical investment thresholds. This combination of high returns and low infrastructure burden highlights the attractiveness of these scenarios under current market and regulatory conditions. Importantly, financial performance in Cluster C3 is achieved without reliance on policy support or cross-subsidization, distinguishing it clearly from the policy-leveraged dynamics observed in Cluster C2.

Overall, Cluster C3 defines a pragmatic, market-driven deployment envelope in which renewable energy systems can be rolled out rapidly and at scale with minimal public intervention. However, this comes at the cost of limited contribution to precinct-level energy autonomy and decarbonization ambition. In this sense, Cluster C3 illustrates the inherent tension between market readiness and transformational energy outcomes, reinforcing the need for complementary policy mechanisms if higher self-sufficiency targets are to be achieved without compromising investor confidence or network stability.

5.4.4.2 S3 Cluster analysis

Building on the clustering framework established for S1, this subsection applies the same stakeholder-aligned classification logic to scenarios within S3. The objective is not to identify alternative "optimal" outcomes, but to examine how the feasibility landscape evolves under a more vertically intensified urban form characterized by higher demand intensity, reduced renewable yield per functional floor area, and tighter network operating margins.

Table 5.26 summarizes the resulting stakeholder-aligned clusters for S3. While all four outcome types identified in S1 are retained conceptually, their distribution, density, and performance characteristics differ markedly. In particular, the overall share of scenarios achieving multi-stakeholder alignment is reduced, and those that do qualify tend to exhibit weaker absolute performance across both energy and economic dimensions. This indicates that, in S3, relative optimization within the design space does not translate into equivalent system-level outcomes.

Table 5.26. Stakeholder-aligned outcome clusters across all scenarios in S3

Stakeholder feasibility alignment	Unique Scenario Count	% of total scenarios	Implications	Cluster ID
Energy ✓ Investor ✓ Network ✓	5	3.45%	Configurations that achieve relative alignment between energy performance, private investment viability, and network feasibility within the S3 urban form.	Table 13.14. S3C1: Balanced outcomes Table 13.11. S1C1: Balanced outcomes
Energy ✓ Network ✓	19	13.10%	Renewable-forward outcomes that achieve relatively higher levels of energy autonomy with minimal infrastructure reinforcement, but require policy or financial support to achieve private investment viability.	Table 13.15. S3C2: Renewable-forward (policy-supported)Table 13.12. S1C2: Renewable-forward (policy-supported)
Investor ✓ Network ✓	23	15.86%	Market-ready and network-compatible outcomes that prioritise financial viability, but deliver limited energy autonomy	Table 13.16. S3C3: Market-ready (conservative)Table 13.13. S1C3: Market-ready (conservative)
Energy ✓ Investor ✓	0	0	Technically and financially attractive outcomes that are constrained by network capacity and therefore require	-

			significant infrastructure upgrades	

Balanced outcomes in S3 represent configurations that achieve relative alignment between energy performance, private investment viability, and network feasibility within a highly constrained urban form. Although these scenarios satisfy all three stakeholder criteria under the adopted tier definitions, their absolute performance levels remain modest compared to equivalent clusters in S1, particularly in terms of self-sufficiency and investment returns. These outcomes therefore reflect localized balance under constraint, rather than genuinely strong multi-objective performance, highlighting the limited headroom available for integrated optimization in S3.

Renewable-forward outcomes in S3 achieve relatively higher levels of energy autonomy while remaining broadly compatible with existing network infrastructure. However, these configurations systematically fail to achieve private investment viability under current cost assumptions, with returns frequently falling below conventional benchmarks. Compared to S1, this cluster is more prominent in relative terms but weaker in absolute performance, indicating that intensified urban form amplifies the economic penalties associated with energy-maximizing strategies and increases reliance on policy or financial support mechanisms.

Market-ready outcomes in S3 prioritize financial viability and network compatibility, but deliver only limited improvements in energy autonomy. While this cluster constitutes the largest share of stakeholder-aligned scenarios in S3, its dominance reflects a contraction of the feasible design space toward conservative configurations rather than strong market performance. Relative to S1, these scenarios achieve lower absolute returns and self-sufficiency levels, underscoring how higher baseline demand intensity and reduced renewable yield per functional floor area constrain the scope for economically attractive energy upgrades.

Notably, the cluster corresponding to simultaneously high energy autonomy (high SSR), strong private investment viability (high IRR), and tolerance for substantial infrastructure upgrades (Cluster C4) does not emerge in either S1 or S3. **The absence of this outcome type across both urban forms indicates that configurations achieving strong energy and economic performance are not those that push the power system to its limits. Rather, scenarios that perform well on both dimensions tend to do so by effectively managing demand, generation profiles, and storage coordination in a way that inherently mitigates network stress.** This suggests that high-performing energy and investment outcomes are more closely associated with system coherence and operational alignment than with aggressive reliance on infrastructure reinforcement.

5.4.4.2.a Cluster S3C1 – Balanced outcomes

Cluster S3C1 represents the subset of scenarios in S3 that satisfy all three stakeholder-aligned criteria under the same badge-based classification applied to S1, namely moderate or higher energy autonomy, acceptable private investment performance relative to the S3-specific IRR distribution, and no more than minor infrastructure reinforcement. Applying an identical clustering framework enables a direct comparison of outcome quality between the two urban forms and reveals how structural constraints in S3 reshape what constitutes a “balanced” configuration.

Table 5.27. Summary table of cluster S3C1

	Min	Max	Median	Mean
• *Design Variables*				
North BIPV	0%	20%	20%	12%
E/W BIPV	50.00%	80.00%	80.00%	68.00%
Battery Capacity (MWh)	38.94	56.10	43.90	44.35
EV uptake	20.00%	20.00%	20.00%	20.00%
• *Key Indicators*				
Infrastructure upgrade cost - AUD	0.00	8572.10	8572.10	5143.26
SSR	11.44%	15.92%	12.65%	12.94%
IRR	3.30%	3.98%	3.60%	3.58%

In absolute terms, however, the performance envelope of S3C1 is markedly weaker than its S1 counterpart. As summarised in Table 5.27, S3C1 scenarios exhibit median SSR values of 12.65% (mean 12.94%), compared with 17.67% in S1C1, indicating a systematic reduction in achievable energy autonomy even among the most favourable S3 configurations. This reduction is consistent with the higher demand intensity and lower renewable yield per unit functional floor area identified earlier for S3.

A similar downward shift is observed in economic performance. While S1C1 scenarios achieve median IRR values of 4.19% (mean 4.23%), comfortably exceeding the assumed WACC of 3.66%, S3C1 exhibits a median IRR of 3.60% and a mean of 3.58%, with individual scenarios ranging from 3.30% to 3.98%. Notably, several S3C1 scenarios fall below the WACC threshold, implying that they would not achieve a positive NPV despite being classified as "balanced" under relative tier-based criteria. This highlights a critical distinction between relative feasibility within a constrained design space and absolute investment viability.

From a design perspective, S3C1 configurations rely on a narrower and more conservative parameter envelope than S1C1. Battery capacities are substantially lower, with a median of 43.9 MWh compared to 79.2 MWh in S1C1. EV uptake is uniformly limited to 20%, indicating that even moderate increases in electrified transport demand would push these scenarios beyond acceptable network or economic limits. East–west BIPV coverage remains high (median 80%), while north-facing BIPV is either absent or limited, reinforcing earlier findings that façade orientation becomes increasingly critical under intensified urban form.

Infrastructure upgrade costs in S3C1 remain low in absolute terms, with a median cost of AUD 8,572 and several scenarios requiring no upgrades at all. Taken together, Cluster S3C1 demonstrates that while "balanced" outcomes are still technically achievable in S3, they represent a compromised equilibrium characterised by lower energy autonomy, weaker economic margins, and reduced tolerance to demand growth or system expansion. The presence of IRR values below WACC within this cluster further confirms that balance in S3 is often achieved at the expense of absolute financial viability. This contrasts sharply with S1, where balanced clusters align more closely with both investor benchmarks and policy objectives.

Accordingly, S3C1 should not be interpreted as an equally desirable analogue to S1C1, but rather as evidence that vertically intensified urban form compresses the feasible solution space and lowers the ceiling of what can be simultaneously achieved. In this sense, S3C1 serves less as a model for optimal deployment and more as a diagnostic benchmark, illustrating the limits of design optimisation under structurally constrained urban conditions.

5.4.4.2.b Cluster S3C2 – Renewable growth and grid compatibility scenarios

Cluster S3C2 represents the renewable-forward, policy-supported regime within the S3 urban form. Analogous to Cluster S1C2, these scenarios prioritize higher levels of energy autonomy through expanded renewable generation and storage deployment, but fail to achieve private investment viability under prevailing market conditions without targeted public intervention. However, in contrast to S1C2, the performance envelope of S3C2 is systematically compressed across energy, economic, and infrastructure dimensions, reinforcing the structurally weaker feasibility landscape associated with the vertically intensified urban form.

As summarized in Table 5.28, Cluster S3C2 exhibits greater dispersion in façade deployment strategies than its S1 counterpart. North-facing BIPV spans a wide range from 0% to 80% (median 50%), while east–west BIPV similarly ranges from 0% to 80% (median 50%). This broader spread reflects an attempt to compensate for higher demand intensity in S3 through more aggressive façade utilization. Nevertheless, the resulting energy gains are more muted than in S1C2, indicating diminishing returns from façade expansion under constrained functional floor area ratios.

Battery capacities in S3C2 range from approximately 39 to 83 MWh, with a median of 57 MWh. While substantial, these capacities remain notably lower than those observed in S1C2 (median 89 MWh), reflecting the reduced spatial scale. EV uptake remains fixed at 20% across all scenarios in this cluster, highlighting that further electrification is largely incompatible with renewable-forward outcomes in S3 without triggering disproportionate infrastructure stress.

Table 5.28. Summary table of cluster S3C2

	Min	Max	Median	Mean
• *Design Variables*				
North BIPV	0%	80%	50%	47%
E/W BIPV	0.00%	80.00%	50.00%	40.00%
Battery Capacity (MWh)	38.94	83.18	57.44	63.32
EV uptake	20.00%	20.00%	20.00%	20.00%
• *Key Indicators*				
Infrastructure upgrade cost - AUD	0.00	70329.00	17144.00	29707.59
SSR	11.73%	22.62%	16.94%	16.92%
IRR	1.14%	3.15%	2.29%	2.26%

From an energy performance perspective, S3C2 delivers moderate improvements relative to balanced S3 outcomes but falls short of the renewable autonomy achieved in S1C2. Self-sufficiency rates range from 11.7% to 22.6%, with a median of 16.9%, compared to a median of 19.6% in S1C2. This downward shift confirms that, even under similarly aggressive renewable deployment strategies, S3's intensified built form dilutes renewable effectiveness when assessed against higher underlying demand.

Economic performance is substantially weaker. IRR values in S3C2 range from 1.14% to 3.15%, with a median of 2.29%, compared to a median of 3.16% in S1C2. Importantly, all S3C2 scenarios remain below the WACC of 3.66% used in the NPV calculation, indicating that none achieve positive NPV under base assumptions. This contrasts with S1C2, where a subset of scenarios approach investment viability and sit closer to conventional return thresholds. The S3C2 cluster therefore represents a structurally loss-making regime under market conditions, rather than a marginally investable one.

Infrastructure upgrade costs in S3C2 remain moderate but non-trivial, ranging from zero to approximately AUD 70,000, with a median of AUD 17,100. While broadly comparable to S1C2 in absolute terms, these costs are incurred in conjunction with weaker energy and economic outcomes, implying a poorer return on network engagement. In this sense, infrastructure stress in S3 yields lower system value per dollar of upgrade relative to S1.

Policy support implications

Table 5.29 quantifies the scale of intervention required to render S3C2 scenarios economically viable. The median total support required per scenario is approximately AUD 22.9 million, almost double that of S1C2 (AUD 12.1 million), with an interquartile range spanning AUD 14.3–35.6 million. When normalised by energy outcome, the median support required per additional 1% SSR increases to AUD 2.20 million, more than twice the corresponding value in S1C2. This indicates that marginal gains in energy autonomy are substantially more expensive to unlock in S3.

Table 5.29. Estimated policy support intensity required for Cluster S3C2 scenarios

	Median	Low - P25	High - P75	Units
Total Support Required	$22,891,000	$14,310,000	$35,558,000	AUD
Support per 1% SSR achieved	$2,204,200	$1,791,000	$2,941,900	AUD per +1% SSR
Support per kW PV/BIPV	$533.17	$391.57	$684.26	AUD per kW PV/BIPV
Support per kWh Battery Capacity	$374,020	$269,240	$477,370	AUD per battery unit
Support per 1% EV uptake	$1,144,500	$715,500.00	$1,777,900	AUD per 1% EV uptake

Generation-focused support remains the most efficient intervention lever, but at significantly higher cost levels than in S1. The median support required per kW of PV/BIPV rises to AUD 533, compared to AUD 198 in S1C2, reflecting reduced generation effectiveness under intensified urban geometry. Battery-focused support is particularly inefficient, requiring a median of AUD 374,000 per kWh of capacity, nearly three times the requirement observed in S1C2. Similarly, EV-linked support remains prohibitively expensive, with a median requirement exceeding AUD 1.14 million per additional 1% EV uptake, reinforcing the role of electrification as a dominant stressor rather than a value driver in S3.

Taken together, these results indicate that while renewable-forward outcomes are technically achievable in S3, they are significantly more policy-dependent and economically fragile than in S1. The same design logic that produces transitional, policy-unlockable regimes in S1 yields a much narrower and costlier feasibility envelope in S3. Public intervention can still enable progress toward higher energy autonomy, but at substantially higher fiscal cost and with weaker absolute performance outcomes.

Overall, Cluster S3C2 illustrates how intensified urban form transforms renewable-forward strategies from marginally investable transition pathways into structurally subsidy-dependent configurations. This reinforces the central conclusion that urban form fundamentally conditions the effectiveness, cost, and scalability of renewable energy transitions, even when identical technologies and optimization frameworks are applied.

5.4.4.2.c Cluster S3C3 – Market ready outcomes

Cluster S3C3 represents market-ready and network-compatible configurations within the intensified urban form, prioritizing private investment viability while maintaining low infrastructure impact. These scenarios mirror the conservative deployment logic observed in S1C3, emphasizing restrained renewable

penetration, modest storage capacity, and controlled electrification to preserve economic performance under prevailing market conditions. As such, S3C3 constitutes the upper bound of what can be achieved through market-driven design alone in S3, without recourse to policy support or major network upgrade.

Table 5.30. Summary table of cluster S3C3

	Min	Max	Median	Mean
• *Design Variables*				
North BIPV	0%	20%	0%	5%
E/W BIPV	0.00%	80.00%	20.00%	26.96%
Battery Capacity (MWh)	6.39	38.94	23.56	21.84
EV uptake	0.00%	50.00%	20.00%	28.26%
• *Key Indicators*				
Infrastructure upgrade cost - AUD	0.00	76335.00	2315.10	23564.29
SSR	1.84%	10.93%	6.81%	6.32%
IRR	3.42%	13.29%	4.48%	5.90%

As summarized in Table 5.30, S3C3 exhibits a consistently conservative deployment profile. North-facing BIPV penetration remains minimal, with a median of 0% and a mean of only 5%, while east–west BIPV coverage spans a wide range (0–80%) but concentrates around a median of 20%. This pattern closely mirrors that of S1C3 (Table 5.25), indicating that market-ready outcomes in both urban forms rely on selective and opportunistic façade deployment rather than systematic capacity maximization.

Battery capacity in S3C3 is notably lower than in its S1 counterpart. Capacities range from 6.4 to 38.9 MWh, with a median of 23.6 MWh, approximately half that observed in S1C3. This reflects tighter economic constraints in the intensified urban form, where the marginal value of storage is reduced by higher baseline demand and less favorable load–generation matching. EV uptake spans 0–50%, with a median of 20%, consistent with a cautious electrification strategy that avoids exacerbating peak demand or triggering infrastructure upgrades.

From a private investment perspective, S3C3 remains viable. IRR values range from 3.42% to 13.29%, with a median of 4.48% and a mean of 5.90%, exceeding the WACC threshold used in the NPV assessment. These values confirm that conservative system designs can still attract private investment under S3 conditions, provided that deployment scales are tightly controlled. However, relative to S1C3, both median and mean IRR values are lower, indicating reduced financial headroom. This suggests that market-ready outcomes in S3 are more sensitive to cost assumptions, tariff structures, and revenue uncertainty, and may be more vulnerable to adverse changes in market conditions. While viable, these configurations offer less resilience than their S1 equivalents.

Taken together, Cluster S3C3 demonstrates that market-ready and network-compatible outcomes remain achievable in intensified urban form, but only within a narrow and conservative design envelope. While the structural characteristics of S3C3 closely resemble those of S1C3, the resulting energy benefits are systematically weaker and financial margins narrower. This cluster therefore represents the ceiling of market-led performance in S3: beyond this point, further gains in energy autonomy cannot be achieved without either compromising private investment viability or invoking explicit policy support. In contrast to S1, where market-ready configurations still deliver meaningful energy contributions, S3C3 highlights the limitations of relying on private incentives alone in high-density urban contexts. In this sense, S3C3 reinforces the broader finding that intensified urban form compresses the feasible solution space,

increasing sensitivity to design choices and constraining the effectiveness of conservative, market-driven deployment strategies.

5.5 Chapter summary and key takeaways

This chapter presented an integrated assessment of urban renewable energy systems, spanning resource availability, system design, operational behavior, and system-level feasibility. The analysis progressed from high-resolution solar potential mapping and shading simulation, through detailed modelling of distributed renewable generation, battery energy storage, electric vehicle uptake, and fuzzy-logic-based energy management strategies, to power network and building energy simulations informed by BIM-based modelling and power network modelling. Together, these components established a physically grounded and operationally consistent modelling framework for evaluating urban energy performance under spatial, technical, and behavioral constraints.

Building on this foundation, the chapter culminated in a techno-economic and stakeholder-oriented feasibility analysis that synthesized energy outcomes, private investment performance, and infrastructure impacts across a wide scenario space. Rather than seeking a single optimal configuration, this final stage revealed how feasibility emerges from the interaction between design choices, network thresholds, and urban morphology, and how trade-offs between stakeholders are structurally embedded in dense urban energy systems. By contrasting a lower-rising reference urban form (S1) with a vertically intensified alternative (S3), the analysis further demonstrated how urban form fundamentally reshapes the achievable balance between energy autonomy, economic viability, and infrastructure compatibility.

The key takeaways presented below distill the central insights from across the chapter, integrating physical modelling results, system behavior, and feasibility outcomes into a coherent set of structural observations, design principles, and policy-relevant implications for urban renewable energy planning.

Key takeaways

1. Overall Structural Insights:

- **Urban renewable systems are governed by an inherent trade-off structure rather than a single optimum.** It is unrealistic to simultaneously maximise energy autonomy, private investor returns, and infrastructure feasibility at scale. This "impossible triangle" arises from network constraints and the uneven distribution of capital costs and benefits across stakeholders.
- **Infrastructure impacts are threshold-driven, not gradual.** EV uptake and north-facing BIPV deployment introduce sharp feasibility transitions, beyond which infrastructure upgrades become unavoidable and escalate rapidly in cost. This threshold is consistent across S1 and S3.
- **Balanced outcomes are rare but achievable.** Only a small subset of scenarios aligns energy performance, private investment viability, and network compatibility, highlighting the importance of targeted design choices rather than broad or uniform deployment strategies.
- **Notably, configurations achieving strong energy and economic performance are usually not those that push the power system to its limits.** Rather, scenarios that perform well on both energy and economic dimensions tend to do so by effectively managing demand, generation profiles, and storage coordination in a way that inherently mitigates network stress.

2. Urban form observations between S1 and S3

- **S3 achieves higher renewable generation intensity when normalised by total project land area**, primarily due to reduced inter-building shading across seasons and improved façade irradiance associated with its taller and more vertically articulated built form.
- **This generation advantage is substantially offset by significantly higher energy demand intensity**, with S3 exhibiting approximately **90% higher energy consumption per unit land area** and **8–13% higher energy consumption per unit functional floor area (FFA)** compared to S1.
- **The elevated energy consumption per unit land area in S3 is a direct consequence of its vertically intensified urban form**, whereby a greater amount of conditioned floor space and activity is concentrated within a smaller land footprint.
- **The higher energy consumption per unit FFA indicates additional operational impacts beyond density alone**, consistent with the consumption modelling results presented in **Section 5.2.2**, which show that S3 experiences **up to 15% higher heating and cooling loads** relative to S1.
- **S3 simultaneously exhibits higher renewable generation per unit land area and lower generation per unit functional floor area**, reflecting its vertically intensified configuration. With an FFA-to-land ratio of approximately **170%**, compared to **~100% in S1**, functional floor area in S3 increases significantly faster with building height than renewable collection surfaces. As a result, renewable yield scales favourably with land use but is diluted when assessed per unit of functional space.
- **Statistical analysis presented in this section further confirms that the intensified concentration of functional floor area in S3 leads to systematically weaker energy performance**, with S3 exhibiting lower overall outcomes across all three indicators (SSR, GLR, and RUR) across the evaluated scenarios.
- Lower self-sufficiency rates (SSR) indicate reduced local energy autonomy in S3 compared to S1, while lower generation-to-load ratios (GLR) reflect a higher demand burden relative to on-site generation capacity. Together with lower renewable utilization rates (RUR), these results indicate that S3 faces structural constraints in both meeting and effectively absorbing its locally generated renewable energy.

3. Energy system design considerations

- **Feasible urban renewable deployment lies within a bounded envelope instead of a single optimal point.** Across the explored design space, balanced and policy-relevant outcomes are typically achieved with:
    - north-facing BIPV and rooftop PV limited to approximately 20%
    - east–west BIPV extending up to 50–80%
    - total battery capacity (household or utility BESS) generally below ~80–90 MWh at the precinct scale,
    - and EV uptake below ~50% of dwellings under current network assumptions.

- **Utility-scale BESS substantially improves economic feasibility but can potentially introduce further capital cost and alter the system physics.** It consistently delivers higher IRR and NPV outcomes due to lower capital cost per kWh. This confirms that the primary advantage of utility BESS in dense urban contexts is economic efficiency rather than additional energy.
- **Utility BESS introduces a quantifiable tolerance for additional capital costs that scales with storage size.** Analysis of NPV differentials shows that the acceptable additional capital cost for utility-scale BESS increases approximately linearly with total battery capacity. For mid-range deployments of **100–140 MWh**, utility BESS can absorb **AUD 75–85 million** in additional capital costs (e.g. land acquisition or site-specific works) while remaining more competitive than household batteries. At very high storage capacities of **180–220 MWh**, this tolerance exceeds **AUD 120 million**.
- **Utility BESS expands the economic envelope but not the infrastructure envelope.** While utility BESS shifts many scenarios from financially unviable to investable, it does not remove the underlying infrastructure thresholds associated with high EV uptake or excessive north-facing BIPV deployment. In other words, utility BESS can make more scenarios economically viable within the existing feasible design envelope, but it may not fundamentally relax network-driven limits on renewable and electrification intensity especially at the higher end of renewable penetration/electrification.
- **EV uptake and north-facing BIPV define the hardest envelope boundaries.** Beyond roughly 50% EV penetration or 50% north-facing façade coverage, infrastructure upgrades become both inevitable and economically significant.
- **Battery storage moderates variability but does not remove envelope limits.** Moderate deployment can alleviate network stress in some configurations, but large-scale battery penetration (typically above ~100–120 MWh) consistently shifts scenarios outside the feasible envelope due to charging synchronisation effects and reverse power flow constraints.
- **East–west BIPV expands the envelope with comparatively low network risk.** High E/W façade coverage increases self-sufficiency without systematically worsening upgrade probability or cost, making it the most infrastructure-resilient pathway for increasing renewable penetration in dense urban contexts.

4. Policy and planning implications

- **Policy interventions reshape the feasible envelope.** Targeted support for renewable-forward but investor-unviable configurations can shift outcomes toward higher energy autonomy without triggering disproportionate infrastructure burdens.
- **Support for PV and BIPV deployment, particularly façade-integrated systems offers the highest return on public expenditure.** Compared with subsidies for batteries or accelerated EV uptake, PV/BIPV support delivers greater system-level energy benefits per unit of funding while imposing lower network stress.

- **Urban renewable planning must be stakeholder-aware by design.** Treating economic, energy, and infrastructure metrics as separable or sequential leads to misleading conclusions; feasibility emerges only when these dimensions are assessed jointly.

6. Conclusion and Recommendations

Sustainable precinct design requires a holistic approach that simultaneously addresses urban heat, water management, embodied carbon, and energy efficiency. As urban areas become denser and climate-related challenges intensify, integrating passive design strategies, renewable energy, and low-carbon materials is critical to achieving both environmental and social resilience.

Urban heat mitigation plays a central role in enhancing thermal comfort and reducing energy demand. Strategic tree placement, vegetation integration, and irrigated green spaces can lower local air temperatures by up to 10.9 °C, improve evaporative cooling, and reduce peak cooling loads. The orientation of streets and buildings, along with adequate setbacks and preserved ventilation corridors, further enhances airflow, optimizes shading, and prevents the formation of hot pockets, highlighting the importance of building morphology alongside material choice.

Water management is equally integral to sustainable precinct design. Active and passive irrigation of street trees and open spaces is essential to maintain vegetation health and cooling potential, particularly in areas facing increasing drought risks due to climate change. Supplementary water sources, rather than relying solely on rainfall, is required to sustain irrigated landscapes that contribute to both thermal comfort and stormwater management.

Embodied carbon in construction materials remains an important contributor to precinct-level emissions. Concrete and steel account for the largest portions of the carbon footprint, making material selection crucial. Incorporating low-carbon alternatives, including lightweight and mass timber construction, and reconsidering the need for basements and carparking, can reduce emissions by over 50%. Taller building height limits potentially reduce the scope of application of light-weight construction methods, increasing embodied carbon. Achieving net-zero targets necessitates integrated, cross-disciplinary assessment methods that evaluate both the operational and embodied carbon impacts across the precinct.

Energy efficiency and renewable integration are closely tied to urban morphology, shading, and building design. Rooftop photovoltaic systems, complemented by façade-integrated PV, provide strong seasonal performance; rooftop PV peaks in summer while façade PV optimizes generation in winter and shoulder seasons. Medium-to-high battery capacity and smart electric vehicle charging schedules are essential to smooth demand, improve consumption efficiency, and maintain system stability. Greening strategies further reduce cooling loads, particularly on lower floors, demonstrating a synergistic effect between vegetation, microclimate improvement, and energy performance.

In conclusion, sustainable precinct design is most effective when it leverages the interplay between urban heat mitigation, water management, embodied carbon reduction, and energy strategies. A coordinated approach that integrates passive design, renewable energy, low-carbon materials, and landscape planning can significantly enhance thermal comfort, resource efficiency, and carbon performance. Such holistic planning is vital for creating resilient, climate-adaptive urban environments that meet operational and environmental goals while supporting Australia's broader net-zero and sustainability commitments. The findings of the study deliver following recommendations:

6.1 Urban heat

- **Create a network of irrigated open spaces spread throughout the precinct that are placed strategically to take advantage of prevailing winds.**
  Open space which has airflow to the south will be able to spread more cool air (specifically in the weather conditions at Sunshine Precinct). It is also important to maintain some gaps in the vegetation in open spaces to enable airflow, provide irrigation to maintain soil moisture, and target daytime actions such as active watering in high temperatures, to provide cooling.
- **Plan for sufficient airflow in the precinct in summer, and moderation of wind speeds in winter.**
  Building height, spacing and podium continuity should be considered as part of heat mitigation. In the Sunshine Precinct context:
  - control wind through use of vegetation on NW/NE streets to prevent wind channelling.
  - avoid long, continuous podium structures, to prevent wind channelling and improve airflow.
  - increase setbacks between towers and buildings, and limit building heights to allow more airflow in summer and prevent hot pockets.
  - avoid trees in the middle of streets where airflow is important.
  - provide for airflow southwards in dead-ends and cul-de-sacs.
- **Plan tree canopy as a spatial system that considers locations where shading and ventilation is required.**
  For the specific context of Sunshine Precinct, that means prioritising the southern sides of E-W streets for shading with overlapping canopy, planting dense irrigated vegetation on the south side and low-density vegetation on the north-side (which is shaded by buildings). For N-S corridors that means balancing shading and ventilation. Shading from buildings can be utilised in summer, allowing somewhat less dense vegetation to enhance airflow. Soil and water infrastructure is required to support vegetation, as outline in the Water section below.
- **Irrigate vegetation and maintain soil moisture to support cooling.** This will also support tree growth, as described in the Water section below.
- **Use climate-responsive material selection at the pedestrian scale.** In highly sun-exposed locations, prioritise high-thermal-mass and low-reflectivity finishes where reflected radiation is likely to affect pedestrians or nearby surfaces. High-reflectivity materials remain appropriate where solar radiation can be reflected primarily toward the sky. These strategies should be applied selectively and, where needed, balanced with measures that support effective nighttime heat release and cooling.
- **Identify, prioritise and treat targeted hotspots through coordinated landscaping, irrigation and built form interventions, rather than focusing on precinct-scale averages.** Micro-climate modelling, such as the Envi-met modelling used in the research, can be used to identify hotspots and test the impact of different interventions.

6.2 Water

- **Ensure soil volume, active and passive irrigation to support overlapping tree canopy growth, particularly in priority areas for shading.** Create 3m verges with structural soil or 5m verges with passive and active irrigation. Passive irrigation is critical to achieving overlapping canopy, while

supplementary active irrigation is important to enable trees to meet maturity more quickly and to protect against drought conditions.

- **Provide *efficient* passive irrigation systems for street trees.** Supply of additional water beyond rainfall is critical to achieving tree canopy in the precinct. There is a significant difference in outcome between efficient and inefficient systems, so investment in a well-designed, efficient system is important.
- **Provide an alternative water capture systems to provide water for active cooling of public open space**, aiming for 11-12ML per annum *above* the amount already allocated to maintain a mid-range sports level. Water capture from low rise commercial and industrial buildings, or other infrastructure, could be good alternatives – if other sources of water (e.g., residential building rooftops and road runoff) is already fully utilised.
- **Encourage capture of alternative water on private land** to support increased soil moisture in summer (for urban cooling purposes) and to support achievement of canopy targets on private land.
- **If a 30% canopy target is a priority, consider options to increase canopy cover across the precinct**, including increasing canopy cover on private land and allocation of additional public open space for greening.

6.3 Embodied carbon

- **Facilitate low-carbon building designs.** Results show that substituting typical construction materials with low carbon equivalents can reduce embodied carbon by 14%. This could be improved to a 46% if low carbon (lightweight and mass timber) approach was adopted.
  As embodied carbon becomes an increasing share of lifecycle emissions, encouraging material changes over the long term will be important to reducing built form emissions. This may entail some changes to built form, as research (Pomponi et al. 2021) suggests that low embodied carbon buildings are easier to achieve when they are shorter.
- **Reduce private car parking.** Carparking within buildings was found to contribute significantly to embodied carbon of the precinct designs assessed. By removing carparking (within the building) from the Base Scenario embodied carbon was reduced by 15%. Moving carparking from basements to the upper floors of buildings had lesser impact, reducing embodied carbon by 4%. Public transport systems will be expected to reduce the embodied carbon of buildings by removing the need for personal carparking space or by shifting such space to lower embodied carbon alternatives (such as remote carparking).
- **Use the Digital Twin to maximise the embodied carbon value of precinct designs while at the same time aiming for a net-zero carbon outcome.** Embodied carbon can be viewed as a cost to development that needs to be managed like any other cost. It was clear from the precinct designs assessed in the study that significant improvements in embodied carbon 'value' were achievable through various initiatives outlined above. It was also clear that none of the precinct designs achieved a 'net zero' carbon outcome over the life cycle, even when the carbon sequestration potential of mass-timber was included. The ability of mass-timber and other biogenic materials to store carbon presents a theoretical opportunity for a precinct to achieve a net-zero carbon outcome if this goal is prioritised.

6.4 Energy

For Distribution Network Service Providers (DNSPs)

- Implement spatially differentiated connection standards and incentives to encourage DER deployment on underutilised feeders.
- Require explicit evening discharge targets and standardised inverter volt–var and volt–watt settings for batteries and PV.
- Prioritise shared or utility-scale BESS where it delivers peak substitution, voltage control, and ramp-rate reduction.
- Use constraint classification frameworks to distinguish between scenarios requiring infrastructure augmentation and those addressable through operational or spatial measures.
- Coordinate EV smart charging programs to target load-factor improvement, not just peak avoidance.

For Planning Authorities

- Develop a strategic direction for energy management at the precinct scale that outlines the extent to which renewable energy and EV deployment is a priority, and how this can be addressed.
- Incentivise east–west façade-integrated PV through planning controls, design guidelines, or floor-space bonuses.
- Require shading, orientation, and energy performance analysis at early design stages for high-density developments to maximise passive heating and cooling and onsite renewable energy usage at a precinct neighbourhood scale.
- Support shared-service PV and battery business models (e.g. precinct energy services, community batteries).
- Understand potential EV loads based on proposed charging infrastructure and carparking capacity in new developments, and engage with DNSPs about the implications
- Encourage smart charging infrastructure.
- Incorporate consideration of urban form in any localised renewable energy deployment strategy.

For Developers and Precinct Proponents

- Design buildings to maximise usable PV surfaces, particularly east–west façades in high-rise contexts.
- Treat rooftop and façade PV as integrated energy assets, not optional add-ons.
- Invest in smart EV charging infrastructure rather than reducing parking capacity – although noting that reduced carparking capacity has positive benefits for embodied carbon.
- Consider shared or utility-scale battery solutions to improve project economics and manage peak demand.
- Evaluate projects using integrated metrics (IRR/NPV, self-consumption, network impacts) from early feasibility stages.

7. Appendix 1 - Sunshine precinct climate analysis

7.1 Air temperature patterns

Air temperature is one of the main climatic factors influencing buildings and urban designs. It must be considered during the design process to provide satisfactory thermal comfort for users of indoor and outdoor spaces. Therefore, understanding the future patterns of air temperature in various seasons and the recommended design temperatures is essential to ensure the users' thermal comfort. Figure 7.1 provides a comprehensive insight into the various air temperature patterns during 2050. The predicted mean highest temperature in 2050 is 41.3 C° on February 25.

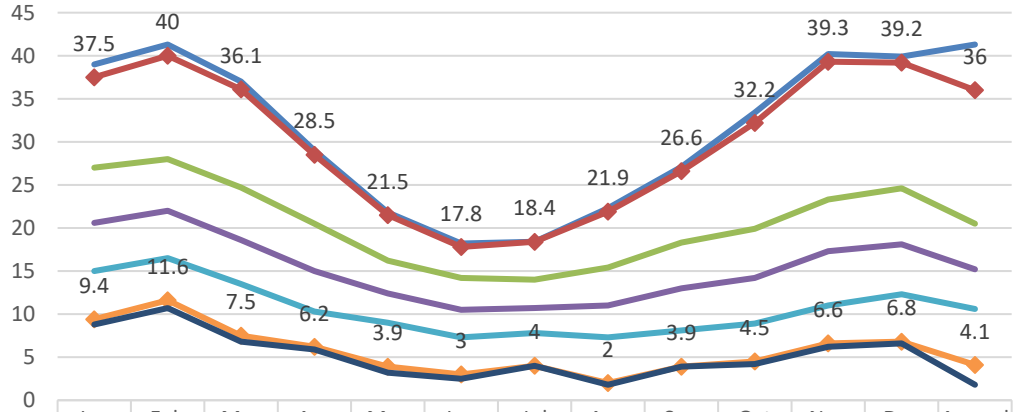

	Jan	Feb	Mar	Apr	May	Jun	Jul	Aug	Sep	Oct	Nov	Dec	Annual
Highest	39	41.3	37	29	21.8	18.2	18.4	22.3	27.1	33.4	40.2	39.9	41.3
Design high	37.5	40	36.1	28.5	21.5	17.8	18.4	21.9	26.6	32.2	39.3	39.2	36
Average high	27	28	24.7	20.5	16.2	14.2	14	15.4	18.3	19.9	23.3	24.6	20.5
Mean	20.6	22	18.6	15	12.4	10.5	10.7	11	13	14.2	17.3	18.1	15.2
Average low	15	16.5	13.5	10.3	9	7.3	7.8	7.3	8.1	8.9	11	12.3	10.6
Design low	9.4	11.6	7.5	6.2	3.9	3	4	2	3.9	4.5	6.6	6.8	4.1
Lowest	8.8	10.7	6.8	5.9	3.2	2.5	4	1.8	3.9	4.2	6.2	6.6	1.8

Figure 7.1. Air temperature patterns during 2050. The design high and low were based on a 0.5% threshold to avoid the extreme temperature conditions that occur for a short time within the month.

By comparing the predicted mean temperatures in 2050 with the mean historical data from 1855 to 2015, it can be seen that there is an increase in the mean temperature of January and a slight decrease in December of about 0.5 C°. February has a notable rise of 1.75°C. This suggests that summers in 2050 will likely be warmer, especially in February, which will experience the most significant rise. This will lead to more intense heat during late summer. In autumn, there is a slight decrease in the mean temperature from April to May, which suggests that late autumn and early winter are expected to be slightly colder in 2050; however, the changes are minor. In winter, there is a notable increase in July of about 0.95 C° with a slight increase in August, which suggests that winter in 2050 will likely be warmer, particularly in July. In Spring, there is a slight fluctuation in temperature, which indicates that Spring will generally be warmer, particularly in November, which sees a notable increase in temperature, while October will experience a

slight cooling trend. Generally, the seasons will be a bit warmer except for autumn, which will be slightly colder.

To ensure satisfactory thermal comfort for internal and external spaces and to provide a more sustainable design, a balance between evaluating the design response to typical and extreme conditions is essential. For instance, if the design evaluation considers only typically hot and cold days, that would provide an average understanding of the design's performance, but this performance might be insufficient during extreme conditions. Therefore, the evaluation should focus on the extreme conditions to provide the high capability for the design to respond to these conditions; in addition, the evaluation should extend to typical conditions to evaluate the sustainability of the design. Based on the climate analysis for 2050, it is recommended to design buildings and precisely HVAC systems sizing to respond to the design high threshold in February, 40 C°, and to the low design threshold in August, 2 C°. This is also recommended for urban designs. However, the evaluation of urban designs is more complicated than that of buildings as the interaction with the climate parameters is direct without an offset due to the various building materials. Therefore, it is recommended that the evaluation be focused on the hottest and coldest days, which are, in the case of Sunshine, February 25 and August 16, respectively. It can be argued that these extreme conditions are unlikely to host significant outdoor crowds. However, the evaluation in these extreme days could provide substantial information for outdoor and indoor spaces, providing comprehensive climate-responsive designs. In addition, the assessment for outdoor spaces should be extended to typical hot and cold days, where typical activities will remain without disturbance from the extreme conditions to evaluate the design's sustainability and responsiveness to the climate conditions. Based on the analysis, the recommended annual design high temperature is 36 C°, and it should be noted that only 41 hours during summer exceed this temperature, with only 27 hours above 37 C°. Two typical days could successfully present this design temperature: February 14 and 24. Thus, continuously evaluating the outdoor spaces for February 24—25 to better understand the typical hot and hottest days is recommended.

It should be noted that the average difference between day and night in Sunshine is significant and ranges between 12.3 C° and 6.2 C°; the highest average is during summer. This suggests that there is no accumulated heat during heatwaves. However, if the design requires an evaluation during a heatwave condition, it can be noticed from the analysis that the period between the sunrise of February 13 to the sunrise of February 16 is a good candidate for the evaluation. These days experience continuous hot days with temperatures almost above human thermal comfort during the night, Figure 7.2.

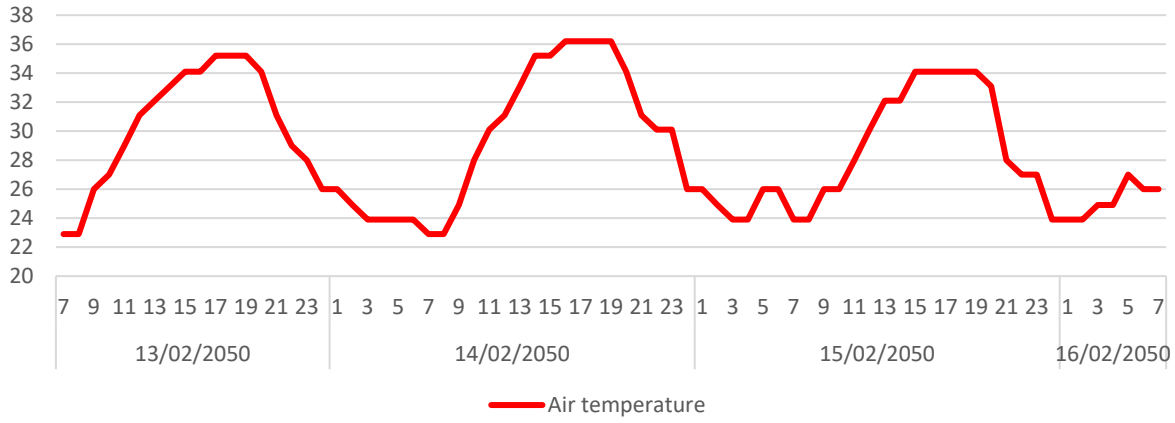

Figure 7.2. Air temperature on February 13-16

7.1.1 Summer wind characteristics

Based on the air temperature analysis, February was the hottest month in 2050, and therefore, it has been selected for this analysis, Figure 7.3.

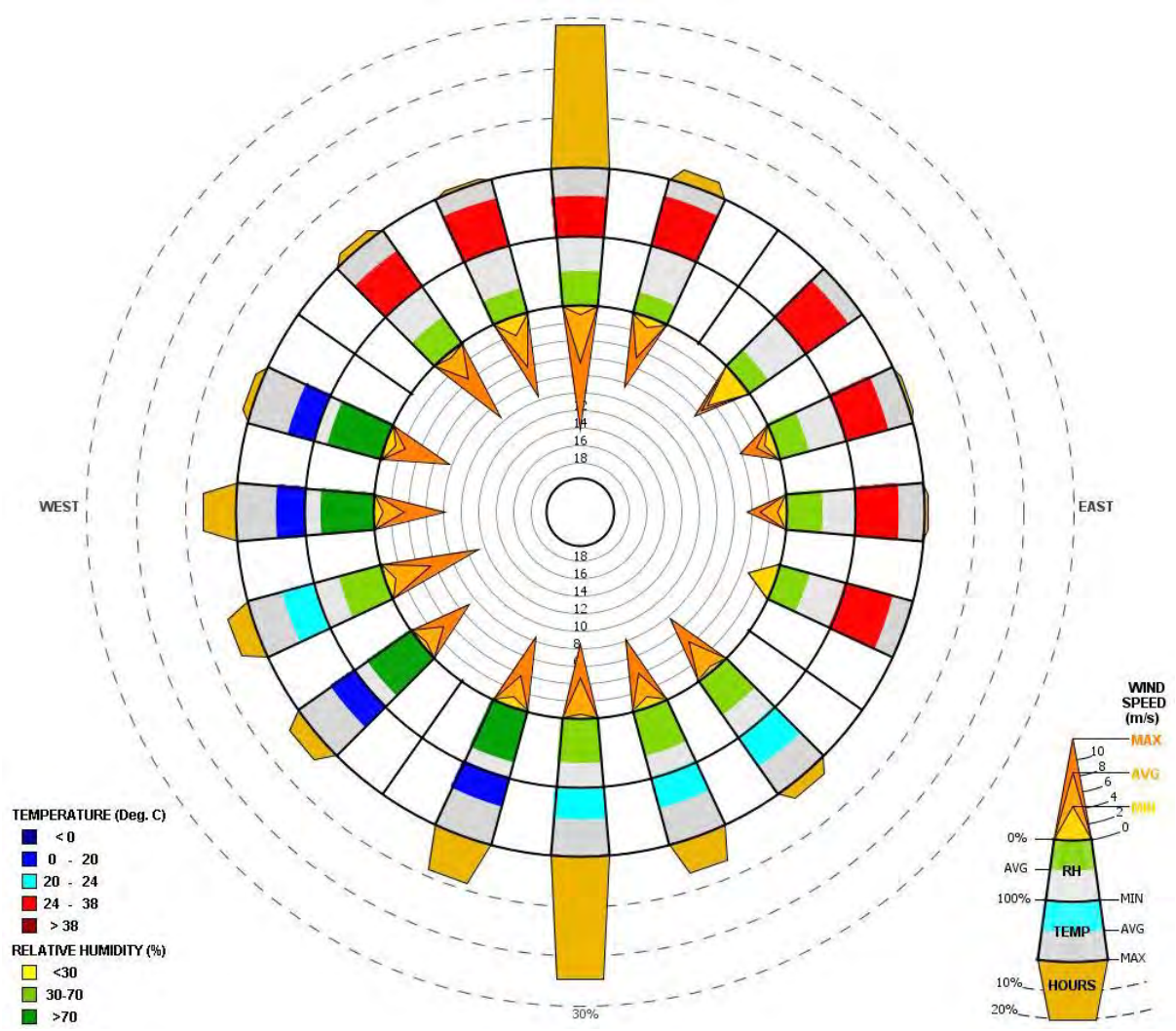

Figure 7.3. Windwheel for Sunshine City representing the wind characteristics in February as a summer representative month. Generated using Climate Consultant.

The prevailing wind direction in February is primarily from the north, making up 29 % of the total wind patterns. Winds from the south constitute 24%, while winds from the west to SS-W (except the south direction) are still considerable and account for 9% to 4%. Winds from the other directions have a minimal effect on the overall wind dynamics.

The highest wind speed is recorded from the north, reaching up to 14 m/s (50 km/h). The next highest wind speed is from WW-S, reaching up to 11m/s (40 km/s), followed by the wind from NN-W and N-W with almost about 10 m/s (36 km/h). The average wind speed is equal to or less than 5m/s except for north, NN-W, and WW-S.

The wind temperature and humidity show similar patterns; the hot wind above the comfort level of 24 C° is usually less humid than the wind temperature within the thermal comfort levels (20-24), which is also less humid than the cool breezes. In general, the wind from EE-S to N-W is relatively hot (above 24 C°), and it should be mitigated. The wind from S-E to south and WW-S have temperatures within the comfort level, while the wind from other directions has a temperature of less than 20 C°, which should be considered a cooling source for outdoor spaces.

7.2 Solar access analysis

As the axial of the Earth is tilted about 23.4°, the sunrise and set positions vary throughout the year by up to 23.4° north or south of due east or west. In Sunshine City, the sun reaches the summer solstice on around 21 December, when the South Pole is most fully orientated towards the Sun. In addition, the Sun reaches winter solstice around 21 June, when the North Pole is most fully orientated towards the Sun. Therefore, understanding the solar angle of these days will significantly enhance design sustainability and allow the integration of passive and active design strategies to control solar access by blocking unwanted solar exposure in summer and allowing solar access during winter.

In the summer solstice, the solar culmination occurs at 1:18 pm, when the sun's altitude is 75.65°, Figure 7.4. The sunrise is at 5:54 am, and the sunset is at 8:42 pm. The daylight lasts about 14 hours and 48 minutes. In the winter solstice, the solar culmination occurs at 12:23 pm, when the sun's altitude is 28.82°. The sunrise is at 7:36 am, and the sunset is at 5:09 pm. The daylight lasts about 9 hours and 34 minutes.

A)

B)

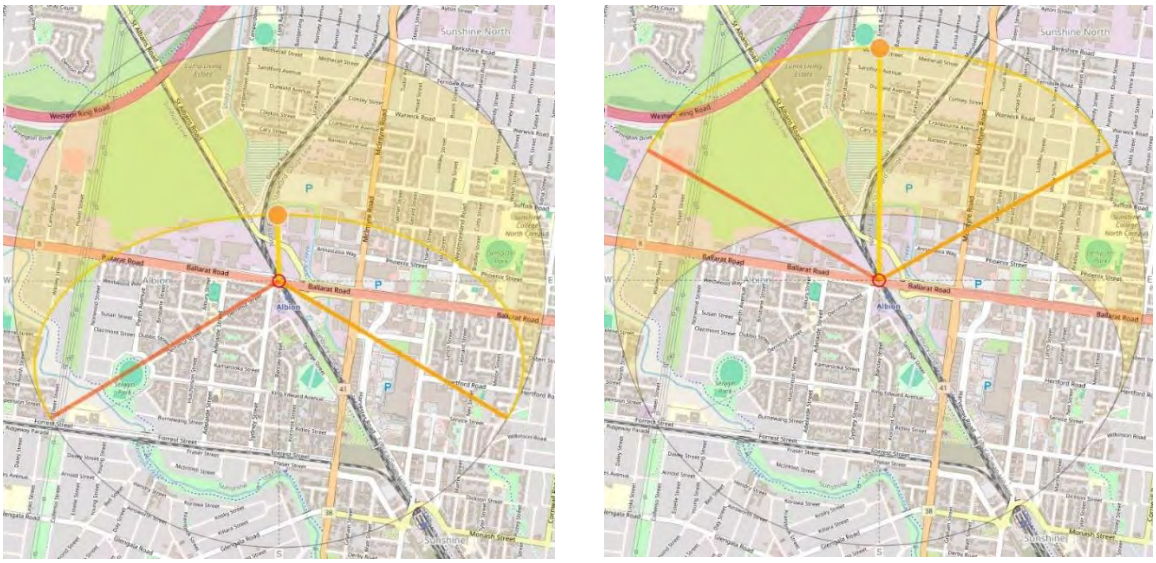

Figure 7.4. Solar access analysis in 2050. A) Summer solstice, 21 December; B) Winter solstice, 21 June. Generated by suncalc.org

The above information helps designers adjust their designs to respond to solar access. The choice of buildings and urban design elements should be evaluated based on allowing or blocking solar radiation to the designed spaces in winter and summer, respectively. My NASA Data (2024) thoroughly discussed the Earth's energy budget, the solar radiation and reflection under normal conditions, and the impact of greenhouse gases, which are the leading cause of climate change, Error! Reference source not found..

Figure 7.5. Earth's energy budget (My NASA Data, 2024)

The built environment alters the absorbed and reflected radiations, increasing the solar concentration in some locations more than others and altering the surface's energy budget, Figure 7.6. This causes the

phenomenon known as urban heat islands, which can also be intensified by other anthropogenic activities. Therefore, urban designs need to carefully consider the solar angles and the various elements and their materials in the solar path to reduce the increased solar reflectance (in general) and absorbance during summer, which has a negative impact on the thermal comfort of space users and increases the energy consumption of HVAC systems. For instance, trees are well known for their various environmental benefits, shading, and cooling effects. However, the wrong tree species in the wrong location may have a negative impact. In Figure 7.6, the tree provides shade for the lower floors of the building, which has a positive impact during summer. However, due to the distance between the tree and the building, the tree shape, and the reflected surfaces in the building facade and the footbath, the tree has some negative impacts that might outweigh the gained benefits, specifically with the absence of irrigation during summer. In addition, if this tree is an evergreen tree, not a deciduous tree, the negative impact will increase as it will block the passive heating during winter.

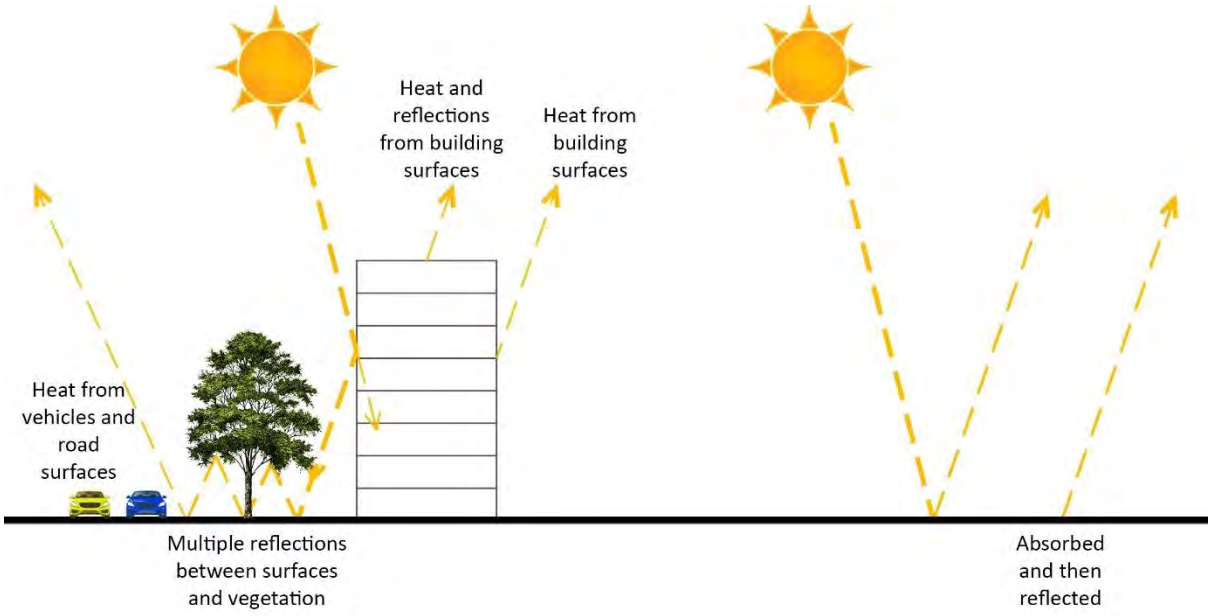

Figure 7.6. Solar reflection and absorbance. The left illustration represents a typical urban area, while the right represents a typical rural area. Created by Majed Abuseif

It can also be noticed from the same illustration that the reflected surfaces in the north elevation and on the ground level intensify the urban heat island effect due to the multiple reflections of radiation, which directly impact the pedestrians. Therefore, it is recommended that reflective surfaces in these areas be avoided to reduce this adverse effect. If the reflective surfaces are essential in the design for various reasons, then the design elements, composition, and angles must be well-evaluated to reduce the solar reflectance toward pedestrians.

Lastly, the shading effect from the vertical and horizontal elements needs to be evaluated to enhance solar access and control in the designed spaces. Vertical objects at 1 m cause 0.26 m shading during summer at culmination time, while in winter, they cause 1.82 m shading. The sun angle must also be considered when designing the horizontal and vertical shading devices at the north, east, and west building facades. Figure 7.7 demonstrates solar access during summer and winter and provides information about the precise design of the horizontal shading devices at the north facades by blocking the solar access to windows in summer and allowing it in winter.

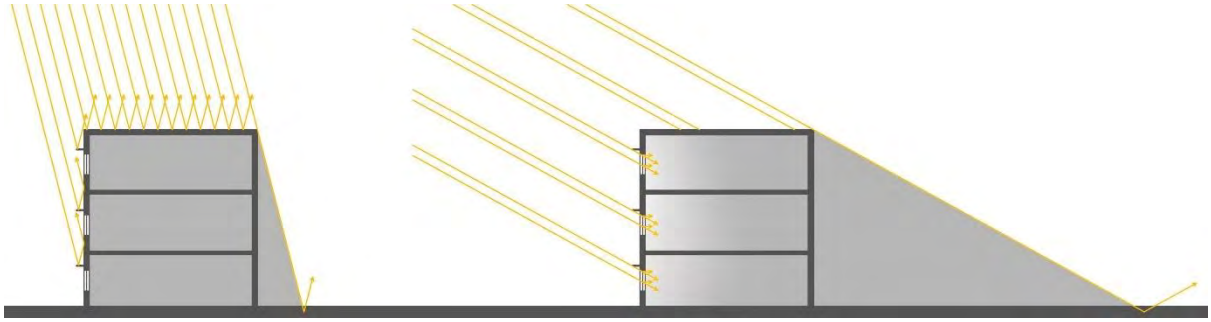

Figure 7.7. Solar access and shading in Sunshine. The left illustration represents summer, and the right one represents winter. Created by Majed Abuseif

7.3 Wind characteristics

The prevailing wind direction throughout 2050 is predominantly from the north, accounting for approximately 30% of the total wind patterns. Winds from the south contribute 15%, followed by winds from the west, which make up around 11%. Winds originating from the northwest and southwest appear intermittently, while those from other directions are negligible due to their minimal influence on the overall wind dynamics, Figure 7.8.

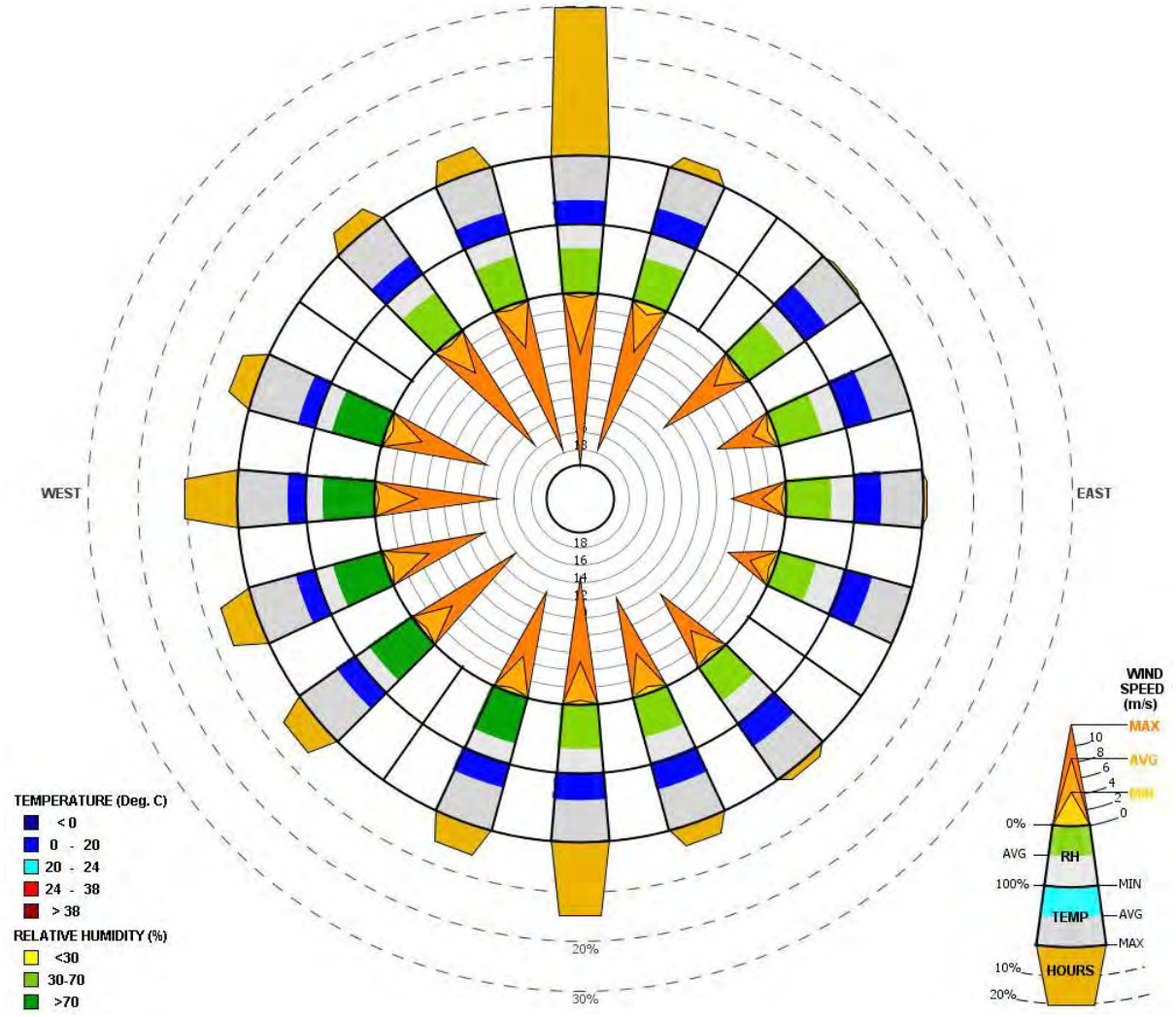

Figure 7.8. Windwheel for Sunshine City representing the average wind characteristics in 2050 (January to December). Generated using Climate Consultant.

The highest wind speeds are recorded from the north, reaching up to 20 m/s (72 km/h), indicating a significant wind force from this direction. Winds from the north-northeast (NN-E) and north-northwest (NN-W) also exhibit substantial wind speeds up to 18 m/s (65 km/h). Winds from the south, west, and southwest show a slightly lower, yet substantial, wind speed of 15 m/s (54 km/h). The average wind speeds were equal to or lower than 5 m/s (18 km/s) —which is considered within the comfort level for walking pedestrians— from all directions except north and NN-E.

In terms of humidity, winds from the northwest-west to the south-southwest (N-WW to SS-W) demonstrate relatively high humidity levels, ranging between 70% and 80%. In contrast, winds from other directions generally exhibit lower humidity, with levels below 65%. This variation in humidity levels may significantly affect the local thermal comfort and urban microclimates, as humid winds alter the heat perception. High humidity during hot days will increase heat perception and reduce the body's ability to cool down, while moderate humidity can enhance passive cooling.

7.3.1 Winter wind characteristics

Based on the air temperature analysis, June was the coldest month in 2050, and therefore, it has been selected for this analysis, Figure 7.9.

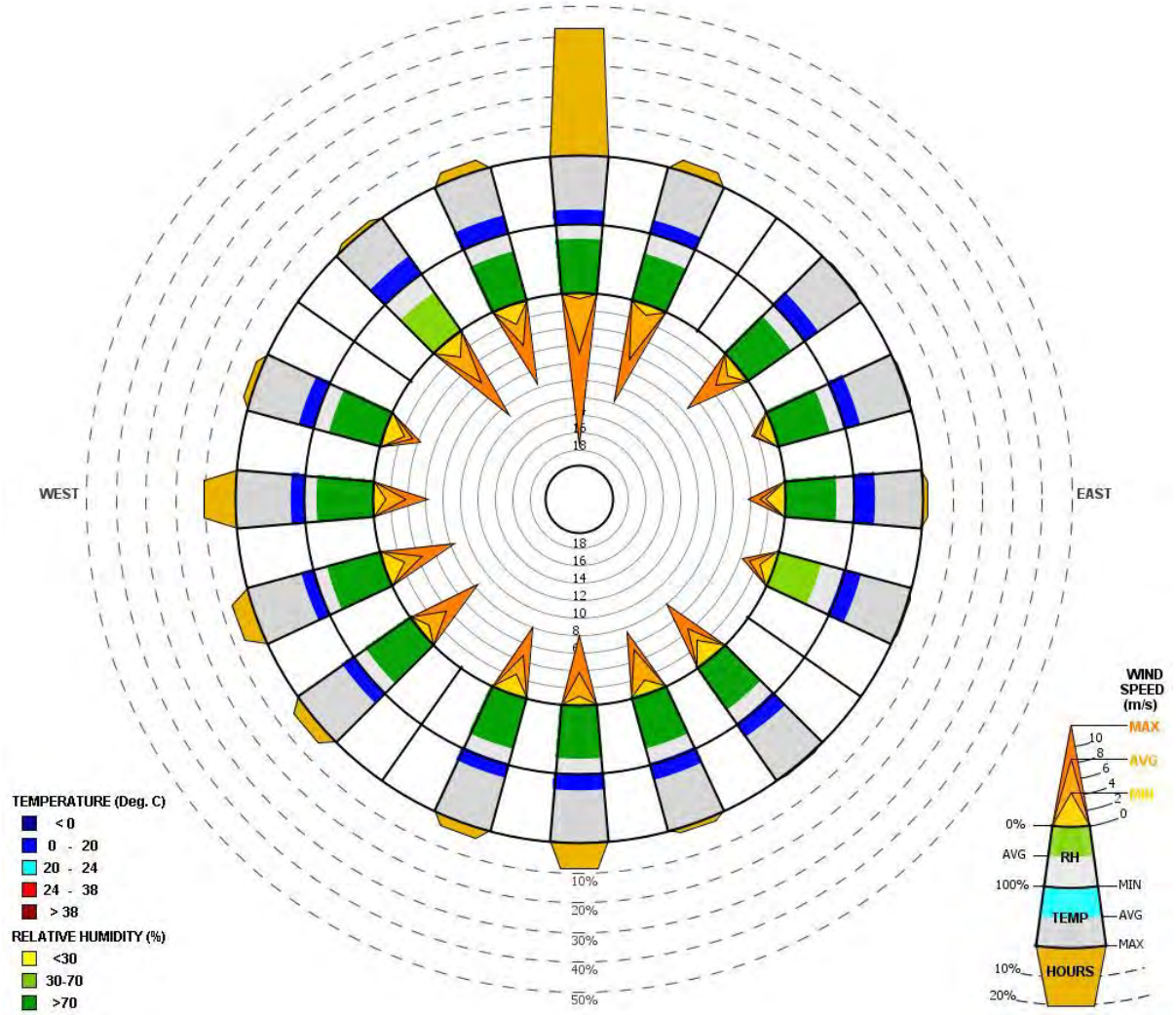

Figure 7.9. Windwheel for Sunshine City representing the wind characteristics in June as a summer representative month. Generated using Climate Consultant.

In June, the prevailing wind direction is predominantly from the north, accounting for around 42% of the total wind patterns. Winds from the south and west contribute approximately 10%, while winds from the other directions make up less than 6%, and notably from N-E to SS-E less than 1%.

The highest wind speeds during this month are recorded from the north, with speeds reaching up to 18 m/s (65 km/h), indicating strong winds, followed by winds from the NN-E and N-W approaching 12 m/s (43 km/h). Winds from the S-W to WW-S almost reach 8 m/s (29 km/h). The average speed remains equal to or less than 5 m/s except for NN-E, north, and NW.

Lastly, the average air temperature was less than 20 C°, with the highest temperature from the east of 19 C°. In addition, the average relative humidity was high and above 65% from all directions.

8. Appendix 2 - Data sources and modelling tools

To support a comprehensive analysis, this study integrated a wide range of data sources across multiple domains. Urban heat and energy simulations draw on spatial, climatic, and infrastructure datasets, enabling high-resolution modelling of thermal performance and energy demand across the precinct. Energy simulations further incorporate inputs such as building typologies, occupancy patterns, and power network data.

Water analysis used meteorological, building/ infrastructural, vegetation, trees, grass and spatial data, allowing for detailed assessment of water balance strategies under changing climate conditions. Embodied carbon calculations rely on building data, building codes and standards, construction specifications, and lifecycle assessment tools to estimate emissions associated with building materials and construction processes. The integration of these diverse datasets ensured a robust and holistic approach to assessing the environmental performance of the precinct through to 2050. Table 8.1 summarises the datasets used in this research.

Table 8.1. Datasets used by the subgroups

Dataset	Purpose	Subgroups
Sunshine Precinct 2.5D and 3D modelling	To deliver the building footprint of Sunshine precinct. To develop the new precinct DSM	All subgroups
CSIRO climate projections (2019) RCP4.5 scenario	To conduct the climate analysis for Sunshine Precinct. To identify the hottest day and select a typical hot day To aid the solar potential mapping and shading analysis To evaluate building energy performance under climate change conditions. To make assumptions related to annual rain fall and evapotranspiration when developing alternative scenarios	Urban heat, Energy, Water
Weather data from BOM (Station: 86282 Melbourne Airport)	Annual rainfall and evapotranspiration	Water
AEMO's 2024 Integrated System Plan	To make assumptions related to distributed generators, electric vehicles and building energy consumption simulation	Energy
National Construction Code 2022	To make assumptions related to urban-scale Rooftop PV Placement Modelling and building energy consumption simulation To make assumptions related to building materials	Energy
Powercor network data for Sunshine region	To conduct the power network analysis	Energy
NABERS and NatHERS rating systems	To make assumptions related to building energy consumption simulation	Energy

Environmental Product Declarations (EPDs)	The Australasian EPD Database was employed for most material related environmental data	Embodied carbon

The subgroups also engaged closely with key industry reference groups such as Development Victoria, Homes Victoria, Department of Energy, Environment and Climate Action (DEECA), Brimbank Council and consultants from DTP to support the design of realistic and contextually grounded scenarios. This collaborative approach ensured that assumptions reflected current policy directions, development intentions, and practical implementation considerations. This engagement with government and industry stakeholders played a critical role in shaping assumptions, validating scenario parameters, and aligning the study with broader strategic frameworks and real-world feasibility.

A range of modelling tools were employed in this study to investigate strategies for urban heat mitigation, water efficiency, embodied carbon reduction, and the transition to renewable energy systems. These tools enabled detailed analysis across various environmental and infrastructural dimensions. Table 8.2 provides a summary of the key modelling tools utilised in the study, along with their respective applications.

Table 8.2. Modelling tools

Modelling tools	Application	Subgroup
ENVI-met	Microclimate simulation	Urban heat
GIS (QGIS, ArcGIS)	Extract and process spatial data Create input files	Urban heat, Energy, Embodied carbon
MATLAB	Energy simulation	Energy
Rhino/Grasshopper	Building energy consumption simulation	Energy
DigiSilient PowerFactory	Power system analysis	Energy
MS Access	Microsoft Access (relational database) was employed for calculating material quantities and carbon impacts from a parametric model	Embodied carbon
Tableau Desktop	Employed for embodied carbon results visualisation.	Embodied carbon

9. Appendix 3 - Geospatial model preprocessing

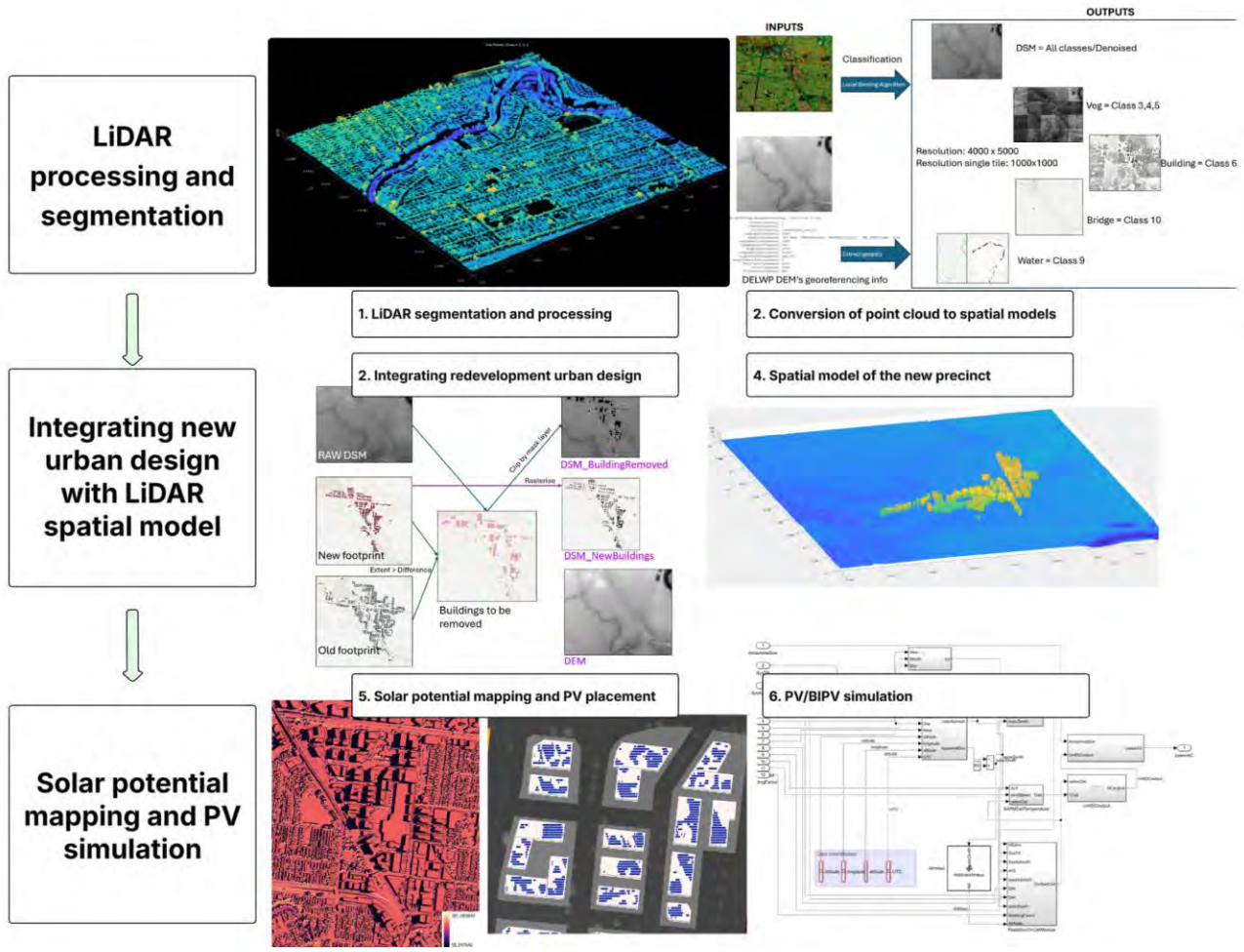

Figure 9.1. Workflow of baking doughnut model into DSM

The project targets a 2050 time horizon; consequently, no future LiDAR is available. The spatial representation of the precinct and its surroundings therefore rely on the Greater Melbourne 2017–18 LiDAR acquisition published by the Department of Environment, Land, Water and Planning (DELWP) in 2019. The dataset covers approximately 12,000 km², was flown between November 2017 and October 2018, and has an average point density of about 8 points per m². Processing includes ICSM Level-2 ground classification and class labels for vegetation (3–5), buildings (6), water (9), and bridges (10). Seamless 1 m DTM and 0.5 m contours are available. These characteristics provide a robust baseline for terrain and above-ground features prior to integrating the 2050 precinct plan.

The DELWP LiDAR derivatives are supplied as 1 km × 1 km tiles (e.g., tile code e306n5814 denotes a tile origin at Easting 306,000 m and Northing 5,814,000 m in MGA Zone 55). For this study, 20 tiles were selected to form a 4,000 m × 5,000 m analysis zone comprising the area of interest (AOI) plus buffer. The extent spans Easting 306,000–310,000 m and Northing 5,814,000–5,819,000 m. All processing is in GDA2020 / MGA Zone 55 (EPSG:7855).

The geospatial preprocessing follows three stages (Figure 9.1). Stage 1: LiDAR denoising and segmentation. Stage 2: DSM construction from the classified point cloud. Stage 3: integration of the 2050

redevelopment planning model (provided by DTP) into the AOI DSM. The outcome is a precinct-ready surface suitable for annual solar-potential and shading simulation.

Stage 1 — Denoising and segmentation. Raw tiles are denoised using a K-nearest neighbour (KNN)–based outlier filter, then segmented to isolate feature classes. Quality checks indicate misrepresentation in some tree classes; water bodies are treated explicitly to avoid downstream artefacts. Identified issues are corrected before rasterization.

Stage 2 — DSM construction. The DELWP DEM provides georeferencing control. A local binning routine converts the classified point cloud to a DSM, and class-specific rasters are produced for vegetation (3, 4, 5), buildings (6), water (9), and bridges (10). Outputs are generated at project resolution (4,000 × 5,000) and as 1 km tiles for memory and performance management. Depending on analytical needs, the DSM is compiled from either all classes or the denoised subset.

Stage 3 — Integration of the 2050 planning model (DTP). Legacy building footprints and conflicting above-ground features (e.g., poles, trees, amenities) are removed where they overlap with planned redevelopment. The DTP building footprints are rasterised and aligned to the DSM/DEM grid. Merging proceeds as follows: (i) mask DSM values where planned buildings occur; (ii) infill masked cells with ground elevation from the DEM; (iii) add the planned-building raster. This prevents vegetation appearing on rooftops and preserves non-building context. The resulting DSM is validated visually against the LiDAR-derived surface and in 3-D views. Conflicting existing buildings are removed, planned buildings inserted, and surrounding context retained.

10. Appendix 4 - Urban Heat

10.1 Base case scenario

10.1.1 Research Process

A robust methodology was developed to study urban microclimates and devise strategies for mitigating urban heat, combining advanced simulation tools, stakeholder engagement, and comprehensive data collection. A detailed literature review assessed various microclimate simulation models, with a focus on urban heat. Specifically, ENVI-met was compared with tools like CFD and UMEP, demonstrating its strength in modelling surface-vegetation-atmosphere interactions, and therefore, ENVI-met 5.6.1 Winter Edition has been selected for this investigation. The collaboration with DTP facilitated the identification and acquisition of critical data, including land use, vegetation, and building material properties, in the form of spatial data as a 3D GIS model. The QGIS plugin for ENVI-met has been utilised for its efficiency in importing GIS data and enhancing spatial data accuracy in urban heat modelling based on the data provided by DTP. The following subsections provide a thorough overview of the methodologies used in urban heat analysis.

10.1.2 Climate data and simulation period

As this project aimed to assess the development of the Albion Quarter in 2050 while enforcing best practices in mitigating climate change, the predictive weather data for building energy modelling, developed by CSIRO for the 2050 RCP4.5 scenario, was used. In addition, based on the climate analysis for Sunshine, the 25th of February was chosen as the representative hottest day to test the development during extreme conditions based on the climate analysis in section 8, Table 10.1. In addition to understanding the development performance during average extreme heat conditions and assessing the need for further analysis to optimise heat mitigation strategies, the study also included a typical hot day, focusing on the central area of the project. Based on the climate analysis, February 24th was selected as a representative day for the typical hot day conditions. It should be noted that multiple-day heatwaves were not simulated in this study.

Table 10.1. An overview of the climatic parameters used in urban heat simulation

Day	Time	Air temperature °C	Relative humidity %	Wind direction	Wind speed	Cloud coverage
24	6	15.7	96	0	2.1	3
24	7	14.7	96	0	1	3
24	8	15.7	90	0	1	3
24	9	20.8	65	22	1	2
24	10	27	48	0	5.9	1
24	11	29	43	0	11.4	1
24	12	31.1	38	0	9.4	1

24	13	33.1	36	0	8.1	1
24	14	34.1	32	0	7.6	1
24	15	36.2	29	0	5.9	1
24	16	36.2	27	0	5.9	1
24	17	37.2	24	0	4.8	1
24	18	37.2	24	0	7	1
24	19	36.2	25	22	7	1
24	20	35.2	28	22	4.5	1
24	21	33.1	32	22	4.1	1
24	22	31.1	36	22	4.5	2
24	23	30.1	38	0	4.5	2
24	24	28	45	0	4.1	2
25	1	28	45	0	4.5	2
25	2	28	45	0	6.5	2
25	3	27	48	0	7	2
25	4	27	48	0	5.6	3
25	5	26	51	0	5.9	3
25	6	26	47	0	6.5	3
25	7	26	47	0	7.6	3
25	8	24.9	51	0	8.9	2
25	9	27	45	0	9.4	1
25	10	30.1	40	0	11.4	1
25	11	33.1	32	0	11.4	1
25	12	35.2	26	0	11.4	1
25	13	37.2	22	0	10.5	1
25	14	38.2	18	0	9.4	1
25	15	40.3	13	0	8.1	1
25	16	40.3	11	337	4.8	1
25	17	41.3	12	315	3.5	1

25	18	41.3	12	315	4.1	1
25	19	40.3	10	0	4.8	3
25	20	38.2	14	0	3.5	3
25	21	33.1	20	0	3	1
25	22	29	37	0	0	1
25	23	28	40	0	0	10
25	24	26	42	0	0	1
26	1	27	39	0	2.4	1
26	2	27	39	0	4.5	1
26	3	26	42	0	4.5	1
26	4	24.9	41	0	4.5	1
26	5	23.9	41	0	4.5	1
26	6	23.9	41	0	4.5	1

10.1.3 Defining the base case scenarios

The target area has a non-uniform layout; however, urban heat modelling in ENVI-met requires the simulation domain to be defined as a continuous rectangular grid with fixed, orthogonal boundaries. To meet this requirement, the areas surrounding the project were included to construct a rectangular domain that fully contains the irregular project footprint, supports stable boundary forcing, and avoids distortions at the model edges. Where necessary, auxiliary boundary extensions were incorporated to approximate the irregular geometry within a uniform rectangular region suitable for ENVI-met simulation, as shown in Figure 10.1.

Figure 10.1. The target area for urban heat simulation, where the building is highlighted in black colour

Large models can consume a significant amount of time during the simulation and are also vulnerable to crashing due to their complexity. In addition, the model resolution is highly important and increasing the resolution can significantly increase the model size, while reducing the resolution can reduce the accuracy. Therefore, a thorough analysis was conducted to determine the ideal model size and resolution by consulting the literature and the ENVI-met team. A decision was made to split the target area into five models, utilising a 5 m grid resolution, as the ideal configuration for this project. A 90 m overlap between the tiles was established to facilitate integration and enhance the quality of the results, Figure 10.2.

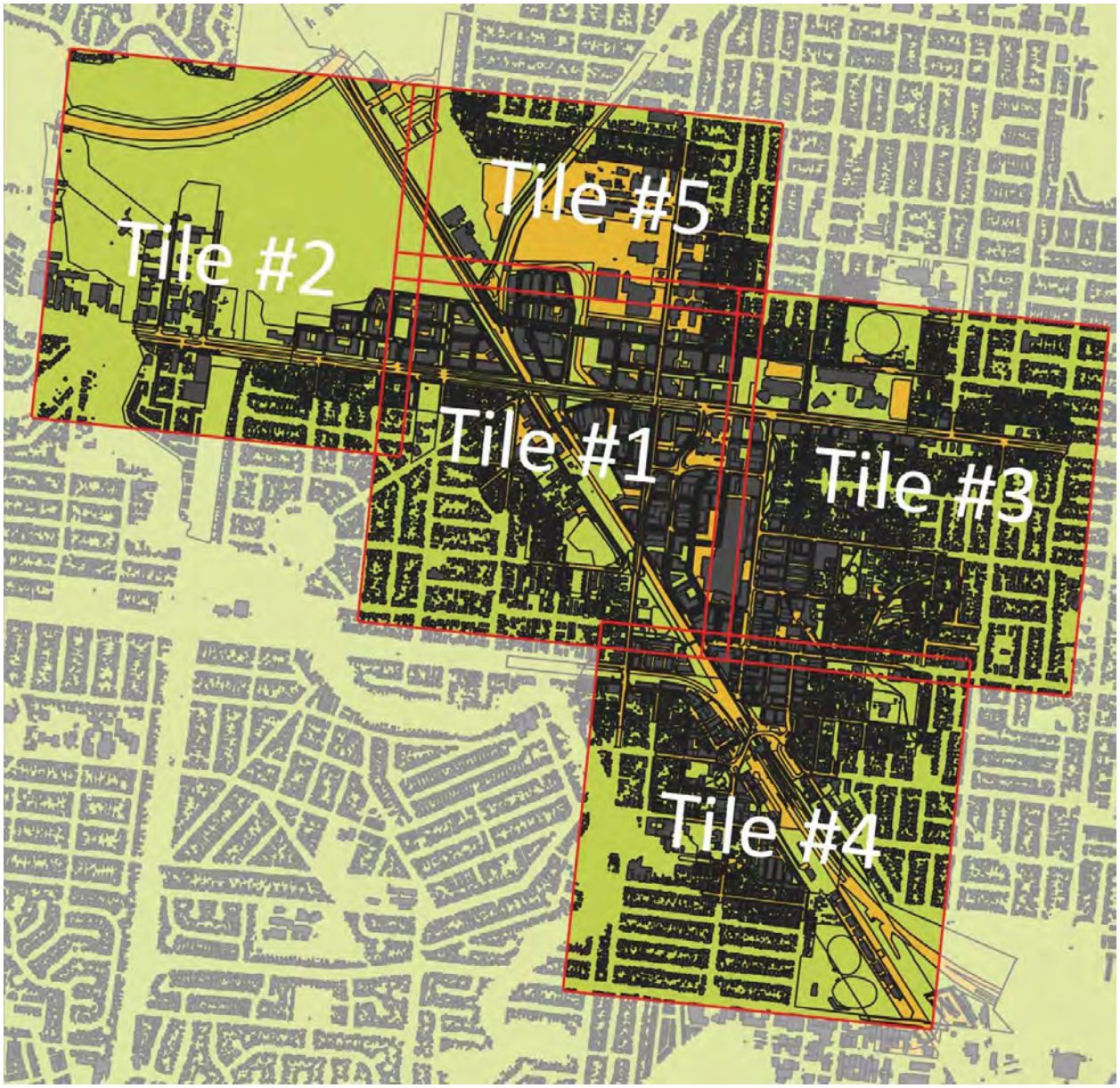

Figure 10.2. The identified tiles for urban heat simulations

10.1.4 Defining the modelling settings

The base case modelling consists of five tiles. Tiles 1-4 were identical in their settings, while Tile 5 shared the same setting except the y-grids, which were less than those of the other models to cover the targeted area. The height of the models consists of 40 grids, with 1 meter as the base for the grids. The first grid at ground level was split into 5 to facilitate modelling low canopy vegetation, and the telescoping option was utilised to expand the model height without sacrificing the simulation time and to enhance its stability. The telescoping factor was set to 30% and started after a height of 30 metres. The length and width of the Tiles were 260 x 260 grids for X and Y, except that Tile 5 was 260 x 136 grids, respectively, and each cell represented an area of 5m x 5m. The Tiles were rotated by 6 degrees to facilitate horizontal modelling and increase the modelling accuracy. A 20-nesting grids were included in the simulation but was excluded from the results to facilitate the wind forcing during the simulation process. Additionally, 7

cells within the Tiles area were used as a buffer zone to enhance simulation stability. These settings resulted in a final modelling area of 1300m x 1300m for Tiles 1-4 and 1300m x 680m for Tile 5. The final heights of the models were 85.41m, and the minimum space between buildings and the model border was 1180m.

10.1.5 Defining alternative scenarios

Various alternative scenarios were proposed to test the impact of alternative settings compared to the base case scenario. The alternative scenarios were not conducted on all the tiles, while they targeted specific tiles based on the aim of the investigation. Table 10.2 summarises the alternative scenarios, their aims, and the targeted Tile for the proposed investigations.

Table 10.2. Alternative scenarios for urban heat

Alternative scenario	Aim	Targeted tile
Drought-resistant trees	Testing the impact of using drought-resistant trees as a strategy to save water for irrigation	Tile 1
Small trees	Testing the impact of including small trees in street canyons, if the soil volume is insufficient in the developed site.	Tile 1
Large trees	Testing the impact of including large trees in street canyons to check the potential of increasing the allocation of soil volume and verges	Tile 1
Proposed irrigation	Testing the impact of irrigating strategic public spaces	Tile 1
Building materials	Testing the impact of high and low embodied carbon materials and their effects on urban heat and energy	Tile 1

10.1.6 Defining the modelling materials

The materials in urban heat were classified into two categories. The first category encompasses the materials used in buildings and surfaces, while the second covers vegetation. The material classifications of surfaces and buildings have been exported from QGIS, and representative of their thermal parameters have been added to the 3d models in ENVI-met. This also includes trees and low vegetation, whether they are irrigated or not. The glass used for windows was clear glass with the following properties: thickness of 0.006 m, absorption of 0.16, transmittance of 0.77, reflection of 0.7, emissivity of 0.9, specific heat capacity of 750 J/kg/K, thermal conductivity of 0.05 W/m/K, and density of 2500 kg/m^3. The water properties included a roughness of 0.01, an albedo of 0, and an emissivity of 0.9. The used soil was a mix of clay and sand with water content at saturation of 0.45 and 0.395, water content at specific field capacity of 0.255 and 0.135, water content at wilting point of 0.175 and 0.07, hydraulic conductivity of 6.3 and 1.76, and volumetric heat capacity of 1.175 and 1.463, respectively. The asphalt and permeable basalt were assigned an albedo of 0.12 and an emissivity of 0.9. Lastly, the used building material properties are summarised in Table 10.3.

Table 10.3. Thermal properties of building materials for urban heat

Materials\ properties	Thickness	absorption	transmission	reflection	emissivity	specific heat	thermal conductivity	density
Glass	0.006	0.05	0.9	0.05	0.9	750	1.05	2500
Air gap-G	0.012	0	1	0	0.96	1006	0.025	1.2
plaster board	0.016	0.5	0.17	0.5	0.93	840	0.6	950
Glass wool insulation	0.075	0.42	0.12	0.5	0.9	670	0.04	200
phenolic composite	0.08	0.42	0.018	0.5	0.9	937	0.043	1440
Alucobond	0.01	0.1	0	0.9	0.18	880	203	2700
Wood timber	0.128	0.15	0.13	0.15	0.7	1800	0.12	450
Particleboard	0.013	0.15	0.1	0.15	0.7	1450	0.045	254
Concrete	0.18	0.7	0	0.3	0.9	850	1.6	2220
Brick	0.1	0.7	0	0.3	0.93	900	0.64	1500
Roof tyles	0.05	0.7	0	0.3	0.93	800	0.84	1900
Steel	0.002	0.3	0	0.7	0.1	420	45	8000

An average of the thermal properties was applied to the materials for building that included various materials in the facade, based on their percentage composition. For instance, if the elevation consists of 30% concrete and 70% glazing, the average properties of the materials were applied in the same proportions. Finally, the construction of the various building assemblies is summarised in Table 10.4.

Table 10.4. Assembly types and associated materials of buildings for urban heat

Assembly type	Assembly composition
Metal	Metal sheet (0.02m)/Air space (0.1m)/Plasterboard (0.016m).
Concrete	Concrete (0.18m)/Insulation (0.05m)/Plasterboard (0.016m).
Brick	Brick (0.10m)/Air space (0.1m)/Plasterboard (0.016m).
Clay tile	Clay tile (0.03 m)/Insulation (0.1 m)/Plasterboard (0.016 m).
Light wood	Plasterboard (0.016m)/ Glass wool (0.075m)/Plasterboard (0.016m)/ Air gap (0.093m)/phenolic composite (0.08).
Mass wood	Alucobond (0.01m)/Air gap (0.05m)/Glass wool (0.05m)/Wood timber (0.128m)/ Particleboard (0.013m).
Windows	Glass (0.006m)/Air gap (0.012m)/ Glass (0.006m).

For the vegetation, a simplified modelling approach was used to classify the trees into 20 different models based on the available trees in the GIS 3D model. A 5-meter-based classification approach was used to allocate the trees in the 20 categories based on their size, including height and width, as per Table 10.4. Going forward in the report, trees with a diameter of 5 m are considered small, 10 m medium, 15 m large, and 20 m extra-large. All the modelled trees were conifers with sparse canopies, with an assigned leaf area density of 1. The CO2 fixation was C3, with foliage shortwave of 0.12, emissivity of leaves 0.96, foliage shortwave transmittance 0.1, leaf weight 100 g/m^2 and isoprene capacity of 12. The root zone of the trees was 70% of the diameter of the tree, and the depth was 16.7% of the tree height. The grass parameters were as follows: albedo 0.2, emissivity 0.97, transmittance 0.3, height 20cm, root zone depth 0.2 cm, with leaf area density of 0.3.

Table 10.5. Tree classification for urban heat modelling

		Height (m)				
		1-5	5-10	10-15	15-20	
Diameter (m)	1-5	05X05L	05X10L	05X15L	05X20L	Height/Diameter
	5-10	10X05L	10X10L	10X15L	10X20L	Height/Diameter
	10-15	15X05L	15X10L	15X15L	15X20L	Height/Diameter
	15-20	20X05L	20X10L	20X15L	20X20L	Height/Diameter

10.1.7 Data analysis and visualisation

Further processing of the simulation results was conducted using BIO-met from ENVI-met to generate Thermal comfort and NetCDF files, facilitating integration with the Digital Twin Victoria portal. The universal thermal index was used to calculate thermal comfort using a typical male setting, with a weight of 75 kg, a height of 1.75 m, and a body surface area of 1.91 m^2. As the analysis is during summer, the static insulation (clo) was set to 0.5 and the metabolic rate (met) to 1.48. The NetCDF files for the various tiles were merged and exported to the Digital Twin Victoria portal. For this report and for the integrated analysis with the energy and embodied carbon groups, Leonardo, MS Excel, and Adobe Photoshop were used. In Leonardo, all the data for this report were extracted at the pedestrian level, 1.5 m above the ground surface. The data was then processed manually using MS Excel to generate charts and Adobe Photoshop to create graphical maps. An automated extraction of the results was conducted for further processing in MS Excel. These results were used to generate climatic data from various models at different heights for specific locations, facilitating the simulation of a few alternative energy scenarios.

10.2 Updated scenario

The climate data, simulation period, materials, and data analysis were identical to the research process of the base case scenario, as outlined in section 10.1. The modelling settings for the Energy Park, which focused on Tile 2, remained identical to those of the original base case. However, for Tile 1, which focuses on the Albion Quarter, the model settings were adjusted to accommodate the increased building heights

introduced in the updated scenarios. To enable a valid comparison, an additional base case scenario was developed and simulated using the same settings as the updated scenarios.

The simulation of this stage was based on four models. The first model focused on an Energy Park following the same design layout of the Energy Park, except for the tree arrangement, which was redesigned and idealised based on the analysis in the base case scenario to free the airflow and enhance the passive cooling, as the park was one of the hottest spots in the base case and mainly due to the tree arrangement. The other three scenarios were developed by DTP for the Albion Quarter and differ in tree distribution, tree size, and irrigation strategies across streets, public open spaces, and the private realm. These scenarios, illustrated in Figure 10.3, are the Best Investment Case (BIC), Reasonable Investment Case (RIC), and Business As Usual (BAU).

Scenario	Streets					Public open space			Private realm			
	Active irrigation priority	Active irrigation all	Tree overlap priority	Tree overlap all	Structural soil	Active irrigation	30% canopy	% hardstand	Active irrigation	10% ground canopy	Podium canopy	Internal streets with trees
Best Investment case	O	O	O	X	O	O 30%	O	X	O 20%	O	X	O
Reasonable investment case	O	X	O	X	O	O 20%	O	X	X	O	X	O
BAU	X	X	X	X	X	X	O	X	X	O	X	O

Assumptions	Definition
Priority Street	Street sides that will be unshaded in summer
All Streets	All street sides, regardless of orientation and shading
Tree Overlap	Trees that are close enough together or large enough that canopy overlaps
Structural Soil	Extra soil put under footpath and on-street carparking to support tree growth and facilitate tree canopy overlap
Active Irrigation	Drip irrigation to enable street tree growth (street trees). For open space, the equivalent of active irrigation for cooling purposes
% hardstand	The amount of open space not covered by grass
30% canopy	Coverage of 30% of open space with tree canopy
Podium canopy	Trees planted on top of carparking podiums

Figure 10.3. Assumptions and definitions of Albion Quarter scenarios for the updated scenario simulations

The height of these models consists of 45 grids, with 1 meter as the base for the grids. The first grid at ground level was split into 5 to facilitate modelling low canopy vegetation. The telescoping option was utilized to expand the model height, allowing for increased building heights without sacrificing simulation time and enhancing stability. The telescoping factor was set to 30% and started after a height of 30m. The length and width of the models were 260 x 260 grids for X and Y, respectively. Each cell represented an area of 5m x 5m. The models were rotated by 6 degrees to facilitate horizontal modelling and increase the modelling accuracy. A 20-nesting grid was included in the simulation but was excluded from the results to enable wind forcing during the simulation process. Additionally, 7 cells within the model's area were used as a buffer zone to enhance simulation stability. These settings resulted in a final modelling area of 1300m x 1300m. The final heights of the models were 247.47m, and the minimum space between buildings and the model border was 1180m. It should be noted that the high-rise buildings were stretched in this model due to the use of the telescoping factor. To ensure accurate results, the input data for these buildings were adjusted accordingly in the GIS model before exporting. This process results in a 3 m

increase or decrease in the height of a few of these buildings, which could be neglected due to the limited impact of these changes on the overall results.

11. Appendix 5 - Water

11.1 Overall water balance

The water balance analysis was conducted on an annual basis using a simplified and conservative framework for both trees and grassed green spaces across the precinct:

Water Balance = Rainwater Supply – Plant Water Demand

Rainwater Supply = Effective rainfall (mm) × soil infiltration area (m^2)

where effective rainfall is 50% of annual rainfall, and soil rooting depth beneath an area is assumed to be 1.0 m.

Plant Water Demand = ET_0 (mm) × Kc (0-1) × Canopy area (m^2).

where ET_0 is potential evapotranspiration for Sunshine (mm); Kc is the Water use coefficient for the plant (between 0 and 1) and Canopy area is for a Tree canopy (m^2) or the Grassed area (m^2).

Annual water balance estimates were made for three climate scenarios:

- C0: Current conditions (annual rainfall: 539mm, annual ET_0: 1364mm)
- C1: 2050 average (–6% current rainfall, +10% ET_0)
- C2: 2050 dry (–13% current rainfall, +10% ET_0)

Within these scenarios, calculations were based on two tree water use coefficients (Kc) and three grass water use coefficients (Kc). Detailed parameter settings and calculation methods can be found in this section.

11.2 Case studies of tree canopy cover and green space area

As the project's built form underwent changes throughout the study period, the analysis was structured into two distinct and logical phases.

- Phase 1: Macro-Scale Assessment based on the base case

The initial phase of the analysis was based on the project's early base case model. The assessment at this stage was macro-level, which aimed to provide a preliminary evaluation of the precinct's overall potential, key constraints, and the total volume of supplementary water sources. The findings from this phase guided the direction for the more detailed investigation that followed.

- Phase 2: Focused Scenario Testing based on Model Stage 3

As the project's planning progressed, the built form evolved into the more detailed Stage 3 Model (S3 Model). To ensure the analytical conclusions would provide practical and relevant guidance for the final design, the core of the study shifted to a focused "Scenario Testing" based on this updated model.

The analysis in this phase was highly focused on street trees. This strategic pivot was informed by the conclusions of Phase 1, which identified that streets, as public realm assets, not only face the most severe

environmental challenges for growth but also offer the most significant and direct opportunities for intervention. Therefore, this phase involved an in-depth sensitivity analysis of street tree growth potential under various design interventions, with the goal of providing specific, quantitative decision support for the final streetscape design.

11.2.1 Phase 1: base case

In phase 1, the total tree canopy rate was estimated to be 16% as shown in Figure 11.1 and Table 11.1.

The base case involved simulating trees in both the existing Sunshine CBD and in the proposed Albion Quarter urban renewal area. The Sunshine CBD has existing tree canopy, whereas there are very few trees in the Albion Quarter. Tree canopy data was developed separately for the two areas.

For the new Albion Quarter renewal area, tree canopy was estimated based on:

- For proposed private land development: assuming a 10% canopy on private land as per the Better Apartment Design Standards (BADS). Trees were assumed to be a mix of medium and large trees, consistent with the BADS requirements. Medium canopy trees are defined as 8m in diameter and large canopy trees are 12m in diameter in the BADS, these were simplified to 10m and 15m crown diameters to align with the 5x5 m model resolution of Envi-met simulations.
- For proposed open space: assuming a 12m separation between extra-large trees along the perimeter of open space, typical of many open space designs in the area. Trees were assumed to be 20m diameter.
- For proposed street trees:
    - All street trees were assumed to be medium size - simplified to 10m in crown diameter to align with Envi-met based model resolution.
    - Trees were arranged on spacing of 8m between tree points, based on advice from Brimbank Council around typical spacing for new street tree planting.
    - Trees were not planted in certain areas, specifically: a 10m offset from intersections and 3m clearance on both sides of driveways.
    - Trees were removed, (25%) to account for expected conflicts with utilities and infrastructure. This was based on work in the City of Sydney (TreeNet, 2020). This City of Sydney study assumed a 20% impact for most of the city and 30% impact for CBD areas.
- For existing streets, Council tree data was used to identify street trees. These were simplified to the nearest 5m diameter.
- For Stony Creek, fairly dense planting was assumed that did not take into account contamination constraints.

Tree canopy data for the Albion Quarter in the Reference Case did not account for any soil or water constraints.

Results of the initial tree data creation for Albion Quarter are outlined below.

Figure 11.1. Proposal tree canopy for the base case

Table 11.1. Breakdown of the canopy rate for the base case

Measure		
Total tree canopy (including overlap)	**20.9%**	**108179 m²**
Total tree canopy (excluding overlap)	**19.9%**	**103194 m²**
Private land	4.6%	23677 m²
Public open space	6.4%	33287 m²
Street trees	9.9%	51215 m²

Note: Total canopy excluding overlap represents the effective canopy area accounting for overlapping tree crowns. Canopy contributions by land type are shown as components of the total effective canopy.

11.2.2 Phase 2: Street and park tree scenario testing

The scenario testing was conducted to move beyond the conceptual assumptions of the initial base case and evaluate the practical feasibility of achieving the target canopy outcomes. In the base case, tree placement was based primarily on spatial design intent without assessing whether soil volume and water availability were adequate to sustain healthy tree growth. As a result, it represented an idealised design rather than an implementable strategy.

Building upon this, the scenario testing aimed to quantify how biophysical constraints, such as rainfall, soil storage, and irrigation potential, would influence the extent of achievable canopy and precinct-scale heat performance. This included:

1. Testing which trees could realistically be delivered based on effective rainfall and available soil volume;
2. Estimating future tree water demand and summer storage requirements under different climate conditions;
3. Estimating irrigation requirements for cooling, given the strong relationship between irrigation and microclimate performance; and
4. Comparing results across typical street cross-section types to understand how verge width and paving configurations affect water and soil supply.

In the meanwhile, the precinct's digital model evolved from the original base case to the updated S3 built form scenario, which introduced significant changes to building massing and height. These modifications affect solar exposure and shading patterns, both of which are critical to tree growth and canopy performance. The scenario testing therefore also explored the interaction between built form and canopy potential, ensuring that the design recommendations remain realistic within future development conditions.

Figure 11.2 presents one proposed scenario of the overall area tested using the S3 model, with Ballarat Road excluded from the analysis as it is expected to remain unchanged.

Figure 11.2. One proposed scenario for the tree canopy plan in the Albion Quarter, developed using the S3 built form model

11.3 Data input for water calculations

11.3.1 Climate-related data

Weather and climate significantly influence the water analysis for this study. Compared to other weather attributes, such as solar irradiance, rainfall patterns are more challenging to predict on a daily basis. However, long-term average predictions are essential for understanding water availability and demand under future climate scenarios.

To address these uncertainties, three weather scenarios have been developed, considering variations in annual rainfall and reference evapotranspiration (ETo).

Table 11.2. Annual rainfall and Annual ETo of three weather scenarios

Parameter	Scenario	Co: Current	C1: 2050 Avg	C2: 2050 Decile 1
Rainfall	Annual (mm)	539	506	469
	Change from Co (%)	/	-6%	-13%
ETo	Annual (mm)	1364	1500	1500
	Change from Co (%)	/	+10%	+10%

Table 11.2 summarizes the value of the annual rainfall and ETo. For the base case Co, the weather data is obtained from BOM (Station: 86282 MELBOURNE AIRPORT). The differences between these scenarios are illustrated in the table above. The projected decrease in annual rainfall is shown, with rainfall expected to decline by up to 13% under the worst-case scenario (C2). The projected increase in annual ETo is presented, indicating a 10% rise for both future scenarios (C1 and C2). These assumptions are made based on CSIRO climate projections (2019) RCP4.5 scenario and the Greater Melbourne Climate Projections (2019). The widening gap between evapotranspiration and rainfall indicates that greater supplementary water will be required for vegetation under future climate scenarios.

11.3.2 Vegetation-related data

11.3.2.1 Crop coefficient (Kc)

The crop coefficient (Kc) is applied in the calculation of vegetation water consumption. A higher Kc indicates greater water demand, as the vegetation requires more water to sustain its growth and maintain its physiological functions.

For trees, two primary categories are considered: medium water-use trees with a Kc of 0.5 and low water-use trees with a Kc of 0.3. For grass, three types are considered, each with distinct water requirements. Kc values are summarized in Table 11.3.

Table 11.3. Kc values for tree and grass

Scenario	*Tree Kc*	*Grass Kc*
Base case	All areas: 0.5	High-range level for sports: 0.8

		Mid-range level for sports: 0.6 unirrigated grass: 0.3
Sensitivity analysis	Public: 0.3 Private: 0.5	High-range level for sports: 0.8 Mid-range level for sports: 0.6 unirrigated grass: 0.3

11.3.2.2 Trees and Grass Spatial Data

To enable further calculations, the tree input data should include several essential attributes. These include the tree location (i.e., whether it is in a public area, private property, or a verge), as this affects management practices and water use scenarios. Tree diameter or radius is necessary for estimating canopy size and, consequently, water consumption. Species information may also be recorded, as different species have varying tree Kc, which influence water demand. In addition, the soil type at the planting site must be considered, as it directly affects water availability and retention. The impact of soil type on summer water storage capacity is discussed in detail in a later section.

For the grass, the total area of the grass is essential for calculating water consumption. Additionally, the purpose of the grass should be specified, whether it is primarily used for cooling or sports, as this can impact its water requirements (directedly related to Kc). Also, it is important to identify whether the grass area has an irrigation system.

11.3.3 Building and road-related data

Building water consumption varies according to building category, with the primary categories being residential and commercial. Water consumption rates are based on advice from Greater Western Water.

- For residential buildings, the consumption rate is 0.12 ML per dwelling per year.
- For commercial buildings, water use is estimated by multiplying the total gross floor area (GFA) by the average consumption rate.

For commercial buildings, average water consumption rates have changed over time:

- Prior to 2021, the average consumption was 362 L/m^2.
- Following the increased prevalence of working from home in 2023–2024, this figure decreased to 191 L/m^2.

On the supply side, building and road water capture are primarily determined by the surface area available for rainwater collection. The calculation method is outlined in the following sections.

11.4 Water calculation methods

11.4.1 Water Balance Principle

The water balance model estimates the water consumption of vegetation and available water supply from rainfall. Key Equations are as follows:

Annual Water demand (mm) = Actual evapotranspiration (ETa) – Effective Precipitation (Pe)

Or

Annual Water demand (L) = Actual evapotranspiration (ETa) x 1m² – Effective Precipitation (Pe) x 1m²

Where:

- Water consumption of vegetation: Annual Actual Evapotranspiration (ETa) = Annual ETo x Kc
- Water supply from rainfall: Pe = Annual Rainfall x Effective rainfall factor

Input data:

- Annual Reference Evapotranspiration (ETo) are detailed in Table 11.2
- Kc refers to Table 11.3
- Annual Rainfall refers to Table 11.2
- Effective Rainfall Factor: An effective rainfall factor of 50% is applied, as suggested by Water Use Efficiency for Irrigated Turf and Landscape (Connellan, 2013), to estimate the portion of rainfall available for plant water use.

11.4.2 Grass water need

For grass, once the grass area is determined, the total amount of water required to meet its water demand, including any potential irrigation, can be calculated.

Grass water demand is calculated as follows:

- Per unit area: Grass water demand (L/m²) = Actual evapotranspiration (ETa) × 1 m²
- Total grass area: Grass water demand (L) = Actual evapotranspiration (ETa) × grass area

The annual water balance for grass is then calculated as:

Annual Water demand (L) = Eta x grass area (m²) – Pe x grass area (m²)

11.4.3 Tree water need

There are two kinds of trees considered in the project: (1) Trees in open space open areas with no root restrictions. (2) Trees in Verges or Tree Pits.

Tree water demand is calculated as follows:

- Per unit area: Tree water demand (L/m²) = Actual evapotranspiration (ETa) × 1 m²
- Per tree: Tree water demand (L) = Actual evapotranspiration (ETa) × tree canopy area

11.4.4 Summer storage capability

Summer water storage days are analysed due to distinct seasonal rainfall patterns and their impact on tree water availability. During December, January, and February, effective rainfall (≥1mm) typically occurs on only 4 to 6 days per month, resulting in limited water availability. Extended dry periods are common in summer, increasing the risk of soil moisture depletion and water stress, particularly for trees with restricted root zones. Additionally, abundant rainfall before summer can enhance soil moisture storage, potentially reducing the need for supplementary water.

The calculation of the summer water storage in days use the following approach:

$$\text{Summer soil storage in day} = \frac{\text{AWHC x soil volume}}{\text{Daily Eta of summer x canopy area}}$$

Where

- Soil volume: 0.6 m3/m² of canopy area as the minimum requirement.
- Available Water Holding Capacity (AWHC): 160 mm/m (representing a loam soil)
- Daily ETa of summer = Daily ETo of summer x Kc
- Daily ETo of summer = mean of monthly ETo (Dec, Jan and Feb), as shown in Table 11.4.

Table 11.4. Daily Eto of summer for different climate scenarios

	Co	C1	C2
Daily ETo of summer (mm)	5.947	6.244	6.244
Change from Co (%)	/	+10%	+10%

From the Equation above, it could be found that:

- An increase in daily ET_0 under future climate scenarios (C1 and C2) will reduce summer soil storage.
- Higher soil quality, such as loam soil with organic content and an available water holding capacity (AWHC) of up to 180 mm/m, increases storage. However, this condition is unlikely to be achieved in roadside verges due to ongoing risks of soil compaction.
- Greater soil volume allows for higher water storage capacity.

A 50-day target for water storage is suggested to ensure trees have sufficient moisture during prolonged dry periods in summer. To achieve this, it is essential to determine the appropriate soil volume that can sustain trees for this duration without relying on additional irrigation.

Therefore, according to the equation above, the soil-to-canopy ratio can be calculated to determine the required soil volume for sustaining tree water demand over the 50-day target period.

If 50 days as a target period, Figure 11.3 illustrates the relationship between Available Water Holding Capacity (AWHC) of the soil (x-axis) and the soil-to-canopy ratio (y-axis) under different climate scenarios. It should also be noted that an AWHC of approximately 120 mm/m is a more realistic value for typical urban verge soils.

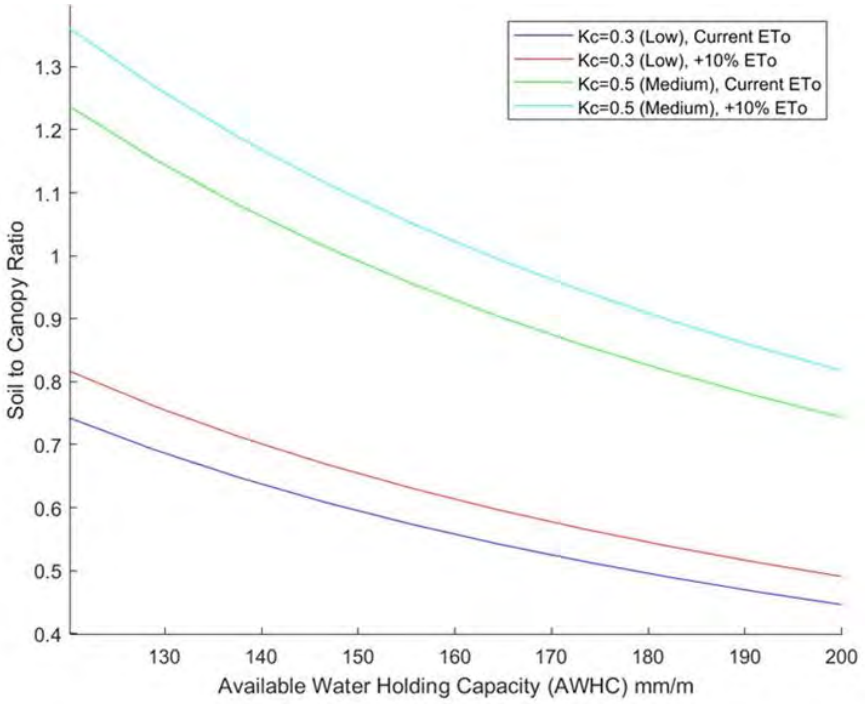

Figure 11.3. Relationship between Available Water Holding Capacity (AWHC) and the soil-to-canopy ratio for a 50-day target under different climate scenarios.

11.4.5 Building and road water capture

11.4.5.1 Building roof capture

The annual volume of rainwater that can be captured from building roofs is calculated as follows:

Roof rainfall capture = Annual rainfall x Roof area x Runoff coefficient x Tank efficiency

Where:

- Roof area: 60% of the building footprint is assumed to be available for rainwater capture (based on advice from DEECA).
- Runoff coefficient: 0.9, reflecting typical values for roof surfaces (Rainwater Tank Design and Installation Handbook, 2008).
- Tank efficiency: 0.7, representing storage and system efficiency.
- No pre-treatment devices are assumed in this calculation.

11.4.5.2 Road capture

The equation used for road water capture is:

Road rainfall capture = Annual rainfall x Road area x Usage percentage

Where:

- Usage Percentage: Two scenarios were modelled to represent varying levels of infrastructure performance:

- Low Efficiency (20%): Represents a sub-optimal passive irrigation design (or standard tree pit) with limited inflow capacity. This capture rate is consistent with findings by Szota et al[9]. (2019).
- High Efficiency (90%): Represents an optimized passive irrigation system incorporating permeable elements, such as kerb inlets (broken kerbs) and swale verges, designed to maximize runoff interception.

11.4.6 100m-based street tree design

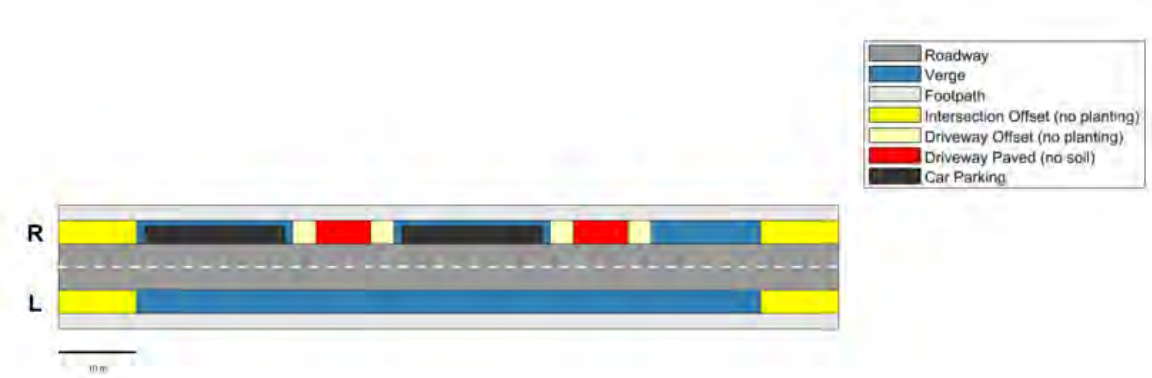

Figure 11.4. A typical living street configuration of 100m

A customizable model was developed to determine how many street trees in a typical 100-meter corridor can sustain at their planned mature size. The model is designed to be highly flexible, accommodating various road cross-sections by allowing users to input specific parameters for elements like footpaths, verges, and roads, as well as site features such as driveways and parking bays. For example, Figure 11.4 illustrates a typical living street configuration. It is reflective of the proposed urban density – where fewer driveways are required compared to low density areas – and future shading patterns, where more canopy is required on the southern side of the street in summer. As such it was modelled with the following parameters:

- Cross-section: A 2-meter footpath, a 3-meter verge, and a 6-meter road.
- Site Features: Two 7-meter-wide driveways and two 18m x 2.3m parking bays on one side.
- Planting Conditions: Street trees are planted within the verge at a soil depth of 1 meter.

By adjusting these inputs, the model can be applied to virtually any street design to test its tree-hosting capacity.

Based on the street cross-section, the analysis compares two distinct approaches to determine their impact on tree capacity:

- Basic approach: This approach represents standard practice. It assumes trees are planted in a 1 m deep verge and rely solely on this soil. No structural soil. There is 20% rainwater capture from the road. All trees are of a uniform size.

[9] *https://www.sciencedirect.com/science/article/pii/S0169204618312222*

- Sophisticated approach: This approach incorporates advanced techniques to improve growing conditions. It includes:
    - Structural soil: 0.9 m depth installed under footpaths and parking bays, with an effective soil ratio of 20%.
    - Road rainwater capture: 20% of annual rainfall from the road surface is used for passive irrigation.
    - Varied tree sizes: A mix of large and small trees is used to optimize for site conditions like sun exposure. In Section 3.4.2.1 the model assumes a tree crown diameter of 7 m for large trees and 4 m for small trees.

The maximum number of trees is determined by the most limiting of three factors: physical spacing, soil capacity, and water balance, based on the following parameters:

- Planning Thresholds: Soil-to-canopy ratio and annual water balance (supply vs. demand).
- Tree Water Use: 450 L/m²/year of canopy (low water use tree).
- Rainfall: 506 mm/yr with Effective Rainfall Rate = 50% (baseline) and 100% (water doubled through active drip irrigation).
- Spacing Rules: A 10 m offset from intersections and a 3 m offset from driveways for visual clearance.

The final approved tree count is the lowest number that meets the constraints. In Section 3.4.2.3, the street tree maps were generated based on parameters summarized in Table 11.5. The tree diameters were set to 5 m and 10 m to align with the Urban Heat Model, which operates at a 5 m spatial resolution.

Table 11.5. Tree number of 100m street used for both the precinct's tree canopy analysis and urban heat modelling

Scenario	Approaches	Trees per 100m	Pattern	Diameter
BAU	Basic Approach	7	Single	5
BAU with water doubled through active drip irrigation	Basic Approach	14	Single	5
Better/Best Practice – non-Prioritized area	Basic Approach	14	Single	5
Better/Best Practice – Prioritized area	Sophisticated Approach - N	16	Single	5
Better/Best Practice – Prioritized area	Sophisticated Approach - S	8	Alternating	10 5
Better/Best Practice – Prioritized area	Sophisticated Approach – W	16	Single	5
Better/Best Practice – Prioritized area	Sophisticated Approach - E	8	Alternating	10 5

12. Appendix 6 – Embodied carbon

The term 'embodied carbon' was used in this study to refer to the climate change impacts associated with materials employed in the construction of the proposed Sunshine Precinct. While lacking the precision of a clearer terminology, such as 'climate change impact of materials', the term 'embodied carbon' was generally understood and preferred by the multi-disciplinary research team and wider stakeholder. While attempts were made to step away from the term to a more precise language, these generally failed as participants tended to return to more familiar language. For this reason, 'embodied carbon' is used throughout to refer to the climate change impacts associated with materials in the precinct.

As the impact of climate change has a growing impact on the lives of Australians (BOM 2024), planners must respond to the dual challenge of adapting to, and mitigating climate change in the built environment. In seeking to mitigate the cause of climate change, the Australian Government has committed to:

> "reducing Australia's net greenhouse gas emissions to zero by 2050" (Climate Change Bill 2022:5)

If the above goal is to be achieved it is essential that the climate change impacts of urban development, such as the Sunshine Precinct, be considered at the planning stage and that the implications of design decisions be comprehended at the point a precinct is proposed. It is within this context that the 'Digital Twin' was considered a possible enabler of improved quantification of climate change impact at the planning stage of development, allowing councils to plan for climate impact or to drive for offsets at the point precincts are proposed.

The goals of the embodied carbon assessment were therefore to provide planners with an estimate of climate change impacts of the materials employed within the proposed precinct, in a manner that was sufficiently transparent to enable causes of impacts to be understood. Transparency of calculation was considered a priority as it was unclear as to exactly how planners might use climate impact information in decision making. The project therefore emphasised the building of a climate impact dataset that could be queried from multiple perspectives and that could be easily reconciled to precinct scale metrics.

In addition to providing climate impact information for planners, the embodied carbon assessment also sought to identify a methodology whereby such information could be provided quickly and consistently with other allied analyses such as precinct energy demand/supply, urban heat island and water use. The ambition of responding in a consistent fashion to a given precinct design was considered a critical enabler of 'clash detection', thereby the avoiding the problem where competing goals of the design tend to contradict one another, leading to unintended burden shifting between design objectives.

The research goals can be summarised as follows:

1. Quantify the embodied carbon of the built environment of the precinct. Such quantification must be transparently calculated and readily connectable to precinct features such as its form and material.
2. Identify possible approaches that could be employed to reduce the embodied carbon of the Sunshine Precinct.
3. Identify a process that leverages the Digital Twin concept to calculate impacts quickly, consistently and transparently in order to support informed decision making.

12.1 Scope of Analysis

The research considered the development of the Sunshine Precinct proposed over the timeframe through to 2050. Focus was placed upon new building development proposed in the sub-precincts Albion Quarter, Sunshine Station and Town Centre, as shown in Figure 12.1.

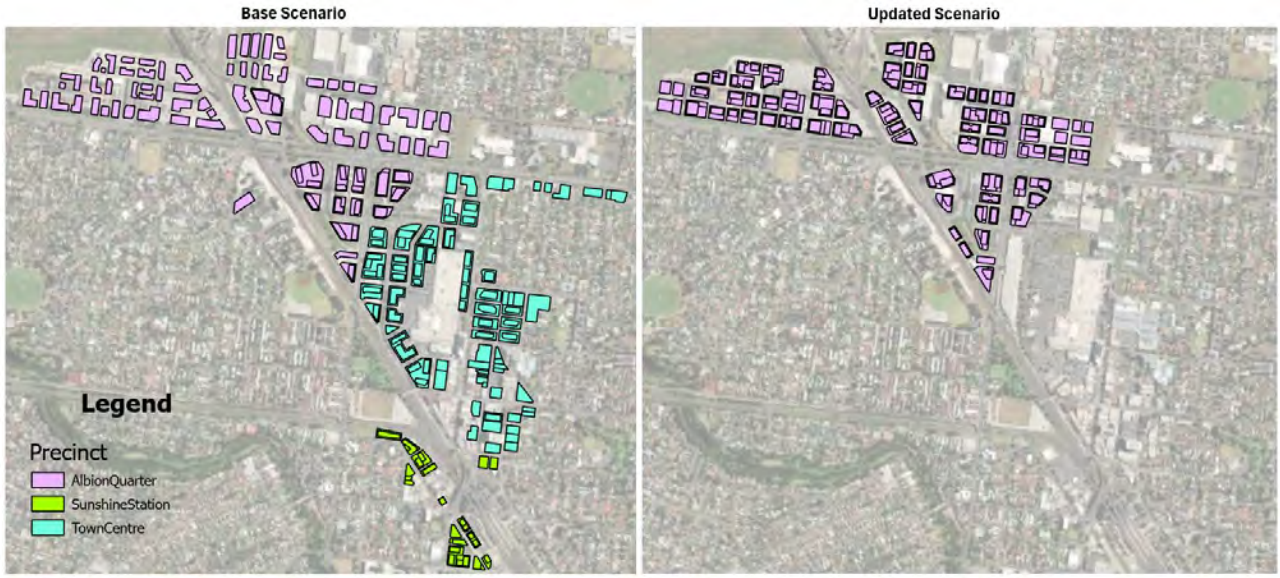

Figure 12.1. Sunshine Precinct showing new buildings considered for the three sub-precincts considered for the Base Scenario and the Updated Scenario. Note that the Updated Scenario was only completed for the Albion Quarter sub-precinct.

Precinct data were provided as a geospatial information system (GIS) representation and a capacity model spreadsheet for the two development scenarios considered. The first scenario, referred to as the 'Base Scenario', represented an initial precinct design. The second scenario, referred to as 'Updated Scenario' represented the most recent design iteration available that could be analysed within the timeframe of the project.

12.1.1 Base Scenario

- GIS Data: BaseCaseV3R1.gdb
- Capacity model data: CapacityModelling_Sunshine_20241008.xlsx
- Scope: Albion Quarter, Sunshine Station and Town Centre

12.1.2 Updated Scenario

- GIS Data: AQSPScenario3R0.gdb
- Capacity model data: DTP_AlbionQuarterCapacity_Scenario_2.1.xlsx
- Scope: Albion Quarter

12.2 Data processing and consistency checking

12.2.1 Base Scenario

As with any such undertaking, multiple data sources, produced at different times and by different people reveal a degree of inconsistency. Indeed, the separation of data sets (GIS/Capacity) appeared as an early

learning from the project as it revealed the inconsistency in decision making data. In this case, precinct function (capacity) had become disconnected from precinct form.

To resolve inconsistencies in the data, the principle that all data must be linked to form was adopted. This was considered essential because so many precinct impacts were related to the detail form, such as building material quantities, shade patterns and therefore energy use and supply, urban heat island and microclimate outcomes, etc. It was also apparent the precinct design itself was described in terms of form, rather than spreadsheets, and would be likely to evolve in three dimensions going forward.

The following assumptions were employed to reconcile the data provided and to produce a singular GIS model from which input data were received to which results would be published.

- GIS footprints assumed to represent buildings, not envelopes
    - The capacity model spreadsheet reduced all footprints by 80% to acknowledge site usage efficiency
    - The subsequently (after calculation of above) reduced all building floor areas by 50% to 80% to reflect internal building usage efficiency
    - No form was provided that was reflective of these assumptions and could not be inferred.
- Carparking basements added, where required, to all buildings in the GIS model, preserving building heights described in the GIS model
    - Number of carpark floors required derived from the capacity model spreadsheet. If a single carpark floor was required then this was accommodated in the basement. If more than one floor was required (fewer than 2% of buildings), then this displaced a functional floor (commercial or residential) thereby preserving building height.

The resulting capacity (in terms of area) of the of the precinct is shown in Table 12.1. Capacities were calculated in terms of gross floor area (no allowance for building efficiency), however were also interpreted in terms of number of carparks (assuming 32m^2 per carpark); number of dwellings (assuming 98m^2 per dwelling); and, in terms of number of residents (assuming 2.2 people per dwelling). All derived functions were rounded to the nearest integer at the building level.

Table 12.1. Capacity of the Base Scenario.

		Floor area by use (m^2)				
		Commercial	Residential	Carpark (above ground)	Carpark (basement)	Grand Total
Building Type	Commercial Tower	376,977	0	0	14,928	391,905
	Residential Tower	0	607,560	13,452	95,570	716,582
	Commercial Tower on Podium	87,119	0	0	0	87,119
	Residential Tower on Podium	0	619,641	0	0	619,641
	Podium	561,098	0	0	124,763	685,861
	Total	1,025,194	1,227,201	13,452	235,261	**2,501,108**
	No of carparks (32 m^2 each)	*NA*	*NA*	*420*	*7,352*	*7,772*
	No of dwellings (98 m^2 each)	*NA*	*12,522*	*NA*	*NA*	*12,522*
	No of residents (2.2 per dwelling)	*NA*	*27,549*	*NA*	*NA*	*27,549*
	Functional Floor Area (m^2 FFA)	*1,025,194*	*1,227,201*	*NA*	*NA*	***2,252,395***

Across the Base Scenario there were 167 stand-alone buildings (Albion Quarter: 81, Sunshine Station: 19, Town Centre: 67) of which the median height was 24 m and the median gross floor area was 11946 m² (overall). The distribution of floor area by stand-alone building is shown in Figure 12.2 broken down by sub-precinct.

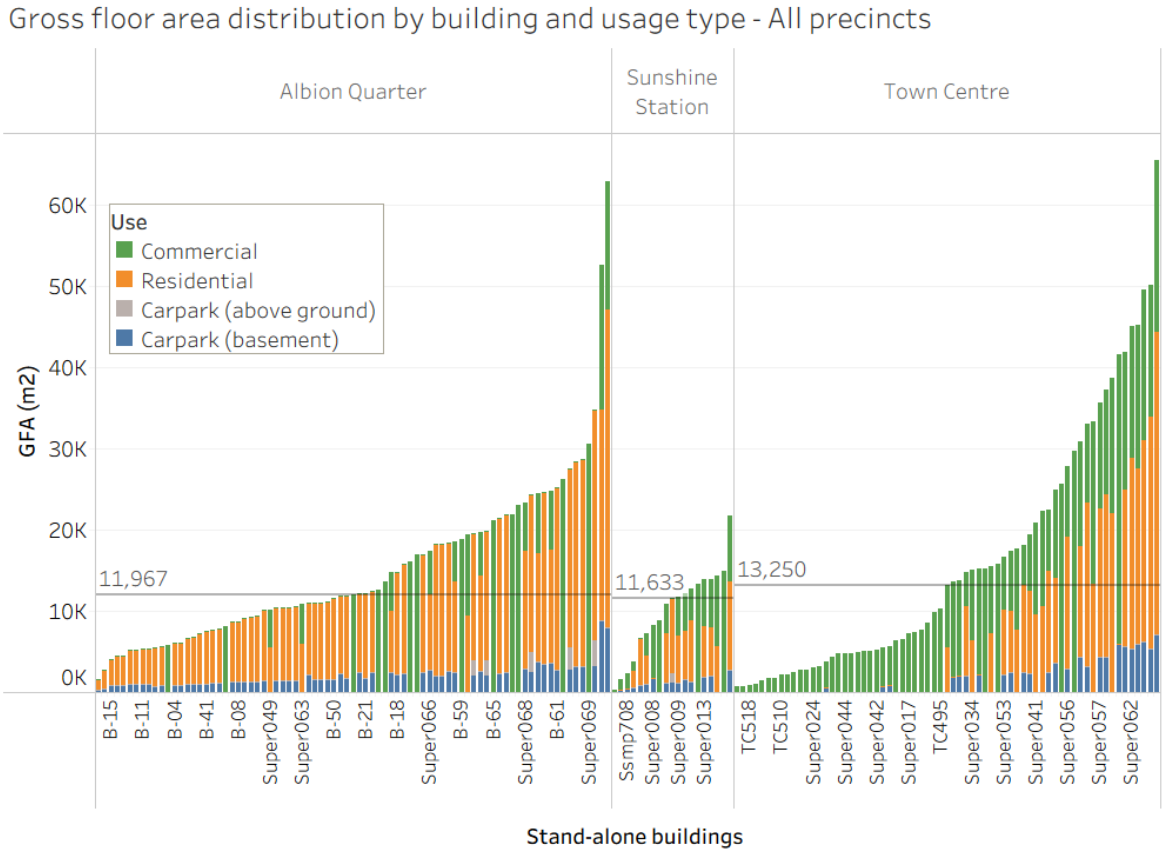

Figure 12.2. Distribution of floor area use type by stand-alone building across all sub-precincts of the Base Scenario. Median building floor area is shown as a line.

12.2.2 Updated scenario

Where possible, the same data processing approach was employed for the Base and Updated precinct designs, although some changes were needed. A challenge of this stage of the analysis was a change in the data structure of the design which moved from describing buildings in terms of footprints with floors of varying function, to describing buildings in terms of footprints with floors of uniform function (i.e. car parking; residential, commercial) that were stacked vertically. The change was made as planners began to consider 'sleeved' development envelopes that sought to minimise exposed carparking buildings along street frontage. This subtle change altered the way analysis had to be undertaken and limited the exploration of alternatives such as basements. Figure 12.3 illustrates the difference in the way building functions were specified between the Base and Updated Scenario as well as the difference in design approach adopted for the Updated Scenario (larger buildings that are taller). In addition, the scope of the Updated Scenario only considered the Albion Quarter sub-precinct (excluding Town Centre and Sunshine Station).

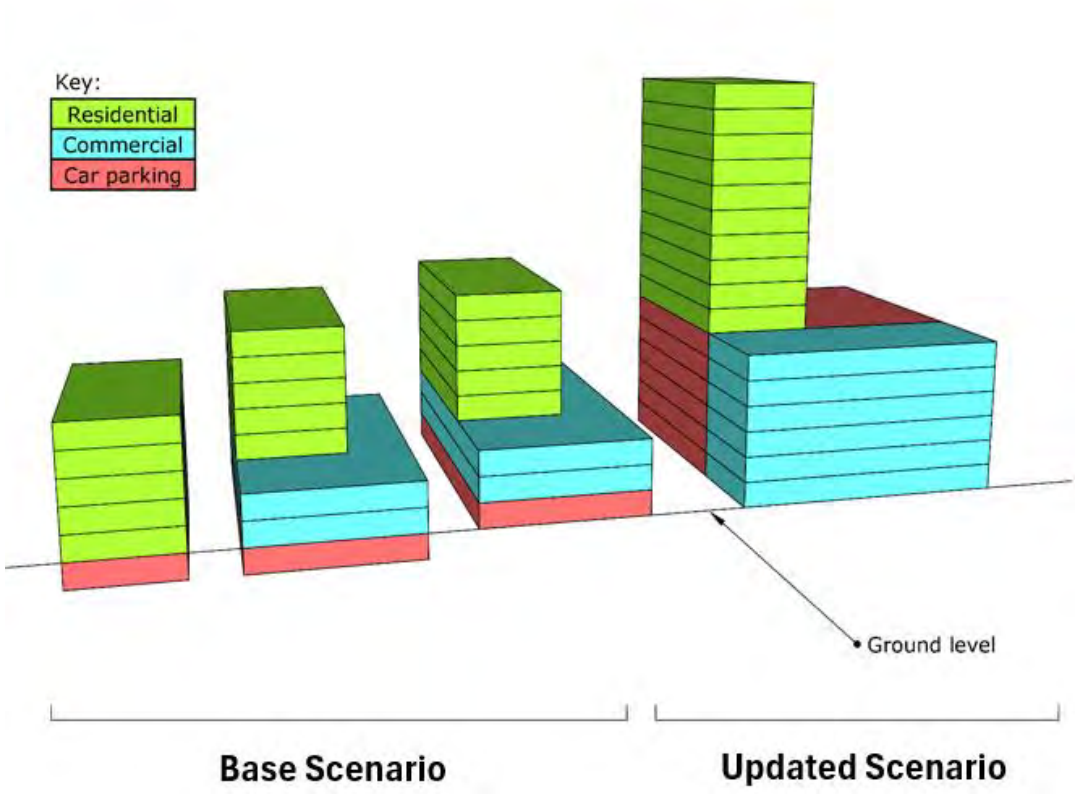

Figure 12.3. Precinct design data structures and building design differences.

As a result of the above differences, analysis of alternative construction and other scenarios was largely completed using the Base Scenario to describe precinct form. Analysis of the Updated Scenario was limited to the consideration of alternative construction approaches of the form as described and did not consider the impact of basements (basement levels were not considered for the Updated Scenario as they had been addressed in the Base Scenario analysis and we considered an unlikely approach given soil

conditions at the site). A detailed description of the scenarios analysed and the precinct designs used is described in Section 12.3.1.

A comparison of the capacity of the Base Scenario with the Updated Scenario is shown in Table 12.2. The table shows an increase in the GFA of the Updated Scenario of 64% over the Base Scenario which is substantially greater than the FFA increase of 28%, indicating a substantial increase in parking area in the Updated Scenario (the number of carparks increased by 300% over the Base design).

Table 12.2. Capacity of the Base Scenario compared to the Updated Scenario for the Albion Quarter.

		Base Scenario - Albion Quarter Floor area by use (m^2)				
		Commercial	Residential	Carpark (above ground)	Carpark (basement)	Grand Total
Building Type	Commercial Tower	174,239	0	0	0	174,239
	Residential Tower	0	592,365	12,289	93,565	698,219
	Commercial Tower on Podium	22,564	0	0	0	22,564
	Residential Tower on Podium	0	167,622	0	0	167,622
	Podium	123,882	0	0	37,255	161,137
	Total	320,685	759,987	12,289	130,820	**1,223,781**
	No of carparks (32 m^2 each)	*NA*	*NA*	*384*	*4,088*	*4,472*
	No of dwellings (98 m^2 each)	*NA*	*7,755*	*NA*	*NA*	*7,755*
	No of residents (2.2 per dwelling)	*NA*	*17,061*	*NA*	*NA*	*17,061*
	Functional Floor Area (m^2 FFA)	*320,685*	*759,987*	*NA*	*NA*	***1,080,672***

		Updated Scenario - Albion Quarter Floor area by use (m^2)				
		Commercial	Residential	Carpark (above ground)	Carpark (basement)	Grand Total
Building Type	Commercial Tower on Podium	301,433	0	0	0	301,433
	Residential Tower on Podium	0	648,675	0	0	648,675
	Commercial Podium	275,443	0	0	0	275,443
	Residential Podium	0	155,210	0	0	155,210
	Parking Podium	0	0	621,698	0	621,698
	Total	576,876	803,885	621,698	0	**2,002,459**
	No of carparks (32 m^2 each)	*NA*	*NA*	*19,428*	*0*	*19,428*
	No of dwellings (98 m^2 each)	*NA*	*8,203*	*NA*	*NA*	*8,203*
	No of residents (2.2 per dwelling)	*NA*	*18,046*	*NA*	*NA*	*18,046*
	Functional Floor Area (m^2 FFA)	*576,876*	*803,885*	*NA*	*NA*	***1,380,761***

Under the Updated Scenario, building floor areas were seen to increase across the Albion Quarter, where such increases were generally achieved by increased building height as shown in Figure 12.4. Median floor area for the Albion Quarter was seen to increase from 11,967 m2 to 24,476 m2, an increase of 105% over the Base Scenario. Median building heights were also seen to increase significantly from 24 m to 66 m, an increase of 175%. The changes seen in the Updated Scenario maintain roughly the same residential floor area as the Base Scenario (6% increase) however commercial (80% increase) and carparking (334% increase) were increased significantly.

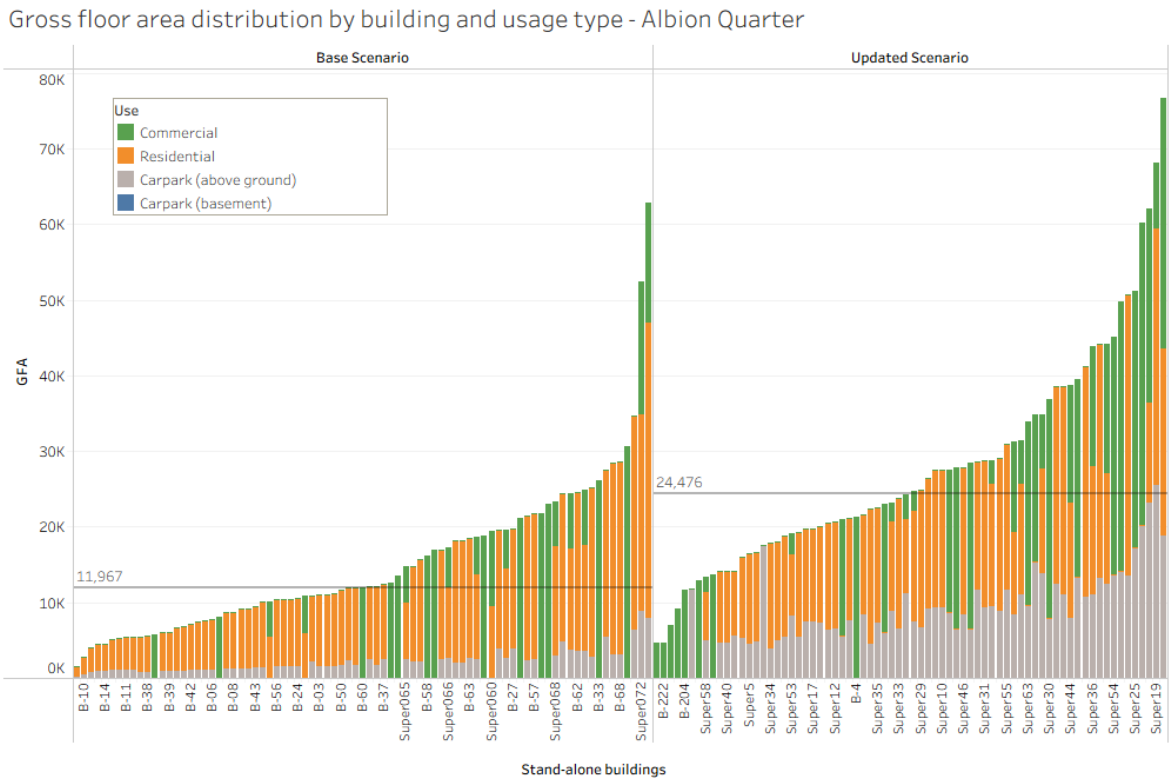

Figure 12.4. Distribution of floor area usage type by stand-alone building across the Albion Quarter. Distribution of the Base is compared to the Updated Scenario, showing median building floor area as a line.

12.2.3 Functional unit

In order to assess the efficiency of the precinct and to enable comparability, a functional unit was identified in a manner consistent with that employed in life cycle assessment. In life cycle assessment the functional unit can be defined as:

> "The functional unit defines the quantification of the identified functions (performance characteristics) of the product. The primary purpose of a functional unit is to provide a reference to which the inputs and outputs are related. This reference is necessary to ensure comparability of LCA results. Comparability of LCA results is particularly critical when different systems are being assessed, to ensure that such comparisons are made on a common basis. It is important to determine the reference flow in each product system, in order to fulfil the intended function, i.e. the amount of products needed to fulfil the function." (ISO 14040 2006)

All buildings within the scope arguably provide for multiple functions. If the functional composition of buildings being compared is identical it can be argued that the systems that support the building life cycle can be reasonably compared. For example: Two buildings are compared with the same footprint area, a single floor of carparking and two floors of commercial space. One building is made from steel and the other from concrete. The two can be compared because their functional floor areas are identical (the material system does not impact their function). In this case the comparison is a fair one because the function provided by the buildings is equivalent. Alternatively: Two buildings of identical footprint area with differing function are compared. One building is made from steel and the other from concrete. One

building has two floors of carparking and one floor of commercial space. The second building has one floor of carparking and one floor of commercial space. In an absolute sense, the second building is smaller than the first, so provides less absolute function. The buildings are not functionally comparable in absolute terms. Even if results are normalised by dividing by the floor area, there is still a functional discrepancy as each building provides a different ratio of commercial to carparking space.

In addition to ensuring functional equivalence when drawing comparisons, it was important to consider the probable impact of building scale on normalised results. This problem comes about because the ratio of total floor area to foundation/roof/wall area typically reduces as a building gets larger. While a larger building will always have a larger carbon footprint in an absolute sense, it typically has a smaller normalised carbon impact (the impact per m^2 floor area). It is therefore problematic to compare the impact of material or construction method changes between large and small buildings as it is difficult to isolate the effect of materials versus the scale effect described above. Such comparisons require both functional AND scale equivalence.

In this research the function of the precinct was defined in terms of the primary functions provided by the precinct – commercial and housing gross floor area (the Functional Floor Area FFA). The resultant functional unit was defined as:

> **Functional unit: Provision of one (1) square meter of functional floor area (commercial and residential) and associated personal transport.**

While the above functional unit facilitated the comparison of various construction strategies within the precinct, it did not enable comparison to other studies of the climate impact of buildings. Such studies typically employ a reference unit (as opposed to functional unit) based on the gross floor area (GFA) provided by the building. To enable the study of the precinct to be compared to other studies of buildings, the following reference unit of climate impact was also assessed:

> **Reference unit: Provision of one (1) square meter of gross floor area (commercial, residential and carparking).**

The reference unit approach was consistent with standards, such as the Whole of Life Carbon Assessment (RICS 2017) which employs a reference unit of 1 m2 of net internal area (NIA)[10], provided for life of building (60 years).

12.2.4 Is car parking a function or is it a burden?

A challenge when considering the carbon footprint of a building or precinct is the treatment of carparking. Carparking may be considered as a useful function by a person purchasing an apartment or commercial office. The car space provides the owner with the ability to store, and perhaps charge, a car on site. In this case, carparking is a form of unique building function that must be considered when drawing comparisons between buildings and precincts (i.e. compared systems must deliver the same quantum of carparking area).

[10] Building areas in this study were coarsely defined. GFA and NIA were assumed to be equivalent.

Alternately, a car park could be viewed as part of a transportation system, in which case a viable substitute for that function would be the provision of public transport. In this case, transport is the function which is provided by the building/precinct system within which carparking is an enabling element. In this case, transport can also be provided by a system which uses public transport and no carparking. The comparison is fair provided the transport function is equivalent.

While both approaches can be argued it is difficult to argue that carparking is not a part of the personal transport system (except for those that attribute value to cars and carparking intrinsically). It therefore reasonable to compare equivalent transport options for a building or precinct, albeit a potentially challenging task, to establish this equivalency. Importantly, when such comparisons are drawn carparking must be viewed as a burden of the transport system and not considered an aspect of building precinct function. In other words, the systems compared must deliver equivalent transport functionality, regardless of carparking area. As a consequence of this, carparking area should not be considered during normalisation. Instead, the functional floor area (FFA) should be employed.

FFA in this study included the primary functions of buildings such as commercial floor area and residential floor area. Unlike GFA, results using FFA are not readily compared to other carbon footprint studies. Hence the use of the FFA as the basis of the functional unit used in this study and the presentation of GFA for comparative reference.

12.2.5 System Boundary

The scope of analysis was defined using the terms described by EN15978 (2011) 'Sustainability of Construction Works - Assessment of Environmental Performance of Buildings - Calculation Method' which defines the building life cycle in terms of the stages shown in Figure 12.5. Using these stages, RICS (2017) define, embodied carbon of a building as including the climate impact associated with producing materials needed to build a building (A1-3), construction of the a building (A4-5), maintenance of the building (B1-5) and disposal of materials at the end of the building's life (C1-4), shown in the green box in Figure 12.5. In this study, this scope was modified to simplify analysis by excluding maintenance and repair systems (B1-5) and is shown in the orange boxes in Figure 12.5.

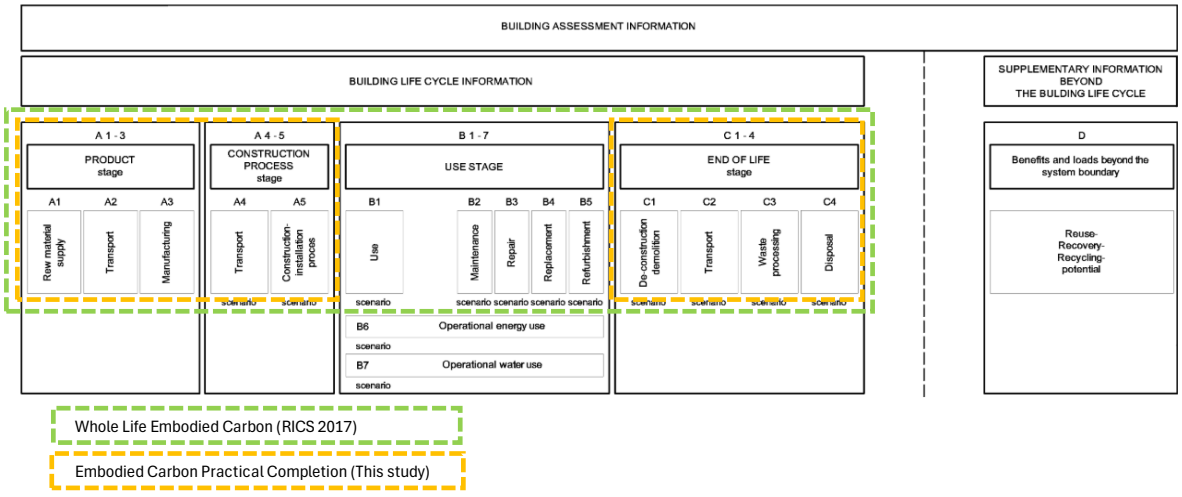

Figure 12.5. Building life cycle stages described by EN 15978 (2011). Stages included in the embodied carbon definition are shown within the dashed boxes.

The modification to the RICS (2017) Whole Life Embodied Carbon was made to remove an area of significant uncertainty from the analysis as it was difficult to find good evidence to support repair and replacements for the materials considered. It was also felt to be a reasonable modification as it retained the important Product (A) and End of Life (C) stages associated with materials and construction (it is important that both stages are considered when assessing impacts of biogenic materials as discussed in Section 12.3.4). The resulting boundary was referred to as Embodied Carbon to Practical Completion (ECPC) and reflects the impact of constructing the precinct and disposing of the materials introduced during initial construction (shown in orange in Figure 12.6). ECPC excludes operation and maintenance impacts (Stage B).

While this standardised approach based on EN15978 (above) provided a sound basis for describing the scope of a building system in isolation it did not handle some of the functionality provided by a precinct, such as transportation. When considering precincts, the standardised approach is silent regarding transport systems so an expanded system boundary was considered as shown in Figure 12.6.

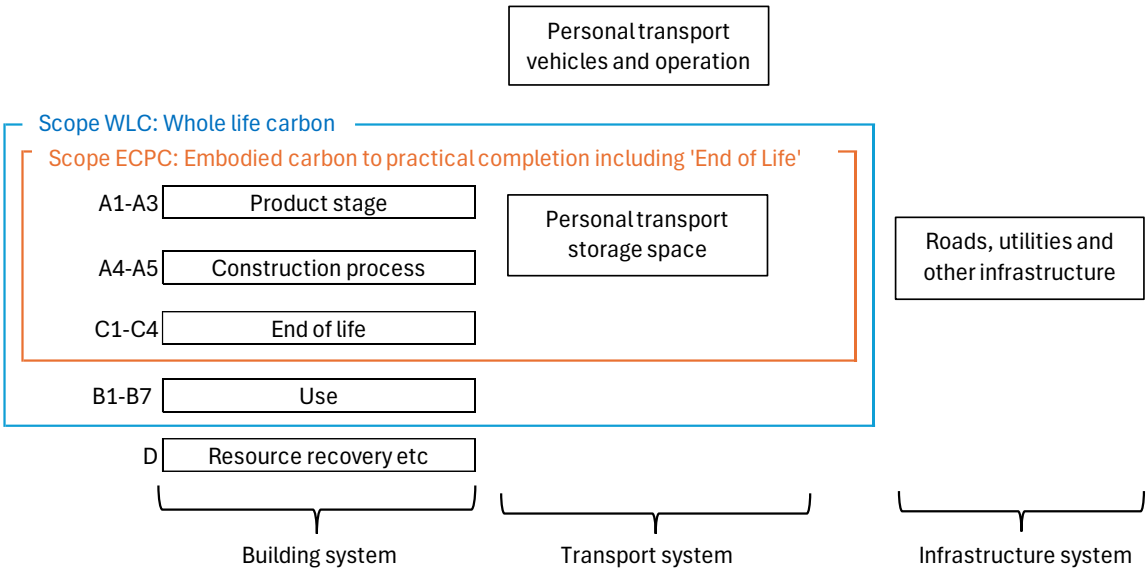

Figure 12.6. System boundaries appropriate to the precinct (rather than building). Whole Life Carbon (WLC) scope is shown in blue and Embodied Carbon to Practical Completion (ECPC) in orange.

Combining a consideration of buildings and transportation, the system boundary diagram presented in Figure 12.6 illustrates the main systems considered by the study scope and draws boundaries around the process groups considered in each scope. Importantly the diagram also indicates the system elements that were not considered by the study such as personal transport vehicles and the precinct infrastructure. Personal transportation vehicles were excluded from consideration due to difficulties in understanding these systems which separate from the precinct planning process which is primarily concerned with space allocation (particularly private transport). The decision to exclude precinct infrastructure was made for more practical reasons as it was thought the impacts of these systems would be too difficult to meaningfully qualify within the resources allocated. Arguably, this aspect should be included within scope in future studies as data and methods become easier to access and implement.

The assessment of the precinct embodied carbon employed the ECPC scope for most calculations except the life cycle assessment completed in Section 4.2.2, which employed the Whole Life Carbon (WLC) scope (shown in blue in Figure 12.6).

12.3 Methodology

The embodied carbon of the precinct was estimated using a parametric approach. Inputs were gathered from the project data provided (the precinct GIS model and the capacity model spreadsheet) and necessary supporting data which included models of building elements by material and environmental product disclosures (EPDs) for the materials considered. These inputs where employed in a parametric model to estimate the material quantities used in the precinct and their associated climate change impacts. The parametric model assessed material quantity, area and embodied carbon at the building level, by building element and life cycle stage for both the functional unit (m^2 FFA) and the reference unit (m^2 GFA). Outputs from the model were then published back to the originating GIS model for spatial representation, and to the data science tool Tableau, for visualisation. A pictograph of the process is shown in Figure 12.7.

A key stage of the process involved the development of a database of element models from existing building carbon assessment studies. Element models were developed to relate the material quantities employed in building elements (such as external walls, roofs, upper floors, foundations, windows etc.) to fundamental building parameters derived from the GIS and capacity models (such as external wall area, roof area, number of upper floors etc.) of the precinct. To create these models, existing studies of buildings were employed that were sufficiently transparent to allow material quantities to be related to building elements. These studies included Carre and Crossin (2015) and Durlinger et al. (2013) from which adapted parametric models of building elements were developed.

Using the basic parameters from the GIS model of the precinct and the capacity model the element models were adjusted linearly to suit a simple cubic geometry for each building. The most important parameters employed included the building footprint perimeter, footprint area and height, from which a façade area, floor area (for all storeys), roof areas and foundation areas could be calculated. Using these areas in combination with the database of element models it was possible to estimate material quantities for all buildings in the precinct, as shown in Figure 12.7.

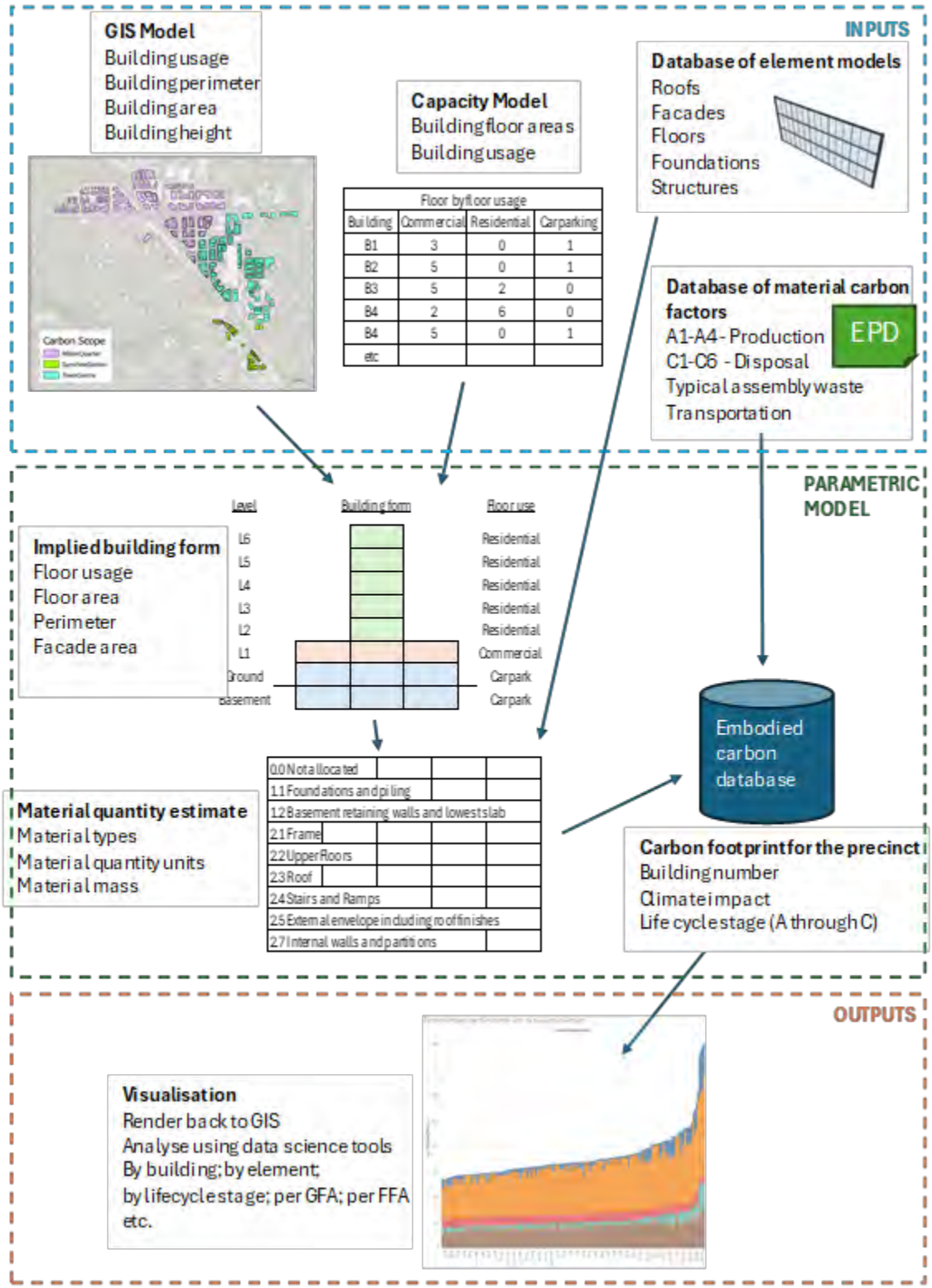

Figure 12.7. Embodied carbon calculation method.

The calculation of climate impacts from material quantities was completed by using carbon factors extracted from published EPD's for materials commonly available in Australia and specialised datasets for transportation and construction (Table 12.3). The approach was adopted because it was relatively simple to apply as all calculations are linear and because it is transparent (it is easy to see where factors have

come from). A limitation of the approach was that it involved bringing together carbon factors that have been calculated using a range of impact assessment methods from datasets with varying degrees of completeness, across a range of timeframes. While these issues limit definitive conclusions being drawn at a building-by-building level, they were thought to provide reasonable estimates at a precinct scale, particularly where various precinct options were being considered. Alternative approaches such as the use of generic Australian datasets (e.g. EPiC) were also considered, however transparency regarding factors from such databases was considered a drawback as well as the limited scope to explore alternative material options. Indeed, by employing EPD's for most carbon data, the method employed was considered consistent with other building assessment tools such as NABERS Embodied Carbon (NABERS 2025).

Table 12.3. Sample database of material and construction carbon factors employed.

			Carbon factors per lifecycle stage (kg CO2e per unit)					
Material Name	**Location**	**Unit**	**A1toA3 Fossil**	**A1toA3 Biogenic**	**A4**	**A5**	**C1toC4**	**Source**
Concrete 40 Mpa	Australia	m3	387	0	8.6	20.2	17.3	In most cases EPD's were used for life cycle stages A1toA3 exclusively. For stages A4 additional transport factors were employed from a range of sources based on typical inbound transport assumptions. Stage A5 employed typical waste rate assumptions by material combined with production impacts from A1toA3. Lastly, stage C1toC4 employed carbon factors from EPD's as well transportation assumptions to disposal. Transport factors were drived from the AusLCI 1.42EF database and EcoInvent (using CML3.11).
Reinforcing and structural steel	Australia	kg	1.7	0	0	0.1	0	
Plasterboard 16mm	Australia	m2	2.5	0	0	0.3	0.4	
Glasswool 215mm	Australia	m2	3.3	0	0	0.2	0	
Double glazing unit	USA	m2	59	0	5.7	0	0.1	
Aluminium section	Australia	kg	9.1	0	0	-0.2	0	
Galvanised steel section	Australia	kg	5.5	0	0	0.2	0	
Phenolic foam panel 90mm	Australia	m2	13.3	0	0	1.3	0.1	
Polymer render	Greece	kg	0.1	0	0.2	0	0	
Cross laminated timber	Australia	m3	248	-740	27.6	-20.3	59	
Softwood timber	Australia	m3	157	-875	49.6	-30.5	59.6	
Laminated veneer lumber	New Zealand	m3	144	-941	17.7	-36	59	
Calcium silicate sheet	Germany	m2	8.7	0	2	1	0	
Magnesium oxide board	USA	m2	51	0	3.5	5.5	0.1	
Aluminium façade panel 4mm	Japan	m2	50.6	0	0.9	-0.3	0.1	
Construction site factors								
Construction Concrete	Australia	m2	0	0	0	27	0	Derived from Sandanayake et al (2017)
Construction Timber	Australia	m2	0	0	0	18.4	0	Concrete scaled according to Huang (2024)
Excavation	Australia	m3	0	0	0	21.2	0	Derived from Sandanayake et al (2017)

Lastly, the resultant database of carbon footprints by building, lifecycle stage and building element was analysed using graphical techniques drawn from data science and by publishing data back to the original spatial GIS model. Given the scale of the precinct, graphical methods such as those supported by the software Tableau Desktop were found to be useful for extracting results while also ensuring internal dataset consistency and transparency. Complementing the analysis, the results were also embedded back into the original spatial model, allowing interested parties to undertake analysis within a GIS structure and potentially in a more widely available online spatial dataset.

12.3.1 Scenarios considered

The embodied carbon assessment employed the parametric model above to consider 12 different ways of providing the functional unit of the precinct that were distinguished by changes to precinct design, changes to built form, changes to carparking and changes to materials used to construct the buildings of the precinct. Two (2) precinct design scenarios, the Base Scenario and the Updated Scenario (explained in Section 12.2) were considered. In addition, two (2) built form alternatives were considered a) using buildings with basement carparking, and b) using buildings with upper floor carparking. The form alternatives were intended to consider the implications of basement excavation and construction versus

upper level carparking provision. Two (2) carparking alternatives were also considered that incorporated a) 100% of planned carparking, and b) no carparking. These alternatives were intended to consider the implications of reduced carparking provision in the event public transportation services could be enhanced to provide these services. Lastly, three (3) construction materials combination alternatives were considered that employed different methods of construction for the buildings in the precinct. The 'Typical' alternative assumed buildings reinforced concrete, steel and glass; the 'Best efforts' alternative assumed the same materials as Typical were employed, however efforts to choose low-carbon versions of materials were employed (informed by EPDs); and finally, the 'Low carbon' alternative assumed that light-weight and mass-timber construction materials were employed (complimented by traditional materials where necessary).

In the 'Low Carbon' materials scenario, light-weight timber structural systems were assumed for residential towers of six (6) floors or fewer, while mass-timber construction was adopted for residential towers exceeding six (6) floors. Commercial towers and podiums maintained the conventional concrete structural systems as described in the Base case. Light-weight timber structures consist of studs, joists, and rafters, combined with typical plasterboard linings for slabs and walls. These systems are well suited for buildings with shorter spans, where structural loads can be effectively transferred through core masonry walls at lift shafts. In contrast, mass-timber structures utilize engineered wood components such as cross-laminated timber (CLT), glued laminated timber (Glulam), and laminated veneer lumber (LVL), enabling support for higher loads and longer spans.

A summary of the alternatives considered is presented in Table 12.4, illustrating the focus on analysis of the Base Scenario under various form, carparking and materials assumptions. The Updated Scenario analysis was limited to changes in materials options. This approach was adopted as it was felt the main benefit of the Updated Scenario analysis was to assess how a planning approach that encouraged larger, taller buildings would impact upon embodied carbon outcomes. Table 12.4 also identifies the scenario names used throughout the report.

Table 12.4. Scenarios considered. Scenario names used throughout the report are noted in bold.

Precinct Design	Precinct considered	Building Form	Car parking*	Materials		
				Typical	Best efforts	Low carbon
Base	Albion Quarter, Town Centre & Sunshine Station	Basement	100%	**B-T (Base case)**	**B-BE**	**B-LC**
		No Basement	100%	**NoB-T**	**NoB-BE**	**NoB-LC**
		No Basement	0%	**NoB-T-CP0**	**NoB-BE-CP0**	**NoB-LC-CP0**
Updated	Albion Quarter	No Basement	100%	**Upd-NoB-T**	**Upd-NoB-BE**	**Upd-NoB-LC**

* Carparking measured as proportion of functional capacity

12.3.2 Validation of parametric estimates of material quantities

Quantity model validation was undertaken in two (2) stages. Firstly, material quantities for concrete and reinforcing steel that were calculated by the parametric model were compared to manual estimates developed from detailed structural designs and quantity surveyor estimates for eight (8) buildings in the precinct (the QS estimates). Secondly, material quantity estimates from the model for a mass-timber and lightweight building example were compared to literature examples of similar scale buildings.

Stage 1 – QS Estimates vs parametric model

In order to complete the QS estimates of material quantities, structural designs were developed for eight (8) buildings in the precinct by a structural engineer (example shown in Figure 12.8) from which building quantities were estimated.

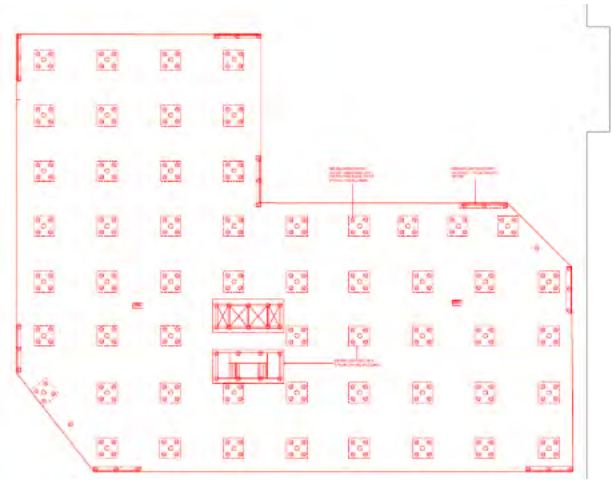

Figure 12.8. Example footing layout for a commercial building in the Base Scenario precinct.

Material quantity estimates generated for the selected buildings using the parametric model were compared to material quantity estimates manually calculated by the QS. After an initial round of adjustments, required to improve consistently between manual and parametric model outcomes, the results of both approaches were compared for the major (largest contribution by mass) materials of concrete and steel, as shown in Figure 12.9. These results showed that for the seven (7) buildings selected from the Base Scenario (covering a range of sizes and primary functions) the parametric model estimated material quantities between 88% and 113% of QS estimate. Given that the QS estimate had the advantage of a detailed structural design to work from, these results were considered reasonable given the broader context of uncertainty associated with the precinct's development. Results were not as good for the Updated Scenario which employed fewer but larger buildings to achieve the FFA.

For the Updated Scenario, the parametric model was found to be less accurate, underestimating material quantities derived from the detailed design (the QS estimate was approximately 150% of the parametric model estimate). A review of the estimate showed that the parametric model did not adequately allow for the foundations, slab thickening and other structural changes needed to support the larger (and taller) buildings of the Updated Scenario. This result indicated that carbon footprint results for the Updated Scenario were likely to be underestimated.

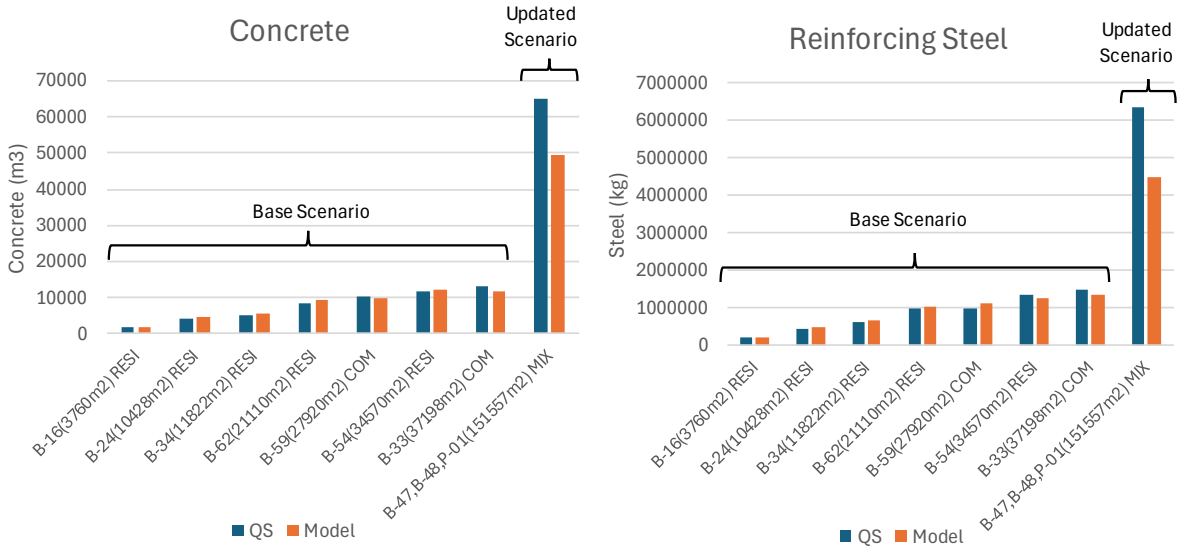

Figure 12.9. Validation of material quantity estimates. 'QS' - Signifies a manual estimate developed by a quantity surveyor based on an engineer's schematic diagram. 'Model' – Signifies an estimate developed by the parametric model using basic building parameter inputs. Base design buildings were generally smaller than the **Updated Scenario** buildings.

It was not possible to test the low carbon approaches using the approach employed in Figure 12.7 for the 'Low Carbon' material scenarios because expertise regarding structural design and quantity estimation could not be found. Instead, literature was used to sense check material quantities for these designs by comparing buildings from the precinct to life cycle assessment reports as follows:

- Light weight construction approach: Carre, A. and E. Crossin (2015). A comparative Life Cycle Assessment of Two Multi Storey Residential Apartment Buildings. Melbourne, Forest and Wood Products Australia.
- Mass timber construction approach: Durlinger, B., et al. (2013). Life Cycle Assessment of a cross laminated timber building. Melbourne, Forest and Wood Products Australia.

A single building from the precinct was compared to the buildings considered in the studies above and the material quantities per square meter (GFA) compared.

Table 12.5 shows the result of the materials comparisons, highlighting the areas where large discrepancies existed between this study and the reference cases considered. While it was not possible to reconcile exactly why these discrepancies existed the result served to highlight that the 'Low Carbon' approaches involve a higher degree of uncertainty than the 'Typical' approaches considered.

Table 12.5. Material quantities per unit area (GFA) compared for selected study buildings and reference buildings. Significant variations in material quantities are highlighted.

	Building 24 (this study) compared to Carre & Crossin 2015 (reference)			Building 70 (this study) compared to Durlinger, Crossing & Wong 2013 (reference)		
	This study	Reference building	Percentage of reference	This study	Reference building	Percentage of reference
Building type	Residential	Residential	NA	Residential & Commercial	Residential	NA
No of floors	5 residential, 1 car park	6 residential, 1 car park		6 residential, 3 commercial, 1 car park	9 residential, 1 commercial	
Building area (m2 GFA)	5315	9022		10876	2431	
Concrete (m3/m2 GFA)	0.2	0.1	233%	0.3	0.3	104%
Steel reinf (kg/m2 GFA)	34.5	9.5	362%	29.3	34.2	86%
Glazing (m2/m2 GFA)	0.1	0.2	61%	0.3	0.0	520%
Kooltherm panel (m2/m2 GFA)	0.1	0.3	53%	NA	NA	NA
Plaster (m2/m2 GFA)	1.5	3.0	51%	4.5	5.5	82%
Cement/MgO Boards (m2/m2 GFA)	1.7	2.4	74%	NA	NA	NA
Wood (m3/m2 GFA)	0.1	0.1	134%	0.3	0.4	88%

12.3.3 Limitations and exclusions

The approach adopted aimed to quantify the carbon footprint of a built form that was not fully defined. While anticipated development footprints and usage types provided an indication of the final form, details regarding these buildings had to be assumed. Furthermore, the scale of the assessment required that certain aspects of building life be excluded from consideration due to complexity. Key exclusions from the analysis were as follows:

- Interior fitout
- Infrastructure including roads, water supply, sewerage, energy supply, energy generation, transport systems
- Private transport vehicles
- Building operation, maintenance and refurbishment (Section B of the life cycle)
- Resource recovery at the end of building life (Section D of the life cycle)

Lastly, the model validation activity showed that the parametric material quantity model was best suited to estimating quantities in the smaller (up to 37198 m^2) buildings seen in the Base Scenario, however tended to underestimate quantities in the larger buildings seen in the Updated Scenario (151557 m^2). Carbon footprints are therefore likely to be underestimated in the Updated Scenario.

12.3.4 Treatment of biogenic carbon

Biogenic carbon refers to the carbon absorbed and emitted by natural products, such as wood, over their life cycle.

> "Biogenic carbon emissions Carbon released as carbon dioxide or methane from combustion or decomposition of biomass or biobased products." (IPCC 2022:1795)

If sustainably produced, such products absorb CO_2 from the atmosphere during the Stage A - production stage of life (e.g. as trees are planted and grow as part of forestry practice). This absorbed carbon is then stored in the materials (e.g. wood products) built into the building for the life of the building. At the end of the building life, Stage C, the biogenic carbon that is stored in materials will be partially or completely released back to the environment, depending on how the materials are disposed of (e.g. repurposed, incinerated, composted or placed in landfill).

Biogenic carbon is considered distinct from fossil carbon because it is related to the natural carbon cycle of life, whereas fossil carbon emissions are considered to contribute entirely to global warming due to human activity. In LCA, there has been a tradition of simplifying analysis using the '0/0 approach' whereby biogenic carbon flows were considered neutral over time, provided absorptions and emissions relate to the gas CO_2. This has meant that traditional analysis would only focus on instances where absorbed CO_2 is converted into a higher potential emission gas, such as CH_4 (e.g. methane generation in landfill. Biogenic methane has 28 times the global warming potential (GWP) of CO_2 (DCCEEW (2024)), ignoring the absorption and emission of CO_2 which would be assumed to offset one another over the lifetime considered when assessing global warming impacts (typically 100 years). In other words, biogenic carbon was typically considered part of a natural cycle and therefore ignored by the analysis, except where a change in GWP occurred.

An alternative to the '0/0 approach' described above is the '-1/+1 approach' whereby biogenic carbon flows are explicitly considered in the climate impact calculation. Using this approach, biogenic carbon absorption is counted during Stage A - production (e.g. the sustainable growing of trees) and emission of biogenic carbon, including conversion to CH_4 (biogenic methane), is counted at the Stage C - end of life. As the '-1/+1' suggests, the absorption of biogenic carbon is counted as a negative emission and the release of biogenic carbon is counted as a positive emission. Importantly, the net climate change impacts under the '-1/+1 approach' are very different depending on how the disposal method employed for the biogenic material.

Differences in climate impact occur under '-1/+1 approach' versus the '0/0 approach' because biogenic carbon is known to be sequestered in landfill (O'Dwyer et al. 2018; Ximenes et al. 2015). While the '0/0 approach' is an appropriate approach when biogenic materials are composted or burned at the end of their lives, it is not appropriate when material is disposed of to landfill – the most likely fate for biogenic construction waste in Australia (FWPA 2022; Hyder Consulting 2011; Taylor and Warnken 2008). The notion of carbon sequestration is not considered under the '0/0 approach' because all carbon is assumed to return to the atmosphere at some stage, despite good evidence that this is not the case when material is disposed of to landfill. For this reason, the '-1/+1 approach' is considered more appropriate in the Australian context and can be practically achieved using the EPD disclosures which report Stage A absorptions and Stage C emissions for biogenic materials.

A further assumption made regarding the treatment of biogenic carbon, in wood predominantly, was to adopt a the Stage C emission profile for wood products based on recent publications regarding the composition of wood in landfill, as recommended in the wood products EPD (FWPA 2022). This recommendation adopts a wood decomposition profile based on laboratory research undertaken by Wang et al. (2011) which assumes a larger quantity of biogenic carbon is stored in landfill than is currently assumed by DCCEEW (2025). As a result of this approach, the net impact of wood products across Stage A and C of life is substantially negative as biogenic carbon is absorbed and stored in the building and ultimately in landfill over a 100-year period. Underpinning this assumption is the equally important assumption that all wood used in the project comes from sustainable forestry sources (plantations; replanting occurs after harvest; only softwood varieties are considered).

12.4 Detailed results

12.4.1 Material quantity results

Material quantity estimates generated by the parametric model, were seen to be dominated by concrete and steel across the scenarios considered (

Table 12.6). Under the B-T scenario, concrete was seen to comprise 94.2% of total precinct mass and steel 4.2% (all other materials were less than 1.6% of mass). Importantly, these materials were also seen to dominate the mass of the B-LC scenario which incorporated mass timber and light-weight buildings because even these buildings employ concrete and steel in foundations, podiums (if present) and other structural elements. For the B-LC scenario, concrete was seen to contribute 78.6% and steel 3.8% of total precinct mass (

Table 12.6). This result demonstrated that even when efforts were made to reduce the climate impacts under the B-LC scenario, concrete and steel still dominated total material mass.

Material intensity (mass per floor area) was seen to vary between scenarios particularly when considering FFA. As FFA does not include the carpark area, the mass associated with carparking construction materials must be carried by the FFA. This is most significant when comparing a scenario with no carparking, such as NoB-T-CP0 (926 kg/m^2 FFA) to one with a large carparking allocation, such as Upd-NoB-T (1493 kg/m^2 FFA), whereby Upd-NoB-T is 567 kg/m^2 (FFA) heavier. While a number of factors lead

to the increased material intensity of Upd-NoB-T, it is the carparking allocation that drives the bulk of the difference in material intensity. When a traditional approach to measuring building functional area is employed that counts carparking area the difference between these scenarios falls to 104 kg/m² (GFA). This smaller difference is due to the difference in the mix of buildings (commercial, residential, podium) and the shapes of the buildings in the two scenarios. As discussed in Section 12.3.2, the parametric model was found to underestimate material quantities for the larger buildings in the Updated Scenario, so this difference would be expected to be a minimum.

Differences in material intensity attributable to changes in material make-up are not as significant as might be expected. Low carbon design scenarios were seen to reduce the material mass from 1076 kg/m² (FFA) for the B-T scenario to 936 kg/m² (FFA) for the B-LC scenario, a reduction of 140 kg/m² (FFA) or 13% (

Table 12.6). **The reduction comes about as concrete and steel in the structure and façade are replaced with wood and other light-weight façade materials. Even in the low carbon scenarios, steel and concrete are still required for foundations and other structural elements, limiting the reduction in mass achievable.**

Table 12.6. Material quantity assessment by scenario.

		Material Mass (tonnes and % of total)											
	Scenario Name	**B-T**	**B-BE**	**B-LC**	**NoB-T**	**NoB-BE**	**NoB-LC**	**NoB-T-CP0**	**NoB-BE-CP0**	**NoB-LC-CP0**	**Upd-NoB-T**	**Upd-NoB-BE**	**Upd-NoB-LC**
	Precinct design	Base	Base	Base	Base	Base	Base	Base	Base	Base	Updated	Updated	Updated
	Precincts considered	Albion Qtr. Town Cen. Sun. Station	Albion Qtr. Town Cen. Sun. Station	Albion Qtr. Town Cen. Sun. Station	Albion Qtr. Town Cen. Sun. Station	Albion Qtr. Town Cen. Sun. Station	Albion Qtr. Town Cen. Sun. Station	Albion Qtr. Town Cen. Sun. Station	Albion Qtr. Town Cen. Sun. Station	Albion Qtr. Town Cen. Sun. Station	Albion Qtr.	Albion Qtr.	Albion Qtr.
	Building form	Basement	Basement	Basement	No basemt.	No basemt.	No basemt.	No basemt.	No basemt.	No basemt.	No basemt.	No basemt.	No basemt.
	Car parking	100%	100%	100%	100%	100%	100%	0%	0%	0%	100%	100%	100%
	Materials	Typical	Best efforts	Low carbon	Typical	Best efforts	Low carbon	Typical	Best efforts	Low carbon	Typical	Best efforts	Low carbon
Materials groups	Aluminium	5,252	5,252	6,556	5,318	5,318	6,622	5,249	5,249	6,553	4,337	4,337	5,848
		0.2%	0.2%	0.3%	0.2%	0.2%	0.3%	0.3%	0.3%	0.4%	0.2%	0.2%	0.3%
	Cement sheet	0	0	26,938	0	0	26,248	0	0	26,248	0	0	0
		0.0%	0.0%	1.3%	0.0%	0.0%	1.2%	0.0%	0.0%	1.5%	0.0%	0.0%	0.0%
	Concrete	2,282,028	2,282,028	1,658,431	2,261,861	2,261,861	1,686,430	1,962,189	1,962,189	1,340,886	1,958,807	1,958,807	1,671,379
		94.2%	94.2%	78.6%	94.3%	94.3%	79.0%	94.0%	94.0%	75.6%	95.0%	95.0%	81.6%
	Glazing	16,594	16,594	16,594	16,594	16,594	16,594	16,594	16,594	16,594	13,358	13,358	13,358
		0.7%	0.7%	0.8%	0.7%	0.7%	0.8%	0.8%	0.8%	0.9%	0.6%	0.6%	0.7%
	Insulation	1,203	1,203	2,126	1,203	1,203	2,113	1,203	1,203	2,113	853	853	735
		0.0%	0.0%	0.1%	0.1%	0.1%	0.1%	0.1%	0.1%	0.1%	0.0%	0.0%	0.0%
	Plaster	16,781	16,781	61,973	16,781	16,781	61,824	16,781	16,781	61,824	11,319	11,319	56,329
		0.7%	0.7%	2.9%	0.7%	0.7%	2.9%	0.8%	0.8%	3.5%	0.5%	0.5%	2.7%
	Render	0	0	1,806	0	0	1,806	0	0	1,806	0	0	0
		0.0%	0.0%	0.1%	0.0%	0.0%	0.1%	0.0%	0.0%	0.1%	0.0%	0.0%	0.0%
	Steel	100,756	100,756	80,566	97,744	97,744	79,412	84,597	84,597	64,401	73,470	73,470	60,286
		4.2%	4.2%	3.8%	4.1%	4.1%	3.7%	4.1%	4.1%	3.6%	3.6%	3.6%	2.9%
	Wood	0	0	253,646	0	0	252,555	0	0	252,555	0	0	240,960
		0.0%	0.0%	12.0%	0.0%	0.0%	11.8%	0.0%	0.0%	14.2%	0.0%	0.0%	11.8%
	Grand Total	2,422,615	2,422,615	2,108,637	2,399,501	2,399,501	2,133,604	2,086,613	2,086,613	1,772,980	2,062,144	2,062,144	2,048,895
		100.0%	100.0%	100.0%	100.0%	100.0%	100.0%	100.0%	100.0%	100.0%	100.0%	100.0%	100.0%
	FFA (m2)	2,252,395	2,252,395	2,252,395	2,252,395	2,252,395	2,252,395	2,252,395	2,252,395	2,252,395	1,380,761	1,380,761	1,380,761
	GFA (m2)	2,501,108	2,501,108	2,501,108	2,501,108	2,501,108	2,501,108	2,252,395	2,252,395	2,252,395	2,002,459	2,002,459	2,002,459
	Mass per FFA (kg/m2	1,076	1,076	936	1,065	1,065	947	926	926	787	1,493	1,493	1,484
	Mass per GFA (kg/m2	969	969	843	959	959	853	926	926	787	1,030	1,030	1,023

12.4.2 Embodied carbon results

Embodied carbon assessment for the scenarios considered followed the material trends identified above. In general, the lower mass solutions tended to also be the lower carbon solutions, however the differences varied across a wider range. Embodied carbon (ECPC scope) was seen to vary between 325 to 790 kt CO_2e across the scenarios considered for the Base Scenario and 271 to 631 kt for the Updated Scenario (**Error! Reference source not found.**). When considered in terms of the functional unit, the r esult across all scenarios varied between 144 kg CO_2e/m2 (FFA) and 457 kg CO_2e/m2 (FFA). The lowest embodied carbon impact was achieved by the NoB-LC-CP0 scenario which eliminated the basement, adopted low carbon construction and eliminated carparking. The highest impact scenario, Upd-NoB-T, had the largest allocation of carparking and adopted a typical construction approach (Table 12.7).

Table 12.7. Embodied carbon assessment for the precinct (ECPC scope).

Scenario Name	**B-T**	**B-BE**	**B-LC**	**NoB-T**	**NoB-BE**	**NoB-LC**	**NoB-T-CP0**	**NoB-BE-CP0**	**NoB-LC-CP0**	**Upd-NoB-T**	**Upd-NoB-BE**	**Upd-NoB-LC**
Precinct design	Base	Base	Base	Base	Base	Base	Base	Base	Base	Updated	Updated	Updated
Precincts considered	Albion Qtr. Town Cen. Sun. Station	Albion Qtr. Town Cen. Sun. Station	Albion Qtr. Town Cen. Sun. Station	Albion Qtr. Town Cen. Sun. Station	Albion Qtr. Town Cen. Sun. Station	Albion Qtr. Town Cen. Sun. Station	Albion Qtr. Town Cen. Sun. Station	Albion Qtr. Town Cen. Sun. Station	Albion Qtr. Town Cen. Sun. Station	Albion Qtr.	Albion Qtr.	Albion Qtr.
Building form	Basement	Basement	Basement	No basemt.	No basemt.	No basemt.	No basemt.	No basemt.	No basemt.	No basemt.	No basemt.	No basemt.
Car parking	100%	100%	100%	100%	100%	100%	0%	0%	0%	100%	100%	100%
Materials	Typical	Best efforts	Low carbon	Typical	Best efforts	Low carbon	Typical	Best efforts	Low carbon	Typical	Best efforts	Low carbon
Total (t CO2e)	789,928	680,589	423,982	761,693	651,595	403,336	676,570	581,142	324,604	631,210	535,762	270,857
Impact per FFA (kg CO2e/m2	**351**	**302**	**188**	**338**	**289**	**179**	**300**	**258**	**144**	**457**	**388**	**196**
Results as a % of Typical	**100%**	**86%**	**54%**	**96%**	**82%**	**51%**	**85%**	**74%**	**41%**	**130%**	**111%**	**56%**
Reference: Impact per GFA (kg CO2e/m2)	*316*	*272*	*170*	*305*	*261*	*161*	*300*	*258*	*144*	*296*	*251*	*127*

When the Base building form was considered, the scenario analysis showed that embodied carbon could be reduced to 86% of the typical scenario (B-T) by selecting equivalent materials with lower carbon intensity (B-BE). When a more ambitious low carbon approach (B-LC) was adopted, this was reduced

further to 54% of the typical scenario. This reduction was achieved without modification to basements or carparking areas, showing that significant embodied carbon reductions were possible without modification to carparking levels. Elimination of carparking and removal of basements (NoB-LC-CP0) was shown to reduce the footprint further to the minimum achieved of 144 kg CO_2e/m2 (FFA), which was 41% of the typical embodied footprint (Table 12.7).

Analysis of the results per functional unit, when broken down by building element, showed that upper floors contributed the most to precinct carbon footprints (Figure 12.10). This element was primarily comprised of the floor slabs in the multistorey buildings considered (shown in green in Figure 12.10). The large reduction in footprint associated with the LC material scenario was due to the use of mass timber (employed in CLT) in the walls and floors of residential towers supported by concrete (low carbon formulations) in the supporting podium structure. This reduction comes about because the mass timber elements have lower emissions intensities to produce and because the sequester carbon over the building life and when disposed of to landfill (refer Section 4.2) shown as negative impact in Figure 12.10 and Figure 12.11.

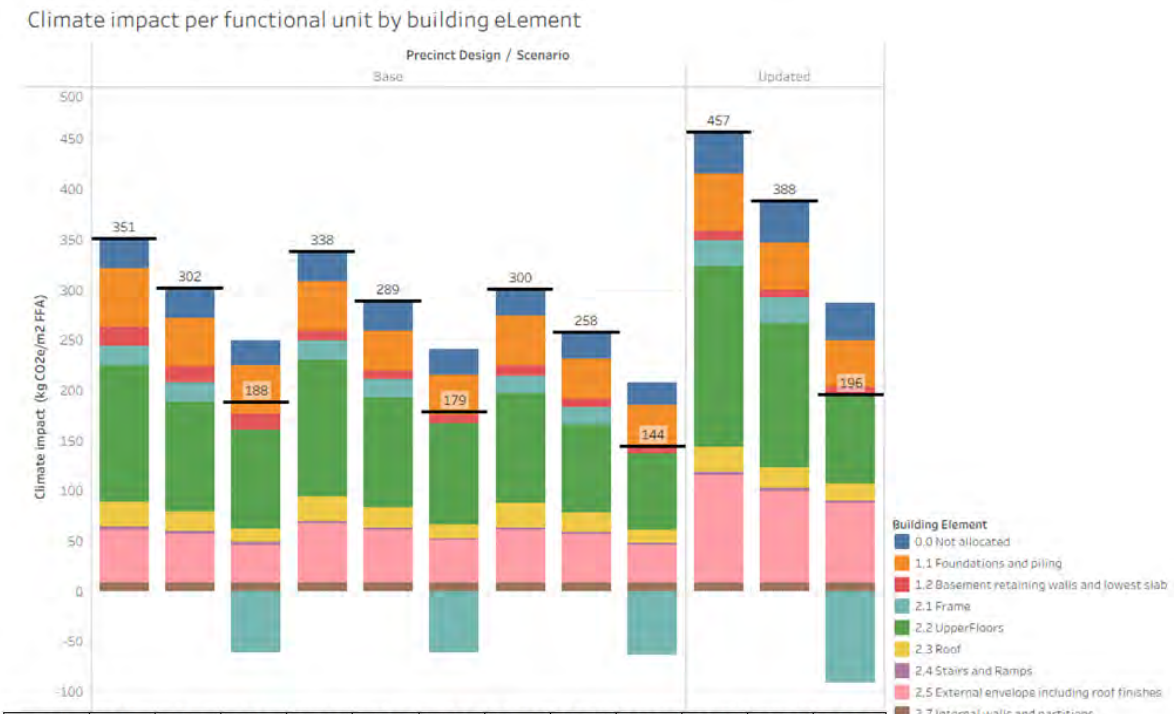

Scenario Name	B-T	B-BE	B-LC	NoB-T	NoB-BE	NoB-LC	NoB-T-CP0	NoB-BE-CP0	NoB-LC-CP0	Upd-NoB-T	Upd-NoB-BE	Upd-NoB-LC
Precinct design	Base	Base	Base	Base	Base	Base	Base	Base	Base	Updated	Updated	Updated
Precincts considered	Albion Qtr. Town Cen. Sun. Station	Albion Qtr. Town Cen. Sun. Station	Albion Qtr. Town Cen. Sun. Station	Albion Qtr. Town Cen. Sun. Station	Albion Qtr. Town Cen. Sun. Station	Albion Qtr. Town Cen. Sun. Station	Albion Qtr. Town Cen. Sun. Station	Albion Qtr. Town Cen. Sun. Station	Albion Qtr. Town Cen. Sun. Station	Albion Qtr.	Albion Qtr.	Albion Qtr.
Building form	Basement	Basement	Basement	No basemt.	No basemt.	No basemt.	No basemt.	No basemt.	No basemt.	No basemt.	No basemt.	No basemt.
Car parking	100%	100%	100%	100%	100%	100%	0%	0%	0%	100%	100%	100%
Materials	Typical	Best efforts	Low carbon	Typical	Best efforts	Low carbon	Typical	Best efforts	Low carbon	Typical	Best efforts	Low carbon

Figure 12.10. Embodied carbon by building element for each scenario (FFA basis). Net embodied carbon shown as black line.

When the embodied carbon result was considered in terms of materials, as shown in Figure 12.11, concrete and steel were seen to be the largest contributors to embodied carbon in all scenarios, together contributing 78% of the footprint for the B-T scenario. The next most significant contributor was the fuel use associated with construction, which contributed 11% of the footprint for the B-T scenario. For the low carbon scenarios, the use of mass timber to store carbon indefinitely, as discussed in Section 4.2,

played a significant role in reducing the embodied carbon emissions associated with these scenarios. For the B-LC sicario, the storage of carbon in timber reduced the embodied emissions of the precinct by 36%.

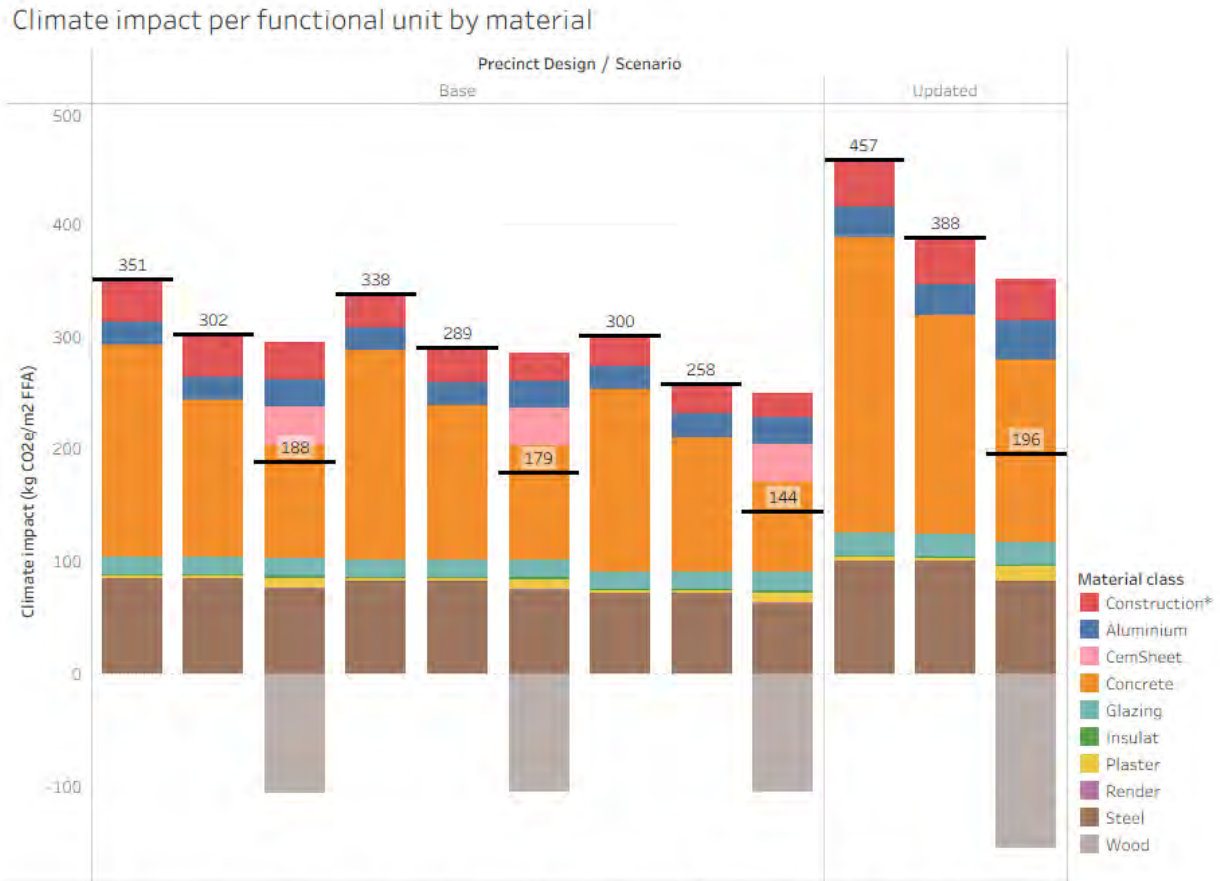

Scenario Name	B-T	B-BE	B-LC	NoB-T	NoB-BE	NoB-LC	NoB-T-CP0	NoB-BE-CP0	NoB-LC-CP0	Upd-NoB-T	Upd-NoB-BE	Upd-NoB-LC
Precinct design	Base	Base	Base	Base	Base	Base	Base	Base	Base	Updated	Updated	Updated
Precincts considered	Albion Qtr. Town Cen. Sun. Station	Albion Qtr. Town Cen. Sun. Station	Albion Qtr. Town Cen. Sun. Station	Albion Qtr. Town Cen. Sun. Station	Albion Qtr. Town Cen. Sun. Station	Albion Qtr. Town Cen. Sun. Station	Albion Qtr. Town Cen. Sun. Station	Albion Qtr. Town Cen. Sun. Station	Albion Qtr. Town Cen. Sun. Station	Albion Qtr.	Albion Qtr.	Albion Qtr.
Building form	Basement	Basement	Basement	No basemt.	No basemt.	No basemt.	No basemt.	No basemt.	No basemt.	No basemt.	No basemt.	No basemt.
Car parking	100%	100%	100%	100%	100%	100%	0%	0%	0%	100%	100%	100%
Materials	Typical	Best efforts	Low carbon	Typical	Best efforts	Low carbon	Typical	Best efforts	Low carbon	Typical	Best efforts	Low carbon

Figure 12.11. Embodied carbon by material for each scenario (FFA basis). Net carbon impact shown as black line.

12.4.3 Results validation

Carbon footprint results were compared to studies which considered similar buildings and scopes as shown in Table 12.8. Results were found to be broadly consistent with other studies where carbon storage in landfill at the end of life had been accounted for.

Table 12.8. This study compared to similar reports in an Australian context.

Source	Carbon footprint kg CO2e/m2 (GFA)	Notes
This research	127 to 316	A + C stages. Multistorey development.
Carre and Crossin (2015)	196	A + C + D stages. Lightweight Mult residential cases
Carre and Crossin (2015)	185	A + C + D stages. Mass timber high-rise
GBCA and Thinkstep (2021)	298	A + C stages. Large Australia sample residential. Excludes carbon storage
GBCA and Thinkstep (2021)	538	A + C stages. Large Australia sample commercial. Excludes carbon storage

12.4.4 Assumptions when looking across the precinct life cycle

A more holistic view of the climate change impact of the precinct was considered by including the operational phase of building life (Stage B in Figure 12.5) in the analysis. To do this the embodied carbon (ECPC scope) of the precinct for Scenario B-T (which covered Stage A and C in Figure 12.5) was added to estimated impacts associated with manufacturing photovoltaics (PV) and battery storage systems (BESS). This total embodied carbon was informed by the Energy Subgroup scenario P01F02N04S04B01E03 which assumed that buildings employed rooftop and façade solar as well as battery storage where possible, to maximise grid stability. Building embodied carbon was assumed to support precinct function over a 60 year period, and PV and BESS 20 years (requiring two replacements over one building life).

Operational impacts (Stage B in Figure 12.5) comprised an estimate for building maintenance and replacements (Stages B1 to B5) combined with an estimate of building electricity draw from the grid for the period (Stage B6). It was assumed that all building loads were satisfied by electricity (either generated on site or imported from the grid). Electrical loads were estimated by the Energy Subgroup and considered building heating and cooling as well as lighting, appliances and hot-water supply. Electricity supply for the precinct was considered under three scenarios, as follows:

Scenario 1: All electricity is supplied by the grid. There is no on-site generation (or associated embodied impacts for manufacturing PV and BESS). Grid emissions intensity (Scope 3) is as it is for Victoria supply in 2025 (0.76 kg CO_2e/kWh).

Scenario 2: Electricity is supplied by a combination of on-site generation and grid supply. Grid emissions intensity (Scope 3) is as it is for Victoria supply in 2025 (0.76 kg CO_2e/kWh).

Scenario 3: As grid emissions intensity is expected to fall over the life of the precinct, a scenario that anticipates this fall was considered based on projections from DCCEEW (2024). Grid emissions intensity (Scope 3) is assumed to be 0.08 kg CO_2e/kWh (the average projected emission intensity over the precinct life). Electricity is supplied by a combination of on-site generation and grid supply, as per Scenario 2.

A summary of the assumptions underpinning the precinct life cycle assessment is shown in Table 12.9.

Table 12.9. Building life cycle assumptions.

Parameter	Scenario 1	Scenario 2	Scenario 3	Source
Precinct life	60 years			RICS (2017)
Embodied carbon (Stage A & C)	BASE-B scenario			Calculated in this study
B1 to B5 building maintenance and replacement emissions	22% of Stages A, B and C (excluding B6)			Estimate from Röck et al. (2020)
Photovoltaic (PV) capacity (20 yr life)	0 kW	21,799 kW		Energy Subgroup scenario: P01F02N04S04B01E03
Battery Energy Storage System (BESS) capacity (20 yr life)	0 kWh	182,657 kWh		
Net electricity import*	80 kWh/m2.a	53 kWh/m2.a		
Emissions factor (EF) electricity	0.87 kg CO_2e per kWh		0.08 kg CO_2e per kWh**	0.87 – emissions factor for Victoria from DCCEEW (2025). 0.08 – Average of emissions projections 2025 to 2085. Projections from DCCEEW (2024).
Embodied carbon of BESS (Stage A)	NA	217 kg CO_2e per kWh		Le Varlet et al. (2020) for LiFePO4 chemistry
Embodied carbon of PV	NA	810 kg CO_2e per kW		Müller et al. (2021)

* Net electricity import represents the total of all electricity drawn from the grid less electricity exported to the grid. This value was calculated hourly.

** Projected emission factor calculated as the total of annual of projections from 2025 to 2040 from DCCEEW (2024) plus the projection for 2040 multiplied by 45 years, all divided by 60 years.

The Energy Subgroup developed as estimate of building loads and electricity supply from PV generation (combined with BESS) per unit area (GFA) using time-step simulation analysis, as shown in Figure 12.12. The figure shows how loads and generation vary over an average day for each season of the year. The black line in Figure 12.12 shows the net electricity draw from the grid that the precinct requires per unit area (GFA) which can be seen to show electricity import during the night-time hours and electricity export during the day (when solar energy can be harvested). The analysis of the precinct life cycle assumed that surplus electricity generation during daytime hours was exported to the grid and effectively offset emissions from the grid at a connected load (e.g. another precinct). In this fashion, all electricity generation was assumed to create a climate benefit.

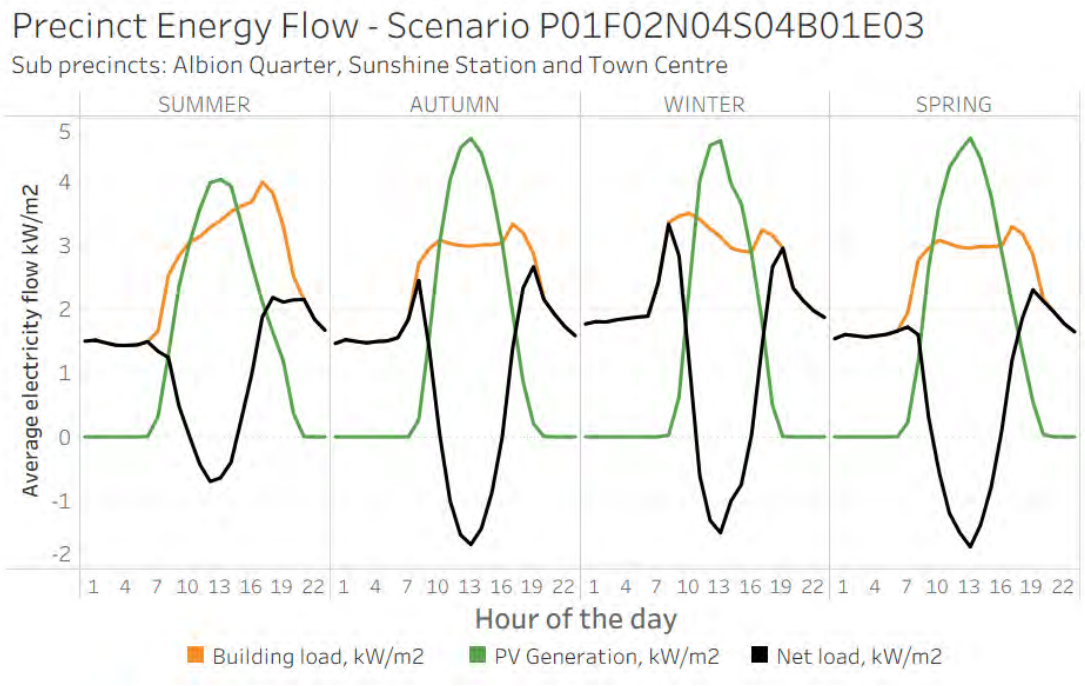

Figure 12.12. Electricity generation, building demand and net demand from the grid by season for Energy Scenario P01F02N04S04B01E03.

When complete, the expanded analysis went beyond the ECPC scope used for embodied carbon, shown in orange in Figure 12.12 to include the precinct operation (Stage), thereby employing the WLC scope shown in blue in Figure 12.12. The expanded scope allowed embodied carbon to be placed into a wider perspective allowing its significance to be assessed.

13. Appendix 7 - Energy

13.1 Summary of methods

The energy subgroup aims to shape the future energy landscape of the Sunshine Precinct towards the more sustainable and resilient energy infrastructure, powered by the community processed distributed assets and flexible energy management strategies. Targeting the different stages of the project, the energy subgroup proposed an iterative process to digitalise and test different energy scenarios as well varies of precinct-level energy options.

Overall, the objectives within the energy subgroup are outlined as follows:

(1) Identify the impacts of future changes to the energy supply and demand, including urban built form, policies, climate changes, electrification, and distributed assets growth (EV, PV, battery, etc.)
(2) Evaluate the potential of renewable energy and energy flexibility within the precinct under different built forms and policies.
(3) Assess the potential impacts to the precinct's energy landscape, including energy consumption efficiency, self-sufficiency, and power grid impacts.

Specifically, along with the precinct modelling process and project stages, the detailed tasks of the energy subgroup are outlined in Figure 13.1.

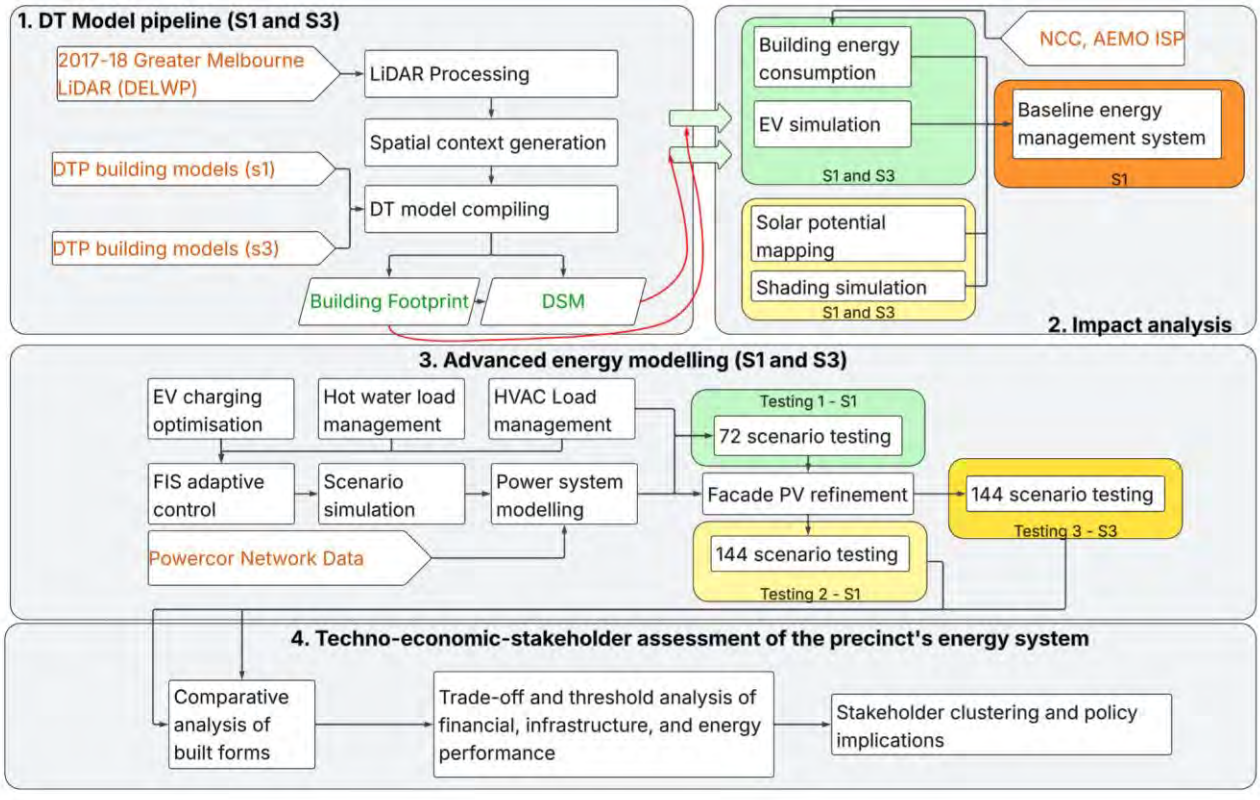

Figure 13.1. Overall workflow of energy modelling process

13.2 Scenario settings

In total, two scenarios were tested within the energy modelling workflow as shown in Table 13.1. Each scenario uses a different built form model. Among the three models, the digital model of S1 covers study areas of Albion Quarter, Town Centre, Sunshine Station, Energy Park, and Significant Sites, while the models of S3 covers only the Albion Quarter.

Table 13.1. Scenario comparison in Energy Subgroup

	S1	S3
Precinct Digital Model Version	S1 model covers full study area (322 buildings)	S3 model (Albion Quarter – 230 buildings)
Solar and shading mapping	Yes	Yes
Renewable generator	Rooftop and façade PV multiple scenarios	Rooftop and façade PV multiple scenarios
Load models	Baseline models + Load adjustment models	Load management models
Energy management system models	Baseline model + Adaptive EMS	Adaptive EMS
Adaptive EMS testing iterations	Two iterations including preliminary 72 scenario settings and expanded 144 scenario settings	One iteration with the expanded 144 scenario settings
Power system analysis	Yes	Yes

For S1 and S3, the load models cover the consumption profiles of various of building loads (HVAC, appliances, hot water, lighting, etc.), and EV charging load determined by the dwelling numbers and carpark ratios. For S1, two categories of load models were developed to reflect the base consumption as of today's typical meteorological year (TMY) and consumption profile, and the projected consumption as of 2050's TMY projection and electrification.

In terms of the precinct-level energy management strategies, the S1 tested two models, namely the baseline operation model and adaptive fuzzy inference system (FIS) based control model. The baseline model was developed to identifying the load impacts of climate changes, increasing density, and electrifications, as well as to understand the capacity of the distributed generators including PV and battery systems. The FIS model was developed to implement the load management strategies that can

achieve load stability within the precinct. In S3, the energy management strategy focuses on only the FIS-based control strategy.

13.2.1 Iterative testing of load and supply options

For both S1 and S3, multiple options were developed to test the different renewable energy, storage, and load options. For S1, two iterations of testing were carried out with option combinations shown in Table 13.2 and Table 13.3. Testing scenario iteration 2. For iteration 1, the purposes were to (1) Validate the effectiveness of FIS framework, (2) Examine the effectiveness of different energy options, and (3) Refine scope and modelling workflow. Following the analysis of the iteration 1, the option combinations were modified to refine the system options for façade PV and to exclude infeasible options in iteration 2. The total number of option combinations is 72 for iteration 1 and 144 for iteration 2. For S3 specifically, only the iteration 2 was tested.

Table 13.2. Testing scenarios iteration 1

Attributes	Option 01	Option 02	Option 03	Option 04
Rooftop PV {P}	20% Coverage	50% Coverage	80% Coverage	-
Façade PV {F}	Excluded	Included	-	-
BESS {B}	Low capacity (70% generation capacity)	Medium capacity (140%)	High capacity (210%)	-
EV {E}	No smart charging + 50% carpark capacity	Smart charging 20% carpark capacity (20% * dwelling number)	Smart charging 50% carpark capacity	Smart charging 80% carpark capacity

Table 13.3. Testing scenario iteration 2

Attributes	Option 01	Option 02	Option 03	Option 04
Rooftop PV {P}	20% Coverage	-	-	-
Façade PV {F}	Excluded	Included	-	-
North BIPV{N}	Excluded	20%	50%	80%
EW-BIPV {S}	Excluded	20%	50%	80%
BESS {B}	Low capacity (70% generation capacity)	Medium capacity (140%)	High capacity (210%)	-

EV {E}	-	Smart charging 20% carpark capacity	Smart charging 50% carpark capacity	Smart charging 80% carpark capacity

13.2.2 Energy supply resources mapping and digitalisation

The simulation adopts the weather data of CSIRO 2050 RCP 4.5 TMY dataset for the closest weather station of the Sunshine Precinct located in Tullamarine Airport, Victoria, Australia. Following open-accessed toolboxes were used:

Urban Multi-scale Environmental Predictor (UMEP): The UMEP Python Toolbox was used for shading simulations for building surfaces within the precinct. The UMEP process GMN General Public License which allows for complete source code modifications. (Link: UMEP/LICENSE at SuPy-QGIS3 · UMEP-dev/UMEP · GitHub)

Sandia National Laboratory's PVLib toolbox MATLAB Version: The PVLib toolbox was used for determining hourly sun path, angular parameters, and solar potential level of the receiving surfaces. The PVLib toolbox processes a BSD-3 Clause license which allows for modification, open-access usage, and redistribution of the source codes given the BSD-3 Clause license notice is maintained and all changes within the source codes are tracked. (Link for citation: PV_LIB Toolbox – PV Performance Modelling Collaborative (PVPMC))

The solar potential and shading impact mapping generates five categories of outputs in raster format, representing:

1. Hourly shading height on wall surface.
2. Hourly shading on horizontal surface.
3. Hourly solar potential (W/m2) on unshaded wall surface.
4. Hourly solar potential (W/m2) on shaded wall surface.
5. Hourly solar potential (W/m2) on horizontal surface.

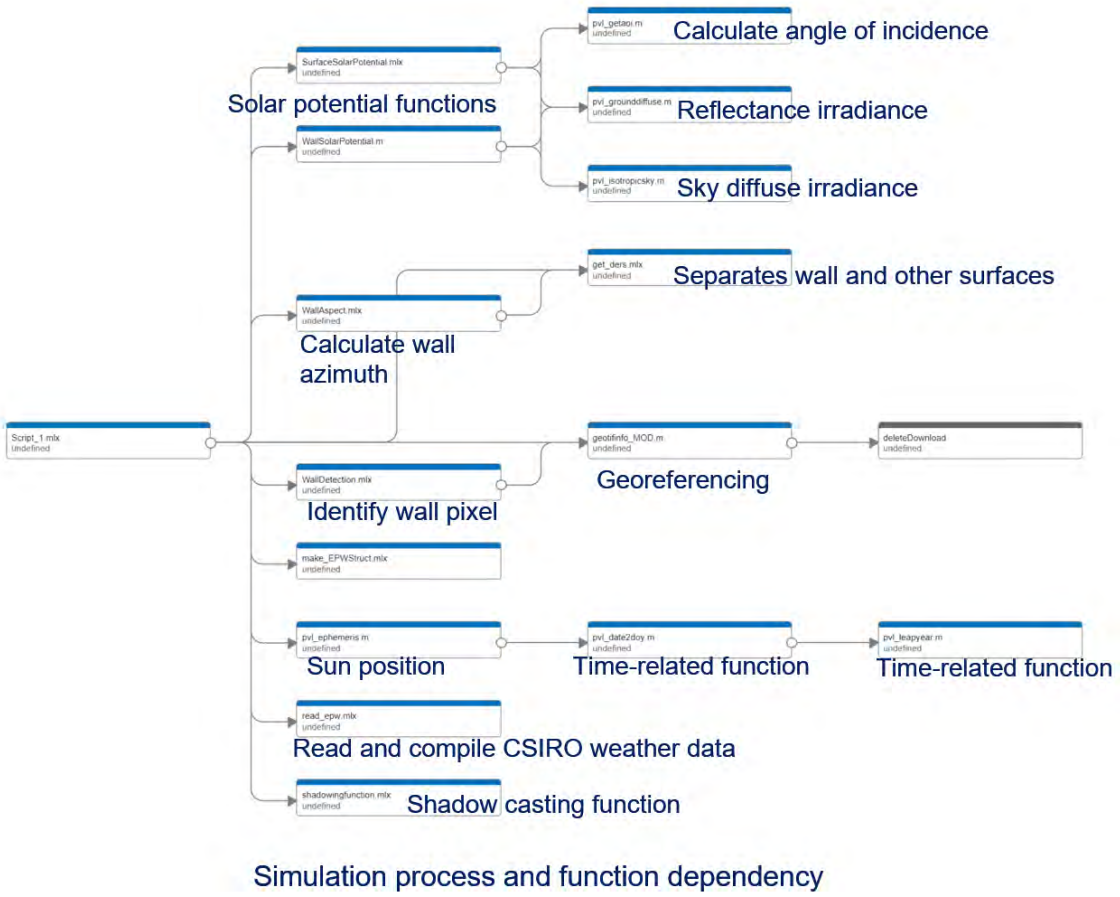

Figure 13.2. Program dependency map of Solar Energy Simulation Workflow

The mapping process excluded the hours in the year that has sun altitude angle below 0° and the hours in the year with total irradiance equals to 0 W/ m2. The simulation was on hourly time interval with 1m-by-1m resolution. In total, this task generated 18,345 (3,669 * 5) raster layers for the five categories above.

The rooftop photovoltaic (PV) panel placement was systematically modelled through georeferencing PV panel polygon shapefiles, linking them accurately to building identifiers (Global ID or BuildingNum when Global ID was unavailable). This approach ensures precise spatial alignment and facilitates reliable integration into building-level energy assessments.

The PV system geometry settings were standardized to enhance consistency across urban-scale analyses, utilizing panels with dimensions of 1 m in width and 2 m in length. An edge distance of 1 m from the roof perimeter was maintained to prevent shading and ease maintenance access. Panels were positioned at a tilt angle of 30° and oriented northward with an azimuth angle of 0°, optimizing exposure to solar radiation. Module spacing was fixed at 0.1 m, while arrays were spaced 1 m apart, balancing density and efficiency of placement.

To address complex urban geometries and regulatory constraints, the placement methodology considered several critical constraints:

- Overlap Management: For overlapping building footprints, panels were exclusively assigned to structures with the highest elevation (Z_max) to prevent shading-induced inefficiencies.

- Special Structural Exclusion: Podium-type buildings were systematically excluded from the PV placement process, adhering to urban planning guidelines and structural limitations.
- Minimum Area Requirement: Buildings with footprints smaller than 55 sqm were omitted, aligning the analysis with the latest requirements outlined in the National Construction Code (NCC).

These constraints were implemented through rigorous geometric filters within the placement algorithm, ensuring compliance, efficiency, and practical feasibility of rooftop solar installations.

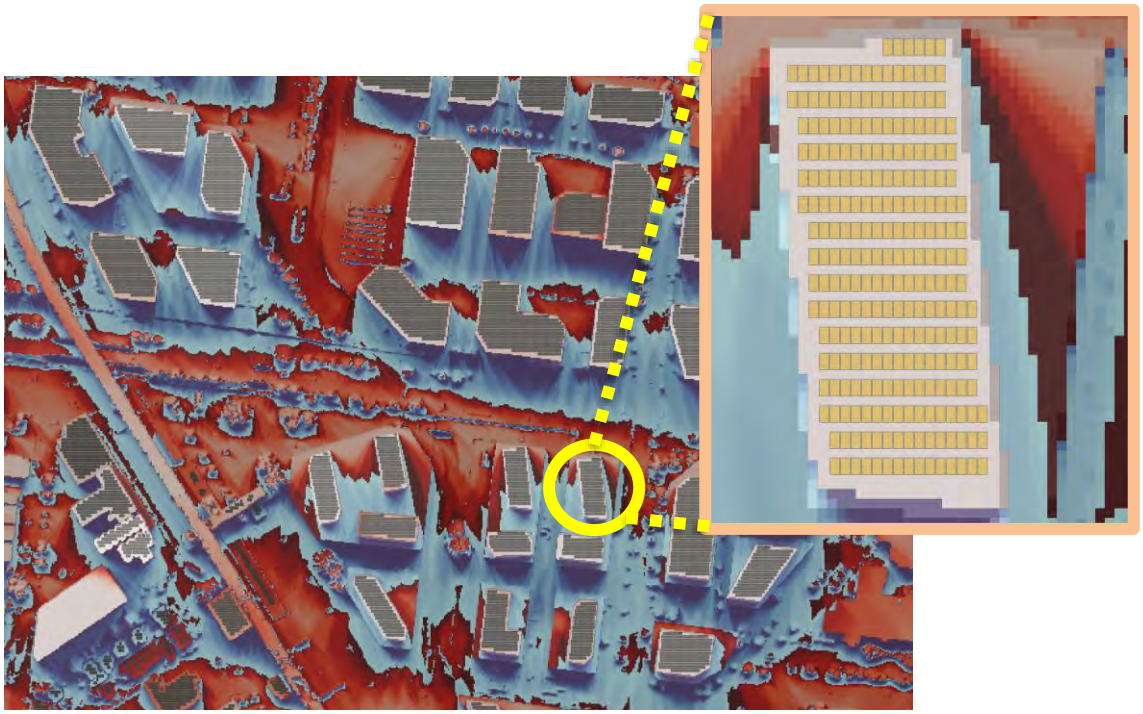

Figure 13.3. Rooftop PV placement

The façade solar PV system modelling (Figure 13.2) further expanded upon the rooftop analysis by considering vertical building surfaces. The simulation accounted for hourly façade PV generation and operating temperature across urban-scale building datasets. The process involved using detailed 3D building vertices to precisely model façade geometries, facilitating accurate representation and analysis of PV deployment potential.

The modelling process assumed a window-to-wall ratio ranging between 40% and 60%, striking a realistic balance between solar harvesting and architectural considerations. Facade PV systems were strategically deployed above the average shading height calculated dynamically between adjacent vertices, thus optimizing energy yield.

Comprehensive data layers generated from the simulation included detailed information summaries for each building and vertex gaps. Key simulation outputs covered deployment heights, total deployment area, estimated installed capacities for glazed and opaque BIPV areas, position indices, and azimuth orientations.

Hourly performance data encompassed both shaded and unshaded conditions, providing granular insights into façade PV operations. These data points included total hourly AC and DC outputs,

temperature profiles for glazed and opaque PV materials, and differentiated performance metrics for shaded versus unshaded façade segments.

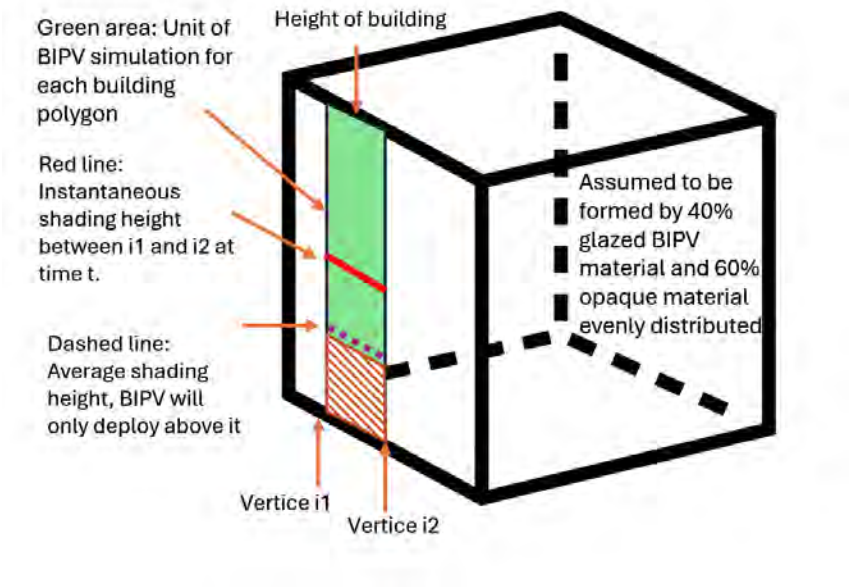

Figure 13.4. Illustration of façade PV system placement

The simulation process for both rooftop and façade PV installations was designed to quantify hourly performance metrics comprehensively, including DC and AC power outputs and module operating temperatures. Inputs for this simulation encompassed detailed PV system settings, accurately georeferenced panel shapefiles, hourly shading, and solar irradiance raster layers, along with inverter system characteristics.

The modelling employed robust simulation algorithms to incorporate temperature-dependent performance variability. PV efficiency was set at 16%, with a temperature coefficient of -0.005, reflecting realistic performance conditions. The inverter was modelled based on NREL's established inverter framework, adopting inverter efficiencies and capacities reflective of industry standards. Specifically, inverter efficiency was set to 96%, and inverter capacity was scaled according to system efficiency and size parameters.

The simulation leveraged a simultaneous efficiency and temperature modelling approach based on the Sandia National Lab's SAPM framework. This methodology integrated multiple environmental parameters such as shading factors, solar zenith and azimuth angles, ambient temperature, and irradiance data. By using this detailed and rigorous approach, the simulation delivered high-resolution, temporally detailed insights into the performance of urban-scale PV deployments.

13.2.3 EV simulation and load management

The scenario design in this project for EV charging load impacts reflects the predicted residential EV uptake. Three carpark capacity scenarios are simulated: 20%, 50%, and 80% of total dwellings in each building. Of the available bays, 90% are assumed to be EV-charging bays, guided by the 2024 Integrated

System Plan (ISP) by AEMO. Fleet composition and per-vehicle energy requirements are instantiated accordingly for each scenario.

Vehicle parameters follow a single reference model for clarity. A Tesla Model 3 (76 kWh usable battery) is adopted as the baseline EV. Daily energy use per vehicle is sampled at random within a realistic range. The sampled use sets the per-EV energy requirement, operationalised in the optimiser as the difference between battery capacity and the specified initial state of charge for each vehicle. This approach produces heterogeneous charging needs while keeping power limits consistent through the common per-EV maximum rate.

The detailed settings are summarised as follows:

Table 13.4. EV charging settings

Reference EV system	TESLA Model 3
Maximum battery capacity	76 kWh (400-500 KM)
Maximum charging power	22 kW
Daily battery usage	20% to 80% of the total battery capacity, following a Poisson distribution with mean of 25% (normalised around 30 KM per day)
User profiles	Each vehicle is randomly assigned with one of the three owner profiles below • Cautious charger – Always charge to 100% whenever the battery is not fully charged • Careless charger – Only charge to 100% when battery capacity is below certain threshold (e.g. 20%) • Weekend charger – Charge to 100% during weekend, and charge to 100% when battery is below 50% during weekdays
Charging window	Regulated window: 9 pm – 5 am Unregulated window: 4 pm onwards until fully charged
Charging power	Unregulated: Charging at maximum power until fully charged. Regulated: Fully charge the vehicles scheduled to be charged within the regulated charging window, and minimise load turbulence during the charging window.

In S1, both unregulated and regulated EV charging schemes were tested to understand the impact of EV charging and effectiveness of defined charging window and strategies. The unregulated charging profile

was established with the daily usage, user profile, and a charging window of 4 pm start. The unregulated charging will charge each EV at maximum charging power until fully charged. On the other hand, the regulated charging applies the same daily battery usage, user profiles, but a different charging window of 9 pm to 5 am. Additionally, a quadratic programming approach is utilized to flatten the total charging load through the charging window.

13.2.4 Fuzzy inference-based energy management system

The project builds a policy-based energy management system at precinct scale. It coordinates rooftop PV, façade PV, batteries, and the charging demand that arrives from residents. The aim is simple: keep electricity use steadier across the day, prefer local solar when it is available, and reduce unnecessary imports from the grid.

Control decisions are produced by a fuzzy inference system (FIS) in the format of transparent "if–then" policies. For example: if current demand is high and the near-term trend is rising, then reduce load; if demand is low and PV is plentiful, then charge the battery. Fuzzy logic is well suited to this task because real signals are noisy and rarely just "high" or "low". It translates shades of grey into smooth actions rather than abrupt on/off decisions.

The energy management system is implemented as a hierarchical Type-1 Mamdani fistree named LoadControlFIS. The topology contains two nodes connected in series. The Load Control node converts real-time system context into a supervisory command (LoadControlCMD). The BESS Control node receives this command together with the photovoltaic (PV) surplus signal and issues two actionable outputs: Battery behaviour and Charging source. This structure reduces rule-base size, preserves interpretability, and separates short-term load assessment from battery dispatch decisions.

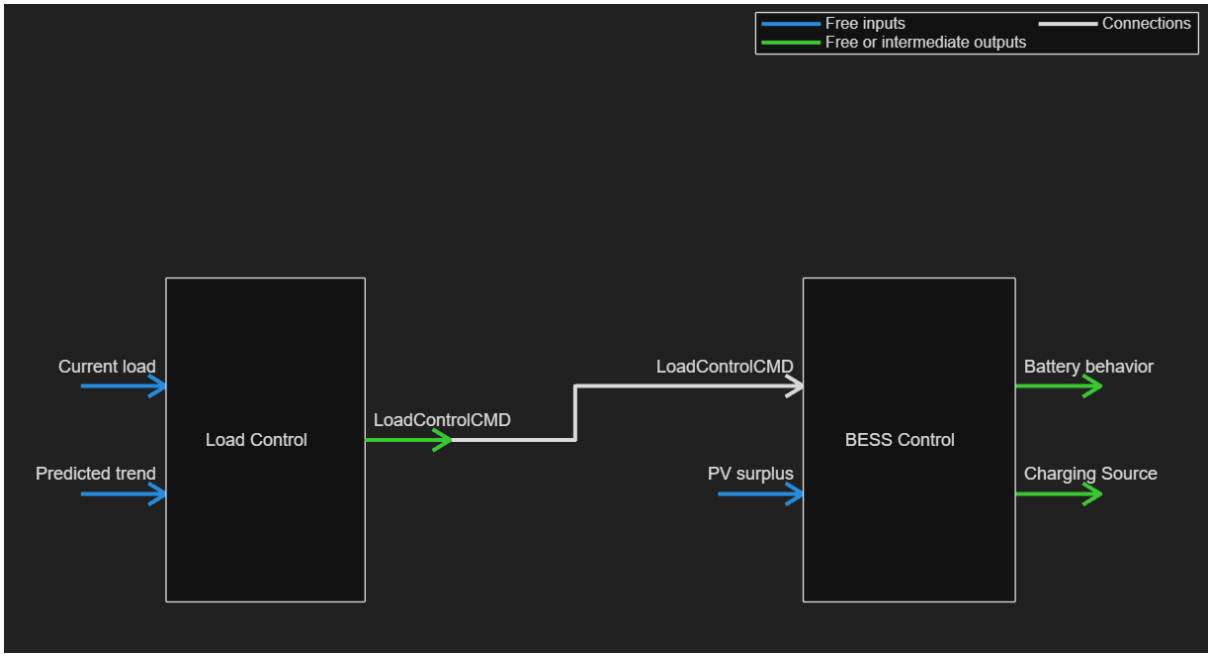

Figure 13.5. Overall FIS structure

The controller has two layers. The first layer, Load Control, looks at the current load and a short-term trend. It issues a supervisory command: reduce, hold, or increase load. The second layer, BESS Control,

takes that command plus the PV surplus and decides what the battery should do: charge, discharge, or idle; as well as where charging energy should come from: PV surplus first, grid second. This hierarchy keeps policies easy to explain and tune, while still capturing the main operational choices.

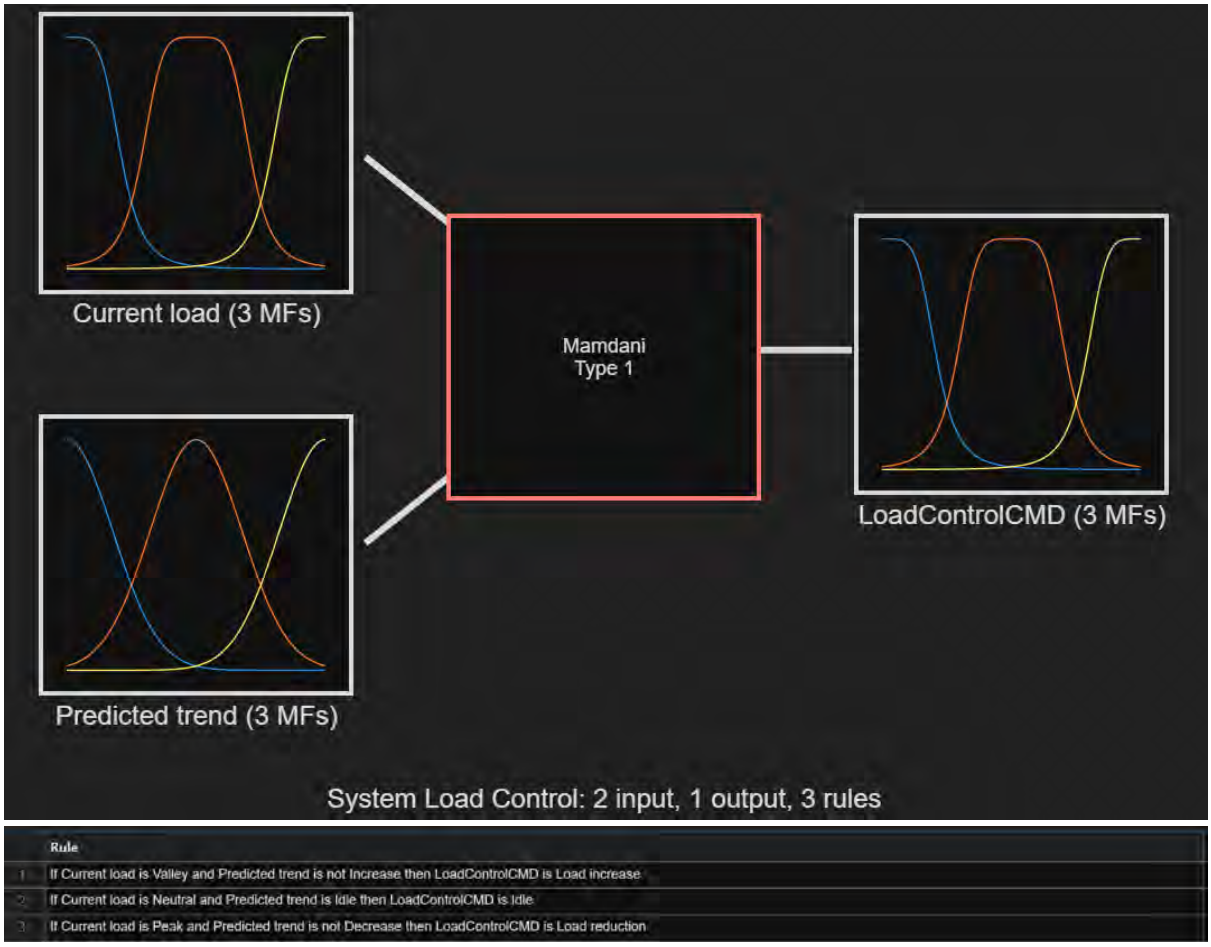

Figure 13.6. Load control unit

For the load control unit, two inputs are defined: Current load and Predicted trend. Each input uses three linguistic terms. For current load these are Valley, Neutral, and Peak. For the trend these are Decrease, Idle, and Increase. The single output is LoadControlCMD with three terms: Load reduction, Idle, and Load increase. Within the load control unit, three rules are defined: When the current load is in a Valley and the trend is not Increase, the controller issues Load increase. When load is Neutral and the trend is Idle, the command is Idle. When load is Peak and the trend is not Decrease, the command is Load reduction. This node therefore promotes valley-filling and peak-shaving behaviour using only three rules.

The second layer is the battery controller takes two inputs of the LoadControlCMD (three states as above) from the load control unit, and PV surplus with three states (Negative, Neutral, Positive). It generates two outputs, including the battery behaviours of discharge, idle, or charge, and the charging/discharging sources/destinations including: PV surplus (negative = load, positive = excessive PV generation), and grid. Eight rules were defined for the battery controller unit to coordinate storage actions with load objectives and PV conditions. When the command is Load increase, the battery charges. If PV surplus is Neutral (no excessive generation power), charging draws from the Grid; if PV surplus is Positive, charging uses PV Surplus. When the command is Load reduction and PV surplus is Negative, the

battery Discharges. If the command is Load reduction and surplus is Non-negative, the battery remains Idle unless surplus is Positive, in which case it Charges from PV Surplus. When the command is Idle, the battery is Idle for Negative or Neutral surplus, and Charges from PV Surplus when surplus is Positive. These eight rules encode a clear priority: satisfy the load-levelling request while maximising self-consumption of local PV and avoiding unnecessary grid imports.

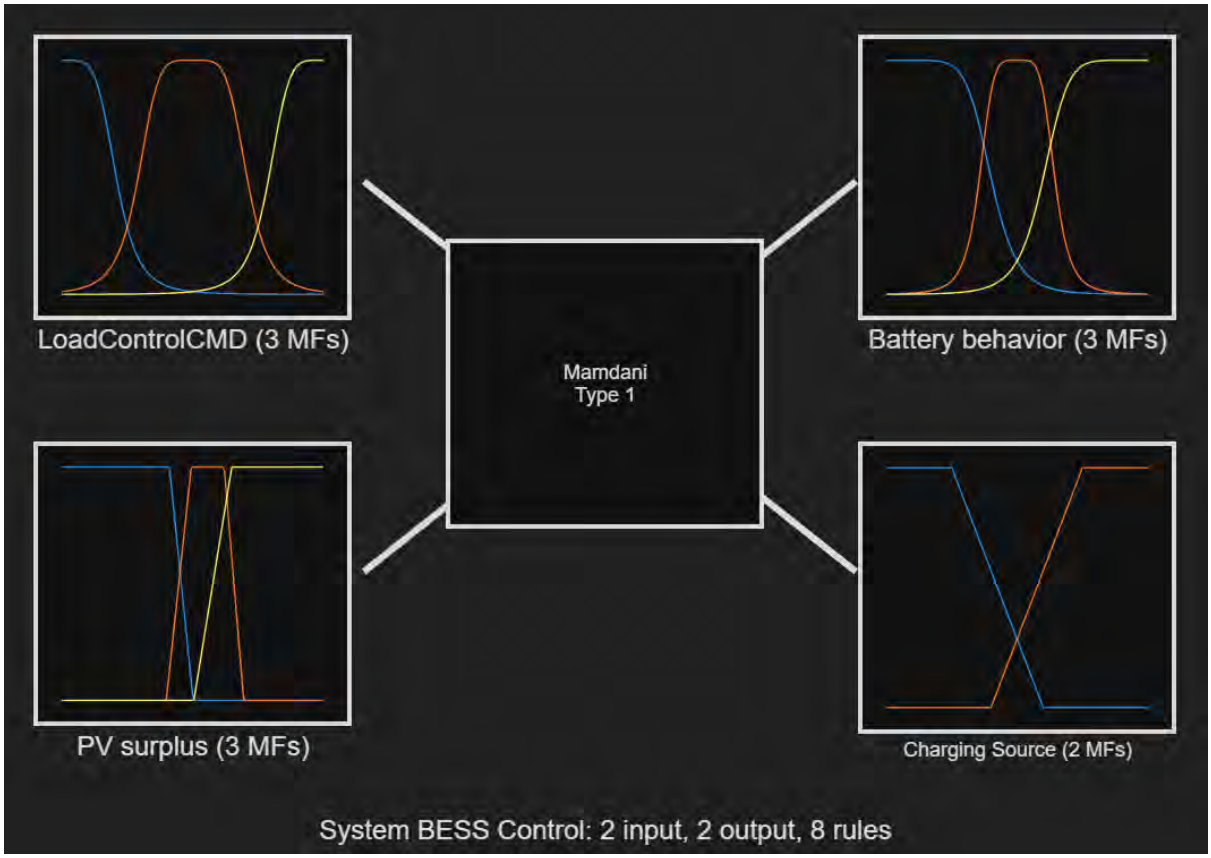

	Rule
1	If LoadControlCMD is Load increase then Battery behavior is Charge, Charging Source is Grid
2	If LoadControlCMD is Load reduction and PV surplus is Negative then Battery behavior is Discharge
3	If LoadControlCMD is Load reduction and PV surplus is not Negative then Battery behavior is Idle
4	If LoadControlCMD is Idle and PV surplus is not Positive then Battery behavior is Idle
5	If LoadControlCMD is Idle and PV surplus is Positive then Battery behavior is Charge, Charging Source is PV Surplus
6	If LoadControlCMD is Load reduction and PV surplus is Positive then Battery behavior is Charge, Charging Source is PV Surplus
7	If LoadControlCMD is Idle and PV surplus is Neutral then Battery behavior is Idle
8	If LoadControlCMD is Load increase and PV surplus is Neutral then Battery behavior is Charge, Charging Source is Grid

Figure 13.7. Subsystem structure of battery behaviour controller

Both nodes use Mamdani Type-1 inference (as indicated in the node diagrams). The hierarchical design keeps each node's rule base small (3 and 8 rules). It also provides transparent intermediate semantics via LoadControlCMD, which can be logged or tuned independently. The combination yields a controller that pushes charging into valleys, curtails charging at peaks, prefers PV energy when available, and uses the grid as a secondary source.

For each building in the precinct, the total building load (including hot-water, EV charging load, HVAC, and other loads), the combined PV generation (rooftop + BIPV), the rooftop PV component (for reporting), and the EV charging trace aligned to the hourly grid. If the building has no PV in a given scenario, the adjusted load is identical to the baseline load by design.

Battery sizing is scenario-dependent and determined by the following factor:

- Energy capacity (kWh): total capacity of PV/façade PV in each scenario;
- Power (kW): the mean of non-zero hourly PV values multiplied by capacity ratio of battery within each scenario;
- Round-trip efficiency: 0.90;
- Initial state of charge (SOC): 20% of capacity.

At each hour, three signals are computed to drive the fistree (LoadControlFIS):

- Normalised current load
- Normalised load trend
- Normalised PV surplus

These form the input vector to the FIS controller to produce the following control commands:

- LoadControlCMD (supervisory intent: load reduction / idle / load increase),
- Battery behaviour (negative = discharge, zero ≈ idle, positive = charge),
- Charging source (negative = PV, positive = grid, near zero = blend).

The output commands is then processed by the load management function to implement the actuation logic subject to the system boundaries (i.e. battery maximum/minimum capacity and maximum charging/discharging power) to charge or discharge the battery from the designated sources, or remain/reset idle state.

13.2.5 Energy load digitalization and simulation

This study developed a city-scale building energy consumption model using the Rhino/Grasshopper platform (Figure 13.8), leveraging the Dragonfly and Honeybee plug-ins within Ladybug Tools to simulate and assess the energy performance of multiple building groups. Model parameters were primarily defined based on the building energy efficiency assessment methodology outlined in J1V3 and J1V5 of the National Construction Code 2022 (NCC2022), supplemented by technical manuals from mainstream rating systems such as NABERS and NatHERS, including building usage, thermal performance of envelope components, HVAC system setups, and operational schedules, etc.

During the modelling process, the Dragonfly plug-in enabled efficient generation of city-scale building models through a streamlined 2D extrusion approach. It supports the integration of diverse geometric data sources such as building footprints, massing models, and floor plans, and automatically constructs simulation-ready structures compatible with EnergyPlus. Each building energy model can be independently converted into an EnergyPlus model, enabling parallel computation and significantly enhancing simulation efficiency. Under complex urban morphology, Dragonfly effectively manages inter-building shading relationships and thermal environmental contexts, offering robust technical support for large-scale urban energy performance evaluations.

Figure 13.8. Simulation flow in Rhino/Grasshopper

Energy simulation is usually based on TMY meteorological data. This study first uses current TMY data to calibrate and verify the input parameters to ensure accuracy of the simulation basis. Following this, the simulation incorporates future climate TMY data under the RCP4.5 scenario for the year 2050 to evaluate building energy performance under climate change conditions. The meteorological files used are 60_CZ0607_TU_NH16_TMY for the current climate and 60_CZ0607_TU_NH16_TMY_RCP45_2050_Mir for the future climate scenario.

This study uses typical building construction types in Melbourne as a basis to construct building envelope models for residential and commercial buildings. For Urban Heat, the settings are more detailed to capture thermal mass and specific heat, as these are essential for Urban heat (but in total the study of urban heat provides the same R-values to the Energy section). The specific parameters are shown in the following table.

Table 13.5. Building Materials

Building Materials	Construction	Total R value {m2-K/W}	Solar absorptance
Basement Floor	Heavyweight concrete/insulation layer	2	-
Basement Wall	Heavyweight concrete/insulation layer	2	-
Exterior Wall	Finishes/Lightweight concrete/insulation layer/Finishes	2.8	0.6

Roof	Finishes/Lightweight concrete/insulation layer/Finishes	3.5	0.6
Interior Wall	Plasterboard partitions	0.3	-
Interior floor	Normalweight concrete/Finishes	0.55	-
		Total U value {m2-K/W}	SHGC
Double Glazed Window (40% WWR) Commercial building	Dbl Low-e 6mm/12mm/6mm Air/Aluminum frame with thermal break	2.7	0.7
Double Glazed Window (40% WWR) Residential building	Dbl Low-e 6mm/12mm/6mm Air/Aluminum frame with thermal break	1.7	0.25

Based on the detailed architectural layout designed by the architect, typical functional zoning settings were made for residential and commercial buildings, as shown in the following table.

Table 13.6. Functional zoning and usage parameters

Residential building	
Common area	0.15
Bedroom	0.3
Livingroom	0.4
Bathroom	0.08
Kitchen	0.07
Commercial building (Retail floor)	
Common area	0.3
Retail	0.65
Toilet	0.05
Commercial building (Office floor)	
Common area	0.2
Office room	0.6
Conference room	0.15
Toilet	0.05

The residential unit area is set to ≤100 m² and the occupancy density is 41.2 m²/person, based on NCC 2022. In commercial buildings, the office area is set to 10 m²/person, and the retail area is set to 3.5 m²/person, based on NABERS' handbook. For the building occupancy sequence, the occupancy curve defined in NCC 2022 is used.

For residential buildings, electrical load includes 4.38 W/m² for socket-type equipment, 36.2 W/m² for kitchen cooking, and 4 W/m² for lighting. Indoor areas are set with thermal zones according to functions: living rooms and bedrooms are air-conditioned areas during the day, and kitchens and bathrooms are

non-air-conditioned areas. Regarding commercial buildings, electrical equipment load is 15 W/m² for offices and 3.2 W/m² for retail spaces; lighting power density is 4.5 W/m² for offices and 14 W/m² for retail areas.

For residential buildings, split air conditioners are adopted. Considering the anticipated improvement in air conditioning efficiency, the coefficient of performance (COP) is set to 4, based on AEMO's assumptions. The heating temperature is set to 20°C from 6:00 to 24:00 and 18°C at night, while the cooling setpoint is 24°C. The fresh air system relies solely on natural ventilation, with no mechanical ventilation, and an air permeability rate of 0.7 air changes per hour. Domestic hot water is supplied by a heat pump water heater, with a daily hot water consumption of 10 L/person/day. The hot water load profile is based on the NatHERS hot water module.

For commercial buildings, a Dedicated Outdoor Air System (DOAS) is used, paired with a Variable Refrigerant Flow (VRF) system for cooling and heating at the terminals. The temperature setpoints are 21°C for heating and 24°C for cooling. Ventilation is provided at a rate of 10 L/s per person, with an air permeability rate of 0.35 air changes per hour. The domestic hot water system also uses a heat pump water heater, and the hot water usage profile is based on the default ASHRAE/NCC settings embedded in Ladybug Tools.

For residential buildings, this study adopts the NatHERS to evaluate and verify the heating and cooling loads. All residential buildings in the base case comply with the NatHERS 7-star standard under the current TMY weather file, with annual total heating and cooling loads not exceeding 99 MJ/m² (approximately 27.5 kWh/m²·year), including a heating load limit of 24.44 kWh/m²·year and a cooling load limit of 13.33 kWh/m²·year.

For commercial buildings, the energy efficiency level is rated and calibrated with reference to actual operational data from historical buildings in the NABERS energy rating system, aiming to achieve an efficiency level equivalent to NABERS 5.5 stars.

To evaluate the impact of the urban heat island effect on building energy consumption, this study extracted the simulation results of key meteorological parameters such as air temperature, relative humidity and wind speed on the hottest day for each scenario based on the simulation results of urban microclimate by ENVI-met. Then, standard EPW file was modified accordingly these results to generate a customized meteorological file that reflects the microclimate differences. Subsequently, the modified EPW file was imported into the simulation environment to analyse the changes in building energy consumption under different strategies and quantify the synergistic effect of various mitigation measures in reducing the urban heat island effect and improving building energy efficiency. The outputs are shown in Section 5.1.3.

13.2.6 EMS system level assessment

1) Load Factor (LF) — consumption efficiency

Load Factor measures how evenly electricity is used over time. It is calculated from hourly data as:

$$LF = \frac{Average\ Load\ over\ a\ period\ of\ time}{Peak\ load} \times 100\%$$

A higher LF means the energy management system has more consistent consumption, fewer spikes, better utilisation of existing network assets, and lower wear on equipment. The lower LFs indicate pronounced peaks and deep valleys, under-utilised infrastructure for most hours, and larger capacity required to meet short spikes.

2) Coefficient of Variation (CV) — short-term stability

$$CV = \frac{Standard\ deviation\ of\ load\ over\ a\ period\ of\ time}{Mean\ load}$$

A lower CV means a steadier, more predictable load; simpler to manage; less need for rapid ancillary responses, while higher CVs indicate spikier profile; greater reliance on fast services and reserve capacity.

13.2.7 Power system analysis

13.2.7.1 Modelling methodology

The detailed methods for constructing the precinct-level power system model involved extensive preprocessing and integration of original GIS data into a functional and accurate electrical network within DIgSILENT PowerFactory. The transformation of geographic data into PowerFactory-compatible elements included the following key stages:

Processing network parameters:

- Raw Data Extraction:
  The original raw GIS files provided spatial coordinates (latitude and longitude) and relevant technical parameters for each transformer and substation within the Sunshine Precinct. Each transformer records initially contained attributes such as geographic coordinates (latitude, longitude) and capacity (kVA rating), as shown in Figure 13.9.
  Transmission lines, initially represented as polyline features within the GIS dataset, were decomposed into a series of sequential geographical points, including the starting point, intermediate points, and endpoints. Each extracted point was then documented, including identifiers for line segments (From, Midpoints, To), alongside precise geographical coordinates (Latitude, Longitude), as illustrated clearly in Figure 13.10
- Coordinate Standardization and Validation:
  Latitude and longitude coordinates extracted from GIS files were standardized into decimal degrees format (WGS84) to ensure compatibility and accurate spatial referencing within PowerFactory. These processed coordinates, along with transformer capacities, were structured into CSV files as demonstrated in Figure 13.11.
- Integration into PowerFactory:
  Each transformer and substation coordinates were manually imported, ensuring the precise placement of each transformer within the DIgSILENT environment as illustrated in Figure 13.12. During the import process, transformer attributes, including rated power (kVA), voltage levels, and geographical coordinates, were verified to match accurately with the original dataset.
  The processed polyline coordinates (start, intermediate, end points) were inputted into PowerFactory's geographical position editor to precisely reconstruct the original geometry and routing of each transmission line segment. Figure 13.13 provides a representative example of a fully integrated transmission line segment displaying the detailed coordinate input within the PowerFactory environment.

This meticulous approach ensured the accurate geographical and technical representation of transmission lines in the digital network model.

Processing Loads (Buildings)

- Raw Building Footprint Data:
  Buildings within the precinct were originally provided as polygonal features representing footprints. To accurately represent load positions within the electrical model, building footprints were processed to identify the centroid (geometric center) of each building polygon, as shown in Figure 13.14.
- Load Positioning and Integration:
  Calculated centroid coordinates for each building were standardized and matched to respective building energy consumption profiles (hourly data) provided by other energy subgroup simulations. Each building's hourly load profile was then assigned and imported into the PowerFactory environment at the identified centroid coordinates.
- Load Aggregation and Validation:
  Load aggregation techniques were applied where necessary to group nearby buildings to a common node or substation feeder, reflecting realistic network configurations. Validation steps were undertaken to ensure each load correctly represented its geographic and electrical characteristics.

Network Model Validation and Completeness Check

- Topological Verification:
  After data import and integration, the constructed digital power network underwent rigorous topological verification within PowerFactory. Each element (transformer, line, load, substation node) was cross-checked against the original GIS spatial dataset, ensuring precise alignment, proper connectivity, and topological consistency, comparison of original GIS and network model as shown in Figure 13.15 and Figure 13.16.
- Electrical Parameter Validation:
  Electrical parameters for each network component were thoroughly reviewed. Voltage levels, transformer capacities, line impedances, and load profiles were verified to match original data accurately, ensuring a high-fidelity model suitable for subsequent simulation analyses.
- Scenario Integration Preparedness:
  Preparations were made to seamlessly integrate future energy scenarios (DER, BESS, EMS strategies) into the established baseline power network model, facilitating comparative analyses and scenario evaluations.

Transformer capacity baseline and group to transformer allocation

- Purpose and scope.
  This subsection specifies how transformer ratings were consolidated and how group loads were assigned to transformers for network analysis.
- Transformer rating register.
  Ratings are drawn from utility records and verified nameplates where available. Conflicts are resolved by preferring the more recent verified source, with the alternate value recorded in a notes column. Apparent power ratings are in kilovolt ampere. Where conversion from kilowatt is required a power factor of zero point nine five is applied unless a better value is documented for a specific asset.
- Allocation of groups to transformers.

Groups are allocated to transformers using feeder service areas and physical proximity. Where a group centroid lies close to a service boundary, the allocation follows the utility service rules used in the study area. The final allocation table records group id, transformer id, feeder id, and the allocation rule applied.

- Capacity criteria.
  Assessment follows the planning aim that the annual maximum loading for every transformer must be at or below ninety percent. The annual average loading should approach sixty percent subject to the maximum constraint. Any asset that approaches ninety percent is flagged as a bottleneck for option testing.
- Validation and freeze.
  The asset list is frozen to a specific date that is stated in the Appendix. Allocation results are validated by a spot check against spatial plots of service areas. Any remaining ambiguity is resolved before scenario studies commence.
- Deliverables.
  A machine readable transformer register with fields transformer id, feeder id, rating in kilovolt ampere, voltage level, data source, last verified date, and notes.
  A cross table with fields group id, transformer id, feeder id, allocation rule.

Scenario Setup and Simulation Readiness

The fully processed and integrated digital network model within PowerFactory served as a robust foundation for executing detailed time-series power flow simulations and scenario analyses. The following analyses were ready to be performed:

- Voltage stability assessments
- Line loss quantification
- DER and BESS integration impact analyses
- Comparative scenario analyses (base scenario, peak load, maximum DER penetration, EMS optimized scenarios, etc.)
- Sensitivity analyses for DER scalability and EV charging load variability

This detailed methodological process allowed for the construction of a realistic, GIS-based digital power system network within DIgSILENT PowerFactory, accurately reflecting real-world geographic distributions and electrical parameters for the Sunshine Precinct. Such rigorously structured and processed data provided a solid foundation for robust, meaningful power system analysis and scenario-based studies.

While the integration of detailed geographic and electrical data into the PowerFactory environment appears labour intensive at face value, the workflow adopted in this study has been substantially automated. All key steps, including extraction of spatial information from GIS files, transformation of geographic coordinates into PowerFactory compatible formats, batch creation of network infrastructure elements, and systematic adjustment of component locations, are implemented through a series of MATLAB scripts.

This scripted workflow represents an optimised and repeatable modelling pipeline rather than a manual, case specific process. Once established, the approach enables efficient re application to alternative precincts or revised development layouts with minimal manual intervention, limited primarily to input data updates. Future iterations of the model could further reduce setup effort through tighter integration with upstream GIS and building energy modelling tools, but the current framework already provides a scalable and reproducible foundation for precinct scale power system studies.

Assumptions

General assumptions:

- All lines operate at a nominal voltage of 22 kV.
- Conductor parameters (R, X, L) for underground cables and overhead lines are based on CSIRO public datasets (Berry *et al.*, 2015) and provided parameters (eg. AAAC KRYPTON 157.60 mm^2 overhead conductor and standard underground cable), as shown in Figure 13.17.
- Transformer and substation characteristics correspond directly to provided field data; transformer parameters and specifications are based on CSIRO public datasets, as shown in Figure 13.18.
- Load profiles accurately reflect the hourly electricity consumption of 321 buildings within the precinct.

Scenario assumptions:

- Load growth, DER distribution, and BESS integration and operational strategies are derived from simulations performed by other energy subgroups.
- All scenarios run over a full calendar year to capture the seasonal and annual variations in energy use and system performance.

Field: Add Calculate Selection: Select By Attributes Zoom To Switch Clear Delete Copy

	FID	Shape *	id	status	primary_vo	secondary_	tertiary_v	NP_RATING_	owner
1	17	Polyline	207849839	in service	22kV	LV	None	750 kVA	Powercor
2	48	Polyline	20489988	in service	22kV	LV	None	750 kVA	Powercor
3	50	Polyline	19863345	in service	22kV	LV	None	750 kVA	Powercor
4	61	Polyline	20581570	in service	22kV	LV	None	750 kVA	Powercor
5	95	Polyline	20657766	in service	22kV	LV	None	750 kVA	Powercor
6	133	Polyline	20489999	in service	22kV	LV	None	750 kVA	Powercor
7	157	Polyline	185164340	in service	22kV	LV	None	750 kVA	Powercor
8	181	Polyline	19861398	in service	22kV	LV	None	750 kVA	Powercor
9	226	Polyline	198077959	in service	22kV	LV	None	750 kVA	Powercor
10	99	Polyline	20585618	in service	22kV	LV	None	63 kVA	Powercor
11	149	Polyline	162163131	in service	22kV	LV	None	63 kVA	Powercor
12	3	Polyline	20643400	in service	22kV	LV	None	500 kVA	Powercor
13	14	Polyline	191194446	in service	22kV	LV	None	500 kVA	Powercor

Figure 13.9. Transformer raw GIS data

line_name	point_type	Latitude	Longitude
15367926	From	-37.78293162	144.809145
	Mid1	-37.78283356	144.8092898
	To	-37.78284638	144.8094289
15370976	From	-37.77922586	144.8280958
	Mid1	-37.77921993	144.8279234
	To	-37.77916704	144.8279049
15370994	From	-37.77961001	144.828081
	Mid1	-37.77958132	144.8278225
	Mid2	-37.77981817	144.8277807
	To	-37.7798192	144.82779
19154689	From	-37.79742979	144.8362767
	Mid1	-37.79742822	144.8362627
	Mid2	-37.79744161	144.8362603
	Mid3	-37.79770383	144.8362107
	To	-37.79771276	144.8361794
19154707	From	-37.79010752	144.8324617
	Mid1	-37.79010459	144.8324574
	Mid2	-37.79011657	144.8324445
	Mid3	-37.79012535	144.8324574
	To	-37.7904505	144.832109
19154713	From	-37.78216298	144.8348747
	Mid1	-37.78220234	144.8335122
	Mid2	-37.78220264	144.833502
	Mid3	-37.78219665	144.8335017
	Mid4	-37.78219746	144.8334772
	Mid5	-37.78219656	144.8334772
	Mid6	-37.78219566	144.8334772
	To	-37.78219475	144.8334771

Figure 13.10. Transmission line with coordinates

id	lon	lat	capacity_kVA
19863004	144.7971508	-37.79796239	300 kVA
162735289	144.7999158	-37.79129069	315 kVA
19862971	144.8055714	-37.77266184	1000 kVA
20643400	144.8097364	-37.77225244	500 kVA
19862960	144.8017927	-37.77218089	200 kVA
164254870	144.8214616	-37.77157277	1500 kVA
19863213	144.7995718	-37.77148652	300 kVA
20645122	144.8115807	-37.77132992	200 kVA
64823268	144.8098698	-37.77099889	200 kVA
19862938	144.8044062	-37.76976241	300 kVA
203552187	144.7975359	-37.76941336	1000 kVA
203551932	144.7975781	-37.76935779	1000 kVA
19862916	144.8185827	-37.76886694	100 kVA
73769168	144.8102769	-37.76878749	315 kVA
191194446	144.8184259	-37.76786234	500 kVA
93937631	144.824055	-37.76694302	200 kVA
41153649	144.8113526	-37.76604827	200 kVA
207849839	144.8196767	-37.76585438	750 kVA
20526967	144.8068956	-37.79620947	25 kVA
19863587	144.8092958	-37.79599461	200 kVA
19863697	144.8048278	-37.79280427	200 kVA
19863488	144.810627	-37.79138847	300 kVA
19863653	144.8048584	-37.78976617	200 kVA
19863477	144.8082385	-37.7881642	300 kVA
160593955	144.8107312	-37.78796672	315 kVA
20556046	144.8062637	-37.78795045	315 kVA
19863664	144.8007759	-37.78786658	200 kVA
163031299	144.7998341	-37.78711021	200 kVA
19863642	144.8033901	-37.78681804	500 kVA
200532726	144.812382	-37.78591271	315 kVA

Figure 13.11. Transformer with coordinates and capacity

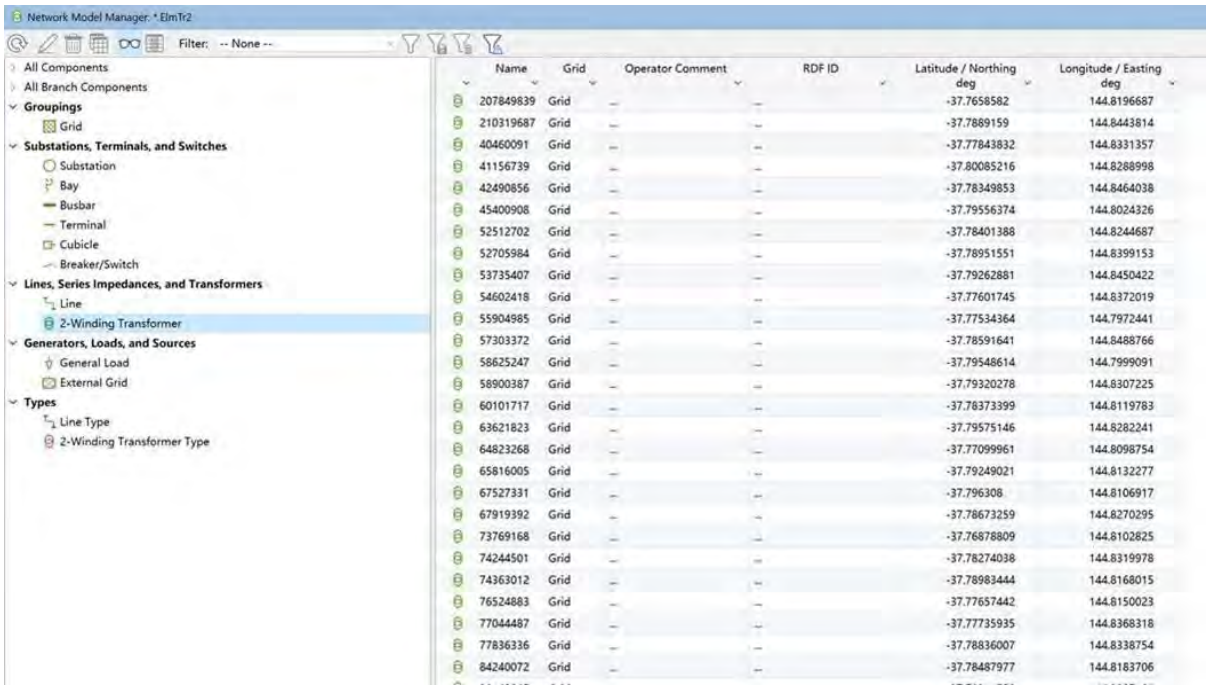

Figure 13.12. Transformer with coordinates in PowerFactory

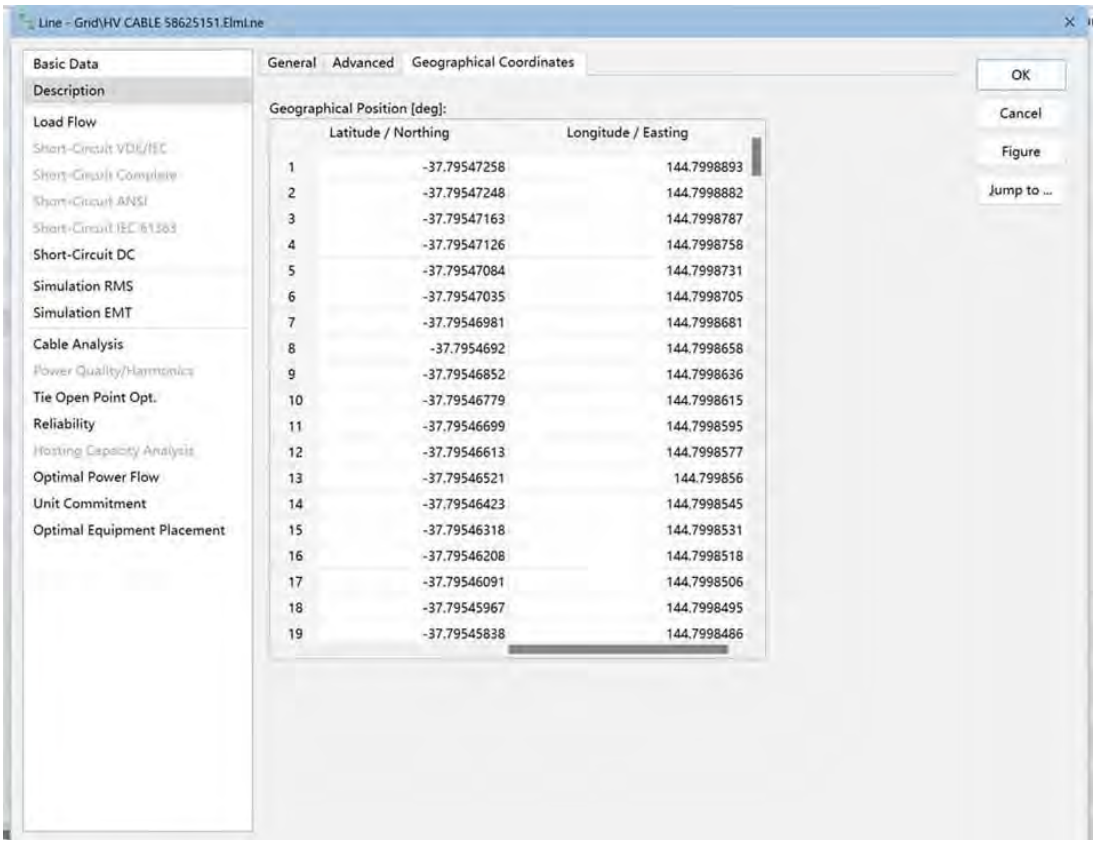

Figure 13.13. One transmission line with coordinates in PowerFactory

	A	B	C
1	GroupID	Lon_E	Lat_S
2	G1	144.8200059	-37.77480292
3	G10	144.8297984	-37.77560185
4	G11	144.8296795	-37.77658
5	G12	144.8259616	-37.77744746
6	G13	144.8280357	-37.77758791
7	G14	144.8182519	-37.77367569
8	G15	144.8198832	-37.77547225
9	G16	144.8210657	-37.77563977
10	G17	144.8221504	-37.77576839
11	G18	144.8238822	-37.77524489
12	G19	144.8249432	-37.77443399
13	G2	144.8191742	-37.7739325
14	G20	144.82551	-37.77330332
15	G21	144.8273952	-37.77534777
16	G22	144.8316111	-37.77681013
17	G23	144.8162452	-37.77441546
18	G24	144.8176948	-37.77463879
19	G25	144.8183734	-37.774722
20	G26	144.8160705	-37.77495922
21	G27	144.8169087	-37.77510759
22	G28	144.8175593	-37.77518737
23	G29	144.8182099	-37.77526714
24	G3	144.8179602	-37.77410912
25	G30	144.819117	-37.77481426
26	G31	144.81901	-37.7753655
27	G32	144.8233189	-37.77475949
28	G33	144.8241924	-37.77572195
29	G34	144.8245554	-37.77607411
30	G35	144.8242493	-37.77316757
31	G36	144.8248771	-37.77322106
32	G37	144.8247573	-37.77385367

Figure 13.14. Building groups with coordinates

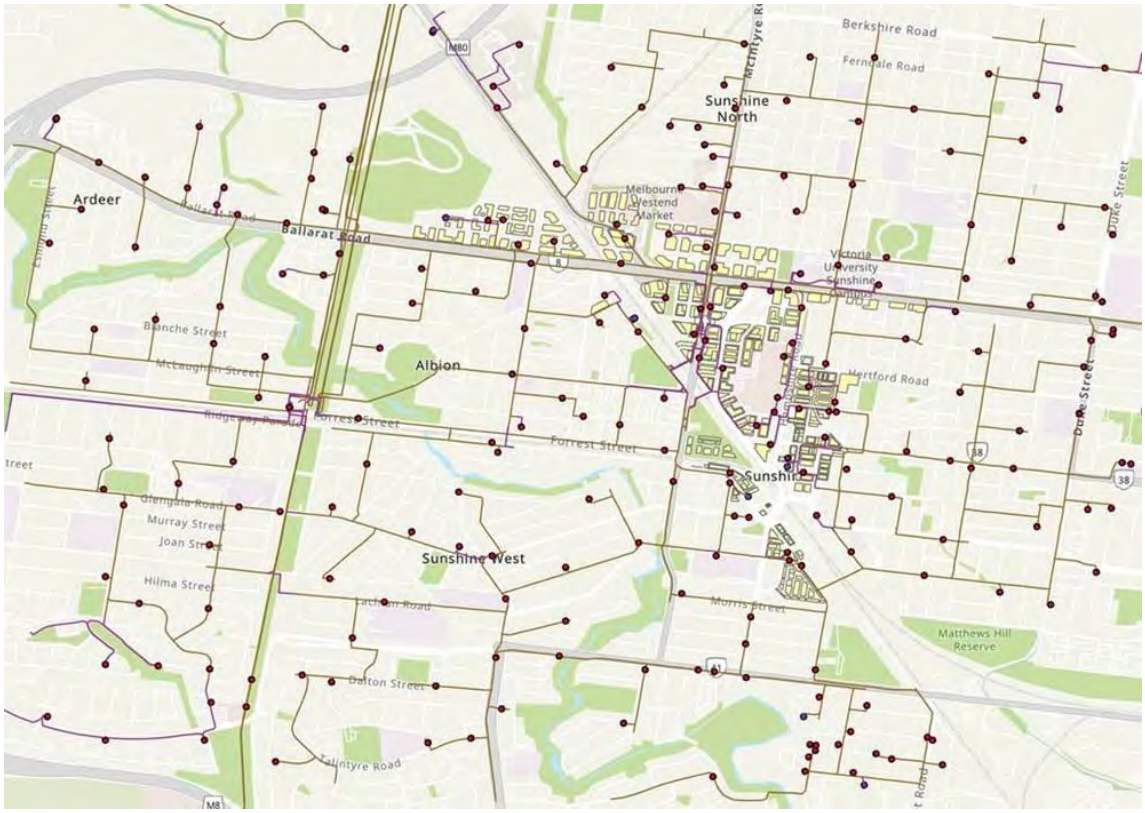

Figure 13.15. Original Network Topology

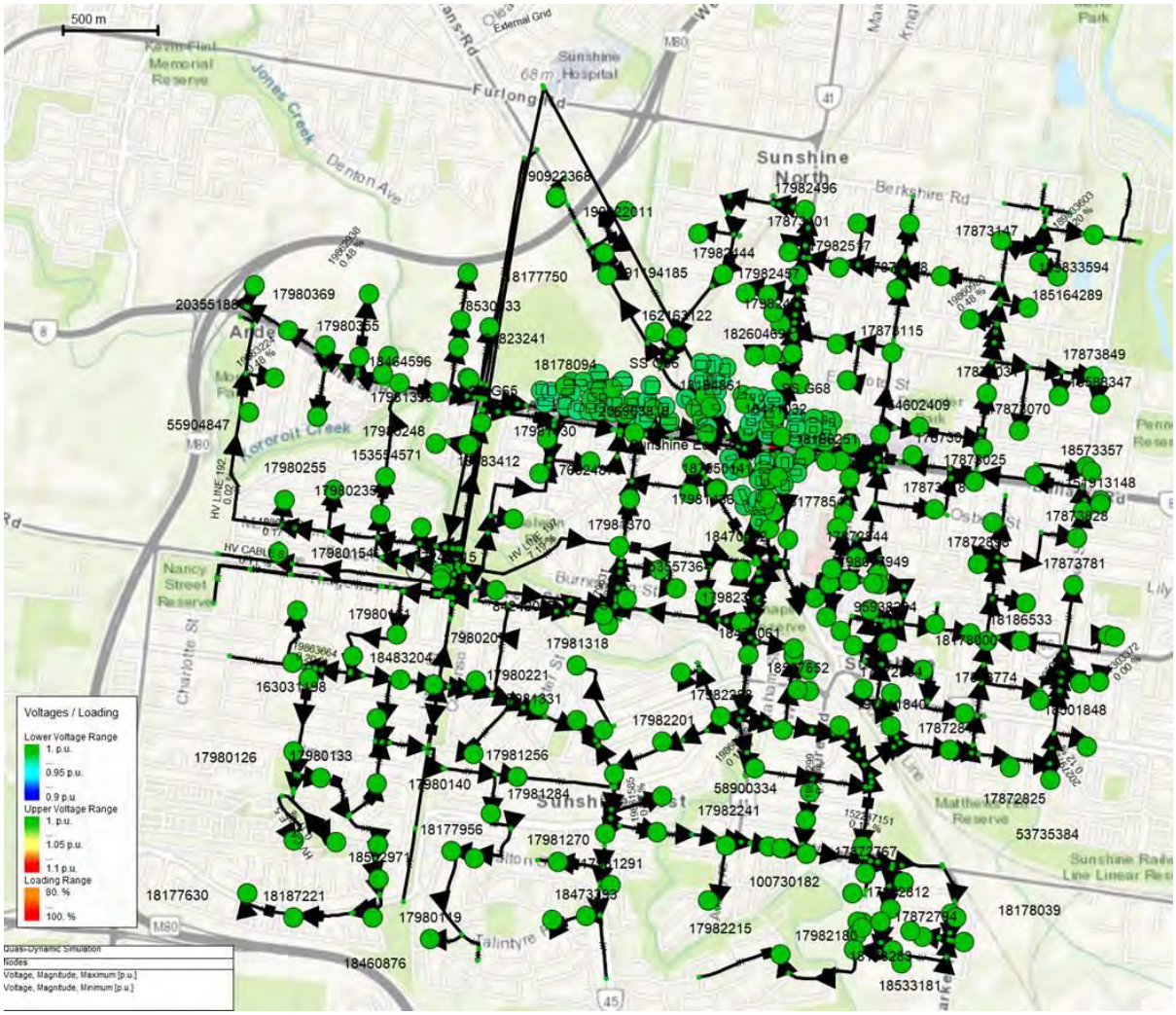

Figure 13.16. Network Topology Simulation in PowerFactory

13.2.7.2 Input data and sources

Table 13.7. Data and source for power system

Data Category	Data Sources	Data Format
Network Topology	Provided GIS network topology	GIS/Coordinate
Transformers & Specifications	Provided GIS network topology; Electrical parameters derived from CSIRO Representative Australian Feeder data	GIS/Coordinate
Distribution Lines& Specifications	Provided GIS network topology; Conductor parameters derived from CSIRO Representative Australian Feeder data	GIS/Coordinate
Substations	Provided GIS network topology	CSV
Hourly Building Load Profiles	Energy subgroup simulation outputs	CSV

Load+DER Capacity, Layout, and Location	Energy subgroup simulation outputs	CSV / GIS coordinates
Battery Energy Storage Systems	Energy subgroup simulation outputs	CSV
EMS Control Logic & Operational output	Energy subgroup simulation outputs	Documentation, CSV

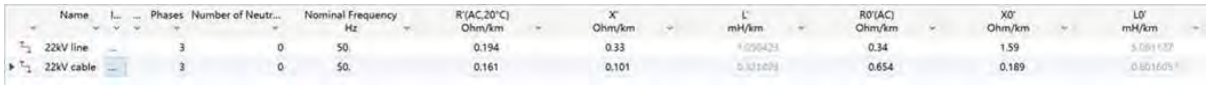

Name	I...	...	Phases	Number of Neutr...	Nominal Frequency Hz	R'(AC,20°C) Ohm/km	X' Ohm/km	L' mH/km	R0'(AC) Ohm/km	X0' Ohm/km	L0' mH/km
22kV line			3	0	50.	0.194	0.33		0.34	1.59	
22kV cable			3	0	50.	0.161	0.101		0.654	0.189	

Figure 13.17. Conductor parameters

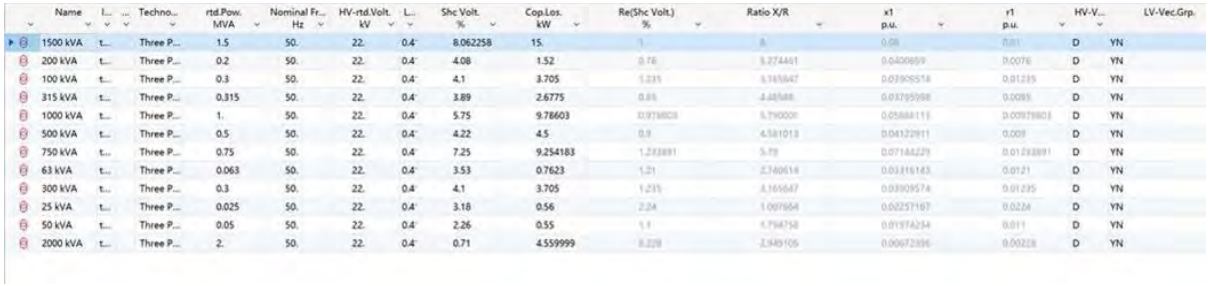

Name	I...	...	Techno...	rtd.Pow. MVA	Nominal Fr... Hz	HV-rtd.Volt. kV	L...	Shc Volt. %	Cop.Los. kW	Re(Shc Volt.) %	Ratio X/R	x1 p.u.	r1 p.u.	HV-V...	LV-Vec.Grp.
1500 kVA	t...		Three P...	1.5	50.	22.	0.4	8.062258	15.					D	YN
200 kVA	t...		Three P...	0.2	50.	22.	0.4	4.08	1.52					D	YN
100 kVA	t...		Three P...	0.3	50.	22.	0.4	4.1	3.705					D	YN
315 kVA	t...		Three P...	0.315	50.	22.	0.4	3.89	2.6775					D	YN
1000 kVA	t...		Three P...	1.	50.	22.	0.4	5.75	9.78603					D	YN
500 kVA	t...		Three P...	0.5	50.	22.	0.4	4.22	4.5					D	YN
750 kVA	t...		Three P...	0.75	50.	22.	0.4	7.25	9.254183					D	YN
63 kVA	t...		Three P...	0.063	50.	22.	0.4	3.53	0.7623					D	YN
300 kVA	t...		Three P...	0.3	50.	22.	0.4	4.1	3.705					D	YN
25 kVA	t...		Three P...	0.025	50.	22.	0.4	3.18	0.56					D	YN
50 kVA	t...		Three P...	0.05	50.	22.	0.4	2.26	0.55					D	YN
2000 kVA	t...		Three P...	2.	50.	22.	0.4	0.71	4.559999					D	YN

Figure 13.18. Transformer specifications

13.2.7.3 Objectives of the power system analysis

The primary objectives of the power system digitalization and integration analysis include:

- Voltage Stability Analysis:
  To evaluate voltage variations at each bus node within the Sunshine Precinct under different operational scenarios, ensuring that node voltages remain within Australian standards (0.95 p.u. – 1.05 p.u.).
- Network Losses Analysis:
  To quantify power line losses across different scenarios, providing insights into network efficiency and economic performance.
- DER Integration Impact Analysis:
  To investigate impacts of integrating distributed energy resources, including rooftop / facade photovoltaic systems and battery energy storage systems (BESS), on grid operation, voltage quality, losses, and capacity utilization.
- Scenario Comparison Analysis:
  To analyse and compare network performance variations across multiple scenarios, such as the baseline scenario, maximum PV generation scenario, peak load scenario, and energy management optimization scenario.

13.2.7.4 Data inputs and model interfaces

The power system model is driven by externally generated, scenario-specific hourly time-series inputs representing net electrical demand at the building level. All demand-side technologies are aggregated prior to network simulation.

Building net load profiles are constructed by combining baseline building electricity demand with on-site distributed energy resources and controllable loads. Specifically, photovoltaic generation, battery energy storage systems (BESS), and electric vehicle (EV) charging are resolved at the building level and aggregated into a single hourly net load profile for each building.

BESS charging and discharging behaviour, as well as EV charging schedules, are defined exogenously based on scenario assumptions. These profiles are not optimised within the power system model and do not respond dynamically to network conditions. The network simulation therefore evaluates system performance under imposed net load trajectories rather than actively managing DER operation.

Each building net load profile is mapped to a corresponding low-voltage load node based on spatial location and feeder assignment. All inputs share a common hourly resolution and simulation horizon. The power system model does not internally alter demand or DER schedules; its role is limited to assessing voltage compliance, thermal loading, and network losses under the specified operating conditions.

This structure ensures that differences in network performance across scenarios arise solely from variations in building-level net load composition and spatial distribution, rather than from model-side control or optimisation logic.

13.2.7.5 Simulation scenario definitions

Two simulation scenario types are considered in this study. All simulations are driven by hourly building-level net load profiles, which are mapped directly to the distribution network model. No optimisation or control is performed within the power system simulation.

Baseline Building Load Scenario: This scenario represents the post-development precinct with new buildings connected to the existing distribution network, but without distributed energy resources. Loads consist solely of building electricity demand. No rooftop PV, BIPV, battery storage, or EV charging is included. Hourly building demand profiles are derived from precinct-scale building energy simulations and aggregated to network load nodes. This scenario establishes a reference operating condition for assessing the incremental impacts of distributed energy resource deployment.

Distributed Energy Resource Scenarios (144 configurations): A total of 144 DER scenarios is simulated to evaluate network performance under varying levels of distributed energy adoption. In all cases, DER impacts are incorporated by modifying building-level net load profiles prior to network simulation.

Each scenario includes a combination of the following parameters:

- Rooftop PV: fixed at 20% coverage
- BIPV coverage: North-facing façades: 0–80%
- East–West façades: 0–80%
- Electric vehicles (EV): 20–80% penetration
- Battery energy storage systems (BESS): low, medium, and high-capacity levels

Photovoltaic generation, EV charging demand, and battery charging/discharging profiles are specified exogenously and combined with baseline building demand to form hourly net load profiles. These net

loads are then used as direct inputs to the distribution network model. Network topology and asset ratings remain unchanged across all DER scenarios.

Across both scenario types, differences in network performance arise exclusively from changes in building-level net load composition, rather than from internal network optimisation, dynamic control, or topology modification.

13.2.7.6 Risk and sensitivity analysis

A sensitivity analysis is included to explore critical uncertainties and risks related to DER and EV integration, focusing specifically on:

- DER Penetration Sensitivity

  Analysis of different DER penetration levels (PV systems and BESS) to assess network impact sensitivity to renewable energy variability.
- Electric Vehicle (EV) Charging Load Sensitivity

  Analysis of the network impacts due to varying EV charging load intensities and timing, evaluating voltage stability and capacity margins under high EV integration scenarios.

This sensitivity analysis enables evaluation of system robustness and adaptability under uncertain future energy transitions.

13.3 Supplementary data and results

13.3.1 Power system analysis results

Based on the defined objectives and scenarios, the analysis will output and examine:

- Voltage Stability:

  Hourly and annual voltage variation profiles at nodes, identifying any potential violations.
- Capacity Margin Analysis:

  Network capacity margin assessments for all defined scenarios, quantifying infrastructure adequacy.
- Network Losses:

  Quantification and comparative analysis of line losses for each scenario.
- DER & BESS Integration Impacts:

  Assessment of voltage profiles, line loading, and system performance changes caused by DER and battery storage systems integration.
- Scenario Comparisons:

  Systematic performance comparison between scenarios, highlighting critical differences and providing insights for planning and operational decision-making.
- Sensitivity Analysis Outcomes:

Outcomes of DER and EV charging load sensitivity analyses, providing a clearer understanding of network resilience under varied future conditions.

Transformer loading and capacity headroom

Table 13.8. Summary of worst-case transformer loading under the Base case for feasible scenarios

Scenarios	worst Device Max Loading/ %	Worst Device Over 80%_hours Count
s49	98.666948	71
s52	98.666422	72
s46	98.666055	66
s28	97.14561	138
s31	97.142341	141
s34	97.139376	142
s40	95.502838	47
s43	95.501625	48
s37	95.50091	42
refer	89.238505	14
s7	87.019096	7
s4	86.974824	7
s1	86.125749	6
s16	83.95079	4
s13	83.905814	3
s10	82.687464	1
s25	79.143633	0
s22	79.099648	0
s19	77.736733	0

This table reports, for each feasible scenario, the maximum annual loading observed on the most heavily loaded distribution transformer and the number of hours for which that transformer operates above eighty percent of its nameplate rating. Results are derived from hourly simulations and are used to identify asset-level binding constraints under the Base case planning envelope.

Table 13.9. Distribution of transformer utilisation levels across the feasible scenarios under the Base case

scenario	over 60% trans Count	over 70% trans	over 80% trans
s1	14	2	1

s4	15	2	1
s7	15	2	1
s10	12	2	1
s13	12	2	1
s16	13	2	1
s19	12	3	0
s22	13	3	0
s25	13	3	0
s28	15	5	2
s31	16	5	2
s34	16	5	2
s37	16	6	2
s40	17	6	3
s43	18	6	3
s46	16	6	2
s49	17	6	2
s52	17	6	2

This table reports the number of distribution transformers operating above sixty percent, seventy percent, and eighty percent of nameplate rating for each feasible scenario, providing a network-wide view of loading dispersion and available headroom.

Table 13.10. Summary of network losses for Base Case

Row	Yearly Total Loss / MWh	Mean Loss / MW	Max Loss / MW	Peak Loss / MW	Peak Share	Mean Abs	P95 Abs Delta / MW	Delta Total Vs Ref / MWh	Delta Total Vs Ref / pct
s52	2637.50	0.30	0.49	450.29	0.17	0.01	0.02	-72.57	-3.00%
s49	2638.71	0.30	0.49	450.07	0.17	0.01	0.02	-71.36	-3.00%
s46	2644.33	0.30	0.49	451.20	0.17	0.01	0.02	-65.73	-2.00%
s43	2646.23	0.30	0.51	452.12	0.17	0.01	0.02	-63.84	-2.00%
s40	2647.85	0.30	0.51	452.15	0.17	0.01	0.02	-62.21	-2.00%

s37	2653.31	0.30	0.51	453.42	0.17	0.01	0.02	-56.75	-2.00%
s34	2662.30	0.30	0.51	451.10	0.17	0.01	0.02	-47.76	-2.00%
s31	2663.85	0.30	0.51	451.48	0.17	0.01	0.02	-46.22	-2.00%
s28	2668.38	0.31	0.50	452.49	0.17	0.01	0.02	-41.68	-2.00%
s25	2674.35	0.31	0.52	453.37	0.17	0.01	0.02	-35.71	-1.00%
s22	2676.38	0.31	0.52	454.00	0.17	0.01	0.02	-33.68	-1.00%
s19	2680.81	0.31	0.52	455.26	0.17	0.01	0.02	-29.25	-1.00%
s16	2689.84	0.31	0.55	456.27	0.17	0.01	0.02	-20.22	-1.00%
s13	2692.01	0.31	0.54	457.20	0.17	0.01	0.02	-18.06	-1.00%
s7	2703.01	0.31	0.56	459.16	0.17	0.01	0.02	-7.06	0.00%
s4	2704.87	0.31	0.56	460.28	0.17	0.01	0.02	-5.19	0.00%
s1	2708.23	0.31	0.55	461.59	0.17	0.01	0.02	-1.83	0.00%
refer	2710.06	0.31	0.58	465.74	0.17	0.01	0.03	0.00	0.00%
s10	2944.79	0.34	0.55	463.37	0.16	0.01	0.06	234.72	9.00%

13.3.2 Clustering results of Scenario 1

Table 13.11. S1C1: Balanced outcomes

Scenario Code	EV uptake (% of Dwelling)	Battery Capacity (MWh)	Roof PV Capacity (MW)	BIPV Capacity (MW)	North BIPV Coverage Ratio	E/W BIPV Coverage Ratio	Infrastructure upgrade cost (AUD)	SSR	IRR
P01F02N02S03B02E02	20%	79.24	9.05	39.74	20%	50%	3941.90	17.73%	4.14%
P01F02N02S03B03E02	20%	79.24	9.05	39.74	20%	50%	3941.90	17.61%	4.51%
P01F02N02S03B03E03	50%	79.24	9.05	39.74	20%	50%	42735.00	16.45%	4.24%
P01F02N02S04B03E02	20%	89.40	9.05	47.15	20%	80%	12577.00	19.50%	4.03%

Table 13.12. S1C2: Renewable-forward (policy-supported)

Scenario Code	EV uptake (% of Dwelling)	Battery Capacity (MWh)	Roof PV Capacity (MW)	BIPV Capacity (MW)	North BIPV Coverage Ratio	E/W BIPV Coverage Ratio	Infrastructure upgrade cost (AUD)	SSR	IRR
P01F02N02S03B01E02	20%	79.24	9054.50	39738.00	20%	50%	3941.90	17.42%	3.61%
P01F02N02S03B01E03	50%	79.24	9054.50	39738.00	20%	50%	42735.00	15.72%	3.44%
P01F02N02S03B02E03	50%	79.24	9054.50	39738.00	20%	50%	42735.00	16.27%	3.93%
P01F02N02S04B01E02	20%	89.40	9054.50	47150.00	20%	80%	12577.00	19.42%	3.18%
P01F02N02S04B01E03	50%	89.40	9054.50	47150.00	20%	80%	51370.00	17.54%	3.04%
P01F02N02S04B02E02	20%	89.40	9054.50	47150.00	20%	80%	12577.00	19.69%	3.68%
P01F02N02S04B02E03	50%	89.40	9054.50	47150.00	20%	80%	51370.00	18.22%	3.52%
P01F02N02S04B03E03	50%	89.40	9054.50	47150.00	20%	80%	51370.00	18.38%	3.78%
P01F02N03S01B01E02	20%	118.59	9054.50	68460.00	50%	0%	44612.00	25.02%	2.37%
P01F02N03S01B02E02	20%	118.59	9054.50	68460.00	50%	0%	50869.00	25.17%	2.80%
P01F02N03S01B03E02	20%	118.59	9054.50	68460.00	50%	0%	50869.00	24.86%	3.13%
P01F02N03S02B01E02	20%	125.36	9054.50	73402.00	50%	20%	45426.00	26.65%	2.26%
P01F02N03S02B02E02	20%	125.36	9054.50	73402.00	50%	20%	51683.00	26.77%	2.68%
P01F02N03S02B03E02	20%	125.36	9054.50	73402.00	50%	20%	51683.00	26.41%	3.00%

Table 13.13. S1C3: Market-ready (conservative)

Scenario Code	EV uptake (% of Dwelling)	Battery Capacity (MWh)	Roof PV Capacity (MW)	BIPV Capacity (MW)	North BIPV Coverage Ratio	E/W BIPV Coverage Ratio	Infrastructure upgrade cost (AUD)	SSR	IRR
P01F01N01S01B01E01	0%	24.81	9054.50	0.00	0%	0%	0.00	6.06%	10.12%
P01F02N01S01B01E02	20%	24.81	9054.50	0.00	0%	0%	0.00	5.49%	11.58%
P01F02N01S01B02E02	20%	24.81	9054.50	0.00	0%	0%	0.00	5.52%	12.37%
P01F02N01S01B02E03	50%	24.81	9054.50	0.00	0%	0%	38793.00	5.02%	12.09%
P01F02N01S01B03E02	20%	24.81	9054.50	0.00	0%	0%	0.00	5.51%	13.12%
P01F02N01S01B03E03	50%	24.81	9054.50	0.00	0%	0%	38793.00	5.02%	12.57%
P01F02N01S02B01E02	20%	31.58	9054.50	4941.60	0%	20%	0.00	7.02%	8.47%

P01F02N01S02B02E02	20%	31.58	9054.50	4941.60	0%	20%	0.00	7.07%	9.09%
P01F02N01S02B02E03	50%	31.58	9054.50	4941.60	0%	20%	38793.00	6.43%	8.80%
P01F02N01S02B03E02	20%	31.58	9054.50	4941.60	0%	20%	0.00	7.07%	9.64%
P01F02N01S02B03E03	50%	31.58	9054.50	4941.60	0%	20%	38793.00	6.44%	9.23%
P01F02N01S03B01E02	20%	41.73	9054.50	12354.00	0%	50%	0.00	9.15%	6.16%
P01F02N01S03B01E03	50%	41.73	9054.50	12354.00	0%	50%	50369.00	8.30%	5.99%
P01F02N01S03B02E02	20%	41.73	9054.50	12354.00	0%	50%	0.00	9.25%	6.71%
P01F02N01S03B02E03	50%	41.73	9054.50	12354.00	0%	50%	38793.00	8.45%	6.48%
P01F02N01S03B03E02	20%	41.73	9054.50	12354.00	0%	50%	0.00	9.23%	7.14%
P01F02N01S03B03E03	50%	41.73	9054.50	12354.00	0%	50%	38793.00	8.49%	6.82%
P01F02N01S04B01E02	20%	51.88	9054.50	19766.00	0%	80%	0.00	11.09%	4.85%
P01F02N01S04B01E03	50%	51.88	9054.50	19766.00	0%	80%	50369.00	10.07%	4.72%
P01F02N01S04B02E02	20%	51.88	9054.50	19766.00	0%	80%	0.00	11.22%	5.36%
P01F02N01S04B02E03	50%	51.88	9054.50	19766.00	0%	80%	38793.00	10.33%	5.20%
P01F02N01S04B03E02	20%	51.88	9054.50	19766.00	0%	80%	0.00	11.15%	5.73%
P01F02N01S04B03E03	50%	51.88	9054.50	19766.00	0%	80%	38793.00	10.38%	5.48%
P01F02N02S01B01E02	20%	62.32	9054.50	27384.00	20%	0%	0.00	13.67%	4.42%
P01F02N02S01B02E02	20%	62.32	9054.50	27384.00	20%	0%	0.00	13.91%	5.00%
P01F02N02S01B02E03	50%	62.32	9054.50	27384.00	20%	0%	41171.00	12.67%	4.72%
P01F02N02S01B03E02	20%	62.32	9054.50	27384.00	20%	0%	0.00	13.89%	5.42%
P01F02N02S01B03E03	50%	62.32	9054.50	27384.00	20%	0%	41171.00	12.81%	5.08%
P01F02N02S02B01E02	20%	69.09	9054.50	32326.00	20%	20%	0.00	15.24%	4.08%
P01F02N02S02B02E02	20%	69.09	9054.50	32326.00	20%	20%	0.00	15.53%	4.65%
P01F02N02S02B02E03	50%	69.09	9054.50	32326.00	20%	20%	41171.00	14.16%	4.38%
P01F02N02S02B03E02	20%	69.09	9054.50	32326.00	20%	20%	0.00	15.48%	5.04%
P01F02N02S02B03E03	50%	69.09	9054.50	32326.00	20%	20%	41171.00	14.32%	4.73%

13.3.3 Clustering results of Scenario 3

Table 13.14. S3C1: Balanced outcomes

Scenario Code	EV uptake (% of Dwelling)	Battery Capacity (MWh)	Roof PV Capacity (MW)	BIPV Capacity (MW)	North BIPV Coverage Ratio	E/W BIPV Coverage Ratio	Infrastructure upgrade cost (AUD)	SSR	IRR
'P01F02N01S04B02E02'	20%	38.94	2.33	23.76	0%	80%	0.00	11.44%	3.60%
'P01F02N01S04B03E02'	20%	38.94	2.33	23.76	0%	80%	0.00	11.50%	3.98%
'P01F02N02S03B02E02'	20%	43.90	2.33	27.38	20%	50%	8572.10	13.21%	3.30%
'P01F02N02S03B03E02'	20%	43.90	2.33	27.38	20%	50%	8572.10	12.65%	3.70%
'P01F02N02S04B03E02'	20%	56.10	2.33	36.29	20%	80%	8572.10	15.92%	3.30%

Table 13.15. S3C2: Renewable-forward (policy-supported)

Scenario Code	EV uptake (% of Dwelling)	Battery Capacity (MWh)	Roof PV Capacity (MW)	BIPV Capacity (MW)	North BIPV Coverage Ratio	E/W BIPV Coverage Ratio	Infrastructure upgrade cost (AUD)	SSR	IRR
'P01F02N01S04B01E02'	20%	38.94	2.33	23.76	0%	80%	0.00	11.73%	3.15%
'P01F02N02S03B01E02'	20%	43.90	2.33	27.38	20%	50%	8572.10	12.62%	2.98%
'P01F02N02S04B01E02'	20%	56.10	2.33	36.29	20%	80%	8572.10	16.94%	2.45%
'P01F02N02S04B02E02'	20%	56.10	2.33	36.29	20%	80%	8572.10	16.69%	3.04%
'P01F02N03S01B01E02'	20%	49.30	2.33	31.32	50%	0%	10887.00	12.43%	2.13%
'P01F02N03S01B02E02'	20%	49.30	2.33	31.32	50%	0%	10887.00	13.17%	2.59%
'P01F02N03S01B03E02'	20%	49.30	2.33	31.32	50%	0%	10887.00	12.81%	2.85%
'P01F02N03S02B01E02'	20%	57.44	2.33	37.26	50%	20%	17144.00	14.97%	2.08%
'P01F02N03S02B02E02'	20%	57.44	2.33	37.26	50%	20%	17144.00	15.55%	2.44%
'P01F02N03S02B03E02'	20%	57.44	2.33	37.26	50%	20%	17144.00	15.54%	2.68%
'P01F02N03S03B01E02'	20%	69.64	2.33	46.17	50%	50%	29658.00	18.76%	1.81%
'P01F02N03S03B02E02'	20%	69.64	2.33	46.17	50%	50%	29658.00	19.06%	2.22%
'P01F02N03S03B03E02'	20%	69.64	2.33	46.17	50%	50%	29658.00	18.74%	2.45%
'P01F02N03S04B01E02'	20%	81.85	2.33	55.08	50%	80%	51558.00	21.50%	1.69%
'P01F02N03S04B02E02'	20%	81.85	2.33	55.08	50%	80%	51558.00	22.31%	2.03%
'P01F02N03S04B03E02'	20%	81.85	2.33	55.08	50%	80%	51558.00	22.62%	2.29%
'P01F02N04S01B01E02'	20%	75.05	2.33	50.12	80%	0%	70329.00	18.56%	1.17%
'P01F02N04S01B03E02'	20%	75.05	2.33	50.12	80%	0%	70329.00	17.21%	1.78%
'P01F02N04S02B01E02'	20%	83.18	2.33	56.06	80%	20%	70329.00	20.31%	1.14%

Table 13.16. S3C3: Market-ready (conservative)

Scenario Code	EV uptake (% of Dwelling)	Battery Capacity (MWh)	Roof PV Capacity (MW)	BIPV Capacity (MW)	North BIPV Coverage Ratio	E/W BIPV Coverage Ratio	Infrastructure upgrade cost (AUD)	SSR	IRR
'P01F01N01S01B01E01'	0%	6.39	2.33	0.00	0%	0%	0.00	2.25%	10.39%
'P01F02N01S01B01E02'	20%	6.39	2.33	0.00	0%	0%	0.00	1.84%	11.71%

'P01F02N01S01B02E02'	20%	6.39	2.33	0.00	0%	0%	0.00	1.93%	12.75%
'P01F02N01S01B03E02'	20%	6.39	2.33	0.00	0%	0%	0.00	1.93%	13.29%
'P01F02N01S02B01E02'	20%	14.53	2.33	5.94	0%	20%	0.00	4.36%	5.61%
'P01F02N01S02B02E02'	20%	14.53	2.33	5.94	0%	20%	0.00	4.35%	6.05%
'P01F02N01S02B02E03'	50%	14.53	2.33	5.94	0%	20%	76335.00	3.85%	5.71%
'P01F02N01S02B03E02'	20%	14.53	2.33	5.94	0%	20%	0.00	4.51%	6.58%
'P01F02N01S02B03E03'	50%	14.53	2.33	5.94	0%	20%	76335.00	3.91%	6.11%
'P01F02N01S03B01E02'	20%	26.73	2.33	14.85	0%	50%	0.00	8.11%	3.98%
'P01F02N01S03B01E03'	50%	26.73	2.33	14.85	0%	50%	70078.00	7.09%	3.77%
'P01F02N01S03B02E02'	20%	26.73	2.33	14.85	0%	50%	0.00	8.31%	4.41%
'P01F02N01S03B02E03'	50%	26.73	2.33	14.85	0%	50%	76335.00	7.50%	4.20%
'P01F02N01S03B03E02'	20%	26.73	2.33	14.85	0%	50%	0.00	8.38%	4.72%
'P01F02N01S03B03E03'	50%	26.73	2.33	14.85	0%	50%	76335.00	7.37%	4.48%
'P01F02N01S04B02E03'	50%	38.94	2.33	23.76	0%	80%	76335.00	10.66%	3.42%
'P01F02N01S04B03E03'	50%	38.94	2.33	23.76	0%	80%	76335.00	10.93%	3.79%
'P01F02N02S01B01E02'	20%	23.56	2.33	12.53	20%	0%	2315.10	6.71%	3.85%
'P01F02N02S01B02E02'	20%	23.56	2.33	12.53	20%	0%	2315.10	6.81%	4.31%
'P01F02N02S01B03E02'	20%	23.56	2.33	12.53	20%	0%	2315.10	6.80%	4.86%
'P01F02N02S02B01E02'	20%	31.69	2.33	18.47	20%	20%	2315.10	9.20%	3.46%
'P01F02N02S02B02E02'	20%	31.69	2.33	18.47	20%	20%	2315.10	9.18%	3.94%
'P01F02N02S02B03E02'	20%	31.69	2.33	18.47	20%	20%	2315.10	9.32%	4.28%

Acknowledgement

The team would like to acknowledge Development Victoria, Greater Western Water, Brimbank City Council, Powercor, and Solar Victoria / the Department of Energy, Environment and Climate Action for their valuable support and guidance throughout the project. We also extend our sincere thanks to Geoff Connellan (G&M Connellan Consultants), Stephen Livesley (The University of Melbourne), and Sujan Dev (HIP V. HYPE) for their expert input and assistance in refining the assumptions applied in this project.

The embodied carbon subgroup would like to acknowledge the contributions of Pranav Jaikant for his assistance during the early stages of project development and material selection. We also thank Malindu Sandanayake for generously meeting with the team and sharing insights from his research on the climate impacts of construction in Melbourne, as well as Slattery Quantity Surveyors for providing early insights into carbon foot printing practices in commercial buildings.

The Energy subgroup would like to acknowledge C4NET for their ongoing guidance and support, and Powercor for providing relevant data.

The team also wishes to acknowledge Bill Lilley (RACE for 2030) and Tosh Szatow (RACE for 2030) for their valuable suggestions and guidance that contributed to improving this work.

The team would also like to acknowledge the DTP team and staff for their constant support, guidance, and coordination throughout the project. The University of Melbourne has provided in-kind contributions to support Prof Rebecca Yang's continued leadership of the project following her transition from RMIT in February 2025.

References

1. Berry, A., Collins, L., Oliver, E. and Perfumo, C. (2015) Representative Australian electricity feeders with load and solar generation profiles. CSIRO Data Access Portal, doi:https://doi.org/10.4225/08/5631B1DF6F1A0.

2. BOM (2024) State of the Climate 2024, Bureau of Meteorology.

3. Carre A and Crossin E (2015) A comparative Life Cycle Assessment of Two Multi Storey Residential Apartment Buildings, Forest and Wood Products Australia, Melbourne.

4. Climate Change Bill 2022, (2022) (The Parliament of the Commonwealth of Australia).

5. DCCEEW (2024) Australia's emissions projections 2024 - November 2024, Department of Climate Change, Energy, the Environment and Water, Canberra.

6. DCCEEW (2025) Australian National Greenhouse Accounts Factors - For individuals and organizations estimating greenhouse gas emissions, Department of Climate Change, Energy, the Environment and Water, Canberra.

7. DCCEEW. (2025). Future climate change. Retrieved 9-12-2025 from https://www.dcceew.gov.au/climate-change/policy/climate-science/climate-science/climate-change-future?

8. Durlinger B, Crossin E and Wong J (2013) Life Cycle Assessment of a cross laminated timber building, Forest and Wood Products Australia, Melbourne.

9. EN 15978 (2011) EN 15978:2011 Sustainability of Construction Works - Assessment of Environmental Performance of Buildings - Calculation Method.

10. Foo, G.S. & Shen, D. 2018, 'Australian commercial buildings window to wall ratios', in P. Rajagopalan & M.M. Andamon (eds), Engaging Architectural Science: Meeting the Challenges of Higher Density: 52nd International Conference of the Architectural Science Association 2018, The Architectural Science Association and RMIT University, Australia, pp. 231–240.

11. FWPA (2022) Environmental Product Declaration - Softwood Timber (v2), Wood Solutions website, accessed 14/8/2023. https://www.woodsolutions.com.au/system/files/2022-03/WS%20EPD%201%20Softwood%2002-22.pdf?check_logged_in=1

12. GBCA and Thinkstep (thinkstep-anz GBCoAa) (2021) Embodied Carbon & Embodied Energy in Australia's Buildings,

13. Huang Z, Zhou H, Miao Z, Tang H, Lin B and Zhuang W (2024) 'Life-Cycle Carbon Emissions (LCCE) of Buildings: Implications, Calculations, and Reductions', Engineering, 35:115–139, doi:https://doi.org/10.1016/j.eng.2023.08.019.

14. Hyder Consulting (2011) Construction and Demolition Waste Status Report - Management of Construction and Demolition Waste in Australia, Department of Sustainability, Environment, Water, Population and Communities Queensland Department of Environment and Resource Management, Melbourne.

15. Infrastructure Australia (2024) Embodied Carbon Projections for Australian Infrastructure and Buildings, Infrastructure Australia, Canberra.

16. IPCC (2022) Annex I: Glossary in IPCC, 2022: Climate Change 2022: Mitigation of Climate Change. Contribution of Working Group III to the Sixth Assessment Report of the Intergovernmental Panel on Climate Change, Intergovernmental Panel on Climate Change, Geneva.

17. ISO 14040 (2006) Environmental management — Life cycle assessment — Principles and framework, International Organization for Standardization.

18. Middel, A., Chhetri, N., & Quay, R. (2015). Urban forestry and cool roofs: Assessment of heat mitigation strategies in Phoenix residential neighborhoods. Urban Forestry & Urban Greening, 14(1), 178-186. https://doi.org/https://doi.org/10.1016/j.ufug.2014.09.010

19. My NASA Data. (2024). Earth's Energy Budget. My NASA Data. https://mynasadata.larc.nasa.gov/basic-page/earths-energy-budget#:~:text=Earth%20strives%20to%20maintain%20a,emits%20energy%20back%20to%20space

20. NABERS (2025) The Rules - Embodied Carbon - Version 2.0 - April 2025, National Australian Built Environment Rating System - New South Wales Government

21. Ng, E., & Cheng, V. (2012). Urban human thermal comfort in hot and humid Hong Kong. Energy and Buildings, 55, 51-65. https://doi.org/https://doi.org/10.1016/j.enbuild.2011.09.025

22. O'Dwyer J, Walshe D and Byrne KA (2018) 'Wood waste decomposition in landfills: An assessment of current knowledge and implications for emissions reporting', Waste Management, 73:181-188, doi:https://doi.org/10.1016/j.wasman.2017.12.002.

23. RICS (2017) Whole Life Carbon Assessment for the Built Environment, Royal Institution of Chartered Surveyors, London.

24. Sandanayake M, Zhang G, Setunge S, Luo W and Li C-Q (2017) 'Estimation and comparison of environmental emissions and impacts at foundation and structure construction stages of a building – A case study', Journal of Cleaner Production, 151:319–329, doi: https://doi.org/10.1016/j.jclepro.2017.03.041.

25. Szota, C., Coutts, A. M., Thom, J. K., Virahsawmy, H. K., Fletcher, T. D., & Livesley, S. J. (2019). Street tree stormwater control measures can reduce runoff but may not benefit established trees. Landscape and Urban Planning, 182, 144-155.

26. Taylor J and Warnken M (2008) Wood recovery and recycling: A source book for Australia, Forest and Wood Products Australia, Melbourne.

27. Thorsson, S., Rocklöv, J., Konarska, J., Lindberg, F., Holmer, B., Dousset, B., & Rayner, D. (2014). Mean radiant temperature–A predictor of heat related mortality. Urban Climate, 10, 332-345.

28. Wang X, Padgett JM, De la Cruz FB and Barlaz MA (2011) 'Wood Biodegradation in Laboratory-Scale Landfills', Environmental Science & Technology, 45(16):6864-6871, doi:10.1021/es201241g.

29. Ximenes F, Björdal C, Cowie A and Barlaz M (2015) 'The decay of wood in landfills in contrasting climates in Australia', Waste Management, 41:101-110, doi:https://doi.org/10.1016/j.wasman.2015.03.032.

30. Zare, S., Hasheminejad, N., Shirvan, H. E., Hemmatjo, R., Sarebanzadeh, K., & Ahmadi, S. (2018). Comparing Universal Thermal Climate Index (UTCI) with selected thermal indices/environmental parameters during 12 months of the year. Weather and climate extremes, 19, 49-57.

RACE for 2030

RELIABLE
AFFORDABLE
CLEAN
ENERGY

info@racefor2030.com.au

UTS
L10 10/235 Jones St Ultimo,
NSW 2007 Australia

ABN 46 640 317 559

Australian Government
Department of Industry, Science and Resources

Cooperative Research Centres Program